UNIVERSITÀ DEGLI STUDI DI MILANO

SCUOLA DI DOTTORATO IN SCIENZE E TECNOLOGIE CHIMICHE
DIPARTIMENTO DI SCIENZE FARMACEUTICHE
CORSO DI DOTTORATO IN CHIMICA DEL FARMACO
CICLO XXVIII

OPTIMIZATION AND APPLICATION OF COMPUTATIONAL METHODS FOR THE DESIGN OF PROTEIN-PROTEIN INTERACTIONS MODULATORS

SETTORE CHIM/06 CHIMICA ORGANICA

Dott.ssa IRENE MAFFUCCI
Matricola: R10080

Tutor: Dr. Alessandro CONTINI
Coordinatore del dottorato: Prof. Marco DE AMICI

ANNO ACCADEMICO
2014/2015

CONTENTS

ABBREVIATIONS

Protein-protein interaction, PPI
Amino acid, AA
Binding free energy, ΔG_{bind}
Solvent accessible surface area, SASA
Non natural amino acid, nnAA
Cα-tretrasubstituted amino acid, CTAA
Chiral CTAA, cCTAA
Molecular dynamics, MD
Born-Oppenheimer, BO
Molecular mechanics-Generalized Born surface area, MM-GBSA
Molecular mechanics-Poisson Boltzmann surface area, MM-PBSA
Thermodynamic integration, TI
Free energy perturbation, FEP
Linear interaction energy, LIE
Replica exchange molecular dynamics, REMD
Intrinsically disordered peptides, IDPs
Potential of mean force, PMF
Quantum theory of atom in molecules, QTAIM
Critical point, CP
Bond critical point, BCP
Right handed, *P*
Left handed, *M*
Helical excess, h.e.
Partial nudged elastic band, PNEB
Radius of gyration, RoG
Circular dichroism, DC
Quantitative structure-property relationship, QSPR
Root mean square displacement, RMSD
Difference in accessible solvent areas, dASA
Atomic unities, au.

1 INTRODUCTION

1.1 PROTEIN-PROTEIN INTERACTIONS: ROLE AND PROPERTIES

Protein-protein interactions (PPIs) are central to the tuning and regulation of the most important biological processes,[1,2] because they play a key role in cell proliferation, growth, differentiation, signal transduction and apoptosis.[3–6] Thus, it is not surprising that PPIs are also involved in many disease states, such as cancer, neurodegeneration, and viral and bacterial infections.[7–9] Therefore, the modulation of PPIs has a great therapeutic potential and, in the last decades, much effort has been paid to the design and development of molecules targeting PPIs known to be involved in pathologic states.[1,3,7,10–14]

However, interfering with PPIs represents a challenging task, because of the poor experience gained so far in this field and the intrinsic complexity of the target. This requires innovation of the methodological approaches used for "classical" targets, such as enzymes or receptors.[2]

Indeed, the structural properties of PPIs differ from those of protein-ligand binding, and this represents the biggest problem when trying to modulate PPIs. First of all, the protein-protein interfaces are usually much larger than the binding sites of classical targets. While the ligand-receptor contact areas are usually of about 300-1000Å^2,[15] protein-protein interfaces are usually of 1500-3000 Å^2 in size, or even larger, as in the case of those G-proteins and components of the signal transduction pathway.[16–19] Furthermore, the interfaces involved in PPIs are usually flat and lacking of the grooves, pockets or indentations found at the binding site of classical targets,[2,7,20] and the interactions between two proteins generally involve not contiguous amino acids (AAs).

Nevertheless, since a huge amount of PPIs occurs in cells, structural and composition differences of the regions involved in the interaction are necessary to have the specificity needed for the formation of the right complex in the crowded cellular environment.[11,21,22] This observation, together with promising

results,[2,7,8,11,14,23–27] gives hope for finding molecules able to target protein-protein interfaces and, thus, modulate PPIs.[7]

Indeed, although protein-protein interfaces are large, they are not energetically homogeneous,[28] and generally specific interface portions, called *hot regions*, mainly contribute to PPIs.[22,29] According to the O-ring theory,[30] in these regions it is possible to identify a core and a rim, where this latter contains more accessible residues sheltering the core AAs from solvent molecules (Figure 1.1). The core residues, known as *hot spots*, are those accounting for most of the binding energy and, if replaced by an alanine, they lead to a change in the binding free energy (ΔG_{bind}) $\geq$ 2 kcal/mol.[31] Hot spots located in the same hot region cooperate in stabilizing the complex,[22,32] while the energetic contributions of two or more regions are additive, suggesting the independency of hot regions.[33]

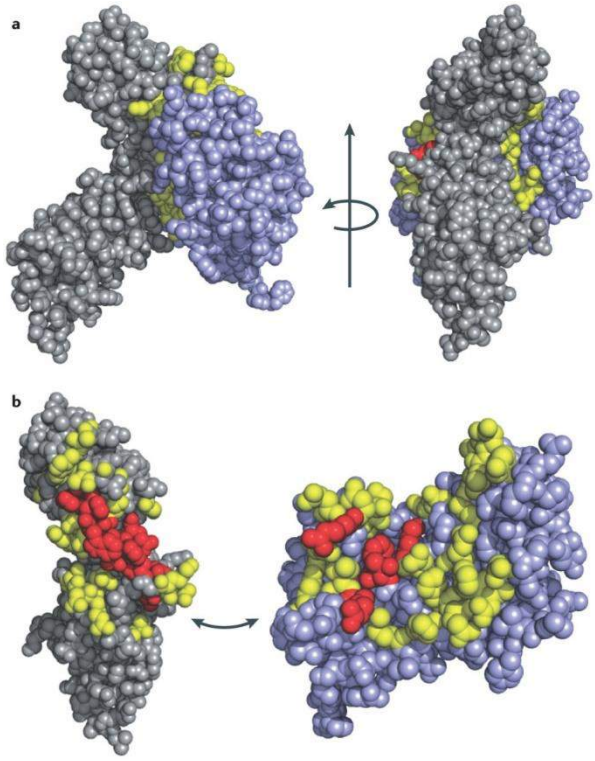

Figure 1.1. Hot spots and O-rings at the protein–protein interface. a) Orthogonal views of the human growth hormone binding protein (GHBP)–growth hormone (GH) complex (PDB ID: 3HHR), with the proteins depicted as atom spheres coloured either purple (GH) or grey (GHBP) except for the hot spot (red) and rim (yellow) residues. b) The complex is shown opening to expose the interacting surface.[34]

Moreover, within hot regions and, most of all, hot spots, there is a strong geometric and energetic complementarity between the proteins involved in the PPI. This complementarity can be enhanced by water mediated interactions,[35,36] where structural water molecules are involved in bridging H-bonds between the two proteins and/or create interfacial dry cores, thus maximizing the interactions between hot spots protected by the rim AAs and water.[37]

Systematic analysis of known hot spots revealed that their composition is not random[38] and that tryptophan, tyrosine, arginine and, at minor extent, isoleucine are the most frequently occurring and the most conserved AAs.[28] Conversely, leucine, serine, threonine and valine are rarely identified as hot spots.[30,39]

Indeed, both tryptophan and tyrosine have a bulky aromatic side chain, which can take part in π interactions and protect fragile H-bonds from water,[40] and they are also able to take part in H-bonds. Moreover, the substitution of tryptophan with an alanine creates a large cavity, causing a destabilization of the PPI, while tyrosine, because of its ability of being involved in H-bonds, has a three times higher probability of being a hot spot than phenylalanine.[30] On the other side, arginine can be responsible of the formation of both salt bridges and H-bonds.

Therefore, although protein-protein interfaces show a high amount of hydrophobic residues, the hydrophobic effect cannot be the only driving force in protein-protein association and the importance of electrostatic interactions is not negligible.[41,42] Indeed, the hydrophobicity degree of protein-protein interfaces is in between the one observed for a protein core and the one of a solvent exposed protein surface, and the composition of hot spots reflects this situation.[38]

The presence of hot spots, where the binding energy is focused, makes the identification of compounds with a relatively low molecular weight more feasible than it would be if the binding energy was equally distributed over the interface. However, this process can be influenced by the druggability of the PPIs.

1.2 DRUGGABILITY OF PPIS

Druggability is defined as the likelihood of identifying a selective, low molecular weight compound with high affinity to the target.[43] It is not an absolute property of the target and, in addition, there is not yet a unified way to determine the druggability of PPIs. However, Chène proposed a useful decision tree to establish if a certain PPI can be considered druggable or not.[11]

First of all, the difficulty in targeting a PPI is related to its half-life: permanent complexes, whose subunits remain associated, or obligate complexes, whose monomers do not exist in the non-associated form in the cellular environment, have a more difficult modulation than transient and non-obligate complexes. Furthermore, an *a priori* knowledge about the presence of cavities, the interfacial hydrophobicity degree, the size and complementarity of the interface helps in targeting PPIs.

The shape of the interface is another factor to take in account, since the less flat the protein interface, the more stable the complex, because one of the partner is more buried. Therefore, transient and hetero-complexes, which are the most attractive for drug discovery, have more planar interfaces.[18] However, the presence of some cavities at the interface is desirable, because they can accommodate molecules and allow specific targeting. Moreover, the hydrophobicity at the interface should be intermediate, allowing the development of molecules with an acceptable trade-off between optimal binding and good pharmacokinetic properties.

Furthermore, it is important to consider the conformational changes eventually occurring upon binding, since when this phenomenon is observed is more difficult to modulate PPIs.

Another important aspect that affects the druggability of a PPI is the presence of helical motifs at the interface. Indeed, because of their frequent occurrence in both protein core and exposed regions, superficial helices are often

responsible of molecular recognition, and the 62% of PPIs reported in databases have helical interfaces.[44,45]

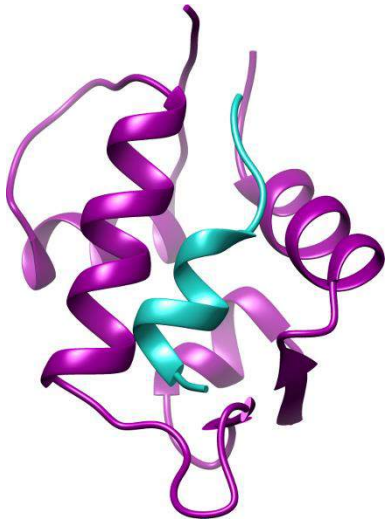

Figure 1.2. X-ray structure of MDM2 (magenta) in complex with the transactivation domain of p53 (turquoise) (PDB ID: 1YCR).[46]

Helical interfaces can be divided into three main categories, which are differently druggable. In detail, to the first class belong proteins whose interface consists in a cleft where a helix can bind and a minimum of two close AAs strongly contribute to the interaction, as happens for the complex between MDM2 and p53 (Figure 1.2).[7,11,46] This situation offers better chances for the design of small molecule able to modulate these PPIs. To the second category belong extended interfaces where the interaction is due to multiple strong contacts between two to five turn helices and a high number of residues. The third category is made of proteins showing both of the described features and quite weak interactions.

All these aspects have to be taken in account when assessing the druggability of a PPI and designing its potential modulators.

1.3 Role of water in PPIs

The importance of water in PPIs has been often underestimated, since the mainstream idea was that protein adhesion was the main actor, while water represented only a spectator in the protein aggregation phenomena. However, as

mentioned before, protein-protein interfaces are enriched in polar and charged residues,[41] and water molecules are often trapped at the interface and are able to satisfy the H-bond network by bridging polar protein-protein interactions which are either too distant of energetically unfavored (Figure 1.3).[47] Therefore, water molecules affect the structure, stability, dynamics and function of biomolecules.

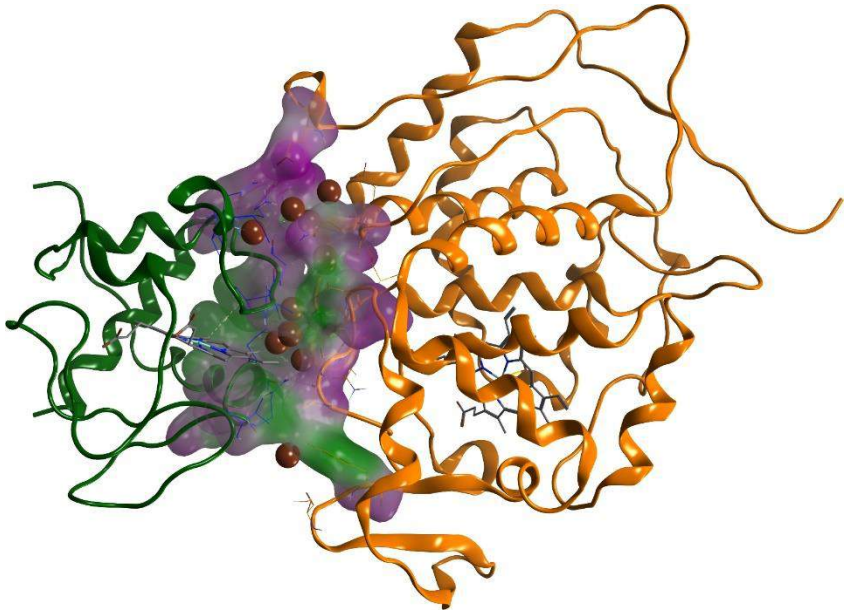

Figure 1.3. Cytochrome C-Cytochrome C peroxidase complex (PDB ID: 2PCC).[48] Protein-protein interface is highlighted and colored depending on lipophilicity (magenta: hydrophilic, green: lipophilic). Interfacial water molecules are depicted as CPK.

Moreover, it has been demonstrated that long-range water-mediated forces, quantified by the hydration free energy, are fundamental for the aggregation of proteins which are approaching each other from a large distance to within a contact distance, as happens in the cellular environment.[49] Nonetheless, water interacting with rim residues allows the formation of dry nuclei at the interface, which enhance the interactions between hot spots,[37] thanks to the hydrophobic effect induced by water.

In a study conducted on 179 high-resolution (< 2.30 Å) X-ray structures of protein-protein complexes[50] it has been showed that of the 4741 interfacial water molecules, 21% were bridging interactions between both proteins and 53% were involved in favorable interactions with only one protein, while the remaining 26%

of water molecules were not interacting with either protein. However, about the half of them showed a solvent accessible surface area (SASA) ≤ 10 Å^2, suggesting that they are buried within the protein-protein interface, often creating hydrophobic bubbles. This kind of water molecules seems fundamental for the mediation and/or lubrication of PPIs,[18] and cannot be neglected when simulating PPIs.

Therefore, as water has been exploited as a component for the design of modulators of classical targets, it can be useful also in the case of PPIs.

1.4 Modulation of PPIs

The modulation of PPIs can be achieved by either stabilization or inhibition of the interaction (Figure 1.4), with the latter being the most explored approach.[7,10,51]

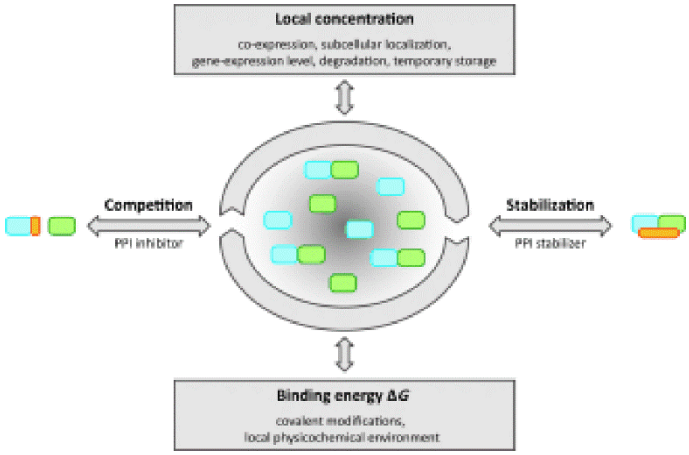

Figure 1.4. Regulatory control mechanisms for the association state of interacting proteins. Adapted from Thiel *et al*.[52]

Furthermore, for both the approaches the modulation can be obtained by either a direct or an allosteric mode of action. When aiming at PPI inhibition by following the former mode, the modulator should directly bind at the interfacial surface of one of the proteins involved in the PPI, preventing the binding of the interaction partner, as observed in the case of the complex Rac1 - Tiam1, whose formation is inhibited by the binding of an inhibitor, such as NSC23766, to Rac1.[53]

Conversely, when the stabilization of the PPI has to be obtained, the modulator binds at the interfacial surface making contacts with both partners and

increasing the mutual binding affinity. In this case, the stabilizing molecule can bind first to one of the interacting proteins, making the interaction surface more adapt to the other protein, as in the case of FKBP binding molecules FK506 and rapamycin.[52] Conversely, the stabilizing molecule can bind to the rim of an already formed protein-protein interface and increase the binding affinity of the two protein partners, as in the case of forskolin binding the C_{1a} and C_{2a} subdomains of adenylyl cyclase, resulting in an increase of the cAMP levels in many tissues.[54]

On the contrary, the allosteric modulation is achieved for both inhibition and stabilization of PPIs by binding to a region of one protein partner not directly involved in the PPI, as in the case of paclitaxel, which, binding to a hydrophobic pocket of polymerized tubulin located only on the β subunit, stabilizes the microtubule structures.[55]

Simultaneously, the modulation of PPIs can be achieved through classical small molecules, which, not necessarily mimicking the secondary structure at the interface, bind to the protein receptor acting as simple functional mimetics.[56,57] These compounds are not versatile, because they are designed for the modulation of a specific target and they can be unlikely exploited for other PPIs.

Conversely, it is possible to obtain the modulation through molecules able to mimic the surface by non-sequential hot spot residues.[58] In this case, it is possible to develop non-peptide scaffolds, known as proteomimetics, witch match the topography of the original secondary structure, usually a helix,[44,45] by spatially orienting their substituents in a way that allows the interaction with the hot spots. For example, the aryl core of 3,2′,2″-terphenyl derivatives (Figure 1.5c) are able to assume a staggered conformation which projects the *ortho* substituents to mimic the positions of the *i*,*i+4* and *i+7* residues of a helix (Figure 1.5a,b). Some of these derivatives proved to inhibit the calmodulin/phosphodiesterase, the Bcl-x_L/Bak and gp41 PPIs with nanomolar IC_{50}.[59–61]

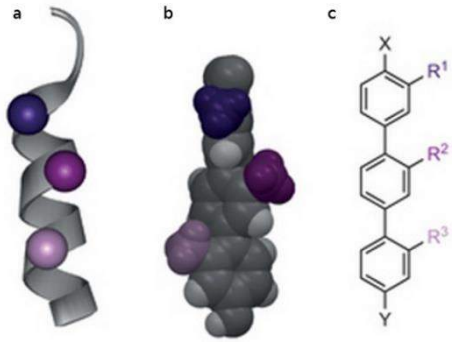

Figure 1.5. a) Representation of an α-helix whose i, i+4 and i+7 residues are highlighted on a single face. b) X-ray structure of a terphenyl derivative. c) 3,2',2"-terphenyl - the first α-helix mimetic. Adapted from Azzarito.[58]

The last and more interesting approach to modulate PPIs is the use of peptide-based molecules. This is particularly useful when targeting helical interfaces, which are the most frequently occurring and structurally stable.[45] Peptides provide a high degree of selectivity and specificity toward the target and a low toxicity.[62–64] However, synthetic peptides are considered therapeutically undesirable because of their poor bioavailability and their sensitivity to proteolytic degradation.[65] Furthermore, synthetic peptides in solution often adopt random conformations, far from those observed in their parent proteins, which have to be maintained to assure the correct interaction with the target protein interface.[58] Therefore, many approaches aimed to solve one or both these problems have been developed. Among these, the most exploited ones consist in the nucleation of the helix formation and/or in the stabilization of the helical conformation (Figure 1.6).

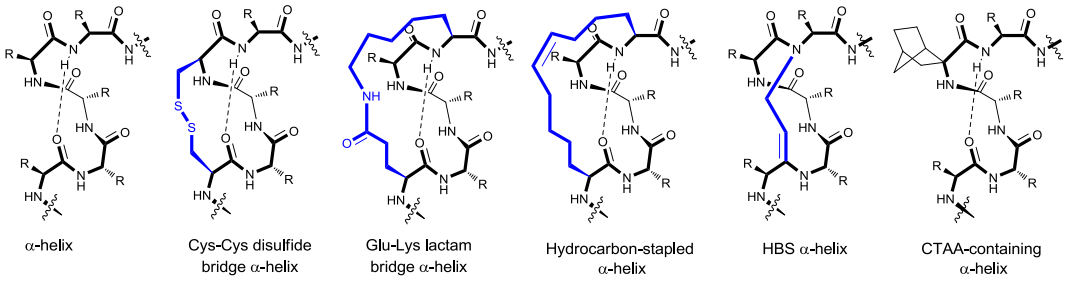

Figure 1.6. Scheme illustrating different approaches for helix stabilization.

In this framework, frequently applied methods are the covalent cyclization, i.e. disulfide or lactam bridges,[66,67] the H-bond surrogate (HBS) method,[68] the

hydrocarbon stapling[69,70] or the use of non natural AAs (nnAAs), such as β-AAs[71] or Cα-tetrasubstituted AAs (CTAAs).[72,73]

1.5 COMPUTATIONAL APPROACHES IN PPIS MODULATION

The exploitation of computational methods has revealed to be extremely helpful for the design of PPIs modulators.[74] Different methods can be applied to each step, from the analysis of the protein-protein interface to the modulators optimization and the estimation of the binding affinity.

For example, although crystallographic structures provide important information about the protein-protein interfaces, different computational methods can be used for the identification of possible binding pockets present at the interface. Some of these methods rely on geometry- or energy-based algorithms,[75] while other techniques are based on structure and sequence comparison[76,77] or on the analysis of the dynamics of proteins through extensive molecular dynamics (MD) simulations.[78,79]

Furthermore, a fundamental step when designing any kind of PPIs modulators is the detection of hot spots. Obviously, this can be done through experimental methods, which, however, are laborious and expensive. Therefore, there is a high demand of computational approaches aimed to this. Among the available methods, the most straightforward is the *in silico* alanine scanning, where selected AAs are mutated to alanine and the effect of the mutation in terms of relative binding free energy are evaluated. Then, a relative binding (free) energy is computed for the wild-type complex and for the complexes carrying the mutations to alanine, often using simple physical models or empirical scoring functions.[80] The computational alanine scanning can be performed on a single complex structure or on an ensemble of conformations obtained from MD simulations, with this approach performing better than the former because the single structure may be not representative if the proteins are flexible.

Another widely used method to establish the contribution of single AAs to the ΔG_{bind} is the Molecular Mechanics Generalized Born/Poisson Boltzmann Surface

Area (MMGB/PBSA), which allow a per-residue decomposition of the ΔG_{bind}.[81] In both methods endpoint free energy calculations are performed to predict the total ΔG_{bind} on an ensemble of states extracted from MD simulations. They also allow the decomposition of the ΔG_{bind} into pairwise contributions, which are useful to detect important interactions between pairs of AAs.

Because of the already mentioned differences between PPIs and classical targets, different approaches for the rational design of molecules targeting PPIs have to be developed.[82] The modulation *via* small molecules is quite difficult, although some successful results have been obtained. Indeed, an extensively developed database of starting structure is still needed and the current chemical libraries lack of a sufficient diversity to reflect PPI drugs. Furthermore, the protein interface might be too flat and without relevant crevices where a small molecule can bind.

Nevertheless, in the case of the design of small molecules, the fragment based ligand design can be applicable, since it allows the introduction of a high degree of chemical diversity and because only the interaction with the hot spots is required.[7]

Conversely, when designing a peptide or peptidomimetic PPI modulator, the hot spot identification is likely to evidence the required peptide function that the modulator needs. However, as previously underscored, in order to obtain a correct spatial orientation of the substituents, it is fundamental to assess the conformation that the modulator will assume in the biological environment. This can be achieved through computational methods such as long classical MD or enhanced sampling MD, which allow the exploration of the whole conformational space and, possibly, the identification of the most energetically stable conformation of the molecule under study.

Furthermore, computational studies using different and complementary approaches can help in the generalization of either the structural features required by small molecules[77] or the secondary structure stabilizing conditions needed by peptides/peptidomimetic ligands.[58,72]

The estimation of some kind of parameter as a measure of the ligand binding affinity is a fundamental step in drug discovery and the application of computational methods at different degree of accuracy and speed can represent a useful tool for this process. These methods can involve the use of scoring function and, therefore, limit the estimation to a single conformation state, or they can be based on the analysis of MD simulations, which provide a statistically meaningful ensemble of conformations for thermodynamic calculations at an acceptable computational cost. Among these latter methods, the most popular are the previously mentioned MMPB/GBSA, the linear interaction energy (LIE),[83] the thermodynamic integration (TI),[84] and the free energy perturbation (FEP).[85] However, because of their good balance between efficiency and accuracy, MMPB/GBSA methods are getting used more and more for the computation of binding energies.

As just evidenced in this section, computational methods can be usefully exploited to target PPIs, although they have to be adapted to those used for classical targets, because of the structural complexity of PPIs.

2 PROJECT OVERVIEW

Among all the research topics concerning the modulation of PPIs, my PhD project has been focused on the optimization of computational methods and protocols for the design of modulators of PPIs, with a particular interest on peptide modulators.

It has to be underlined that my work has been mainly methodological and it aimed to provide basic knowledge and computational tools for the design of well-structured peptides[72,86–88] and for the prediction of binding energies with a good correlation with experimental data.[89,90]

Therefore, I initially evaluated the ability of some of the modern force fields coupled to different implicit solvent models of reproducing and, thus, predicting the main peptide secondary structure motifs, such as helices, β-sheets and random coils.[88] Indeed, as previously underscored, the *a priori* knowledge of which conformation a peptide designed as PPI modulator will more likely assume in the biological environment is fundamental to verify the correct spatial orientation of the side chains for the interaction with the protein target and to assure the interaction with the target protein interface.[58] Therefore, I selected and submitted to Replica Exchange Molecular Dynamics (REMD) simulations eight peptides: two helical, three β-hairpins and three intrinsically disordered peptides (IDPs).[88]

As evidenced in the previous chapter, helical protein-protein interfaces are frequently occurring in nature[44,45] and different approaches to stabilize the helical secondary structure in synthetic peptides have been developed.[58] Among these, the insertion of CTAAs in the peptide sequence can lead to peptides inherently stable to proteases and peptidases[91], and folding into well-ordered helices.[58,73,87] Furthermore, this approach together with the synthesis of chiral CTAAs (cCTAAs) is of high interest in my research group.[73,87,92,93] Therefore, taking in account the information gained from the previous study,[88] I applied theoretical methods to identify some intuitive descriptors that can be applied to predict how a given

cCTAA can affect the peptide folding, as well as to compare different cCTAAs in terms of stabilization efficacy.[72]

Moreover, since the ability of a cCTAA to influence the helical screw sense of a peptide might depend on its Cα stereochemistry,[93–96] and because in nature the right-handed (*P*) helix is found more frequently than the left-handed (*M*) helix,[97,98] I extended the previous study by investigating the cCTAAs features which are most responsible of the helical screw sense selectivity.[86]

In this context, by collaborating with Prof. Jonathan Clayden at the University of Manchester, I also studied the mechanisms involved in the helical screw sense inversion, whose knowledge can be exploited either for signal transmission in the cellular environment, as aimed by Prof. Clayden's group,[99] or for a conformation-controlled modulation of PPIs.[100]

Successively, because many efficient and reliable computational approaches for determining the protein-protein interface and identifying hot spots were already available,[28,101] I preferred to focus on the development and optimization of a MMGBSA based protocol for the estimation of relative binding energies of PPIs involving complexes providing a good correlation with experimental data. This approach, named Nwat-MMGBSA consists in considering the effect of water on the binding affinity by including a selected number of water molecules (Nwat) which are the closest to the ligand or to selected residues frame by frame during the MD simulation time, as part of the receptor in the MMGBSA analysis. Therefore, I initially applied this approach to the simplest situation, represented by classical protein-ligand systems with known experimental activities.[89]

Once assessed the reliability and validity of the Nwat-MM-GBSA method, I applied it to PPI systems. In detail, I initially performed a methodological investigation on a dataset of hetero-dimeric PPIs with known experimental ΔG_{bind}. Aiming to identify the most critical variables affecting the correlation of predicted and experimental energies, I tested two different recent AMBER force fields (e.g. ff99SBildn and ff14SB), two implicit solvent models (e.g. GB-OBC(II) and GB-

Neck2) and two explicit solvent models (e.g. TIP3P and TIP4PEW) on 12 ns simulations, which were analyzed through Nwat-MMGBSA at the fourth and at the last ns with different ways to select the protein-protein interface. Consequently, I applied the best protocol to five PPI systems consisting in one of the two interacting proteins inhibited by small molecules or peptidomimetics with known activities.

After a brief chapter summarizing the bases of the computational methods applied throughout the project, each part will be discussed in a dedicated chapter, which will be organized as follows: a) an introduction to the study, aimed to contextualize it within the project and to summarize it; b) a results and discussion session; and c) protocols details.

3 METHODS

3.1 MOLECULAR DYNAMICS (MD)

Molecular Dynamics (MD) is a computational method used to study the time dependent behavior of proteins and other macromolecules, providing atomistic information on the fluctuations and conformational changes of biosystems. This method is extensively applied for the investigation of structure, dynamics and thermodynamics of biological molecules and their complexes.

MD method is based on the Newton's second law, also known as equation of motion, expressed as $F_i = m_i a_i$, where F_i is the force, usually depending on the temperature, exerted on a particle i having mass m and acceleration a, which can also be expressed as $\frac{d^2 r_i}{dt^2}$, with r_i being the vector of the Cartesian atomic coordinates.

Therefore, from the knowledge of the force acting on each atom it is possible to determine the acceleration of each atom of the simulated system. The integration of the equation of motion on small time intervals through different algorithms yields a trajectory describing how atomic positions, velocities and accelerations vary with time.

The force acting on a particle, F_i, can also be expressed as the gradient of the potential energy of the system (V): $F_i = -\nabla_i V$, which, combined with the previous equation, gives $-\frac{dV}{dr_i} = m_i \frac{d^2 r_i}{dt^2}$.

Thus, starting from known initial coordinates, usually derived from experiments such as NMR or X-ray analyses, initial distribution of velocities and forces applied on the system, it is possible to generate the trajectory of the system as a function of the simulation time. Moreover, it allows to relate the derivative of the potential energy to the changes in position as a function of time.

At the light of this, the potential energy function is fundamental for performing MD simulations and, being a function of the atomic positions r, takes in account for both the interactions between bonded atoms and those between

atoms which are not directly bound. Commonly, the potential energy function is represented in its basic form as the following Hamiltonian:

$$V(\overrightarrow{R}) = \sum_{bonds} k_d\,(d - d_0)^2 + \sum_{angle} k_\theta\,(\theta - \theta_0)^2 + \sum_{dihedrals} k_\varphi(1 + \cos(n\varphi - \delta)) + \sum_{non-bond}\left\{\epsilon_{ij}\left[\left(\frac{R_{ij}^{min}}{R_{ij}}\right)^{12} - \left(\frac{R_{ij}^{min}}{R_{ij}}\right)^{6}\right] + \frac{q_i q_j}{\epsilon_l r_{ij}}\right\},$$

which collects the "bonded" energy terms, such as the stretching energy associated to the bond length, the bending energy associated to the angles variations, the torsion energy which derives from the torsion of dihedral angles, and the "non-bonded" energy terms comprising van der Waals and electrostatic forces.[102]

Being a Molecular Mechanics (MM) method, MD relies on the Born-Oppenheimer (BO) approximation, which allows to consider the potential energy as a function of the nuclear coordinates only. The BO approximation is based on the assumption that, since the nuclei are much heavier than electrons, the atoms can be described as spheres with a certain radius, mass and a point charge, which simulates the effect of merging electrons and nuclei, located in the center of the sphere.

The Hamiltonian and the related parameters, comprising atomic radii and point charges, are contained in a force field. Several force fields are available, differing in parameterization methods and/or in the form of the energy functions. Moreover, within a force field family (i.e. the Amber force field), few differences can also be observed, usually related to torsion angle parameters.

Since MD simulations aim to reproduce what happens in the biological environment, the solvent, usually water, has to be considered during the simulation. This can be done by using either implicit or explicit solvent models. In the former, the solvent is considered as a continuous medium with a certain dielectric constant. In explicit models water molecules are included during the simulation, making the simulation more realistic, although increasing the computational time.

In addition, for the reproduction of the experimental conditions, it is possible to use different thermodynamic ensembles, where the total number of particles (N) is kept constant together with a) volume (V) and total energy (E), known as microcanonical ensemble (NVE), b) volume and temperature (T), known as canonical ensemble (NVT) or c) pressure (P) and temperature, known as isothermal-isobaric ensemble (NPT).

However, when dealing with MD simulations, it is important to bear in mind that many approximations are introduced during the calculations, mainly related to the use of the force field and to the solvent model used. Furthermore, the feasible simulation time is only up to nano- or, maximum, microseconds, therefore the simulation of, for example, conformational changes occurring in a millisecond scale still represents a challenge.

3.2 Replica Exchange Molecular Dynamics (REMD)

Peptide folding simulations through classical all atoms MD need an extremely long computational time to converge, because simulated peptides tend to get trapped in local energy minima, from which it is hard to escape at the simulation temperature (usually 300 K).

Therefore, Sugita and Okamoto developed the REMD method, which belongs to the class of enhanced sampling MD. [103] REMD performs simulations based on essentially known non-Boltzmann probability weight factors, realizing a random walk in the temperature space. This random walk induces a random walk in the energy space, which allows the simulation to escape from local minima energy states.

Concretely, many MD simulations of a system, named *replica*, are performed at different temperatures starting from the same system coordinates. During the REMD simulation the temperatures are exchanged between the replica (Figure 3.1).

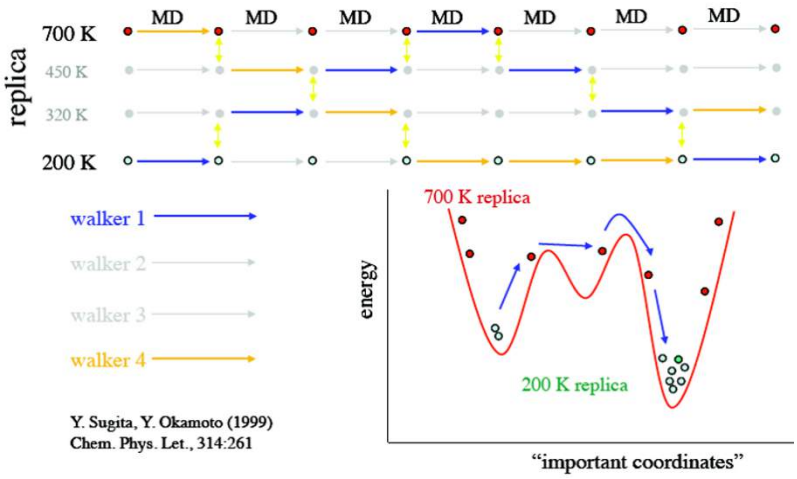

Figure 3.1. REMD simulation method scheme.

The number of replicas and the temperature interval (usually between 200 and 700 K) are chosen depending on the size of the system. At low temperatures the sampled conformations are stable but unlikely escaping from the local energy minima; conversely, at high temperatures it's easier to escape from these minima, but the sampled geometries are not stable, since classical force-fields are not designed to operate at high temperatures. Therefore, moving a geometry obtained at high temperatures to a simulation at low temperature allows to benefit of both simulation conditions.

Successively, the trajectory at the temperature of interest (around 300 K) is extracted and analyzed, in order to obtain information about the conformational changes of the system under study.

3.3 POTENTIAL OF MEAN FORCE (PMF)

For investigating some biological events, such as peptide/protein folding or the conformational changes to which a protein undergoes upon its activation or inactivation, it can be helpful to study how the free energy profile changes as a function of one or more inter- or intramolecular coordinate, such as atom distances or torsion angles. The free energy surface along the defined coordinate is known as PMF (Figure 3.2).[104]

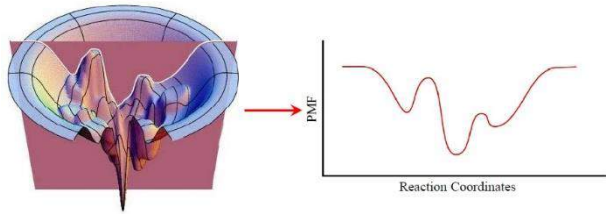

Figure 3.2. From the free energy surface to the free energy as a function of a reaction coordinate.

Therefore, the PMF $\omega(\chi)$ along the coordinate χ is defined from the average distribution function $\langle\rho(\chi)\rangle$ through this relationship:

$$\omega(\chi) = \omega(\chi^*) - k_B T ln\left[\frac{\langle\rho(\chi)\rangle}{\langle\rho(\chi^*)\rangle}\right]$$

Where $\omega(\chi^*)$ and $\langle\rho(\chi^*)\rangle$ are arbitrary reference values. $\langle\rho(\chi)\rangle$ is obtained from a Boltzmann weighted average. This quantity cannot be obtained by a classical MD simulation, because of the poor sampling of high energy configurations, but it can be computed from REMD simulations.

3.4 QUANTUM THEORY OF ATOM IN MOLECULES (QTAIM)

QTAIM method[105] has been developed by Richard Bader in the early 1960s and represents a model of molecular and condensed matter electronic systems (i.e. crystals) where atoms and bonds are expressions of the electron density distribution function. In particular, the nucleus acts as a point attractor immersed in a cloud of negative charge, the electronic density $\rho(r_c)$, which describes how the electronic charge is distributed throughout the space. The electronic density is a maximum at the position of each nucleus and decays quickly away from these position (Figure 3.3).

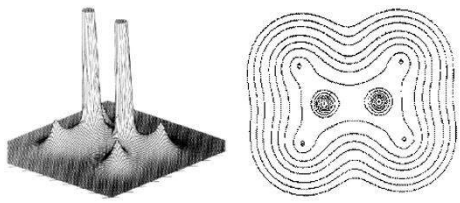

Figure 3.3. The electron density in the plane containing the two carbon and four hydrogen nuclei of the ethene molecule.

However, to extrapolate information about the electronic density it is fundamental to consider the field obtained by following the trajectories traced out by the gradient vectors of the density. The gradient of $\rho(r_c)$ is a vector pointing toward the maximum increase in the density, thus, since the density has a maximum at the position of each nucleus, the traced trajectories terminate at each nucleus. These trajectories allows the definition of the atomic basins, which are the space regions traversed by trajectories and terminating at a given nucleus, as showed in Figure 3.4.

Nuclei correspond to a kind of critical points (CP), where a CP is a point in the space where the first derivative of the density ($\nabla\rho(r_c)$ is null. To CPs is associated a set of trajectories starting at infinity and terminating at CP (Figure 3.4), which define an interatomic surface separating the basins of two neighboring atoms. A unique pair of trajectories originates at each CP and terminates, one each, at the neighboring nucleus. This pair defines a line through the space along which the $\rho(r_c)$ is a maximum. This line, called bond path, indicates that an interaction between the two atoms occur. Therefore, the related CP, which is the point with the lowest electronic density along the bond path, is called bond critical point.

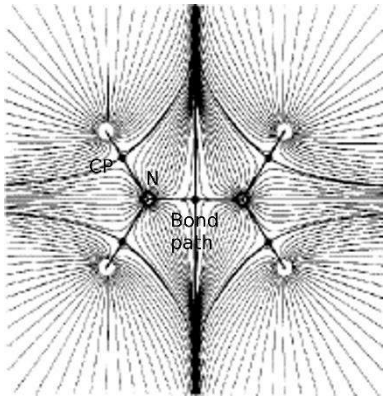

Figure 3.4. Trajectories that terminate at the nuclei (N), including the bond path and the bond critical point (CP). Each trajectory is arbitrarily terminated at the surface of a small circle centered on the nucleus.

CPs are classified by two values: their rank and their signature. The former is the number of non-zero curvatures of the electron density at the CP, which are

always 3 if the system is at an equilibrium charge distribution state. The latter is the algebraic sum of the signs of the curvatures and it is equal to -3 if the CP is a local maximum (i.e. the nucleus), -1 if it is a bond critical point, because it is a minimum on the plane perpendicular to the bond path and a maximum along it.

The $\rho(r_c)$ at the bond CP defines the strength of the chemical bond, while the sum of the three curvatures of the density at the CP ($\nabla^2\rho(r_c)$) is < 0 if the interaction between the two atoms is covalent, > 0 if it's electrostatic. A third parameter, called ellipticity (ε), measures the stability of the interaction, because it indicates the extent to which density is preferentially accumulated in a given plane containing the bond path. If $\varepsilon = 0$, the bond is cylindrically symmetrical and stable.

Therefore, QTAIM can be exploited for the characterization of covalent and noncovalent interactions within a molecules in terms of strength ($\rho(r_c)$), nature ($\nabla^2\rho(r_c)$) and stability (ε).[106]

3.5 PARTIAL NUDGED ELASTIC BAND (PNEB)

Many MD based approach for the study of conformational changes occurring along a defined path have been developed, however most of them are computationally expensive and require a prior definition of a reaction coordinate along which biasing the simulation. This represents a limit for systems involving many degrees of freedom.

A possible alternative is to use chain-of-states methods, where two images are used as initial and final seeds, and additional images are generated between them and optimized.

Among these methods, the nudged elastic band (NEB)[107,108] allows the definition of a minimum energy path of a conformational transition given only initial and the final structures and uses multiple simulations of the system, called images, to map the conformational change. Indeed, these images are pulled into an interpolating path between the two endpoint conformations, then the initial path is optimized, by, for example, simulation annealing, to minimize the energy pathway and the minimum potential energy path is obtained. The images are connected to

their neighbor images by virtual springs, which are needed to force the images to stay at an average separation between their partner images along the path.

In the plain elastic band method spring forces could interfere with the energy of each image, because too rigid spring constants cause an image overestimation of the energy in the saddle points, determining corner cutting and unresolved saddle point structures. Conversely, for weak spring constants, the forces acting on the images are too prominent, thus the images slide down the path back to the minima.

NEB solves this problem by using a tangent vector to the path for decoupling the force to a perpendicular component, described by the force field, and a parallel component, described by the springs, which are only needed to keep the images evenly spaced along the path. Therefore, the force described by the force field is only applied perpendicular to the path tangent and, thus, it is projected out from each image and not along the path between images.

Beyond the endpoint structures, which are not submitted to NEB, additional images can be chosen as seeds for the initial path, but they are not exempt from NEB force calculation.

Recently, a partial nudged elastic band (PNEB)[109] implementation has been introduced, allowing the NEB method to be applied to a desired subset of the system, whereas the non-NEB part acts as a standard MD simulation. With this implementation NEB can be used in large systems where a local transition is desired, or in explicitly solvated systems.

3.6 Molecular Mechanics Poisson-Boltzmann/Generalized Born Surface Area (MMPB/GBSA)

The drug design process often benefits of computational methods for the prediction of binding energies.[110,111] Many of these methods are MD-based, because MD provides statistically meaningful conformational ensembles for thermodynamic calculations in an acceptable computational time. Among the MD-based methods, Molecular Mechanics Poisson-Boltzmann/Generalized Born Surface Area (MMPB/GBSA)[112,113] is one of the most popular for drug

design/discovery purposes, because of its balance between reliability and computational cost.[114]

MMPBSA and MMGBSA methods combine molecular mechanics (MM) energies, polar and nonpolar solvation contributes, and an entropy term to approximate the binding free energy of a ligand to a receptor. More in detail, with these methods the binding free energy is calculated as reported in eq. 1:

$$\Delta G^0_{bind,solv} = \Delta G^0_{bind,vacuum} + \Delta G^0_{solv,complex} - (\Delta G^0_{solv,ligand} + \Delta G^0_{solv,receptor}) \quad (1)$$

Where $\Delta G^0_{bind,vacuum}$ results from the calculation of the average energy of interaction between receptor and ligand and by evaluating the entropic contribute, usually with normal-mode analysis. Conversely, the solvated free energies of complex, receptor and ligand are calculated through the linearized Poisson-Boltzmann (PB) equation[115] or the Generalized Born (GB)[116,117] model, as showed by eq. 2. PB or GB equations solutions provide the electrostatic contribute (ΔG_{el}) to the solvation free energy, which is calculated as the sum of ΔG_{el} and a nonelectrostatic contribute (ΔG_{nonel}) considered proportional to the solvent accessible surface area (SA).[112]

In both the approaches, the solvent is treated implicitly and considered as a continuous medium with a certain dielectric constant ϵ_{solv}, which is 80 for water, and a low dielectric constant ϵ_{in} is assigned to the solute (usually ϵ_{in} = 1 for proteins).

$$G_{solv,PB(GB)}(X) = \frac{1}{2}\sum_{i,j\in X} q_i q_j g_{ij}^{PB(GB)} \quad (2)$$

Where X is the complex, the receptor or the ligand, q_i and q_j are the atomic charges and $g_{ij}^{PB(GB)}$ is the solution of PB (eq. 3) or GB equations (eq. 4).

$$\vec{\nabla}\left[\varepsilon\left(\vec{r}\right)\vec{\nabla}\psi\left(\vec{r}\right)\right] = -4\pi\rho\left(\vec{r}\right) - 4\pi\sum_i c_i^{\infty} q_i^{ion}\lambda\left(\vec{r}\right)\cdot e^{\frac{-q_i^{ion}\psi\left(\vec{r}\right)}{k_B T}},\ \varepsilon = 80 \text{ and } 1 \quad (3)$$

Variable	Definition
$\left(\underset{r}{\rightarrow}\right)$	Position dependence
$\underset{\nabla}{\rightarrow}\psi$	Gradient of the electorstatic potential
ρ	Solute charge distribution
c_i^{∞}	Bulk charge density of ion q_i^{ion}
λ	Accessibility of position $\left(\underset{r}{\rightarrow}\right)$ to the ions in solution
k_B	Boltzmann constant
T	Absolute temperature

$$g_{ij}^{GB} = \left(\frac{1}{\varepsilon_{solv}} - \frac{1}{\varepsilon_{in}}\right)\left[r_{ij}^{n} + \alpha_i\alpha_j exp\left(-\frac{r_{ij}^{n}}{A\alpha_i\alpha_j}\right)\right]^{-1/n} \quad (4)$$

where *A* and *n* are constants and r_{ij}^{n} is the distance between atoms *i* and *j*.

When performing MMPB/GBSA calculations, a fixed number of frames of the explicit solvent MD trajectory of the complex is analyzed in order to obtain the average of the interaction energies between receptor and ligand, taking each free energy component of eq. 1 from the single MD trajectory of the complex.

However, because of the use of an implicit solvent model, the standard MMPB/GBSA approach does not consider the effect on the binding free energy of water molecules present at the binding site or at the protein-protein interface, which can mediate H-bonds between the receptor and the ligand or between the two protein partners, or stabilize the complex.[118,119]

A way to overcome this limit is represented by the application of the Nwat-MMPB/GBSA approach, described in Chapter 8.[89,90,120]

Part 1:

Designing well-structured helical peptides containing chiral Cα-tetrasubstituted amino acids

4 PROTOCOL OPTIMIZATION FOR PEPTIDE FOLDING PREDICTION

4.1 INTRODUCTION

As previously evidenced, PPIs occur through the interaction of protein domains with a well-defined secondary structure. Therefore, when designing peptide modulators of PPIs it is important to verify if they fold in the correct conformation. Several efforts has been thus devoted to the design of peptidomimetics[121] or peptide drugs,[122] as well as to the development of computational methods for the prediction of the secondary structure of peptides[73,93,123–125] or mini-proteins.[126–129] Indeed, we lately assisted to an improvement in computer hardwares[130–132] and to the development of enhanced sampling methods,[103,133,134] aiming to overcome the limit represented by the long and CPU intensive simulations needed to extensively sample the conformational space of peptides. Among the enhanced sampling techniques, REMD has been successfully applied for the prediction of folding behavior of many peptides.[73,87,93,103]

However, a limit to the accuracy of REMD simulations in predicting peptide secondary structures might be represented by the choice of the molecular mechanics force field. The existing force fields have been mostly derived from quantum mechanics calculations or from experiments and, recently, new force fields were obtained through refinement of old ones in order to improve their accuracy.[135,136] Therefore, a plethora of force fields differing only in a few parameters associated to specific torsion angles is currently available.

Nevertheless, except for some studies,[137–141] the comparison of force fields accuracy in predicting peptide folding behavior has been focused on a limited number of test systems.[142–152] Furthermore, with some exceptions,[137,153,154] current force fields have been validated by focusing on α-helix and β-hairpin secondary structures, with less attention being paid to intrinsically disordered peptides (IDPs),[137,138,148,149,155] and principally performing the simulations in explicit solvent.[140,142–144,146–149,153,156–158] Concerning this latter aspect, REMD simulation

time dramatically increases in explicit solvent conditions, thus a large CPU power is needed when simulating long peptides or a large number of systems. Therefore, in drug discovery the use of an implicit solvent model may be advantageous, as long as the secondary structure prediction accuracy is maintained.[159–162]

Moreover, although challenging, the accurate modelling of disordered states of proteins and peptides is fundamental, since IDPs are involved in important biological processes, such as signaling and regulation,[163,164] and their conformational flexibility can be crucial in mediating PPIs.[165,166]

At the light of these considerations, we used REMD simulations to test the ability of some AMBER force fields, namely ff96,[167] ff99SB,[141] ff99SBildn,[136] ff99SBildn-φ,[168] ff12SB[169] and ff14SB[170], and implicit solvation models, namely GB-HCT,[171] GB-OBC(II)[172] and GB-Neck2,[173] to reproduce the folding behavior of 8 peptides. Among these, the QK VEGF modulator (**H1**)[174] and the Ac-Ala-Aib-Ala-Aib-Ala-NHMe peptide (**H2**)[175] are known to be helical; the C-terminus of protein G (**B1**, PDB code 2GB1),[176] the trpzip2 trypthophan zipper (**B2**, PDB code 1LE1)[177] and the N-terminus of ubiquitin (**B3**, PDB code 1UBQ)[178] fold into β-hairpins, while Polybia-MPII (**ID1**),[179] the TRTK-12 CapZ peptide (**ID2**)[180] and the C-terminus of p53 (**ID3**)[181,182] are IDPs (Table 4.1).

Table 4.1. Peptides considered for the protocol optimization.

Peptide	Sequence	Secondary Structure	Experimental Data
H1	Ac-KLTWQELYQLKYKGI-NH_2	Helix	CD (water, 20 °C, pH 7.1)
H2	Ac-Ala-Aib-Ala-Aib-Ala-NHMe	3_{10}-Helix	X-ray
B1	GEWTYDDATKTFTVTE	β-hairpin	NMR (H_2O/10% D_2O, pH 6.3)
B2	SWTWENGKWTWK	β-hairpin	NMR (H_2O/8% D_2O, pH 5.5)
B3	QIFVKTLTGKTITLE	β-hairpin	X-ray
ID1	INWLKLGKMVIDAL-NH_2	IDP	CD (water, 25 °C
ID2	TRTKIDWNKILS	IDP	NMR (H_2O/10% D_2O, pH 7.2)
ID3	Ac-STSRHKKLMTKTE	IDP	NMR (D_2O, 37°C)

In particular, the two latter peptides adopt an α-helical secondary structure when bound to S100B protein, while they are IDP in the unbound state,[180,181,183] thus representing an interesting test for the considered force fields and implicit solvent models. We decided to study only two helical peptides, because modern force fields generally overpopulate the α-region,[140] thus we chose to stress more on β-hairpin and IDP predictions.

This study was aimed to identify which is the most reliable combination of force field and implicit solvent model for the reproduction of a certain secondary structure and to evaluate if a protocol for the prediction of an unknown secondary structure can be defined.

4.2 RESULTS AND DISCUSSION

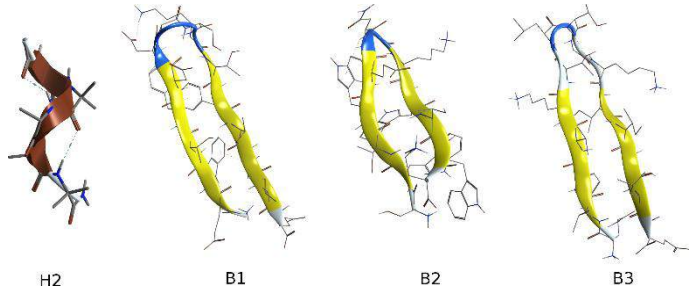

Figure 4.1. Native structures of peptides **H2**, **B1-B3**.

Helical Peptides. As previously underscored, although the latest force fields were specifically developed to provide a better balance between the helical and the other conformations by adding specific torsional parameters,[136,141,167,169] it has been reported that most modern force fields are still biased toward the helical structure.[140] Therefore, this observation together with the strong helicity of peptide **H1** explain why all the combinations used for the simulations on peptide **H1** led to a helical conformation. Indeed, the principal cluster obtained from the analysis of the REMD simulations had in all cases a helical representative structure and a population (pop%) higher than 50% (Figure 4.2). The only exceptions were represented by the combination ff99SBildn-φ/GB-HCT, which gave a helical

population of 46.4% and ff99SBildn-φ/GB-Neck2, whose corresponding representative structure is only partially folded into a helix. The best results, in terms of both helicity of the representative structure of the most populated cluster and its pop%, were obtained for the simulations performed using the combinations ff96/GB-OBC(II), ff99SB/GB-HCT, ff12SB/GB-Neck2 and ff14SB/GB-OBC(II) (Figure 4.2).

These observations were confirmed by the total DSSP average helical content (h_{tot}%, Table 4.2), which were all above 60%, except for the analysis of the ff99SB/GB-HCT trajectory. In this case, the low h_{tot}% (39.9%) was compensated by the presence of a significant amount of turn-like structures (26.1%) which are however clustered with helical geometries, thus explaining the high pop% obtained for the principal cluster. This suggests that the **H1** helix is predicted as less stable by this combination. Indeed, helical H-bonds occupancies are lower than those observed for the other well-performing combinations (Annex 4.A). Moreover, DSSP analysis for ff12SB/GB-OBC(II) also provided a h_{tot}% (67.9%) as high as that obtained for the ff12SB/GB-Neck2 combination, although the population of the principal cluster was lower. However, the representative structure of the second cluster (Figure 4.3) is still helical at the N-terminus, thus explaining the relatively high h_{tot}% obtained by DSSP.

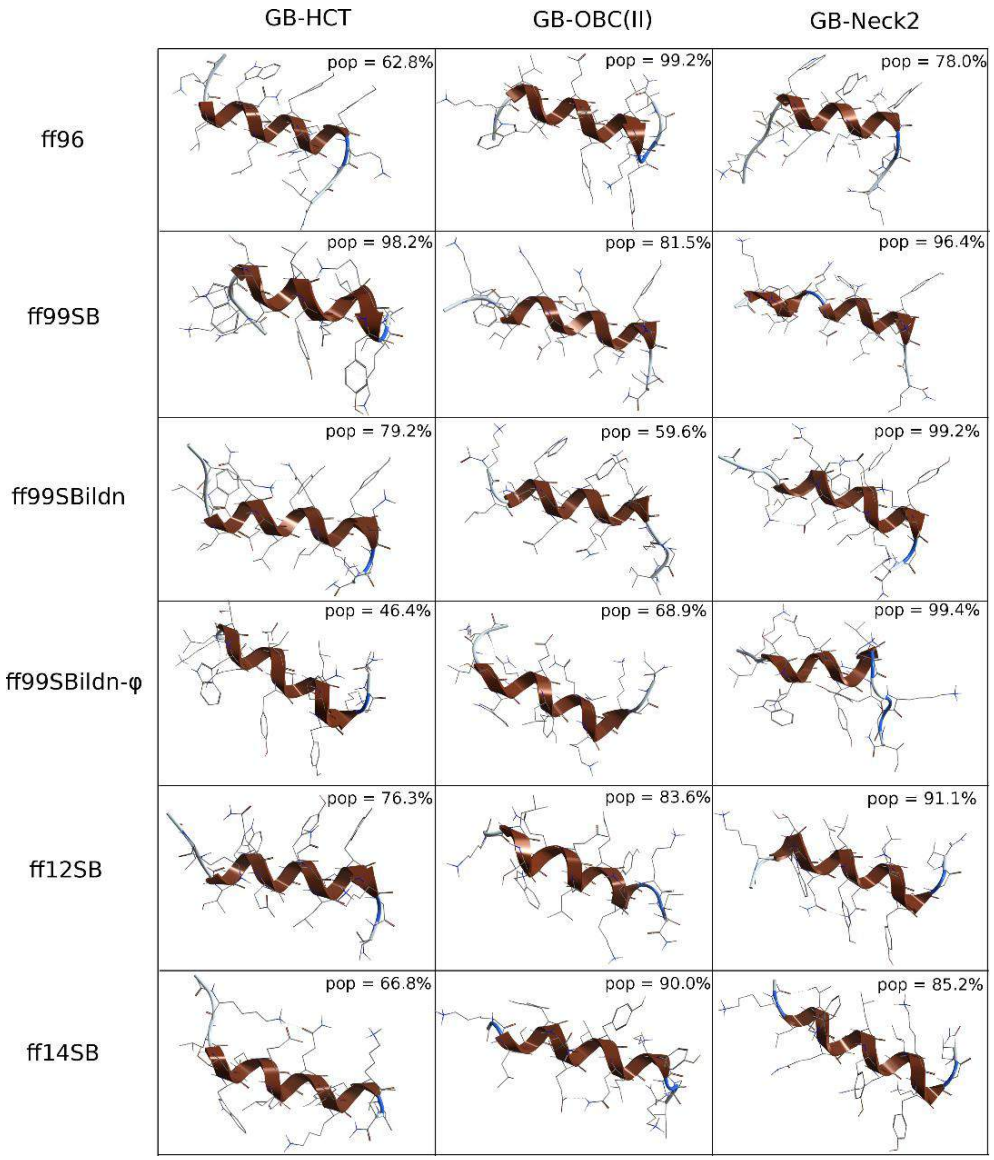

Figure 4.2. Representative structure and populated of the most population cluster from the 300.37 K trajectory extracted from REMD simulations of peptide **H1**.

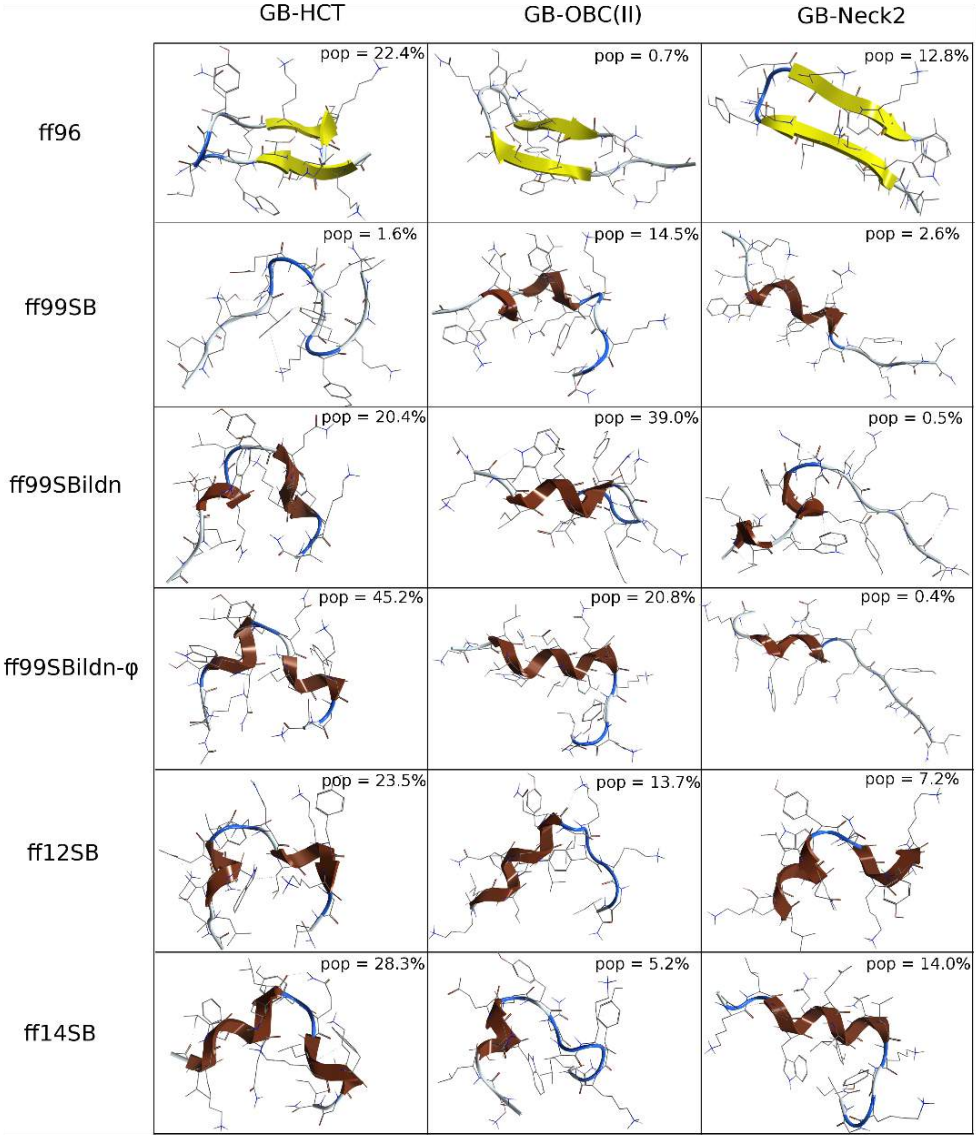

Figure 4.3. Representative structure and populated of the second cluster from the 300.37 K trajectory extracted from REMD simulations of peptide **H1**.

Furthermore, both cluster and DSSP analyses showed that the REMD simulations with ff96/GB-HCT and ff96/GB-Neck2 predicted a significant amount of β-hairpin (Figure 4.3 and Table 4.2), which is not consistent with experimental findings.[174]

Table 4.2. DSSP analysis of 300.37 K trajectory extracted from REMD simulations of peptide **H1**. Data are reported as averaged percentages.

Force field/implicit solvent model	Para	Anti	3-10	Alpha	Pi	Turn	Bend	other
ff96/GB-HCT	1.37	5.78	0.17	34.79	2.01	11.08	11.22	33.56
ff96/GB-OBC(II)	0.01	0.34	0.08	63.03	0.37	6.16	2.59	27.41
ff96/GB-Neck2	0.04	8.26	0.05	40.65	0.04	6.73	4.82	39.42
ff99SB/GB-HCT	0.30	0.16	7.38	32.56	0.49	26.06	6.84	26.21
ff99SB/GB-OBC(II)	0.01	0.07	6.17	38.50	0.28	20.30	6.39	28.28
ff99SB/GB-Neck2	0.00	0.03	5.26	39.82	0.22	18.46	5.77	30.44
ff99SBildn/GB-HCT	0.03	0.13	9.89	26.55	0.33	29.76	7.34	25.97
ff99SBildn/GB-OBC(II)	0.02	0.34	9.39	26.63	0.21	26.58	7.32	29.51
ff99SBildn/GB-Neck2	0.01	0.09	8.46	33.84	0.20	19.64	6.74	31.00
ff99SBildn-φ/GB-HCT	0.01	0.01	8.25	34.39	0.29	27.57	5.30	24.18
ff99SBildn-φ/GB-OBC(II)	0.01	0.02	7.01	40.96	0.06	21.59	5.17	25.17
ff99SBildn-φ/GB-Neck2	1.36	0.04	7.51	33.97	0.18	22.55	5.88	28.51
ff12SB/GB-HCT	0.01	0.00	4.68	52.18	0.14	17.74	2.52	22.73
ff12SB/GB-OBC(II)	0.01	0.00	1.52	66.39	0.00	12.33	1.14	18.61
ff12SB/GB-Neck2	0.00	0.00	2.43	63.82	0.03	11.84	1.29	20.59
ff42SB/GB-HCT	0.03	0.00	6.85	49.10	0.05	21.66	2.99	19.33
ff42SB/GB-OBC(II)	0.00	0.01	5.34	56.32	0.03	17.51	2.78	18.02
ff42SB/GB-Neck2	0.00	0.02	6.08	53.42	0.03	16.87	2.50	21.08

When considering peptide **H2**, which is shorter and contains the helix stabilizer α-aminoisobutyric acid (Aib),[184–186] ff96 fails in predicting the helical secondary structure, independently from the implicit solvent model. Indeed, in all cases the representative structures of the two most populated clusters showed a RMSD from the native-like structure (Figure 4.1) of 2.9 Å or more (Figures 4.4 and 4.5). These results were confirmed by both the DSSP and H-bond analyses: the former gave $h_{tot}\% < 10\%$ (Table 4.3) and the latter could not detect H-bonds with ff96/GB-Neck2, and only a weakly occupied Aib6→Ala2 H-bond with GB-HCT or GB-OBC(II) (Annex 4.B).

On the other hand, most of the other representative structures of the principal cluster well reproduced the crystallographic structure, although with relatively low pop% (about 40-50%; Figure 4.4), except for those resulting from the analysis of ff12SB/GB-OBC(II) and ff14SB/GB-HCT simulations. However, both DSSP and H-bonds analyses showed that ff12SB and ff14SB with any implicit solvent model overestimate the α-helical content at the expense of the 3_{10}-helix, while this happened at lower extent with the ff99SB series combined to GB-HCT and GB-Neck2 (Table 4.3 and Annex 4.B).

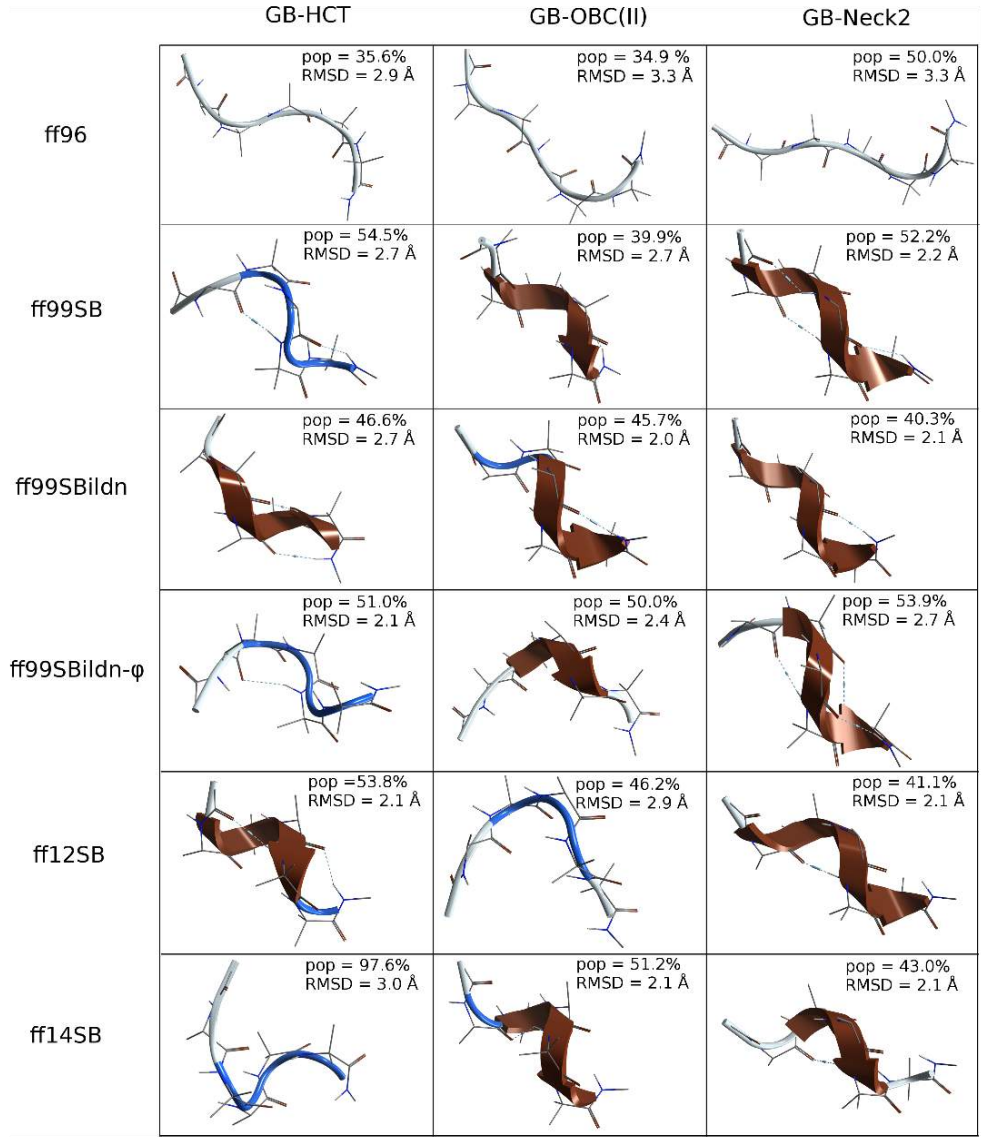

Figure 4.4. Representative structure and population of the most populated cluster from the 308.5 K trajectory extracted from REMD simulations of peptide **H2**.

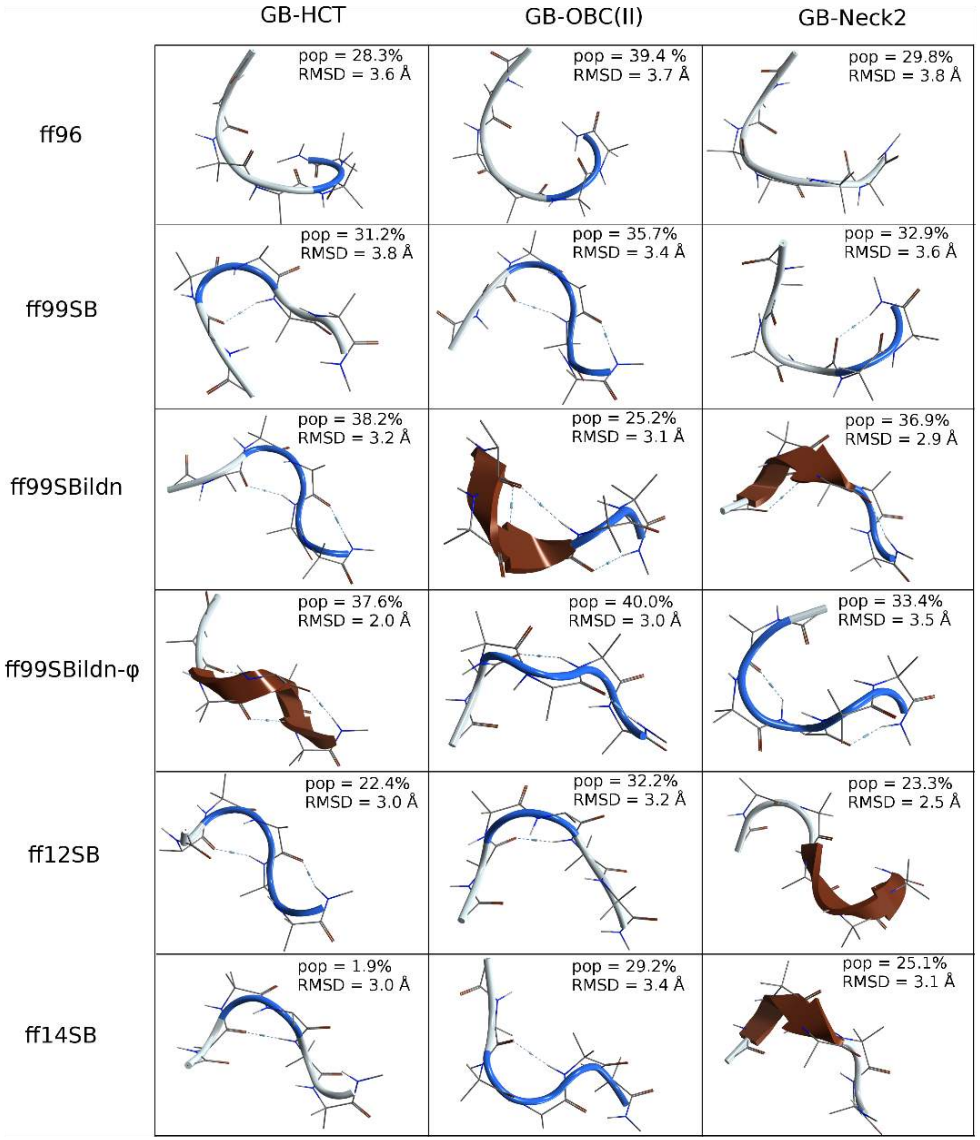

Figure 4.5. Representative structure and population of the second cluster from the 308.5 K trajectory extracted from REMD simulations of peptide **H2**.

Table 4.3. DSSP analysis of 308 K trajectory extracted from REMD simulations of peptide **H2**. Data are reported as averaged percentages.

Force field/implicit solvent model	Para	Anti	3-10	Alpha	Pi	Turn	Bend	other
ff96/GB-HCT	0.01	0.22	2.60	3.86	0.00	20.86	6.55	65.89
ff96/GB-OBC(II)	0.01	0.12	2.16	6.88	0.00	18.48	6.23	66.13
ff96/GB-Neck2	0.00	0.06	0.80	0.56	0.00	11.20	7.63	79.75
ff99SB/GB-HCT	0.00	0.00	32.42	6.11	0.00	38.11	2.14	21.21
ff99SB/GB-OBC(II)	0.00	0.00	33.91	5.53	0.00	37.57	2.23	20.75
ff99SB/GB-Neck2	0.00	0.00	35.97	3.39	0.00	34.15	2.78	23.71
ff99SBildn/GB-HCT	0.00	0.00	34.20	5.27	0.00	39.10	1.86	19.57
ff99SBildn/GB-OBC(II)	0.00	0.00	36.25	6.69	0.00	34.66	2.08	20.32
ff99SBildn/GB-Neck2	0.00	0.01	36.88	2.28	0.00	36.31	2.47	22.06
ff99SBildn-φ/GB-HCT	0.00	0.00	34.86	5.96	0.00	38.68	1.66	18.84
ff99SBildn-φ/GB-OBC(II)	0.00	0.00	36.00	6.79	0.00	38.15	1.49	17.57
ff99SBildn-φ/GB-Neck2	0.00	0.00	37.25	3.34	0.00	35.04	2.11	22.27
ff12SB/GB-HCT	0.00	0.00	22.87	20.85	0.00	31.52	1.08	23.68
ff12SB/GB-OBC(II)	0.00	0.00	23.63	17.68	0.00	32.79	1.26	24.64
ff12SB/GB-Neck2	0.00	0.00	27.70	8.57	0.00	32.35	1.79	29.59
ff42SB/GB-HCT	0.00	0.00	21.66	18.20	0.00	33.28	1.27	25.58
ff42SB/GB-OBC(II)	0.00	0.00	24.07	20.35	0.00	31.41	1.05	23.12
ff42SB/GB-Neck2	0.00	0.00	25.71	8.69	0.00	33.96	1.97	29.67

Therefore, the structure of medium-to-long natural peptides having a native helical geometry is well reproduced by all force field/GB model combinations used. Conversely, short helical peptides containing non natural amino acids are well simulated by using any of the ff99SB/ildn/ildn-φ force fields coupled with GB-OBC(II) or GB-Neck2 models, since the above combinations provide a significant amount of native-like conformations and, at the same time, discriminate well between α- and 3_{10}-helix, in line with previously reported results.[73,93,187]

β-Hairpins Peptides. Because of the helical propensities of modern force fields[140,141,188,189] and problems in correctly estimating salt bridges given by the implicit solvent models,[137,150,151,190,191] the prediction of β-hairpins can be more challenging than that of helices. Therefore, it is not surprising that most of the REMD simulations performed on peptide **B1** failed in predicting the native-like β-hairpin conformation,[176] as observed from cluster (Figure 4.6), DSSP (Table 4.4) and H-bond (Annex 4.C) analyses.

In detail, DSSP analysis showed that the best, although far from the ideal, results were obtained with the ff96/GB-Neck2 simulation, with an anti-parallel β-sheet content of 12.8% and an irrelevant h_{tot}% (< 1%; Table 4.4). Moreover, none of the H-bonds present in the native-like structure were detected by the H-bond analysis, while those actually found where characterized by low occupancies (Annex 4.C). An RMSD of 3.6 Å from the native conformation was found for the representative structure of the most populated cluster, which is the lowest found among all the simulations of this peptide (Figure 4.6) and lower than that reported in the literature for similar studies.[137]

Acceptable results were obtained for ff96/GB-HCT combination, where the second most populated cluster had a relevant pop% (39.5%) and a representative structure with a RMSD from the native-like peptide of 2.7 Å (Figure 4.7). However, DSSP analysis gave an average anti-parallel β-sheet content of only 9.7% and a high α-helical content (Table 4.4), which is consistent with results from H-bond analysis (Annex 4.C).

All the other force field/GB model combinations led to worse results, favoring the $\alpha/3_{10}$-helix or disordered conformations. The bias toward the helix conformation was particularly strong for the simulation with ff14SB coupled to any of the GB models (Table 4.4), suggesting that the use of this force field with implicit solvation should be avoided when simulating the folding of β-hairpin peptides.

Table 4.4. DSSP analysis of 300.37 K trajectory extracted from REMD simulations of peptide **B1**. Data are reported as averaged percentages.

Force field/implicit solvent model	Para	Anti	3-10	Alpha	Pi	Turn	Bend	other
ff96/GB-HCT	0.59	9.68	0.15	23.19	0.52	8.78	13.43	43.66
ff96/GB-OBC(II)	0.55	0.75	0.13	25.58	0.05	7.70	7.99	57.25
ff96/GB-Neck2	0.01	12.75	0.08	0.33	0.00	10.78	10.77	65.28
ff99SB/GB-HCT	0.00	0.37	12.90	15.44	0.07	25.38	13.60	32.24
ff99SB/GB-OBC(II)	0.14	4.01	11.27	12.77	0.02	19.68	12.12	40.00
ff99SB/GB-Neck2	0.02	0.01	12.38	20.34	0.04	21.46	8.50	37.27
ff99SBildn/GB-HCT	0.02	2.31	10.57	8.43	0.05	23.67	17.00	37.95
ff99SBildn/GB-OBC(II)	0.05	0.06	8.53	10.97	0.02	21.73	12.40	46.24
ff99SBildn/GB-Neck2	0.06	0.18	12.48	11.08	0.02	22.64	9.73	43.82
ff99SBildn-φ/GB-HCT	0.00	0.05	13.96	12.68	0.03	25.26	14.95	33.08
ff99SBildn-φ/GB-OBC(II)	0.01	0.00	13.00	13.61	0.02	20.58	11.94	40.84
ff99SBildn-φ/GB-Neck2	0.00	0.13	14.16	16.07	0.03	22.04	8.75	38.83
ff12SB/GB-HCT	0.02	0.23	14.34	14.00	0.08	28.84	9.33	33.15
ff12SB/GB-OBC(II)	0.00	0.04	15.33	13.67	0.09	24.09	7.98	38.80
ff12SB/GB-Neck2	0.01	0.01	17.38	15.22	0.07	22.13	8.07	37.11
Ff14SB/GB-HCT	0.00	0.01	5.13	52.67	0.01	10.97	5.28	25.92
Ff14SB/GB-OBC(II)	0.01	0.00	4.89	45.76	0.00	8.00	4.60	36.75
Ff14SB/GB-Neck2	0.00	0.00	1.42	60.80	0.00	5.67	2.43	29.68

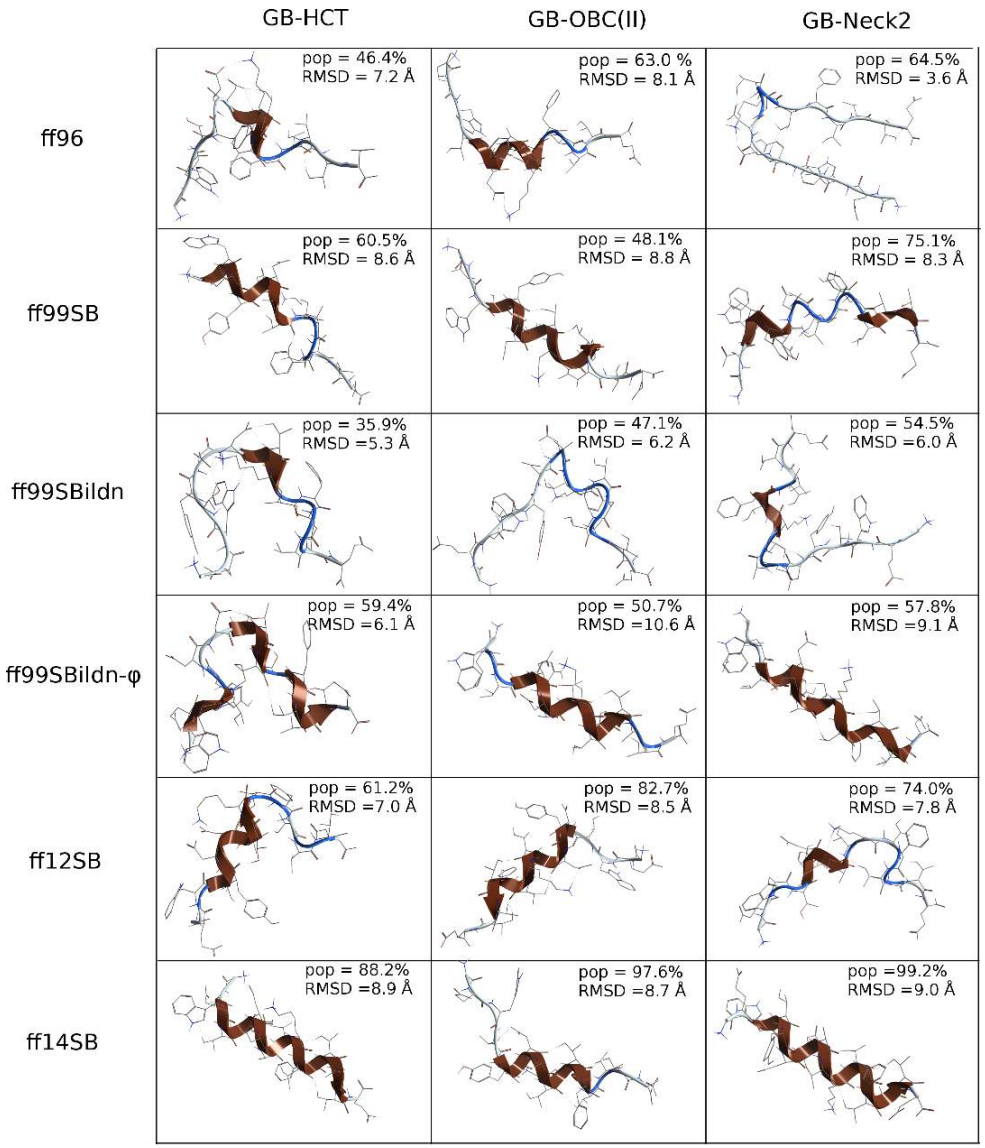

Figure 4.6. Representative structure and populated of the most populated cluster from the 300.37 K trajectory extracted from REMD simulations of peptide **B1**.

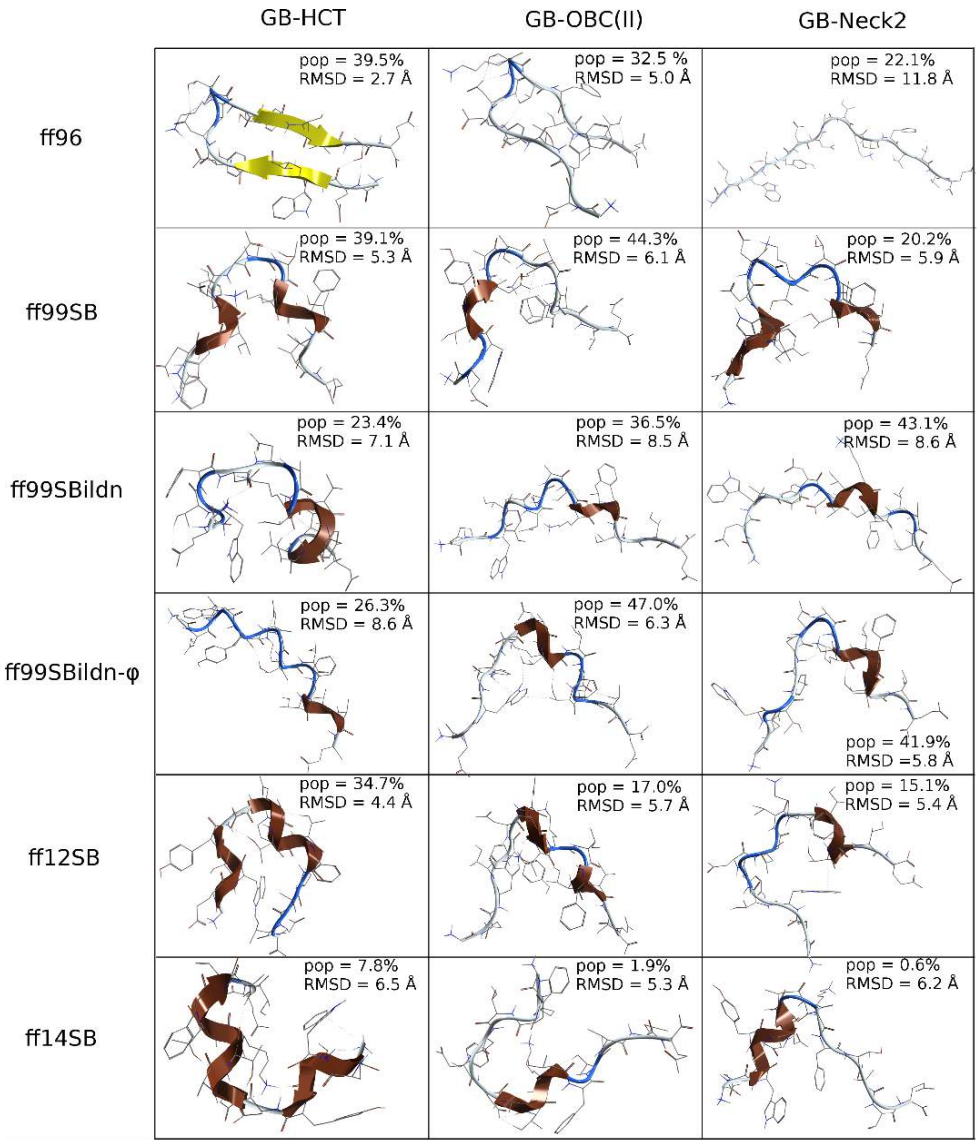

Figure 4.7. Representative structure and populated of the second cluster from the 300.37 K trajectory extracted from REMD simulations of peptide **B1**

Our results apparently disagree with those obtained by Shell and coworkers,[137] who found that the ff96/GB-OBC(II) combination was able to reproduce the native structure of **B1**. However, their REMD simulations were run by using the native structure as the starting conformation and a 10 ns length for each replica, with analyses performed on the last ns. Furthermore, NMR studies in water showed that the hairpin population of **B1** was about 40%.[176] Moreover, it has been reported that continuum solvent models favors non-native **B1** structures, since they push the charged side chains to form salt bridges, instead of being fully solvated, thus overwhelming the hydrophobic interactions needed to form the β-hairpin.[137,151] In detail, the salt bridge between Lys10 and Asp6 brings the latter residue, which is near to the β-hairpin turn, in close contact to Lys10, causing the expulsion of Tyr5 and Phe12 side chains from the hydrophobic core.[151] An H-bond between Asp6 and Lys10 with a significant occupancy was found in all the simulations except those with GB-Neck2 (Annex 4.C), suggesting that this model allows a better description of ion pairing. However, a force field-dependent effect altering the salt-bridge populations, as already hypothesized,[143] or introducing a conformational bias toward helices cannot be excluded. Indeed, ff14SB/GB-Neck2 model gave no salt bridges, but still predicted a helical conformation (Table 4.4 and Annex 4.C). We also studied the folding behavior of peptide **B2**, which has been proved to be a stable monomeric β-hairpin by NMR experiments in water[177]. In this case also, most of the force field/GB model combinations failed in predicting the native structure. Indeed, except for ff96 coupled to GB-HCT or GB-OBC(II), the representative structures of the principal cluster (pop% > 50%) showed a RMSD from the native structure of about 5 Å or more (Figure 4.8). These results were confirmed by DSSP and H-bond analyses (Table 4.5 and Annex 4.D), which evidenced the presence of a reasonable amount of average anti-parallel β-sheet content and a negligible helical content for ff96/GB-HCT or GB-OBC(II), while with GB-Neck2 only disordered conformations were found. For all the other simulations, it can still be noticed a bias toward the helical conformation (h_{tot}% > 20%), with a maximum observed for ff14SB with any GB model (Table 4.5). However, H-bond analysis evidenced $i+3 \rightarrow i$ or $i+4 \rightarrow i$ H-bonds with occupancies < 30%, showing that the preference for the helical secondary structure, although present (Annex 4.D), is less marked for this system compared to **B1**, and probably limited to a force field effect. Indeed, no persistent ionic interactions were observed in **B2** simulations except those with ff12SB, ff14SB coupled to any GB model and, to a minor extent, the one with ff96/GB-HCT (Annex 4.D), where a salt bridge between Lys8 and Glu5 was sampled. However, while the two former methods predicted a high helical content, the latter ended in an acceptable native-like β-hairpin conformation.

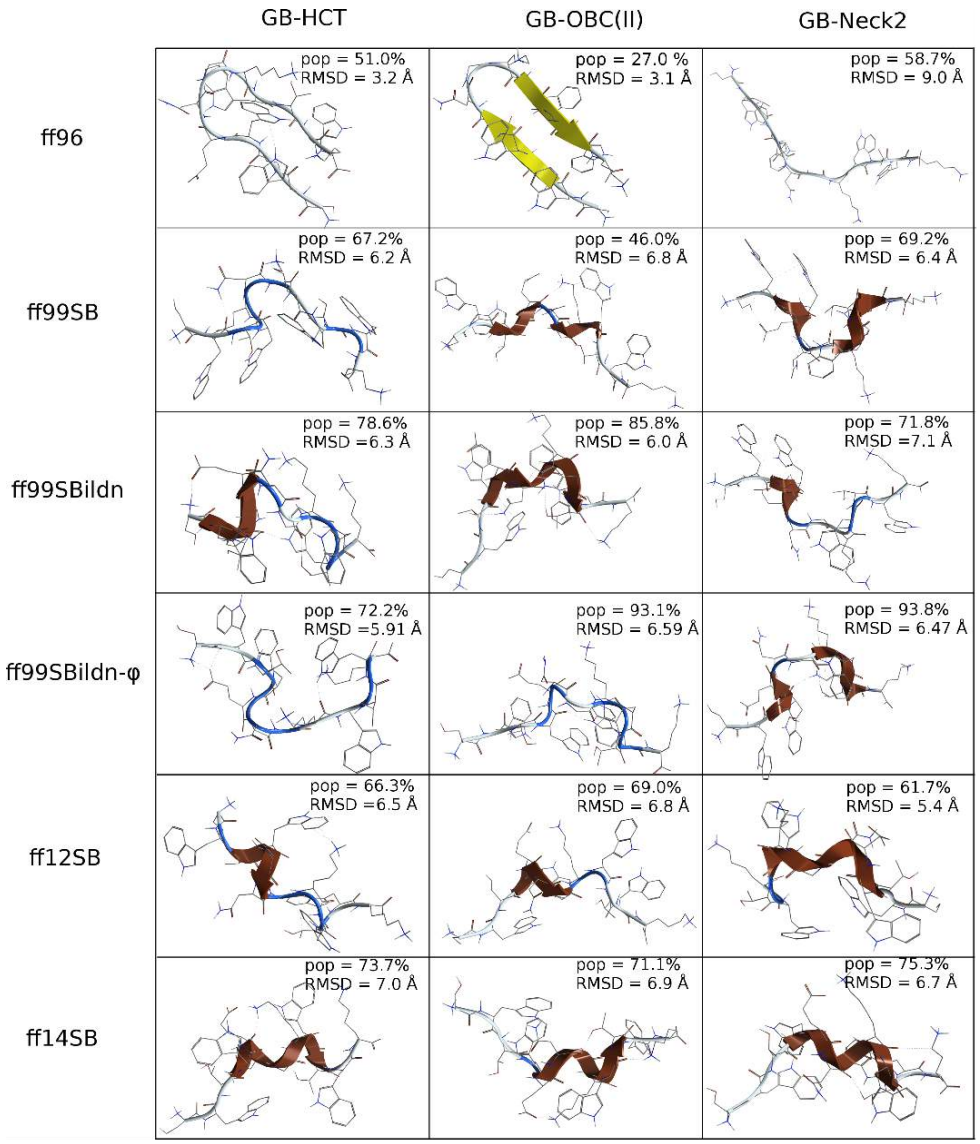

Figure 4.8. Representative structure and populated of the most populated cluster from the 300.37 K trajectory extracted from REMD simulations of peptide **B2**.

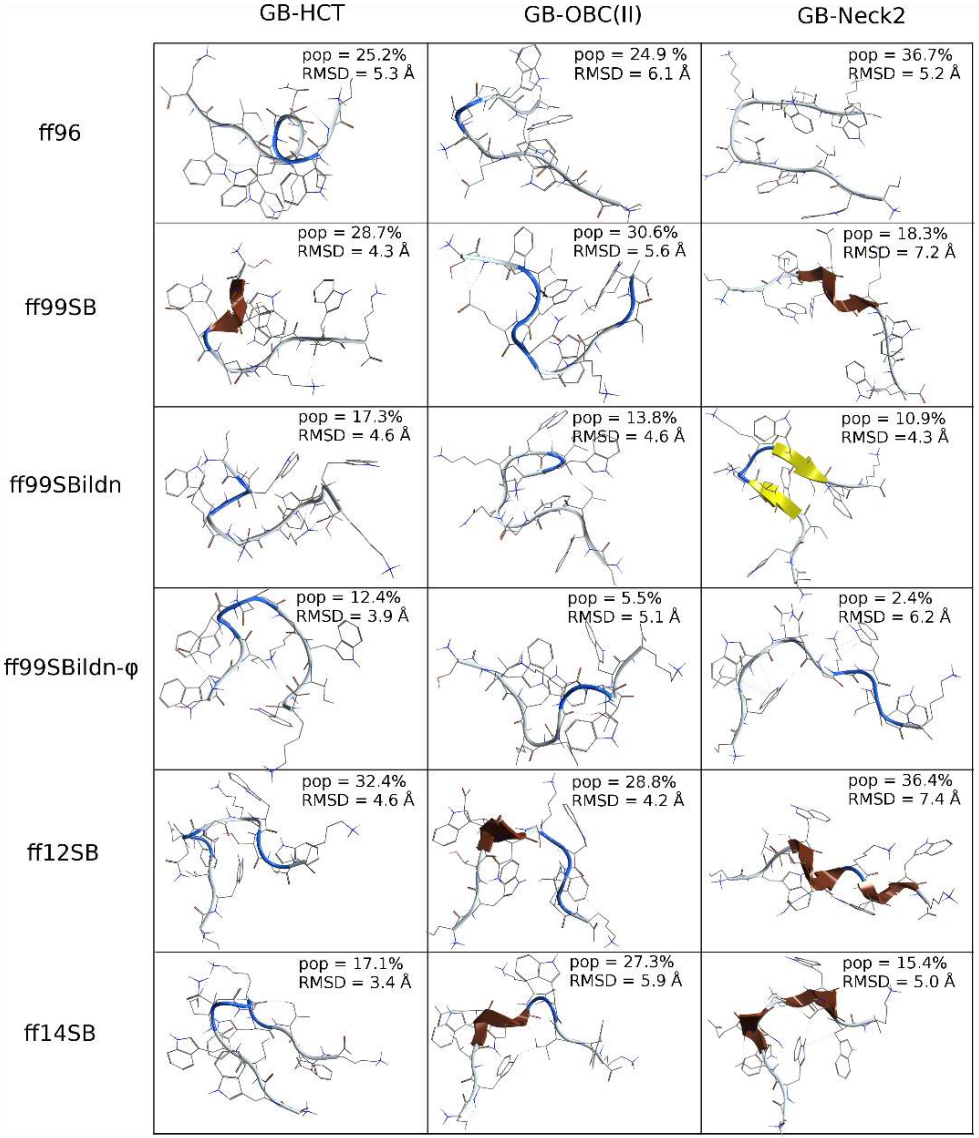

Figure 4.9. Representative structure and populated of the second cluster from the 300.37 K trajectory extracted from REMD simulations of peptide **B2**

Table 4.5. DSSP analysis of 300.37 K trajectory extracted from REMD simulations of peptide **B2**. Data are reported as averaged percentages.

Force field/implicit solvent model	Para	Anti	3-10	Alpha	Pi	Turn	Bend	other
ff96/GB-HCT	1.96	14.08	0.12	4.00	0.22	14.42	17.44	47.76
ff96/GB-OBC(II)	1.83	10.35	0.11	1.49	0.04	7.40	15.67	63.13
ff96/GB-Neck2	0.53	3.54	0.06	0.47	0.00	3.21	12.26	79.93
ff99SB/GB-HCT	0.22	0.36	7.66	13.18	0.14	25.39	13.98	39.08
ff99SB/GB-OBC(II)	0.18	0.65	9.64	4.26	0.01	19.80	15.90	49.56
ff99SB/GB-Neck2	0.44	0.40	9.80	8.13	0.01	18.52	13.60	49.11
ff99SBildn/GB-HCT	0.05	0.41	8.37	15.39	0.16	25.49	12.04	38.09
ff99SBildn/GB-OBC(II)	0.07	1.19	9.65	7.43	0.05	18.17	17.57	45.87
ff99SBildn/GB-Neck2	0.24	1.43	10.03	6.97	0.02	19.94	12.28	49.08
ff99SBildn-φ/GB-HCT	0.06	0.43	10.95	13.90	0.13	26.89	10.97	36.68
ff99SBildn-φ/GB-OBC(II)	0.00	0.15	14.46	7.21	0.03	20.17	11.70	46.28
ff99SBildn-φ/GB-Neck2	0.11	0.29	13.83	9.32	0.02	20.21	11.15	45.06
ff12SB/GB-HCT	0.03	0.03	0.32	13.24	15.79	0.02	24.12	46.43
ff12SB/GB-OBC(II)	0.02	0.04	14.72	7.68	0.01	20.68	8.16	48.69
ff12SB/GB-Neck2	0.12	0.60	16.34	6.61	0.02	18.76	8.99	48.57
ff42SB/GB-HCT	0.02	0.80	14.90	20.48	0.04	20.87	5.62	37.28
ff42SB/GB-OBC(II)	0.04	0.06	18.07	11.15	0.01	16.43	7.43	46.82
ff42SB/GB-Neck2	0.01	0.03	17.01	16.87	0.01	13.03	6.30	46.75

As an additional example of a β-hairpin, we performed REMD simulations on peptide **B3**, which is the N-terminal sequence of ubiquitin.[178] Consistently with what observed for **B2** and, to a minor extent, **B1**, the best results were obtained with ff96 force field coupled with GB-HCT, although the other GB models also gave acceptable performances. In detail, cluster analysis performed on the ff96/GB-HCT simulation resulted in a principal cluster with an excellent pop% (92.7%) and a representative structure which deviates from the native structure of only 0.95 Å (Figure 4.10). Similar, although slightly worse, results were obtained with ff96 and either GB-OBC(II) or GB-Neck2. Coherently, DSSP analysis showed that the simulations performed with ff96 had an antiparallel β-sheet content of about 20-30%, with the highest and lowest percentages obtained for GB-HCT and GB-OBC(II), respectively, and an irrelevant h_{tot}% (< 2%) (Table 4.6). H-bond analysis of ff96/GB-HCT and GB-OBC(II) trajectories evidenced the presence of 5 out of the 6 native H-bonds involving the peptide backbone, although with poor occupancies, while none of the native H-bonds was found with GB-Neck2 (Annex 4.E). However, it has to be underscored that helical H-bonds were poorly sampled as well, while some H-bonds, principally involving Leu14 and Phe3 or Lys5 and Ile12, were identified, particularly by using ff96/GB-Neck2 (Annex 4.E). This is indicative of the presence of β-hairpin-like conformations with the turn between the two β-strands being shifted toward the N-terminus compared to the native structure (Figure 4.12).

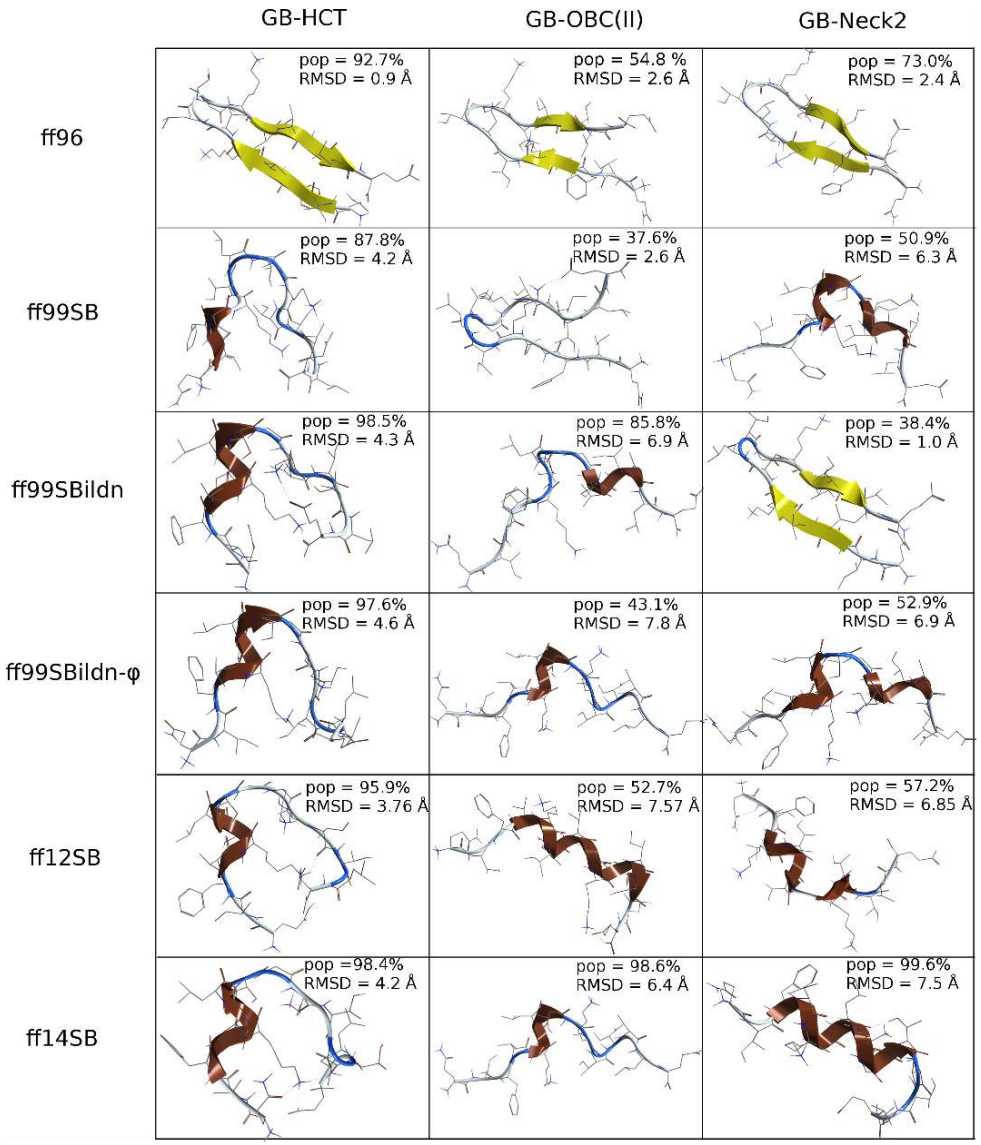

Figure 4.10. Representative structure and populated of the most populated cluster from the 300.37 K trajectory extracted from REMD simulations of peptide **B3**.

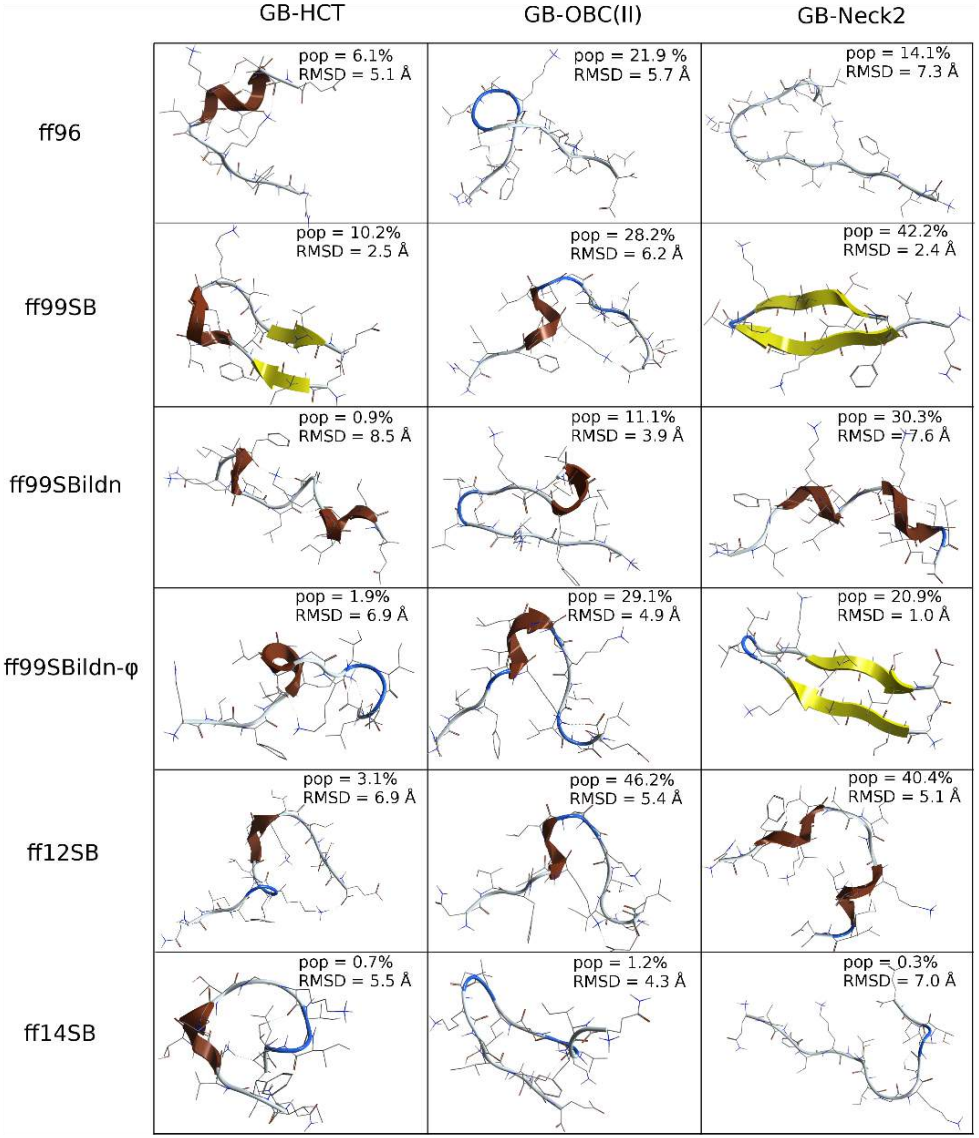

Figure 4.11. Representative structure and populated of the second cluster from the 300.37 K trajectory extracted from REMD simulations of peptide **B3.**

Contrary to what observed for peptides **B1** and **B2**, ff99SBildn/GB-Neck2 and ff99SB/GB-Neck2 were also able to reasonably predict a native-like conformation for peptide **B3**. Indeed, the principal cluster (pop% = 38.4%) obtained by the former method and the second cluster (pop% = 42.2%) obtained by the latter had a representative structure with rather low RMSDs from the native structure (1.01 and 2.45 Å, respectively; Figures 4.10 and 4.11). Furthermore, these force field/GB model combinations gave an average antiparallel β-sheet content of about 20%, although a certain amount of helix was at the same time found (h_{tot}% > 10%; Table S13), coherently with results from H-bond analysis (Annex 4.E).

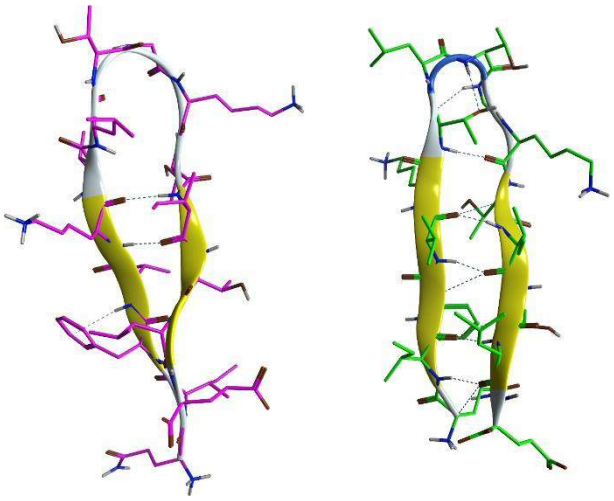

Figure 4.12. Representative structure of the top cluster of the 300.37 K ff96/GB-Neck2 trajectory of peptide **B3** (magenta) and native structure of peptide **B3** (green).

Table 4.6. DSSP analysis of 300.37 K trajectory extracted from REMD simulations of peptide **B3**. Data are reported as averaged percentages.

Force field/implicit solvent model	Para	Anti	3-10	Alpha	Pi	Turn	Bend	other
ff96/GB-HCT	1.01	36.86	0.04	1.98	0.30	7.59	16.73	35.49
ff96/GB-OBC(II)	0.18	20.64	0.03	0.85	0.04	6.95	19.12	52.18
ff96/GB-Neck2	0.17	31.43	0.02	0.01	0.00	2.74	15.96	49.68
ff99SB/GB-HCT	0.01	4.91	6.19	16.71	0.07	26.31	9.19	36.61
ff99SB/GB-OBC(II)	0.25	11.54	3.38	8.06	0.04	21.15	12.11	43.46
ff99SB/GB-Neck2	0.04	24.79	5.76	8.41	0.07	17.34	6.49	37.09
ff99SBildn/GB-HCT	0.06	0.49	8.84	15.43	0.05	27.35	9.20	38.58
ff99SBildn/GB-OBC(II)	0.04	2.85	4.71	12.12	0.16	21.25	10.75	48.11
ff99SBildn/GB-Neck2	0.11	20.55	6.21	6.38	0.04	16.59	8.70	41.42
ff99SBildn-φ/GB-HCT	0.01	1.71	9.79	17.70	0.01	24.64	7.65	38.49
ff99SBildn-φ/GB-OBC(II)	0.38	1.88	5.40	11.55	0.09	22.12	10.25	48.33
ff99SBildn-φ/GB-Neck2	0.38	9.26	10.68	12.89	0.04	17.13	8.14	41.48
ff12SB/GB-HCT	0.01	0.10	11.12	19.09	0.08	20.51	9.23	39.86
ff12SB/GB-OBC(II)	0.71	1.00	11.44	13.33	0.05	21.45	9.36	42.67
ff12SB/GB-Neck2	1.37	0.09	16.62	12.16	0.08	20.28	9.45	39.96
ff42SB/GB-HCT	0.00	0.12	8.21	30.67	0.00	19.71	4.72	36.57
ff42SB/GB-OBC(II)	0.02	0.18	6.73	33.89	0.02	14.02	5.27	39.86
ff42SB/GB-Neck2	0.04	0.01	5.23	53.78	0.00	9.64	2.56	28.73

Except for ff99SB/GB-OBC(II), which also behaved fairly, the other combinations showed a preference for the helical conformation, as evidenced by cluster, DSSP and H-bond analyses. This

might be due to the combined effect of the force field biases and salt bridges overestimation by the implicit solvent model, with ff14SB being the most helical and GB-HCT the most salt bridge stabilizer. Indeed, salt bridges between Lys5 or Lys10 and Glu15 were sampled in all simulations performed with GB-HCT, except those based on the ff96 force field (Annex 4.E), thus leading to misfolded conformations (Figure 4.13).

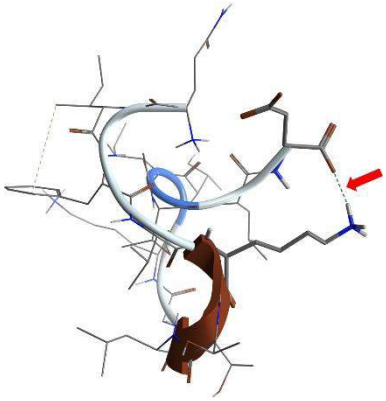

Figure 4.13. Misfolded conformation of peptide **B3** extracted from the 300.37 K trajectory performed with ff14SB and GB-HCT. The salt bridge is highlighted with the red arrow.

At the light of this, we can conclude that the choice of a proper combination of force field and solvent model for the prediction of β-hairpins is not trivial and strictly dependent on the system to be simulated. Indeed, ff96 force field always gave the best results, but with different GB models (GB-Neck2, GB-HCT or -OBC(II) and GB-HCT for B1, B2 and B3, respectively). Moreover, while ff12SB and ff14SB are clearly not suited for the simulation of β-hairpin peptides in implicit solvent, ff99SB or ff99SBildn might represent an alternative to ff96, especially if combined with GB-Neck2.

Intrinsically Disordered Peptides. As previously underscored, the discrimination of disordered from well-structured peptide states is of fundamental interest, because of the role of IDPs in biological events.[153,154,163–166] Moreover, testing the force field/GB model combinations on IDPs allows a better evaluation of their eventual biases toward a particular secondary structure.

Indeed, when considering **ID1**, ff96/GB-HCT, GB-OBC(II) and, to minor extent, GB-Neck2 combinations favored a β-hairpin secondary structure. Cluster analysis performed on the corresponding 300.37 K trajectories gave a highly populated top cluster whose representative structure is a β-hairpin-like geometry (Figure 4.14). Moreover, DSSP analysis showed a high amount of β-sheet content, only marginally compensated by other secondary structures (Table 4.7) and the radius of gyration profiles showed peaks suggesting the presence of compact structures (Figure 4.16).

Although less intense, the same peaks were observed for ff12SB and ff14SB, which showed a helical bias in this case also. Indeed, the representative structure of the most populated cluster (pop% > 70%) obtained from the analysis of the related trajectories (Figure 4.14) was helical. DSSP analysis also gave levels of helical propensity significantly higher than the average percentages of other structures (h_{tot}% > 40%; Table 4.7).

Similar observations can be done for ff99SB and ff99SBildn-φ coupled with GB-HCT or GB-OBC(II), and for ff99SBildn coupled with GB-OBC(II), although h_{tot}% was lower than that observed for ff12SB and ff14SB force fields (Table 4.7) and the representative structure of the main clusters were not perfectly helical (Figure 4.14). Conversely, ff99SB/GB-Neck2 and ff99SBildn/GB-HCT or GB-Neck2 gave a representative structure of the most populated cluster which was helical only at the C-terminus, while a β-hairpin was obtained as the representative conformation of the second cluster (Figure 4.15), in agreement with the average secondary structure amount obtained by DSSP analysis (Table 4.7). The ff99SBildn-φ/GB-Neck2 simulation gave similar results, although a geometry with a high helical content was obtained as the representative structure of the principal cluster (Figure 4.14). Moreover, H-bond analysis found H-bonds corresponding to both turn- and β-sheet-like conformations with moderately low occupancies (Annex 4.F), thus explaining the broader distribution of the radius of gyrations profiles (Figure 4.16).

Therefore, although a trajectory without a detectable amount of defined secondary structures was never obtained for **ID1**, the ff99SB series of force fields provided an acceptable description of a disordered conformation. In particular, when using the GB-Neck2 model, the trajectory analyses showed a similar amount of helical and β-hairpin content, which can be interpreted as a warning of structural instability and a suggestion that the system under study is an IDP. Conversely, ff96, ff12SB and ff14SB combined to any GB model not seem to be suited to simulate unstructured peptides.

The analyses performed on **ID2** and **ID3** trajectories gave similar results, although some differences need to be underlined. First of all, the ff96/GB-OBC(II) combination unexpectedly turned out to have a helical preference, very evident for **ID2** (Figures 4.17 and 4.18, Table 4.8) and weak for **ID3** (Figures 4.19 and 4.10, Table 4.9).

On the contrary, ff96/GB-Neck2 was the best combination in predicting the disordered conformation of both **ID2** and **ID3**, as showed by DSSP analysis, where no preferential secondary structure was found, by the radius of gyration profile, which had a rather broad distribution (Figure 4.16), and by the absence of persistent H-bonds (Annexes 4.G and 4.H). The ff99SB, ff99SBildn and ff99SBildn-φ force fields coupled with GB-Neck2 also represent an acceptable choice when simulating IDPs, although a small bias toward the helical structure was observed.

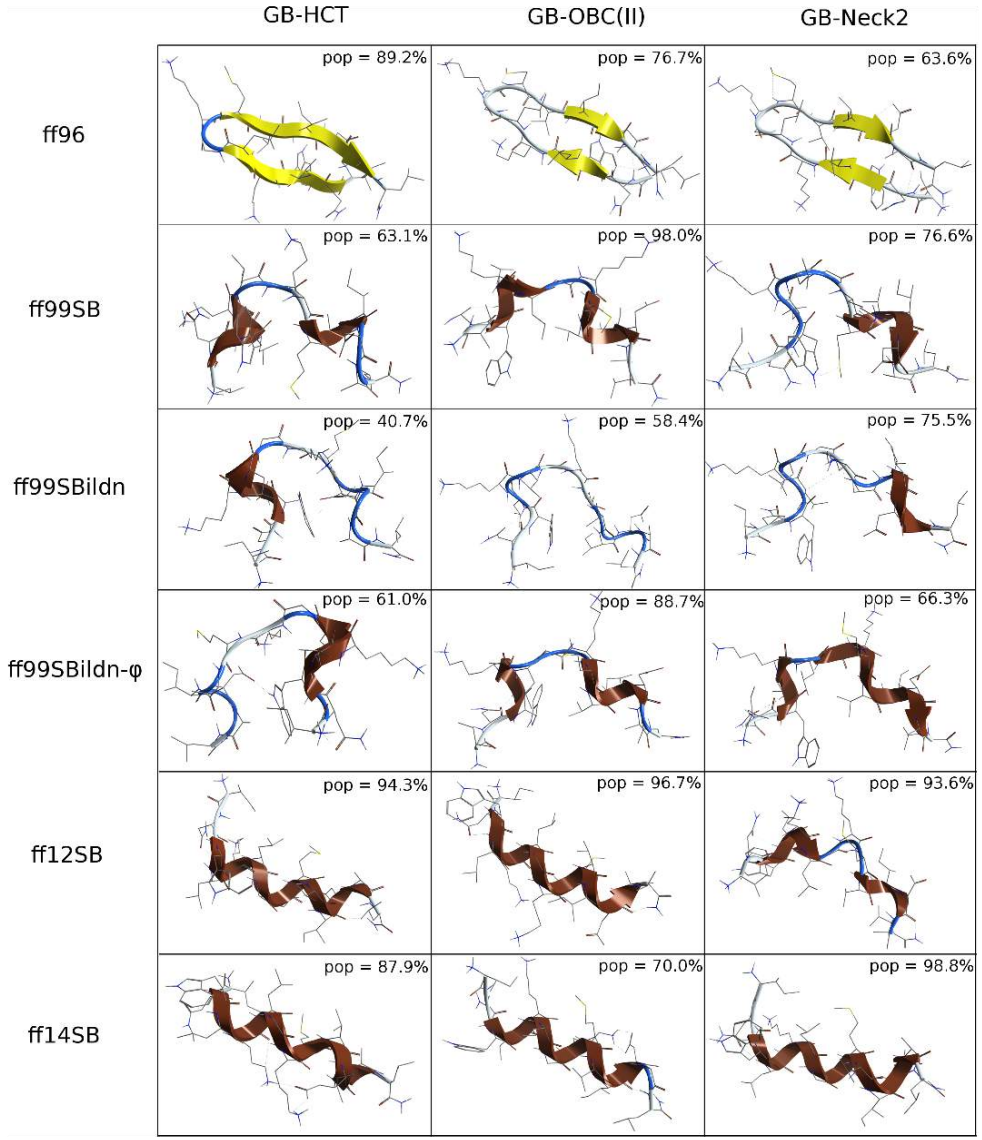

Figure 4.14. Representative structure and populated of the most populated cluster from the 300.37 K trajectory extracted from REMD simulations of peptide **ID1**.

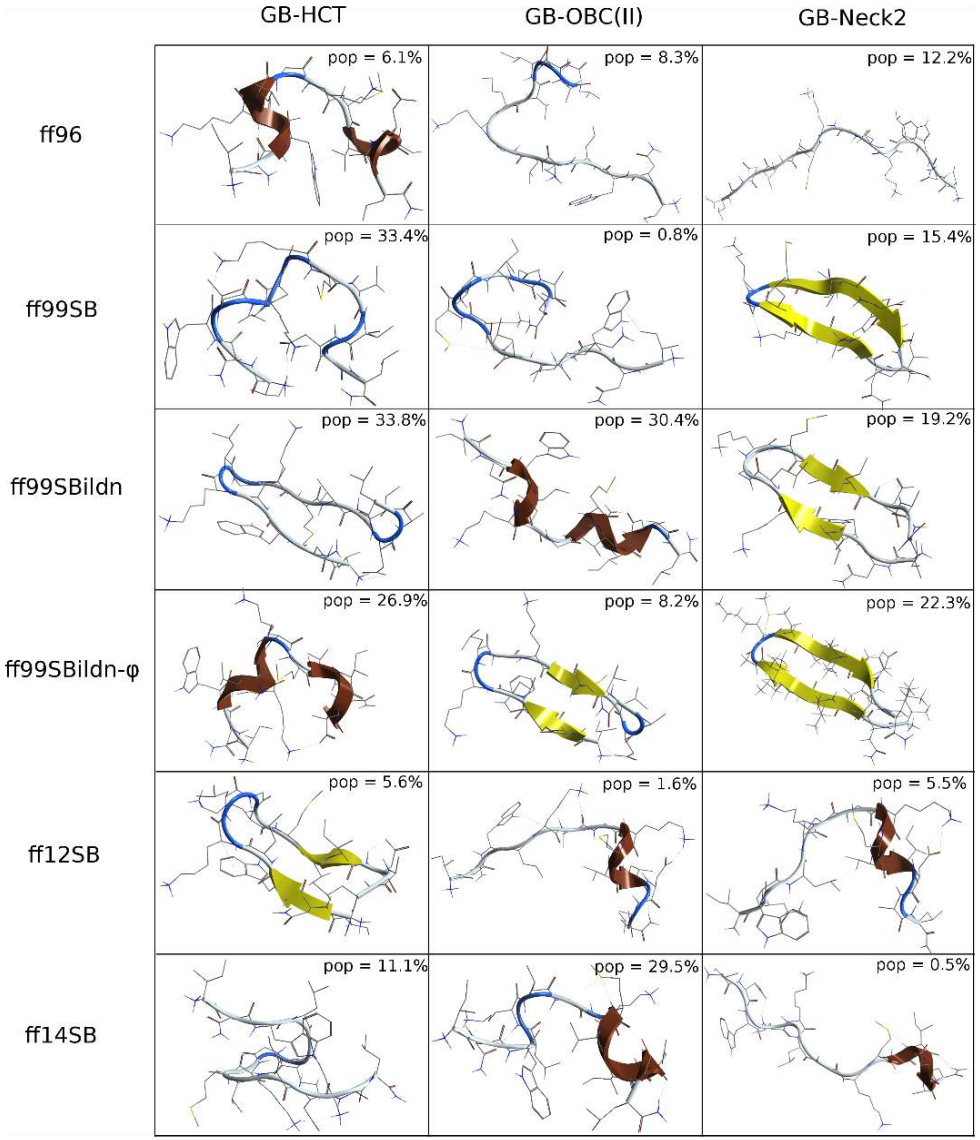

Figure 4.15. Representative structure and populated of the second cluster from the 300.37 K trajectory extracted from REMD simulations of peptide **ID1**

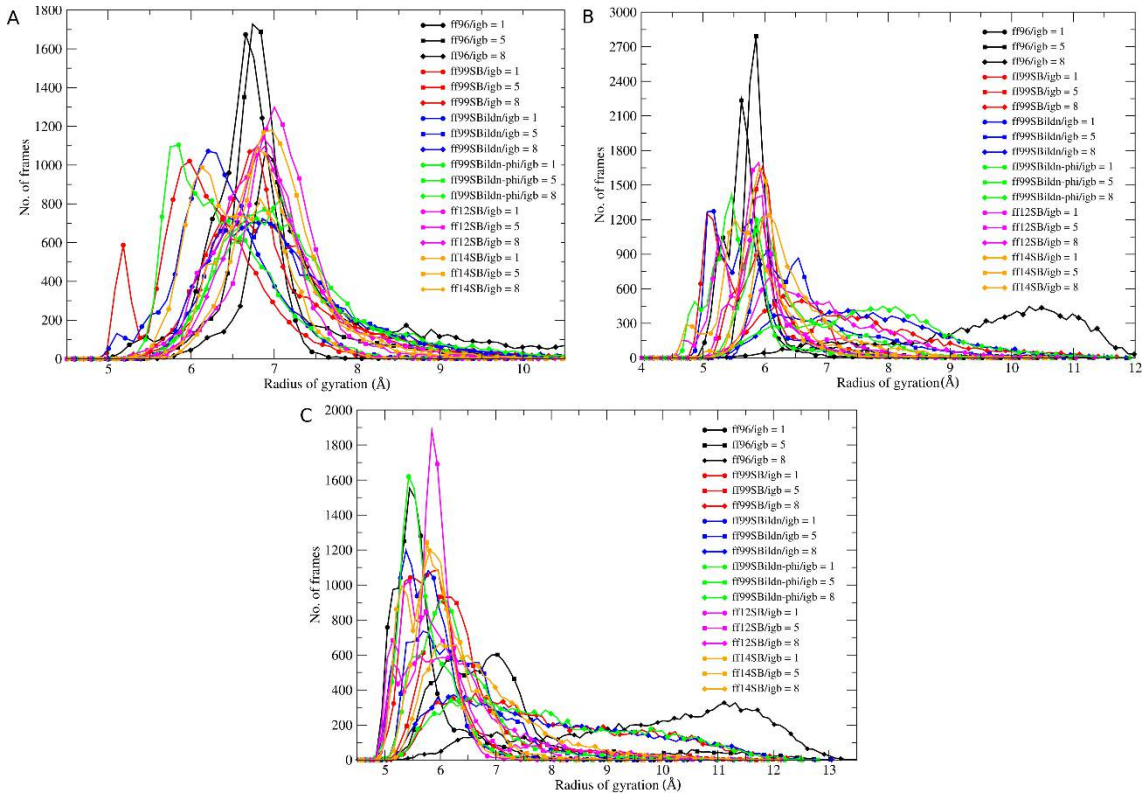

Figure 4.16. Frequency of radii if gyrations for the 300.37 K trajectories extracted from the REMD simulations of A) **ID1**, B) **ID2**, and C) **ID3**.

Table 4.7. DSSP analysis of 300.37 K trajectory extracted from REMD simulations of peptide **ID1**. Data are reported as averaged percentages.

Force field/implicit solvent model	Para	Anti	3-10	Alpha	Pi	Turn	Bend	other
ff96/GB-HCT	0.42	43.05	0.05	1.11	0.03	11.24	13.61	30.49
ff96/GB-OBC(II)	0.67	35.28	0.06	2.46	0.30	7.65	13.76	39.82
ff96/GB-Neck2	0.73	26.89	0.10	1.45	0.01	8.42	12.12	50.28
ff99SB/GB-HCT	1.18	0.63	6.34	17.99	0.20	30.36	10.25	33.04
ff99SB/GB-OBC(II)	0.12	0.17	9.77	24.33	0.07	22.87	7.63	35.04
ff99SB/GB-Neck2	0.11	10.78	8.36	16.91	0.07	20.14	7.68	35.95
ff99SBildn/GB-HCT	0.42	11.59	5.85	9.42	0.07	27.39	10.44	34.82
ff99SBildn/GB-OBC(II)	0.68	1.93	10.04	12.02	0.09	23.67	11.10	40.46
ff99SBildn/GB-Neck2	1.60	5.62	9.76	9.84	0.08	23.48	9.04	40.57
ff99SBildn-φ/GB-HCT	0.72	1.02	9.55	13.15	0.14	30.67	10.73	34.03
ff99SBildn-φ/GB-OBC(II)	0.52	2.27	11.39	17.04	0.03	24.15	7.99	36.61
ff99SBildn-φ/GB-Neck2	0.07	11.39	8.37	8.60	0.03	19.83	10.23	41.48
ff12SB/GB-HCT	0.05	1.68	6.26	37.97	0.16	23.04	4.34	26.50
ff12SB/GB-OBC(II)	0.01	0.01	7.10	46.67	0.04	16.32	3.20	26.63
ff12SB/GB-Neck2	0.01	0.09	9.65	35.31	0.05	18.42	4.99	31.47
ff42SB/GB-HCT	0.05	0.37	6.97	30.77	0.20	22.70	7.09	31.86
ff42SB/GB-OBC(II)	0.00	0.01	7.33	43.28	0.06	16.63	3.96	28.72
ff42SB/GB-Neck2	0.03	0.03	10.28	37.10	0.08	16.96	4.58	30.94

Table 4.8. DSSP analysis of 300.37 K trajectory extracted from REMD simulations of peptide **ID2**. Data are reported as averaged percentages.

Force field/implicit solvent model	Para	Anti	3-10	Alpha	Pi	Turn	Bend	other
ff96/GB-HCT	0.05	18.77	0.42	6.40	0.03	9.03	23.63	41.67
ff96/GB-OBC(II)	0.00	0.28	0.13	43.13	0.00	2.28	4.43	49.75
ff96/GB-Neck2	0.00	1.13	0.21	0.59	0.00	1.34	11.18	85.56
ff99SB/GB-HCT	0.42	1.64	8.35	7.98	0.00	23.49	17.50	40.62
ff99SB/GB-OBC(II)	0.00	0.13	4.36	25.73	0.02	19.78	8.47	41.51
ff99SB/GB-Neck2	0.00	0.21	9.02	10.72	0.01	15.69	8.64	55.71
ff99SBildn/GB-HCT	0.03	8.29	3.77	8.42	0.02	21.19	18.27	40.02
ff99SBildn/GB-OBC(II)	0.00	0.33	5.72	5.87	0.01	12.21	20.30	55.56
ff99SBildn/GB-Neck2	0.53	1.47	7.07	9.99	0.04	13.51	9.14	58.26
ff99SBildn-φ/GB-HCT	0.09	7.36	7.82	10.56	0.01	20.96	15.27	37.93
ff99SBildn-φ/GB-OBC(II)	0.00	0.13	7.05	14.39	0.04	14.75	15.03	48.62
ff99SBildn-φ/GB-Neck2	0.15	0.12	7.13	8.49	0.04	13.05	10.92	60.11
ff12SB/GB-HCT	0.00	0.89	6.02	19.99	0.01	18.04	13.08	41.97
ff12SB/GB-OBC(II)	0.04	0.02	5.66	31.32	0.01	10.20	6.70	46.04
ff12SB/GB-Neck2	0.12	0.53	9.35	23.53	0.04	14.57	5.67	46.20
ff42SB/GB-HCT	0.03	0.03	7.05	22.56	0.04	24.33	9.24	36.72
ff42SB/GB-OBC(II)	0.00	0.74	4.83	28.89	0.01	15.63	5.48	44.42
ff42SB/GB-Neck2	0.02	0.04	6.16	41.49	0.04	9.97	2.49	39.79

Table 4.9. DSSP analysis of 300.37 K trajectory extracted from REMD simulations of peptide **ID3**. Data are reported as averaged percentages.

Force field/implicit solvent model	Para	Anti	3-10	Alpha	Pi	Turn	Bend	other
ff96/GB-HCT	0.36	9.18	0.23	14.26	0.58	8.58	28.11	38.72
ff96/GB-OBC(II)	0.17	2.37	0.10	5.66	0.06	10.17	21.76	59.71
ff96/GB-Neck2	0.08	3.21	0.19	4.46	0.01	2.51	10.70	78.84
ff99SB/GB-HCT	0.89	0.59	9.34	16.06	0.20	26.08	14.10	32.73
ff99SB/GB-OBC(II)	0.04	0.04	9.83	11.08	0.10	21.26	18.04	39.60
ff99SB/GB-Neck2	0.16	4.17	8.70	8.06	0.07	18.74	12.26	47.84
ff99SBildn/GB-HCT	1.79	0.63	7.94	19.66	0.29	26.03	12.86	30.80
ff99SBildn/GB-OBC(II)	0.00	0.97	8.04	9.20	0.18	20.08	19.81	41.72
ff99SBildn/GB-Neck2	0.74	1.00	10.34	4.90	0.02	19.52	14.11	49.37
ff99SBildn-φ/GB-HCT	1.74	0.36	6.69	16.67	0.17	26.01	13.26	35.08
ff99SBildn-φ/GB-OBC(II)	0.03	0.45	7.52	13.60	0.13	24.55	14.94	38.77
ff99SBildn-φ/GB-Neck2	0.21	1.65	8.62	5.97	0.05	17.92	15.08	50.52
ff12SB/GB-HCT	0.13	0.11	5.65	46.71	0.01	15.39	5.21	26.78
ff12SB/GB-OBC(II)	0.06	1.49	6.99	20.77	0.00	26.65	9.94	34.09
ff12SB/GB-Neck2	0.30	0.05	10.21	34.93	0.01	16.73	8.95	28.82
ff42SB/GB-HCT	0.06	0.81	10.36	28.24	0.02	21.32	9.65	29.54
ff42SB/GB-OBC(II)	0.00	0.04	8.30	19.53	0.09	21.02	15.05	35.98
ff42SB/GB-Neck2	0.08	0.12	12.86	29.25	0.00	17.33	8.99	31.38

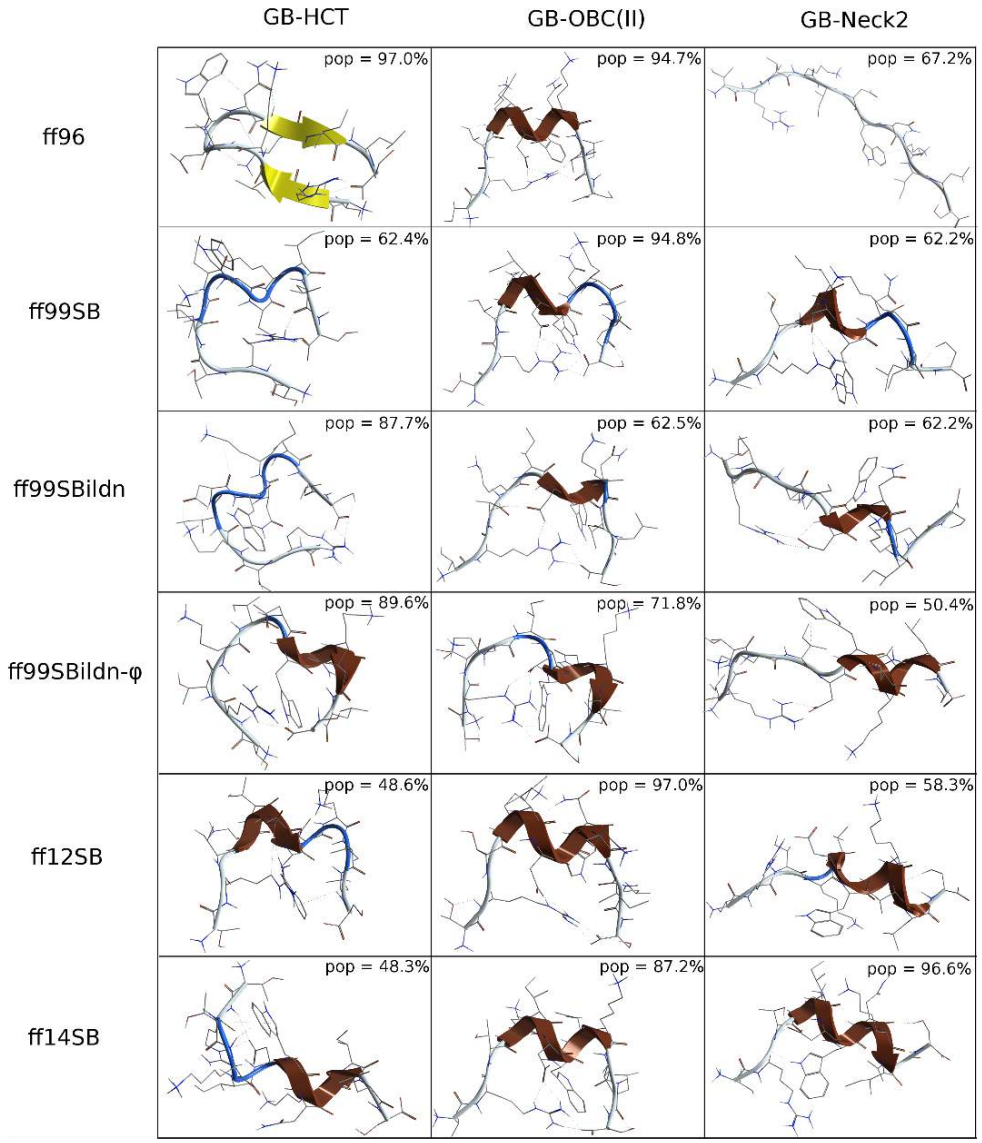

Figure 4.17. Representative structure and populated of the most populated cluster from the 300.37 K trajectory extracted from REMD simulations of peptide **ID2**.

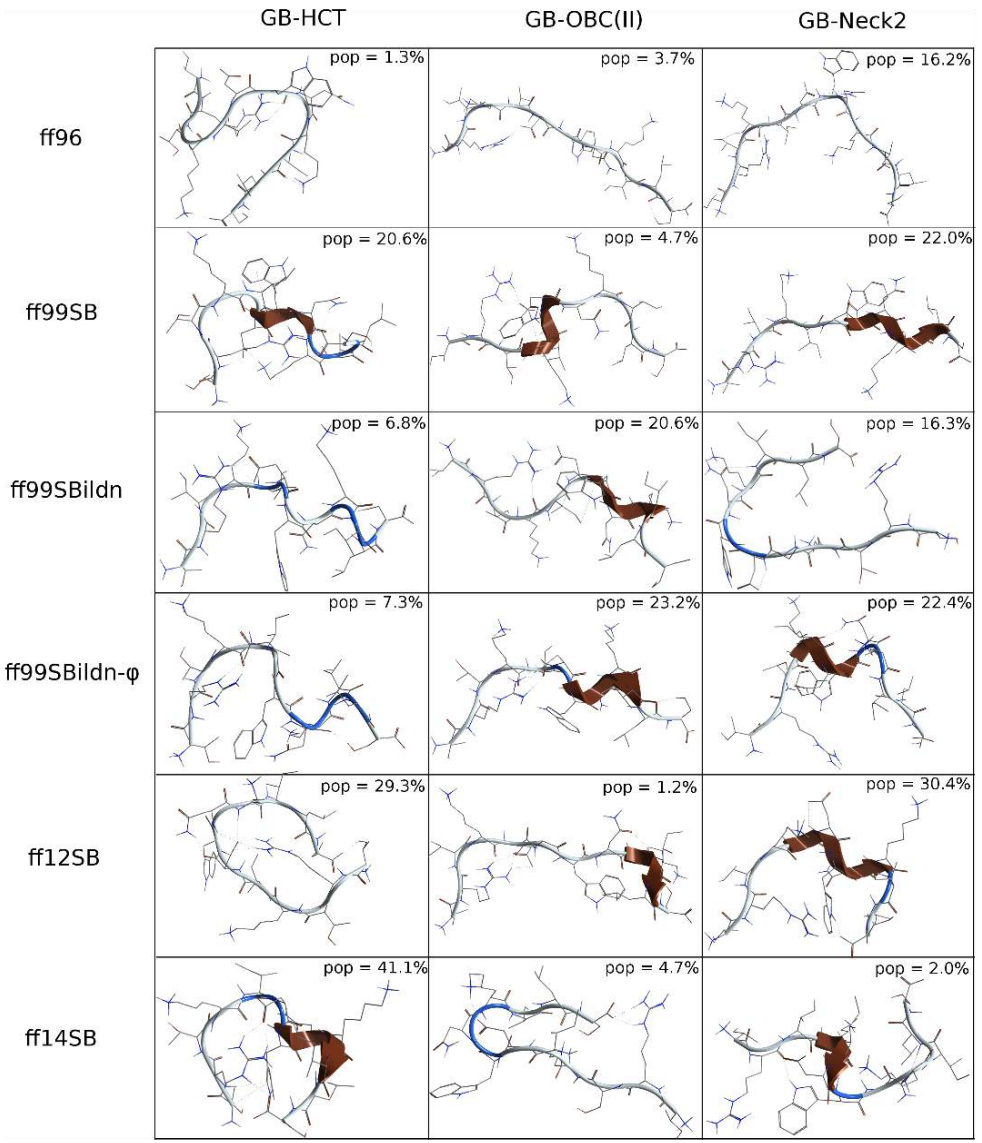

Figure 4.18. Representative structure and populated of the second cluster from the 300.37 K trajectory extracted from REMD simulations of peptide **ID2**.

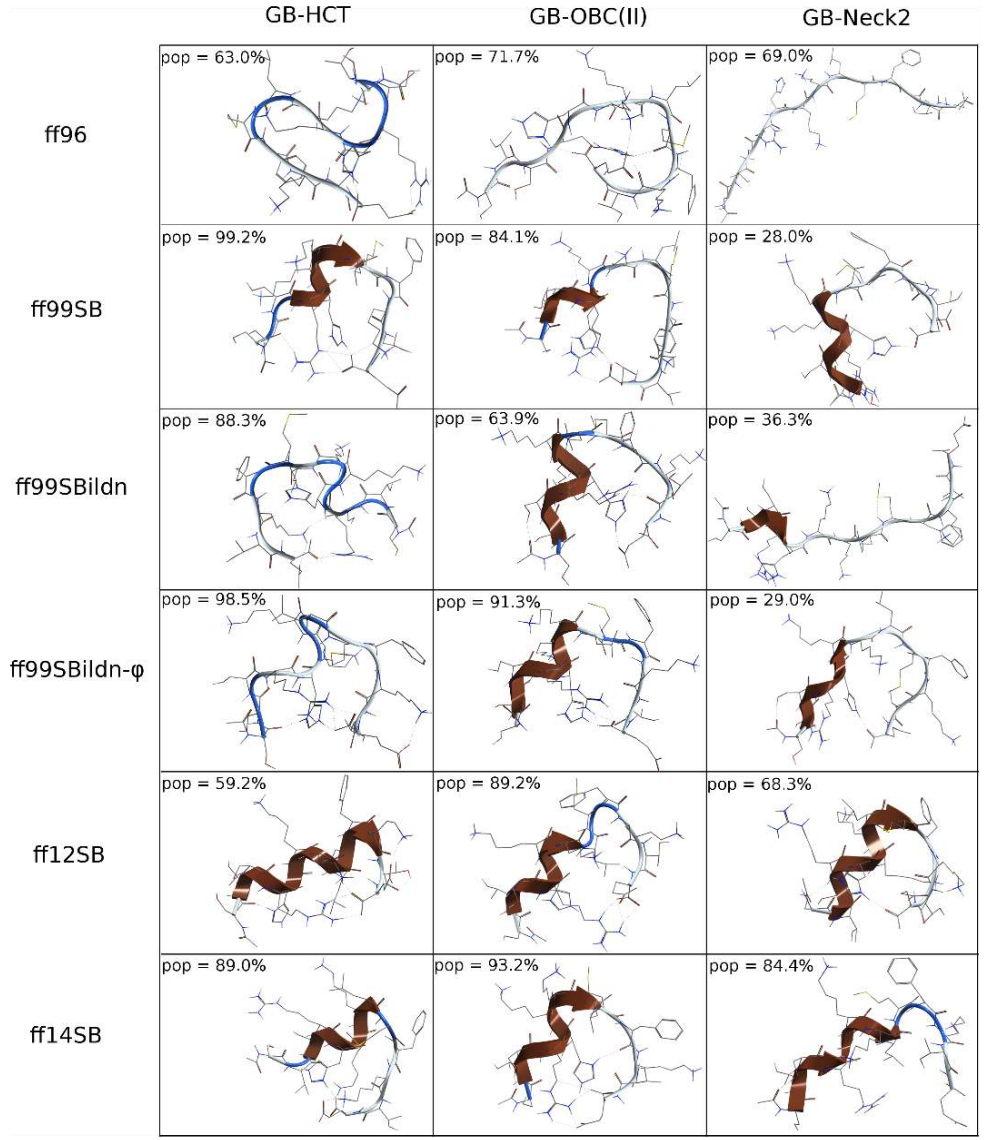

Figure 4.19. Representative structure and populated of the most populated cluster from the 300.37 K trajectory extracted from REMD simulations of peptide **ID3**.

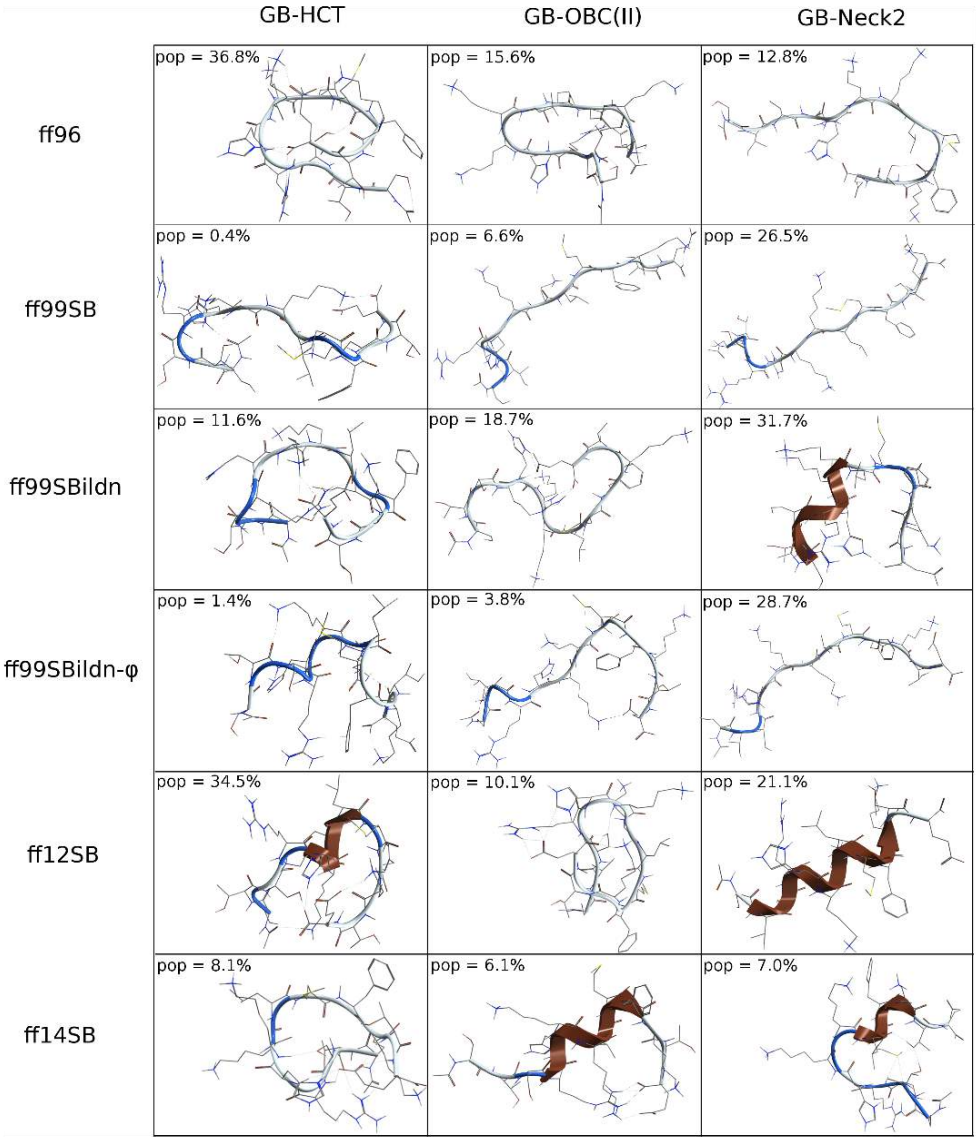

Figure 4.20. Representative structure and populated of the second cluster from the 300.37 K trajectory extracted from REMD simulations of peptide **ID3**

4.3 MATERIALS AND METHODS

REMD simulations. REMD simulations were performed on the selected peptides built with the *tLEaP* module of AMBER 14[192] starting from both an extended conformation (φ = ψ = ω = 180°) and a misfolded conformation (i.e. β-hairpin for **H1** and **H2**, α-helix for **B1**-**B3** and **ID1**-**ID3**), for convergence test. The parameters of Aib were obtained from the RED database. For simulations with GB-HCT, GB-OBC(II) and GB-Neck2 (igb = 1, 5 and 8, respectively) the *bondi*, *mbondi2* and *mbondi3* sets of radii were used, respectively. The number of replicas, which were 12 for peptide **H2**, 20 for the others, and the temperature ranges were selected through the T-REMD server. Each simulation was run with steps of 50 ns until convergence considering all the mentioned combinations of force field and solvent model. The trajectories at 308.5 K of the REMD simulations on peptide **H2** and at 300.37 K of all the other simulations were extracted and the analysis were performed on 25 ns time intervals to check the convergence. The convergence was checked in terms of frequency of RMSD, DSSP analysis, H-bonds occupancies and conformation of the representative structures of the two most populated clusters.

Cluster analyses were conducted with *cpptraj* sampling one every two frames using the average-linkage algorithm and the pairwise mass-weighted Root Mean Square Displacement (RMSD) on backbone heavy atoms as a metric and requesting five clusters.

Secondary structure analyses were performed on the basis of DSSP with *cpptraj*. H-bonds were computed with VMD 1.9.1 by setting a donor-acceptor distance threshold of 4.0 Å and an angle cutoff of 30° and considering only H-bonds with an occupancy ≥ 5%. Radii of gyration (RoG) of **ID1-ID3** were computed on backbone heavy atoms with *cpptraj*.

5 MECHANISM OF HELIX SECONDARY STRUCTURE STABILIZATION BY CCTAAS

5.1 INTRODUCTION

As previously underlined, the high occurrence of helical motifs at protein-protein interfaces[44,45] leads to the necessity of stabilizing a defined secondary structure, in this case the helix, when designing peptide-based PPIs modulators.[58] Indeed, it is fundamental to guarantee the correct orientation of peptide side chains to allow the interaction with the target protein, resulting in high selectivity and specificity.[62–64] As already mentioned, a way to stabilize the helix peptide conformation is represented by the insertion of CTAAs in the sequence, which can also increase the resistance to proteases and peptidases.[91] Among the CTAAs, the achiral α-aminoisobutyric acid (Aib) together with one of its higher homologues Cα,α-diethylglycine and cyclic derivatives (i.e. 1-aminocyclopropane-1-carboxylic acid and 1-aminocyclopentane-1-carboxylic acid) are the most studied[184–186,193–197] and their helical propensity has been attributed to a limitation of the peptide backbone conformational freedom.[64,193,198,199] However, chiral CTAAs (cCTAAs) have also been synthetized and exploited,[93,200–204] and configuration at Cα has been observed to affect both the helical stabilization and the screw sense preference.[93,205–211]

Therefore, the choice of a given cCTAA has to be made depending on both the desired features of the cCTAA side chain (i.e. hydrophobicity, acidity, H-bond capability and so on), and the folding preference of the cCTAA. At the light of this, it would be important to have intuitive descriptors that can be used to predict how a cCTAA can drive the peptide folding or for the comparison of different cCTAAs in terms of stabilization efficacy.

With this aim, using REMD simulations and QTAIM analyses, we investigated the conformational behaviour of selected cCTAAs (Figure 5.1) when inserted in the Ac-L-Ala-cCTAA-L-Ala-Aib-L-Ala-NHMe sequence, a model peptide which have been already used in similar studies.[92,126]

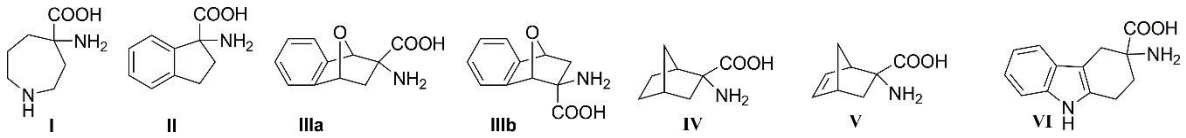

Figure 5.1. Selection of cCTAAs used for this study.

We found that the inclusion of cCTAAs in the chosen peptide model limits the backbone freedom thanks to at least two complementary mechanisms: 1) steric hindrance mainly located in the (+x,+y,-z) sector of the right-handed 3D Cartesian space (Figure 5.2), where the +z → -z axis coincides with the N → C helical axis and the cCTAA Cα lies on the +y axis, and 2) the presence of additional intramolecular C-H···O=C interactions.[72]

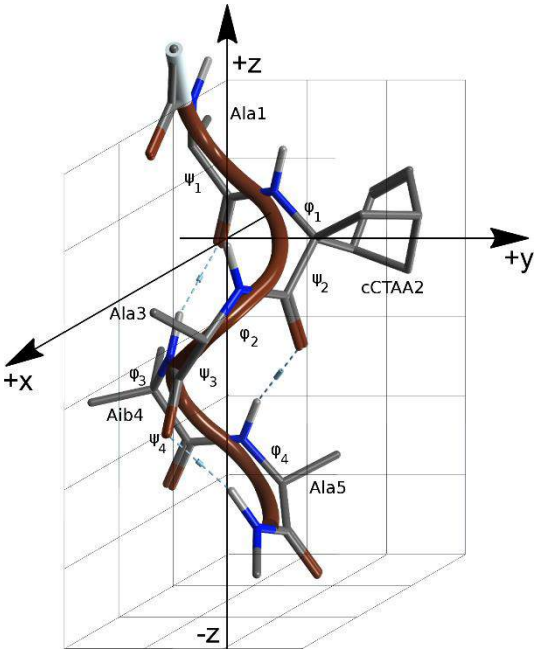

Figure 5.2. 3D Cartesian space used for the representation of helical peptides containing cCTAAs. The ideal right-handed helix of Ac-L-Ala-(1*R*,2*R*,4*R*)-**V**-L-Ala-Aib-L-Ala-NHMe is shown.

5.2 Results and Discussion

Cluster, DSSP and H-bond analysis (Tables 5.1 and 5.2) performed on the 300 K REMD trajectories of peptides **1-15** show that all the peptides, except **8** and **12**, mainly fold into a *P*-helix, as indicated by the average population of helical geometries ($pop_{h\%}$) obtained from the cluster analysis, the DSSP helical content ($h_{\%}$) and the occupancies of $i+3 \rightarrow i$ H-bonds.

Concerning peptide **8**, containing (*S*)-**I**, circular dichroism (DC) in MeOH and NMR experiments in CD_3CN solution already showed that this peptide do not fold into an ordered secondary structure.[93] Conversely, peptide **12**, containing (1*R*,2*S*,4*S*)-**IV**, is the only one having a *M*-helix as the most populated cluster, although a minor amount of *M*-helix is observable also for peptides **15**, **1** and **5** (cCTAA = Aib, (*R*)-**I** and (1*S*,2*R*,4*R*)-**IV**, respectively).

Table 5.1. Average Helical Population from Cluster Analysis ($pop_h\%$) and Average DSSP Helical Content ($h_{\%}$) Obtained from the REMD Trajectories of Ac-L-Ala-CTAA-L-Ala-Aib-L-Ala-NHMe Peptides **1-15**.[a] Differences Between Peptides Containing CTAAs of Opposite Stereochemistry ($\Delta pop_h\%$ and $\Delta h_{\%}$) are also reported.

#	(*R*)-*c*CTAAs[b]	$pop_{h\%}$	$h_{\%}$	#	(*S*)-*c*CTAA[b]	$pop_{h\%}$	$h_{\%}$	$\Delta pop_{h\%}$	$\Delta h_{\%}$
1	(*R*)-**I**	43.2±3.3	46.7±1.0	**8**	(*S*)-**I**	n.a.[c]	23.1±1.2	0.5	23.5
2	(*R*)-**II**	85.1±0.9	85.8±0.6	**9**	(*S*)-**II**	76.6±3.1	68.1±1.7	8.5	17.7
3	(1*R*,2*R*,4*R*)-**IIIa**[d]	73.3±2.0	80.0±0.2	**10**	(1*S*,2*S*,4*S*)-**IIIa**[d]	72.2±1.7	73.6±1.8	1.1	6.4
4	(1*S*,2*R*,4*S*)-**IIIb**[d]	79.7±1.5	82.0±0.7	**11**	(1*R*,2*S*,4*R*)-**IIIb**[d]	90.4±1.8	90.5±0.4	-20.3	-8.5
5	(1*S*,2*R*,4*R*)-**IV**	61.9±2.6	56.5±1.4	**12**	(1*R*,2*S*,4*S*)-**IV**	30.6±2.7[e]	35.8±1.1	31.3	20.7
6	(1*R*,2*R*,4*R*)-**V**	82.5±1.6	82.9±0.5	**13**	(1*S*,2*S*,4*S*)-**V**	84.8±2.1	69.0±0.8	-2.3	+13.9
7	(*R*)-**VI**	83.1±2.4	84.1±1.3	**14**	(*S*)-**VI**	81.6±1.8	73.5±1.1	1.5	10.6

[a]The $pop_h\%$ and h% values obtained from the REMD trajectory of the reference Ac-Ala-Aib-Ala-Aib-AlaNHMe achiral peptide **15** are 51.3±4.9 and 51.8±1.2, respectively. [b]The stereochemical descriptor refers to the Cα configuration. [c]The

representative geometry of the most populated cluster does not correspond to a helix. [d]Experimental **IIIa**:**IIIb** ratio = 7:1.[198,201] [e]The representative geometry of the most populated cluster corresponds to a *M*-helix.

Table 5.2. H-bond Analysis of REMD Trajectories of Ac-L-Ala-CTAA-L-Ala-Aib-L-Ala-NHMe peptides **1-15** (donor: N-H; acceptor: C=O).[a]

#	CTAA	donor	acceptor	occ%	#	CTAA	donor	acceptor	occ%
1	(*R*)-**I**	Aib4	Ala1	39.00	**8**	(*S*)-**I**	Aib4	Ala	Aib4
		Ala5	**I**	12.94			Ala5	**I**	Ala5
		Ala5	Ala1	7.11					
2	(*R*)-**II**	Aib4	Ala1	69.72	**9**	(*S*)-**II**	Aib4	Ala1	62.91
		Ala5	**II**	57.57			Ala5	**II**	52.06
3	(1*R*,2*R*,4*R*)-**IIIa**	Aib4	Ala1	64.15	**10**	(1*S*,2*S*,4*S*)-**IIIa**	Aib4	Ala1	60.07
		Ala5	**IIIa**	47.11			Ala5	**IIIa**	51.79
4	(1*S*,2*R*,4*S*)-**IIIb**	Aib4	Ala1	63.84	**11**	(1*R*,2*S*,4*R*)-**IIIb**	Aib4	Ala1	72.81
		Ala5	**IIIb**	58.91			Ala5	**IIIb**	65.69
5	(1*S*,2*R*,4*R*)-**IV**	Aib4	Ala1	41.55	**12**	(1*R*,2*S*,4*S*)-**IV**	Aib4	Ala1	31.89
		Ala5	**IV**	25.30			Ala5	**IV**	38.40
		Ala5	Ala1	11.20					
6	(1*R*,2*R*,4*R*)-**V**	Aib4	Ala1	65.78	**13**	(1*S*,2*S*,4*S*)-**V**	Aib4	Ala1	62.08
		Ala5	**V**	55.69			Ala5	**V**	60.69
7	(*R*)-**VI**	Aib4	Ala1	70.17	**14**	(*S*)-**VI**	Aib4	Ala1	72.60
		Ala5	**VI**	60.13			Ala5	**VI**	54.16

[a]The reference H-bonds occ% obtained from the REMD trajectory of the Ac-Ala-Aib-Ala-Aib-AlaNHMe achiral peptide **15** are 4→1 45.01%, 5→2 26.55% and 5→1 6.82%.

Furthermore, from the analyses performed on the 300 K REMD trajectories it can be observed that the cCTAAs with the highest ability of helix stabilization are (1*R*,2*S*,4*R*)-**IIIb**, (*R*)-**II**, (*R*)-**VI** and (1*R*,2*R*,4*R*)-**V** which, once included in the peptide model, give $pop_{h\%}$ and $h_{\%}$ above 80%.

It has to be underlined that the stereochemistry at Cα, or better the spatial orientation of the substituents at Cα, influences at different extents the ability of each cCTAA to stabilize the helical conformation and, therefore, in all the examples a "eutomer", i.e. the enantiomer having the highest stabilization effect, and a "distomer", i.e. the enantiomer having the poorest stabilization effect, can be found. Obviously, the behavior as eutomer or distomer depends on the stereochemistry of the other residues in the peptide chain, because L-Ala can affect the peptide conformation. These differences are highlighted by the $\Delta pop_{\%}$ and $\Delta h_{\%}$ reported in table 4.1 and are particularly relevant for **IV**.

At the light of this, the following discussion is focused on the peptides containing the "eutomers" cCTAAs (*R*)-**I**, (*R*)-**II**, (1*R*,2*R*,4*R*)-**IIIa**, (1*S*,2*R*,4*R*)-**IV**, (1*R*,2*R*,4*R*)-**V**, (*R*)-**VI**, (1*R*,2*S*,4*R*)-**IIIb**.

Furthermore, simulations of peptide **1**, **5** and **15** (cCTAA = (*R*)-**I**, (1*S*,2*R*,4*R*)-**IV** and Aib, respectively) also sampled α-helices, although poorly, as showed by low occupancy $i+4 \rightarrow i$ H-bonds (Table 5.2).

These results were confirmed by 2D-PMF as a function of φ_1-ψ_2 and φ_2-ψ_3 dihedral pairs (Figures 5.3 and 5.4), directly involving the cCTAA and the cCTAA + 1 residues, which show the statistical accessibility of these dihedrals pairs in the REMD trajectory.

In these profiles it can be generally observed the presence of a global minimum corresponding to the *P*-helix, which has wider wells for 2D-PMF(φ_2,ψ_3), and a local one corresponding to the *M*-helix, with (1*R*,2*R*,4*R*)-**V** and (1*R*,2*S*,4*R*)-**IIIb** being the most selective toward the *P*-helix. Indeed, 2D-PMF profiles of peptides **1**, **3**, **5** and **15** (cCTAA = (*R*)-**I**, (1*R*,2*R*,4*R*)-**IIIa**, (1*S*,2*R*,4*R*)-**IV** and Aib, respectively) showed an additional minima corresponding to β-strands or polyproline helices (Figures 5.3 and 5.4), while peptide **2** (cCTAA = (*R*)-**II**) had an additional minimum in 2D-PMF(φ_1,ψ_2) in a region which is not corresponding to any well-defined secondary structure ($-130° \leq \varphi_1 \leq -180°$; $-60° \leq \psi_2 \leq +30°$). The 2D-PMF($\varphi_1$,$\psi_2$) of peptide **7** (cCTAA = (*R*)-**VI**), on the other hand, only showed the minima corresponding to the *P*- and *M*-helices, but with an apparently lower ΔE if compared to peptide **6** and **11** (Figure 5.3).

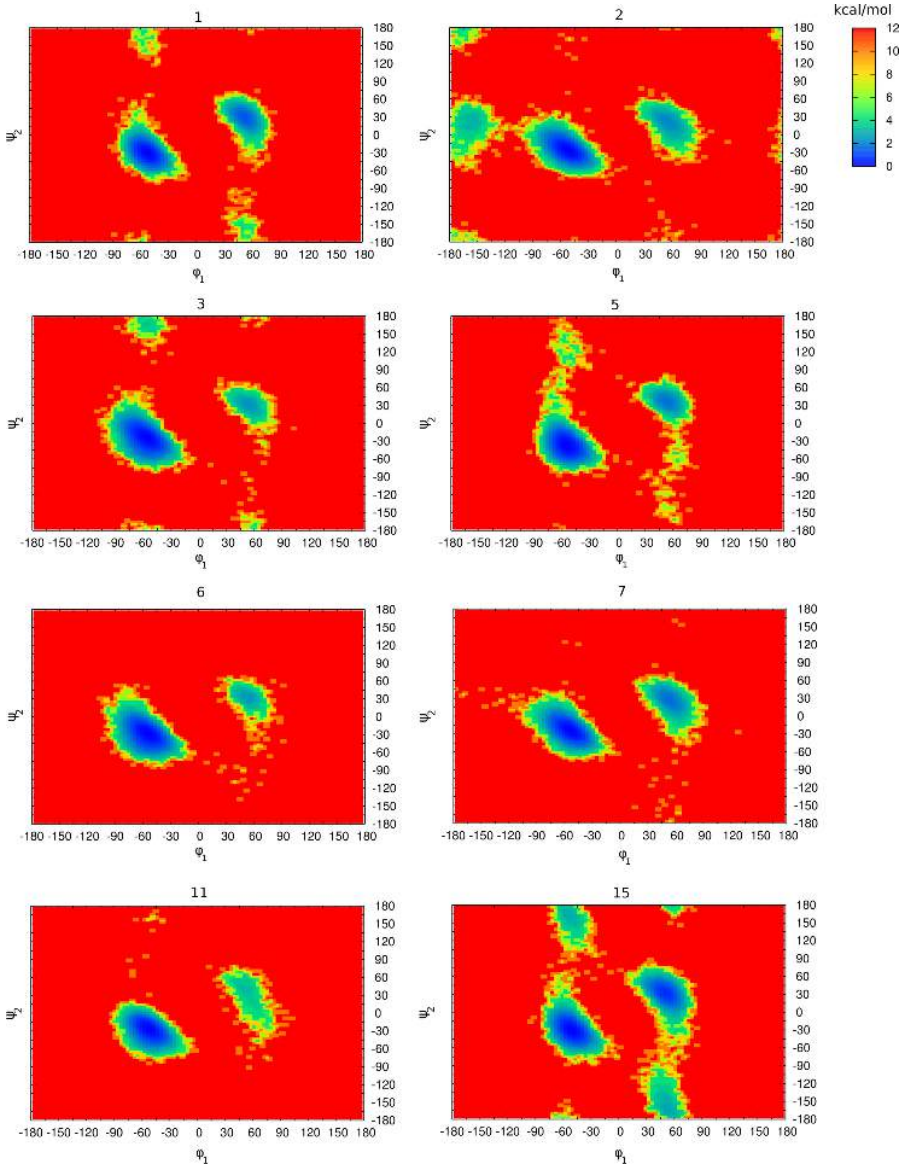

Figure 5.3. 2D-PMF profiles (kcal/mol) as a function of φ_1-ψ_2 dihedral pair obtained from REMD simulations of peptides **1-3**, **5-7**, **11** and **15** containing (*R*)-**I**, (*R*)-**II**, (1*R*,2*R*,4*R*)-**IIIa**, (1*S*,2*R*,4*R*)-**IV**, (1*R*,2*R*,4*R*)-**V**, (*R*)-**VI**, (1*R*,2*S*,4*R*)-**IIIb** and Aib, respectively.

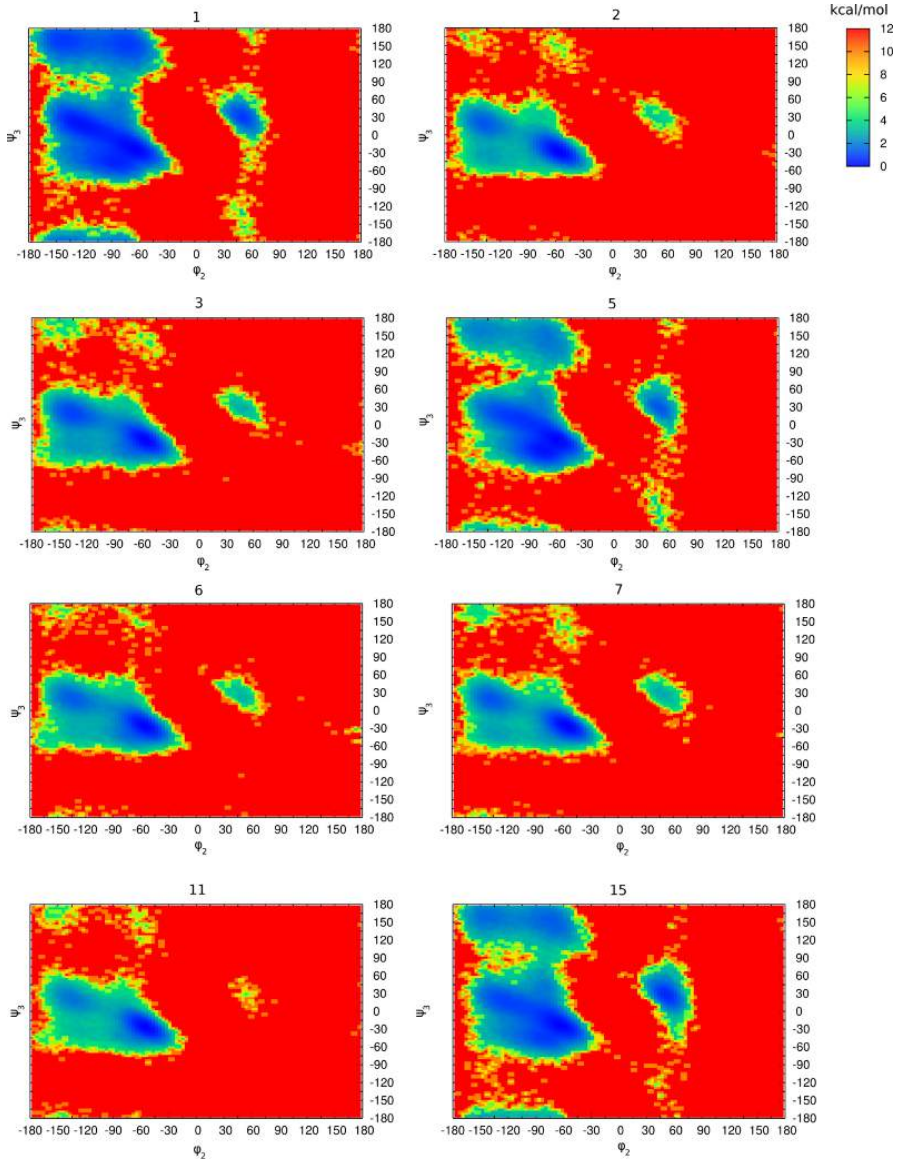

Figure 5.4. 2D-PMF profiles (kcal/mol) as a function of φ_2-ψ_3 dihedral pair obtained from REMD simulations of peptides **1-3**, **5-7**, **11** and **15** containing (*R*)-**I**, (*R*)-**II**, (1*R*,2*R*,4*R*)-**IIIa**, (1*S*,2*R*,4*R*)-**IV**, (1*R*,2*R*,4*R*)-**V**, (*R*)-**VI**, (1*R*,2*S*,4*R*)-**IIIb** and Aib, respectively.

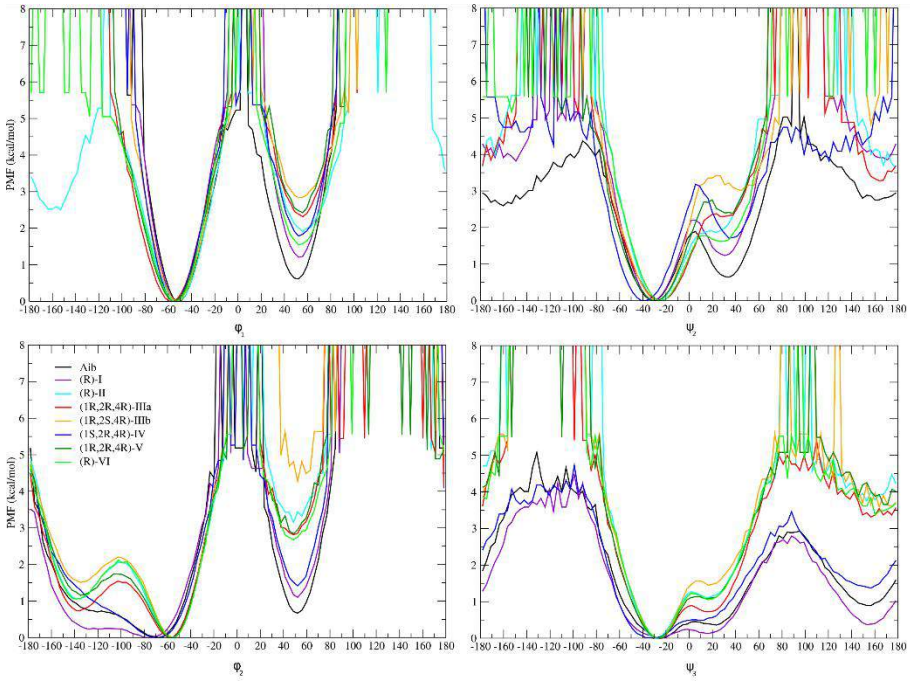

Figure 5.5. PMF profiles (kcal/mol) obtained from REMD simulations of peptides **1-3**, **5-7**, **11** and **15** containing (*R*)-**I**, (*R*)-**II**, (1*R*,2*R*,4*R*)-**IIIa**, (1*S*,2*R*,4*R*)-**IV**, (1*R*,2*R*,4*R*)-**V**, (*R*)-**VI**, (1*R*,2*S*,4*R*)-**IIIb** and Aib, respectively. Dihedrals associated with PMF higher than 6 kcal/mol were not sampled at the 260-335 K range temperature.

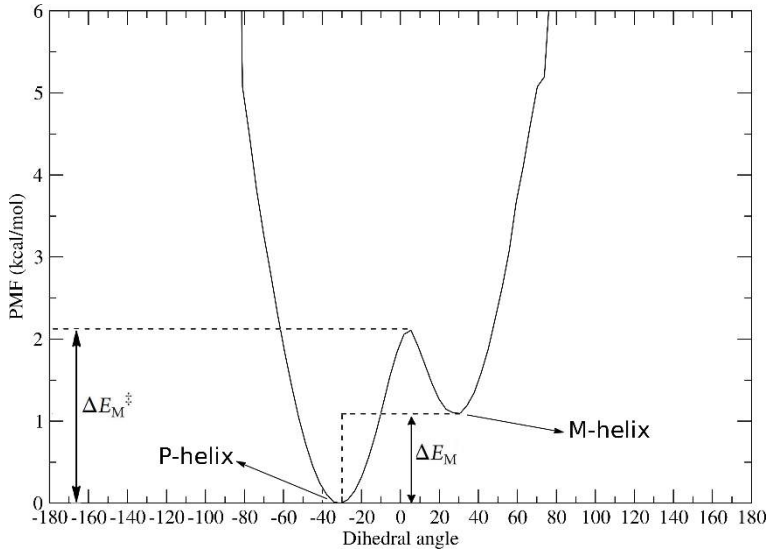

Figure 5.6. PMF profiles descriptors.

A more detailed description of the Δ*E* associated to the rotation of single dihedrals (e.g. φ_1, ψ_2, φ_2, ψ_3) is obtained from monodimensional PMF (Figure 5.5). Concerning PMF(φ_1) and PMF(φ_2) profiles, it can be observed that the energy difference between the two helical minima (Figure 5.6, ΔE_M) is somehow correlated with the h% and the pop$_{h\%}$ (Table 5.1), which are here used as a measure of the helix stabilization ability of the cCTAAs. However, the energy barrier between the minima (Figure 5.6, $\Delta E_M^{\ddagger}$) is quite high, suggesting that the interconversion from *P*- to *M*-helix and *vice versa* is unlikely to occur at the simulation time and temperature. This high $\Delta E_M^{\ddagger}$ is not observed for the PMF(ψ_2) and PMF(ψ_3), where both ΔE_M and $\Delta E_M^{\ddagger}$ seem to reflect the h% and the pop$_{h\%}$. Moreover, for peptides containing Aib, (*R*)-**I** and (1*S*,2*R*,4*R*)-**IV** the barrier for the conversion between helix and β-

strand can be overcome, suggesting a lower ability in stabilizing the helix secondary structure if compared to other cCTAAs here studied.

In addition, to investigate if the relative helical tendency of cCTAAs is influenced by the presence of Aib in the peptide chain, we also simulated the behavior of Ac-L-Ala_2-cCTAA-L-Ala_2-NHMe peptide models, where cCTAA = (*R*)-**I** or (1*R*,2*R*,4*R*)-**V**, which are the worst and the best performing cCTAAs, respectively. Table 5.3 shows that both cCTAAs maintain their helical stabilizing ability and, most of all, their hierarchy in terms of helical propensity.

Table 5.3. DSSP Helix Content ($h_{\%}$)[a] and H-bond analyses of 100 ns REMD Trajectories of Ac-L-Ala_2-cCTAA-L-Ala_2-NHMe Pentapeptides **16**-**17**.

			H-Bond		
#	cCTAA	$h_{\%}$	donor	acceptor	$occ_{\%}$
16	(*R*)-**I**	42.9±1.4	Ala4	Ala1	32.04
			Ala5	Ala2	35.85
			Ala5	Ala1	7.09
17	(1*R*,2*R*,4*R*)-**V**	81.9±0.4	Ala4	Ala1	38.81
			Ala5	Ala2	60.32
			Ala5	Ala1	5.61

[a] Calculated as the sum of 3_{10}- and α-helix content of CTAA, averaged with respect to the 25-50, 50-75, 75-100 ns time intervals.

Although these results give valuable insights about the folding preferences of peptides containing cCTAAs, they could not provide an explanation of the mechanisms behind the helix stabilization. It is known that cCTAAs' additional alkyl group at Cα limits the φ_1 conformational freedom, although this cannot explain the differences in the helix stabilizing ability among sterically similar cCTAAs, such as **IV** and **V**. The helical conformational preferences of some natural AAs have been suggested to depend on side chain entropic and steric factors,[212,213] together with the ability to strengthen the helical H-bond network.[214–218] Consistently, cCTAAs might affect the helical conformation stability by similar mechanisms.

Therefore, for a preliminary investigation of the structure-"activity" relationships of the considered cCTAAs, where the "activity" corresponds to the ability in helical conformation stabilization/induction, we evaluated the role played by steric hindrance through a 3D quantitative structure-property relationship (QSPR) analysis using the PHASE software.[219] This is a frequently applied medicinal chemistry tool for the derivation of predictive 3D-pharmacophore models, starting from a set of compounds with known activity data.[220]

We preliminary discarded from this analysis peptides **8** and **12**, because a *P*-helix conformation was not found by cluster analysis; then the ideal models of *P*-helix conformations of peptides **1**-**7**, **9**-**11**, and **13**-**15** have been aligned and submitted to a QSPR analysis using the $h_{\%}$ values obtained from

DSSP as the "activity" field. The obtained results were visualized with a 3D plot, where blue and red cubes represent the regions where hydrophobic substituents positively or negatively affect the helical content, respectively (Figure 5.7).

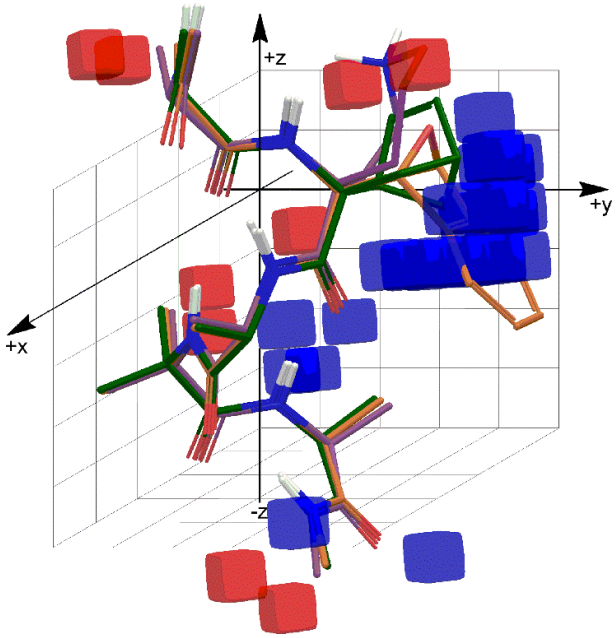

Figure 5.7. 3D QSPR plot obtained from PHASE analysis of ideal *P*-helices of peptides **1**-**7**, **9**-**11**, and **13**-**15**. Blue and red cubes correspond to regions where hydrophobic substituents positively and negatively affect the helix content, respectively. Peptides **1** (purple), **6** (green) and **11** (orange) are showed as reference.

It can be observed that a positive effect on the helix stabilization is exerted by the presence of hydrophobic substituents in the (+x, +y, ± z) sectors of the Cartesian space, although this is more evident for the (+x, +y, -z) sector, probably because the considered peptide models have the cCTAA in position 2, thus closer to the N-terminus. Indeed, steric hindrance in this latter sector limits the rotational freedom of ψ_2, as showed by PMF (Figure 5.5). For example, the best performing cCTAA is (1*R*,2*S*,4*R*)-**IIIb**, which has its aryl group in this sector, while its enantiomer has a lower helix stabilizing ability, since its aryl group is located in the (-x, +y, -z) sector.

Furthermore, (1*R*,2*R*,4*R*)-**IIIa**, whose side chain points toward the (-x, +y, +z) sector, has both $h_{\%}$ and $pop_{h\%}$ lower than those of (1*R*,2*S*,4*R*)-**IIIb**, together with reduced ΔE_M and $\Delta E_M^{\ddagger}$ in the PMF profiles (Figure 5.5), although its performance is still good. Since the QSPR plot (Figure 5.7) shows that steric hindrance in the (-x, +y, +z) sector has limited effects on the helical stability, the lower helix stabilizing ability of (1*R*,2*R*,4*R*)-**IIIa** could be attributed to its reduced steric hindrance in the (+x, +y, -z) sector.

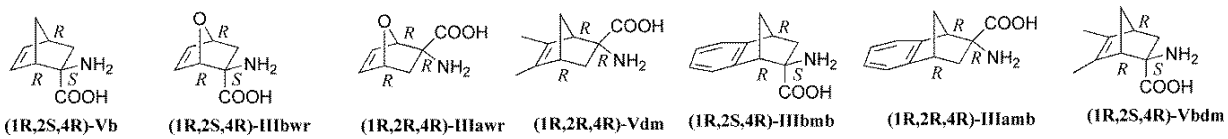

Figure 5.8. Modified cCTAAs.

In order to prove the validity of the results obtained by the preliminary QSPR analysis, we investigated the folding behavior of hypothetical (thus never synthesized) cCTAAs (Figure 5.8), structurally related to the actual cCTAAs studied here (Figure 5.1).

First of all, we evaluated how $pop_{h\%}$ and $h_{\%}$ were affected by the inclusion in the peptide model of a modified cCTAA, called (1*R*,2*R*,4*R*)-**IIIawr** (Figure 5.8), where the aromatic ring of the benzoxanorbornene group of (1*R*,2*R*,4*R*)-**IIIa** was deleted. As expected, the $pop_{h\%}$ and $h_{\%}$ for this peptide were equivalent to those of peptide **3** (Tables 5.1 and 5.4). Furthermore, PMF profiles as a function of the considered single dihedrals are comparable, except for a slight difference (0.5 kcal/mol) in ΔE_M in PMF(φ_1) and PMF (ψ_2) (Figure 5.9).

Table 5.4. Average helical population ($pop_{h\%}$) from cluster analysis, average DSSP helical content ($h_{\%}$) and H-bonds occupancies ($occ_{\%}$)obtained from the analysis of the REMD trajectories (308 K) of the Ac-L-Ala-cCTAA-L- Ala-Aib-L-Ala-NHMe peptides containing modified CTAAs.

cCTAA	$pop_{h\%}$	$h_{\%}$	H-Bond		
			donor	acceptor	$occ_{\%}$
(1*R*,2*S*,4*R*)-**Vb**	84.1 ± 1.7	83.6 ± 0.2	Aib4	Ala1	66.12
			Ala5	cCTAA	58.1
(1*R*,2*S*,4*R*)-**IIIbwr**	84.0 ± 2.4	86.2 ± 0.6	Aib4	Ala1	69.5
			Ala5	cCTAA	57.3
(1*R*,2*R*,4*R*)-**IIIawr**	71.6 ± 1.8	79.1 ± 0.3	Aib4	Ala1	63.0
			Ala5	cCTAA	44.2
(1*R*,2*S*,4*R*)-**IIIbmb**	90.6 ± 1.5	88.8 ± 0.4	Aib4	Ala1	71.1
			Ala5	cCTAA	66.0
(1*R*,2*R*,4*R*)-**IIIamb**	84.2 ± 1.3	83.8 ± 0.3	Aib4	Ala1	67.4
			Ala5	cCTAA	57.8
(1*R*,2*S*,4*R*)-**Vbdm**	91.4 ± 1.3	90.2 ± 0.4	Aib4	Ala1	71.4
			Ala5	cCTAA	66.2
(1*R*,2*R*,4*R*)-**Vdm**	84.5 ± 2.1	83.5 ± 0.9	Aib4	Ala1	65.9
			Ala5	cCTAA	58.0

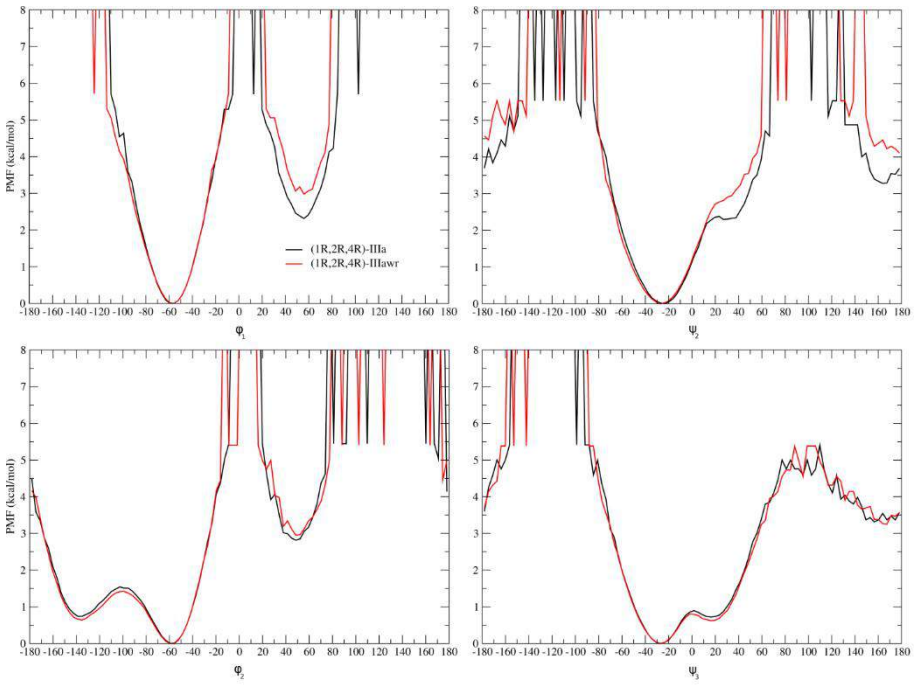

Figure 5.9. Comparison of PMF profiles, as a function of φ_1, ψ_2, φ_2 and ψ_3 dihedrals, of peptides containing (1*R*,2*R*,4*R*)-**IIIa** (black) and (1*R*,2*R*,4*R*)-**IIIawr** (red).

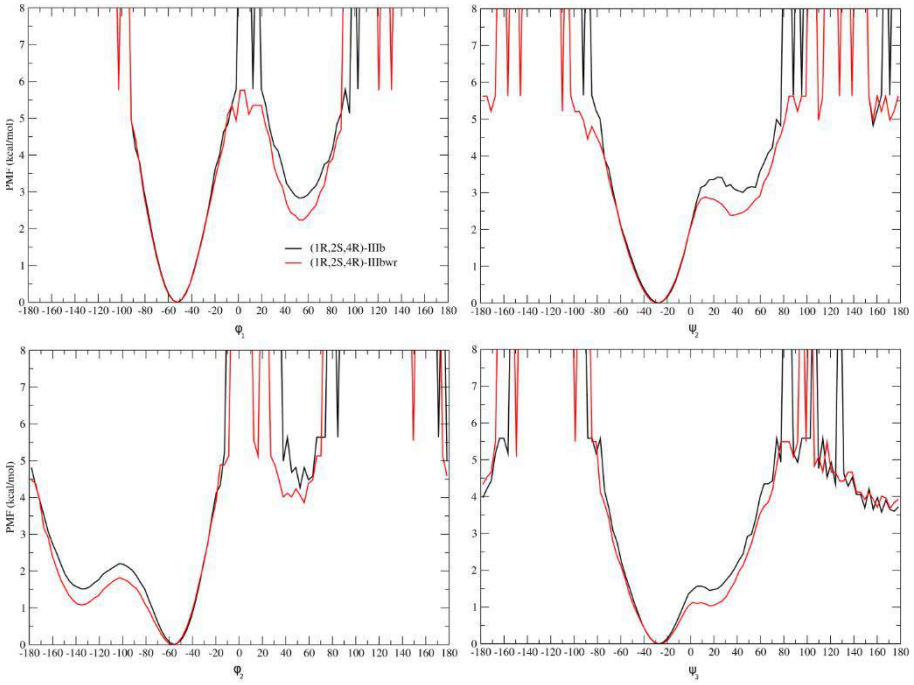

Figure 5.10. Comparison of PMF profiles, as a function of φ_1, ψ_2, φ_2 and ψ_3 dihedrals, of peptides containing (1*R*,2*S*,4*R*)-**IIIb** (black) and (1*R*,2*S*,4*R*)-**IIIbwr** (red).

The cCTAA (1*R*,2*S*,4*R*)-**IIIb** was similarly modified, obtaining (1*R*,2*S*,4*R*)-**IIIbwr** (Figure 5.8). This latter residue, once inserted in the peptide model, gave $pop_{h\%}$ and $h_{\%}$ only 6 and 4% lower, respectively, than those obtained for peptide **11** (Table 5.4). Moreover, their PMF(φ_1), PMF(ψ_2) and PMF(ψ_3) only slightly differ in terms of both ΔE_M and $\Delta E_M^{\ddagger}$ (Figure 5.10). The differences in helical stabilization ability of these two cCTAAs resulted lower than expected, considering their large

difference in size, but it can be observed that the H-C=C-H bridge of (1*R*,2*S*,4*R*)-**IIIbwr** is still located in the (+x, +y, -z) sector and the oxo-bridge points toward the (+x, +y, +z) area (Figure 5.11A).

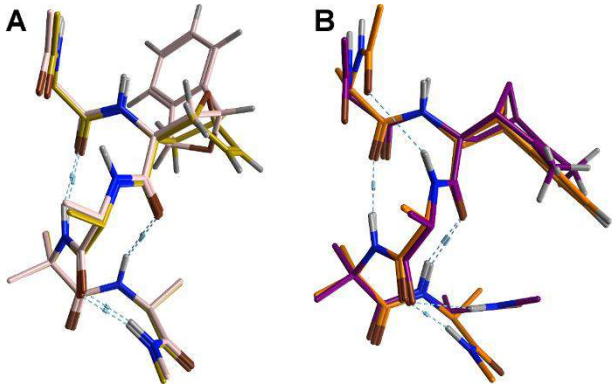

Figure 5.11. A) Superimposed right-handed 3_{10}-helices of peptides **3** ((1*R*,2*R*,4*R*,)-**IIIa**; pink) and Ala-(1*R*,2*S*,4*R*)-**IIIbwr**-Ala-Aib-Ala (ochre). B) Superimposed right-handed 3_{10}-helices of peptides **11** ((1*R*,2*S*,4*R*)-**IIIb**; orange) and Ala-(1*R*,2*S*,4*R*)-**Vbdm**-Ala-Aib-Ala (purple).

Successively, we evaluated the role of the oxo or methylene bridge through the comparison of the folding behaviors of model peptides containing (1*R*,2*S*,4*R*)-**Vb** (Figure 5.8), which is the non-isolated regioisomer of (1*R*,2*R*,4*R*)-**V**,[221] and (1*R*,2*S*,4*R*)-**IIIbwr**. Only minor differences can be observed in cluster and DSSP analyses ($\Delta pop_{h\%}$ = 1.4 and $\Delta h_{\%}$ = 2.6 in favor of (1*R*,2*S*,4*R*)-**IIIbwr**) (Table 4.4). Consistently, monodimensional PMF profiles were similar, except for an increased $\Delta E_M^{\ddagger}$ in PMF(φ_1) for (1*R*,2*S*,4*R*)-**Vb** (Figure 5.12), indicating that a *P*→*M* helix conversion is disfavored.

As a further proof, we replaced the oxygen of the oxo-bridge in (1*R*,2*S*,4*R*)-**IIIb** with a methylene group, obtaining (1*R*,2*S*,4*R*)-**IIIbmb** (Figure 5.8). As expected, we could not observe any significant difference in the cluster, DSSP and PMF analyses (Tables 5.1, 5.4 and Figure 5.13), driving to the conclusion that the oxo-bridge in the **III** does not play an important role in the helix stabilization.

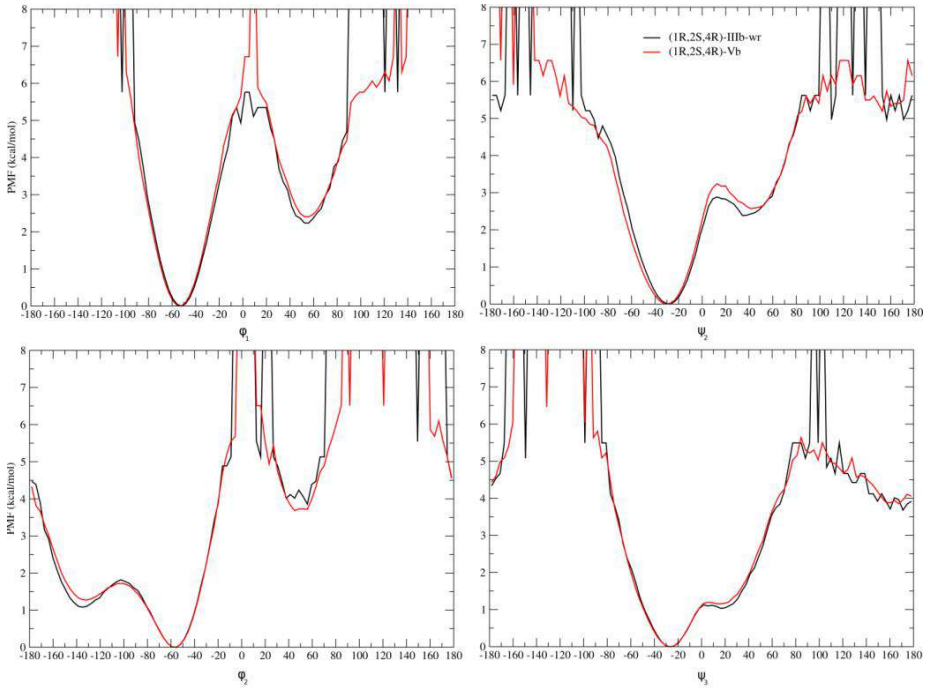

Figure 5.12. Comparison of PMF profiles, as a function of φ_1, ψ_2, φ_2 and ψ_3 dihedrals, of peptides containing (1*R*,2*S*,4*R*)-**IIIbwr** (black) and (1*R*,2*S*,4*R*)-**Vb** (red).

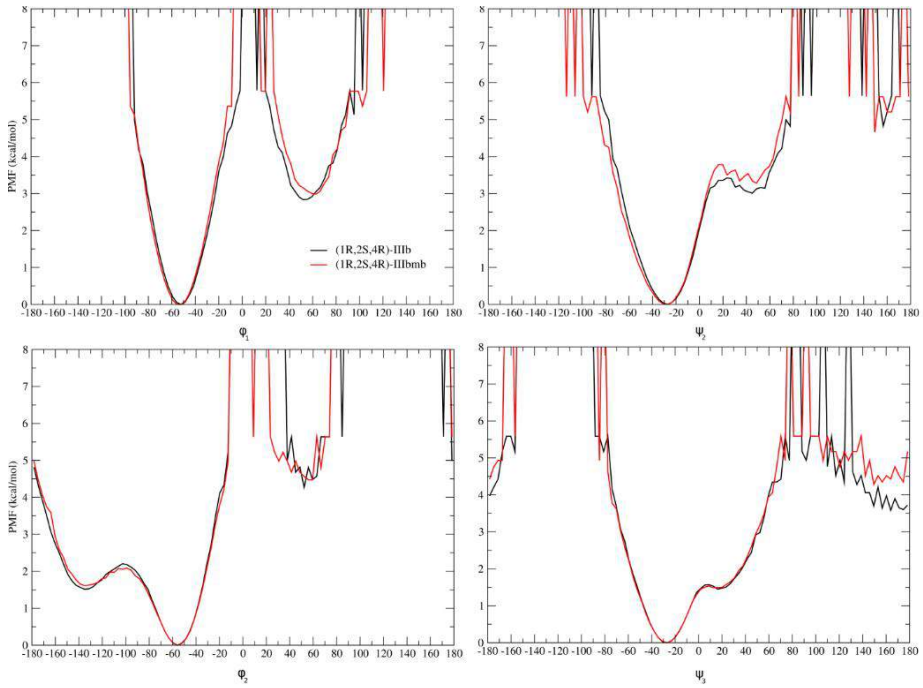

Figure 5.13. Comparison of PMF profiles, as a function of φ_1, ψ_2, φ_2 and ψ_3 dihedrals, of peptides containing (1*R*,2*S*,4*R*)-**IIIb** (black) and (1*R*,2*S*,4*R*)-**IIIbmb** (red).

Subsequently, we evaluated if the positive effect on the helix stabilization of the aryl group of the **IIIb** can be attributed to an electronic effect, due its aromatic nature, or to a simple steric effect. Therefore, we compared the folding behavior of peptide **11** (cCTAA = (1*R*,2*S*,4*R*)-**IIIb**) with that of a model peptide containing the hypothetical cCTAA (1*R*,2*S*,4*R*)-**Vbdm**, bearing a methyl group at C5 and C6 (Figure 5.8). Cluster and DSSP analyses showed an improvement of about 7% in both $pop_{h\%}$ and $h_{\%}$ of (1*R*,2*S*,4*R*)-**Vbdm** compared to (1*R*,2*S*,4*R*)-**Vb**, with the former having a behavior equivalent to that of (1*R*,2*S*,4*R*)-**IIIb**. Furthermore, the PMF profiles of (1*R*,2*S*,4*R*)-**Vbdm** and (1*R*,2*S*,4*R*)-**IIIb** are closely related, although those of (1*R*,2*S*,4*R*)-**Vbdm** show a more limited conformational freedom (Figure 5.14), which can be attributed to the higher steric hindrance parallel to the z axis (Figure 5.11B).

A rather high helical amount, with $pop_{h\%}$ and $h_{\%}$ only 5% lower than those of peptide **11** (cCTTA = (1*R*,2*S*,4*R*)-**IIIb**), was observed for peptide **7**, containing (*R*)-**VI**. From Figure 5.15A and C it can be noticed that only the saturated ring of the tetrahydrocarbazole moiety of (*R*)-**VI** is located in the (+x, +y, -z) sector, with the remaining part of its side chain lying in the (-x, +y, -z) area. In addition, PMF profiles of peptide **7** reproduce those of peptide **11**, although lower ΔE_M and $\Delta E_M^{\ddagger}$ together with an increased population in the β-strand region can be observed (Figure 5.14). Consistently, the folding behavior of peptide **4**, whose $pop_{h\%}$ and $h_{\%}$ are about 10% lower than those of peptide **11**, can be ascribed to the positioning of its benzoxanorbornene core in the (-x, +y, -z) area (Figure 5.15).

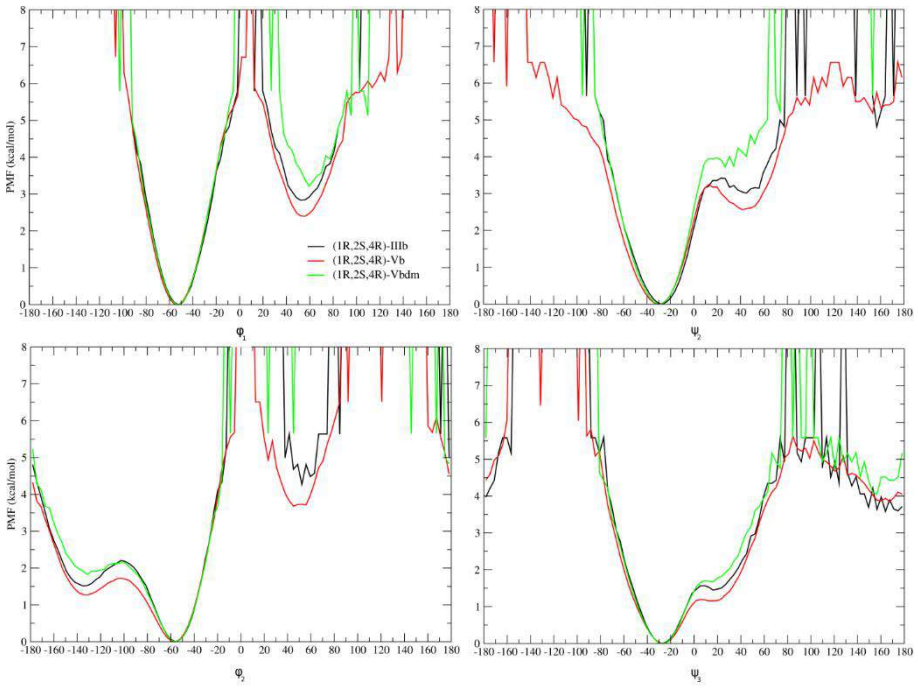

Figure 5.14. Comparison of PMF profiles, as a function of φ_1, ψ_2, φ_2 and ψ_3 dihedrals, of peptides containing (1*R*,2*S*,4*R*)-**IIIb** (black), (1*R*,2*S*,4*R*)-**Vb** (red) and (1*R*,2*S*,4*R*)-**Vbdm** (green).

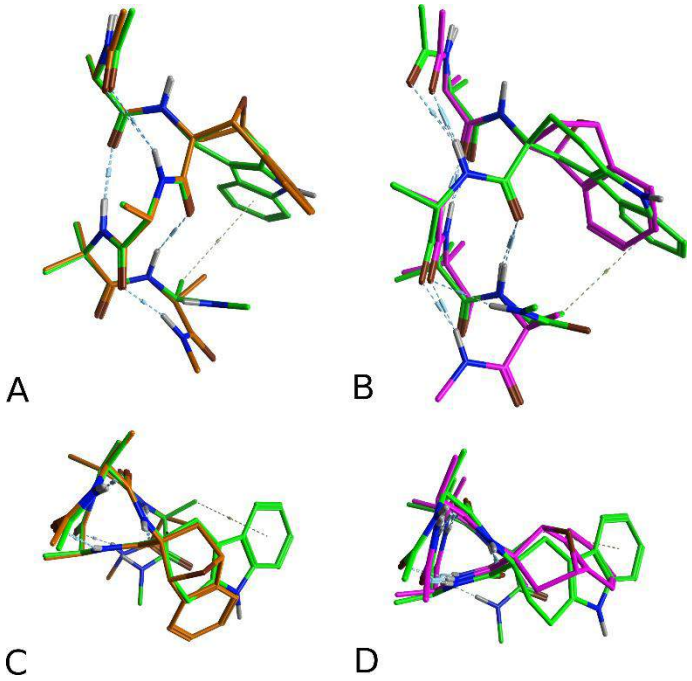

Figure 5.15. Front (A, B) and top (C, D) views of superimposed right-handed 3_{10}-helices of peptides **7** ((*R*)-**VI**; green), **11** ((1*R*,2*S*,4*R*,)-**IIIb**; orange) and **4** ((1*S*,2*R*,4*S*)-**IIIb**;magenta).

Steric hindrance by itself, however, is not enough to explain why structurally unrelated cCTAAs, such as (*R*)-**VI**, (*R*)-**II** and (1*R*,2*R*,4*R*)-**V** ($h_{\%}$ = 84.1, 85.8, and 82.9, respectively) behave similarly, and why related cCTAAs, such as (1*S*,2*R*,4*R*)-**IV** and (1*R*,2*R*,4*R*)-**V** have significantly different stabilizing effects ($h_{\%}$ = 56.5 and 82.9, respectively).

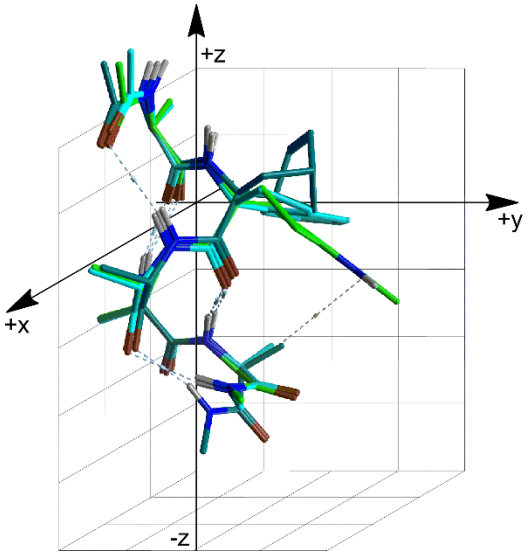

Figure 5.15. Superimposed right-handed 3_{10}-helices of peptides **2** ((*R*)-**II**; cyan), **6** ((1*R*,2*R*,4*R*)-**V**; blue) and **7** ((*R*)-**VI**; green) in the Cartesian space.

Indeed, (*R*)-**VI**, (*R*)-**II** and (1*R*,2*R*,4*R*)-**V** have their bulky groups lying in different regions of the Cartesian space (Figure 5.16), with only (*R*)-**VI** side chain being partially located in the (+x, +y, -z) sector. Conversely, the side chain of (1*R*,2*R*,4*R*)-**V** is lying in the (-x, +y, +z) sector, which should not affect the helix stabilization, whereas the indane moiety of (*R*)-**II** is located on the +y axis.

Therefore, other mechanism might be affecting the helix stabilization. Since differences in the H-bond networks were found to affect helix stability in natural peptides,[214,222] we employed QTAIM calculations to evidence and evaluate the differences in H-bonding, considering both classical and weak H-bonds, in the peptides studied here.

For all the peptides, focusing on the *P*-helix conformation, the BCP network comprises the helical $i+3 \rightarrow i$ N-H···O=C BCPs with $\rho(r_c)$ in the range of classical H-bonds (0.002 – 0.022 au),[223,224] a positive Laplacian, indicating an electrostatic interaction, and a low ε, proving the stability of H-bonds. Furthermore, Cβ-H···O=C $i+3 \rightarrow i$ BCPs, observed also in natural peptides,[214,222] with $\rho(r_c)$ of 0.003 – 0.009 au were detected. In addition, in both helical and extended conformations (Table 5.11), it can be observed the presence of an additional Aib4 → Ala3 Cβ-H···O=C BCP (Figure 4.16) with a $\rho(r_c)$ = 0.011 – 0.012 au, a quite high value for a C-H···O interaction involving a hydrogen bound to a sp^3 carbon.

Some of the considered peptides, in the *P*-helical conformation, have peculiar BCP networks which can explain well the particular behaviors of (*R*)-**II**, (1*R*,2*R*,4*R*)-**V** and (*R*)-**VI** (Tables 5.5, 5.6 and 5.10). For example, peptide **7** (cCTAA = (*R*)-**VI**) has only the BCP network typical of helical secondary structures (Table 5.5), with a $\sum\rho(r_c)$ = 0.1002 au. Conversely, peptide **6** (cCTAA = (1*R*,2*R*,4*R*)-**V**) has an additional intra-residue C-H···O=C BCP involving the methylene C7-H and the backbone carbonyl group of the cCTAA with a $\rho(r_c)$ = 0.0135 au, corresponding to a strong H-bond (Figure 5.17 and Table 5.6).

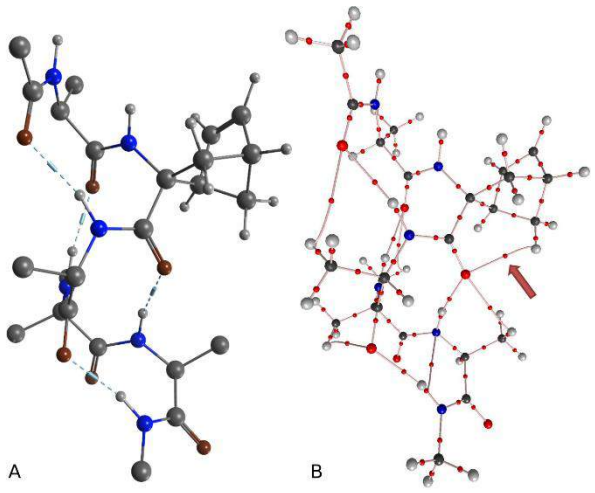

Figure 5.17. (A) Ball and stick representation and (B) QTAIM molecular graph of the optimized right-handed 3_{10}-helical conformation of Ac-Ala-(1*R*,2*R*,4*R*)-**V**-Ala-Aib-Ala-NHMe. The red arrow indicates the intra-residue C-H···O.

This H-bond constrains the ψ_2 dihedral to a value corresponding to a *P*-helix, thus providing an additional stabilization to the helical secondary structure of peptide **6**. This particular C-H···O=C H-bond can also be observed in the X-ray structure of an Ala-Aib pentapeptide containing at position 2 a β-benzylsulfanylnorbornene cCTAA.[87,225]

In addition, a $\Delta\sum\rho(r_c)$ = 0.0153 au, which can be compared to the electronic density of a single H-bond, can be observed between peptide **6** and **7** indicating that the strong helical stabilizing ability of (1*R*,2*R*,4*R*)-**V** is due to a strengthening of the H-bond network. Indeed, it has been showed that $\Delta\sum\rho(r_c)$ of about 0.0020 au is enough to explain differences in the helical stabilization exerted by natural AAs.[226]

Table 5.5. Types and properties of BCPs for the Ala-(*R*)-**VI**-Ala-Aib-Ala peptide **7** in the *P*- 3_{10}-helical conformation. All parameters are reported in a.u.

N-H···O BCP	**$\rho(r_c)$**	**λ_1**	**λ_2**	**λ_3**	**$\nabla^2\rho(r_c)$**	**ε**
Ala3···ACE	0.0187	-0.0217	-0.0205	0.1000	0.0578	0.0585
Aib4···Ala1	0.0198	-0.0233	-0.0219	0.1076	0.0624	0.0639
Ala5···VI	0.0196	-0.0229	-0.0217	0.1062	0.0616	0.0553
NME···Ala3	0.0217	-0.0264	-0.0248	0.1193	0.0681	0.0645
$\Sigma\rho(r_c)$ at N-H···O	0.0798				0.2499	
Cβ-H···O BCP						
Ala3···ACE	0.0048	-0.0030	-0.0022	0.0242	0.0190	0.3636
Aib4···Ala3	0.0113	-0.0097	-0.0058	0.0562	0.0407	0.6724
Ala5···VI	0.0043	-0.0032	-0.0022	0.0227	0.0173	0.4545
$\Sigma\rho(r_c)$ at C-H···O	0.0204				0.0770	
$\Sigma\rho(r_c)$ tot	**0.1002**				0.3269	

Table 5.6. Types and properties of BCPs for peptides **5** and **6** in the *P*-3_{10}-helical conformation. All the parameters are reported in a.u.

peptide 5; (1*S*,2*R*,4*R*)-**IV**				**peptide 6**; (1*R*,2*R*,4*R*)-**V**			
N-H···O BCP	$\rho(r_c)$	$\nabla^2\rho(r_c)$	ε	N-H···O BCP	$\rho(r_c)$	$\nabla^2\rho(r_c)$	ε

Ala3···Ac	0.0176	0.0542	0.0579	Ala3···Ac	0.0174	0.0536	0.0535
Aib4···Ala1	0.0181	0.0562	0.0619	Aib4···Ala1	0.0191	0.0598	0.0622
Ala5···IV	0.0190	0.0593	0.0580	Ala5···V	0.0193	0.0602	0.0566
NHMe···Ala3	0.0191	0.0594	0.0616	NHMe···Ala3	0.0195	0.0606	0.0599
Σρ(r$_c$) at N-H···O	0.0738				0.0753		
C$_\beta$-H···O BCP				**C$_\beta$-H···O BCP**			
Ala3···Ac	0.0045	0.0178	0.3684	Ala3···Ac	0.0045	0.0179	0.3684
Aib4···Ala1	0.0055	0.0218	0.7647	Aib4···Ala1	0.0056	0.0223	0.7222
Aib4···Ala3	0.0117	0.0419	0.5373	Aib4···Ala3	0.0119	0.0425	0.5000
IV···IV*	0.0126	0.0449	0.4868	V···V*	0.0135	0.0476	0.3298
Ala5···IV	0.0046	0.0181	0.3600	Ala5···V	0.0047	0.0184	0.3077
Σρ(r$_c$) at C-H···O	0.0389				0.0402		
Σρ(r$_c$) tot	**0.1127**				**0.1155**		

*The donor group is C5-H.

Differences in the strength of the BCP networks can also explain why (1*R*,2*R*,4*R*)-**IIIa** has a worse performance than (1*R*,2*R*,4*R*)-**V** (Table 5.1), although their side chains occupy the same area of the Cartesian space. Indeed, the C-H···O=C BCP found in peptide **6** cannot be observed in peptide **3** and its $\sum \rho(r_c)$ is 0.0131 au less than that of peptide **6** (Table 5.7). Analogous considerations are valid for the comparison of the behaviors of peptide **6** and that containing the hypotetical cCTAA (1*R*,2*R*,4*R*)-**IIIawr** (Tables 5.6 and 5.8).

Table 5.7. Types and properties of BCPs for the Ala-(1*R*,2*R*,4*R*)-**IIIa**-Ala-Aib-Ala peptide **3** in the *P*- 3_{10}-helical conformation. All parameters are reported in a.u.

N-H···O BCPs	**ρ(r$_c$)**	**λ$_1$**	**λ$_2$**	**λ$_3$**	**$\nabla^2\rho(r_c)$**	**ε**
Ala3···ACE	0.0213	-0.0257	-0.0242	0.1160	0.0661	0.0620
Aib4···Ala1	0.0179	-0.0204	-0.0192	0.0951	0.0555	0.0625
Ala5···IIIa	0.0212	-0.0254	-0.0239	0.1167	0.0674	0.0628
NME···Ala3	0.0212	-0.0255	-0.0240	0.1160	0.0665	0.0625
Σρ(r$_c$) at N-H···O	0.0816					
C$_\beta$-H···O BCP						
Ala3···ACE	0.0051	-0.0026	-0.0017	0.0245	0.0202	0.5294
Aib4···Ala3	0.0111	-0.0094	-0.0056	0.0549	0.0399	0.6786
Ala5···IIIa	0.0046	-0.0034	-0.0023	0.0238	0.0181	0.4783
Σρ(r$_c$) at C-H···O	0.0208					
Σρ(r$_c$) tot	**0.1024**					

Table 5.8. Types and properties of BCPs for the Ala-(1*R*,2*R*,4*R*)-**IIIawr**-Ala-Aib-Ala peptide in the *P*-3_{10}-helical conformation. All parameters are reported in a.u.

N-H···O BCPs	**ρ(r$_c$)**	**λ$_1$**	**λ$_2$**	**λ$_3$**	**$\nabla^2\rho(r_c)$**	**ε**
Ala3···ACE	0.0147	-0.0147	-0.0133	0.0775	0.0495	0.1053
Ala5···Ala1	0.0122	-0.0127	-0.0119	0.0686	0.0440	0.0672
Ala5···IIIawr	0.0030	-0.0014	-0.0011	0.0152	0.0127	0.2727
NME···Ala3	0.0208	-0.0250	-0.0234	0.1131	0.0647	0.0684

Aib4···ACE	0.0181	-0.0205	-0.0197	0.0999	0.0597	0.0406
Σρ(r$_c$) at N-H···O	0.0688					
C$_\beta$-H···O BCP						
Ala3···ACE	0.0059	-0.0048	-0.0040	0.0301	0.0213	0.2000
Aib4···Ala1	0.0086	-0.0076	-0.0072	0.0433	0.0285	0.0556
Aib4···Ala3	0.0110	-0.0091	-0.0051	0.0541	0.0399	0.7843
Ala5···IIIawr	0.0025	-0.0016	-0.0012	0.0119	0.0091	0.3333
Σρ(r$_c$) at C-H···O	0.0280					
backbone N···O BCPs						
Aib4···Ala1	0.0076	-0.0047	-0.0029	0.0318	0.0242	0.6207
Σρ(r$_c$) tot	**0.1044**					

In addition, the substitution of the oxygen at position 7 of the (1*R*,2*R*,4*R*)-**IIIa** benzoxanorbornene core by a methylene group (Figure 5.8) seems not to affect helix stability. Indeed, QTAIM analysis of the *P*-helix conformation of the peptide containing (1*R*,2*R*,4*R*)-**IIIamb**, gave a $\sum \rho(r_c)$ equivalent to that of peptide **6** (Tables 5.6 and 5.9) and an intra-residue C-H···O=C BCP, involving the cCTAA, with a $\rho(r_c)$ = 0.0137 au. Therefore, this cCTAA resulted to be as strong as (1*R*,2*R*,4*R*)-**V** in stabilizing the helical secondary structure (Tables 5.1 and 5.4).

Table 5.9. Types and properties of BCPs for the Ala-(1*R*,2*R*,4*R*)-**IIIamb**-Ala-Aib-Ala peptide in the *P*-3$_{10}$-helical conformation. All parameters are reported in au.

N-H···O BCPs	**ρ(r$_c$)**	**λ$_1$**	**λ$_2$**	**λ$_3$**	**$\nabla^2\rho(r_c)$**	**ε**
Ala3···ACE	0.0198	-0.0233	-0.0220	0.1065	0.0612	0.0591
Aib4···Ala1	0.0191	-0.0221	-0.0208	0.1023	0.0594	0.0625
Ala5···IIIamb	0.0174	-0.0197	-0.0186	0.0927	0.0544	0.0591
NME···Ala3	0.0200	-0.0237	-0.0224	0.1084	0.0623	0.0580
Σρ(r$_c$) at N-H···O	0.0763					
C$_\beta$-H···O BCP						
Ala3···ACE	0.0048	-0.0028	-0.0020	0.0241	0.0193	0.4000
Aib4···Ala1	0.0057	-0.0033	-0.0018	0.0281	0.0230	0.8333
Aib4···Ala3	0.0116	-0.0101	-0.0064	0.0580	0.0415	0.5781
IIIamb···IIIamb*	0.0137	-0.0128	-0.0093	0.0708	0.0487	0.3763
Ala5···ONBmb2	0.0045	-0.0033	-0.0024	0.0234	0.0177	0.3750
Σρ(r$_c$) at C-H···O	0.0403					
Σρ(r$_c$) tot	**0.1166**					

*The donor group is C5-H.

QTAIM analysis performed on peptide **2** (cCTAA = (*R*)-**II**) resulted in a $\sum \rho(r_c)$ = 0.1150 au and showed a peculiar and strong ($\rho(r_c)$ = 0.0110 au) *i*+ *1* → *i* C-H···O=C BCP between C7-H of the cCTAA aromatic ring and the carbonyl group of Ala1 (Table 5.10). Therefore, (*R*)-**II** exerts its helical stabilizing effect through the combination of its steric hindrance and this additional C-H···O=C H-bond, although neither of the two features are fully satisfied. Indeed, the steric hindrance of this cCTAA is mainly located in the (+x, +y, 0) sector while the $\rho(r_c)$ of the just described BCP is slightly

lower than that observed for (1*R*,2*R*,4*R*)-**V**. In addition, the PMF(φ_1) and PMF(ψ_2) profiles of peptides **6** and **7** (cCTAAs = (1*R*,2*R*,4*R*)-**V** and (*R*)-**II**, respectively) are different, probably because of the ability of (1*R*,2*R*,4*R*)-**V** to form an intra-cCTAA interaction, while (*R*)-**II** is involved in a C-H···O=C interaction with Ala1, resulting in a wider conformational freedom of the cCTAA backbone.

Table 5.10. Types and properties of BCPs for the Ala-(*R*)-**II**-Ala-Aib-Ala peptide **2** in the *P*-3_{10}-helical conformation. All parameters are reported in au.

N-H···O BCP	**$\rho(r_c)$**	**λ_1**	**λ_2**	**λ_3**	**$\nabla^2\rho(r_c)$**	**ε**
Ala3···ACE	0.0197	-0.0233	-0.0219	0.1062	0.0610	0.0639
Aib4···Ala1	0.0207	-0.0246	-0.0232	0.1142	0.0664	0.0603
Ala5···II	0.0210	-0.0251	-0.0237	0.1153	0.0665	0.0591
NME···Ala3	0.0210	-0.0253	-0.0239	0.1152	0.0660	0.0586
$\Sigma\rho$(rc) at N-H···O	0.0824					
C_β-H···O BCP						
Aib4···Ala1	0.0052	-0.0022	-0.0012	0.0245	0.0211	0.8333
Aib4···Ala3	0.0114	-0.0099	-0.0062	0.0569	0.0408	0.5968
Ala5···II	0.0049	-0.0036	-0.0027	0.0258	0.0195	0.3333
(C_{ring}-H)II···Ala1	0.0111	-0.0103	-0.0093	0.0588	0.0392	0.1075
$\Sigma\rho(r_c)$ at C-H···O	0.0326					
$\Sigma\rho(r_c)$ tot	**0.1150**					

The explanation of the differences in the helix stabilizing ability between the structurally related (1*S*,2*R*,4*R*)-**IV** and (1*R*,2*R*,4*R*)-**V** required the analysis of additional conformations. Indeed, peptide **5** (cCTAA = (1*S*,2*R*,4*R*)-**IV**) has a $pop_{h\%}$ and $h_{\%}$ about 20% lower than peptide **6** (cCTAA = (1*R*,2*R*,4*R*)-**V**) and peptide **12**, containing the (1*R*,2*S*,4*S*)-**IV** enantiomer, folds into a *M*-helix, while peptide **13**, containing (1*S*,2*S*,4*S*)-**V**, folds into a *P*-helix (Table 5.1).

PMF(φ_1) and PMF(ψ_2) profiles of peptide **5** have ΔE_M and $\Delta E_M^{\ddagger}$ (Figure 5.6) of about 1 and 1.5 kcal/mol lower than those of peptide **6**, while PMF(φ_2) and PMF(ψ_3) profiles of peptide **5** show a reduction in both ΔE_M and $\Delta E_M^{\ddagger}$ between the minima corresponding to helical conformations and in the $\Delta E^{\ddagger}$ between the helical and the extended conformations (Figure 5.5) and the ψ_3 is accessible for the whole ±180° interval.

At the light of this, the lower helix stabilization ability of (1*S*,2*R*,4*R*)-**IV** can be ascribed to a reduced stabilization of the *P*-helix and/or to an increased stabilization of the extended conformation, compared to the related (1*R*,2*R*,4*R*)-**V**.

Table 5.11. Types and properties (a.u.) of BCPs for peptides **5** and **6** in the extended conformation.

peptide 5; (1*S*,2*R*,4*R*)-IV				**peptide 6**; (1*R*,2*R*,4*R*)-V			
N-H···O BCPs	**$\rho(r_c)$**	**$\nabla^2\rho(r_c)$**	**ε**	**N-H···O BCPs**	**$\rho(r_c)$**	**$\nabla^2\rho(r_c)$**	**ε**
Ala1···Ala1	0.0215	0.0914	0.9231	Ala1···Ala1	0.0215	0.0912	0.8992
Ala3···Ala3	0.0226	0.0928	0.7113	Ala3···Ala3	0.0221	0.0918	0.7879
Aib4···Aib4	0.0273	0.1047	0.3115	Aib4···Aib4	0.0276	0.0788	0.3012
Ala5···Ala5	0.0225	0.0921	0.6993	Ala5···Ala5	0.0223	0.0919	0.7299

$\Sigma\rho(r_c)$ at N-H···O	0.0939				0.0935		
C-H···O BCPs				**C-H···O BCPs**			
IV (C_α)···Ala1	0.0173	0.0588	0.1548	V (C_α)···Ala1	0.0198	0.0655	0.0950
IV (C5)···Ala1	0.0092	0.0331	0.1905				
Aib4(C_β)···Ala3	0.0119	0.0421	0.3210	Aib4(C_β)···Ala3	0.0122	0.0430	0.2727
Aib4(C_β)···Ala4	0.0121	0.0426	0.3059	Aib4(C_β)···Ala4	0.0116	0.0411	0.3377
$\Sigma\rho(r_c)$ at C-H···O	0.0505				0.0436		
$\Sigma\rho(r_c)$ tot	**0.1444**				**0.1371**		

QTAIM analyses on the *P*-helix of peptides **5** and **6** resulted in qualitatively similar BCPs (Table 5.6), however the BCP network of the latter peptide turned out to be of about 0.0030 au stronger than that of peptide **5**, which has been already considered significant to explain the different helix stabilization propensities of natural AAs).[214] On the other hand, QTAIM analyses performed on the extended conformations of the same peptides (Table 5.11) showed a $\Delta\sum\rho(r_c)$ = 0.0073 au in favor of peptide **5**, because its BCP network is characterized by the presence of an additional C-H···O=C interaction between C5-H and Ala1, which is lacking in the extended conformation of peptide **6** (Figure 5.18). Consequently, the extended conformation of peptide **5** is relatively more stable than that of peptide **6**.

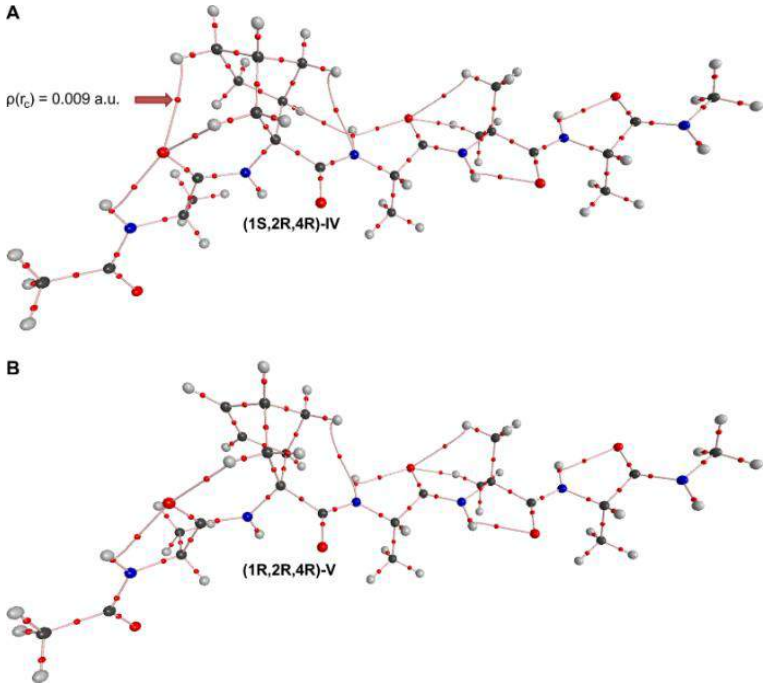

Figure 5.18. QTAIM molecular graph of the optimized extended conformation of Ac-Ala-(1*S*,2*R*,4*R*)-**IV**-Ala-Aib-Ala-NHMe (A) and Ac-Ala-(1*R*,2*R*,4*R*)-**V**-Ala-Aib-Ala-NHMe (B). The red arrow indicates the additional C-H···O observed for the norbornane CTAA -(1*S*,2*R*,4*R*)-**IV**.

It has to be underlined that, although the $\sum\rho(r_c)$ are higher for the extended conformations than for the *P*-helices, the BCPs of the extended structures have also higher ε, indicating a lower stability of

these interactions if compared to those of the helical conformations and a preference for the helix in both cases.

QTAIM analysis can also explain why (1*R*,2*S*,4*S*)-**IV** stabilizes the *M*-helix, while (1*S*,2*S*,4*S*)-**V**, like its enantiomer, stabilizes the *P*-helix.[123] Indeed, peptide **12** (cCTAA = (1*R*,2*S*,4*S*)-**IV**) has a $\Delta \sum \rho(r_c)$ between *M*- and *P*-helix of 0.0035 au in favor of the *M*-helix (Table 4.12). Moreover, the *M*-helix conformation has a strong BCP network, although the number of BCP is lower than that of the *P*-helix. On the contrary, peptide **13** (cCTAA = (1*S*,2*S*,4*S*)-**V**) BCP network indicates that the *P*-helix is favored of 0.0059 au compared to the *M*-helix (Table 5.13).

Table 5.12. Types and properties of BCPs for the Ala-(1R,2S,4S)-**IV**-Ala-Aib-Ala peptide **12** in the *P*- and *M*- 3_{10}-helical conformation. All parameters are reported in au.

peptide **12**, ***P*-helix**				peptide **12**, ***M*-helix**			
N-H···O BCP	**$\rho(r_c)$**	**$\nabla^2\rho(r_c)$**	**ε**	**N-H···O BCP**	**$\rho(r_c)$**	**$\nabla^2\rho(r_c)$**	**ε**
Ala3···ACE	0.0200	0.0621	0.0580	Ala3···ACE	0.0231	0.0736	0.0672
Aib4···Ala1	0.0179	0.0551	0.0628	Aib4···Ala1	0.0179	0.0558	0.0567
Ala5···IV	0.0191	0.0598	0.0622	Ala5···IV	0.0223	0.0715	0.0664
NME···Ala3	0.0207	0.0647	0.0601	NME···Ala3	0.0227	0.0726	0.0646
$\Sigma\rho(r_c)$ at N-H···O	0.0777			**$\Sigma\rho(r_c)$ at N-H···O**	0.0860		
C_β-H···O BCP				**C_β-H···O BCP**			
Ala3···ACE	0.0050	0.0197	0.3636	Aib4···Ala3	0.0109	0.0395	0.9362
Aib4···Ala1	0.0054	0.0213	0.8125	IV···IV*	0.0128	0.0453	0.4557
Aib4···Ala3	0.0120	0.0428	0.4930	Ala5···Aib4	0.0107	0.0389	0.8958
IV···IV*	0.0123	0.0435	0.1875				
Ala5···IV	0.0045	0.0177	0.3750				
$\Sigma\rho(r_c)$ at C-H···O	0.0392			**$\Sigma\rho(r_c)$ at C-H···O**	0.0344		
$\Sigma\rho(r_c)$ tot	**0.1169**			**$\Sigma\rho(r_c)$ tot**	**0.1204**		

*The donor group is C5-H, the acceptor is C=O

Table 5.13. Types and properties of BCPs for the Ala-(1S,2S,4S)-**V**-Ala-Aib-Ala peptide **13** in the *P*- and *M*-3_{10}-helical conformation. All parameters are reported in au.

Peptide **13**, ***P*-helix**				Peptide **13**, ***M*-helix**			
N-H···O BCP	**$\rho(r_c)$**	**$\nabla^2\rho(r_c)$**	**ε**	**N-H···O BCP**	**$\rho(r_c)$**	**$\nabla^2\rho(r_c)$**	**ε**
Ala3···ACE	0.0197	0.0610	0.0594	Ala3···ACE	0.0225	0.0715	0.0615
Aib4···Ala1	0.0189	0.0587	0.0580	Aib4···Ala1	0.0193	0.0603	0.0610
Ala5···V	0.0181	0.0562	0.0564	Ala5···V	0.0220	0.0702	0.0677
NME···Ala3	0.0207	0.0646	0.0598	NME···Ala3	0.0229	0.0735	0.0639
$\Sigma\rho(r_c)$ at N-H···O	0.0774			**$\Sigma\rho(r_c)$ at N-H···O**	0.0867		
C_β-H···O BCP				**C_β-H···O BCP**			
Ala3···ACE	0.0050	0.0196	0.3478	V···V*	0.0140	0.0489	0.3069
Aib4···Ala1	0.0054	0.0217	0.8125	Ala5···Aib4	0.0107	0.0388	0.8958
Aib4···Ala3	0.0121	0.0432	0.5000				
V···V*	0.0129	0.0436	0.1818				
Ala5···V	0.0045	0.0178	0.3200				

$\Sigma\rho(r_c)$ at C-H···O	0.0399	**$\Sigma\rho(r_c)$ at C-H···O**	0.0247
$\Sigma\rho(r_c)$ tot	**0.1173**	**$\Sigma\rho(r_c)$ tot**	**0.1114**

*The donor group is C5-H.

Summarizing, two complementary mechanisms can contribute to the helix stabilization by reducing the backbone conformational freedom: the first depends on the steric hindrance exerted by the cCTAA in an area parallel to the peptide helix axis and downstream of the cCTAA itself, whereas the second consists in the strengthening of the helical H-bond network thanks to peculiar C-H···O=C interactions. Therefore, this knowledge can be exploited to design peptides folding into stable helices, although the choice has to be accompanied by the knowledge of the structural requirements for the cCTAA side chain.

5.3 Materials and Methods

REMD simulations. CTAAs were designed using MOE,[227] capped respectively with an acetyl (Ac) and a NHMe group at the N- and C-termini and submitted to a "Low Mode" conformational search (MMFF94x force field, Born solvation, iteration limit = 40000, MM iteration limit = 2500, rejection limit = 500). The two lowest energy conformations having φ and ψ dihedrals matching a right- or a left-handed helix (φ = ±60°, ψ = ±45°) were selected to derive partial charges with the R.E.D.IV software.[228] Each geometry was optimized at the HF/6-31G(d) level and two different spatial orientations were used to derive orientation- and conformation-independent RESP-A1 charges. Charge restraints of −0.4157, 0.2719, 0.5973 and −0.5679 were imposed to the backbone nitrogen, hydrogen, carbonyl carbon and oxygen, respectively, as observed for standard AAs in the AMBER ff99SB force field.[141]

REMD simulations were carried out on each Ac-L-Ala-CTAA-L-Ala-Aib-L-Ala-NHMe peptide by starting from an extended conformation (ψ=φ=ω= 180°). 12 replicas were run at temperatures from 260.00 to 658.94 K, using the ff99SB/GB-OBC(II)[172] force field and solvent model combination with a simulation time of 250 ns per replica, for a total of 3 μs of simulation for each peptide. REMD simulations were conducted with the pmemd module of the Amber12 suite. The trajectories were extracted at 308.53 K, unless stated otherwise. The simulation convergence was assessed on the basis of cluster analyses performed at 50-100, 100-150, 150-200 and 200-250 ns time intervals. We considered a simulation converged when the standard deviation of the main cluster population ($\sigma_{pop\%}$), averaged with respect to the different intervals, was below 5%. Cluster analyses were performed with ptraj by using the average-linkage algorithm and by sampling one every four frames.[192] The pairwise mass-weighted root mean squared displacement (RMSD) on Cα was used as a metric and a total of five clusters were requested on the basis of pseudo-F statistics and SSR/SST ratio.[229] Secondary structure analyses were performed by DSSP[230] on the 50-250 ns trajectories every Δt = 50 ns, coherently with cluster analyses, using the ptraj "secstruct" command. H-bonds were analyzed with

VMD 1.9.1[231] over the whole 250 ns trajectory, with a donor−acceptor distance threshold of 4.0 Å and an angle cutoff of 30°. Only H-bonds with an occupancy ($occ_{\%}$) greater than 5% were considered.

Mono and bidimensional (2D) Potentials of Mean Force (PMF) were obtained with Amber software coupled with the Weighted Histogram Analysis Method (WHAM) and WHAM-2d,[232] respectively. PMF were calculated over the 250 ns trajectory by setting a histogram limit of ±180°, 100 bins and a tolerance of 0.01. Selected dihedrals (*φ1*, *φ2*, *ψ2* and *ψ3*, accordingly to Figure 4.2) were obtained from the REMD trajectories at 260, 283, 308 and 335 K.

QTAIM calculations. Selected geometries were fully optimized with Gaussian09[233] at the MPWB95/6-31+G(d,p) level,[234] a method that had proved reliable in previous studies from our group,[235] with the CPCM solvation model for water.[236] Vibrational analyses were performed at the same level to confirm optimized geometries as a minimum (no imaginary frequencies observed) (Annex 5.A). QTAIM calculations were performed with AIM2000 on the obtained wave functions.[237] The maximum number of Newton iterations and the step-size were set to 400 and 0.5, respectively, while other parameters were left as default. N-H···O, C-H···O and backbone N···O BCPs were analyzed and $\rho(r_c)$, the sign of the Laplacian, and ellipticity (ε) were used to characterize the BCP network in terms of strength, type and stability of each BCP. BCPs with ε > 1 were considered as unstable and consequently discarded.

6 ORIGIN OF HELIX SCREW SENSE SELECTIVITY BY cCTAAS IN AIB-BASED PEPTIDES

6.1 INTRODUCTION

It has just been underlined that enantiomers of cCTAAs can differently affect the stabilization of the helical secondary structure. These differences can be poor, as in the case of (1*R*,2*R*,4*R*)-**IIIa** and its enantiomer (1*S*,2*S*,4*S*)-**IIIa** (Table 5.1), or dramatic, as observed for the (1*S*,2*R*,4*R*)-**IV** and (1*R*,2*S*,4*S*)-**IV** enantiomers, where the former stabilizes the *P*-helix and the latter the *M*-helix in the (L)-Ala-Aib pentapeptide model.

The knowledge of the mentioned different behaviors can be exploited for the design of peptides with a desired handedness. Indeed, in some cases it has been observed that the inclusion of even one chiral α-AA can be sufficient to favor one screw sense in an otherwise achiral peptide.[94,207,209,210,238]

In literature several examples are reported where helices containing cCTAAs with a *R* configuration at Cα have a *P*-conformation, whereas cCTAAs with *S* configuration at Cα stabilize *M*-helices,[93,175,211,239,240] although some exceptions have been found.[241–244]

Therefore, it is important to clarify the rationale behind the screw sense selectivity, defined as the capability to preferentially stabilize a *P*- or a *M*-helix in a peptide. Thus, the same methods used for the investigation on helix stabilization (e.g. REMD simulations, PMF and QTAIM analysis) have been applied to study the helical screw sense selectivity following the inclusion of selected cCTAAs (Figure 6.1) in Ac-Aib$_2$-cCTAA-Aib$_2$-NHMe peptide models. This dataset does not include **I**, because it turned out to be a poor helical stabilizer, while other cCTAAs with a norbornane core substituted at C3 (e.g. **VII** and **VIII**) have been considered, because of the peculiarities observed for **IV** and **V** in the previous study.[72]

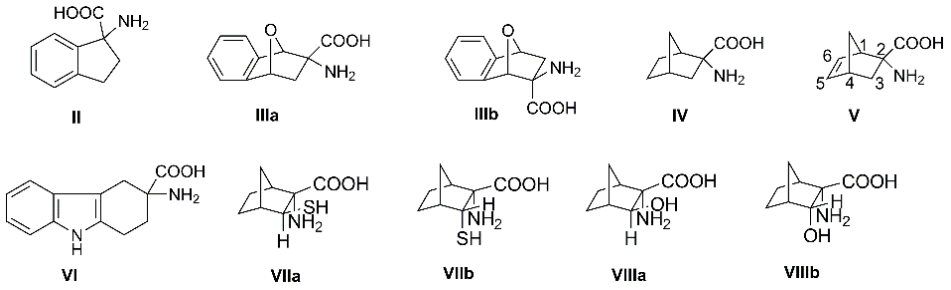

Figure 6.1. Selected cCTAAs used for the investigation of helical screw sense selectivity.

Our investigation was focused on the enantiomers found to be selective for the *P*-helix, because this screw sense is the most frequently observed in nature.[97,98]

We found that the helical screw sense selectivity toward the *P*-helix is enhanced by cCTAA steric hindrance in the (+x, +y, -z) and (-x, +y, +z) sectors of a right-handed 3D-Cartesian space (Figure 6.2), where the *P*-helix has the same position as in the previous study: the +z → -z axis correspond to the N → C helical axis and the Cα of the cCTAA lies on the +y axis (0, +y, 0). Analogous considerations are valid for the *M*-helical screw sense selectivity, with the cCTAA Cα lying on the (0, -y, 0) semiaxis.

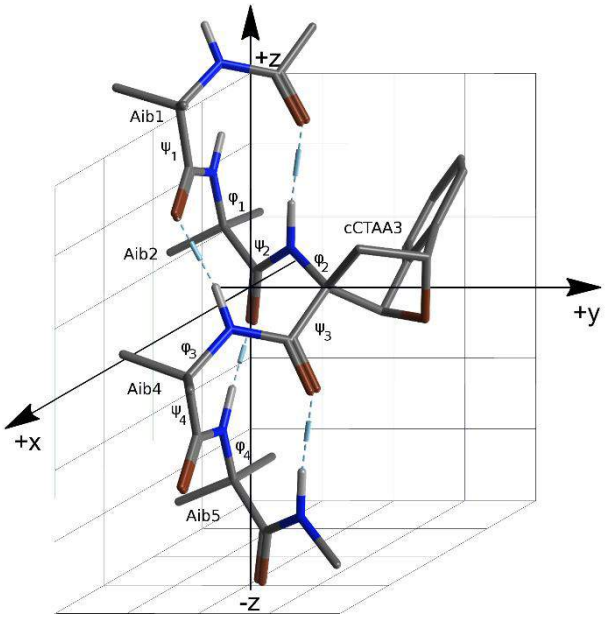

Figure 6.2. Representative geometry of the most populated cluster obtained from the analysis of the 308 K REMD trajectory of Ac-Aib$_2$-(1*R*,2*R*,4*R*)-**IIIa**-Aib$_2$-NHMe included in the 3D-Cartesian space used for the description.

Moreover, additional intramolecular C-H···O=C and backbone N···O interactions,[72,214,222] together with an overall stabilization or destabilization of noncovalent interactions within a defined conformer, can affect the helical screw sense selectivity exerted by cCTAAs. Taking the cue from the helical excess (h.e.) evaluated from NMR studies in fast and slow exchange régimes,[245] the percentage h.e. was here evaluated as the ratio (P% - M%)/(P% + M%), where P% and M% are the *P*- and the *M*-helical populations from cluster analysis of REMD simulations. In this way, a quantitative comparison of the screw sense preferences of the selected peptides was provided.[86]

In the following discussion, all the considered peptides are identified by an Arabic number preceded by *R* or *S* according to the Cα cCTAA stereochemistry. All the cCTAAs are indicated with their full stereochemical notation followed by the cCTAA name as showed in Figure 6.1.

6.2 Results and Discussion

Table 6.1. Average *P*-helical (P%) and *M*-helical (M%) populations[a], average global helical content (H%) and helical excess (h.e., %) obtained from cluster analyses of the 308 K REMD trajectories of Ac-Aib$_2$-cCTAA-Aib$_2$-NHMe peptides with a preference for the *P*-helix (***R*-1**, ***R*-2**, ***S*-3**, ***R*-4**, ***R*-5**, ***S*-6**, ***R*-7**, ***R*-8**, ***S*-9**, ***S*-10**) and **11**[b].

#	cCTAA[c]	P% ± SD	M% ± SD	H% ± SD	h.e. ± SD
***R*-1**	(*R*)-**II**	59.3±1.3	27.5±0.8	86.8±1.5	36.6±1.9
***R*-2**	(1*R*,2*R*,4*R*)-**IIIa**[d]	88.7±1.2	1.2±0.4	89.9±1.3	97.3±2.0
***S*-3**	(1*R*,2*S*,4*R*)-**IIIb**[d]	81.0±2.1	13.7±2.9	94.7±3.6	71.1±3.8
***R*-4**	(1*S*,2*R*,4*R*)-**IV**	83.2±0.9	4.7±0.3	87.9±0.9	89.3±1.4
***R*-5**	(1*R*,2*R*,4*R*)-**V**	76.6±3.0	12.8±2.4	89.4±3.8	71.4±5.3
***S*-6**	(*S*)-**VI**	76.7±3.1	15.2±3.3	91.9±4.5	66.9±4.9
***R*-7**	(1*S*,2*R*,3*S*,4*R*)-**VIIa**	60.1±2.6	n.a	60.1±2.6	100.0±6.1

***R*-8**	(1*S*,2*R*,3*R*,4*R*)-**VIIb**	78.4±2.0	9.9±1.4	83.3±2.4	77.6±3.5
***S*-9**	(1*S*,2*S*,3*S*,4*R*)-**VIIIa**	45.8±3.1	0.4±0.2	46.2±3.1	98.3±6.7
***S*-10**	(1*S*,2*S*,3*R*,4*R*)-**VIIIb**	85.2±0.9	3.7±0.7	88.9±1.1	91.7±1.3

[a]Averaged with respect to the 50-100, 100-150. 150-200, 200-250 ns time intervals. [b]For Ac-Aib_5-NHMe peptide **11** P% = 47.7 ± 3.1, M% = 43.3 ± 3.5, H% = 91.0 ± 4.7 and h.e. < 5%. [c]The stereochemical descriptors refers to the Cα configuration. [d]Experimental **IIIa**:**IIIb** ratio = 7:1.[198,246]

Table 6.2. Average *P*-helical (P%) and *M*-helical (M%) populations[a], average global helical content (H%) and helical excess (h.e., %) obtained from cluster analyses of the 308 K REMD trajectories of Ac-Aib_2-cCTAA-Aib_2-NHMe peptides with a preference for the *M*-helix (***S*-1**, ***S*-2**, ***R*-3**, ***S*-4**, ***S*-5**, ***R*-6**, ***S*-7**, ***S*-8**, ***R*-9**, ***R*-10**).

#	CTAAs[b]	P% ± SD	M% ± SD	H% ± SD	h.e.% ± SD
***S*-1**	(*S*)-**II**	27.0±1.6	60.2±2.1	87.2±2.6	-38.1±3.0
***S*-2**	(1*S*,2*S*,4*S*)-**IIIa**[d]	1.2±0.2	87.0±2.0	88.2±2.0	-97.3±2.3
***R*-3**	(1*S*,2*R*,4*S*)-**IIIb**[d]	13.5±1.1	81.7±1.9	95.2±2.2	-71.6±2.8
***S*-4**	(1*R*,2*S*,4*S*)-**IV**	5.3±0.7	80.7±1.1	86.0±1.3	-87.7±1.5
***S*-5**	(1*S*,2*S*,4*S*)-**V**	12.1±1.6	76.5±1.7	88.6±2.3	-72.7±2.6
***R*-6**	(*R*)-**VI**	15.9±3.4	75.8±3.6	91.7±5.0	-65.3±6.4
***S*-7**	(1*R*,2*S*,3*R*,4*S*)-**VIIa**	n.a	59.3±1.2	59.3±1.2	-100.0±2.0
***S*-8**	(1*R*,2*S*,3*S*,4*S*)-**VIIb**	12.8±2.3	75.9±1.5	88.7±2.7	-71.1±3.1
***R*-9**	(1*R*,2*R*,3*R*,4*S*)-**VIIIa**	0.2±0.06	41.4±2.0	41.6±2.0	-99.0±6.8
***R*-10**	(1*R*,2*R*,3*S*,4*S*)-**VIIIb**	3.2±0.6	86.0±1.6	89.2±1.7	-92.8±2.6

[a]Averaged with respect to the 50-100, 100-150. 150-200, 200-250 ns time intervals. [b]The stereochemical descriptors refers to the Cα configuration. [d]Experimental **IIIa**:**IIIb** ratio = 7:1.[198,246]

Cluster analysis of the 308 K REMD trajectories showed in all cases the presence of both *P*- and *M*-3_{10}-helices (Tables 6.1 and 6.2), except for peptides ***R*-7** and ***S*-7** (cCTAA = (1*S*,2*R*,3*S*,4*R*)-**VIIa** and (1*R*,2*S*,3*R*,4*S*)-**VIIa**, respectively), and ***R*-9** and ***S*-9** (cCTAA = (1*R*,2*R*,3*R*,4*S*)-**VIIIa** and (1*S*,2*S*,3*S*,4*R*)-**VIIIa**, respectively). Only the *P*-conformation was significantly sampled for ***R*-7** and ***S*-9** and only the *M*-helix was observed for ***S*-7** and ***R*-9**. This uncommon behavior resulted in a complete selectivity for one of the two helical screw senses (h.e. ~ 100%), but P% of peptides ***R*-7** and ***S*-9** and M% of peptides ***S*-7** and ***R*-9** were quite low if compared to those observed for the other peptides, a poor total helical amount (H%) was obtained (Tables 6.1 and 6.2). For the other peptides, H% was greater than 80%, confirming the good-to-excellent helical stabilizing properties of cCTAAs.[72]

For peptides reported in Table 6.1 (e.g. ***R*-1**, ***R*-2**, ***S*-3**, ***R*-4**, ***R*-5**, ***S*-6**, ***R*-7**, ***R*-8**, ***S*-9**, ***S*-10**) the representative structure of the most populated cluster was a *P*-helix, whereas, as expected, their stereoisomers (e.g. ***S*-1**, ***S*-2**, ***R*-3**, ***S*-4**, ***S*-5**, ***R*-6**, ***S*-7**, ***S*-8**, ***R*-9**, ***R*-10**; Table 6.2) had the opposite behavior. It is obvious that screw sense preference and Cα stereochemistry are somehow related, however the obtained data do not indicate any correlation between the absolute configuration of Cα and screw sense preference. Although, it has to be noted that opposite configurations, attributed on the

basis of a variation in formal Cahn – Ingold – Prelog priorities, do not always reflect a change in the spatial orientation of the physicochemical properties of Cα substituents. Thus, for example, peptides ***R*-7** and ***S*-9** have similar screw sense preferences but opposite Cα configurations. However, it can be observed that the norbornane cores of the two cCTAAs are perfectly superimposable, and the same is valid for ***R*-8** and ***S*-10**.

Therefore, focusing on *P*-helix inducers, except for peptides ***R*-7** and ***S*-9**, whose particular behavior has already been introduced, cluster analyses indicate that peptides ***R*-2**, ***S*-10**, and ***R*-4** (cCTAAs = (1*R*,2*R*,4*R*)-**IIIa**, (1*S*,2*S*,3*R*,4*R*)-**VIIIb**, and (1*S*,2*R*,4*R*)-**IV**, respectively) are the most selective toward the *P*-helix (h.e. = 97.3 ± 2.0, 91.7 ± 1.3, and 89.3 ± 1.4%, respectively). Conversely, the lowest selectivity was observed for peptide ***R*-1** (h.e. = 36.6 ± 1.9%), containing (*R*)-**II**, which, however, was a good helix stabilizer (Table 5.1),[72] suggesting that screw sense selectivity and helix stabilization exerted by cCTAAs might follow different mechanisms. As happened in the previous study, the structurally related cCTAAs (1*S*,2*R*,4*R*)-**IV** and (1*R*,2*R*,4*R*)-**V** showed highly different helical screw sense preferences, whose causes will be clarified in the following discussion.

2D-PMF as a function of φ_2-ψ_3 and φ_3-ψ_4 dihedrals pairs (Figures 6.3 and 6.4), which involve the cCTAA and cCTAA+1 residues, confirmed the results of cluster analysis and show the effect of the presence of the cCTAA on both the upstream and downstream dihedrals. In these profiles, it can be always observed the presence of a global and a local minimum. In most of the cases, the former corresponds to the *P*-helix, while the latter corresponds to the *M*-helix. As expected, the 2D-PMF profiles of the Aib pentamer (peptide **11**) presented 2 isoenergetic minima, whereas a low ΔE_M (the energy difference between the minima, Figure 5.6) was observed for peptide ***R*-1** in both the profiles, and only in PMF(φ_3-ψ_4) profiles for peptides ***R*-7** and ***S*-9**. On the other side, PMF(φ_3-ψ_4) profiles of these two peptides have the highest energy *M*-helix minimum with the narrowest well among those analyzed, and an additional minimum corresponding to a γ-turn (φ = +75°, ψ = -64°)[247] is observable. These results are consistent with the absence, for peptides ***R*-7** and ***S*-9,** of a significant *M*-helix population which is replaced by a well populated cluster (39.6 ± 2.6% and 53.5 ± 3.2 %, respectively) whose representative structure has a *P* screw sense upstream and a *M* screw sense downstream of the cCTAA (Figure 6.5). Therefore, it seems that both (1*S*,2*R*,3*S*,4*R*)-**VIIa** and (1*S*,2*S*,3*S*,4*R*)-**VIIIa** are able to stabilize the *P*-helix toward the N-terminus, but they do not seem to induce any screw sense preference toward the C-terminus.

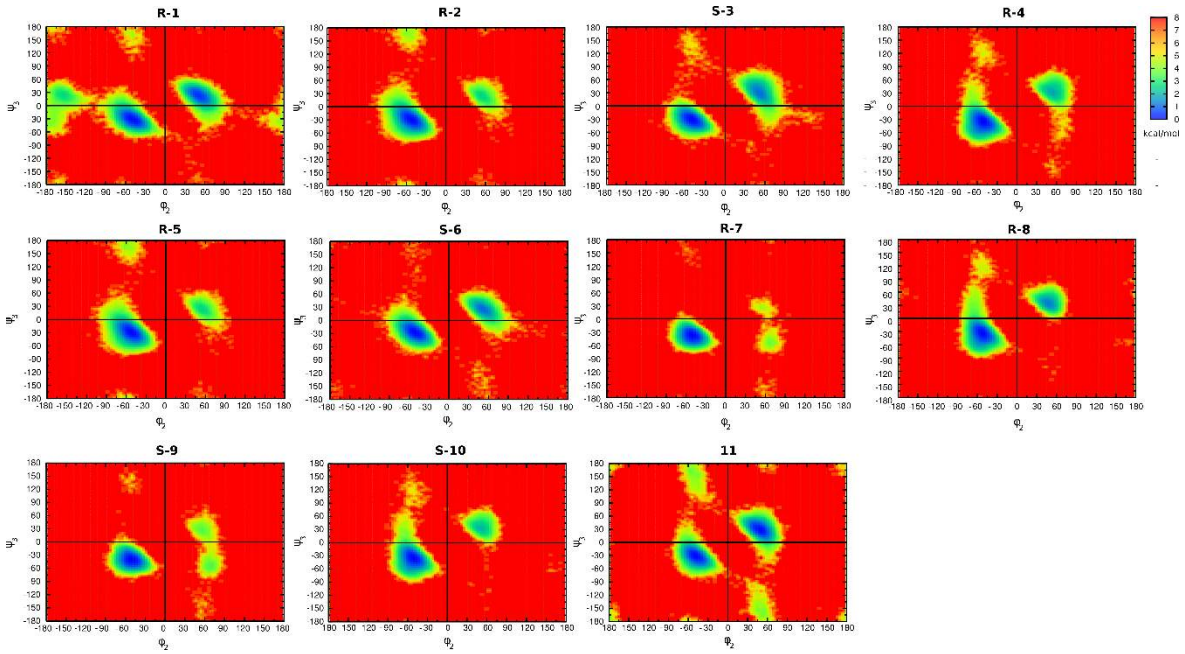

Figure 6.3. PMF profiles (kcal/mol) as a function of φ_2-ψ_3 dihedral pairs obtained from REMD simulations of peptides ***R*-1**, ***R*-2**, ***S*-3**, ***R*-4**, ***R*-5**, ***S*-6**, ***R*-7**, ***R*-8**, ***S*-9**, ***S*-10** and **11** containing (*R*)-**II**, (1*R*,2*R*,4*R*)-**IIIa**, (1*R*,2*S*,4*R*)-**IIIb**, (1*S*,2*R*,4*R*)-**IV**, (1*R*,2*R*,4*R*)-**V**, (*S*)-**VI**, (1*S*,2*R*,3*S*,4*R*)-**VIIa**, (1*S*,2*R*,3*R*,4*R*)-**VIIb**, (1*S*,2*S*,3*S*,4*R*)-**VIIIa**, (1*S*,2*S*,3*R*,4*R*)-**VIIIb** and Aib, respectively.

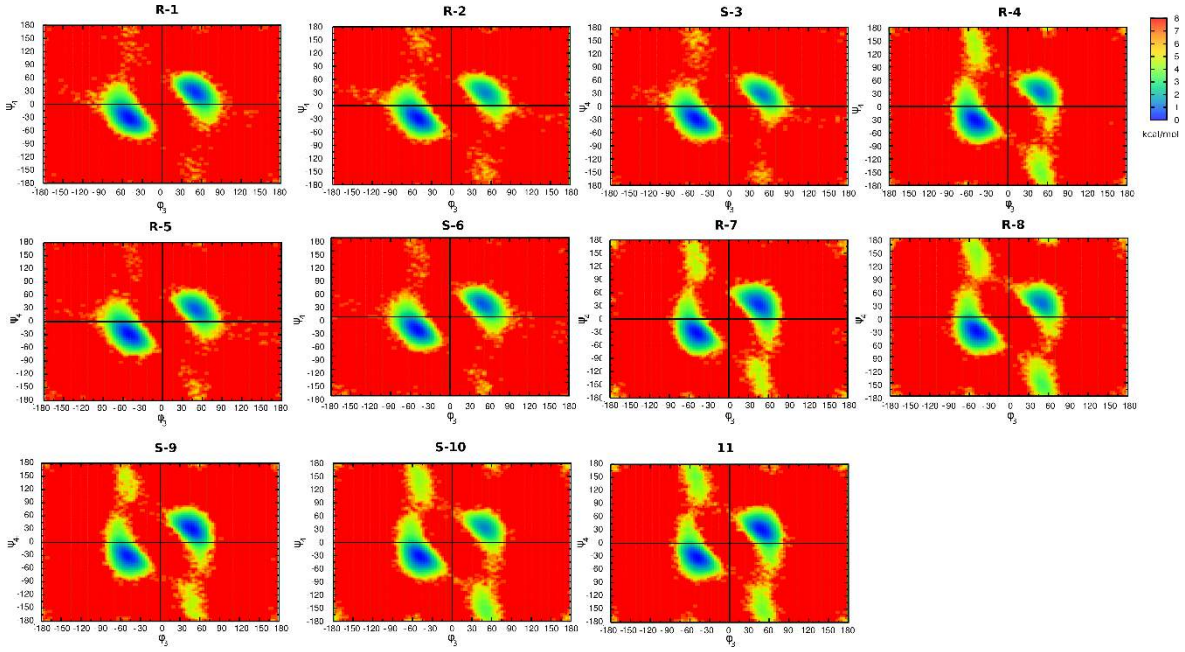

Figure 6.4. PMF profiles (kcal/mol) as a function of φ_3-ψ_4 dihedral pairs obtained from REMD simulations of peptides ***R*-1**, ***R*-2**, ***S*-3**, ***R*-4**, ***R*-5**, ***S*-6**, ***R*-7**, ***R*-8**, ***S*-9**, ***S*-10** and **11** containing (*R*)-**II**, (1*R*,2*R*,4*R*)-**IIIa**, (1*R*,2*S*,4*R*)-**IIIb**, (1*S*,2*R*,4*R*)-**IV**, (1*R*,2*R*,4*R*)-**V**, (*S*)-**VI**, (1*S*,2*R*,3*S*,4*R*)-**VIIa**, (1*S*,2*R*,3*R*,4*R*)-**VIIb**, (1*S*,2*S*,3*S*,4*R*)-**VIIIa**, (1*S*,2*S*,3*R*,4*R*)-**VIIIb** and Aib, respectively.

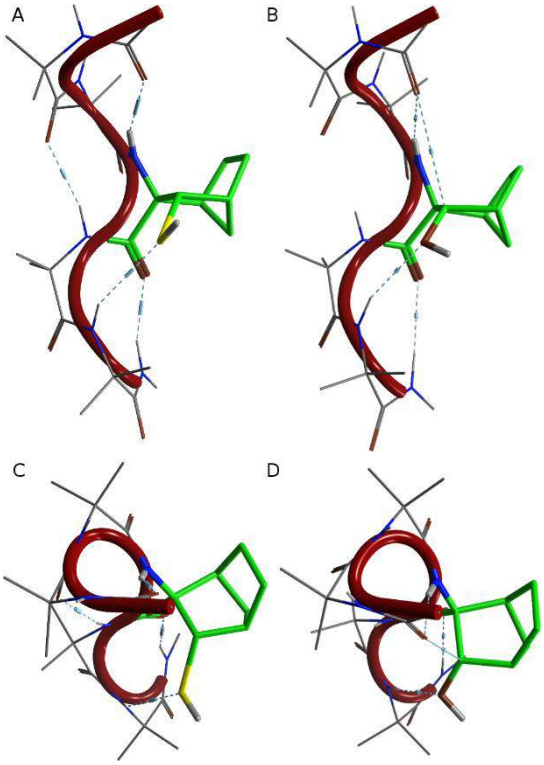

Figure 6.5. Front (A and B) and top (C and D) views of representative structures of the second most populated cluster of peptides ***R*-7** (A and C) and ***S*-9** (B and D), containing (1*S*,2*R*,3*S*,4*R*)-**VIIa** and (1*S*,2*S*,3*S*,4*R*)-**VIIIa** highlighted in green.

This is confirmed by cluster analyses performed on REMD trajectories of Ac-cCTAAs-Aib$_5$-NHMe peptides (Table 6.3). Indeed, when cCTAA = (1*S*,2*R*,3*S*,4*R*)-**VIIa** and (1*S*,2*S*,3*S*,4*R*)-**VIIIa** (peptides ***R*-25** and ***S*-27**), h.e. (6.5 ± 4.8 and -7.7 ± 2.4%, respectively) were only marginally different from those obtained for the achiral peptide **11** (Table 6.1), proving that these cCTAAs lose their screw sense selectivity if moved from the third position to the N-terminus of the peptide chain.

Table 6.3. Average *P*-helical (P%) and *M*-helical (M%) populations, average global helical content (H%) and helical excess (h.e., %) obtained from cluster analyses of the 308 K REMD trajectories of Ac-cCTAA-Aib$_5$-NHMe Peptides.

#	cCTAA	*P*% ± SD	*M*% ± SD	H% ± SD	h.e. ± SD
***R*-19**	(*R*)-**II**	61.1±3.8	30.0±4.1	91.1±5.6	34.1±6.5
***R*-20**	(1*R*,2*R*,4*R*)-**IIIa**	62.2±5.8	28.9±5.6	91.1±8.1	36.6±9.4
***S*-21**	(1*R*,2*S*,4*R*)-**IIIb**	70.8±3.5	18.3±3.2	89.1±4.7	58.9±6.2
***R*-22**	(1*S*,2*R*,4*R*)-**IV**	67.6±5.7	25.7±2.3	93.3±6.1	44.9±7.2
R-23	(1*R*,2*R*,4*R*)-**V**	57.9±1.7	32.7±1.8	90.7±2.5	27.8±2.8
***S*-24**	(*S*)-**VI**	56.3±3.6	34.9±3.6	91.2±5.1	23.5±5.7
***R*-25**	(1*S*,2*R*,3*S*,4*R*)-**VIIa**	48.6±3.4	42.7±2.7	91.3±4.3	6.5±4.8
***R*-26**	(1*S*,2*R*,3*R*,4*R*)-**VIIb**	76.0±5.7	18.4±2.2	94.4±6.1	61.0±7.6
***S*-27**	(1*S*,2*S*,3*S*,4*R*)-**VIIIa**	42.4±1.5	49.5±1.6	91.9±2.2	-7.7±2.4
***S*-28**	(1*S*,2*S*,3*R*,4*R*)-**VIIIb**	80.6±2.5	17.4±2.3	98.0±3.4	64.5±4.1

It should also be noticed that the other cCTAAs still maintain a certain ability of inducing the *P*-helix, however the h.e. of all the Ac-cCTAA-Aib$_5$-NHMe models are reduced. This decrease can be attributed to both the loss of the upstream stabilization effect and to a reduced "spatial memory" of the cCTAA after 3 – 5 Aib residues along the peptide chain.

As noticed in the previous work, PMF(φ_2-ψ_3) and PMF(φ_3-ψ_4) profiles of peptide **11** showed local minima corresponding to β-strands or polyproline-like conformations, whereas for peptides ***R*-4** (cCTAA = (1*S*,2*R*,4*R*)-**IV**), ***R*-7** (cCTAA = (1*S*,2*R*,3*S*,4*R*)-**VIIa**), ***R*-8** (cCTAA = (1*S*,2*R*,3*R*,4*R*)-**VIIb**), ***S*-9** (cCTAA = (1*S*,2*S*,3*S*,4*R*)-**VIIIa**), and ***S*-10** (cCTAA = (1*S*,2*S*,3*R*,4*R*)-**VIIIb**) those conformations were only observed in PMF(φ_3-ψ_4). Moreover, as observed while studying the helix stabilization mechanism, the PMF(φ_2-ψ_3) profile of peptide ***R*-1** (cCTAA = (*R*)-**II**) has an additional minimum at ($-130° \leq \varphi_2 \leq -180°$; $-60° \leq \psi_3 \leq +30°$).

Additional information concerning the rotational energy profile of the single considered dihedrals can be obtained by monodimensional PMF (Figure 6.6).

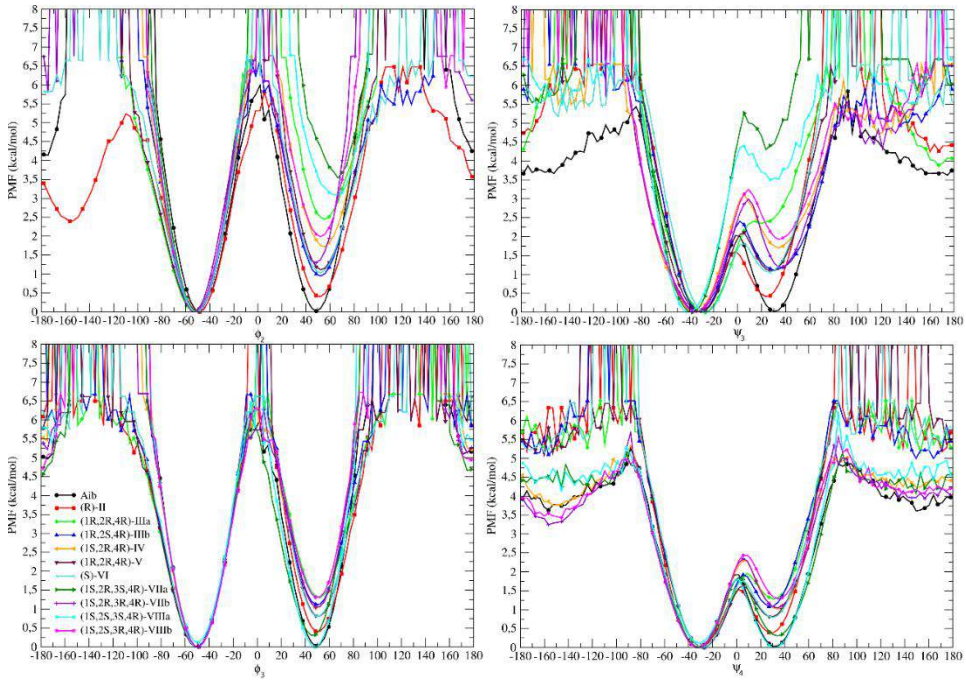

Figure 6.6. PMF profiles from the analyses of trajectories at 260, 283, 308 and 335 K of peptides containing Aib and the cCTAAs selective towards the *P*-helix. Dihedrals associated with PMF higher than 8 kcal/mol were not sampled at the selected temperatures.

In details, PMF(φ_2) and PMF(ψ_3) have a ΔE_M which correlates to h.e., suggesting that φ_2 and ψ_3 coordinates are relevant in the $P \rightarrow M$ interconversion. Moreover, the achiral peptide **11** has a $\Delta E_M = 0$ kcal/mol, while peptides ***R*-7** and ***S*-9** (h.e. ~ 100%) have the highest ΔE_M observed for both PMF(φ_2) (about 3.5 and 3.0 kcal/mol for R-7 and S-9, respectively), and PMF(ψ_3) (abut 4.0 and 3.5 kcal/mol for R-7 and S-9, respectively). As observed in the previous study, the interconversion barrier $\Delta E_M^{\ddagger}$ in PMF(φ_2) profiles is relatively difficult to overcome at the considered temperatures in all cases, except for ***R*-1**, ***S*-3** and **11**. This suggests that the cCTAAs included in these latter peptides, namely (*R*)-**II**, (1*R*,2*S*,4*R*)-**IIIb** and Aib, respectively, have a lower ability in stabilizing the *P*-helix upstream of the

cCTAA itself. Conversely, $\Delta E_M^{\ddagger}$ in PMF(ψ_3) profiles are low enough to allow the interconversion between *P*- and *M*-helices for all the considered peptides, although a peculiar trend cannot be clearly identified.

The ΔE_M of PMF(φ_3) and PMF(ψ_4) profiles are lower than those observed for PMF(φ_2) and PMF(ψ_3), although the correlation with h.e. is maintained. ***R*-7** and ***S*-9** are an exception, since their cCTAAs lose their *P*-screw sense selectivity on the downstream dihedrals, as also showed by 2D-PMF (Figure 6.4) and REMD simulations performed on Ac-cCTAA-Aib$_5$-NHMe peptide models (Table 6.3). In addition, peptides **11**, ***R*-4**, ***S*-6**, ***R*-7**, ***R*-8**, and ***S*-10** (cCTAAs = Aib, (1*S*,2*R*,4*R*)-**IV**, (*S*)-**VI**, (1*S*,2*R*,3*S*,4*R*)-**VIIa**, (1*S*,2*R*,3*R*,4*R*)-**VIIb**, and (1*S*,2*S*,3*R*,4*R*)-**VIIIb**, respectively) have PMF(φ_3) profiles with easily surmountable $\Delta E_M^{\ddagger}$, indicating that their cCTAAs exert their *P*-screw sense selectivity mainly upstream of the cCTAA itself (Figure 6.6).

As previously stated in Chapter 5, PMF analysis provided highlighting information on the helical screw sense preferences of the selected cCTAAs, in particular those related to the cCTAAs effects on the upstream and downstream dihedrals. However, they do not provide a clear explanation of the mechanisms involved in the helical screw sense selectivity.

Recently, no better specified steric hindrance and geometrical factors have been invoked as a possible explanation of screw sense selectivity exerted by cCTAAs,[248] however further investigations in this directions are required. Therefore, consistent with what done for the study of the helix secondary structure stabilization, the effect of steric factors has been preliminarily evaluated through a 3D QSPR analysis with PHASE,[219] by superposing the ideal *P*-3$_{10}$-helices of peptides ***R*-1**, ***R*-2**, ***S*-3**, ***R*-4**, ***R*-5**, ***S*-6**, ***R*-7**, ***R*-8**, ***S*-9**, ***S*-10** and **11** and setting the h.e. as the "activity". A 3D plot where blue and red cubes indicate areas where steric hindrance has a positive and negative effect on the h.e., respectively, was obtained (Figure 6.7).

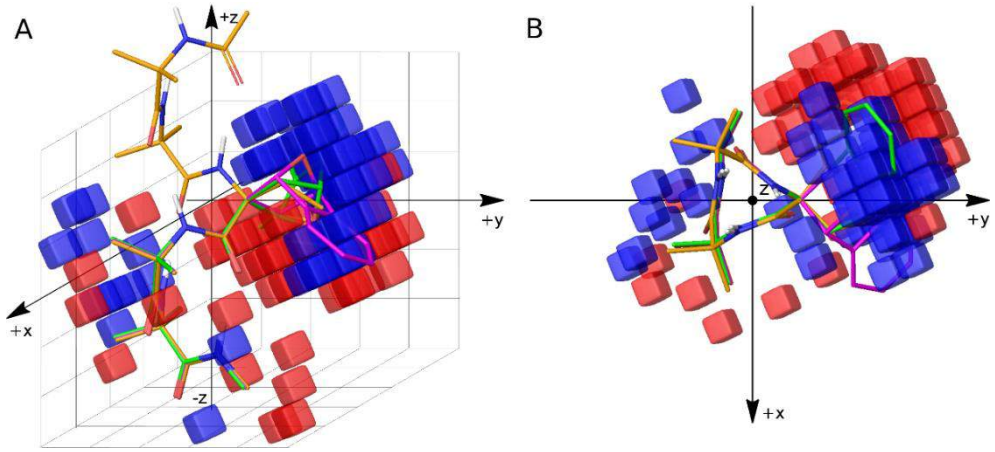

Figure 6.7. Front and top view of 3D plot of QSPR areas obtained through PHASE analysis of peptides ***R*-1**, ***R*-2**, ***S*-3**, ***R*-4**, ***R*-5**, ***S*-6**, ***R*-7**, ***R*-8**, ***S*-9**, ***S*-10** and **11**. Blue and red cubes represent areas where a steric hindrance has a positive or negative effect on the h.e., respectively. Peptides ***R*-1** (orange), ***R*-2** (green) and ***S*-3** (magenta) are shown as a reference.

From Figure 6.7 it can be observed that hydrophobic substituents in the (-x, +y, +z), (+x, +y, -z) and, to minor extent, (+x, +y, +z) sectors of the Cartesian space positively contribute to the *P*-screw

sense selectivity exerted by the cCTAA. Conversely, steric hindrance in the (-x, +y, -z) sector reduces the h.e. Indeed, the side chains of the highly performing cCTAAs (h.e. > 60%) are located in the (-x, +y, +z) or (+x, +y, -z) sectors, whereas for the least selective cCTAA, namely (*R*)-**II**, is predominantly located in the (-x, +y, -z) area.

Following the same procedure previously described (see Chapter 5), hypothetical cCTAAs with ad-hoc structural modifications were investigated to confirm or rebut 3D QSPR suggestions (Figure 6.8).

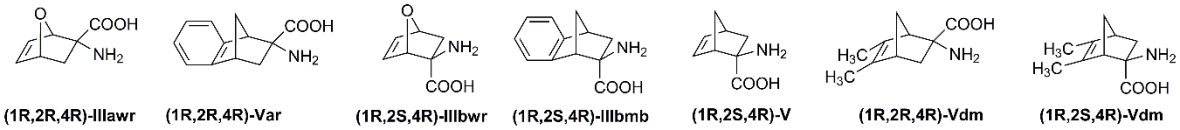

Figure 6.8. Structurally modified cCTAAs used for the study of mechanisms of helical screw sense preferences.

Therefore, to verify the importance of steric hindrance in the (-x, +y, +z) sector, the excellent performing (1*R*,2*R*,4*R*)-**IIIa**, whose side chain lies on that sector, was modified by deleting its aromatic ring, thus obtaining (1*R*,2*R*,4*R*)-**IIIawr** (Figure 6.8). When included in the Ac-Aib$_2$-cCTAA-Aib$_2$-NHMe peptide model (peptide ***R*-12**), this cCTAA gave a reduction of about 17% in the h.e. compared to its parental cCTAA (Table 6.4). PMF profiles as a function of φ_2, ψ_3, φ_3 and ψ_4 dihedrals became comparable to those of peptide ***R*-5**, whose cCTAA ((1*R*,2*R*,4*R*)-**V**) is structurally related to (1*R*,2*R*,4*R*)-**IIIawr**, except for the methylene bridge instead of the oxo-bridge (Figure 6.9).

As a counterproof, (1*R*,2*R*,4*R*)-**V** was modified by adding an aromatic ring, 1*R*,2*R*,4*R*)-**Var** (Figure 6.8), thus increasing its steric hindrance in the (-x, +y, +z) sector. As expected, h.e. increased of about 15%, compared to peptide ***R*-5**, reaching a h.e. (96.0 ± 3.2%) which is equivalent to that of peptide ***R*-2** (cCTAA = (1*R*,2*R*,4*R*)-**IIIa**). The respective PMF also overlapped (Figure 6.9).

Table 6.4. Average *P*-helix (*P*%) and *M*-helix (*M*%) populations, average global helical content (H%) and helical excess (h.e.) obtained from cluster analyses performed on the 308 K REMD trajectories of Ac-Aib2-cCTAA-Aib2-NHMe peptides **12-18**.

#	modified CTAA	P% ± SD	M% ± SD	H% ± SD	h.e. ± SD
***R*-12**	(1*R*,2*R*,4*R*)-**IIIawr**	77.7±3.2	8.7 ±2.1	86.4±3.8	79.9±5.7
***R*-13**	(1*R*,2*R*,4*R*)-**Var**	88.7±2.0	1.8 ±0.5	90.5±2.1	96.0±3.2
***R*-14**	(1*R*,2*R*,4*R*)-**Vdm**	87.6±1.3	1.0 ±0.4	88.6±1.4	97.7±2.1
***S*-15**	(1*R*,2*S*,4*R*)-**V**	87.3±2.1	7.0 ±1.2	94.3±2.4	85.2±3.4
***S*-16**	(1*R*,2*S*,4*R*)-**Vdm**	97.0±0.5	2.0 ±0.3	99.0±0.6	96.0±0.8
***S*-17**	(1*R*,2*S*,4*R*)-**IIIbwr**	73.6±2.9	20.0 ±1.9	93.6±3.5	57.3±4.3
***S*-18**	(1*R*,2*S*,4*R*)-**IIIbmb**	95.3±0.5	3.0 ±0.4	98.3±0.6	93.9±0.9

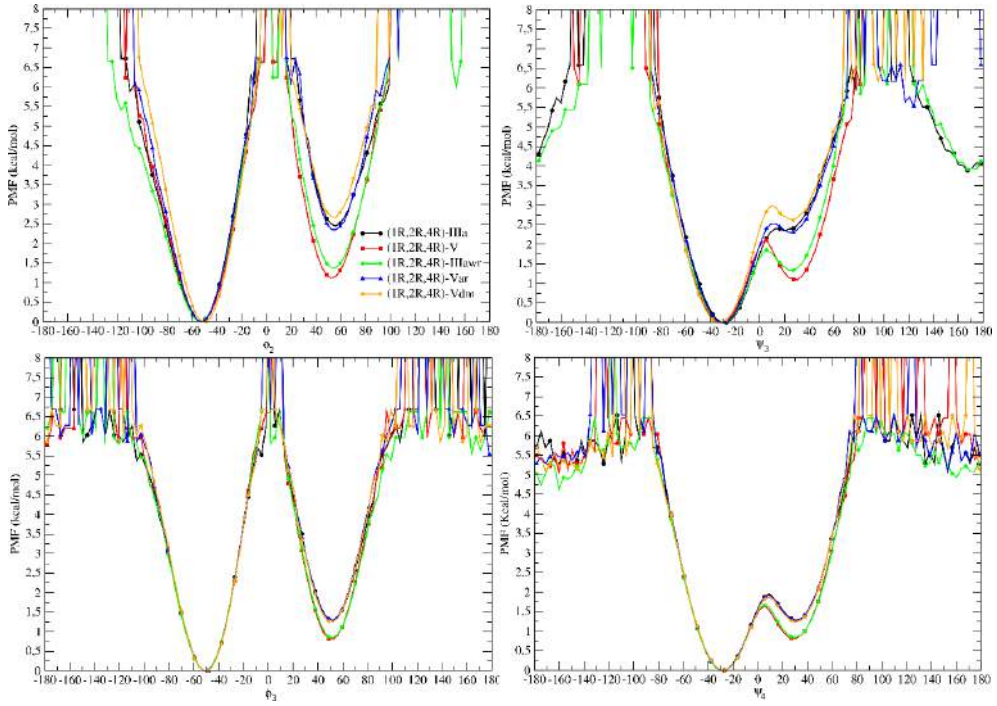

Figure 6.9. Comparison of PMF profiles, as a function of φ_2, ψ_3, φ_3 and ψ_4 dihedrals, of peptides containing (1*R*,2*R*,4*R*)-**IIIa**, (1*R*,2*R*,4*R*)-**V**, (1*R*,2*R*,4*R*)-**IIIawr**, (1*R*,2*R*,4*R*)-**Var** and (1*R*,2*R*,4*R*)-**Vdm** cCTAAs.

In order to understand if the positive effect on the helical screw sense selectivity of (1*R*,2*R*,4*R*)-**IIIa** and (1*R*,2*R*,4*R*)-**Var** is ascribable to an electronic effect of the aromatic ring or to its steric hindrance, a derivative of (1*R*,2*R*,4*R*)-**V**, with two methyl groups at C5 and C6, named (1*R*,2*R*,4*R*)-**Vdm** (Figure 6.8), was designed. Both the h.e. (Table 6.4) and PMF profiles (Figure 6.9) of the corresponding peptide ***R*-14** were comparable to those of peptides ***R*-2** and ***R*-13** (cCTAAs = (1*R*,2*R*,4*R*)-**IIIa** and (1*R*,2*R*,4*R*)-**Var**, respectively), proving that the contribution to the helical screw sense selectivity is principally given by steric hindrance in the (-x, +y, +z) sector.

An analogous approach was followed to evaluate the role of steric hindrance in the (+x, +y, -z) sector. Therefore, the aromatic ring of (1*R*,2*S*,4*R*)-**IIIb** was deleted, obtaining (1*R*,2*S*,4*R*)-**IIIbwr** (Figure 6.8), which, once included in the peptide model ***S*-17**, reduced the h.e. of about 14% compared to ***S*-3**, which contains the parental cCTAA (Tables 5.2 and 5.4). Conversely, the PMF profiles showed only slight differences (Figure 6.9), although a decrease in both ΔE_M and $\Delta E_M^{\ddagger}$ was observable in all the considered PMF profiles for peptide ***S*-17**, suggesting that the deletion of the aromatic ring equally affects the upstream and downstream dihedrals.

The stereoisomer (1*R*,2*S*,4*R*)-**V** (never isolated experimentally) was also studied. Its model peptide ***S*-15** unexpectedly gave a h.e. about 14% and 30% higher than that of peptides ***S*-3** (cCTAAs = (1*R*,2*S*,4*R*)-**IIIb)** and ***S*-17** (cCTAAs = (1*R*,2*S*,4*R*)-**IIIbwr**), respectively (Tables 5.1 and 5.4). PMF(ψ_3) and PMF(φ_3) confirmed these results, because ΔE_M and $\Delta E_M^{\ddagger}$ computed for ***S*-15** were 0.5-1.0 kcal/mol higher than those of peptides ***S*-3** and ***S*-17**, whereas PMF(ψ_4) and PMF(φ_2) profiles were

equivalent to those of peptide ***S*-3** (cCTAA = (1*R*,2*S*,4*R*)-**IIIb**) (Figure 6.10). This indicates that the methylene bridge of the norbornene core might play some role in favoring the *P*-helix.

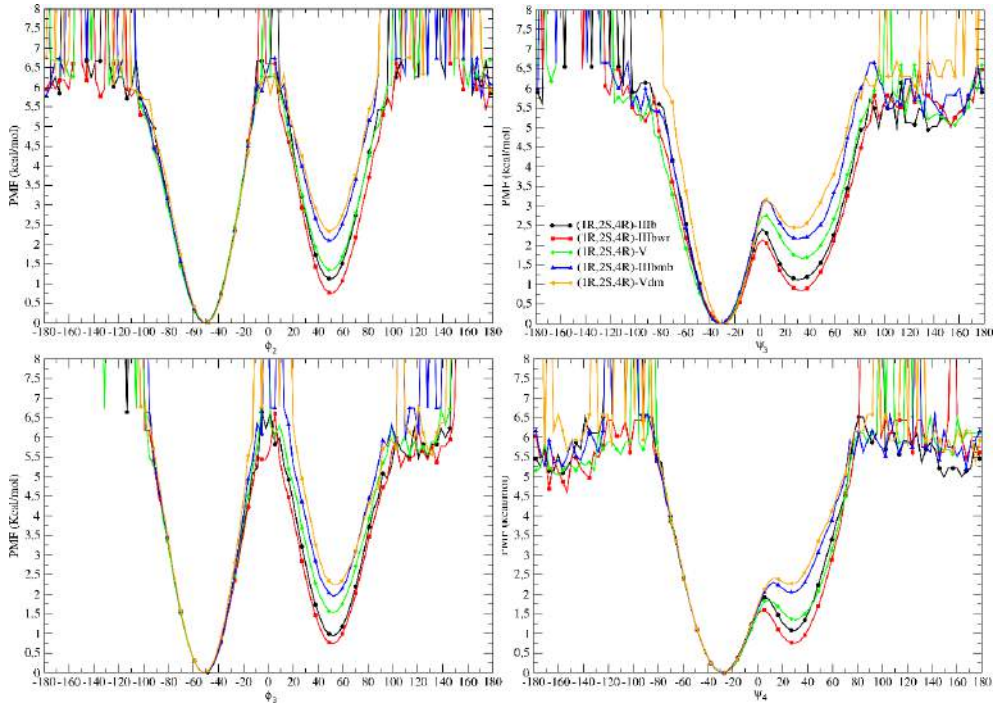

Figure 6.10. Comparison of PMF profiles, as a function of φ_2, ψ_3, φ_3 and ψ_4 dihedrals, of peptides containing (1*R*,2*S*,4*R*)-**IIIb**, (1*R*,2*S*,4*R*)-**IIIbwr**, (1*R*,2*S*,4*R*)-**V**, (1*R*,2*S*,4*R*)-**IIIbmb** and (1*R*,2*S*,4*R*)-**Vdm** cCTAAs.

Therefore, we analyzed the screw sense preferences of peptide ***S*-18**, containing (1*R*,2*S*,4*R*)-**IIIbmb** which is derived from (1*R*,2*S*,4*R*)-**IIIb** by substituted the oxo-bridge with a methylene bridge (Figure 6.7). As previously observed, analysis of ***S*-18**gave an increased h.e. (93.9 ± 0.9 %) (Tables 5.1 and 5.4) and PMF profiles showing ΔE_M and $\Delta E_M^{\ddagger}$ higher than those obtained for peptide ***S*-3** containing the parent cCTAA (Figure 6.10).

In this case also, we evaluated if the positive effect on h.e. was due to a steric hindrance or to electronic properties of the aromatic ring. Therefore, we studied the behavior of peptide ***S*-16**, containing (1*R*,2*S*,4*R*)-**Vdm** which is derived from (1*R*,2*S*,4*R*)-**V** (Figure 6.7) by addition of two methyl groups at C5 and C6. Peptides ***S*-16** and ***S*-18** gave comparable results in terms of h.e. (Table 6.4) and PMF profiles (Figure 6.10), confirming the positive effect on h.e. is simply due to steric hindrance in the (+x, +y, -z) sector.

The relative importance of steric hindrance in (-x, +y, +z) or (+x, +y, -z) sectors have been investigated as well. (1*R*,2*R*,4*R*)-**IIIa**, whose side chain is located in the (-x, +y, +z) sector, has a h.e. 25% higher than that of (1*R*,2*S*,4*R*)-**IIIb**, which, instead, mainly lies in the (+x, +y, -z) sector. However, the deletion of the aromatic ring in both cCTAAs led to an equal reduction of the h.e. obtained for the corresponding ***R*-12** and ***S*-17** peptides (Table 6.4).

However, steric hindrance by itself cannot explain the different levels of *P*-screw sense selectivity obtained for structurally related cCTAAs, such as (1*R*,2*R*,4*R*)-**IV** and (1*R*,2*R*,4*R*)-**V** or (1*R*,2*R*,4*R*)-**V** and (1R,2R,4R)-**IIIawr** pairs (Tables 5.1 and 5.4).

Since the role of classical and weak H-bonds has been proved as relevant for the stabilization of peptide secondary structures,[72,214,222] QTAIM analyses were performed in this case also to investigate whether differences in H-bond networks of both *P*- and *M*-helices could explain the unexpected differences in h.e. (Table 6.5).

Table 6.5. Useful Quantities Derived from QTAIM Calculations

Symbol	Expression	Description
ρ_P	$\sum \rho(r_c)_P$	BCP total density for a given peptide in P conformation
ρ_M	$\sum \rho(r_c)_M$	BCP total density for a given peptide in M conformation
$\Delta\rho_{P-M}$	$\sum \rho(r_c)_P - \sum \rho(r_c)_M$	difference between ρ_P and ρ_M for a given peptide
$\Delta_{A-B}\rho_P$	$\left(\sum \rho\,(r_c)_P\right)_A - \left(\sum \rho\,(r_c)_P\right)_B$	Difference of BCP total densities between peptides "A" and "B" in P conformation
$\Delta_{A-B}\rho_M$	$\left(\sum \rho\,(r_c)_M\right)_A - \left(\sum \rho\,(r_c)_M\right)_B$	Difference of BCP total densities between peptides "A" and "B" in M conformation
$\Delta\rho_{A-B}$	$\Delta_{A-B}\rho_P - \Delta_{A-B}\rho_M$	Difference between two above differences

In this case also, the BCP network consisted of $i + 3 \rightarrow i$ N – H···O=C BCPs with $\rho(r_c)$ values typical for classical H-bonds (0.002 – 0.022 au)[223,224] or slightly higher, a positive Laplacian, indicating that the nature of the interaction is electrostatic, and a low ε, which indicates stable BCPs. In addition, $i + 3 \rightarrow i$ C – H···O=C BCPs with $\rho(r_c)$ higher than those observed in natural peptides[214,222] were found. Moreover, consistent to what reported for some natural peptides,[214] N···O BCP involving the backbone of cCTAA and Aib ($\rho(r_c) \approx 0.0120$ au) was detected within the *P*-helix of peptides ***R*-2**, ***R*-4**, ***R*-5**, ***R*-7**, ***R*-8**, and ***S*-10** and within the *M*-helix of peptide ***R*-1**. An analogous interaction, but involving Aib4 and Aib2, was found for peptides ***R*-7** and ***S*-9** in the *M* and *P* conformations, respectively. Additional $i + 1 \rightarrow i$ (with $i \neq$ cCTAA) Cβ – H···O=C BCPs ($\rho(r_c)$ = from 0.0102 to 0.0126 au) were present between Aib5 and Aib4 in all peptides, and between Aib2 and Aib1 only in the *P*-helix of peptides ***R*-2**, ***R*-4**, ***R*-5**, ***R*-7**, ***R*-8**, and ***S*-10** and in the *M*-helix of peptide ***R*-1** (Figure 6.11). Furthermore, peculiar BCPs involving the cCTAAs were detected in all cases and will be helpful in the following discussion.

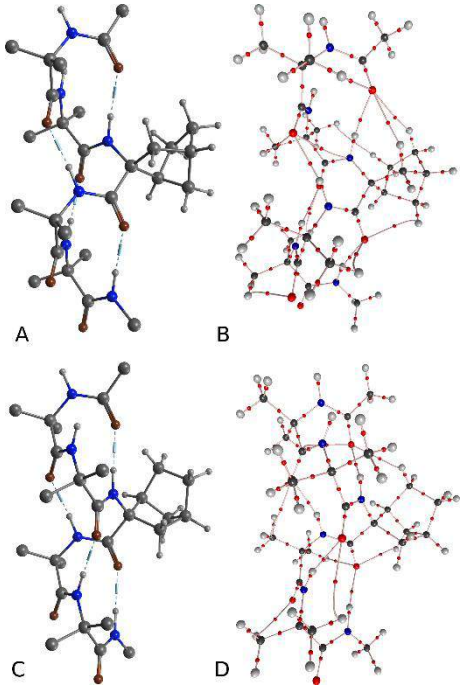

Figure 6.11. (A and C) Ball-and-stick representation and (B and D) QTAIM molecular graph of the optimized *P*- (top) and *M*- (bottom) 3_{10}-helix of Ac-Aib$_2$-(1*S*,2*R*,4*R*)-**IV**-Aib$_2$-NHMe peptide

As previously observed, ***R*-4** and ***R*-5** peptides (cCTAAs = (1*S*,2*R*,4*R*)-**IV** and (1*R*,2*R*,4*R*)-**V**, respectively) had significantly different h.e., although their cCTAAs are structurally similar. QTAIM analyses performed on their *P*-helices (Tables 5.6 and 5.7) gave similar BCP total densities ($\Delta_{4-5}\rho_P$ = 0.0004 au), although peptide ***R*-4** had an additional C – H···O=C BCP between the C5 of (1*S*,2*R*,4*R*)-**IV** and the carbonyl oxygen of the acetyl cap ($\rho(r_c)$ = 0.0037 au). Conversely, the same analysis performed on the *M*-helices provided qualitatively equivalent BCP networks, but a higher difference in BCP total density for peptide ***R*-5** ($\Delta_{4-5}\rho_M$ = -0.0027 au). In addition, the differences in electronic densities between *P*- and *M*-helices $\Delta\rho_{P-M}$ of peptides ***R*-4** and ***R*-5** were of 0.0182 and 0.0151 au, respectively, with a ΔΔρ of 0.0031 au. At the light of this, it can be concluded that the *P*-screw sense selectivity exerted by (1*S*,2*R*,4*R*)-**IV** and (1*R*,2*R*,4*R*)-**V** is increased by rather strong C – H···O=C interactions involving the cCTAA, and the higher h.e. showed by peptide ***R*-4** is ascribable to a lower stabilization of noncovalent interactions in the *M*-helix compared to peptide ***R*-5**. Indeed, a $\Delta\rho_M$ of about 0.0030 au was considered sufficient to explain differences in helical stability observed in natural peptides.[214,222]

Table 6.6. Types and properties of BCPs of the Ac-Aib$_2$-(1*S*,2*R*,4*R*)-**IV**-Aib$_2$-NHMe peptide ***R*-4** in the *P*- and *M*-helix conformation. All parameters are reported in au.

Peptide ***R*-4, *P*-helix**				Peptide ***R*-4, *M*-helix**			
N-H···O BCP	**$\rho(r_c)$**	**$\nabla^2\rho(r_c)$**	**ε**	**N-H···O BCP**	**$\rho(r_c)$**	**$\nabla^2\rho(r_c)$**	**ε**
IV···Ac	0.0203	0.0636	0.0580	IV···ACE	0.0170	0.0531	0.0795
Aib4···Aib1	0.0197	0.0620	0.0502	Aib4···Aib1	0.0213	0.0676	0.0583
Aib5···Aib2	0.0185	0.0580	0.0603	Aib5···Aib2	0.0161	0.0502	0.0473
NMe···IV	0.0215	0.0687	0.0612	NMe···IV	0.0220	0.0704	0.0677
$\Sigma\rho(r_c)$ at NH···O	0.0800			**$\Sigma\rho(r_c)$ at NH···O**	0.0764		

Cβ-H···O BCP				**Cβ-H···O BCP**			
IV(C3-H)···Ac	0.0101	0.0370	0.0833	IV(C6-H)···Ac	0.0080	0.0281	0.1034
IV(C5-H)···Ac	0.0037	0.0135	0.6250	Aib5···Aib2	0.0055	0.0217	0.5714
Aib2···Aib1	0.0104	0.0379	0.8085	IV(C7-H···IV	0.0136	0.0461	0.1574
Aib5···Aib2	0.0055	0.0220	0.5238	Aib4···IV	0.0118	0.0427	0.8704
IV(C7-H)···IV	0.0114	0.0412	0.8269	Aib5···Aib4	0.0123	0.0436	0.4474
Aib5··Aib4	0.0126	0.0445	0.4304				
Σρ(r$_c$) at C-H···O	0.0537			**Σρ(r$_c$) at C-H···O**	0.0512		
N···O CPs							
IV···Aib1	0.0121	0.0385	0.9394				
Σρ(r$_c$) at N···O	0.0121						
Σρ(r$_c$) tot	**0.1458**			**Σρ(r$_c$) tot**	**0.1276**		

Table 6.7. Types and properties of BCPs of the Ac-Aib$_2$-(1*R*,2*R*,4*R*)-**V**-Aib$_2$-NHMe peptide ***R*-5** in the *P*- and *M*-helix conformation. All parameters are reported in au.

peptide ***R*-5, *P*-helix**				peptide ***R*-5, *M*-helix**			
N-H···O BCP	$\rho(r_c)$	$\nabla^2\rho(r_c)$	ε	**N-H···O BCP**	$\rho(r_c)$	$\nabla^2\rho(r_c)$	ε
V···ACE	0.0199	0.0620	0.0548	V···ACE	0.0176	0.0551	0.0707
Aib4···Aib1	0.0197	-0.0343	0.0455	Aib4···Aib1	0.0216	0.0688	0.0571
Aib5···Aib2	0.0195	0.0612	0.0660	Aib5···Aib2	0.0168	0.0521	0.0565
NMe···V	0.0217	0.0697	0.0605	NMe···V	0.0219	0.0699	0.0640
$\sum\rho(r_c)$ **at N-H···O**	0.0808			$\sum\rho(r_c)$ **at N-H···O**	0.0779		
Cβ-H···O BCP				**Cβ-H···O BCP**			
V(C3-H)···Ac	0.0100	0.0369	0.0941	V(C6-H)···Ac	0.0091	0.0324	0.1370
Aib2···Aib1	0.0102	0.0374	0.9070	Aib5···Aib2	0.0055	0.0218	0.5238
Aib5···Aib2	0.0055	0.0220	0.5238	V(C7-H)···V	0.0138	0.0462	0.1441
V(C7-H)···V	0.0139	0.0488	0.3333	Aib4···V	0.0116	0.0422	0.9038
Aib5··Aib4	0.0126	0.0448	0.4250	Aib5···Aib4	0.0124	0.0439	0.4231
$\sum\rho(r_c)$ **at C-H···O**	0.0522			$\sum\rho(r_c)$ **at C-H···O**	0.0524		
N···O CPs							
V···Aib1	0.0124	0.0394	0.8611				
$\sum\rho(r_c)$ **at N···O**	0.0124						
$\sum\rho(r_c)$ **tot**	**0.1454**			$\sum\rho(r_c)$ **tot**	**0.1303**		

Similarly to what observed for peptide ***R*-4**, peptide ***R*-2** in the *P* conformation showed a very strong noncovalent interactions network (Table 6.8), although not directly involving (1*R*,2*R*,4*R*)-**IIIa**. At the same time, the steric hindrance of this cCTAA in the (-x, +y, +z) sector is larger than that of (1*S*,2*R*,4*R*)-**IV**; therefore, the complete fulfilment of steric requirements together with the strengthening of noncovalent interactions selectively in the *P*-helical conformation made (1*R*,2*R*,4*R*)-**IIIa** one of the best performing cCTAAs in terms of screw sense selectivity.

Indeed, (1*R*,2*R*,4*R*)-**IIIa** also exerted a screw sense selectivity higher than that of its Cα epimer (1*R*,2*S*,4*R*)-**IIIb** (Table 6.1, Δh.e. ~ 26%), although steric hindrance in (-x, +y, +z) or in (+x, +y, -z) was found to equally affect the h.e. Conversely, QTAIM analysis performed on both ***R*-2** and ***S*-3** peptides (cCTAAs = (1*R*,2*R*,4*R*)-**IIIa** and (1*R*,2*S*,4*R*)-**IIIb**, respectively) showed that this latter peptide had a significantly lower ρ_P ($\Delta_{2-3}\rho_P$ = 0.0165 au) and a higher ρ_M ($\Delta_{2-3}\rho_M$ = -0.0121 au) than

peptide ***R*-2**, although they have qualitatively similar BCP networks (Tables 5.8 and 5.9). In other words, the decrease in h.e. of peptide ***S*-3** is explained by observing that this peptide in the *P*-conformation has a less stable noncovalent interaction network than peptide ***R*-2**, whereas the stability of its interactions is higher in the *M*-conformation.

It is important to underline that, although peptide ***S*-3** showed a ρ_M higher than ρ_P, DFT calculations performed at the CPCM-mPW1B95/6-31+G(d,p) level gave a ΔE_{P-M} = -2.8 kcal/mol. This result suggests that the *P*-conformation of peptide ***S*-3** is anyway more stable than its *M*-conformation, probably because of the cCTAA side chain steric hindrance correctly located in the (+x, +y, -z) sector (Annex 6.A).

Table 6.8. Types and properties of BCPs of the Ac-Aib$_2$-(1*R*,2*R*,4*R*)-**IIIa**-Aib$_2$-NHMe peptide ***R*-2** in the *P*- and *M*-helix conformation. All parameters are reported in au.

peptide ***R*-2**, ***P*-helix**				peptide ***R*-2**, ***M*-helix**			
N-H···O BCP	$\rho(r_c)$	$\nabla^2\rho(r_c)$	**ε**	**N-H···O BCP**	$\rho(r_c)$	$\nabla^2\rho(r_c)$	**ε**
III···Ac	0.0223	0.0703	0.0630	III···Ac	0.0138	0.0445	0.0815
Aib4···Aib1	0.0216	0.0679	0.0484	Aib4···Aib1	0.0202	0.0642	0.0580
Aib5···Aib2	0.0159	0.0495	0.0545	Aib5···Aib2	0.0163	0.0508	0.0526
NMe···III	0.0234	0.0754	0.0623	NMe···III	0.0205	0.0650	0.0652
$\sum\rho(r_c)$ **at N-H···O**	0.0832			$\sum\rho(r_c)$ **at N-H···O**	0.0708		
Cβ-H···O BCP				**Cβ-H···O BCP**			
III(C3-H)···Ac	0.0104	0.0370	0.1111	III(C_{ar}-H)···Ac	0.0113	0.0376	0.1515
Aib2···Aib1	0.0112	0.0401	0.5410	Aib4···Aib1	0.0067	0.0267	0.6667
Aib4···Aib1	0.0056	0.0226	1.0000	Aib5···Aib2	0.0055	0.0218	0.6842
Aib5···Aib2	0.0051	0.0204	0.7059	Aib4···III	0.0126	0.0453	0.6471
Aib5··Aib4	0.0119	0.0423	0.4789	Aib5···Aib4	0.0122	0.0434	0.4533
$\sum\rho(r_c)$ **at C-H···O**	0.0442			$\sum\rho(r_c)$ **at C-H···O**	0.0483		
N···O BCP							
III···Aib1	0.0113	0.0351	0.2564				
$\sum\rho(r_c)$ **at N···O**	0.0113						
$\sum\rho(r_c)$ **tot**	**0.1387**			$\sum\rho(r_c)$ **tot**	**0.1191**		

Table 6.9. Types and properties of BCPs of the Ac-Aib$_2$-(1*R*,2*S*,4*R*)-**IIIb**-Aib$_2$-NHMe peptide ***S*-3** in the *P*- and *M*-helix conformation. All parameters are reported in au.

peptide ***S*-3, *P*-helix**				peptide ***S*-3, *M*-helix**			
N-H···O BCP	$\rho(r_c)$	$\nabla^2\rho(r_c)$	**ε**	**N-H···O BCP**	$\rho(r_c)$	$\nabla^2\rho(r_c)$	**ε**
III···Ac	0.0213	0.0673	0.0583	III···Ac	0.0212	0.0666	0.0546
Aib4···Aib1	0.0187	0.0594	0.0588	Aib4···Aib1	0.0193	0.0608	0.0519
Aib5···Aib2	0.0178	0.0555	0.0582	Aib5···Aib2	0.0178	0.0558	0.0635
NMe···III	0.0214	0.0680	0.0617	NMe···III	0.0212	0.0672	0.0625
$\sum\rho(r_c)$ **at N-H···O**	0.0792			$\sum\rho(r_c)$ **at N-H···O**	0.0795		
Cβ-H···O BCP				**Cβ-H···O BCP**			
C1H(III)···Ac	0.0087	0.0335	0.0857	C3H(III)···Ac	0.0103	0.0376	0.1011
Aib4···Aib1	0.0051	0.0204	0.7692	Aib5···Aib2	0.0052	0.0206	0.5882
Aib5···Aib2	0.0057	0.0228	0.5909	C6(III)···III	0.0134	0.0448	0.5156
Aib4···III	0.0109	0.0396	0.9348	Aib4···III	0.0108	0.0392	0.8936

Aib5··Aib4	0.0126	0.0445	0.4304	Aib5···Aib4	0.0120	0.0424	0.4722
$\sum \rho(r_c)$ **at C-H···O**	0.0430			$\sum \rho(r_c)$ **at C-H···O**	0.0517		
$\sum \rho(r_c)$ **tot**	**0.1222**			$\sum \rho(r_c)$ **tot**	**0.1312**		

Analogous considerations can be made when comparing peptide ***S*-15** (cCTAA = (1*R*,2*S*,4*R*)-**V**) and ***S*-3**, whose Δh.e. ~ 14% (Table 6.1 and 5.4) is justified by a $\Delta_{15-3}\rho_P$ = 0.0052 au and $\Delta_{15-3}\rho_M$ = -0.0034 au (Tables 5.9 and 5.10).

Table 6.10. Types and properties of BCPs of the Ac-Aib$_2$-(1*R*,2*S*,4*R*)-**V**-Aib$_2$-NHMe peptide ***S*-15** in the *P*- and *M*-helix conformation. All parameters are reported in au.

peptide ***S*-15**, ***P*-helix**				peptide ***S*-15**, ***M*-helix**			
N-H···O BCP	$\rho(r_c)$	$\nabla^2\rho(r_c)$	**ε**	**N-H···O BCP**	$\rho(r_c)$	$\nabla^2\rho(r_c)$	**ε**
V···ACE	0.0213	0.0672	0.0625	V···ACE	0.0201	0.0628	0.0588
Aib4···Aib1	0.0185	0.0577	0.0448	Aib4···Aib1	0.0197	0.0620	0.0502
Aib5···Aib2	0.0195	0.0608	0.0613	Aib5···Aib2	0.0200	0.0631	0.0636
NMe···V	0.0216	0.0688	0.0610	NMe···V	0.0227	0.0735	0.0568
$\sum \rho(r_c)$ **at N-H···O**	0.0809			$\sum \rho(r_c)$ **at N-H···O**	0.0825		
Cβ-H···O BCP				**Cβ-H···O BCP**			
C1H(V)···Ac	0.0068	0.0270	0.1628	C3H(V)···Ac	0.0104	0.0381	0.0909
Aib2···Aib1	0.0104	0.0378	0.7872	Aib5···Aib2	0.0057	0.0230	0.4783
Aib5···Aib2	0.0058	0.0234	0.5909	Aib5···Aib4	0.0127	0.0449	0.4198
Aib4···V	0.0109	0.0395	0.9565	C6H(V)···Nme	0.0010	0.0036	0.7500
Aib5··Aib4	0.0126	0.0445	0.4304	C6(V)···V	0.0155	0.0537	0.3012
$\sum \rho(r_c)$ **at C-H···O**	0.0465			$\sum \rho(r_c)$ **at C-H···O**	0.0453		
$\sum \rho(r_c)$ **tot**	**0.1274**			$\sum \rho(r_c)$ **tot**	**0.1278**		

Conversely, the difference of about 22% in helical screw sense selectivity observed between peptides ***S*-18** (cCTAA = (1*R*,2*S*,4*R*)-**IIIbmb**) and ***S*-3** is difficult to explain. Indeed, the higher h.e. of peptide ***S*-18** is only supported by a slight increase in cCTAA steric hindrance in the (+x, +y, +z) in the *P*-conformation and by a limited weakening of the covalent interactions in the *M*-helix ($\Delta_{3-18}\rho_M$ = 0.0020 au; Tables 5.9 and 5.11). However, in this case also, DFT calculations supported the results of REMD simulations, since for both peptides ***S*-18** and ***S*-3** the obtained ΔE_{P-M} were of -3.6 kcal/mol and -2.8 kcal/mol, respectively (Annex 6.A). Therefore, it seems that some other factors, not detected by QTAIM analysis, might play a role in this particular example.

Table 6.1**1**. Types and properties of BCPs of the Ac-Aib$_2$-(1*R*,2*S*,4*R*)-**IIIbmb**-Aib$_2$-NHMe peptide ***S*-18** in the *P*- and *M*-helix conformation. All parameters are reported in au.

peptide ***S*-18**, ***P*-helix**				peptide ***S*-18**, ***M*-helix**			
N-H···O CPs	$\rho(r_c)$	$\nabla^2\rho(r_c)$	**ε**	**N-H···O CPs**	$\rho(r_c)$	$\nabla^2\rho(r_c)$	**ε**
IIIbmb···Ac	0.0214	0.0674	0.0622	IIIbmb···ACE	0.0206	0.0644	0.0570
Aib4···Aib1	0.0194	0.0614	0.0514	Aib4···Aib1	0.0198	0.0622	0.0502
Aib5···Aib2	0.0178	0.0555	0.0579	Aib5···Aib2	0.0183	0.0576	0.0558
NMe···IIIbmb	0.0225	0.0725	0.0615	NMe···IIIbmb	0.0220	0.0705	0.0635
$\sum \rho(r_c)$ **at N-H···O**	0.0811			$\sum \rho(r_c)$ **at N-H···O**	0.0807		
Cβ-H···O CP				**Cβ-H···O CP**			

C1H(IIIbmb)···Ac	0.0069	0.0274	0.1304	C3H(IIIbmb)···Ac	0.0104	0.0377	0.0899
Aib2···Aib1	0.0103	0.0376	0.9762	Aib2···Aib1	0.0104	0.0378	0.9302
Aib4···Aib1	0.0053	0.0211	1.0000	Aib5···Aib2	0.0053	0.0210	0.5556
Aib5···Aib2	0.0057	0.0225	0.5217	C6(IIIbmb)···IIIbmb	0.0104	0.0474	0.5303
Aib5··Aib4	0.0126	0.0445	0.4125	Aib5···Aib4	0.0120	0.0426	0.4722
$\sum \boldsymbol{\rho(r_c)}$ **at C-H···O**	0.0408			$\sum \boldsymbol{\rho(r_c)}$ **at C-H···O**	0.0485		
$\sum \boldsymbol{\rho(r_c)}$ **tot**	**0.1219**			$\sum \boldsymbol{\rho(r_c)}$ **tot**	**0.1292**		

On the contrary, QTAIM analysis well explained why peptide ***R*-12** (cCTAA = (1*R*,2*R*,4*R*)-**IIIawr**) had a h.e. of about 8% higher than that of peptide ***R*-5** (cCTAA = (1*R*,2*R*,4*R*)-**V**). Indeed, although these cCTAAs has structurally similar side chains, similarly located in the Cartesian space, the $\Delta\rho_{P-M}$ of peptide ***R*-12** is 0.0082 au higher than that of peptide ***R*-5** (Tables 5.7 and 5.12).

Table 6.12. Types and properties of BCPs of the Ac-Aib$_2$-(1*R*,2*R*,4*R*)-**IIIawr**-Aib$_2$-NHMe peptide ***R*-12** in the *P*- and *M*-helix conformation. All parameters are reported in au.

peptide ***R*-12, *P*-helix**				peptide ***R*-12, *M*-helix**			
N-H···O BCP	$\boldsymbol{\rho(r_c)}$	$\boldsymbol{\nabla^2\rho(r_c)}$	**ε**	**N-H···O BCP**	$\boldsymbol{\rho(r_c)}$	$\boldsymbol{\nabla^2\rho(r_c)}$	**ε**
IIIawr···ACE	0.0218	0.0688	0.0607	IIIawr···ACE	0.0190	0.0590	0.0735
Aib4···Aib1	0.0197	0.0621	0.0500	Aib4···Aib1	0.0221	0.0706	0.0553
Aib5···Aib2	0.0178	0.0559	0.0688	Aib5···Aib2	0.0163	0.0508	0.0588
NMe···IIIawr	0.0215	0.0688	0.0615	NMe···IIIawr	0.0221	0.0708	0.0632
$\sum \boldsymbol{\rho(r_c)}$ **at N-H···O**	0.0808			$\sum \boldsymbol{\rho(r_c)}$ **at N-H···O**	0.0795		
Cβ-H···O BCP				**Cβ-H···O BCP**			
C3H(IIIawr)···Ac	0.0098	0.0358	0.1084	C5H(IIIawr)···Ac	0.0107	0.0374	0.1319
Aib2···Aib1	0.0106	0.0386	0.7400	Aib5···Aib2	0.0053	0.0213	0.4762
Aib5···Aib2	0.0054	0.0217	0.5238	Aib5···Aib4	0.0124	0.0438	0.4416
Aib5··Aib4	0.0125	0.0445	0.4487				
$\sum \boldsymbol{\rho(r_c)}$ **at C-H···O**	0.0383			$\sum \boldsymbol{\rho(r_c)}$ **at C-H···O**	0.0284		
N···O CPs							
IIIawr···Aib1	0.0121	0.0386	0.9091				
$\sum \boldsymbol{\rho(r_c)}$ **at N···O**	0.0121						
$\sum \boldsymbol{\rho(r_c)}$ **tot**	**0.1312**			$\sum \boldsymbol{\rho(r_c)}$ **tot**	**0.1079**		

Peptide ***S*-6** (cCTAA = (*S*)-**VI**) had an h.e. comparable to that of ***S*-3** and ***R*-5**, although its side chain is not well located in either (-x, +y, +z) or (+x, +y, -z). However, the good h.e. can be attributed to the strong noncovalent interaction network, involving the cCTAA, of peptide ***S*-6** in the *P* conformation, together with a poor interaction network observed in the *M*-conformation, where the cCTAA is only marginally involved (Table 6.13).

Table 6.13. Types and properties of BCPs of the Ac-Aib$_2$-(*S*)-**VI**-Aib$_2$-NHMe peptide ***S*-6** in the *P*- and *M*-helix conformation. All parameters are reported in au.

peptide ***S*-6, *P*-helix**				peptide ***S*-6, *M*-helix**			
N-H···O BCP	$\boldsymbol{\rho(r_c)}$	$\boldsymbol{\nabla^2\rho(r_c)}$	**ε**	**N-H···O BCP**	$\boldsymbol{\rho(r_c)}$	$\boldsymbol{\nabla^2\rho(r_c)}$	**ε**
VI···ACE	0.0190	0.0601	0.0637	VI···ACE	0.0172	0.0539	0.0734
Aib4···Aib1	0.0196	0.0616	0.0553	Aib4···Aib1	0.0205	0.0649	0.0614
Aib5···Aib2	0.0172	0.0536	0.0492	Aib5···Aib2	0.0178	0.0554	0.0415

NMe···VI	0.0216	0.0684	0.0650	NMe···VI	0.0201	0.0629	0.0628
$\sum \rho(r_c)$ at N-H···O	0.0774			**$\sum \rho(r_c)$ at N-H···O**	0.0756		
Cβ-H···O BCP				**Cβ-H···O BCP**			
VI(C-H)···Ac	0.0075	0.0296	0.0926	VI(C-H)···Ac	0.0107	0.0350	0.0521
VI(CH_2)··Aib1(CH_3)	0.0037	0.0129	0.3125	Aib5···Aib2	0.0050	0.0200	0.6000
Aib5···Aib2	0.0051	0.0203	0.5882	VI···Aib2	0.0142	0.0493	0.2718
VI···Aib2	0.0127	0.0452	0.5417	Aib4···VI	0.0120	0.0431	0.6308
Aib4···VI	0.0111	0.0402	0.8600				
Aib5··Aib4	0.0123	0.0436	0.4286				
$\sum \rho(r_c)$ at C-H···O	0.0524			**$\sum \rho(r_c)$ at C-H···O**	0.0544		
$\sum \rho(r_c)$ tot	**0.1298**			**$\sum \rho(r_c)$ tot**	**0.1300**		

When comparing peptides ***R*-8** (cCTAA = (1*S*,2*R*,3*R*,4*R*)-**VIIb**) and ***S*-10** (cCTAA = (1*S*,2*S*,3*R*,4*R*)-**VIIIb**), it can be noticed that the former peptide has a h.e. of about 13% lower than that of ***S*-10**. This difference cannot be ascribed to differences in steric hindrance between the two cCTAAs, which is equivalent; however, QTAIM calculations gave a $\Delta\rho_{P-M}$ of 0.0032 and 0.0127 au for peptides ***R*-8** and ***S*-10**, respectively (Tables 5.14 and 5.15), indicating that the difference in helical screw sense selectivity of these cCTAAs is only depending on their electronic properties.

Table 6.14. Types and properties of BCPs of the Ac-Aib_2-(1*S*,2*R*,3*R*,4*R*)-**VIIb**-Aib_2-NHMe peptide ***R*-8** in the *P*- and *M*-helix conformation. All parameters are reported in au.

peptide ***R*-8**, ***P*-helix**				peptide ***R*-8**, ***M*-helix**			
N-H···X BCP	$\rho(r_c)$	$\nabla^2\rho(r_c)$	ε	**N-H···O BCP**	$\rho(r_c)$	$\nabla^2\rho(r_c)$	ε
VIIb···ACE	0.0126	0.0399	0.0424	VIIb···ACE	0.0133	0.0426	0.0952
Aib4···Aib1	0.0152	0.0477	0.0318	Aib4···Aib1	0.0209	0.0670	0.0596
Aib5···Aib2	0.0190	0.0594	0.0637	Aib5···Aib2	0.0195	0.0626	0.0607
NMe···VIIb	0.0214	0.0680	0.0571	NMe···VIIb	0.0219	0.0706	0.0595
VIIb(SH)···Ac	0.0201	0.0657	0.0931				
$\sum \rho(r_c)$ at N-H···O	0.0883			**$\sum \rho(r_c)$ at N-H···O**	0.0756		
Cβ-H···X BCP				**Cβ-H···O BCP**			
Aib1··VIIb(SH)	0.0047	0.0162	0.3174	VIIb(C6-H)···Ac	0.0087	0.0309	0.1094
Aib2···Aib1	0.0108	0.0385	0.5893	VIIb(C3-H)··VIIb	0.0200	0.0791	0.7838
Aib5···Aib2	0.0057	0.0227	0.5217	VIIb(C7-H)···VIIb	0.0138	0.0484	0.2979
Aib5··Aib4	0.0126	0.0447	0.4375	Aib5···Aib4	0.0124	0.0439	0.4359
$\sum \rho(r_c)$ at C-H···O	0.0338			**$\sum \rho(r_c)$ at C-H···O**	0.0549		
N···O CPs							
VIIb···Aib1	0.0116	0.0363	0.3191				
$\sum \rho(r_c)$ at N···O	0.0116						
$\sum \rho(r_c)$ tot	**0.1337**			**$\sum \rho(r_c)$ tot**	**0.1305**		

Table 6.15. Types and properties of BCPs of the Ac-Aib_2-(1*S*,2*S*,3*R*,4*R*)-**VIIIb**-Aib_2-NHMe peptide ***S*-10** in the *P*- and *M*-helix conformation. All parameters are reported in au.

peptide ***S*-10**, ***P*-helix**				peptide ***S*-10**, ***M*-helix**			
N-H···O BCP	$\rho(r_c)$	$\nabla^2\rho(r_c)$	ε	**N-H···O BCP**	$\rho(r_c)$	$\nabla^2\rho(r_c)$	ε
VIIIb···ACE	0.0157	0.0476	0.0385	VIIIb···ACE	0.0174	0.0546	0.0773
Aib4···Aib1	0.0164	0.0512	0.0345	Aib4···Aib1	0.0214	0.0682	0.0576
Aib5···Aib2	0.0194	0.0608	0.0664	Aib5···Aib2	0.0144	0.0455	0.0548

NMe···VIIIb	0.0213	0.0676	0.0576	NMe···VIIIb	0.0218	0.0694	0.0688
VIIIb(OH)··Ac	0.0252	0.0930	0.0811	VIIIb(OH)···Aib2	0.0222	0.0743	0.0513
$\sum \rho(r_c)$ **at N-H···O**	0.0980			$\sum \rho(r_c)$ **at N-H···O**	0.0972		
Cβ-H···O BCP				**Cβ-H···O BCP**			
Aib1···Ac	0.0105	0.0382	0.7826	VIIIb(C6-H)···Ac	0.0081	0.0286	0.1034
VIIIb(C4-H)···Ac	0.0081	0.0278	0.2241	VIIIb(C7-H)···VIb	0.0147	0.0498	0.1405
Aib2···Aib1	0.0110	0.0392	0.5000	Aib4···VIIIb	0.0122	0.0439	0.6984
Aib5···Aib2	0.0053	0.0213	0.5882	Aib5···Aib4	0.0121	0.0428	0.4459
Aib5··Aib4	0.0124	0.0440	0.4605				
$\sum \rho(r_c)$ **at C-H···O**	0.0473			$\sum \rho(r_c)$ **at C-H···O**	0.0471		
N···O BCP							
VIIIb···Aib1	0.0118	0.0371	0.3043				
$\sum \rho(r_c)$ **at N···O**	0.0118						
$\sum \rho(r_c)$ **tot**	**0.1571**			$\sum \rho(r_c)$ **tot**	**0.1443**		

Summarizing, REMD simulations together with QTAIM calculations on Ac-Aib$_2$-cCTAA-Aib$_2$-NHMe model peptides showed that the *P*-helical screw sense selectivity is due to steric hindrance exerted by the the cCTAA parallel to the peptide helix axis, without particular preferences for the region downstream and upstream of the cCTAA itself. However, when the side chain is located in the upstream semiaxis, it also has to point toward the opposite direction of the helical screw sense (i.e. the (-x, +y, +z) sector of the Cartesian space indicated in Figure 6.2). On the contrary, if the side chain is located in the downstream semiaxis, its encumbrance needs to follow the helical screw sense direction (i.e. the (+x, +y, -z) sector). In addition, quite strong noncovalent interactions consisting of classical N – H···O=C H-bonds and weak C – H···O=C interactions can improve the helical screw sense selectivity exerted by cCTAAs.

At the light of this, (1*S*,2*R*,4*R*)-**IV** turned out to be a modest helical stabilizer,[72] but an excellent *P*-helix inducer. Indeed, this CTAA develops its steric hindrance in the upstream direction and is able to strengthen the peptide noncovalent interaction network only in the *P*-helix configuration. Conversely, (1*R*,2*R*,4*R*)-**V** resulted an excellent helical stabilizer, but a relatively poor *P*-helix inducer.

Therefore, the design of a peptide including one or more cCTAAs and with well-defined helical secondary structure requires to seek a reasonable compromise between structural features of the cCTAA, needed to allow the binding efficiently to the protein target, and those required to obtain a stable helix and with a defined screw sense.

6.3 Material and Methods

REMD Simulations. Force-field parameters for Aib, **II**, **IIIa**, **IIIb**, **IV**, **V** and **VI** were taken from previous work (Annex 5.B),[72] while **VIIa**, **VIIb**, **VIIIa** and **VIIIb** cCTAAs were parameterized by following the same protocol adopted before.[72]

The *pmemd* module of the Amber14 suite[192] was used to perform REMD simulations of Ac-Aib$_2$-cCTAA-Aib$_2$-NHMe peptides, starting from extended conformations ($\varphi = \psi = \omega = 180°$) and applying the protocol previously described.[72] Briefly, the combination of AMBER *ff99SB* force field[141] and

OBC(II) (igb = 5) solvent model[172] was chosen, and 12 replicas of 250 ns each were run spanning a temperature range from 260.00 to 658.94 K, for a total of 3 μs simulation for each peptide.

The trajectories extracted at 308.53 K were submitted to cluster analyses with *cpptraj*[192] at 50-100, 100-150, 150-200, 200-250 ns time intervals using the previously reported protocol.[72] Here, the simulation was considered converged when the standard deviations of the cluster populations corresponding to *P*- and *M*-helices ($\sigma_{P\%}$ and $\sigma_{M\%}$, respectively) were less than 5% among all intervals. We also verified that simulations conducted on peptides containing enantiomeric CTAAs gave equal and opposite h.e., within the threshold of 5%. As expected, peptide **11** which contains only Aib, also gave h.e. below 5%.

Mono and bidimensional potentials of mean force (PMF) were computed using the weighted histogram analysis method (WHAM and WHAM-2d)[232] on the φ_2, ψ_3, φ_3 and ψ_4 dihedrals obtained from the whole 250 ns trajectories at 260, 283, 308 and 335 K extracted from the REMD simulations. The histogram limit was set to ±180° over 100 bins with a tolerance of 0.01.

QTAIM Calculations. Gaussian 09[233] was used to optimize the *P*- and *M*-helices of selected peptides using the mPW1B95/6-31+G(d,p) level of theory[234] and the CPCM solvent model for water,[236] a combination successfully used by our group in similar instances.[72,249] The same level of theory was used to confirm, by vibrational analyses, that the optimized geometries were true minima. The obtained wave functions were submitted to QTAIM calculations with the AIM2000 software[250] by setting the same parameters used previously.[72] In this case also, N-H···O, C-H···O and backbone N···O bond critical points (BCPs) were evaluated in terms of strength, type and stability by calculating their electronic density $\rho(r_c)$, the sign of the Laplacian $\nabla^2(r_c)$ and their ellipticity ε; BCPs with ε > 1 were considered unstable and discarded.

7 MECHANISMS OF HELICAL SCREW SENSE INVERSION

7.1 INTRODUCTION

Beyond the knowledge of the mechanisms involved in the helix secondary structure stabilization[72] and in the helical screw sense selectivity[86] exerted by cCTAAs, understanding how the interconversion between *P*- and *M*-helices occurs represents an important, although challenging, goal.

Indeed, many events in biological systems involve the coupling of selective molecular recognition to a conformational response,[100,251] leading to modulation of function in peptides, proteins or nucleic acids.[99]

In PPIs modulation, the switch from an inactive to an active conformation of a peptide modulator can represent an advantage if it allows a control of its kinetics and site of action.[252] For example, the possibility of regulating PPI inhibitors activity with light was investigated by introducing photo-sensitive cross-linkers in the peptide chain.[253–255]

Since the secondary structure motif is fundamental in protein-protein recognition, one of the two helical screw senses can represent the inactive conformation (or a prodrug, in the case of switchable peptides), because the AAs side chains are differently oriented in space. Therefore, a detailed knowledge on how the helical screw sense inversion occurs can be helpful for the design of screw sense switchable PPI modulator.

At the light of this, in collaboration with Professor Jonathan Clayden's group at the University of Manchester, the mechanisms involved in this process have been studied.

Clayden's group synthesized Cbz-(*S*)-αMeVal$_2$-Aib$_5$-(*S*)-αMeVal$_2$-NHMe (peptide **1**) and Cbz-(*S*)-αMeVal$_2$-Aib$_5$-(*R*)-αMeVal$_2$-NHMe (**2**) peptides. As expected, the former peptide, containing only (*S*)-αMeVal, had a X-ray structure corresponding to a *P*-3$_{10}$-helix conformation (Figure 7.1A), since it has been proved that (*S*)-αMeVal induces a *P* conformation once inserted in an otherwise achiral helical peptide.[96] Conversely, peptide **2**, bearing (*S*)-αMeVal at the N-termini and (*R*)-αMeVal at the C-termini, gave a X-ray structure corresponding to a *P*-3$_{10}$-helix from the N-terminus to Aib5 and to a *M*-helix from Aib5 to the C-terminus (Figure 7.1B). However, these peptides and their relative crystallographic structures could not provide satisfactory information about either the mechanism involved in the helical screw sense inversion or the energy barriers associated to the migration of the screw sense inversione along the peptide chain.

Therefore, REMD simulations were performed to obtain statistically relevant conformations of the two peptides. PMF analysis was then applied to evaluate the energy barriers associated to the migration of the reverse along the peptide chain. Furthermore, PNEB simulations were carried out on achiral Aib-containing peptides with the aim of describing qualitatively the mechanism behind the helical screw sense inversion.

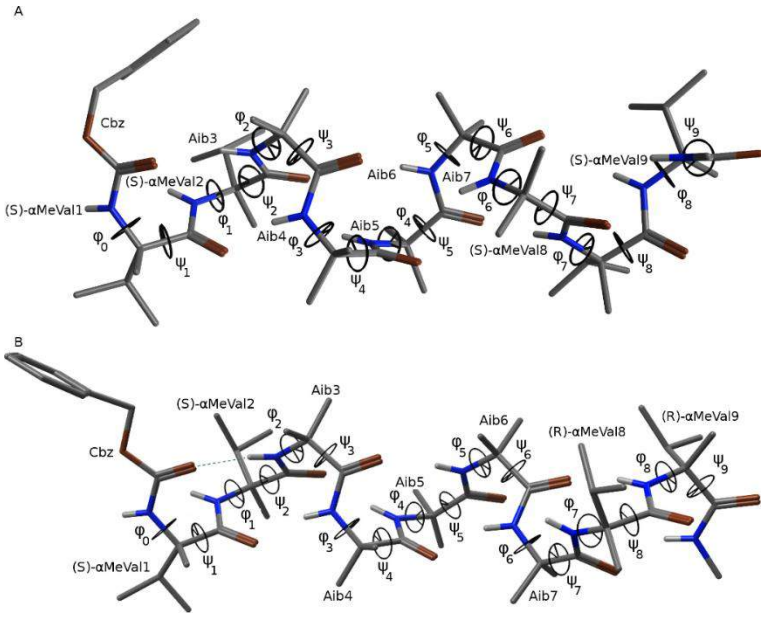

Figure 7.1. X-ray structures of Cbz-(*S*)-αMeVal$_2$-Aib$_5$-(*S*)-αMeVal$_2$-NHMe peptide **1** (A) and Cbz-(*S*)-αMeVal$_2$-Aib$_5$-(*R*)-αMeVal$_2$-NHMe peptide **2** (B).

7.2 Results and Discussion

The results of cluster analyses performed on the 297.31 K implicit solvent trajectories of peptides **1** and **2**, reported in Tables 6.1, showed that in both cases the REMD simulations were able to reproduce the crystallographic data (Figure 7.2). Indeed, the most populated clusters of peptides **1** and **2** (90.1% and 69.3%, respectively) have a RMSD from the backbone of the correspondent X-ray structures of 1.4 Å and 1.0 Å, respectively, and the structures are superimposable to the crystallographic ones (Figure 7.2). As expected, peptide **1** is a complete right-handed 3_{10}-helix, whereas peptide **2** corresponds to a right-handed 3_{10}-helix from the N-terminus to Aib5 and to a left-handed 3_{10}-helix from Aib5 to the C-terminus.

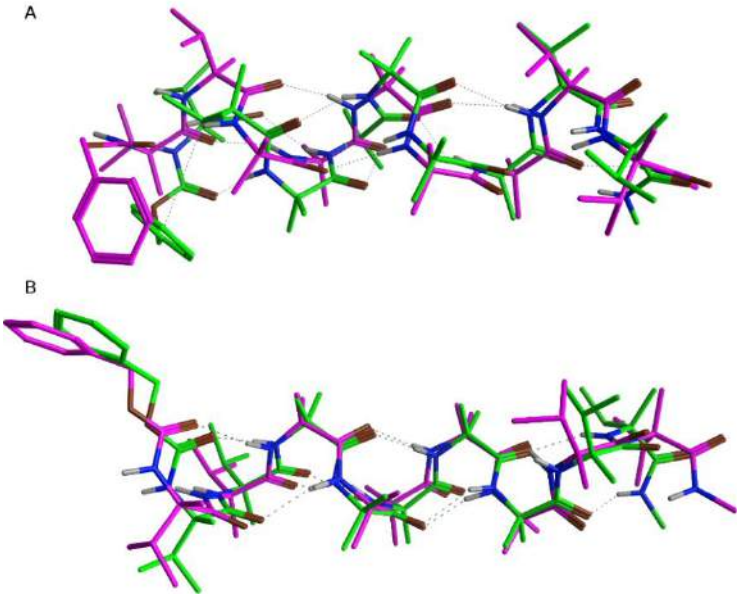

Figure 7.2. A) Superposition of X-ray structure (green) and representative structure of the most populated cluster (magenta) of peptide **1** from the analysis of the 297.31 K REMD trajectory. B) Superposition of X-ray structure (green) and representative structure of the most populated cluster (magenta) of peptide **2** from the analysis of the 297.31 K REMD trajectory.

Moreover, the most stable H-bonds (occupancies > 50%), which are those identifiable in the X-ray structures also (Figure 7.1 and Table 7.3), involve *i+3* and *i* residues, indicating the presence of a 3_{10}-helix or a β-turn. It has to be noted that the occupancies of the H-bonds between (*R*)-αMeVal8 and Aib5 and between (*R*)-αMeVal9 and Aib6 of peptide **2** are about 20% lower than those between (*S*)-αMeVal8 and Aib5 and between (*S*)-αMeVal9 and Aib6 of peptide **1**. This can be explained by the reduced stability of the screw sense preference of peptide **2**, due to the competition between the (*S*)- and (*R*)-αMeVal residues located at the N- and C-terminus, respectively. This is also demonstrated by considering the difference between the two percentages of the most populated clusters: while REMD simulation of peptide **1** mostly resulted in a unique preferential conformation, corresponding to the right-handed 3_{10}-helix, REMD performed on peptide **2** gave additional minor clusters with helical screw sense inversion occurring at different points along the chain (Table 7.1).

Table 7.1. Cluster analyses of the final 50 ns of the 297.31 K REMD trajectories of peptide **1** and **2**.

1	**pop%**	φ_0	ψ_1	φ_1	ψ_2	φ_2	ψ_3	φ_3	ψ_4	φ_4	ψ_5	φ_5	ψ_6	φ_6	ψ_7	φ_7	ψ_8	φ_8	ψ_9	**RMSD**
X-ray		-55.0	-37.5	-52.1	-34.2	-49.8	-39.5	-53.0	-40.6	-57.2	-40.0	-57.6	-32.8	-60.2	-20.9	-44.0	-49.9	-58.3	-38.5	
c0	90.1	-62.9	-13.7	-61.5	-23.3	-34.8	-32.0	-46.3	-31.0	-48.3	-24.8	-50.8	-15.4	-52.3	-35.7	-42.5	-24.9	-61.7	-17.3	1.4 Å
c1	8.6	-64.4	-0.9	-64.1	-8.4	45.9	24.3	49.7	27.8	53.7	18.8	46.9	34.1	56.0	26.3	-68.5	-3.8	-57.9	-30.4	2.3 Å
c2	1.2	-53.8	-33.1	-65.8	-14.0	51.7	38.1	53.0	26.8	47.1	29.3	44.9	38.1	43.6	23.0	48.2	17.5	-50.7	-30.1	2.3 Å
c3	0.1	-50.2	-29.2	-44.1	-39.8	-51.6	-25.2	-45.2	-37.5	-51.3	-33.8	-39.6	-36.5	-48.7	-26.6	60.5	20.4	51.4	11.2	2.1 Å
c4	0.0	-54.6	-24.0	-56.3	-21.7	-47.0	-35.2	-52.9	-8.8	37.3	44.1	62.5	25.4	-46.4	157.4	-52.6	-19.6	-59.2	-1.8	3.3 Å
2																				
X-ray		-55.3	-37.7	-46.5	-33.6	-55.2	-27.4	-51.0	-27.6	-61.6	-19.4	-48.4	-39.9	49.5	42.8	51.6	34.2	56.5	36.6	
c0	69.3	-41.2	-25.1	-52.6	-35.4	-51.7	-25.4	-54.1	-17.1	-52.4	-39.0	-40.2	-19.9	56.0	11.3	65.3	9.6	50.4	28.9	1.0 Å
c1	26.7	-49.7	-21.7	-51.1	-34.7	-39.5	-29.8	-51.6	-11.8	-56.4	-33.0	-37.6	-33.2	-54.7	-19.0	49.4	26.2	55.7	11.2	2.0 Å
c2	3.7	-54.5	-30.0	-67.1	-19.0	-47.7	-45.4	-62.8	-7.5	-53.1	-16.4	-47.2	-33.9	-56.5	-19.3	-41.1	-39.3	58.0	23.5	1.9 Å
c3	0.3	-39.3	-24.4	-50.9	-7.3	-51.9	-4.9	47.1	26.0	56.2	28.7	43.4	47.3	49.7	26.7	-68.9	-42.2	-59.7	-13.2	2.6 Å
c4	0.0	-74.8	3.5	-57.9	-18.7	-40.5	-35.7	-46.9	-23.7	-60.6	-15.6	-46.0	-10.3	51.1	-153.9	39.5	27.5	50.5	10.5	2.6 Å

Table 7.2. Cluster analysis of the final 60 ns of the 303.60 K REMD trajectory of peptide **2** in explicit methanol.

	pop%	φ_0	ψ_1	φ_1	ψ_2	φ_2	ψ_3	φ_3	ψ_4	φ_4	ψ_5	φ_5	ψ_6	φ_6	ψ_7	φ_7	ψ_8	φ_8	ψ_9	**RMSD**
X-ray		-55.3	-37.7	-46.5	-33.6	-55.2	-27.4	-51.0	-27.6	-61.6	-19.4	-48.4	-39.9	49.5	42.8	51.6	34.2	56.5	36.6	
c0	53.5	-71.1	-18.3	-45.6	-13.0	-52.9	-13.3	-53.9	-21.5	-50.5	-31.2	50.6	18.6	48.4	31.8	51.8	7.2	53.2	16.7	2.1 Å
c1	12.7	62.9	23.6	39.3	21.5	54.6	35.5	44.8	29.0	42.1	40.1	55.5	13.5	56.3	0.9	60.8	13.8	48.1	6.1	2.1 Å
c2	10.0	-44.6	-31.8	-52.3	-19.4	-45.5	-18.5	-44.6	-26.3	-47.7	-19.4	-56.6	-16.2	47.7	27.3	48.7	35.7	59.8	12.7	0.9 Å
c3	8.9	-51.2	-18.7	-52.5	-24.2	-30.7	-55.5	-37.9	-32.1	-50.6	-31.7	-43.1	-18.7	-47.4	-8.1	52.4	17.2	58.3	26.3	2.0 Å
c4	7.9	-68.9	9.4	-55.8	-18.6	-51.2	-33.4	62.1	9.2	37.1	29.4	48.5	19.9	49.8	7.7	36.9	20.2	71.9	18.2	2.0 Å
c5	3.1	-49.8	-22.4	-60.0	-20.7	-55.0	-28.6	-56.0	-26.4	-56.6	-19.5	-47.5	-43.1	-48.7	-19.8	53.1	17.8	75.3	8.9	2.2 Å
c6	1.8	-63.9	-17.9	-57.2	-8.7	-52.7	-15.4	-44.8	-29.1	-53.1	-23.3	-35.6	-30.8	-65.2	-16.3	-44.8	0.5	48.3	25.5	2.1 Å
c7	1.4	-53.6	-20.0	-56.2	-40.0	-44.8	-22.5	-64.2	-24.2	-46.2	-10.9	-62.6	-19.3	-51.8	-22.3	-50.6	-14.7	72.8	9.7	1.9 Å
c8	0.4	-47.8	-32.8	-71.1	1.6	-21.2	-49.3	-44.5	-26.7	-46.4	-17.9	-51.2	-18.7	-61.7	-4.2	-56.5	11.0	52.0	8.7	2.3 Å
c9	0.2	-51.8	-14.8	-58.0	-10.8	-47.2	-14.3	-47.1	-27.6	-46.6	-28.9	-43.6	-29.2	-40.7	-36.9	-49.6	-28.1	-40.4	-40.3	1.7 Å
c10	0.1	-56.0	-16.3	-44.3	-22.7	-62.0	-31.2	-31.5	-30.2	-42.9	-30.4	-71.2	11.3	-42.1	-47.9	53.4	-4.0	129.3	-3.1	2.0 Å
c11	0.0	40.3	39.2	50.9	25.8	52.1	29.4	40.0	30.7	55.3	18.2	46.3	25.5	40.2	41.9	65.1	14.0	110.1	10.7	2.0 Å

c12	0.0	-33.9	-40.3	-42.7	-29.9	-60.0	-23.7	-55.1	8.8	-51.4	-31.8	46.6	26.0	48.3	27.1	24.9	35.2	71.4	19.8	2.5 Å
c13	0.0	-53.5	-20.2	-61.4	-27.9	-46.0	-14.1	-49.9	-27.6	-56.3	-21.5	-70.3	-5.2	-42.4	-25.0	59.4	-8.0	71.3	12.0	1.9 Å
c14	0.0	-43.6	-22.3	-59.4	-13.3	-37.5	-49.3	-49.2	-30.0	-71.5	-18.6	-64.0	-10.7	-50.4	-34.0	-61.4	13.0	56.4	9.1	1.9 Å

Table 7.3. H-bond analyses of 297.31 K implicit solvent REMD trajectories of peptides **1** and **2** (Donor, N-H; Acceptor, C=O).

peptide **1**			peptide **2**		
donor	**acceptor**	**occupancy**	**donor**	**acceptor**	**occupancy**
Aib4	(*S*)-αMeVal1	90.24%	Aib4	(*S*)-αMeVal1	88.43%
Aib5	(*S*)-αMeVal2	93.05%	Aib5	(*S*)-αMeVal2	86.74%
Aib6	Aib3	92.92%	Aib6	Aib3	86.11%
Aib7	Aib4	92.74%	Aib7	Aib4	86.95%
Aib7	Aib5	6.52%	Aib7	Aib5	8.42%
(*S*)-αMeVal8	Aib5	73.44%	(*R*)-αMeVal8	Aib5	56.07%
(*S*)-αMeVal8	Aib6	7.46%	(*R*)-αMeVal8	Aib6	10.50%
(*S*)-αMeVal9	Aib6	77.69%	(*R*)-αMeVal9	Aib6	59.00%
(*S*)-αMeVal9	Aib7	6.91%	(*R*)-αMeVal9	Aib7	8.40%

Furthermore, in the representative structure of the most populated cluster of peptide **2**, the carbonyl group of Aib5 and the amino group of (*R*)-αMeVal8 are not involved in any H-bond, as also observed in the X-ray structure. However, from H-bond analysis we noticed the presence of both *i+3→i* and *i+2→i* H-bonds involving Aib5 and (*R*)-αMeVal8, underscoring the presence of β- and γ-turns, respectively. Moreover, even if the H-bonds corresponding to γ-turns are also present in the simulation performed on peptide **1**, their occupancies are higher for peptide **2** (Table 7.3). The low occupancy (around 10%) of these H-bonds means that γ-turns are only transient and the differences showed analyzing the REMD trajectories of the two peptides suggest that γ-turns occur more frequently where the competition between the two helical screw senses is more pronounced. Thus, we can hypothesize that γ-turns can play an active role in the inversion of the helical screw sense. The presence of γ-turns with poor occupancies in the trajectory of peptide **1** can be attributed to the mild effect of the achiral residues, which, in principle, can equally assume both the *P*- and the *M*-conformations. Indeed, for peptide **1**, the *i+2→i* H-bond with the highest occupancy is the one involving (*S*)-αMeVal8 and Aib6, which is the Aib residue less effected by the presence of the (*S*)-αMeVal at the N-terminus.

The different behavior of the two peptides is confirmed by monodimensional PMF profiles as a function of φ and ψ dihedrals (Figure 7.3). Indeed, for both peptides we only observed the presence of two minima corresponding to the *P*- and *M*-helical conformations. However, only the PMF profiles as a function of φ_1, φ_2, ψ_2 and ψ_3 dihedrals, which are those where the Cα*S* enantiomer is involved, are identical in the two peptides, showing a global and a local minimum corresponding to the *P*-helix and *M*-helix, repsectively. PMF profiles of peptide **1** always resulted in a preference for the right-handed helical conformation; conversely, for peptide **2** the PMF as a function of $\varphi_{3\text{-}5}$ and $\psi_{4\text{-}6}$ showed a progressive reduction in the energy difference between the two minima (Figure 5.6, ΔE_M), which culminated in an inversion of the screw sense preference in PMF($\varphi_{6\text{-}8}$) and PMF($\psi_{5\text{-}9}$), where the global minimum corresponded to the *M*-helix.

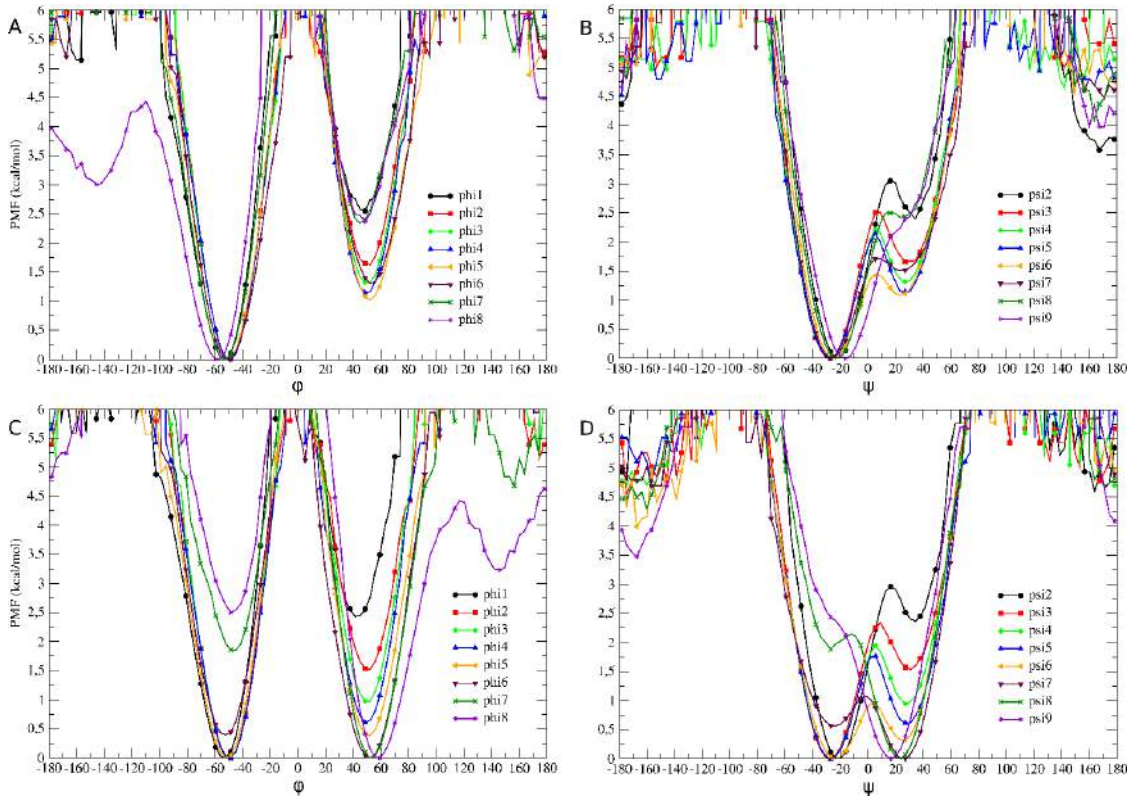

Figure 7.3. PMF as a function of φ (A) and ψ (B) dihedrals for peptide **1** and PMF as a function of φ (C) and ψ (D) dihedrals for peptide **2**.

In details, concerning peptide **1**, ΔE_M for PMF(φ_0) is of about 2.5 kcal/mol in favor of the *P*-helix at the considered temperatures; then, it drops of about 1 kcal/mol from PMF(φ_1) to PMF(φ_2), together with a further decrease of less than 0.5 kcal/mol from PMF(φ_2) to PMF(φ_3). The ΔE_M value for PMF($\varphi_{4\text{-}5}$) remained constant, while ΔE_M for PMF($\varphi_{7\text{-}8}$) increased again up to 2.5 kcal/mol, always favoring the *P*-helix.

The same behavior is observable for PMF on ψ dihedrals, although in this case the energy barrier between the two minima ($\Delta E_M^{\ddagger}$) can be overcome at the analyzed temperatures, as previously observed.[72,86] In this case, $\Delta E_M^{\ddagger}$ decreased progressively from a maximum of 3 kcal/mol reached for PMF(ψ_2) to 1.5 kcal/mol showed by PMF(ψ_6) and then increased again to 2.5 kcal/mol for PMF(ψ_8). It should be noticed that PMF(ψ_9) showed a unique minimum corresponding to the *P*-helix, suggesting that the effect of (*S*)-αMeVal is particularly strong on this dihedral.

On the contrary, PMF profiles for peptide **2** as a function of φ dihedrals showed a progressive ΔE_M decrease from a maximum of 2.5 kcal/mol in favor of the *P*-helical

conformation, observed for PMF(φ_1), to a minimum of less of 0.5 kcal/mol for PMF(φ_5). Successively, PMF as a function of $\varphi_{6\text{-}8}$, showed again an increase of ΔE_M up to 2.5 kcal/mol, but favoring the *M*-helix. PMF profiles as a function of ψ dihedrals gave the same trend, although, in this case also, the $\Delta E_M^{\ddagger}$ resulted surmountable. Moreover, as happened for peptide **1**, PMF (ψ_9) showed only one minimum, which however corresponded to the *M*-helical conformation.

In order to verify if the solvent can significantly affect the results of the simulation,[256,257] we performed a REMD simulation of peptide **2** in explicit methanol. The choice of carrying out the simulation just on this peptide was due to the fact that the screw sense inversion occurs only in peptide **2**, which is the one having enantiomers cCTAAs at the N- and C-termini. Moreover, REMD simulations in explicit solvent resulted extremely time consuming on the available hardware.

The simulation carried out in explicit MeOH led to slightly different results. Indeed, in the representative structure of the most populated cluster (53.5%) the helical screw sense inversion from *P*- to *M*-helix is observed at Aib4, and the RMSD from the crystallographic structure is of 2.06 Å (Figure 7.4A and Table 7.2). Nonetheless, the representative structure of cluster c2 (10.0%) had a conformation which is superimposable to the X-ray structure and with a RMSD of 0.90 Å (Figure 7.4B and Table 7.2), and, considering the representative structures of the other minor clusters, the inversion of the helical screw sense can involve any peptide residue. Moreover, in some minor clusters (e.g. c6, c8, c12-14, see Table 7.2 and Figure 7.5) the presence of γ-turns at different points along the chain is clearly observable. It can also be noticed that γ-turns are located where the helical switch takes place, giving a further proof to the hypothesis that *i*+2→*i* H-bonds are involved in the helical screw sense inversion mechanism.

This can also be confirmed by the H-bond analysis of the intramolecular interactions (Table 7.4). Indeed, in the simulation of peptide **2** conducted in implicit solvent *i*+2→*i* H-bonds were only observed between Aib7 and Aib5, αMeVal8 and Aib6 and between αMeVal9 and Aib7 (Table 7.3), i.e. where the helical screw sense inversion can occur, as showed by cluster analysis and PMF (Table 7.1 and Figure 7.3,

respectively). Conversely, in the case of the explicit MeOH simulation, γ-turns can involve any peptide residue and, as expected, the reverse can occur at different points all along peptide **2**, as showed in Figure 7.5. However, it should be underscored that also in explicit solvent the *i*+*2*→*i* H-bonds having the highest occupancies are those between Aib7 and Aib5, (*R*)-αMeVal8 and Aib6 and (*R*)-αMeVal9 and Aib7, proving the consistency between the two simulations and confirming that the inversion of the helical screw sense preferentially takes place at this point of the peptide chain. Although, it is clear that methanol some way affects the process, by stabilizing the γ-turns and allowing the reverse from right- to left-handed helix and *vice versa* to occur anywhere along the peptide chain.

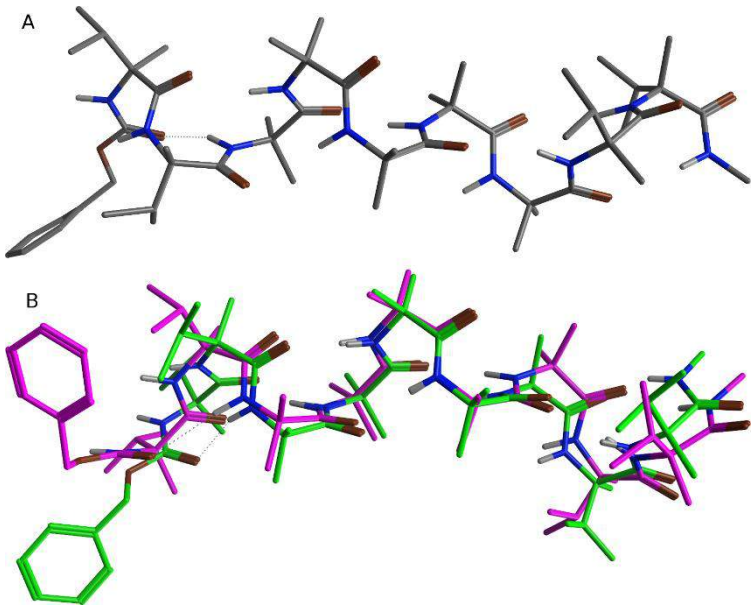

Figure 7.4. A) Representative structure of the most populated cluster of REMD trajectory in explicit solvent at 303.60 K. B) Superposition of crystallographic structure of peptide **2** (green) and the representative structure of cluster c2 (magenta)of REMD trajectory in explicit solvent at 303.60 K.

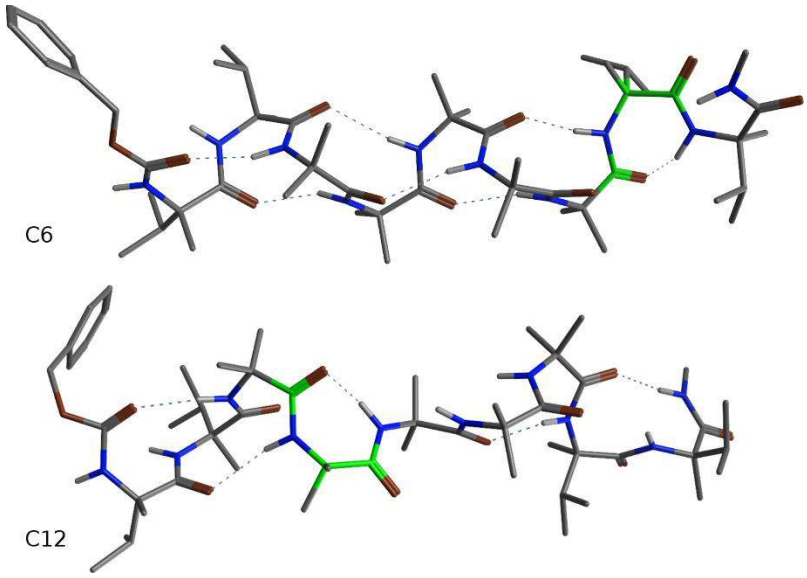

Figure 7.5. Representative structures of clusters C6 (top) and C12 (bottom) of REMD trajectory in explicit methanol at 303.60 K. The γ-turn is highlighted in green.

Indeed, it's not surprising that (*S*)-αMeVal1, (*S*)-αMeVal2, (*R*)-αMeVal8 and (*R*)-αMeVal9 are the residues most frequently involved in H-bonds with solvent molecules, since their backbone -NH and -C=O groups can't be involved in intra-peptide H-bonds. However, also the backbone atoms of the central residues are also able to interact with the solvent (Table 7.4). Thus, methanol seems to contribute to the stabilization of the chain reversal by establishing H-bonds with the residues involved in the helical screw sense inversion, whose amine and carbonyl groups would otherwise be free as observed for the simulation in implicit solvent.

The stabilizing effect of methanol can also be verified by observing the PMF as a function of φ and ψ dihedrals (Figure 7.6). Indeed, if compared to those obtained in implicit solvent (Figure 7.3), the PMF(φ) profiles show a global reduction of both ΔE_M and $\Delta E_M^{\ddagger}$, except for PMF(φ_8) profile, whose ΔE_M is slightly higher in explicit solvent than in the implicit solvent simulation. In addition, $\Delta E_M^{\ddagger}$ from PMF($\varphi_{2\text{-}5}$) can be overcome at the analyzed temperatures, ΔE_M from PMF(φ_4) is zeroed while from PMF(φ_5) the *M*- helix results slightly favored. The same trend can be observed for PMF as a function of ψ dihedrals: ΔE_M are reduced of about 0.5-1.0 kcal/mol, all the $\Delta E_M^{\ddagger}$ are lower than 2.0 kcal/mol compared to those obtained from implicit solvent

REMD, and the inversion of the screw sense preference occurs at ψ_5, although for this dihedral the ΔE_M is close to zero.

Table 7.4. H-bond analysis of explicit solvent REMD trajectory of peptide **2**.

donor	acceptor	occ%		donor	acceptor	frac%§	donor	acceptor	frac%§
Aib4	αMeVal1	82.8		αMeVal1	MeOH	70.4	MeOH	αMeVal9	71.5
Aib3	αMeVal1	7.4		αMeVal2	MeOH	41.5	MeOH	αMeVal8	61.0
Aib5	αMeVal2	81.4		Aib6	MeOH	11.9	MeOH	Aib7	41.7
Aib4	αMeVal2	5.9		Aib5	MeOH	11.4	MeOH	Aib3	34.5
Aib6	Aib3	79.5		Aib7	MeOH	9.85	MeOH	Aib4	31.5
Aib5	Aib3	6.1		Aib4	MeOH	7.09	MeOH	Aib5	29.8
Aib7	Aib4	81.8		αMeVal8	MeOH	3.79	MeOH	αMeVal2	26.7
Aib6	Aib4	5.5		Aib3	MeOH	3.6	MeOH	αMeVal1	24.7
αMeVal8	Aib5	73.43		αMeVal9	MeOH	0.83	MeOH	Aib6	22.45
Aib7	Aib5	8.93							
αMeVal9	Aib6	75.51							
αMeVal8	Aib6	14.83							
αMeVal9	Aib7	11.41							

§ The frac% doesn't represent a real occupancy, since for any given frame more than one solvent molecule can bind to the same place.

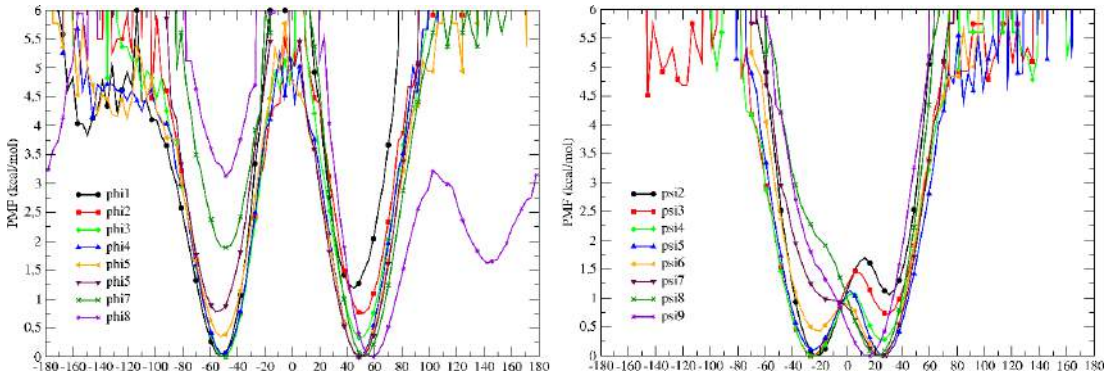

Figure 7.6. PMF as a function of φ (left) and ψ (right) dihedrals for peptide **2**.

To further verify the involvement of γ-turns in the screw sense inversion mechanism, we qualitatively studied the process leading from a *P*- to a *M*-helix by PNEB simulations on Ac-Aib$_n$-NH$_2$ peptides, with n = 4, 6, 8 and 20. Different peptide lengths were used to assess the independency of the simulations from the number of amino acid residues considered. Moreover, these peptides were chosen because they equally exist in both the right- and the left-handed conformations, which can be therefore selected as initial and final images for the simulations (Figure 7.7A and 7.7H, respectively).

The following discussion is mainly focused on the PNEB simulations performed on the hexapeptide, although it is valid for all the peptide considered here. Indeed, the Ac-Aib_6-NH_2 is sufficiently long to be taken as a model for the whole process, but at the same time is easier to handle than its higher homologues due to its lower number of degrees of freedom. The octa- and eicosapeptide have been taken in account to extend the obtained results to longer peptides, while the tetrapeptide has been useful to gain the details of the switch from β- to β'-turn, which represents one of the main steps in the helical inversion.

First of all, a defined propagation direction of the helical inversion is not detectable: the process always starts with the break of one or two internal H-bonds. Apparently, this starting point could seem unrealistic, since the internal H-bonds are stronger than the terminal ones. However, with PNEB simulations the minimum energy pathway from a state to another one is found;[258] thus, although the break of terminal H-bonds is more likely occurring, their re-forming is equally probable without any significant conformational change. Conversely, the break of an internal H-bond can be the initial seed for the inversion, because the system evolution toward the other conformation is less hampered once this high energy H-bond is broken.

After this initial step, in all cases we observe a relaxation of the peptide structure, which assumes a sigmoidal shape stabilized by β-turns (Figure 7.7B-D). Independently from the type of β-turn formed, this seems to be fundamental for the helical inversion, since it creates local C-shaped conformations favoring the subsequent dihedral switch.

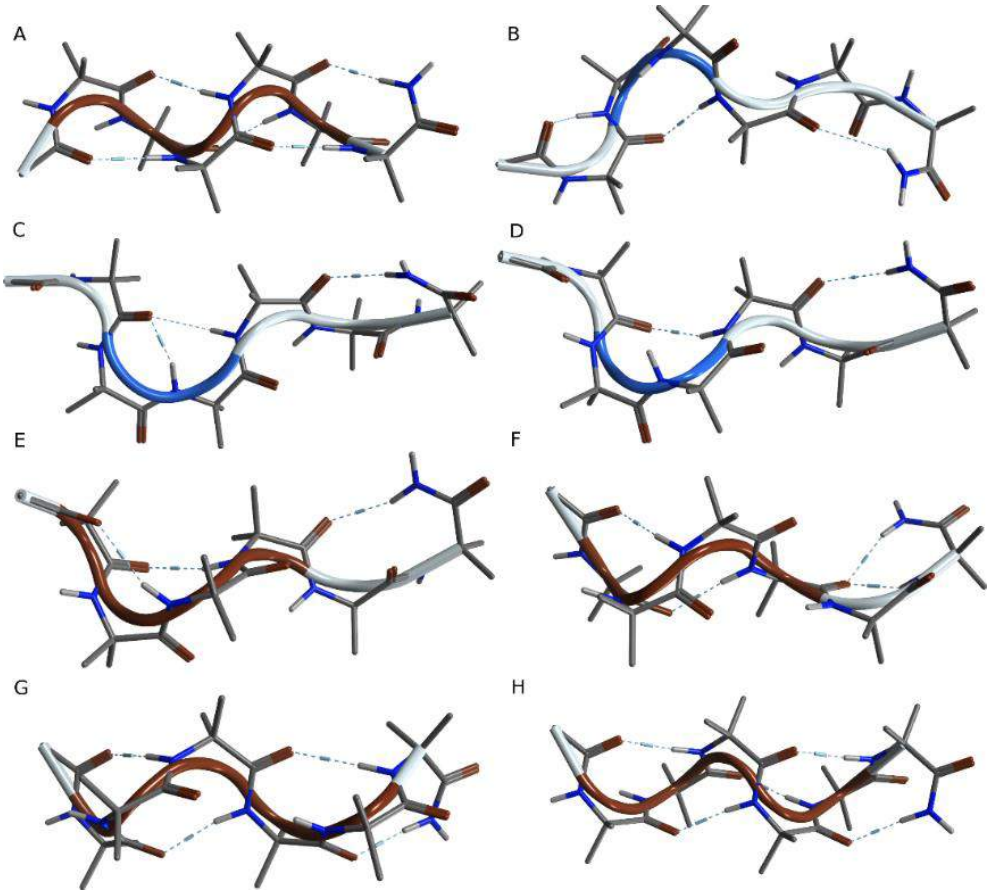

Figure 7.7. Conformations extracted from the PNEB simulation of the Ac-Aib_6-NH_2 peptide (run 5) representing the main steps in the helical screw sense inversion.

Indeed, the inversion of the screw sense takes place individually in each fragment identified by a β-turn and it involves the creation of γ-turns (Figure 7.7B, 6.7C and 6.7F), which can be detected by the H-bond analysis performed on the trajectories extracted from the PNEB simulations (Table 7.5). From a visual inspection and from the measurement of the dihedrals (Figure 7.7C and 6.7F), the observed γ-turns represent the obligated intermediate step in between the switch from β to β' type I turns, which, if repeatedly present in the peptide, lead to a right- and left-handed 3_{10}-helix, respectively.

Table 7.5. H-bond analyses on PNEB simulations of Ac-Aib$_n$-NH$_2$ (n = 4, 6, 8 and 20). Donor (D) and acceptor (A) are NH and C=O groups, respectively.

n = 4		run1	run2	run3	run4	run5	run6	run7	run8	run9	run10
D	**A**	**occ%**	**occ%**	**occ%**	**occ%**	**occ%**	**occ%**	**occ%**	**occ%**	**occ%**	**occ%**
NH_2	Aib2	20.8	8.3	8.3	25.0	8.3	25.0	12.5	8.3	29.2	12.5
Aib4	Aib1	100.0	100.0	100.0	100.0	95.8	95.8	95.8	95.8	100.0	95.8
Aib3	Ac	29.2	37.5	37.5	12.5	37.5	33.3	25.0	33.3	29.2	25.0
Aib4	Aib2	4.2	4.2	4.2	n.a	4.2	4.2	8.3	8.3	n.a	4.2
NH_2	Aib3	4.2	8.3	8.3	4.2	8.3	4.2	4.2	8.3	4.2	8.3
Aib2	Ac	29.2	25.0	25.0	20.8	29.2	16.7	29.2	16.7	20.8	33.3
Aib3	Aib1	8.3	33.3	33.3	4.2	4.2	4.2	8.3	8.3	20.8	8.3
n = 6		run1	run2	run3	run4	run5	run6	run7	run8	run9	run10
D	**A**	**occ%**	**occ%**	**occ%**	**occ%**	**occ%**	**occ%**	**occ%**	**occ%**	**occ%**	**occ%**
Aib6	Aib3	30.56	30.56	36.11	38.89	11.11	16.67	8.33	16.67	8.33	13.89
NH_2	Aib4	100.00	100.00	97.22	13.89	100.00	75.00	100.00	100.00	83.33	100.00
Aib4	Aib1	52.78	88.89	100.00	75.00	97.22	91.67	88.89	44.44	41.67	80.56
Aib5	Aib2	44.44	33.33	25.00	19.44	22.22	13.89	36.11	30.56	13.89	33.33
Aib3	Ac	25.00	13.89	44.44	50.00	44.44	44.44	63.89	66.67	44.44	52.78
Aib2	Ac	16.67	11.11	8.33	19.44	25.00	8.33	8.33	16.67	44.44	30.56
Aib3	Aib1	38.89	n.a	5.56	8.33	5.56	2.78	5.56	13.89	5.56	11.11
Aib6	Aib4	5.56	2.78	5.56	11.11	2.78	5.56	8.33	5.56	n.a	2.78
Aib4	Aib2	5.56	36.11	n.a	2.78	n.a	13.89	8.33	n.a	n.a	n.a
Aib5	Aib3	27.78	44.44	22.22	11.11	19.44	25.00	16.67	19.44	19.44	30.56
Aib4	Ac	11.11	n.a	n.a	n.a	n.a	n.a	11.11	30.56	5.56	n.a
NH_2	Aib5	n.a	n.a	n.a	n.a	n.a	n.a	n.a	n.a	8.33	n.a
n = 8		run1	run2	run3	run4	run5	run6	run7	run8	run9	run10
D	**A**	**occ%**	**occ%**	**occ%**	**occ%**	**occ%**	**occ%**	**occ%**	**occ%**	**occ%**	**occ%**
NH_2	Aib6	50.0	77.1	8.3	54.2	12.5	43.8	50.0	77.1	45.8	83.3
Aib7	Aib4	97.9	22.9	100.0	95.8	100.0	83.3	58.3	50.0	75.0	52.1

Aib5	Aib2	58.3	81.3	70.8	66.7	68.8	81.3	77.1	41.7	31.3	79.2
Aib6	Aib3	20.8	54.2	31.3	16.7	27.1	14.6	27.1	54.2	20.8	16.7
Aib4	Aib1	10.4	31.3	20.8	8.3	20.8	10.4	20.8	37.5	10.4	8.3
Aib3	Ac	66.7	37.5	45.8	37.5	89.6	54.2	52.1	45.8	45.8	58.3
Aib8	Aib5	50.0	33.3	14.6	8.3	22.9	8.3	22.9	68.8	8.3	14.6
Aib5	Aib3	16.7	33.3	25.4	62.5	56.3	66.7	37.5	20.8	43.8	33.3
Aib8	Aib6	4.2	4.2	45.8	8.3	10.4	14.6	4.2	16.7	6.3	8.3
Aib7	Aib5	4.2	22.9	n.a	n.a	4.2	37.5	4.2	n.a	2.1	n.a
Aib2	Ac	20.8	25.0	4.2	18.8	4.2	14.6	16.7	10.4	10.4	18.8
Aib3	Aib1	25.0	8.3	31.3	33.3	6.3	20.8	20.8	10.4	14.6	n.a
NH_2	Aib7	4.2	4.2	4.2	2.1	2.1	2.1	6.3	4.2	2.1	2.1
Aib6	Aib4	n.a	10.4	6.3	4.2	31.3	25.0	6.3	8.3	29.2	18.8
Aib6	Aib2	n.a	4.2	n.a	n.a	n.a	n.a	n.a	n.a	n.a	n.a
NH_2	Aib5	n.a	n.a	n.a	n.a	n.a	n.a	n.a	16.7	n.a	6.3
Aib4	Aib2	n.a	n.a	n.a	n.a	n.a	n.a	n.a	6.3	n.a	n.a

n = 20		run1	run2	run3	run4	run5	run6	run7	run8	run9	run10
D	**A**	**occ%**	**occ%**	**occ%**	**occ%**	**occ%**	**occ%**	**occ%**	**occ%**	**occ%**	**occ%**
Aib13	Aib10	99.0	100.0	63.5	53.1	85.4	81.3	95.8	96.9	55.2	100.0
Aib15	Aib12	69.8	53.1	53.1	55.2	89.6	58.3	45.8	57.3	58.3	67.7
Aib12	Aib9	71.9	25.0	64.6	35.4	37.5	52.1	69.8	42.7	67.7	69.8
Aib10	Aib7	66.7	13.5	61.5	53.1	36.5	61.5	52.1	16.7	95.8	52.1
Aib9	Aib6	20.8	7.3	49.0	35.4	64.6	57.3	44.8	13.5	80.2	0.1
Aib7	Aib4	53.1	19.8	55.2	33.3	37.5	53.1	52.1	61.5	55.2	60.4
Aib6	Aib3	17.7	16.7	33.3	33.3	51.0	63.5	15.6	35.4	67.7	27.1
Aib5	Aib2	58.3	56.3	79.2	81.3	43.8	72.9	38.5	86.5	88.5	84.4
Aib4	Aib1	17.7	11.5	24.0	10.4	94.8	57.3	19.8	29.2	40.6	26.0
Aib3	Ac	64.6	26.0	55.2	62.5	46.9	63.5	76.0	65.6	84.4	67.7
NH2	Aib18	89.6	60.4	57.3	18.8	60.4	79.2	72.9	83.3	88.5	43.8
Aib20	Aib17	66.7	38.5	67.7	84.4	58.3	46.9	41.7	80.2	79.2	40.6

Aib19	Aib16	92.7	92.7	100.0	93.8	46.9	100.0	95.8	90.6	93.8	100.0
Aib18	Aib15	77.1	54.2	56.3	45.8	59.4	54.2	64.6	40.6	40.6	64.6
Aib17	Aib14	100.0	88.5	83.3	70.8	67.7	93.8	79.2	97.9	51.0	95.8
Aib16	Aib13	67.7	49.0	28.1	62.5	57.3	57.3	47.9	17.7	55.2	52.1
Aib14	Aib11	72.9	22.9	75.0	64.6	34.4	51.0	32.3	21.9	72.9	69.8
Aib11	Aib8	99.0	100.0	63.5	53.1	85.4	81.3	95.8	96.9	55.2	100.0
Aib8	Aib5	69.8	53.1	53.1	55.2	89.6	58.3	45.8	57.3	58.3	67.7
Aib5	Aib3	71.9	25.0	64.6	35.4	37.5	52.1	69.8	42.7	67.7	69.8
Aib9	Aib7	66.7	13.5	61.5	53.1	36.5	61.5	52.1	16.7	95.8	52.1
Aib8	Aib6	20.8	7.3	49.0	35.4	64.6	57.3	44.8	13.5	80.2	0.1
Aib11	Aib9	53.1	19.8	55.2	33.3	37.5	53.1	52.1	61.5	55.2	60.4
Aib14	Aib12	17.7	16.7	33.3	33.3	51.0	63.5	15.6	35.4	67.7	27.1
Aib20	Aib18	58.3	56.3	79.2	81.3	43.8	72.9	38.5	86.5	88.5	84.4
Aib15	Aib13	17.7	11.5	24.0	10.4	94.8	57.3	19.8	29.2	40.6	26.0
Aib13	Aib11	64.6	26.0	55.2	62.5	46.9	63.5	76.0	65.6	84.4	67.7
Aib12	Aib10	89.6	60.4	57.3	18.8	60.4	79.2	72.9	83.3	88.5	43.8
NH2	Aib19	66.7	38.5	67.7	84.4	58.3	46.9	41.7	80.2	79.2	40.6
Aib18	Aib16	92.7	92.7	100.0	93.8	46.9	100.0	95.8	90.6	93.8	100.0
Aib17	Aib15	77.1	54.2	56.3	45.8	59.4	54.2	64.6	40.6	40.6	64.6
Aib6	Aib4	100.0	88.5	83.3	70.8	67.7	93.8	79.2	97.9	51.0	95.8
Aib2	Ac	67.7	49.0	28.1	62.5	57.3	57.3	47.9	17.7	55.2	52.1
Aib16	Aib14	72.9	22.9	75.0	64.6	34.4	51.0	32.3	21.9	72.9	69.8
Aib3	Aib1	99.0	100.0	63.5	53.1	85.4	81.3	95.8	96.9	55.2	100.0
Aib7	Aib5	69.8	53.1	53.1	55.2	89.6	58.3	45.8	57.3	58.3	67.7
Aib10	Aib8	71.9	25.0	64.6	35.4	37.5	52.1	69.8	42.7	67.7	69.8
Aib19	Aib17	66.7	13.5	61.5	53.1	36.5	61.5	52.1	16.7	95.8	52.1
Aib4	Aib2	20.8	7.3	49.0	35.4	64.6	57.3	44.8	13.5	80.2	0.1

As can be noticed from most of the trajectories extracted from the PNEB simulations, the *i+2→i* H-bonds are frequently found in peptide **2** with β-turns (Figure 7.7C and 6.7F), but are transient since their presence increases the conformational energy, as showed by the relative energy plot associated to the helical inversion of the Ac-Aib$_4$-NH$_2$ peptide (Figure 7.8). In the simulations of the tetrapeptide the global maximum corresponds to a conformation where the carbonyl group of Aib1 is involved in H-bonds with the NH of both Aib3 and Aib4, while the local maxima or other high energetic conformations show the presence of γ-turns at either the N- or the C-terminus. For longer peptides these observations are less significant, because the energies extrapolated from the PNEB simulations are associated to the whole conformation of each image and the effect of γ-turns can be reduced by the presence of other stabilizing interactions or enhanced if there are other steric clashes.

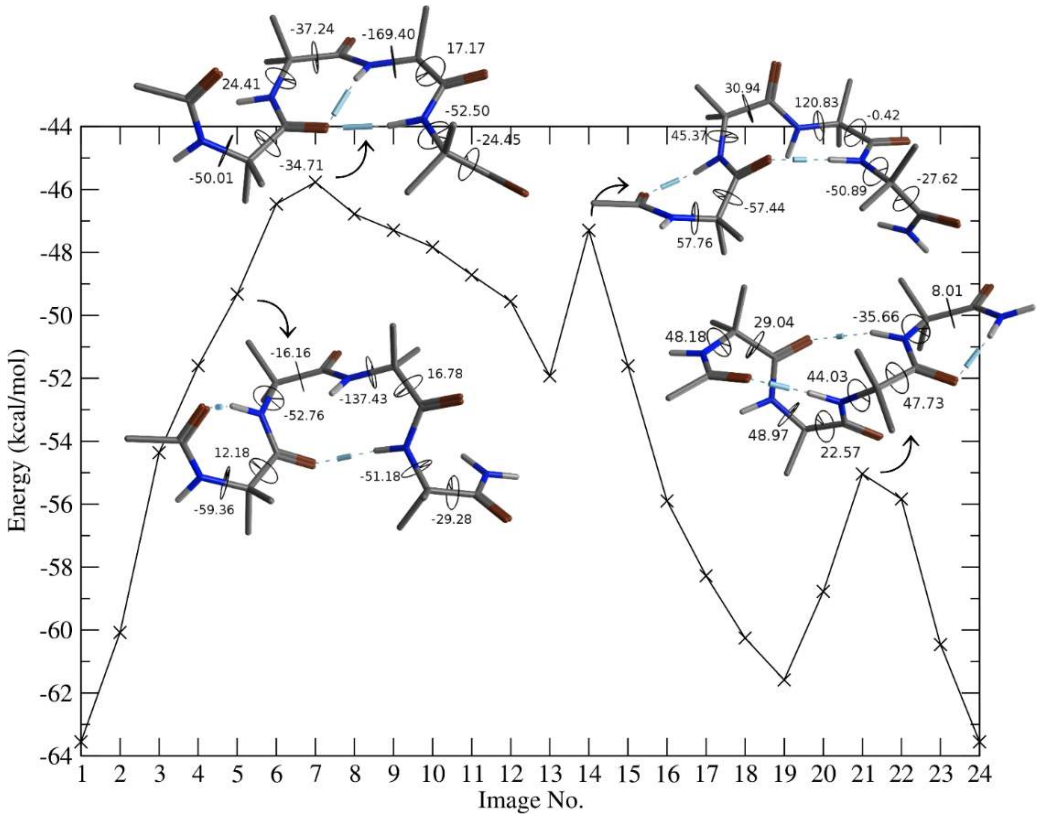

Figure 7.8. Total energies in kcal/mol extracted from the PNEB simulation (run 2) of Ac-Aib$_4$-NH$_2$ peptide with relevant conformations.

Summarizing, the application of computational techniques gave further insights for the study of both the conformational equilibria and the energetics in peptides containing chiral amino acids at the N- and C-termini. In particular, REMD simulations showed that, while peptide **1** is unequivocally a stable *P*-3_{10}-helix, in peptide **2** the presence of enantiomeric αMeVal at the two termini produces a competition for the global helical screw sense: the Cα*S*-enantiomer imposes the *P*-helix, while the Cα*R*-enantiomer induces the *M* conformation. From the PMF profiles as a function of φ and ψ dihedrals, obtained from the REMD simulations of peptide **2**, we can see that the switch from one screw sense to the other is more probable when the $\Delta E_M^{\ddagger}$ and ΔE_M are lower than 1 kcal/mol, both in implicit and explicit solvent. In principle, the helical inversion can occur at any point along the peptide chain, however it is more frequently observed at Aib6 or Aib7, the residues just above the two chiral ones. Moreover, it is clear that methanol reduces the energetic barrier between the *P*- and the *M*-helix, since it might stabilize high energy conformations by creating H-bonds with the backbone atoms.

Furthermore, PNEB simulations allowed to clarify how the inversion from one helical screw sense to the other takes place and, thus, to qualitatively prove the hypothesis that γ-turns are intermediates in the screw sense inversion. Indeed, we found that this process does not show any recurring propagation direction, but, on the contrary, it implies the break of internal H-bonds, leading to a sigmoidal conformation characterized by the presence of multiple β-turns of any type. These turns create local conformations where the switch from β- to β'-turn independently occurs. An obligated step at this point is the formation of transient γ-turns, which are required in order to switch from negative to positive dihedral values and *vice versa*.

In conclusion, in this part of the project we developed some basic knowledge that might be useful for the design of well-structured helical peptide, containing cCTAAs as helical stabilizers, and with a defined helical screw sense. At the same time, we investigated the mechanisms behind the helical screw sense inversion, which might be exploited to design switchable helical peptide that can be activated to PPI modulators by inducing a conformational change.

7.3 MATERIALS AND METHODS

REMD Simulations. Aib, (*R*)- and (*S*)-αMeVal amino acids and the Cbz protecting group were designed using MOE.[227]. The formers were capped with an acetyl (Ac) and a NHMe group at the N- and C-termini, respectively, while the latter was only capped by NHMe at the C-termini. They were then submitted to a "Low Mode" conformational search by setting MMFF94x as force field, Born solvation model, iteration limit = 40000, MM iteration limit = 2500, and rejection limit = 500. For each molecule, the two conformations showing the lowest energy and, in the case of the three amino acids, with the φ and ψ dihedrals corresponding to the right- and left-handed helical ones (φ = ±60° and ψ = ±45°) were chosen for partial charges derivation performed by the R.E.D.IV software[228]. For this step, the selected geometries were optimized at the HF/6-31G(d) level of theory and the RESP-A1 charges were derived using two different spatial orientations, in order to have an orientation- and conformation-independent charges. Moreover, the charges ofbackbone nitrogen, hydrogen, carbonyl carbon and oxygen were fixed at the same values reported in the AMBER *ff99SBildn-φ* force field[168] for standard amino acids (e.g. -0.4157, 0.2719, 0.5973 and -0.5679, respectively).

Cbz-(*S*)-αMeVal$_2$-Aib$_5$-(*S*)-αMeVal$_2$-NHMe (peptide **1**) and Cbz-(*S*)-αMeVal$_2$-Aib$_5$-(*R*)-αMeVal$_2$-NHMe (peptide **2**) peptides were built by imposing an extended conformation (φ = ψ = ω = 180°). REMD simulations in implicit solvent of the two peptides were performed using the AMBER *ff99SBildn-φ* force field coupled with the implicit solvent model GB-Neck2 (igb = 8),[173] combination that proved to give the best results in predicting peptides secondary structures.[88] 16 replica, spanning temperatures between 260.00 K and 690.08 K with a 0.5 probability exchange, were run for 100 ns each, for a total of 1.6 μs of simulation for each peptide, using the *pmemd* module of the Amber14 package.[259] Unless stated otherwise, the trajectories at 297.31 K were extracted and analyzed on the 50-100 ns time interval.

For the REMD simulations in explicit methanol, the Cbz-(*S*)-αMeVal$_2$-Aib$_5$-(*R*)-αMeVal$_2$-NHMe peptide in the extended conformation was solvated with an octahedral box of 1290 MeOH molecules (closeness = 8.0 Å) and preliminarily

submitted to minimization and equilibrations cycles. Initially 5000 cycles of hydrogens minimization (1000 cycles of steepest descent and 4000 cycles of conjugated gradient), followed by 5000 cycles of solvent minimization (2000 cycles of steepest descent and 3000 cycles of conjugated gradient) were carried out. Then, the solvent box was equilibrated at 300 K by 1ns of NVT equilibration and 1ns of NPT equilibration using the Langevin thermostat with a frequency collision of 2.0. This step was followed by 5000 cycles (2500 of steepest descent and 2500 of conjugated gradient) of solvent and sidechains minimization and by 5000 cycles (2500 of steepest descent and 2500 of conjugated gradient) of total minimization. The last step consisted in 100 ps of NVT and 100 ps of NPT equilibration of the whole system. The REMD simulation of the equilibrated system was carried out with the AMBER *ff99SBildn-φ* force field and by performing 40 replica of 120 ns each (4.8 μs totally) between 290.00 K and 511.61 with an exchange probability of 0.20. The trajectory at 303.60 K was extracted, the solvent was stripped out and the simulation convergence was checked every 10 ns by assuring that the conformations obtained during the 10 ns time intervals were similar on the base of the Root Mean Square Deviation (RMSD) (Annex 7.A).

Cluster analyses were performed with *cpptraj* (Amber14)[259] using the average-linkage algorithm and the pairwise mass-weighted RMSD on the Cα of residues 7-11, in order to identify where the screw sense inversion occurs. For the simulations conducted in implicit solvent the 50-100 ns time interval was analyzed by sampling one every four frames and by requesting 5 clusters on the basis of pseudo-F statistics and SSR/SST ratio.[260] As regards the REMD in explicit solvent, since convergence was reached after 50 ns, the last 60 ns were submitted to cluster analysis, sampling one every four frames and requesting 15 clusters.

H-bonds occupancies during the simulations were computed with VMD 1.9.1[231] over the whole trajectories for the simulations in implicit solvent and on the last 60 ns for that in explicit methanol, with a donor-acceptor distance limit of 4.0 Å and an angle cutoff of 60°. This very low angle acceptance threshold was chosen in order to be able to identify the presence of γ-turns, since it has been showed that the hydrogen

bond in γ-turns is highly bent[261] and the N-H-O angle can reach values of 110-130°. Only H-bonds with an occupancy greater than 5% were considered. The H-bond analysis between peptide **2** and methanol molecules was performed with Amber14 *cpptraj*, using successively the backbone carbonyl oxygen atoms as acceptor atoms and setting methanol molecules as solvent donor, then the methanol residues were considered as solvent acceptor and the backbone amidic hydrogens were considered as donor atoms. In this case the distance cutoff was set to 4.0 Å and the minimum angle accepted was fixed at 150°, as for standard H-bonds.

Potential of Mean Force (PMF) as a function of φ and ψ dihedrals were computed with Amber software coupled with the Weighted Histogram Analysis Method (WHAM)[262] over the whole implicit solvent trajectories and over the last 60 ns for the explicit methanol simulation by setting a histogram limit of ±180°, 100 bins and a tolerance of 0.01. Temperatures between 260.00 K and 317.73 K were considered. A threshold of 6 kcal/mol has been fixed for the non-accessible conformations.

NEB simulations. Minimized structures of ideal *M*- and *M*-3_{10}-helices of Ac-Aib_n-NH_2 peptides (n = 4, 6, 8 and 20) were used as initial and final conformations, respectively, for the Partial Nudged Elastic Band (PNEB) simulation of the transition pathway between right- and left-handed helices. The AMBER *ff99SBildn-φ* force field coupled with the GB-Neck2 solvent model was used. For n = 4, 6, 8 and 20, 24, 36, 48 and 96 images, respectively, where chosen and the simulations were repeated 10 times for each peptide to test the reproducibility of the minimum energy pathway. The NEB forces were applied only to the backbone nitrogen, Cα and carbonyl carbon atoms, while the RMS fitted the system on all the atoms. The system was initially heated from 0 K to 300 K in 20 ps, using a spring constant of 10 $kcal \cdot mol^{-1} \cdot Å^{-2}$ and the Langevin thermostat with a collision rate of 1000 ps^{-1}. In the next 100 ps the system was submitted to a MD at 300 K with a spring constant of 50 $kcal \cdot mol^{-1} \cdot Å^{-2}$. Successively, the system was heated from 300 K to 700K and subsequently cooled back to 300 K over 750 ps. The cooling to 0 K to remove kinetic energy was performed in 120 ps and quenched MD was run over 200 ps. The final pathway was

extracted and analyzed. The reproducibility of the simulations was checked by comparing the behavior of φ and ψ dihedrals.[109,263,264]

H-bond analyses were conducted on the extracted trajectory with VMD 1.9.1 with the same parameters used for the analysis of the REMD simulations.

Part 2:

Development and optimization of a MMGBSA protocol for the prediction of the activities of PPIs modulators

8 NWAT-MMGBSA: A MMGBSA-BASED APPROACH TO IMPROVE THE CORRELATION BETWEEN PREDICTED BINDING ENERGIES AND EXPERIMENTAL ACTIVITIES

As previously underlined, the prediction of the activity of a designed molecule toward a defined target represents a fundamental, although challenging, goal of the drug discovery process. The combination of MD simulations and MMPB/GBSA calculations has been frequently used to compute binding free energies in classical protein-ligand,[27] DNA-ligand,[265] or PPIs.[266] However, the correlation between MMPB/GBSA predicted binding energies and biological activity was often protocol-dependent. Indeed, in literature extensive studies on the sensitivity of MMPB/GBSA results to protocol changes can be found.[114,267,268]

In this context, much attention has been paid to tune the solvation term in its electrostatic component, with a particular interest on the parameters common to both PB and GB equations (eq. 3 and 4).[90] In this framework, studies on the effects of a variation if the internal dielectric constant ϵ_{in} on the correlation between experiments and predicted binding energies showed that this parameter highly affects the calculation. Moreover, an universal value for this constant, i.e. suitable for all the protein systems, cannot be found and this choice necessarily depends on an analysis of the properties of the binding pocket.[267–270] Therefore, if a good dataset of known ligands with known activity data is not available, the variation of ϵ_{in} should seldom be done.

Another approach to increase the correlation between experimental activities and MMPB/GBSA predicted binding energies consists in the inclusion of selected explicit water molecules in the calculation. This approached stemmed from the previously underlined observation that water can play a relevant role in both receptor-ligand and protein-protein interactions, because it can takes part in water-mediated H-bonds or it can stabilize the complex through transient H-bonds.[90,120,271]

The selection of the water molecules to be included in the calculation can be done in different ways. The most intuitive consists in including the solvent molecules that

are known to mediate receptor-ligand binding or PPI from crystallographic data.[272,273] However, this approach can lead to detrimental results,[274] because, during the MD simulation water molecules can rapidly exchange their positions. Therefore, although a water mediated H-bond can be detected during the whole simulation time, the water residue involved in it can be not always the same.

To overcome this issue, a possible approach, that proved to increase the correlation between experimental and predicted data, is represented by the inclusion of water molecules identified from MD trajectory analysis through H-bond analysis,[275] B-factor analysis[119] or water density/occupancy analysis,[276] or by selecting those water residues which are, frame by frame, the closest to the ligand or to the residues involved in the PPI.[89]

Although all these approaches have the advantage of their generalizability and reproducibility, because the selected water residues are those which pass a defined numerical threshold, the last one is the easiest to automatize, thanks to the *cpptraj* "*closest*" command[192] (Figure 8.1). This command allows the user to process the explicit solvent MD trajectory to save a new trajectory, containing only a fixed number of the closest water molecules (Nwat) to a residue or atom mask during the whole simulation time, which can be directly used for the MMPB/GBSA calculation (see Annex 10.A and 11.F).

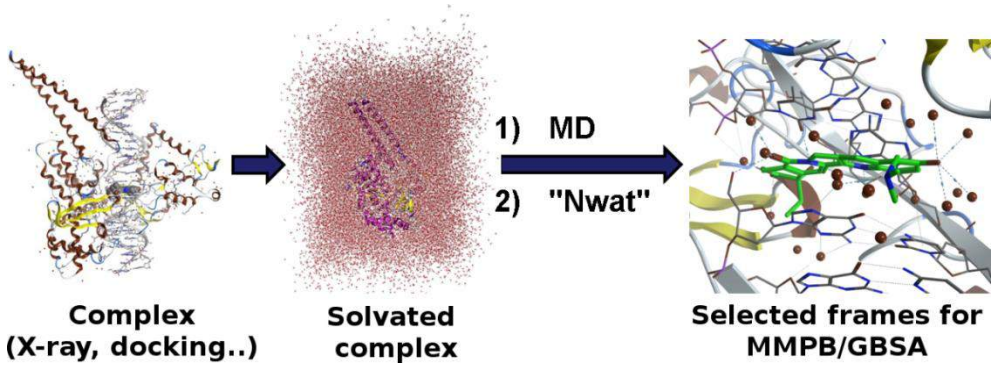

Figure 8.1. Nwat-MMPB/GBSA approach scheme.

Therefore, we decided to initially test this approach on classical receptor-ligand complexes, for which experimental activities were available, in order to verify its reliability and its benefit compared to the standard MMPB/GBSA method (Chapter 9).

Then, we optimized the protocol for the binding affinity prediction in PPIs (Chapter 10), because these systems, as observed in Chapter 1, are structurally different from classical receptor-ligand systems.

Finally, at the light of the good obtained results, we automatized the process by writing a script that performs the setup, calculations and analysis and evaluated the optimized protocol for the prediction of activities of a set of small molecules or peptide-like ligands targeting PPIs and having known activity data (Chapter 11).

9 APPLICATION OF NWAT-MMGBSA TO CLASSICAL RECEPTOR-LIGAND COMPLEXES

9.1 INTRODUCTION

Bearing in mind that water can contribute to the binding free energy of receptor-ligand complexes and that it is often found at protein binding sites,[119,271,275,277] we initially applied the Nwat-MMPB/GBSA approach to four different protein systems, namely topoisomerase I-DNA, α-thrombin, penicillopepsin and avidin complexes, to evaluate both the reliability and robustness of the protocol.

In particular, the topoisomerase I-DNA system was selected because it is known that water plays an important role in mediating H-bond interactions between the topoisomerase I and camptothecin (CPT)-like inhibitors,[278] α-thrombin and penicillopepsin complexes were chosen because previously reported MMPB/GBSA results were poorly correlated with experiments, when using the default ϵ_{in}.[267] Conversely, the avidin system was considered because of the high correlation coefficient obtained with the standard dielectric constant, in order to observe if the Nwat-MMPB/GBSA protocol was detrimental for systems where water does not seem to play a role in the receptor ligand interaction.[267,268,279]

Therefore, we considered the complexes of topoisomerase I – DNA and 9 CPT derivatives with known IC_{50} (Figure 9.1), 7 α-thrombin–ligand and 7 penicillopepsin–igand and 7 avidin–ligand complexes with known ΔG_{bind} (Figure 9.2, 9.3, and 9.4, respectively).

Each system will be discussed independently, in order to provide a clear explanation about the reproducibility, reliability and robustness of the Nwat-MMGBSA approach, evaluated in terms of squared Pearson's correlation coefficient (r^2) between computed binding energies and available experimental data. Although, additional investigations have been performed on the topoisomerase I – DNA system, because of the known importance of water in the interaction between topoisomerase and CPT derivatives (Figure 9.5).[278]

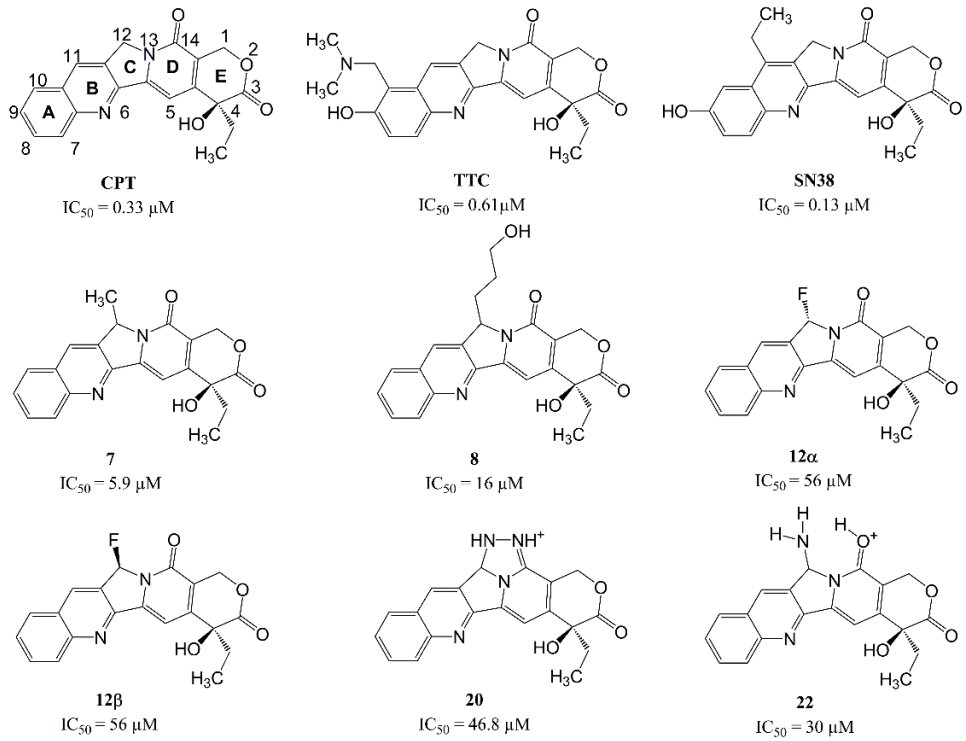

Figure 9.1. Considered topoisomerase I ligands at the protonation state used for the analyses; experimental IC_{50}s are also reported.[280]

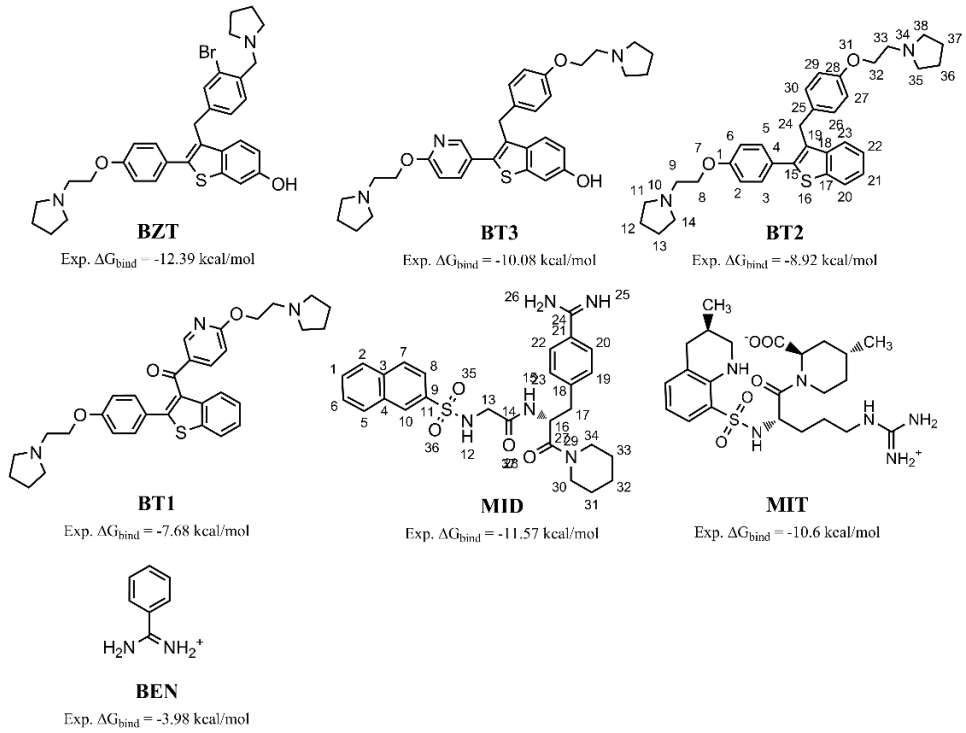

Figure 9.2. Considered α-thrombin ligands; experimental free energies of binding (ΔG_{bind}) are also reported.[267]

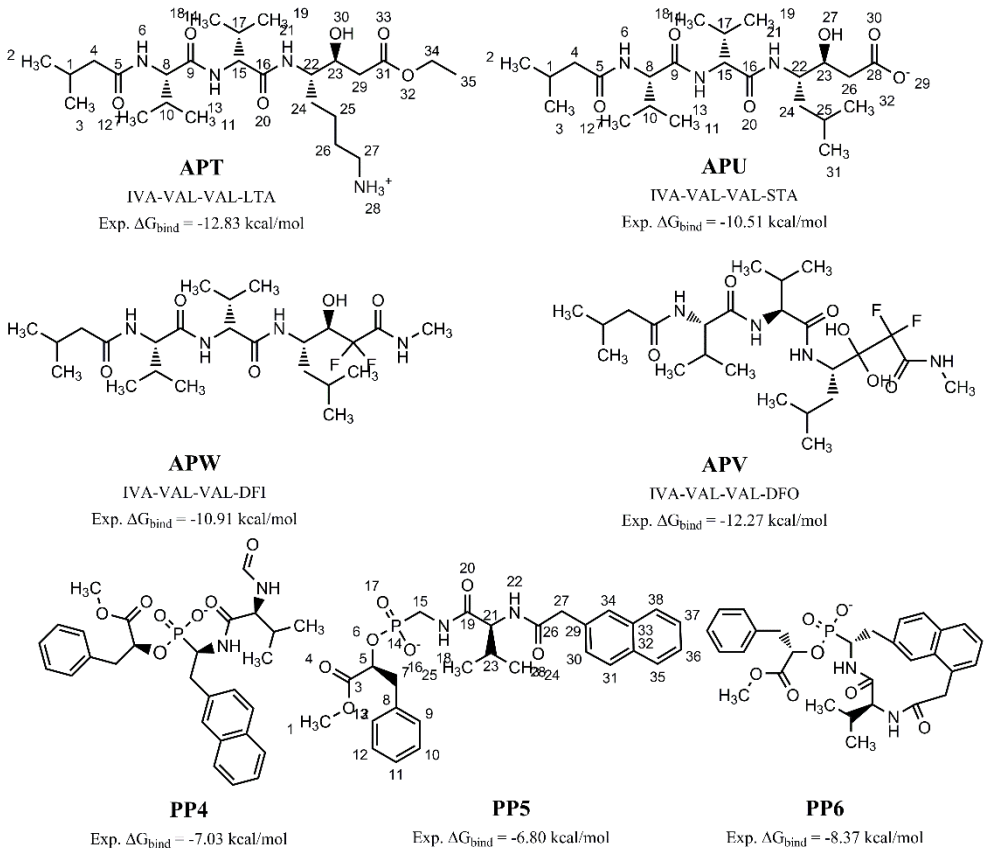

Figure 9.3. Considered penicillopepsin ligands; experimental free energies of binding (ΔG_{bind}) are also reported.[267]

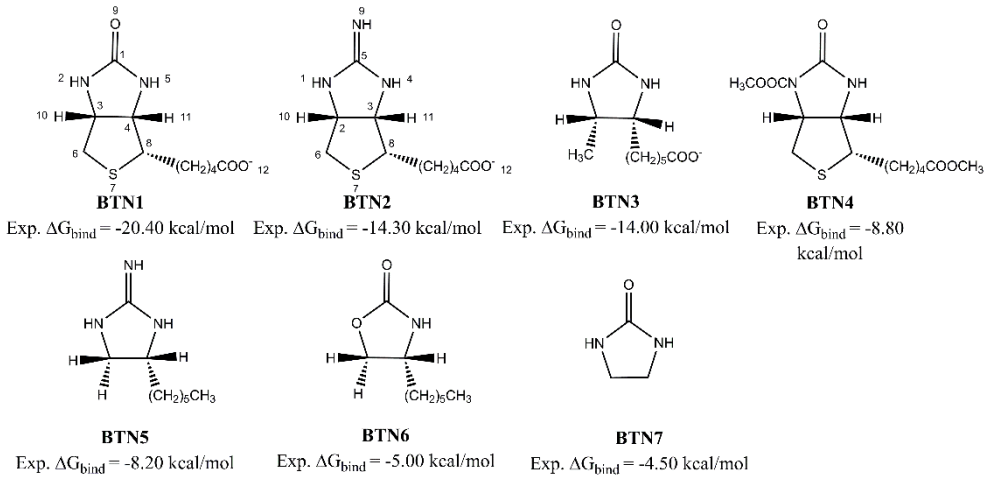

Figure 9.4. Considered avidin ligands; experimental free energies of binding (ΔG_{bind}) are also reported.[267]

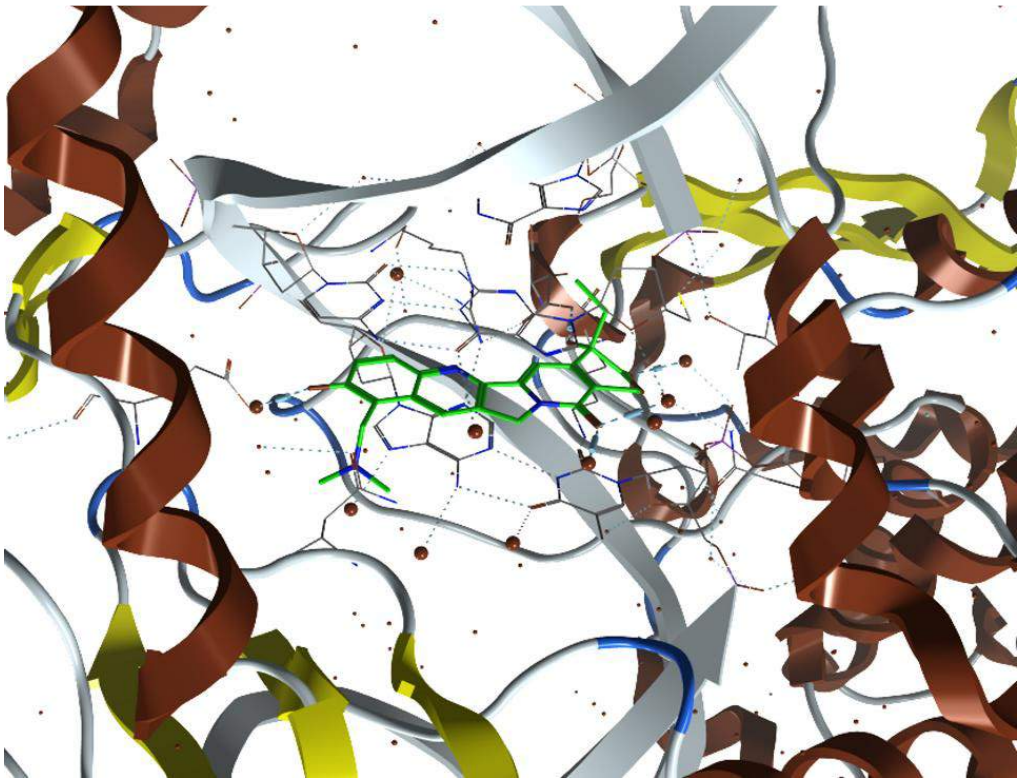

Figure 9.5. Crystallographic structure of the topoisomerase I – DNA – topotecan (TTC) complex (PDB code: 1K4T). Crystallographic waters interacting with both the protein and the ligand are highlighted.

9.2 Results and Discussion

Topoisomerase I - DNA. H-bond analyses performed on TTC and SN38 complexes confirmed the previously underlined observation that even hydrogen-bound waters can rearrange, and a specific residue is replace by a neighboring one. Indeed, for example, the C3=O of TTC takes part in a H-bond with water for the 73% of the simulation time, although 5 different water residues determine this occupancy, namely WAT1638 (37.4%), WAT20971 (25.6%), WAT28324 (4.3%), WAT22562 (3.2%), and WAT20947 (2.5%). Analogous considerations can be done for all the TTC atoms able to take part in H-bonds, namely, C14=O, N6, O2, and C9 – OH (Table 9.1). This latter interacts with 10 different water residues for about the 20% of the simulation time. The simulation of the SN38 complex led to consistent results, although in this case SN38 interacted with about 20 water molecules during the simulation time (Table 9.2).

Table 9.1. H-bonds between TTC and water during the last ns of MD simulation. D, A and Occ are the donor atom, the acceptor atom and the occupancy, respectively.

D	A	Occ	D	A	Occ
WAT20971-O	TTC-O=C3	25.6%	TTC-OH(C9)	WAT3805-O	2.0%
WAT16448-O	TTC-OH(C9)	1.4%	TTC-OH(C4)	WAT30530-O	0.1%
WAT25062-O	TTC-O=C14	2.0%	TTC-OH(C9)	WAT10204-O	1.3%
WAT22562-O	TTC-O=C3	3.2%	WAT25062-O	TTC-OH(C9)	4.7%
WAT25062-O	TTC-N13	0.4%	WAT20998-O	TTC-O=C14	0.1%
WAT28324-O	TTC-O=C3	4.3%	WAT12379-O	TTC-OH(C9)	1.0%
WAT20971-O	TTC-O2	3.6%	TTC-OH(C9)	WAT18473-O	0.4%
WAT28324-O	TTC-O2	0.2%	WAT3805-O	TTC-OH(C9)	0.1%
WAT20947-O	TTC-O=C3	2.5%	WAT24732-O	TTC-OH(C9)	0.6%
WAT16384-O	TTC-O=C3	37.4%	WAT10910-O	TTC-O=C14	2.0%
WAT3278-O	TTC-OH(C9)	0.2%	WAT10910-O	TTC-N13	0.4%
TTC-OH(C9)	WAT16448-O	0.2%	WAT24111-O	TTC-N6	0.3%
WAT20947-O	TTC-O2	0.1%	TTC-OH(C9)	WAT8209-O	7.3%
TTC-OH(C9)	WAT12379-O	0.6%	WAT24111-O	TTC-OH(C9)	2.0%
WAT10204-O	TTC-OH(C9)	7.8%	WAT10910-O	TTC-N6	0.5%
WAT16384-O	TTC-O2	3.9%	WAT10910-O	TTC-OH(C9)	0.2%
WAT16025-O	TTC-OH(C9)	2.2%			

Table 9.2. H-bonds between SN38 and water during the last ns of MD simulation. D, A and Occ are the donor atom, the acceptor atom and the occupancy, respectively.

D	A	Occ	D	A	Occ
SN38-OH(C9)	WAT9324-O	35.7%	WAT10865-O	SN38-OH(C9)	1.0%
WAT14674-O	SN38-O=C3	66.8%	WAT9324-O	SN38-OH(C9)	1.4%
WAT9756-O	SN38-O=C14	18.4%	SN38-OH(C9)	WAT20864-O	0.2%
WAT16826-O	SN38-OH(C9)	0.5%	WAT14633-O	SN38-O=C3	0.1%
WAT14674-O	SN38-O2	4.1%	WAT14422-O	SN38-O=C3	0.2%
WAT21099-O	SN38-OH(C9)	1.4%	WAT10627-O	SN38-OH(C9)	14.7%
WAT9756-O	SN38-N13	0.3%	SN38-OH(C4)	WAT14422-O	0.1%
WAT19706-O	SN38-O=C3	0.3%	WAT21173-O	SN38-O=C14	8.0%
SN38-OH(C9)	WAT17717-O	2.9%	SN38-OH(C9)	WAT5781-O	4.3%
WAT11350-O	SN38-OH(C9)	0.6%	SN38-OH(C9)	WAT10627-O	2.2%
WAT20864-O	SN38-OH(C9)	1.3%	WAT6006-O	SN38-OH(C9)	0.4%
WAT28324-O	SN38-O=C14	0.2%	SN38-OH(C9)	WAT16853-O	5.6%
WAT5781-O	SN38-OH(C9)	3.8%	SN38-OH(C9)	WAT9756-O	1.1%
WAT22614-O	SN38-O=C14	38.3%	WAT26026-O	SN38-OH(C9)	0.1%
WAT22614-O	SN38-N13	0.4%	WAT14422-O	SN38-OH(C4)	0.1%
WAT16853-O	SN38-OH(C9)	4.4%	WAT6651-O	SN38-OH(C9)	0.2%

These results are not in conflict with the X-ray data, because crystallographic residues are identified as a mean electron density, which can be determined by different water molecules which concur to occupy the same position.[281] Indeed, the grid analysis performed for water oxygen atoms showed that the high-water-density regions match with crystallographic water molecules of the X-ray structure (Figures 9.5 and 9.6).

Therefore, standard MMPBSA and MMGBSA (Nwat = 0) calculations and Nwat-MMPBSA and MMGBSA analyses with Nwat = 10, 20, 30, 40, and 50 were performed and the results were correlated to $-\log_{10}(IC_{50})$ (Figures 9.8 and 9.9).

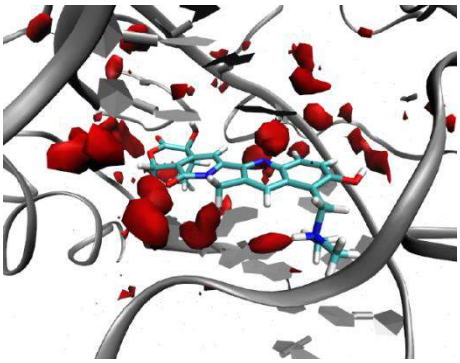

Figure 9.6. Water density plots obtained by grid analysis (ptraj; grid box = 50x50x50 Å, mesh = 0.5 Å; visualization with VMD specifying an isovalue = 45) of topoisomerase-DNA-TTC complex.

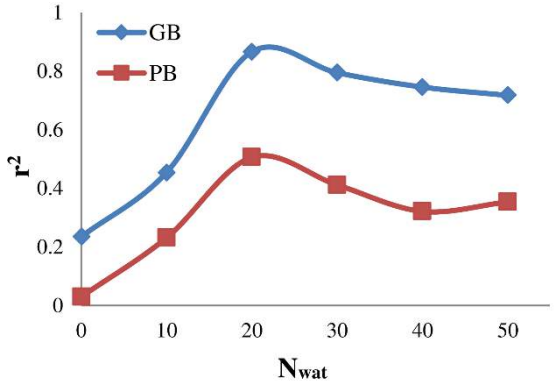

Figure 9.7. Trend of r^2 as a function of Nwat for topoisomerase – DNA complexes.

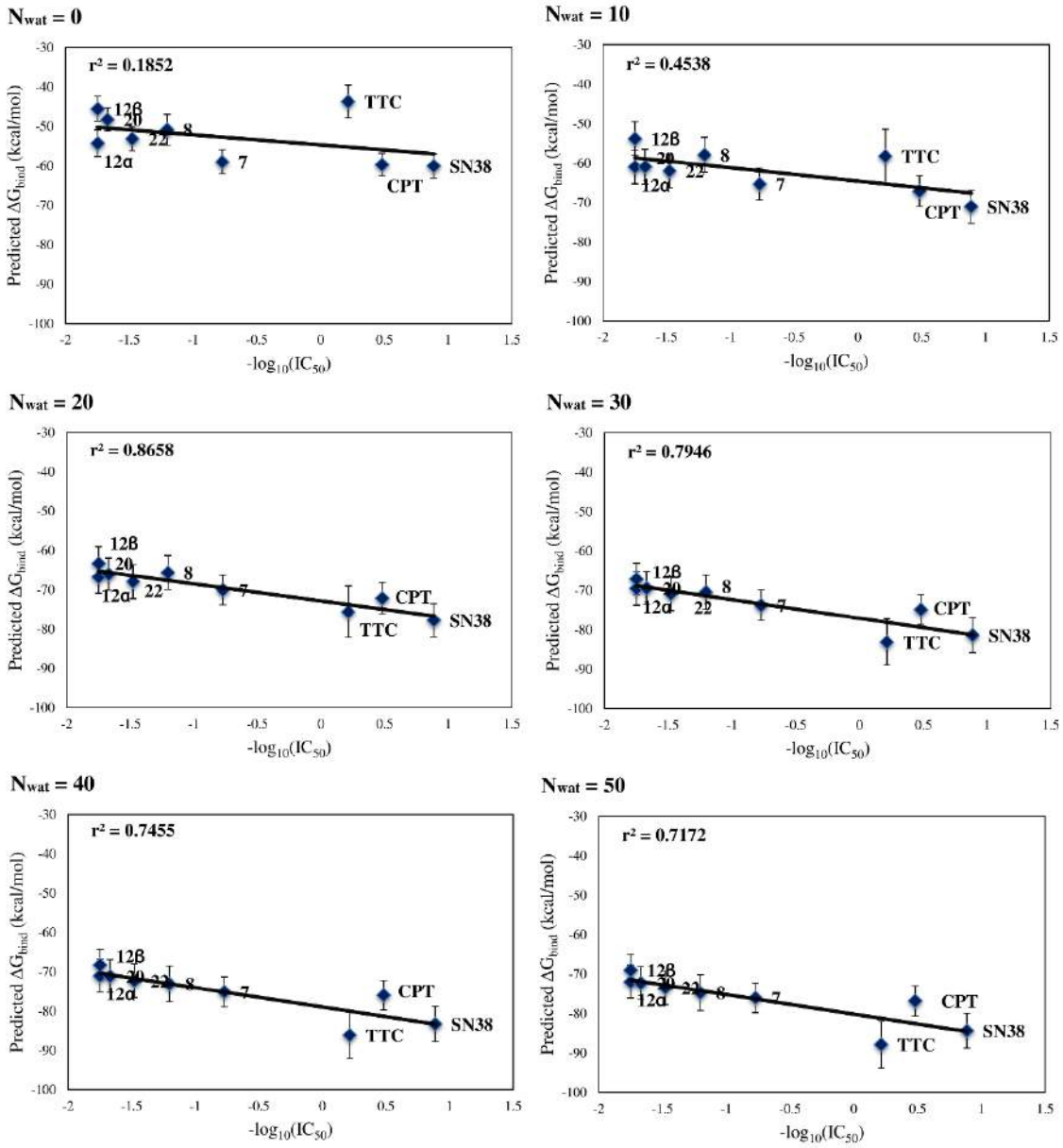

Figure 9.8. Correlations between MMGBSA predicted binding energies and experimental $-\log_{10}(IC_{50})$ for topoisomerase – DNA complexes.

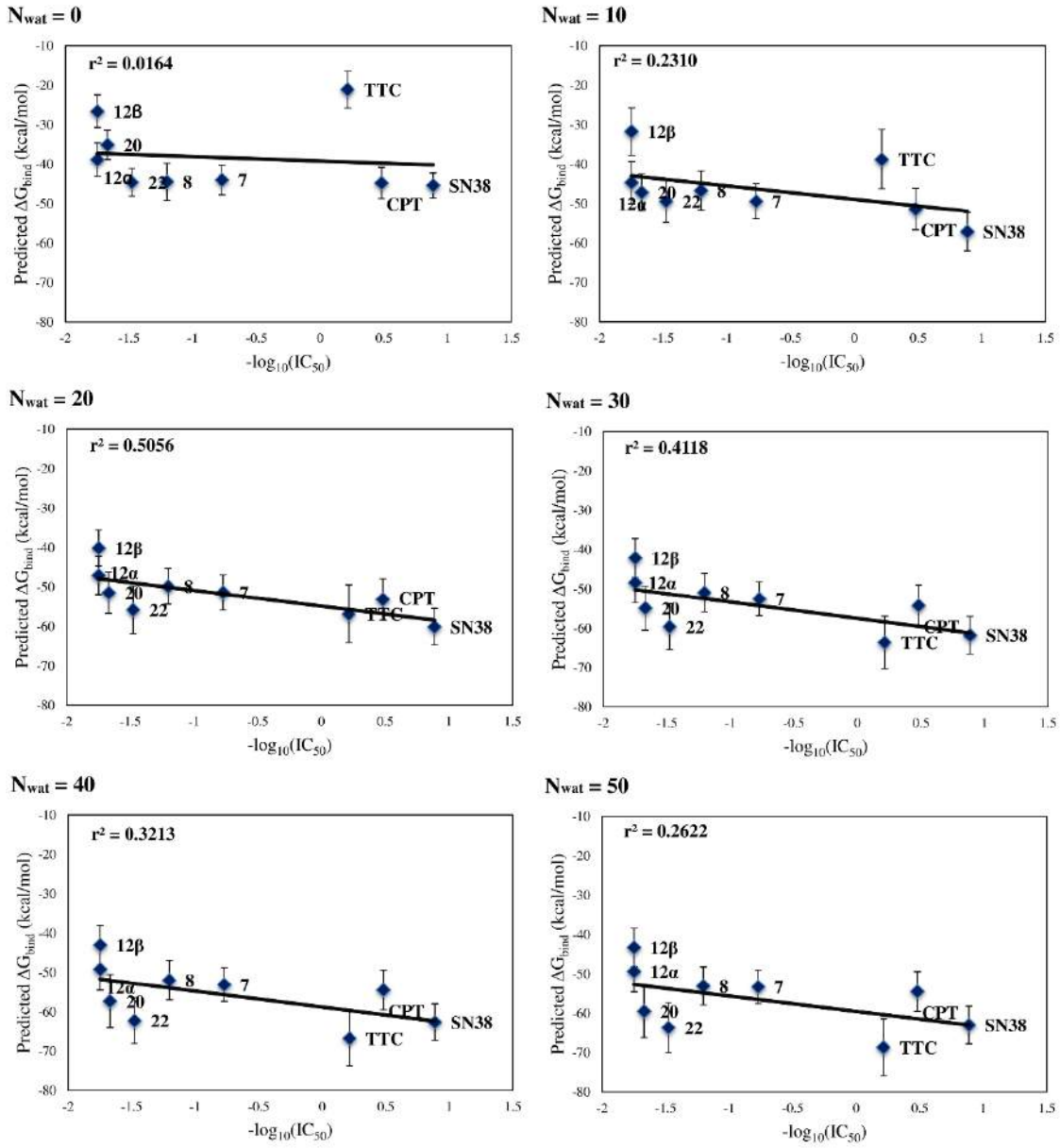

Figure 9.9. Correlations between MMPBSA predicted binding energies and experimental $-\log_{10}(IC_{50})$ for topoisomerase – DNA complexes.

Figures 9.7, 9.8 and 9.9 show that the Nwat-MMPBSA and Nwat-MMGBSA protocols gave for any Nwat better correlations with experiments than the standard MMPBSA and MMGBSA, being the best results those obtained with Nwat = 20 for both PB and GB (r^2 = 0.51 and 0.87, respectively). In detail, the correlation sharply increases with Nwat switching from 10 to 20, while it slowly decreases with 30 or more water molecules, although maintaining an acceptable correlation.

Therefore, it seems that the inclusion of only 10 water molecules around the ligand is not sufficient to take in account all the explicit interactions between the solute and the solvent. Conversely, in this case the use of Nwat > 20 turned out to be slightly detrimental, probably because of the background noises due to the inclusion of a number of solvent molecules larger than needed.

From Figures 9.8 and 9.9, it can be noticed that the improvement in the r^2 is mainly due to a better description of a single ligand, TTC. An explanation of this is given by the comparison of the H-bond analyses performed on the Nwat = 10 and 20 trajectories for TTC and SN38, with this latter weakly affecting the r^2 (Tables 9.3, 9.4, 9.5). The H-bonds with an occupancy greater than 5% detected for the SN38 trajectories remained constant at the increase of Nwat, whereas for TTC an increase of H-bonds were observed when shifting from Nwat = 10 to Nwat = 20. These results provide an explanation to the fact the best r^2 was obtained with Nwat = 20, and suggest that a better correlation can be obtained by considering not only those few water molecules making stable water-mediated H-bonds between the ligand and the receptor, but also those waters involved in transient interactions, but that still contribute to the determination of a water buffer between the ligand and the binding site residues.

Table 9.3. H-bonds between TTC and water of the Nwat= 10 trajectory (occupancy ≥ 5%).

Donor Atom	Acceptor Atom	Occ	Donor Atom	Acceptor Atom	Occ
TTC-N28	WAT611-O	11.8%	WAT616-O	TTC-O18	9.3%
WAT616-O	TTC-N10	8.3%	WAT620-O	TTC-N10	5.5%
WAT618-O	TTC-O23	8.8%	WAT615-O	TTC-O18	6.9%
WAT613-O	TTC-O26	12.9%	WAT617-O	TTC-O26	7.4%
TTC-O26	WAT611-O	60.2%	WAT619-O	TTC-O26	7.2%
WAT618-O	TTC-O18	12.2%	TTC-N28	WAT612-O	10.4%
WAT614-O	TTC-O26	10.2%	WAT619-O	TTC-O18	12.1%
WAT616-O	TTC-O26	7.9%	TTC-O26	WAT612-O	10.3%
WAT613-O	TTC-N10	5.4%	WAT618-O	TTC-N10	8.1%
WAT619-O	TTC-O23	7.4%	WAT620-O	TTC-O23	6.3%
WAT620-O	TTC-O26	9.0%	WAT615-O	TTC-N10	6.5%
WAT619-O	TTC-N10	6.8%	WAT614-O	TTC-N10	7.5%
WAT620-O	TTC-O18	11.5%	WAT612-O	TTC-O26	7.5%
WAT617-O	TTC-O18	10.5%	WAT617-O	TTC-N10	9.1%
WAT615-O	TTC-O26	9.6%	WAT618-O	TTC-O26	6.5%

Table 9.4. H-bonds between TTC and water of the Nwat = 20 trajectory (occupancy ≥ 5%).

Donor Atom	Acceptor Atom	Occ	Donor Atom	Acceptor Atom	Occ
TTC-N28	WAT611-O	11.8%	WAT620-O	TTC-N10	5.5%
WAT616-O	TTC-N10	8.3%	WAT624-O	TTC-O23	6.0%
WAT618-O	TTC-O23	8.8%	WAT623-O	TTC-O23	8.3%
WAT613-O	TTC-O26	12.9%	WAT624-O	TTC-O18	6.5%
TTC-O26	WAT611-O	60.2%	WAT624-O	TTC-O26	6.9%
WAT618-O	TTC-O18	12.2%	WAT621-O	TTC-O18	9.8%
WAT614-O	TTC-O26	10.2%	WAT622-O	TTC-O26	9.2%
WAT616-O	TTC-O26	7.9%	WAT615-O	TTC-O18	6.9%
WAT613-O	TTC-N10	5.4%	WAT617-O	TTC-O26	7.4%
WAT619-O	TTC-O23	7.4%	WAT619-O	TTC-O26	7.2%
WAT620-O	TTC-O26	9.0%	TTC-N28	WAT612-O	10.4%
WAT623-O	TTC-O26	6.4%	WAT619-O	TTC-O18	12.1%
WAT626-O	TTC-O26	5.9%	TTC-O26	WAT612-O	10.3%
WAT619-O	TTC-N10	6.8%	WAT618-O	TTC-N10	8.1%
WAT617-O	TTC-O18	10.5%	WAT620-O	TTC-O23	6.3%
WAT620-O	TTC-O18	11.5%	WAT615-O	TTC-N10	6.5%
WAT615-O	TTC-O26	9.6%	WAT614-O	TTC-N10	7.5%
WAT616-O	TTC-O18	9.3%	WAT622-O	TTC-O18	7.8%
WAT621-O	TTC-O23	9.6%	WAT612-O	TTC-O26	7.5%
WAT627-O	TTC-O26	5.7%	WAT625-O	TTC-O26	5.1%
WAT621-O	TTC-O26	8.3%	WAT617-O	TTC-N10	9.1%
WAT622-O	TTC-O23	6.4%	WAT618-O	TTC-O26	6.5%
WAT623-O	TTC-O18	7.9%			

Table 9.5. H-bonds between SN38 and water of the Nwat = 10 (left) and 20 (right) trajectories (occupancy ≥ 5%).

Nwat = 10			**Nwat = 20**		
Donor Atom	**Acceptor Atom**	**Occ**	**Donor Atom**	**Acceptor Atom**	**Occ**
SN38-OH(C9)	WAT611-O	82.4%	SN38-OH(C9)	WAT611-O	82.4%
WAT617-O	SN38-O=C3	7.0%	WAT617-O	SN38-O=C3	7.0%
WAT612-O	SN38-O=C14	8.0%	WAT612-O	SN38-O=C14	8.0%
WAT615-O	SN38-O=C3	12.0%	WAT615-O	SN38-O=C3	12.0%
WAT613-O	SN38-O=C3	8.3%	WAT613-O	SN38-O=C3	8.3%
WAT619-O	SN38-OH(C9)	7.3%	WAT619-O	SN38-OH(C9)	7.3%
WAT616-O	SN38-OH(C9)	7.6%	WAT616-O	SN38-OH(C9)	7.6%
WAT612-O	SN38-O=C3	6.0%	WAT612-O	SN38-O=C3	6.0%
WAT613-O	SN38-OH(C9)	7.2%	WAT613-O	SN38-OH(C9)	7.2%
WAT615-O	SN38-OH(C9)	8.4%	WAT615-O	SN38-OH(C9)	8.4%
WAT618-O	SN38-O=C14	6.3%	WAT618-O	SN38-O=C14	6.3%
WAT616-O	SN38-O=C3	7.6%	WAT616-O	SN38-O=C3	7.6%
WAT613-O	SN38-O=C14	10.5%	WAT613-O	SN38-O=C14	10.5%

WAT615-O	SN38-O=C14	9.2%	WAT615-O	SN38-O=C14	9.2%
WAT614-O	SN38-O=C3	10.5%	WAT614-O	SN38-O=C3	10.5%
WAT618-O	SN38-O=C3	5.1%	WAT618-O	SN38-O=C3	5.1%
WAT614-O	SN38-OH(C9)	6.9%	WAT614-O	SN38-OH(C9)	6.9%
WAT618-O	SN38-OH(C9)	8.4%	WAT618-O	SN38-OH(C9)	8.4%
WAT614-O	SN38-O=C14	10.5%	WAT614-O	SN38-O=C14	10.5%
WAT617-O	SN38-OH(C9)	8.1%	WAT617-O	SN38-OH(C9)	8.1%
WAT616-O	SN38-O=C14	8.6%	WAT616-O	SN38-O=C14	8.6%
WAT617-O	SN38-O=C14	6.8%	WAT617-O	SN38-O=C14	6.8%

The Nwat-MMPB/GBSA approach also allows a better estimation of the activity of the fluorinated derivative **12**. The analysis of IC_{50} suggests that substitutions at the C12 of the C-ring decreases the activity of CPT derivatives (compounds **7**, **8**, **12**, **20** and **22**), with a more pronounced detrimental effect observed when the C12 substituent is an H-bond acceptor. In addition, although the **12α** and **12β** epimers had the same IC_{50},[280] the standard MMPB/GBSA calculation (Nwat = 0) overestimated the activity of **12α**, while the application of the Nwat-MMPB/GBSA approach gave converged binding energies, thanks to a better estimation of **12α**. This is explained by observing that, during the MD simulation, **12α** F atom is more exposed to the solvent than the F atom of **12β**, as showed by the water density plots obtained from grid analysis on the trajectories (Figure 9.10).

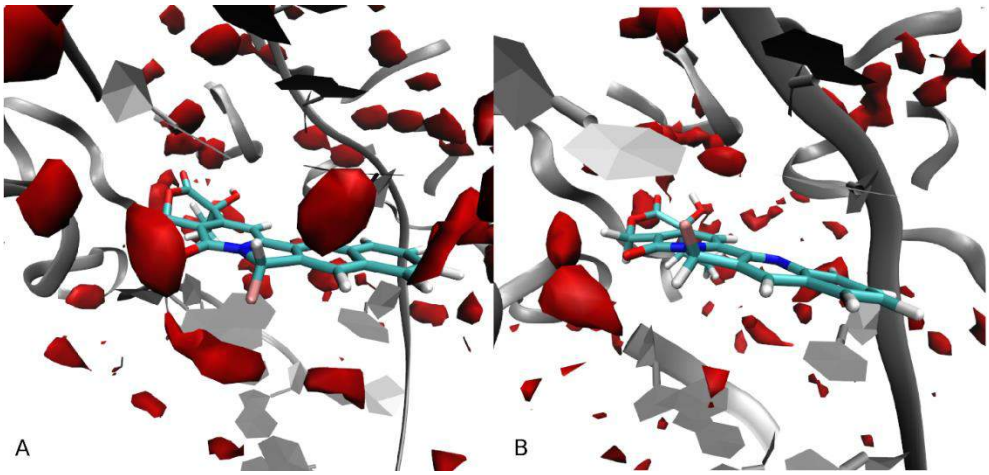

Figure 9.10. Water density plots obtained by grid analysis (ptraj; grid box = 50x50x50 Å, mesh = 0.5 Å**;** visualization with VMD**,** isovalue = 45) of topoisomerase-DNA-**12α** (A) and **12β** (B) complexes.

It has to be underlined that the GB method gave better results than PB, in agreement with that observed by other authors.[267,279,282] Therefore, GB seems to be

better suited for drug design/discovery purposes, especially considering its significantly lower computational cost compared to PB (in the present study, GB required 1/6 of the computational time needed by PB).

At the light of this, although both MMPBSA and MMGBSA analyses were performed (see Annex 9.A for MMPBSA results), the discussion of the remaining systems will be focused on the latter method.

α-Thrombin. Standard MMGBSA calculations (Nwat = 0) on this system already gave acceptable correlation between computed binding energies and experimental binding free energies (r^2 = 0.67, r_s = 0.82). The application of the Nwat-MMGBSA approach (Nwat = 10, 20, 30, 40, 50, 60 and 70) gave different results from those observed for the topoisomerase – DNA systems. Indeed, the inclusion of only 10 water molecules caused the decrease of the r^2 (Figures 9.10 and 9.12), suggesting that a small hydration shell around the ligand introduces noise and it does not improve the treatment of solute-solvent interactions. However, with higher Nwat the r^2 increases, up to 0.78 (Nwat = 50). To check the calculation convergence, the analyses with Nwat = 60 and 70 were also performed, showing a negligible increase in the correlation (r^2 = 0.83).

Therefore, for the α-thrombin system the improvement in the correlation between computed and experimental ΔG_{bind} was less significant than that observed in the previous example, and it could only be noticed with the inclusion of a rather large hydration shell (Nwat = 50 – 70). At the light of this, it can be hypothesized that in this case water plays a less relevant role in mediating receptor-ligand binding. Indeed, H-bond analyses performed on the MID and BT2 trajectories showed the presence of H-bond with negligible occupancies (between 0.10 and 3.70%, Table 9.6) and the water density around the ligand showed by grid analysis (Figure 9.11) was poor compared to that observed for topoisomerase (Figure 9.10).

Therefore, in this case, the mild r^2 improvement given by the application of the Nwat-MMGBSA approach is probably ascribable to a contribution given to the receptor-ligand interaction by transient H-bonds involving water molecules.

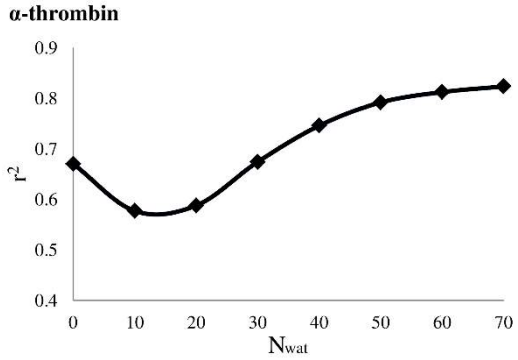

Figure 9.10. Trend of r^2 as a function of Nwat for α-thrombin system.

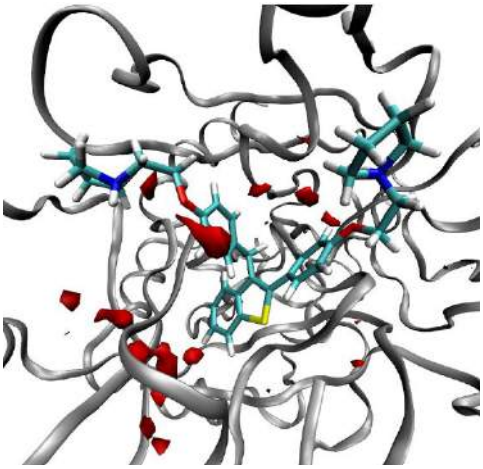

Figure 9.11. Water density plots obtained by grid analysis (ptraj; grid box = 50x50x50 Å, mesh = 0.5 Å**;** visualization with VMD**,** isovalue = 45) of BT2-α-thrombin complex.

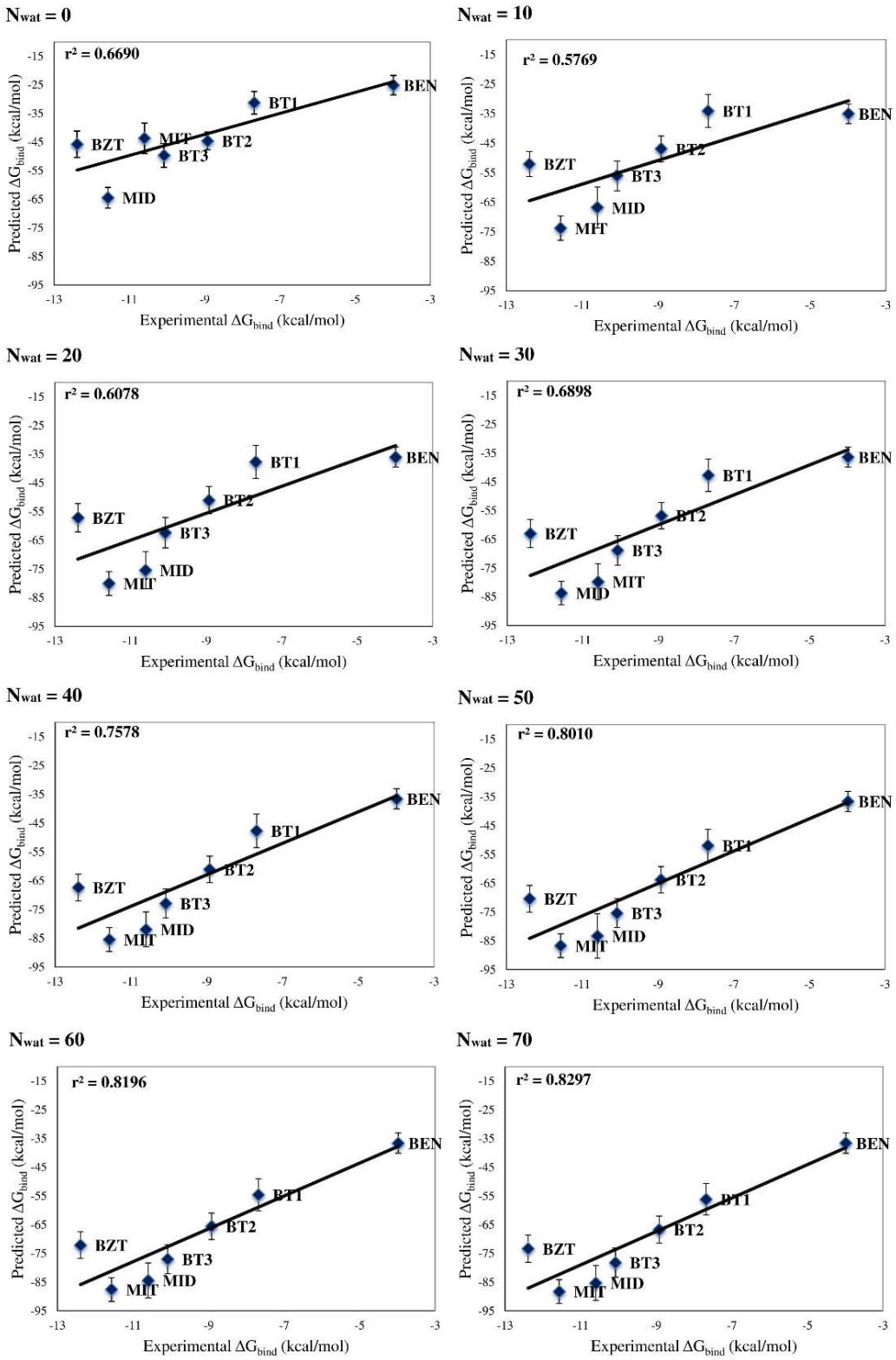

Figure 9.12. Correlations between MMGBSA predicted binding energies and experimental ΔG_{bind} for α-thrombin complexes.

Table 9.6. H-bonds between MID/BT2 and water during the last ns of MD simulation.

MID			BT2		
Donor Atom	**Acceptor Atom**	**Occupancy**	**Donor Atom**	**Acceptor Atom**	**Occupancy**
WAT5573-O	MID-O=S11	2.2%	WAT863-O	BT2-O1	0.4%
WAT5573-O	MID-S11	0.2%	BT2-N34	WAT1148-O	0.2%
WAT8805-O	MID-N26	0.2%	WAT1148-O	BT2-O3	0.1%
WAT9812-O	MID-N12	0.9%	BT2-N10	WAT863-O	0.5%
WAT9812-O	MID-O=S11	2.6%	WAT8353-O	BT2-S16	0.2%
WAT9812-O	MID-S11	1.5%	BT2-N34	WAT8533-O	0.9%
WAT924-O	MID-O=S11	3.7%	WAT4716-O	BT2-O1	0.2%
WAT924-O	MID-S11	0.5%	BT2-N10	WAT4716-O	0.2%
MID-N15	WAT9812-O	0.2%	WAT3398-O	BT2-O1	0.2%
WAT3348-O	MID-O=S11	0.3%	BT2-N10	WAT4423-O	0.3%
WAT3348-O	MID-S11	0.1%	WAT2725-O	BT2-O1	0.1%
WAT8182-O	MID-O=S11	1.2%	WAT4687-O	BT2-S16	0.5%
WAT8182-O	MID-S11	0.7%	BT2-N34	WAT7785-O	0.6%
WAT8182-O	MID-N12	0.1%	WAT7785-O	BT2-N34	0.1%
WAT10308-O	MID-O=S11	1.1%			
WAT10308-O	MID-S11	0.3%			
WAT11327-O	MID-O=S11	0.2%			

Penicillopepsin. For penicillopepsin, the standard MMGBSA calculations (Nwat = 0) gave a modest correlation between predicted and experimental ΔG_{bind} (r^2 = 0.46, r_s = 0.68). Conversely, the Nwat-MMGBSA approach, with Nwat = from 10 to 70, gave a significant improvement of r^2 value (Figures 9.13 and 9.15).

For this system, the r^2 constantly improved with increasing Nwat, although a sharp hike was observed for Nwat = 20-30 (r^2 = 0.70), followed by the convergence to a plateau value of 0.79 (Nwat = 70). The positive effect on correlation between predicted and experimental ΔG_{bind} can be explained by observing the presence of quite wide areas of high water density around the ligand highlighted by the grid analysis (Figure 9.14).

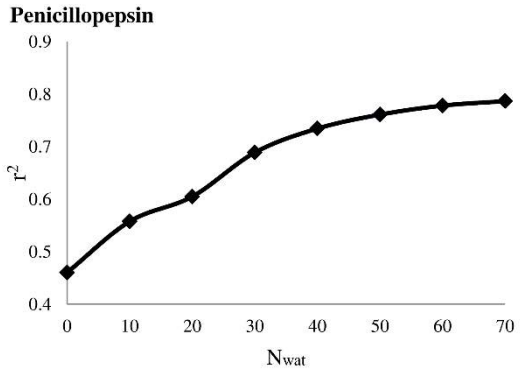

Figure 9.13. Trend of r^2 as a function of Nwat for penicillopepsin system.

The estimation of the binding affinity of the APU ligand was the most affected by the application of the Nwat-MMGBSA approach (Figure 9.15), because its binding energy was highly underestimated by the standard protocol. Therefore, H-bond analyses were performed on the Nwat = 10 and 20 trajectories of APU and APT (Tables 9.7, 9.8 and 9.9), with this latter being a complex not affected by the explicit inclusion of water molecules in MMGBSA calculations.

As previously observed for TTC (Tables 9.3 and 9.4), the number of H-bonds between APU and water molecules increased from 41 to 70 when passing from Nwat = 10 to Nwat = 20 (Tables 9.7 and 9.8), while the APT complex simulation had only 6 H-bonds between APT and water with Nwat = 20, compared to Nwat = 10 (Table 9.9).

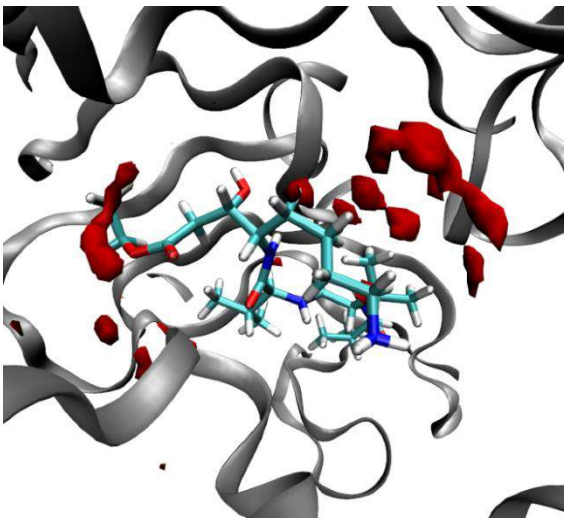

Figure 9.14. Water density plots obtained by grid analysis (ptraj; grid box = 50x50x50 Å, mesh = 0.5 Å; visualization with VMD**,** isovalue = 45) of APT-penicillopepsin complex.

It has to be noted that in this case MMPBSA gave better r^2 than MMGBSA (Annex 9.A), however positive ΔG_{bind} have been obtained with the former method.

Table 9.7. H-bonds between APU and water of the Nwat = 10 trajectory (occupancy ≥ 5%).

Donor Atom	Acceptor Atom	Occ	Donor Atom	Acceptor Atom	Occ
WAT334-O	IVA-O=C5	8.8%	WAT333-O	STA-O29	11.3%
WAT335-O	VAL326-O=C16	7.3%	WAT333-O	IVA-O=C5	6.8%
WAT330-O	STA-O29	9.5%	WAT337-O	VAL326-O=C16	8.0%
WAT329-O	STA-O29	5.6%	WAT329-O	STA-O=C28	5.3%
WAT332-O	STA-O29	12.0%	WAT330-O	IVA-O=C5	5.6%
VAL325-N6	WAT328-O	35.7%	VAL325-N613	WAT329-O	17.4%
WAT333-O	VAL326-O=C16	8.1%	WAT335-O	IVA-O=C5	7.1%
WAT331-O	STA-O29	11.0%	WAT329-O	VAL326-O=C16	5.6%
WAT337-O	STA-O29	12.4%	WAT336-O	STA-O=C28	17.0%
WAT336-O	STA-O29	13.5%	WAT334-O	STA-O=C28	15.5%
WAT337-O	STA-O=C28	14.0%	WAT337-O	IVA-O=C5	6.6%
WAT331-O	STA-O=C28	13.6%	WAT331-O	IVA-O=C5	5.9%
WAT336-O	IVA-O=C5	6.9%	WAT332-O	VAL326-O=C16	7.1%
WAT334-O	VAL326-O=C16	5.7%	WAT336-O	VAL326-O=C16	6.5%
WAT335-O	STA-O=C28	16.7%	VAL325-N66	WAT329-O	11.3%
WAT330-O	STA-O=C28	8.2%	STA-OH-C23	WAT328-O	34.0%
WAT332-O	STA-O =C28	16.7%	STA-OH-C23	WAT329-O	6.7%
WAT335-O	STA-O29	12.8%	VAL325-N66	WAT330-O	7.0%
WAT334-O	STA-O29	13.3%	STA-N21	WAT328-O	26.1%
WAT331-O	VAL326-O=C16	6.9%	STA-N21	WAT329-O	5.9%
WAT333-O	STA-O=C28	18.7%			

Table 9.8. H-bonds between APU and water of the Nwat = 20 trajectory (occupancy ≥ 5%).

Donor Atom	Acceptor Atom	Occ	Donor Atom	Acceptor Atom	Occ
WAT342-O	IVA-O=C5	7.4%	WAT340-O	STA-O=C28	11.1%
WAT334-O	IVA-O=C5	8.8%	WAT344-O	IVA-O=C5	5.0%
WAT335-O	VAL326-O=C16	7.3%	WAT337-O	VAL326-O=C16	8.0%
WAT330-O	STA-O29	9.5%	WAT329-O	STA-O=C28	5.3%
WAT343-O	STA-O=C28	8.8%	WAT330-O	IVA-O=C5	5.6%
WAT329-O	STA-O29	5.6%	WAT338-O	STA-O29	10.7%
WAT338-O	STA-O=C28	13.0%	VAL326-N13	WAT329-O	17.4%
WAT332-O	STA-O29	12.0%	WAT335-O	IVA-O=C5	7.1%
VAL326-N13	WAT328-O	35.7%	WAT329-O	VAL326-O=C16	5.6%
WAT333-O	VAL326-O=C16	8.1%	WAT336-O	STA-O=C28	17.0%
WAT341-O	STA-O=C28	10.6%	WAT341-O	VAL326-O=C16	5.0%
WAT331-O	STA-O29	11.0%	WAT342-O	STA-O29	6.5%
WAT344-O	STA-O29	6.4%	WAT345-O	STA-O29	5.0%

WAT337-O	STA-O29	12.4%	WAT334-O	STA-O=C28	15.5%
WAT336-O	STA-O29	13.5%	WAT337-O	IVA-O=C5	6.6%
WAT337-O	STA-O=C28	14.0%	WAT342-O	STA-O=C28	9.1%
WAT341-O	STA-O29	8.7%	WAT339-O	STA-O29	9.9%
WAT331-O	STA-O=C28	13.6%	WAT341-O	IVA-O=C5	5.2%
WAT336-O	IVA-O=C5	6.9%	WAT331-O	IVA-O=C5	5.9%
WAT334-O	VAL326-O=C16	5.7%	WAT332-O	VAL326-O=C16	7.1%
WAT343-O	STA-O29	6.0%	WAT345-O	STA-O=C28	6.1%
WAT335-O	STA-O=C28	16.7%	WAT339-O	STA-O=C28	11.4%
WAT339-O	IVA-O=C5	6.8%	WAT343-O	IVA-O=C5	5.6%
WAT338-O	VAL326-O=C16	6.4%	WAT336-O	VAL326-O=C16	6.5%
WAT335-O	STA-O29	12.8%	WAT340-O	STA-O29	7.5%
WAT330-O	STA-O=C28	8.2%	WAT346-O	STA-O=C28	5.5%
WAT332-O	STA-O=C28	16.7%	WAT340-O	VAL326-O=C16	5.7%
WAT334-O	STA-O29	13.3%	WAT344-O	STA-O=C28	7.1%
WAT338-O	IVA-O=C5	5.8%	WAT347-O	STA-O=C28	6.0%
WAT331-O	VAL326-O=C16	6.9%	VAL325-N6	WAT329-O	11.3%
WAT333-O	STA-O=C28	18.7%	STA-OH-C23	WAT328-O	34.0%
WAT340-O	IVA-O=C5	5.6%	STA-OH-C23	WAT329-O	6.7%
WAT339-O	VAL326-O=C16	6.4%	VAL325-N6	WAT330-O	7.0%
WAT333-O	STA-O29	11.3%	STA-N21	WAT328-O	26.1%
WAT333-O	IVA-O=C5	6.8%	STA-N21	WAT329-O	5.9%

Table 9.9. H-bonds between APT and water of the Nwat = 10 (left) and 20 (right) trajectories (occupancy ≥ 5%).

Nwat = 10			**Nwat = 20**		
Donor Atom	**Acceptor Atom**	**Occ**	**Donor Atom**	**Acceptor Atom**	**Occ**
LTA-N28	WAT328-O	59.2%	LTA-N28	WAT328-O	58.4%
WAT336-O	IVA-O=C5	10.3%	WAT336-O	IVA-O=C5	11.7%
LTA-N28	WAT329-O	49.3%	LTA-N28	WAT329-O	48.1%
WAT332-O	IVA-O=C5	5.1%	WAT332-O	IVA-O=C5	6.0%
WAT333-O	IVA-O=C5	6.3%	WAT340-O	IVA-O=C5	8.7%
WAT337-O	IVA-O=C5	12.0%	WAT339-O	IVA-O=C5	10.8%
WAT335-O	IVA-O=C5	8.8%	WAT333-O	IVA-O=C5	6.8%
LTA-N28	WAT331-O	7.9%	WAT337-O	IVA-O=C5	11.0%
LTA-N28	WAT330-O	30.7%	WAT335-O	IVA-O=C5	10.6%
LTA-OH-C23	WAT328-O	14.3%	WAT343-O	IVA-O=C5	5.4%
WAT334-O	IVA-O=C5	6.2%	WAT341-O	IVA-O=C5	6.9%
WAT330-O	VAL326-O=C16	10.9%	LTA-N28	WAT331-O	7.3%
VAL326-N13	WAT330-O	6.0%	WAT334-O	IVA-O=C5	7.8%
WAT329-O	VAL326-O=C16	14.4%	WAT342-O	IVA-O=C5	6.6%
WAT328-O	VAL326-O=C16	17.3%	LTA-N28	WAT330-O	25.8%
			LTA-OH-C23	WAT328-O	14.3%

	WAT338-O	IVA-O=C5	10.0%
	WAT330-O	VAL326-O=C16	9.5%
	VAL326-N13	WAT330-O	6.1%
	WAT329-O	VAL326-O=C16	14.8%
	WAT328-O	VAL326-O=C16	18.4%

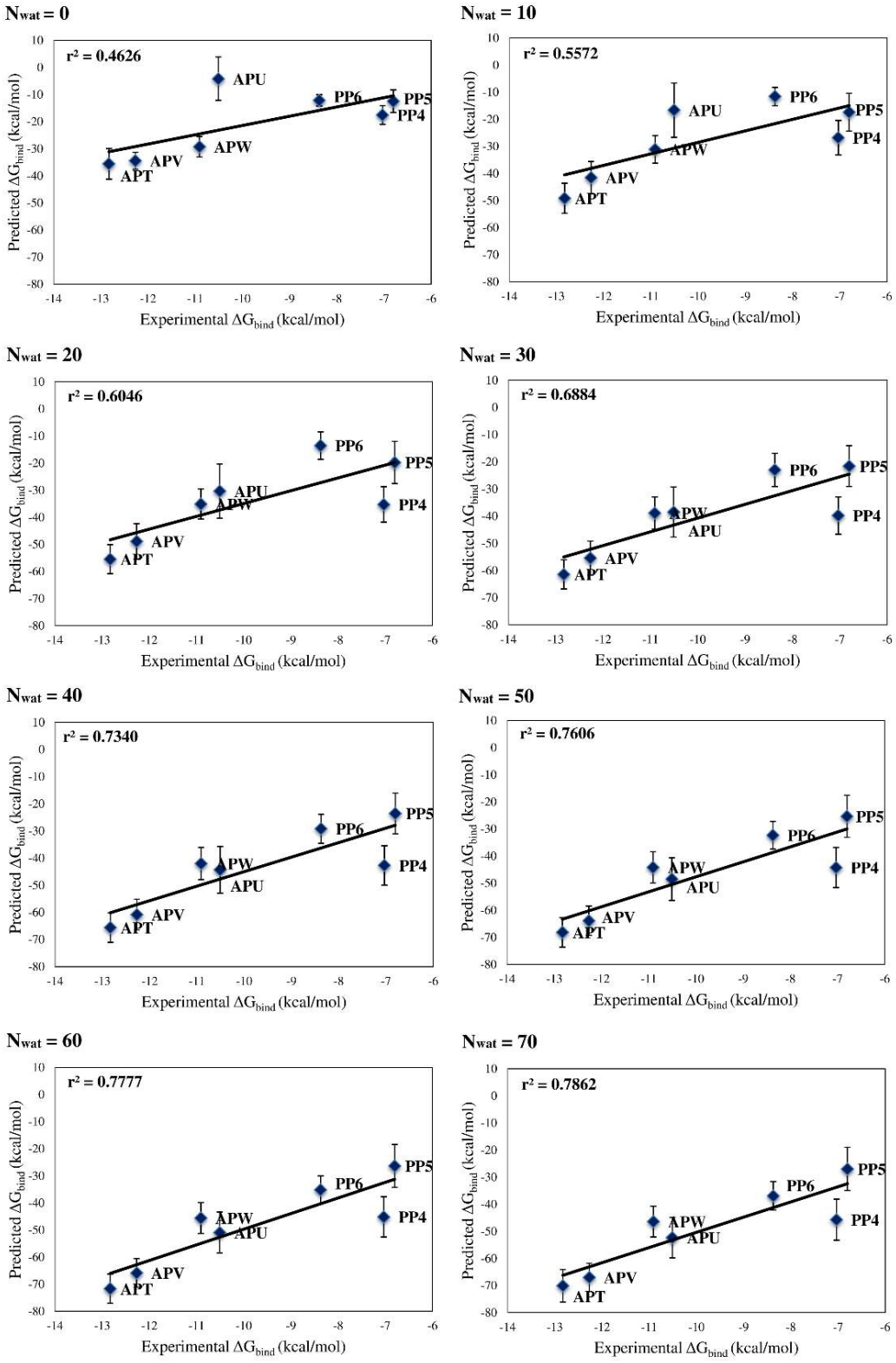

Figure 9.15. Correlations between MMGBSA predicted binding energies and experimental ΔG_{bind} for penicillopepsin complexes.

Avidin. This system was selected because it already gave good correlation with the standard MMGBSA approach.[267,283] Thus, it was not surprising that the good r^2 value of 0.72 was obtained with Nwat = 0 and only minor improvements were given by using Nwat = 10-70 (Figures 9.16 and 9.17).

The small increase in r^2 obtained with the application of the Nwat-MMGBSA method may be attributed to transient interactions between the solute and the solvent. Moreover, the poor relevance of water in this system is also highlighted by the grid analysis of the complex between avidin and BTN2, which showed the absence of high water density around the ligand (Figure 9.18). In addition, no H-bonds with occupancies > 5% were found between water residues and the ligand for BTN1 and BTN2 trajectories (Table 9.10).

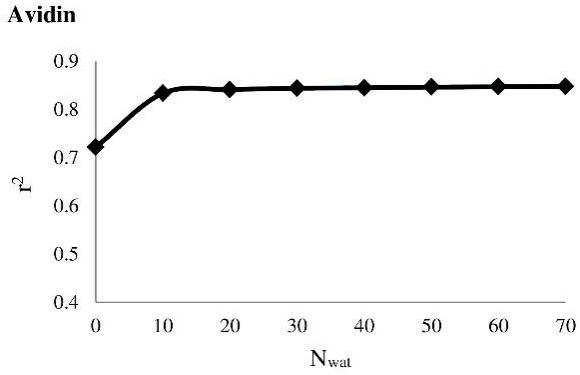

Figure 9.16. Trend of r^2 as a function of Nwat for avidin system.

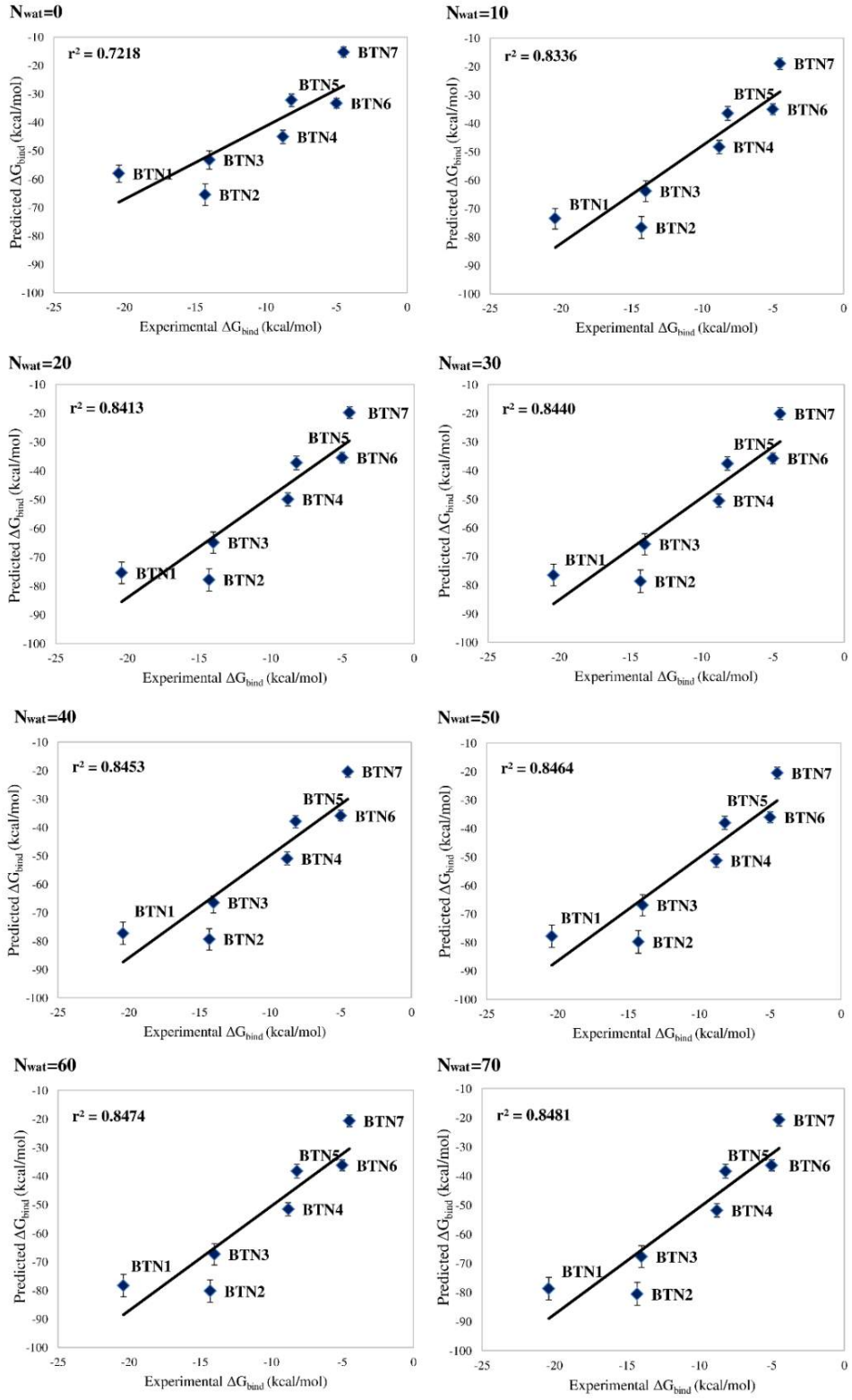

Figure 9.17. Correlations between MMGBSA predicted binding energies and experimental ΔG_{bind} for avidin complexes.

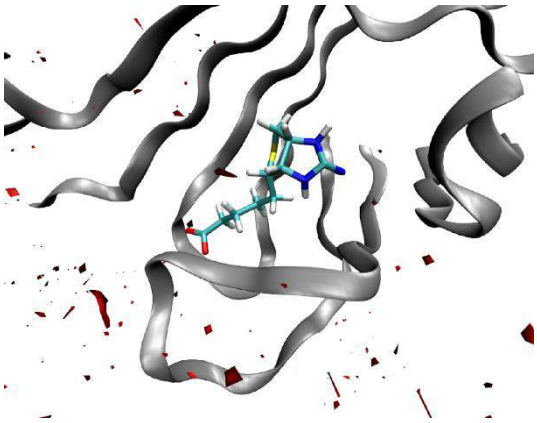

Figure 9.18. Water density plots obtained by grid analysis (ptraj; grid box = 50x50x50 Å, mesh = 0.5 Å; visualization with VMD, isovalue = 25) of avidin-BTN2 complex.

Table 9.10. H-bonds between BTN1 (left) or BTN2 (right) and water during the last ns of MD simulation.

BTN1			**BTN2**		
Donor Atom	**Acceptor Atom**	**Occ**	**Donor Atom**	**Acceptor Atom**	**Occ**
WAT6517-O	BTN1-O=C12	2.7%	WAT523-O	BTN2-O$^-$(C12)	0.5%
WAT6517-O	BTN1-O$^-$(C12)	0.2%	WAT12292-O	BTN2-N4	0.1%
WAT6498-O	BTN1-O=C12	4.1%	WAT12292-O	BTN2-N1	0.1%
WAT6498-O	BTN1-O$^-$(C12)	0.4%			
WAT13708-O	BTN1-O=C12	0.1%			
WAT2867-O	BTN1-O$^-$(C12)	3.7%			
WAT2867-O	BTN1-O=C12	0.1%			

At the light of the results of this study, it appears that the Nwat-MMGBSA approach represents a useful way to improve the correlation between MMPBG/GBSA predicted binding energies and experimental activities of the ligands, without significantly affecting the required computational time.

Although the optimal Nwat was system-dependent, a Nwat = 30 could be considered as a default value in MMPB/GBSA calculations for classical receptor-ligand complexes. Indeed, also in those cases where water has not a significant role in protein-ligand interaction, the inclusion of a hydration shell made of 30 water molecules was not detrimental.

It has also to be underlined that only the correlation between predicted binding energies and biological activities increases, while the estimation of absolute binding

free energy (which also imply the estimation of binding entropies) might be worsened by the presence of water. However, being relative binding energies the most relevant quantity in drug design/discovery, and being calculation time a particularly valuable resource, this approach might be particularly suited for medicinal chemistry applications.

9.3 Materials and Methods

Preparation of Complexes.

Topoisomerase. All models were derived from the 1K4T crystal structure.[278] The considered system is made of human topoisomerase I B, 22 pairs of bases of double helix DNA and Topotecan (TTC) as the ligand (Figure 9.19A). The DNA filament composed by nucleotides 1-22 is cleaved between thymine 10 and guanidine 11, this latter replaced by its 5'-thio derivative (TGP) due to technical reasons related to X-ray resolution. Accordingly to the topoisomerase I cleaving mechanism,[284] the dangling 3' phosphate group of thymine 10 is covalently bound to the Tyr 723 residue.

For those reasons, to prepare a suitable system for MD simulations, the TGP residue was replaced by guanosine monophosphate. A special attention has been given to the covalently bounded thymidine-phosphotyrosine system, for which the definition and charge parameterization of two non-standard residues (DTP and TYP for thymidine and phosphotyrosine, respectively) was mandatory. Conformation and orientation independent partial charges for non-standard residues were derived with the R.E.D. IV software,[228] accordingly to the *ff99SB* force field (RESP-A1 charge model),[141] using two conformations and four orientations for each structure. It's necessary to underline that in the Amber *ff99SB* force field a total charge of −1.0, −0.3079 and −0.6921 is attributed to internal bases, 5' bases ,and 3' bases, respectively.[141] Moreover, when considering the binary complex between DNA and topoisomerase, there is an intact DNA strand, with an integer total charge of −21.0, and two cleaved strands: one is free and has an integer charge of −11.0, the other one has a free 5' end, while the 3' end is covalently bound to TYP 723. Since an integer

charge is requested for the protein-DNA system, the charge of the TYP residue has been restrained to −0.6921 while DTP has been treated as an internal base.

For DTP, an -OMe group has been used to cap the 5' phosphate and the parameterization has been carried by restraining to −1.0 the final total charge of the uncapped DTP. Conversely, to parameterize the TYP residue three caps were added (Figure 9.20) and charge restraints were imposed as follow: a NH-methyl cap on C-terminus with charge of 0.0, an acetyl cap on N-terminus with charge of 0.0 and, on the phosphate group, a methoxyl cap with a charge of −0.3079, as this cap simulates the covalently bounded DNA strand. The backbone N and C atoms were restrained to the same charge value as reported in the force field for the standard tyrosine.[141] Finally, bending parameters for angles involving CA-OS-P and C-OS-P atom types have been calculated from the QM optimized structure using the *parmchk* tool of the Amber 11 suite.[285] Finally, the covalent bond between the phosphotyrosine and the thymidine residues has been created using the LEaP *bond* command (Figure 9.19B).

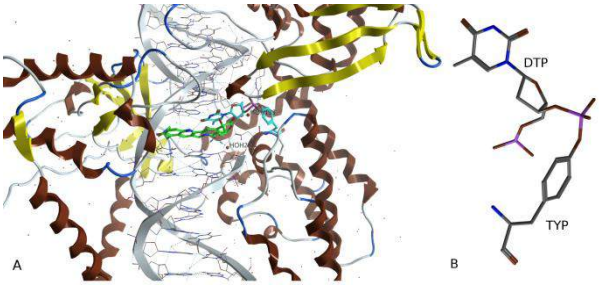

Figure 9.19. A) complex between topoisomerase, DNA and topotecan (carbons colored in green); evidence on TYP and DTP residues (carbons colored in cyan). B) covalent bond between DTP and TYP.

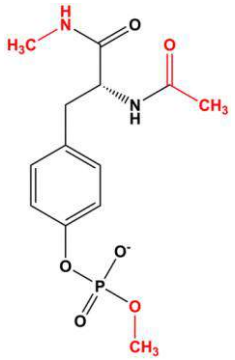

Figure 9.20. TYP residue; the caps (red) have been applied for the charge parameterization step.

The complex between DNA and topoisomerase has been finally processed by H++ server[286] by choosing default settings, in order to establish the correct protonation state for each residue under physiological conditions. The resulting total charge of the DNA-topoisomerase complex was −12, HIS 22, 146, 167, 311, 376 and 342 were protonated on the N^{ε}, while HIS 66, 199, 206 and 315 were protonated on both N^{ε} and N^{δ}.

The ligand test set was made of camptothecin (CPT), topotecan (TTC) and other seven derivatives, for which an experimental IC_{50} value was available in the literature.[280] For ligands characterized by an additional stereocenter at position 5, experimentally evaluated as racemates,[29] both the α and β epimers were considered in MM-PB/GBSA calculation only for compound **12**, as previously reported docking calculations evidenced a significant difference among predicted binding energies for this compound, while only the β epimer was considered for compounds **7**, **8**, **20** and **22**. Regarding this latter derivative, a keto-enol tautomerism might be possible through an intramolecular H-transfer between the C-5 ammonium and the amidic carbonyl (T1 and T2, Figure 9.20). Both tautomers were evaluated, but only the T2 tautomer, which is stabilized by resonance, provided significant correlation with experiments and was thus considered in the following discussion.

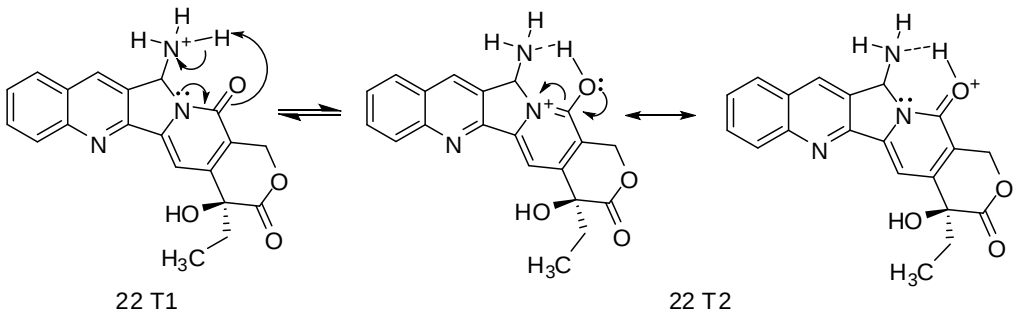

Figure 9.20. Tautomerism for derivative **22**.

Each derivative has then been docked with MOE[227] (placement = Alpha Triangle, 800000 minimum iterations and 5000000 maximum iterations; scoring = Affinity dG; the top 30 structures were subjected to force field refinement up to a gradient = 0.01 and rescored with Affinity dG). A simple pharmacophore (Figure 9.21) consisting of

an H-bond acceptor feature centered on the lactone moiety (F1, radius of 2.8 Å) and an aromatic feature centered on the quinolone moiety (F2, radius of 2.5 Å) based on the crystal structure of topotecan was designed and used as a pharmacophore restraint in all dockings.

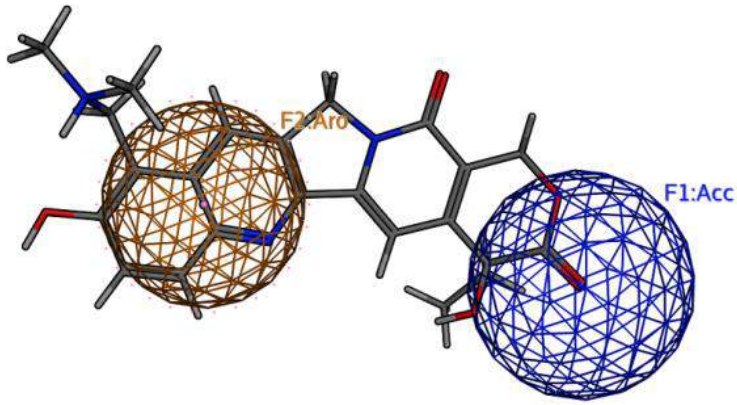

Figure 9.21. Pharmacophore created from bounded TTC and used as a pharmacophore restraint while docking topoisomerase I ligands. F1 = H-bond acceptor; F2 = Aromatic.

The top-ranked conformations were then used to build the complexes. Partial charges were then calculated by following the RESP-A1 model with R.E.D.IV, using two conformations and four orientations.

α-thrombin and penicillopepsin. Since the crystallographic structures of the α-thrombin and penicillopepsin complexes with all the considered ligands were available (PDB codes for α-thrombin: 1D3D, 1D3P, 1D3Q, 1D3T, 1DWB, 1DWC, 1DWD; PDB codes for penicillopepsin: 1APU, 1APT, 1APV, 1APW, 2WEA, 2WEB, 2WEC), no further action, save the protonation of the two proteins with the H++ server, was necessary to build starting geometries for MD simulations. A total charge of −2 was obtained for α-thrombin. HIS 72, 95, 116, 145 and 271 of 1DWB, 1DWC and 1DWD structures and HIS 71, 94 115, 144 and 263 of 1D3D, 1D3P, 1D3Q and 1D3T were protonated at N^{ε}. A total charge of −22 was obtained for penicillopepsin, where HIS 54, 98 and 159 were protonated at N^{ε}. Partial charges for the α-thrombin ligands were derived as previously described for camptothecin derivatives.[89]

Penicillopepsin ligands APT, APU, APV and APW were considered as non-natural tetrapeptides containing a divaline group substituted with isovaleric acid (IVA) at the N-terminus and with one of the non-standard residues LTA, STA, DFI or DFO at the C-terminus. Partial charges were thus derived for IVA (capped with a NH-methyl group), and LTA, STA, DFI and DFO (all capped with acetyl groups) and corresponding force field libraries were generated. Conformations were generated through the low-mode molecular dynamics conformational search implemented in MOE by using default parameters and charges computed with R.E.D.IV as explained above. Conversely, charge parameterization for PP4, PP5 and PP6 ligands was done on the complete structures by restraining the atoms corresponding to the central valine residue to the same charge value as reported in the *ff99SB* force field for valine.[287]

1.3 Avidin. Since the crystallographic structure of avidin-biotin (BTN1) was the only one available (1AVD),[288] the starting geometries of the six biotin analogues (BTN2-BTN7) were manually generated on the basis of the avidin-biotin complex using MOE software. It has been shown that the neutral form of the guanidinium group in BTN2 and BTN5 is dominant when it is bound to the protein,[289] therefore, the neutral form of the guanidinium group for these ligands was used in our simulations. Partial charges for the biotin analogues were derived as previously described for camptothecin derivatives.

The protein structure was protonated through the H++ server, obtaining a total charge of +9 with HIS 48 and 172 being protonated at N^{ε}.

In all cases, QM geometry optimization and electrostatic potential calculation were performed at the HF/6-31G* level, accordingly to the *ff99*SB force field, by using the Gaussian09 software package.[233]

Molecular dynamics

MD simulations were carried out with the *pmemd* module of the Amber 11 package[285] using the *ff99SB*[141] and *gaff* force fields. In each case, the system total charge was neutralized by adding the proper number of Na^+/Cl^- ions and solvent, a cubic box of TIP3P water, has been added up to a distance of 10 Å from the solute. The systems were then relaxed by minimizing hydrogens, ions and waters (1000

cycles of steepest descent and 5000 cycles of conjugated gradient). The solvent box was then equilibrated at 300 K by 45 ps of NVT and 45 ps of NPT simulation. This step was followed by a minimization involving side chains, water and ions and by a total minimization (2500 cycles of steepest descent and 5000 cycles of conjugated gradient) with restraints applied on backbone atoms (10.0 kcal/mol) and on ligands (5.0 kcal/mol). The systems were then heated up to 300 K in 6 steps of 20 ps each (ΔT 50 K), where backbone and ligand restraints were reduced from 10.0 to 5.0 and from 5.0 to 0.5 kcal/mol, respectively. Full equilibration was then performed in NVT ensemble (100 ps, with a restraint of 10.0 and 5.0 kcal/mol on the backbone and ligands, respectively) and in the NPT ensemble (4 steps of 100 ps each, reducing backbone and ligand restraints from 5.0 to 2.0 and from 0.5 to 0.2 kcal/mol, respectively, followed by a 1 ns NPT equilibration with backbone and ligand restraints of 1.0 and 0.1 kcal/mol, respectively). Finally, unrestrained production runs were performed at 300 K for 4 ns, a length considered adequate for similar calculations.[267] A cut-off for electrostatic of 8.0 Å, a time step of 0.002 ps and the SHAKE algorithm, constraining bonds involving hydrogens, were applied to all calculations. Root-mean-square deviation (RMSD) analyses of receptor backbone and ligand atoms were made to assess the system stability. As regards avidin complexes, the analyses has been conducted on each of the two monomers, because the avidin sites are independent of each other.[290]

In some cases (CPT, 7, 12β, BEN, MIT, PP4 and PP6), poor RMSD convergence was observed, so the NPT equilibration step was then extended to 2 ns.

Both MM-PBSA and MM-GBSA analyses were performed by using the MMPBSA.py python script implemented in the Amber 11 package. Analyses were conducted on the 4th ns of production run trajectory by selecting 100 evenly spaced out snapshots. The atomic radii developed by Onufriev and coworkers (*igb*=5)[172] was chosen for all GB calculation, and a salt molar concentration in solution was at 0.15 M in both GB and PB calculations (*saltcon* and *istrng* parameters, respectively). The default PB solver implemented in the sander module was used for PB calculation and, unless differently specified, default parameters were adopted.

The entropy term in the herein reported binding energy calculations was neglected, considering that the benefits of including this term are controversial[119,267,269,283] and entropy estimations by normal mode analysis are rather consuming in terms of CPU time.

When a ligand hydration shell had to be considered in MM-PB/GBSA analyses, corresponding trajectories were obtained using the *ptraj* keyword "*closest*", which allows to retain only the requested number of those water molecules that, in each frame of the solvated MD trajectory, are the closest to the atoms specified in the mask (the ligand atoms, in our case). For performance reason, it has been found convenient to sample the requested snapshots with the *ptraj* "*offset*" keyword, and successively perform the "*closest*" analysis on the reduced trajectory. MM-PB/GBSA were then run by setting "*strip_mdcrd*=0" (avoid the stripping of water molecules) and "*interval=1*" (consider all frames in the MD trajectory) in the input file. The water molecules (10, 20, 30, 40, 50, 60 or 70, depending from the chosen N_{wat}) defining the ligand hydration shell were then included in both the complex and receptor files and considered as part of the receptor atoms. Indeed, we noticed that considering water molecules as part of the ligand atoms provided worse correlation and higher standard deviations to the computed ΔG_{bind}.

Unless differently specified, the square of Pearson's correlation coefficient (r^2) between computed binding energies and available experimental values such as the $-\log_{10}(IC_{50})$ (for topoisomerase) and ΔG_{bind} (for α-thrombin, penicillopepsin and avidin) was used as an evaluation metric.

As regards avidin complexes, MM-PB/GBSA analyses were performed on separate monomers and the results averaged.

All H-bond analyses of ligand-water interactions were performed on the 4th ns of production run with VMD,[231] requesting a donor-acceptor distance of 4.0Å, an angle cutoff of 30°. The same software has been used to visualize grid density maps, generated with a *ptraj* analysis of the whole production run by setting a cubic box (50x50x50 Å, mesh 0.5 Å) centered on the ligand center of mass.

10 TEST AND OPTIMIZATION OF NWAT-MMPB/GBSA METHOD ON PPIS

10.1 INTRODUCTION

As previously observed, water molecules are often found at protein-protein interfaces, and solvent can play a role in PPIs by bridging interactions between the protein partners o by stabilizing their interaction. [47,50] Therefore, the Nwat-MMPB/GBSA approach could improve the correlation between experimental ΔG_{bind} and predicted binding energies also for PPI systems.

However, the Nwat-MMPB/GBSA protocol previously applied to classical receptor-ligand complexes might not be suitable for protein-protein complexes, because of their different structural properties, which have been highlighted in Chapter 1. Indeed, the large interaction surface[15] might need the inclusion in the hydration shell of more than 30-50 water molecules, or the big PPI complexes might necessitate more than 4 ns of production run to achieve the best results in terms of r^2. In addition, more recent force fields, or explicit and implicit solvation models might affect the prediction of the binding energies. Moreover, the selection of the protein-protein interfacial residues, to which the hydration shell has to be centered, is nontrivial.

At the light of this, 20 heterodimeric PPI complexes without ions and missing residues at the interface and with known experimental ΔG_{bind} (Table 10.1)[291] have been selected and submitted to explicit solvent MD and to the Nwat-MMPB/GBSA approach by using different simulation conditions, with the aim of both optimizing the Nwat-MMPB/GBSA method for PPIs and assessing the robustness of the method. In particular, for the MD simulations, we tested two different AMBER force fields, namely the ff14SB[135] and the ff99SBildn[136], two different explicit solvent models, namely TIP3P[292] and TIP4P-Ew[293], and 4 ns and12 ns MD simulation lengths. Concerning the Nwat-MMPB/GBSA protocol, we tested both the PB and GB methods, two implicit solvent models, namely GB-OBC(II)[172] and GB-Neck2[173], and

Nwat = 0 - 50. The effects of these parameters have been evaluated in terms of correlation between experimental ΔG_{bind} and computed binding energies.

In addition, the interface residues have been selected through an automatic *python* script (Annex 10.A), which selects as interfacial residues those whose difference in SASA (dASA) from the complex to a single chain is greater than a given cutoff, whose effect on the r^2 has also been tested by setting it to 0.50 and 0.75.

Furthermore, we verified the effect of including all the interfacial residues or only the polar ones as the residues mask used for the selection of Nwat water molecules.

All the considered variables are summarized in Table 10.2.

Moreover, the whole process has been automatized through a *tcsh* script reported in Annex 10.A.

Table 10.1. PDB ID and experimental ΔG_{bind} of the selected PPI complexes.

PDB ID	Exp. ΔG_{bind} (kcal/mol)	PDB ID	Exp. ΔG_{bind} (kcal/mol)
1ACB[294]	-13.05	1ZHI[295]	-9.08
1AVX[296]	-12.50	2HLE[297]	-10.09
1AY7[298]	-13.23	2HRK[299]	-10.98
1BVN[300]	-15.06	2OOB[301]	-5.66
1EMV[302]	-18.58	2OUL[303]	-11.96
1FLE[304]	-12.28	2SIC[305]	-13.84
1GLA[306]	-6.76	2SNI[307]	-15.96
1KAC[308]	-10.68	2UUY[309]	-11.26
1R0R[310]	-14.17	3BZD[311]	-9.57
1YVB[312]	-11.17	3SGB[313]	-14.51

Table 10.2. Protocol variables considered in the present study.

MD		Nwat-MMPB/GBSA	
Force field	ff14SB, ff99SBildn	Method	GB, PB
Explicit solvent model	TIP3P, TIP4P-Ew	Nwat	0 - 50
Simulation length	4 ns, 12 ns	Implicit solvent model	GB-OBC(II), GB-Neck2
		dASA cutoff	0.50, 0.75
		Interfacial residues mask	All, polar

10.2 Results and Discussion

The setup of an appropriate and automatic way to select the interfacial residues has been nontrivial, therefore this aspect will be explained as first. Indeed, the selection of interfacial residues is necessary to define the Nwat water molecules (0 – 50) to be considered during the Nwat-MMPB/GBSA calculations.

A straight approach to identify the interfacial residues consists in the selection of those residues whose dASA from the PPI complex to the single protein chain is greater than a cutoff, which, however, has to be determined. In addition, the relevance of selecting all interfacial residues or only the polar one, which most likely will be those majorly solvated, needed to be evaluated.

In detail, the optimization of the protocol for the interfacial residues selection included the comparison of MMGBSA analysis of:

- 4th ns of ff99SBildn[136] / TIP3P[292] explicit solvent model MD simulations
- 4th ns of ff14SB[135] / TIP3P[292] explicit solvent model MD simulations

by setting for MMGBSA calculations

- GB-OBC(II)[172] or GB-Neck2[173] as implicit solvent model
- Nwat = 0 – 50 (ΔNwat = 10)
- dASA = 0.50 or 0.75
- the selection of all or only the polar interfacial residues.

The predicted binding energies have been then correlated to the experimental ΔG_{bind} (Figures 10.12 – 10.37)

Surprisingly, independently from the simulation and analysis conditions, the correlation between experimental and predicted binding energies in terms of r^2 was not significantly affected by the selection method for the interfacial residues (Figure 10.1).

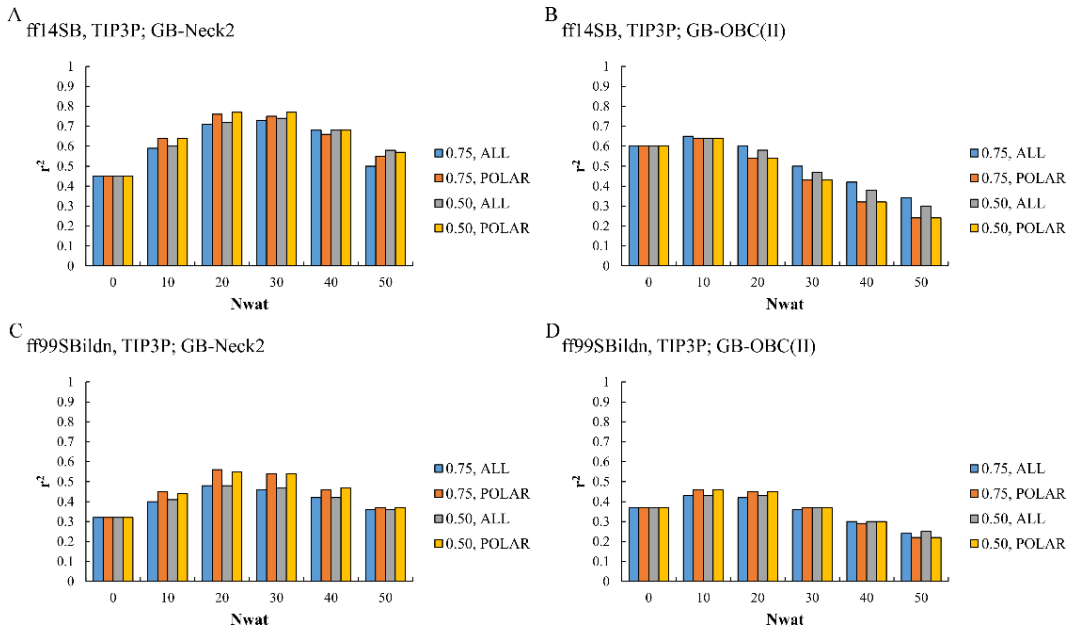

Figure 10.1. Variation of r^2 in dependency of Nwat for Nwat-MMGBSA analysis performed on the 4th ns of the MD simulations. The MD simulation and Nwat-MMGBSA conditions are reported on the top of each plot. See figure 10.12 – 10.37 for details.

This result is explained by observing that the water molecules included during the Nwat-MMGBSA analysis are the same (red oxygen water molecules in Figure 10.2), except for few residues (blue/yellow oxygen water molecules in Figure 10.2), with a cutoff of either 0.50 or 0.75 and with the selection of either all or only polar interfacial residues. This is probably due to the fact that water molecules are anyway mainly located in proximity of polar residues, thus the different parameters acting on the interfacial residues identification do not strongly affect the water molecule selection. Therefore the small and not statistically significant differences in the r^2 that are observed by acting only on the interface selection are due to these nonmatching residues.

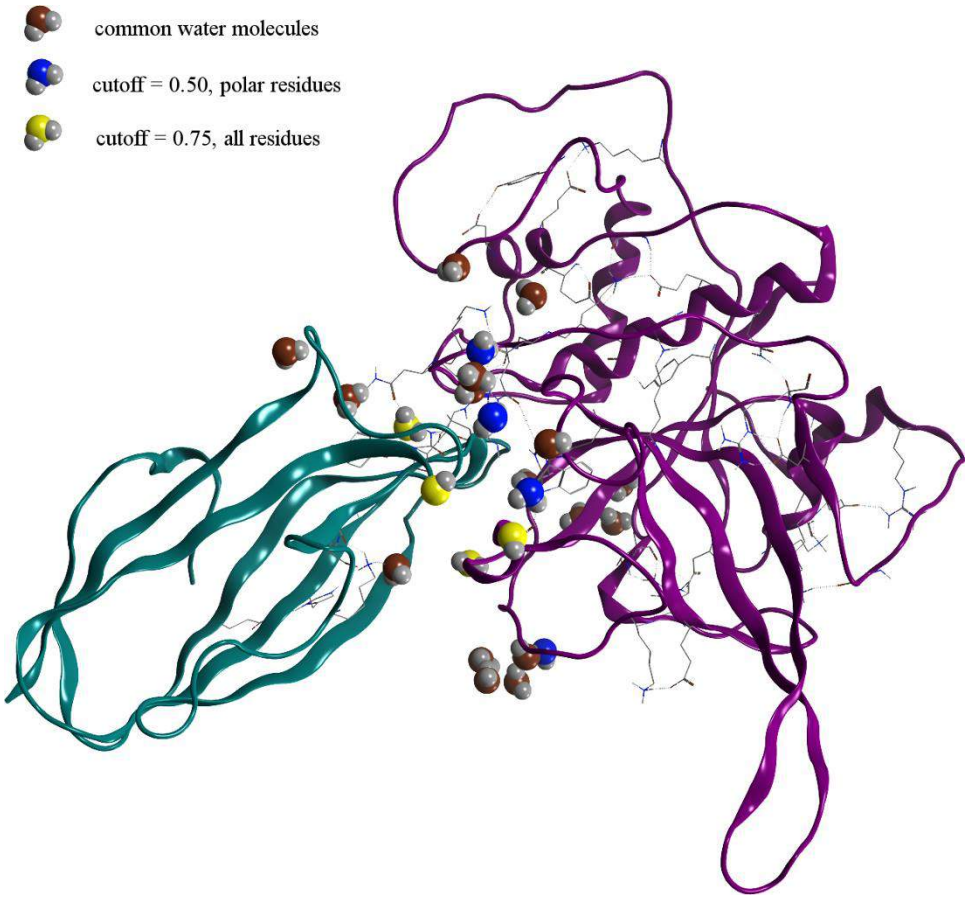

Figure 10.2. Frame of the 2OUL complex MD simulation (ff14SB, TIP3P) submitted to Nwat-MMGBSA (Nwat =20; GB-Neck2) after selecting a) all the residues with a dASA cutoff of 0.75 b) only polar residues with a dASA cutoff of 0.50 as residues to which the 20 water molecules are close during the simulation time. Water molecules with a red oxygen are those residues which have been selected with both the approaches; water molecules with yellow oxygen are those selected only by a); water molecules with blue oxygen are those selected only by b).

It has to be underscored that cutoff values of 0.25, 0.10 and 0.05 have also been tested, but they led to the same selection obtained with a cutoff of 0.50. Analogously, a cutoff value of 1.0 or 0.75 provided the same selection.

At the light of this, only the results obtained using a cutoff of 0.50 and selecting only polar residues will be discussed, whereas those obtained with a cutoff of 0.75 and selecting all the residues whose dASA satisfied this threshold were taken in account as countercheck.

Successively, the performances of both PB and GB were tested despite the poor performances previously observed for PB methods.[89]

As expected, at all the considered conditions, MMPBSA gave worse correlation between experimental and predicted binding energies than MMGBSA (Figures 10.1 and 10.3). The best r^2 values (~ 0.20) were obtained with Nwat = 0, although positive binding energies were predicted, making the results unreliable (Figure 10.3). The inclusion of water molecules during the MMPBSA analysis partially solved this problem, but high standard deviations (> 20%) (Figures 10.18, 10.19, 10.20 and 10.21) were observed together with poor or completely absent correlation between experimental and predicted data ($0.26 < r^2 < 0.0$).

In addition, one or few complexes, which, if discarded, significantly improved the correlation index, could not be found, although it can be observed that for some of them, such as 1YVB and 2SIC, the predicted binding energy is only slightly affected by the inclusion of explicit solvent molecules. The binding energy of other complexes, such as 1EMV, is highly overestimated when applying the Nwat-MMPBSA protocol. This opposite behavior showed by some complexes is the main responsible of the r^2 decrease given by MMPBSA calculations.

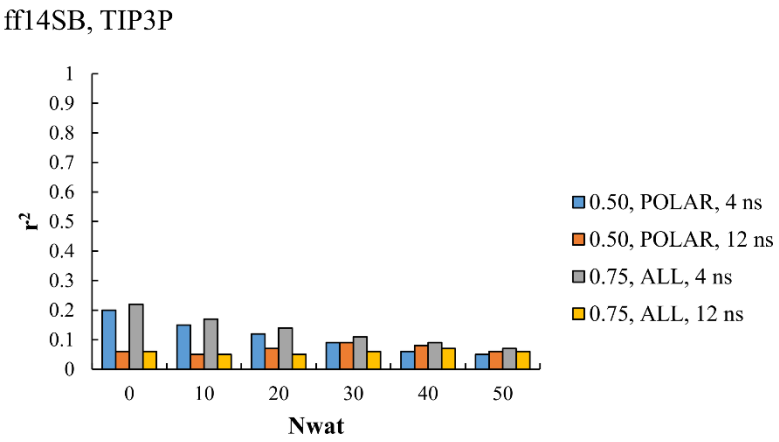

Figure 10.3. Variation of r^2 in dependency of Nwat for Nwat-MMPBSA analysis performed on the 4th and 12th ns of the MD simulations. The MD simulation and Nwat-MMPBSA conditions are reported on the top of the plot. See Figures 10.18 – 10.21 for details.

Although it has been reported that the MMPBSA method gives better correlation with experiments when performed on longer simulations because of its high dependency from the analyzed conformations,[268,314] a dependency of r^2 from the simulation length could not be observed.

Furthermore, analogously to what stated for classical receptor-ligand complexes,[89] the use of the PB method, beyond being detrimental, is also extremely time consuming, compared to the well performing GB method. Therefore, MMGBSA can represent a good choice for the correlation between experimental activities and predicted binding energies for PPIs.

Focusing on MMGBSA results, it can be noticed that, a positive effect on the r^2 values is obtained at any simulation condition when increasing the Nwat from 0 to 20 – 30, except for the analyses performed on the simulations where the TIP4P-Ew explicit solvent model was used (Figures 10.22 and 10.23). Indeed, in this case the correlation between experimental and predicted binding energies obtained with Nwat = 0 (r^2 = 0.31, Figures 10.22 and 10.23) was equivalent to that obtained from MD simulations with TIP3P solvent model ($0.30 < r^2 < 0.45$, Figure 10.1, and Figures 10.13 – 10.14). Conversely, when Nwat ≠ 0, the MMGBSA results coming from the analysis of the TIP4P-Ew MD simulations did not correlate with experimental ΔG_{bind} and positive binding energies were predicted (Figures 10.22 and 10.23). This is necessarily due to the presence of an additional pseudoatom in the water molecules of the TIP4P-Ew model, namely EPW, which has only a point charge, but not a radius.[293] This atom has been introduced to mimic the free electron pair of the water molecule, but, clearly, it is also responsible of the failure of the MMGBSA calculations when water is explicitly included during the analysis.

As previously observed for MMPBSA calculations, the correlations coefficient r^2 is not improved by longer MD simulations. Indeed, in the case of the MD simulations with ff14SB as force field, the MMGBSA analyses performed on the 4th ns gave r^2 values of about 20% higher than those obtained by analyzing the 12th ns (Figure 10.4 and Figure 10.5). This difference can be mainly attributed to complexes 1AVX and 2HLE, whose binding energy are overestimated when the 12th ns of the MD simulation is analyzed (Figure 10.5). The 2HLE misbehavior is due to the fact that during the 12th ns conformations with higher RMSD from the crystallographic structure are sampled, compared to those sampled during the 4th ns (Figure 10.6A), indeed it is an outlier with both Nwat = 0 and Nwat = 30. This is still true, but less

evident for 1AVX complex, whose predicted binding energy has, however, one of the highest standard deviations (> 10%) observed, suggesting that the conformations sampled for the MMGBSA calculation are significantly different. Nevertheless, although for this force field short simulations lead to good results in terms of r^2, it has to be underlined that the trend of the r^2 as a function of Nwat is equivalent, showing an increase of about 20-25% when passing from Nwat = 0 to Nwat = 20-30 followed by a slight decrease with higher Nwat.

Conversely, the MMGBSA analyses performed on the ff99SBildn simulations did showed differences in r^2 related to the analyzed time interval of about 10% and, therefore, statistically nonsignificant. Indeed, although 1AVX became an outlier on the analysis performed on the 12th ns (Figure 10.7) with this force field also, this is not due to difference in the RMSD from the crystallographic structure (Figure 10.8) as previously observed (Figure 10.6B), indeed, the r^2 obtained with Nwat = 0 are equivalent, although poor. However, in this case, the misbehavior of 1AVX is compensated by a better correlation of all the other complexes, for which longer simulations are, therefore, useful.

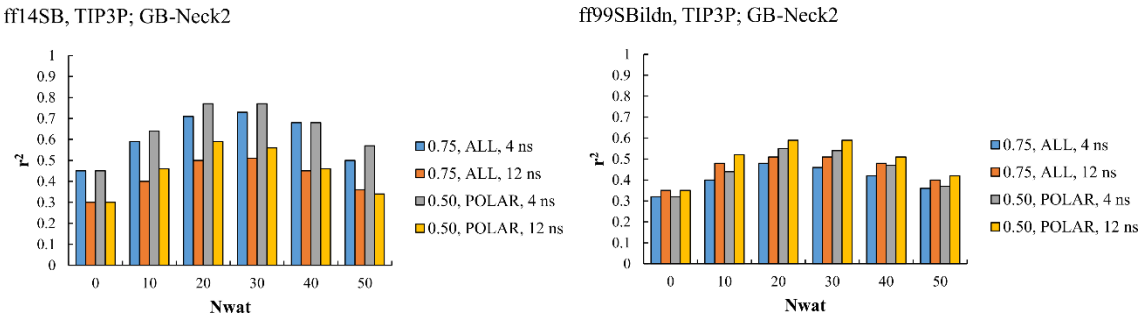

Figure 10.4. Variation of r^2 in dependency of Nwat for Nwat-MMGBSA analysis performed on the 4th ns and 12th ns of the MD simulations. The MD simulation and Nwat-MMGBSA conditions are reported on the top of each plot. (See Figures 10.12 – 10.37 for details)

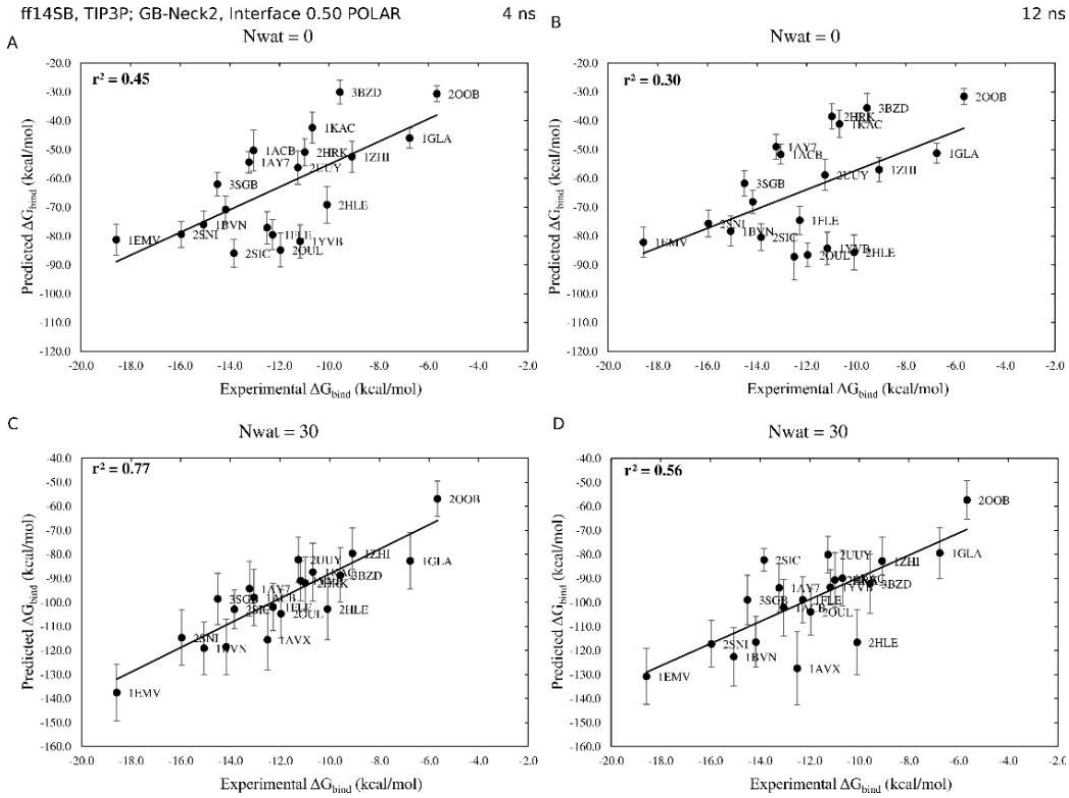

Figure 10.5. Correlation between experimental ΔG_{bind} and predicted binding energies obtained from the analysis MMGBSA analysis (cutoff = 0.50, polar interfacial residues, GB-Neck2) of the 4th (A, C) and 12th (B, D) ns of MD simulations (ff14SB, TIP3P).

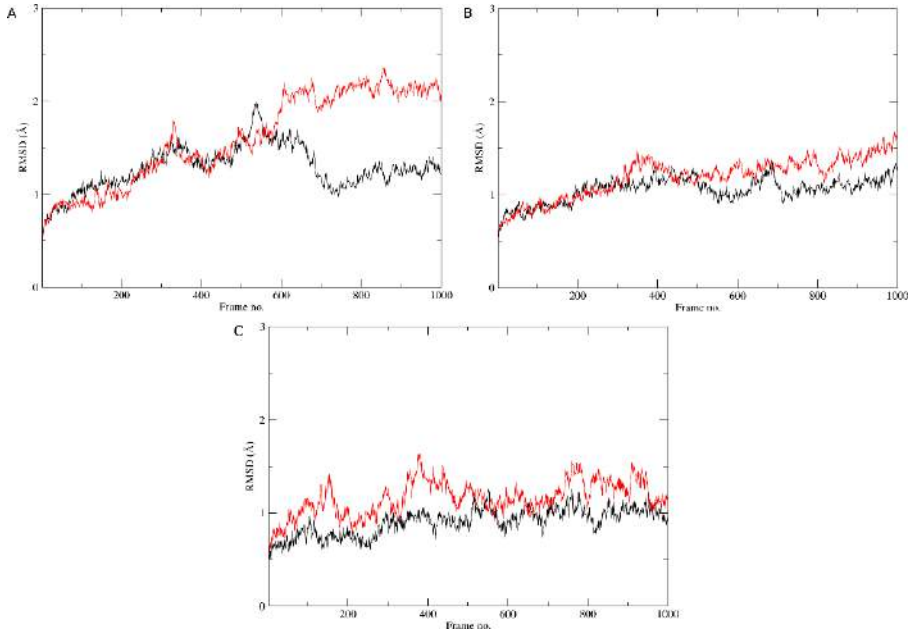

Figure 10.6. RMSD from the crystallographic structure of A) 2HLE, B) 1AVX and C) 2OOB complexes computed on the 4th ns (black) and at the 12th ns (red) of the MD simulation (ff14SB, TIP3P).

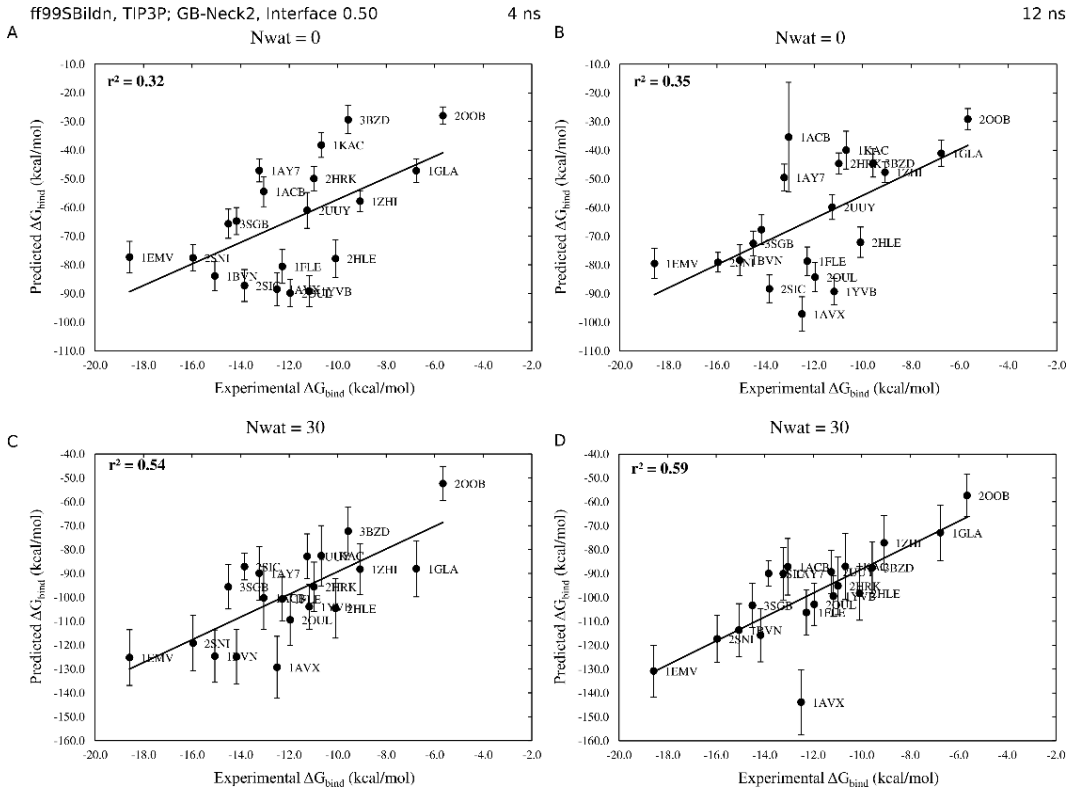

Figure 10.7. Correlation between experimental ΔG_{bind} and predicted binding energies obtained from the analysis MMGBSA analysis (cutoff = 0.50, polar interfacial residues, GB-Neck2) of the 4th (A, C) and 12th (B, D) ns of MD simulations (ff99SBildn, TIP3P).

The overestimation of the binding energy of 1AVX can be explained by comparing the occupancies of stable (occupancy > 20%) water-bridged H-bonds during the 4th and 12th ns of the simulations of 1AVX and 2SNI, chosen as a reference as its behavior is equivalent during both the time intervals (Tables 8.13 and 8.14). Indeed, for the former complex 6 additional water-mediated H-bonds are detected with a longer simulation, and the H-bond involving Ile30 and Asn31 is about 20% more stable (Table 10.3). Conversely, for 2SNI only 3 additional water-mediated interactions are detected by analyzing the 12th ns, and the occupancy are not significantly different (Table 10.4).

Probably, for the correct treatment of the solute-solvent interactions in the 1AVX complex the consideration of other water-bridged H-bonds is needed. Indeed, the analysis of the 1AVX water-mediated interactions on the 4th ns of the ff14SB simulation showed a high number of these interactions with an occupancy of about 20

– 60%). However, compared to the ff99SBildn MD, in this simulation additional water-mediated interactions, such as the one between HIS40 and HIS294 (Figure 10.9), are found.

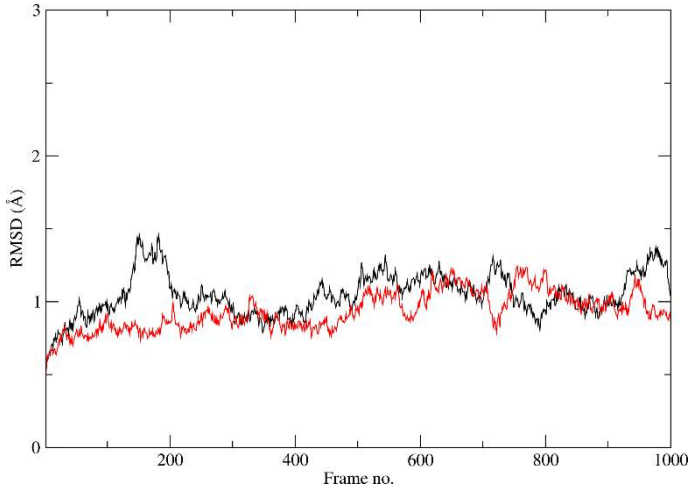

Figure 10.8. RMSD from the crystallographic structure of 1AVX complex computed on the 4th ns (black) and at the 12th ns (red) of the MD simulation (ff99SBildn, TIP3P).

Table 10.3. Water-mediated H-bonds with occupancy > 20% detected from the analysis of the 4th and 12th ns of the simulation of 1AVX (ff99SBildn, TIP3P).

4th ns		**12th ns**	
Residues involved	**Occ%**	**Residues involved**	**Occ%**
30:ILE 31:ASN	64.0	30:ILE 31:ASN	83.0
68:ALA 69:LYS	62.0	24:PHE 25:CYX	61.0
364:GLU 365:ASP	61.0	68:ALA 69:LYS	57.0
24:PHE 25:CYX	60.0	364:GLU 365:ASP	52.0
44:SER 224:ASP	55.0	235:GLU 288:ARG	46.0
16:VAL 28:SER	36.0	16:VAL 28:SER	44.0
175:GLY 177:SER	35.0	195:TYR 202:LYS 286:ARG	35.0
235:GLU 288:ARG	30.0	231:GLY 352:ASN	34.0
20:SER 47:GLN	29.0	80:THR 364:GLU	31.0
224:ASP 292:GLU	26.0	342:ARG 364:GLU	30.0
364:GLU 365:ASP 366:ASP	24.0	78:GLY 364:GLU	30.0
195:TYR 202:LYS 286:ARG	22.0	222:ALA 223:ASN	27.0
398:LYS 400:ASP	22.0	129:SER 131:TYR 236:ASN	27.0
342:ARG 364:GLU	22.0	125:LYS 174:GLN	27.0
231:GLY 352:ASN	21.0	364:GLU 365:ASP 366:ASP	26.0
		365:ASP 366:ASP	26.0
		346:VAL 347:SER	25.0
		20:SER 47:GLN	24.0
		347:SER 351:PHE	23.0

	79:ASN 364:GLU	23.0
	20:SER 45:ARG	22.0

Table 10.4. Water-mediated H-bonds with occupancy > 20% detected from the analysis of the 4th and 12th ns of the simulation of 2SNI (ff99SBildn, TIP3P).

4th ns		**12th ns**	
Residues involved	**Occ%**	**Residues involved**	**Occ%**
155:ASN 221:SER	68.0	39:HIE 209:LEU	73.0
39:HIE 209:LEU	67.0	155:ASN 221:SER	69.0
318:ARG 321:ARG	64.0	323:ARG 337:ARG	68.0
323:ARG 337:ARG	61.0	218:ASN 316:GLU 317:TYR	58.0
99:ASP 101:SER	56.0	99:ASP 101:SER	55.0
316:GLU 321:ARG	53.0	71:THR 207:SER	55.0
95:VAL 96:LEU	50.0	298:ASP 299:LYS	44.0
325:PHE 334:GLU	49.0	197:ASP 198:VAL	42.0
62:ASN 314:THR	47.0	325:PHE 334:GLU	41.0
218:ASN 316:GLU 317:TYR	45.0	62:ASN 314:THR	38.0
197:ASP 198:VAL	43.0	316:GLU 339:GLY	35.0
71:THR 207:SER	39.0	334:GLU 337:ARG	35.0
334:GLU 337:ARG	36.0	60:ASP 63:SER	33.0
16:LEU 17:HIE	35.0	95:VAL 96:LEU	32.0
120:ASP 121:VAL	33.0	323:ARG 337:ARG 339:GLY	32.0
323:ARG 337:ARG 339:GLY	31.0	323:ARG 339:GLY	32.0
323:ARG 339:GLY	31.0	156:GLU 159:SER	29.0
99:ASP 323:ARG	29.0	317:TYR 338:VAL	27.0
333:ALA 334:GLU	25.0	156:GLU 164:THR	27.0
60:ASP 63:SER	22.0	104:TYR 311:THR	26.0
67:HIE 68:VAL	21.0	16:LEU 17:HIE	26.0
10:GLN 184:ASN	21.0	333:ALA 334:GLU	25.0
		120:ASP 121:VAL	21.0
		218:ASN 317:TYR	21.0
		156:GLU 337:ARG	21.0

Table 10.5. Water-mediated H-bonds with occupancy > 20% detected from the analysis of the 4th ns of the simulation of 1AVX (ff14SB, TIP3P).

Residues involved	**Occ%**
365:ASP 366:ASP	63.0
24:PHE 25:CYX	56.0
342:ARG 343:LEU	53.0
342:ARG 365:ASP	48.0
30:ILE 31:ASN	43.0

235:GLU 288:ARG	40.0
63:GLN 97:ASN	39.0
40:HID 294:HIE	38.0
244:SER 249:PHE	37.0
364:GLU 367:LYS	35.0
68:ALA 69:LYS	35.0
222:ALA 223:ASN	31.0
364:GLU 366:ASP	29.0
155:GLN 156:ILE	26.0
131:TYR 235:GLU 236:ASN	26.0
80:THR 155:GLN	26.0
79:ASN 365:ASP	25.0
398:LYS 400:ASP	25.0
171:ASP 199:GLN 202:LYS	22.0
175:GLY 177:SER	22.0
28:SER 29:LEU	22.0
80:THR 82:ASP	22.0
131:TYR 236:ASN	21.0

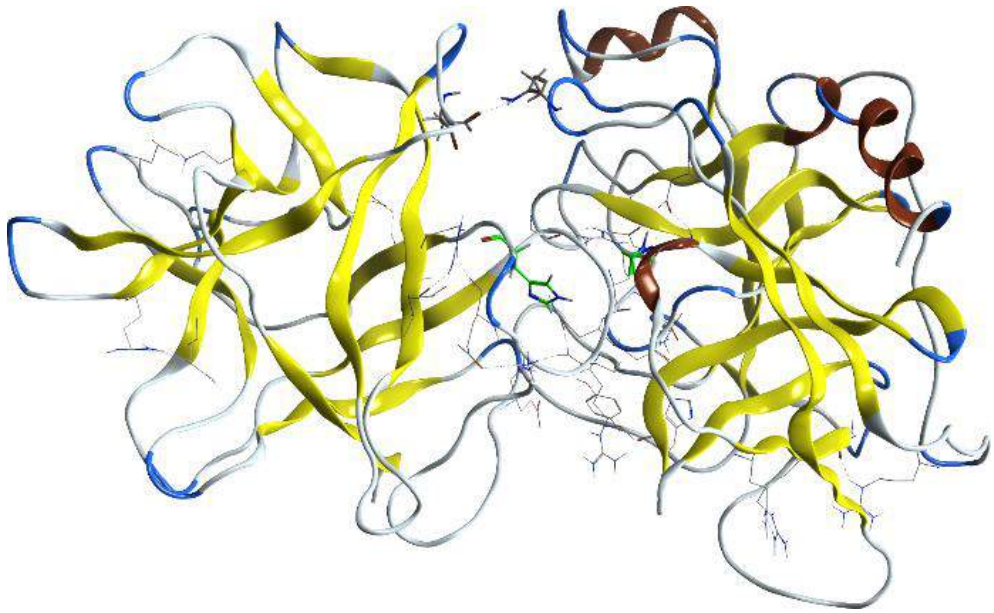

Figure 10.9. 1AVX complex. HIS40 and HIS294 are highlighted in green.

The worse correlation of the 1AVX binding energy when analyzing the 12th MD ns was compensated by a better evaluation of all the other complexes in the case of the ff99SBildn simulations, because in this case the inclusion of 30 water molecules during the MMGBSA analysis worsened the problem showed by 1AVX. However, it

has to be underlined that the correlation between experimental and predicted binding energies improves of about 25% when increasing the Nwat value from 0 to 30, suggesting the overall robustness of the Nwat-MMGBSA approach. In addition, the use of short MD simulations is an advantage when this method is applied for drug design/discovery purposes.

Concerning the effect of the force field for the MD simulations on the Nwat-MMGBSA protocol, it can be observed that the best correlations between experimental and predicted binding energies are obtained with the ff14SB (Figure 10.1), with or without explicit solvent molecules during the MMGBSA calculation. Indeed, the r^2 obtained from the analysis of the simulations with this force field were higher than those obtained with the ff99SBildn force field, under equivalent analysis conditions. In detail, this difference is only marginal when Nwat = 0, while it becomes significant ($\Delta r^2 = 0.20 – 0.26$) when considering Nwat $\neq$ 0 (Table 10.6).

Table 10.6. Values of r^2 obtained from the Nwat-MMGBSA analysis (GB-Neck2) of the 4th ns of the MD simulations performed with either ff14SB or ff99SBildn.

Nwat	**r^2 (ff14SB; cutoff = 0.50, polar)**	**r^2 (ff14SB; cutoff = 0.75, all)**	**r^2 (ff99SBildn; cutoff = 0.50, polar)**	**r^2 (ff99SBildn; cutoff = 0.75, all)**
0	0.45	0.45	0.32	0.32
10	0.64	0.59	0.44	0.40
20	0.77	0.71	0.55	0.48
30	0.77	0.73	0.54	0.46
40	0.68	0.68	0.47	0.42
50	0.57	0.50	0.37	0.36

However, it has to be noticed that with either ff14SB or ff99SBildn force fields the same trend in the correlation index can be observed, because under both conditions the r^2 value improved of about 20% when increasing Nwat from 0 to 20-30, and, then, it slightly decreased with Nwat = 40 -50, indicating that the consideration of 20 – 30 water molecules at the protein-protein interface has a positive effect when correlating MMGBSA binding energies with experiments (Figure 10.1).

The slight difference observed in the correlation index when Nwat = 0 can be completely ascribed to the differences in the two considered force fields, which are

mainly related to parameters associated to side chains and backbone torsional angles and which make ff14SB the force field of election when simulating proteins and peptides in explicit solvent.[135] Conversely, the differences observed with Nwat = 30, i.e. when the maximum r^2 is reached, are only partially attributable to the force fields. Indeed, if the common outlier 1AVX is discarded, the analyses performed on the ff99SBildn simulations give predicted binding energies equivalent to those obtained from the ff14SB simulations. Moreover, the same correlation with experiments is obtained if the simulation time is prolonged to 12 ns (Figure 10.10), whereas MMGBSA analyses with Nwat = 0 are not significantly affected by this complex. This suggests that, as previously hypothesized, the ff99SBildn simulations require longer simulations to allow a correct positioning of water molecules around interacting side-chains, and consequently a proper evaluation of solute-solvent interactions during the MMGBSA analysis.

However, contrarily to what observed for ff99SBildn simulations, the MMGBSA analyses performed on the ff14SB simulations are not affected by either the simulation length or the consideration of particular complexes, such as 1AVX. In addition, at any simulation and analysis condition, this force field provided predicted energies well-to-excellently correlating with experimental data, with the best being those obtained by including 20 – 30 water molecules during the MMGBSA calculations.

Furthermore, Nwat-MMGBSA analysis were also conducted on 4ns ff14SB trajectory using the GB-OBC(II) solvent model, instead of the well performing GB-Neck2, in order to check if the choice of implicit solvent model is critical in the adopted conditions.

The use of this implicit solvent model turned out to have a positive effect when Nwat = 0, while it was detrimental when Nwat ≠ 0 (Table 10.7). Although, the best results are those obtained by setting Nwat = 10, and the inclusion of 20 water molecules provided equivalent results to those obtained with Nwat = 0. In addition, the excellent r^2 value of 0.77 obtained by including 20 – 30 water molecules in the MMGBSA analysis with GB-Neck2 as implicit solvent model and performed on the

4th ns of the ff14SB simulations could not be reached when the GB-OBC(II) implicit solvent model was used.

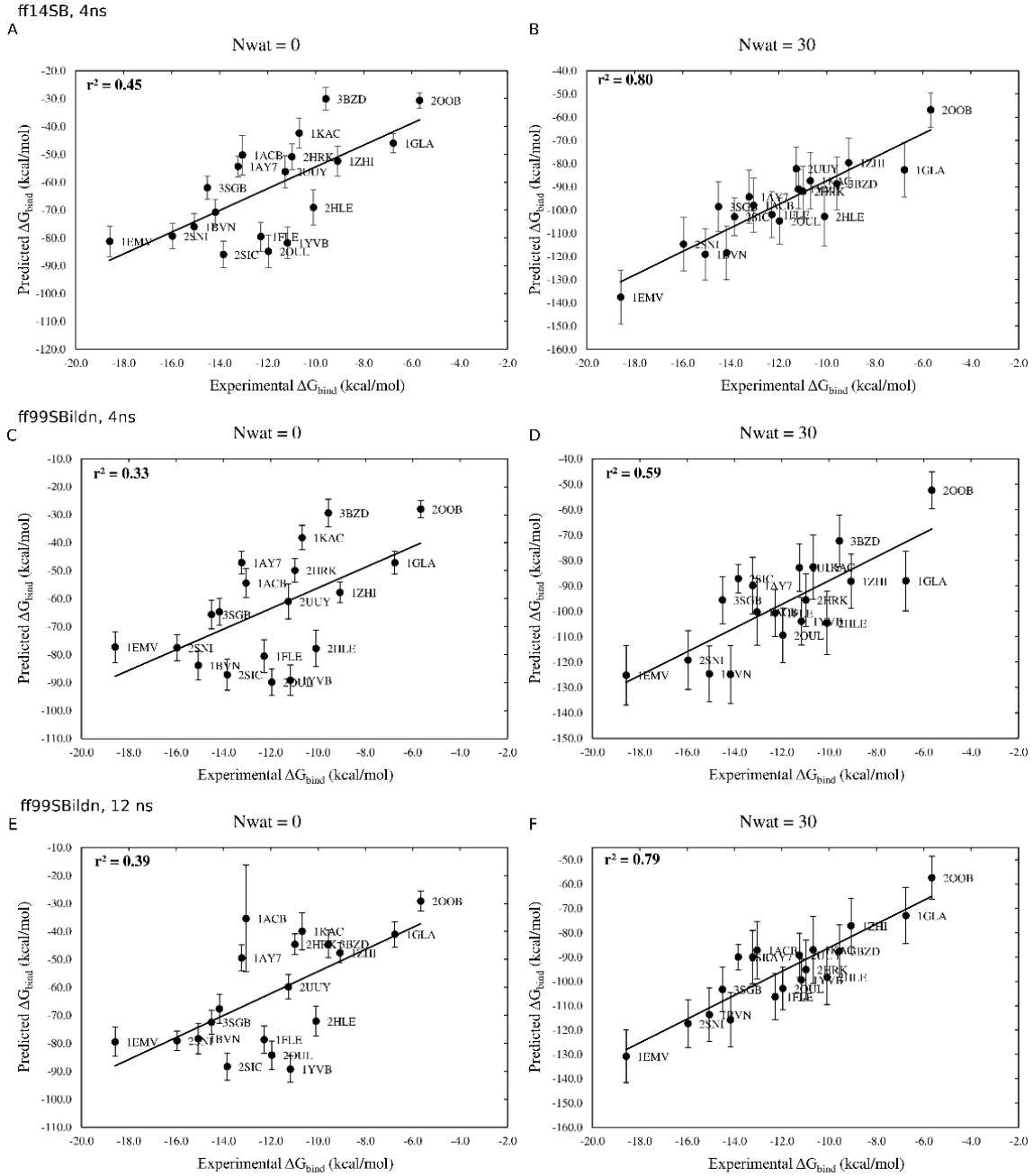

Figure 10.10. Correlation between experimental ΔG_{bind} and predicted binding energies obtained from the analysis MMGBSA analysis (cutoff = 0.50, polar interfacial residues, GB-Neck2) of the 4th ns of the ff14SB (A, B) and ff99SBildn (C, D) MD simulations with Nwat = 0 (A, C) and Nwat = 30 (B, D) and of the 12th ns ff99SBildn simulations (E, F) with Nwat = 0 (E) and Nwat = 30 (F). Complex 1AVX was discarded.

Table 10.7. Values of r^2 obtained from the Nwat-MMGBSA analysis (GB-OBC(II)) of the 4th ns of the MD simulations performed with ff14SB.

Nwat	r^2 **(cutoff = 0.50, polar)**	r^2 **(cutoff = 0.75, all)**
0	0.60	0.60
10	0.64	0.65
20	0.54	0.60
30	0.43	0.50
40	0.32	0.42
50	0.24	0.34

Therefore, referring to the overall best conditions (e.g. 4ns, ff14SB, TIP3P MD simulations, dASA cutoff = 0.50, polar residues, GB-Neck2), the inclusion of 20 – 30 water molecules during the MMGBSA calculations positively affected the correlation between experimental and predicted binding energies, because water-mediated interactions within one of the two interacting proteins or between the protein partners are taken in account during the analysis (Table 10.5, Figure 10.2 as an example). Although all the complexes benefit of this protocol (Figure 10.5), the inclusion of 20 – 30 water molecules is particularly advantageous for some of them, such as 1YVB, 2OUL, and 3BZD, while it weakly affected the calculations performed on other complexes, such as 1ZHI. In particular, the binding energy of 3BZD was underestimated, suggesting that water plays an important role in mediating H-bond between the two protein partners involved in the PPI. Indeed, water-mediated H-bond analysis (Table 10.8) together with the water density plot obtained from grid analysis (Figure 10.11) of the 4ns ff14SB MD simulation of 3BZD showed that many high water density areas are found at the protein-protein interface, compared to those observed for 1ZHI. Moreover, stable (occupancy > 20%) water-mediated H-bonds between the two protein partners are found (Table 10.8) when analyzing the MD simulation of 3BZD, while for 1ZHI, which is only slightly affected by the inclusion of explicit water, only few water-mediated interactions are found, and with lower occupancies than those observed for 3BZD (Table 10.8).

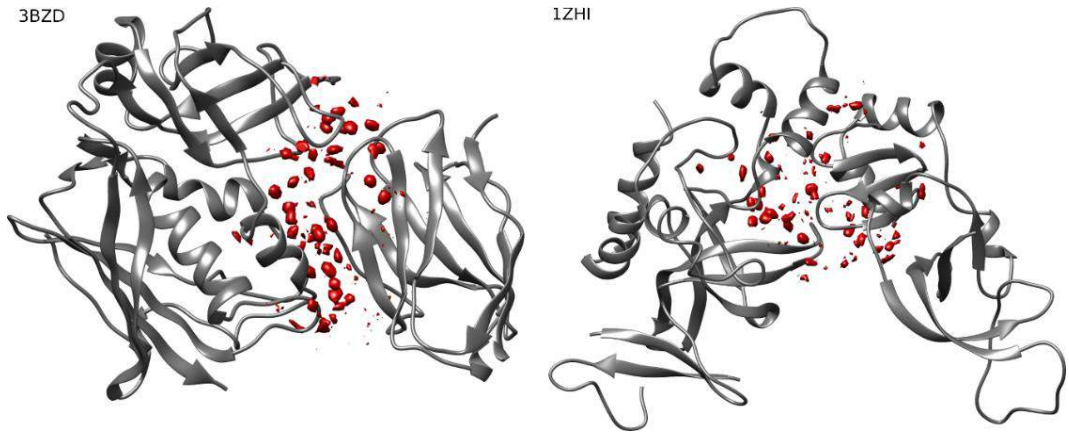

Figure 10.11. Water density plots obtained by grid analysis of the 3BZD (left) and 1ZHI (right) complexes.

Table 10.8. Water-mediated H-bonds with occupancy > 20% detected from the analysis of the 4th ns of the simulation of 3BZD and 1ZHI (ff14SB, TIP3P). The water-mediated H-bonds between the two protein partners are reported in bold.

3BZD		**1ZHI**	
Residues involved	**Occ%**	**Residues involved**	**Occ%**
53:SER 55:GLU	75.0	233:THR 234:LEU	69.0
70:GLN 71:GLU 169:ASN	**67.0**	56:GLN 57:GLU	65.0
55:GLU 56:LYS 129:THR	**65.0**	153:ARG 154:ASP	64.0
55:GLU 313:ASP	**61.0**	131:ILE 132:ARG	45.0
289:GLU 290:THR	59.0	201:GLU 202:GLU	42.0
55:GLU 315:PHE	**59.0**	110:THR 111:ALA	36.0
45:ILE 46:HID	58.0	221:GLU 273:LYS	31.0
334:SER 335:VAL	53.0	**48:GLY 217:ASP**	**29.0**
137:TYR 138:ASP	45.0	221:GLU 271:PHE	27.0
70:GLN 211:TRP	**44.0**	101:ASN 104:ASN	26.0
24:GLN 67:ARG	41.0	56:GLN 189:GLN	26.0
55:GLU 129:THR	**40.0**	202:GLU 203:TYR	25.0
71:GLU 169:ASN	**38.0**	**76:ARG 219:ALA 220:GLU**	**23.0**
51:ALA 199:TYR 200:VAL 317:GLN	**38.0**	**45:GLU 230:ARG**	**22.0**
282:GLU 283:PHE	37.0	**76:ARG 220:GLU**	**21.0**
71:GLU 168:LYS 169:ASN	34.0	108:SER 109:GLU	21.0
216:THR 217:CYX	34.0	220:GLU 222:LYS	21.0
133:MET 134:LYS	32.0	150:ASP 152:GLU	21.0
71:GLU 168:LYS	**31.0**		
59:ILE 61:ASP	31.0		
249:THR 250:ILE	30.0		
68:PRO 135:TYR	**29.0**		
5:GLN 104:THR	27.0		
150:VAL 151:ASP	26.0		

63:TYR 284:ASN	**26.0**	
281:TYR 282:GLU	26.0	
311:PRO 314:LYS	24.0	
25:THR 26:ASN	24.0	
69:SER 72:GLN	23.0	
310:ALA 314:LYS	22.0	

Conversely, 1YVB and 2OUL binding energies were overestimated with Nwat = 0, while with Nwat = 20 – 30 their predicted values well correlated with experimental ΔG_{bind}.

Contrarily to what observed for the complex where ΔG_{bind} was underestimated, the overestimation is not explained by the lacking of consideration of water-mediated interactions between the two protein partners. Conversely, according to equation 1, it can be hypothesized that the contribute associated to one of the proteins in the complex is underestimated, possibly because the monomer is stabilized by H-bonds with the solvent. Indeed, water-mediated H-bond analysis performed on the 1YVB simulation showed that most of the water-mediated interactions only involve the falcipain 2 (chain A, residues 1-241), stabilizing it, whereas only few waters mediate the interactions between falcipain 2 and cystatin or intramolecular interactions only involving cystatin (chain B, residues 242-352) (Table 10.9). Analogous observations can be done for 2OUL, for which the water mediated interactions mainly involve falcipain 2 (chain A, residues 1-241), while few interactions are found within chagasin (chain B, residues 242-348) or between the two proteins (Table 10.10).

Therefore, for overestimated complexes, the Nwat-MMGBSA approach with Nwat = 20 – 30 allows a better evaluation of the contribute associated to only one of the two protein partners, leading to a global improvement in the correlation with experimental ΔG_{bind}.

Table 10.9. Water-mediated H-bonds with occupancy > 20% detected from the analysis of the 4th ns of the simulation of 1YVB (ff14SB, TIP3P).

Residues involved	**Occ%**	**Chains involved**
46:SER 148:ILE	87.0	A
159:TYR 217:ASN	73.0	A
281:VAL 282:ARG	65.0	B

149:SER 234:ASP	59.0	A
126:LYS 127:ASN	59.0	A
305:THR 306:THR	54.0	B
284:ILE 285:SER	52.0	B
153:SER 167:GLU	42.0	A
179:VAL 180:GLY	36.0	A
38:ASN 109:ASP	36.0	A
159:TYR 210:TRP	36.0	A
325:MET 326:ALA	35.0	B
347:LEU 348:GLU	35.0	B
39:CYX 106:TYR	34.0	A
154:ASP 155:ASP	31.0	A
43:TRP 82:GLY	31.0	A
233:THR 234:ASP	28.0	A
152:VAL 171:GLN	28.0	A
35:ASP 206:TRP	27.0	A
50:SER 147:SER	27.0	A
154:ASP 296:TYR	26.0	AB
44:ALA 45:PHE	26.0	A
154:ASP 255:GLU	23.0	AB
81:ASN 289:GLN	23.0	AB
159:TYR 211:GLY	22.0	A
170:ASP 171:GLN	22.0	A
85:ILE 234:ASP	21.0	A
160:LYS 161:GLU	20.0	A
242:ARG 243:LEU	20.0	B
341:LEU 343:GLN	20.0	B

Table 10.10. Water-mediated H-bonds with occupancy > 20% detected from the analysis of the 4th ns of the simulation of 2OUL (ff14SB, TIP3P).

Residues involved	**Occ%**	**Chains involved**
46:SER 148:ILE	86.0	A
159:TYR 217:ASN	75.0	A
339:GLU 340:ARG	57.0	B
149:SER 234:ASP	52.0	A
154:ASP 275:TYR	46.0	AB
179:VAL 180:GLY	42.0	A
154:ASP 309:GLU	41.0	AB
288:MET 289:PHE	36.0	B
154:ASP 272:PHE	34.0	AB
126:LYS 127:ASN	33.0	A
327:TYR 339:GLU	29.0	B

43:TRP 82:GLY	29.0	A
50:SER 147:SER	27.0	A
6:GLU 7:VAL	26.0	A
329:ARG 332:THR	26.0	B
281:LYS 282:GLU	25.0	B
173:ASN 174:HIP	25.0	A
157:ALA 159:TYR	25.0	A
233:THR 234:ASP	23.0	A
300:SER 302:LEU	22.0	B
209:GLN 332:THR	21.0	AB
159:TYR 211:GLY	21.0	A
44:ALA 45:PHE	20.0	A

The inclusion of a number of water molecules greater than 30 caused a decrease in the r^2 values, probably because a large number of water molecules at the protein-protein interfaces generates background noises counteracting the benefits of the explicit consideration of solute – solvent interactions, as previously observed for classical receptor – ligand complexes.

Moreover, although protein-protein interfaces are wider than classical binding pockets, the number of explicit water to be included during the MMGBSA analysis to improve the correlation with experiments should not be over 50. This is probably due to the presence of a high number of hydrophobic residues at the protein-protein interface. Indeed, for all complexes, a maximum of 30 polar residues have been individuated at the interface.

It has to be emphasized that, as observed in Chapter 9, the Nwat-MMGBSA approach improves the correlation between predicted and experimental data improved with the Nwat-MMGBSA approach, but it has not been tested on the prediction of the absolute binding free energies, since the entropic term is neglected. However, this protocol seems to be useful for drug discovery purposes, also because it can be easily automatized (Annex 10.A).

Furthermore, the Nwat-MMGBSA method revealed to be quite robust to changes in the simulation protocol, except for the use of TIP4P-Ew explicit solvent mode. Although the best results have been obtained by analyzing 4 ns MD simulations

performed with the ff14SB force field and the TIP3P explicit solvent model, and with using the GB-Neck2 as implicit solvent model during the MMGBSA calculations.

10.3 Materials and Methods

Structure preparation. Initially, crystallographic water molecules were removed from the PDB files of the PPI complexes. Consequently, the *structure preparation* tool of MOE[227] has been used to cap with an acetyl and a methyl-amino group the N- and C-termini, respectively, of those protein chains having more than 3 missing residues, and to protonate all the considered complexes, in order to build the starting geometries for the MD simulations.

MD simulations. MD simulations were performed with the *pmemd* module of Amber14 package,[192] using either the ff99SBildn[136] or the ff14SB[135] force fields. In each complex, the total charge was neutralized by adding an adequate number of Na^+/Cl^- ions, and the systems were solvated with an octahedral box of either TIP3P[292] or TIP4P-Ew[293] water added up to a distance of 10 Å from the solute. The systems where then relaxed by minimizing hydrogens (1000 cycles of steepest descent and 5000 cycles of conjugated gradient), ions and waters (2000 cycles of steepest descent and 5000 cycles of conjugated gradient). The solvent box was equilibrated at 300 K by 100 ps of NVT and 100 ps of NPT simulation using a Langevin thermostat with a collision frequency of 2.0 ps^{-1}. Successively, a minimization of side chains, water and ions with backbone restraints of 25 kcal/mol and a total minimization with backbone restraints of 10 kcal/mol (2500 cycles of steepest descent and 5000 cycles of conjugated gradient) were performed. The systems were then heated up to 300 K in 6 steps of 5 ps each (ΔT = 50 K), where backbone restraints were reduced from 10.0 kcal/mol to 5 kcal/mol. Full equilibration was performed in the NVT ensemble (100 ps, backbone restraints = 5.0 kcal/mol) and in the NPT ensemble (1 step of 200 ps, backbone restraints = 5 kcal/mol; 3 steps of 100 ps each, reducing the backbone restraints from 5.0 kcal/mol to 1.0 kcal/mol, and 1 step 1 ns with 1.0 kcal/mol of backbone restraints). Finally, unrestrained production runs were run at 300K for 4 to 12 ns. An electrostatic cutoff of 8.0 Å, and the SHAKE algorithm were applied to all the calculations.

RMSD analyses of backbone atoms were made to assess the system stability. H-bonds analysis of solute – solvent interaction (donor – acceptor distance = 4.0 Å, angle = 150°) and grid analyses (cubic box 50 Å ×50 Å ×50 Å, mesh = 0.5 Å, centered on interfacial residues) were also performed with *cpptraj*.

Nwat-MMPB/GBSA. Both MMPBSA and MMGBSA analyses were performed with the MMPBSA.py python script implemented in the Amber14 package. The analyses were conducted on either the 4th or the 12th ns of the production runs by selecting 100 evenly spaced out snapshots. Either the GB-Neck2 or the GB-OBC(II) implicit solvent models were chosen for the GB calculations, and a salt molar concentration in solution was set at 0.15 M. The PB solver implemented in the *sander* module was applied for PB calculations, using the default parameters. During the analyses the entropic term was neglected.

When explicit water molecules were considered during the MMPB/GBSA calculations the same approach described in Chapter 8.1.3 was followed, although the water molecules were selected among those being closest to the interfacial residues. These residues were automatically selected with a pymol script (Annex 10.A) which, given two protein chains, considers as interfacial residues only those whose dASA from the complex to a single chain is greater than a defined cutoff, which in this study was set to either 0.75 or 0.50. Water molecules selection was made by either considering all interfacial residues or only the polar ones.

The water molecules (10, 20, 30, 40 or 50, depending on the chosen Nwat) were considered as part of the protein considered as the receptor, always the first chain of the PDB file.

The square of Pearson's correlation coefficient (r^2) between experimental ΔG_{bind} and computed binding energies was used as an evaluation metric.

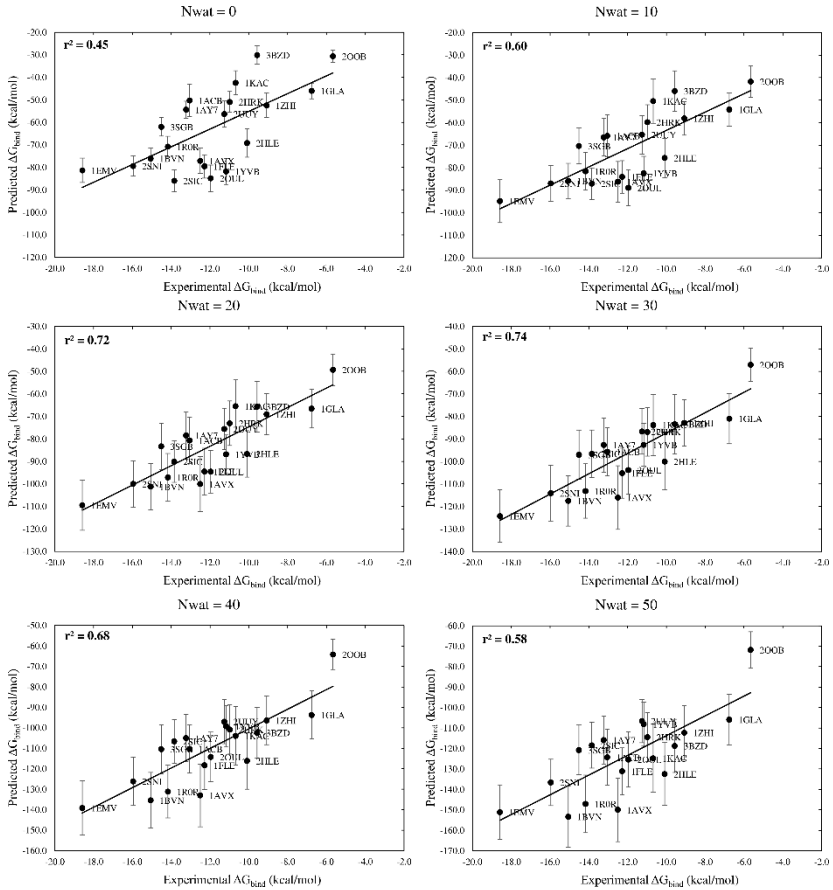

Figure 10.12. Correlation between experimental ΔG_{bind} and predicted binding energies obtained from the analysis MMGBSA analysis (cutoff = 0.50, ALL interfacial residues, GB-Neck2) of the 4th ns of the ff14SB, TIP3P MD simulations.

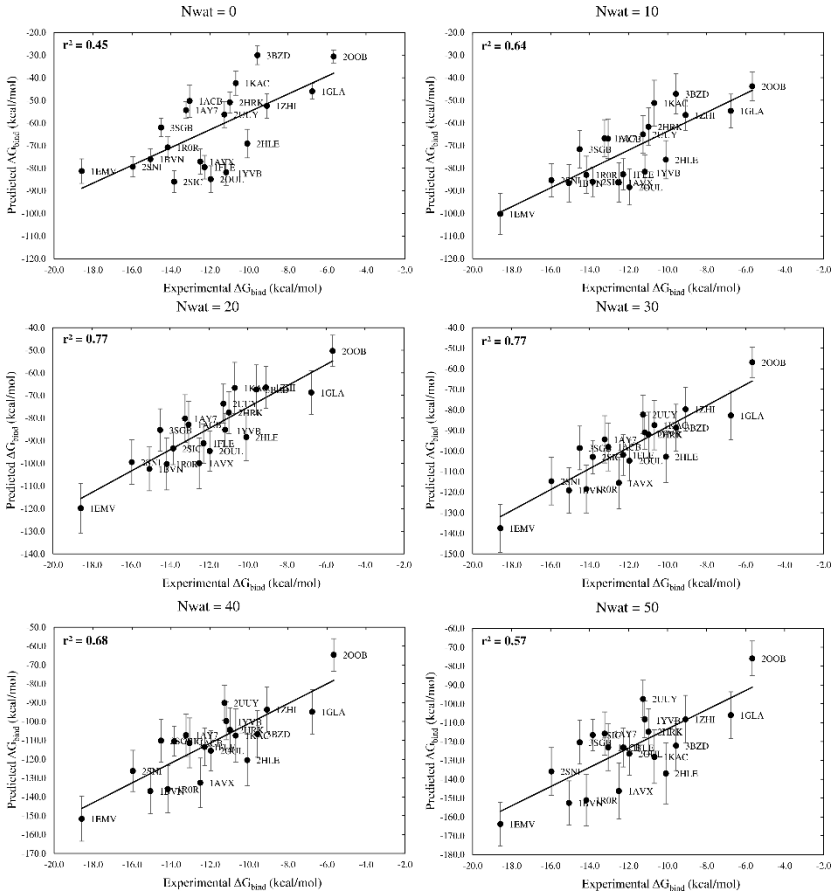

Figure 10.13. Correlation between experimental ΔG_{bind} and predicted binding energies obtained from the analysis MMGBSA analysis (cutoff = 0.50, POLAR interfacial residues, GB-Neck2) of the 4th ns of the ff14SB, TIP3P MD simulations.

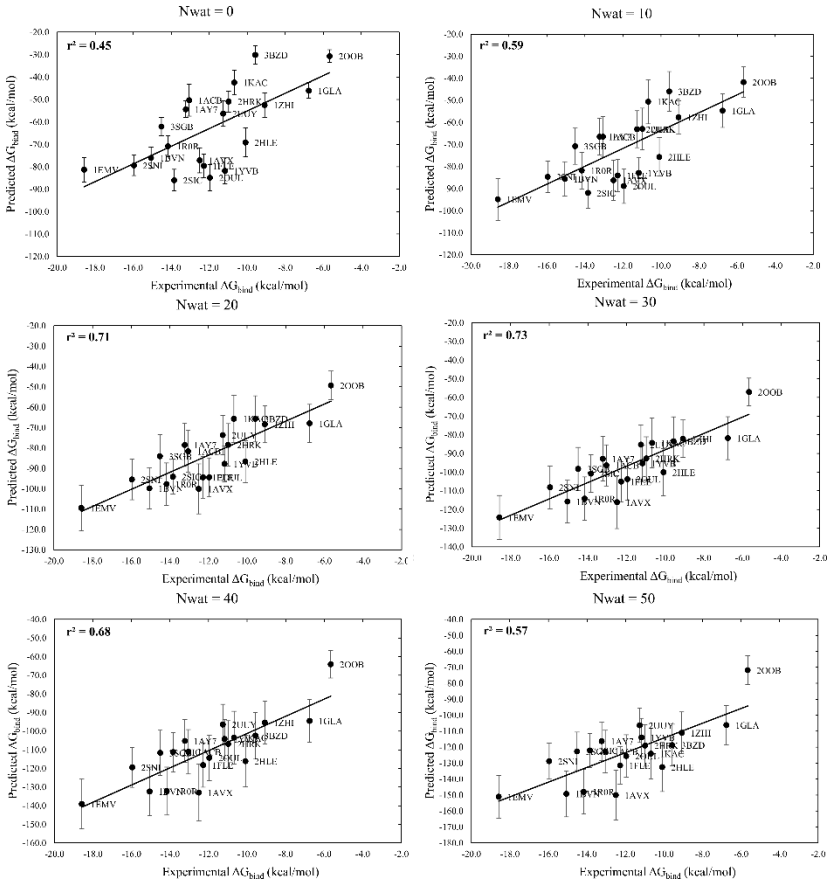

Figure 10.14. Correlation between experimental ΔG_{bind} and predicted binding energies obtained from the analysis MMGBSA analysis (cutoff = 0.75, ALL interfacial residues, GB-Neck2) of the 4th ns of the ff14SB, TIP3P MD simulations.

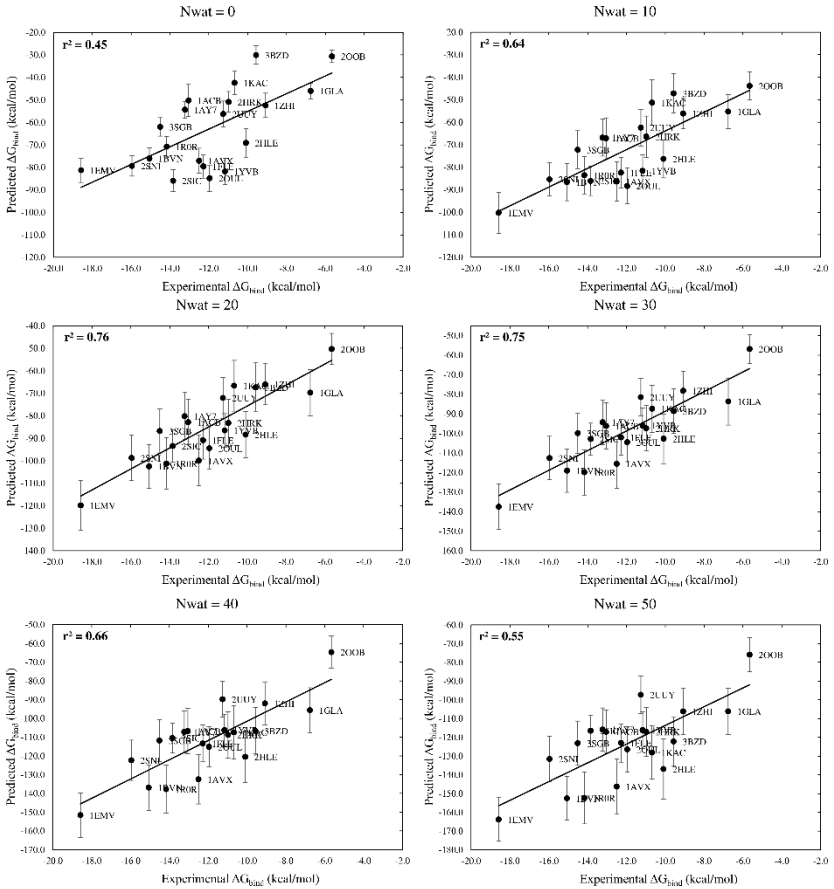

Figure 10.15. Correlation between experimental ΔG_{bind} and predicted binding energies obtained from the analysis MMGBSA analysis (cutoff = 0.75, POLAR interfacial residues, GB-Neck2) of the 4th ns of the ff14SB, TIP3P MD simulations.

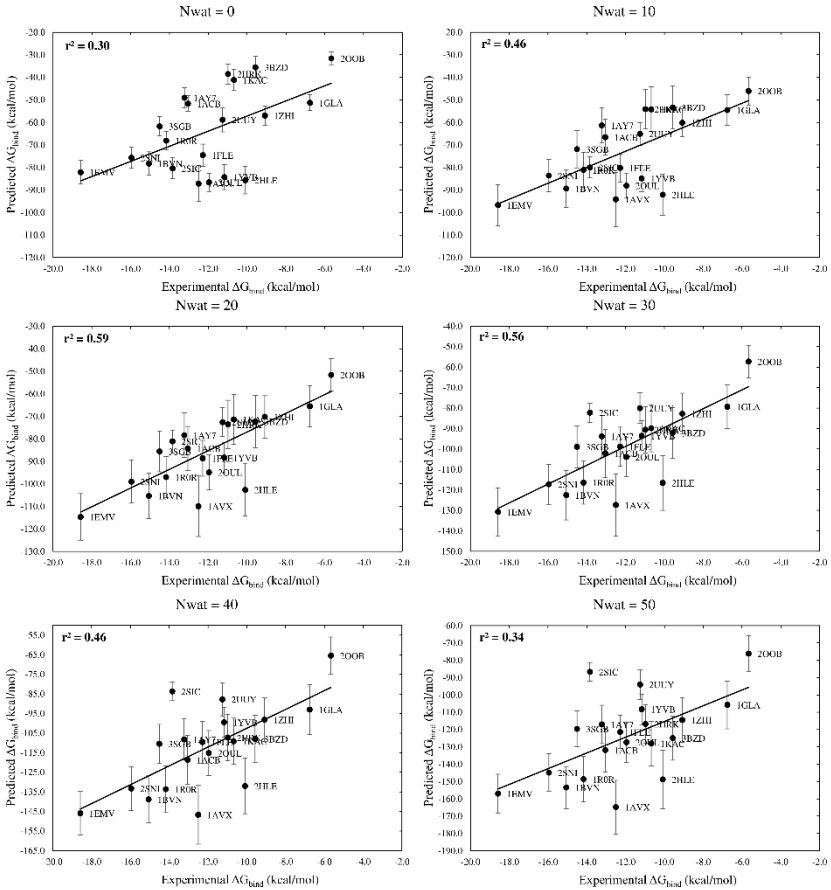

Figure 10.16. Correlation between experimental ΔG_{bind} and predicted binding energies obtained from the analysis MMGBSA analysis (cutoff = 0.50, POLAR interfacial residues, GB-Neck2) of the 12th ns of the ff14SB, TIP3P MD simulations.

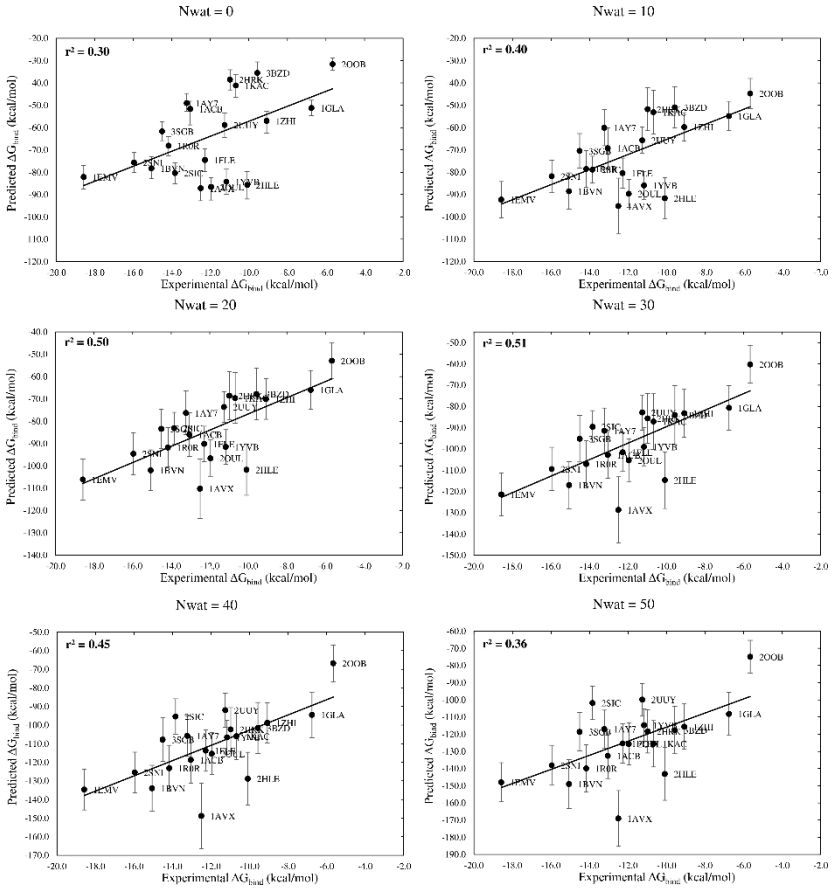

Figure 10.17. Correlation between experimental ΔG_{bind} and predicted binding energies obtained from the analysis MMGBSA analysis (cutoff = 0.75, ALL interfacial residues, GB-Neck2) of the 12th ns of the ff14SB, TIP3P MD simulations.

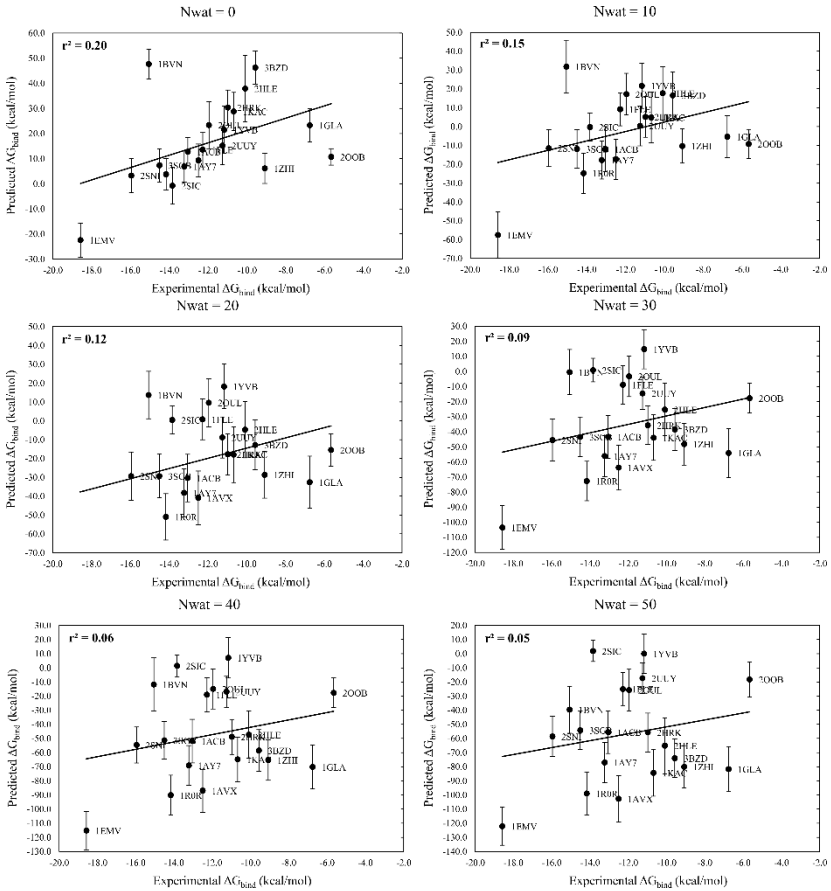

Figure 10.18. Correlation between experimental ΔG_{bind} and predicted binding energies obtained from the analysis MMPBSA analysis (cutoff = 0.50, POLAR interfacial residues) of the 4th ns of the ff14SB, TIP3P MD simulations.

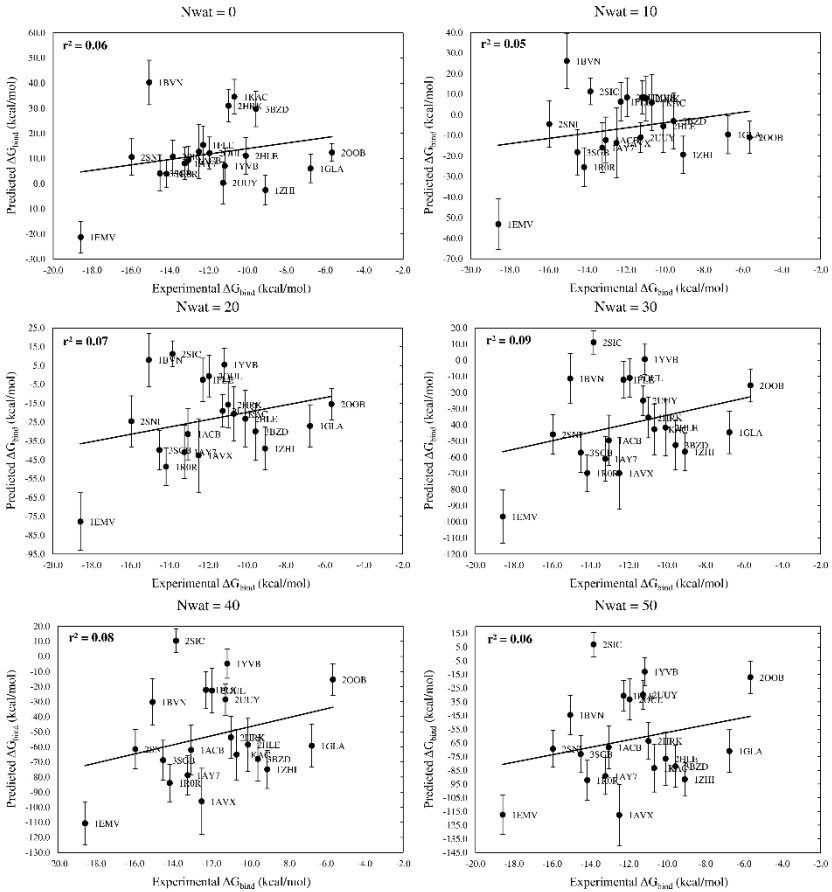

Figure 10.19. Correlation between experimental ΔG_{bind} and predicted binding energies obtained from the analysis MMPBSA analysis (cutoff = 0.50, POLAR interfacial residues) of the 12th ns of the ff14SB, TIP3P MD simulations.

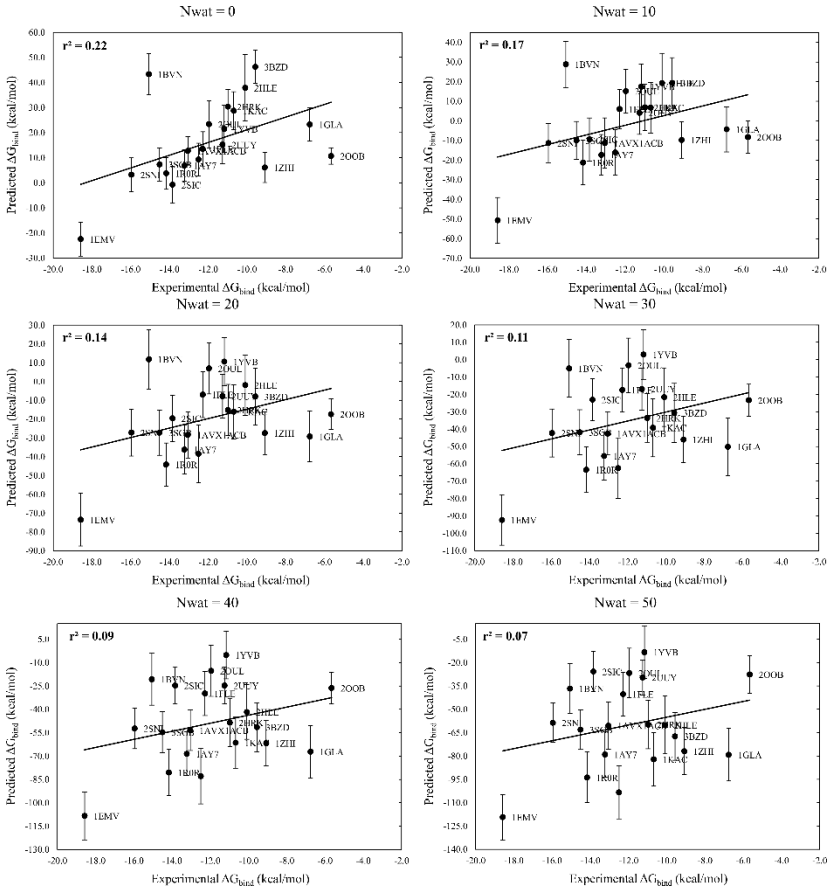

Figure 10.20. Correlation between experimental ΔG_{bind} and predicted binding energies obtained from the analysis MMPBSA analysis (cutoff = 0.75, ALL interfacial residues) of the 4th ns of the ff14SB, TIP3P MD simulations.

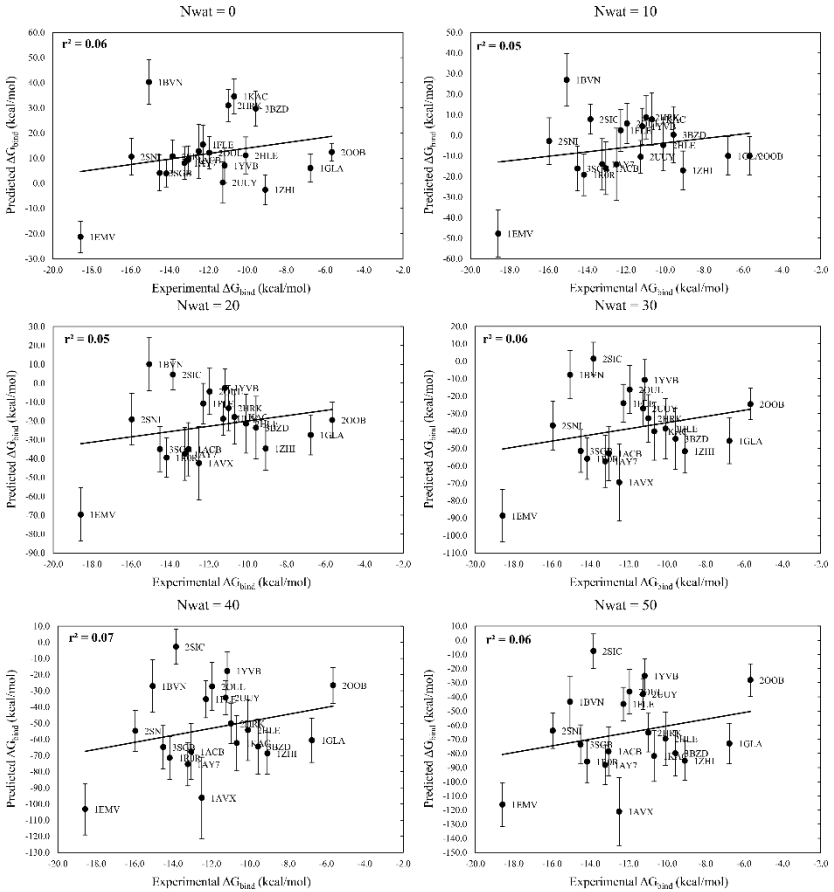

Figure 10.21. Correlation between experimental ΔG_{bind} and predicted binding energies obtained from the analysis MMPBSA analysis (cutoff = 0.75, ALL interfacial residues) of the 12th ns of the ff14SB, TIP3P MD simulations.

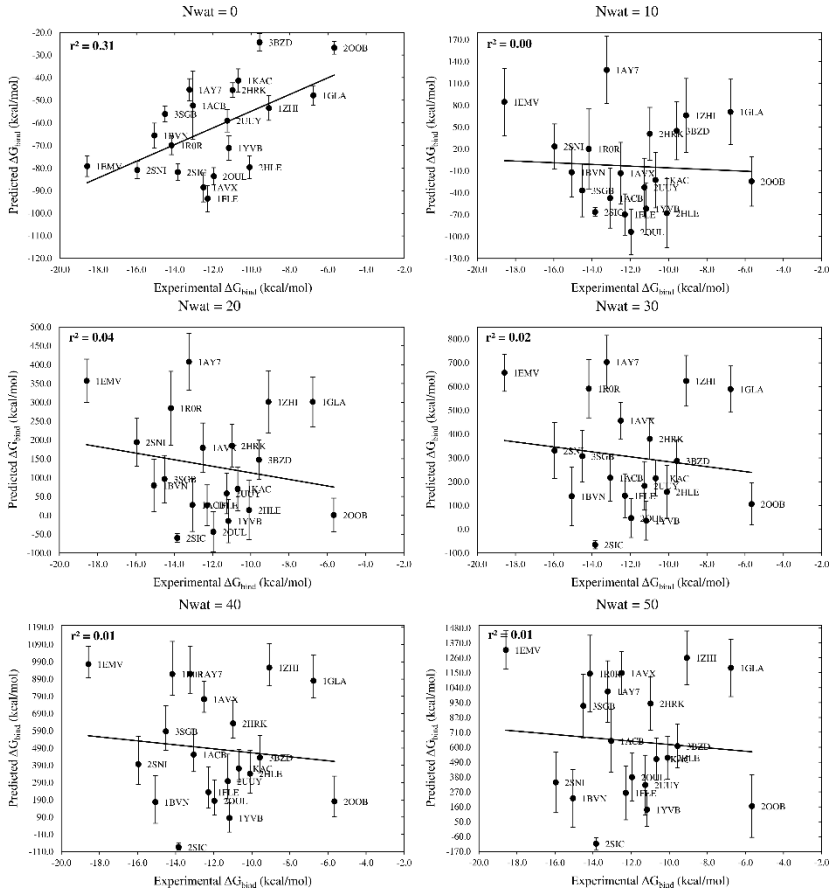

Figure 10.22. Correlation between experimental ΔG_{bind} and predicted binding energies obtained from the analysis MMGBSA analysis (cutoff = 0.50, POLAR interfacial residues, GB-Neck2) of the 4th ns of the ff14SB, TIP4P-Ew MD simulations.

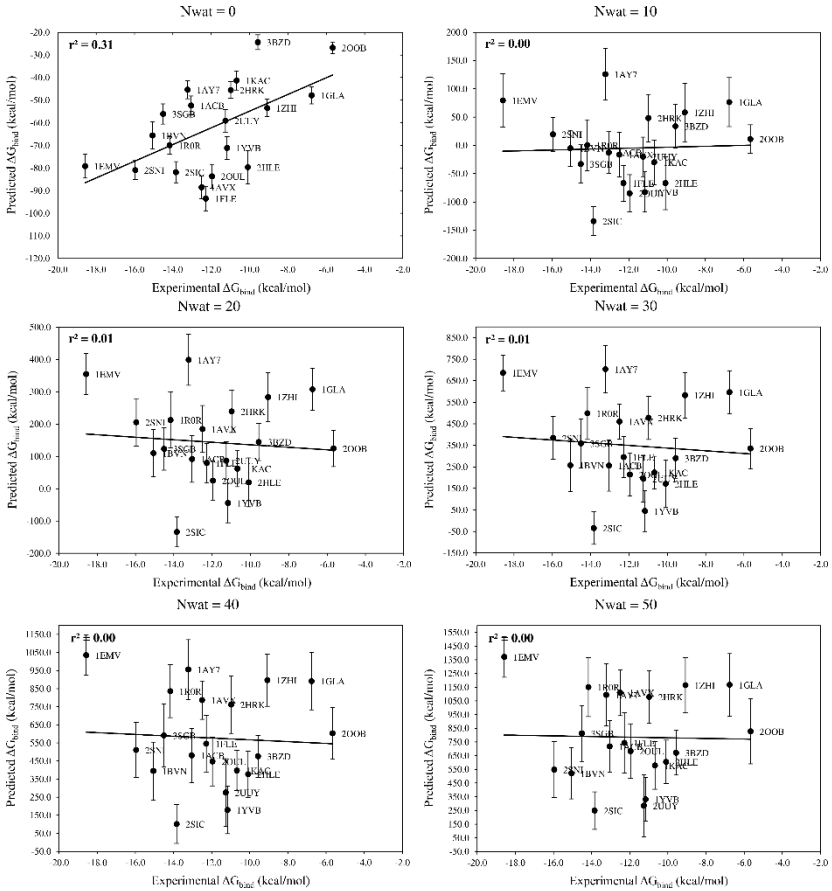

Figure 10.23. Correlation between experimental ΔG_{bind} and predicted binding energies obtained from the analysis MMGBSA analysis (cutoff = 0.75, ALL interfacial residues, GB-Neck2) of the 4th ns of the ff14SB, TIP4P-Ew MD simulations.

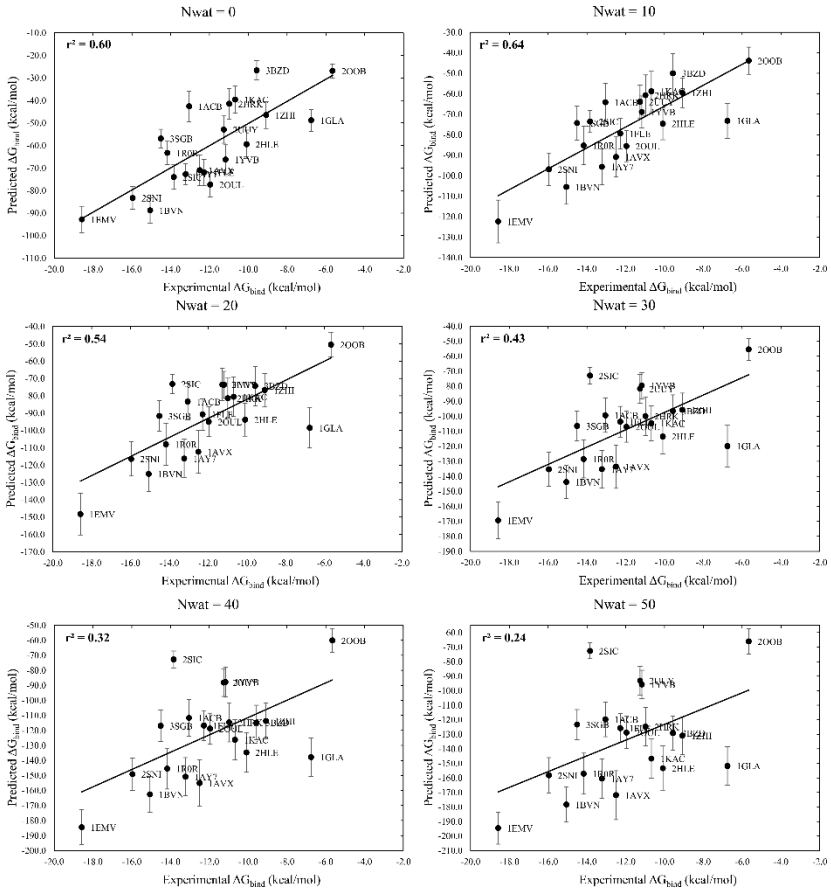

Figure 10.24. Correlation between experimental ΔG_{bind} and predicted binding energies obtained from the analysis MMGBSA analysis (cutoff = 0.50, POLAR interfacial residues, GB-OBC(II)) of the 4th ns of the ff14SB, TIP3P MD simulations.

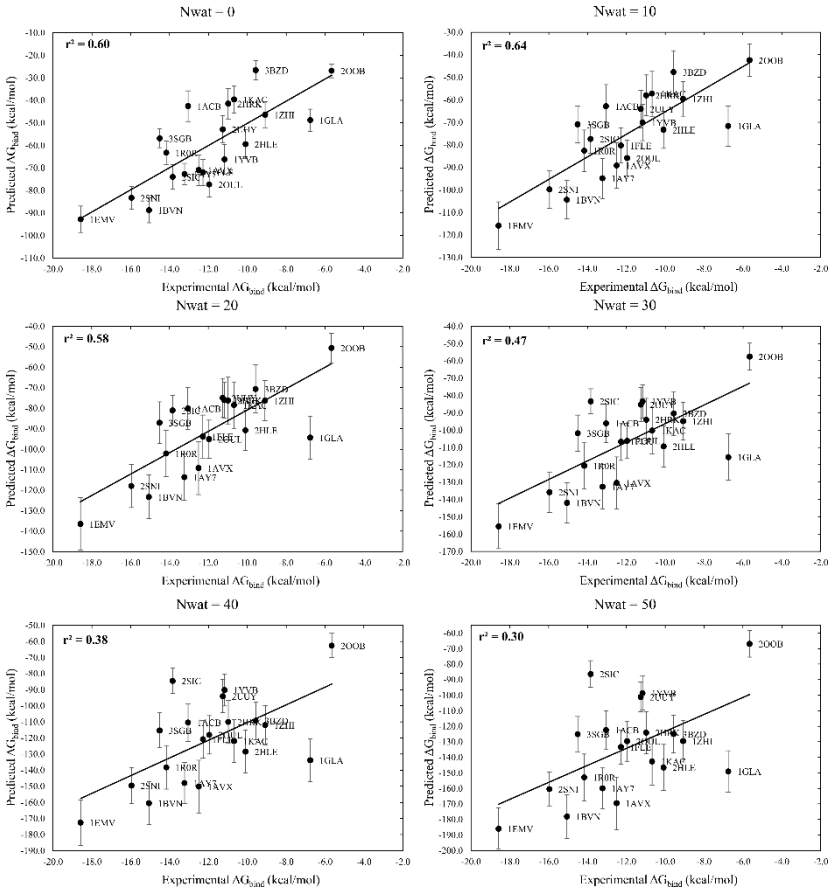

Figure 10.25. Correlation between experimental ΔG_{bind} and predicted binding energies obtained from the analysis MMGBSA analysis (cutoff = 0.50, ALL interfacial residues, GB-OBC(II)) of the 4th ns of the ff14SB, TIP3P MD simulations.

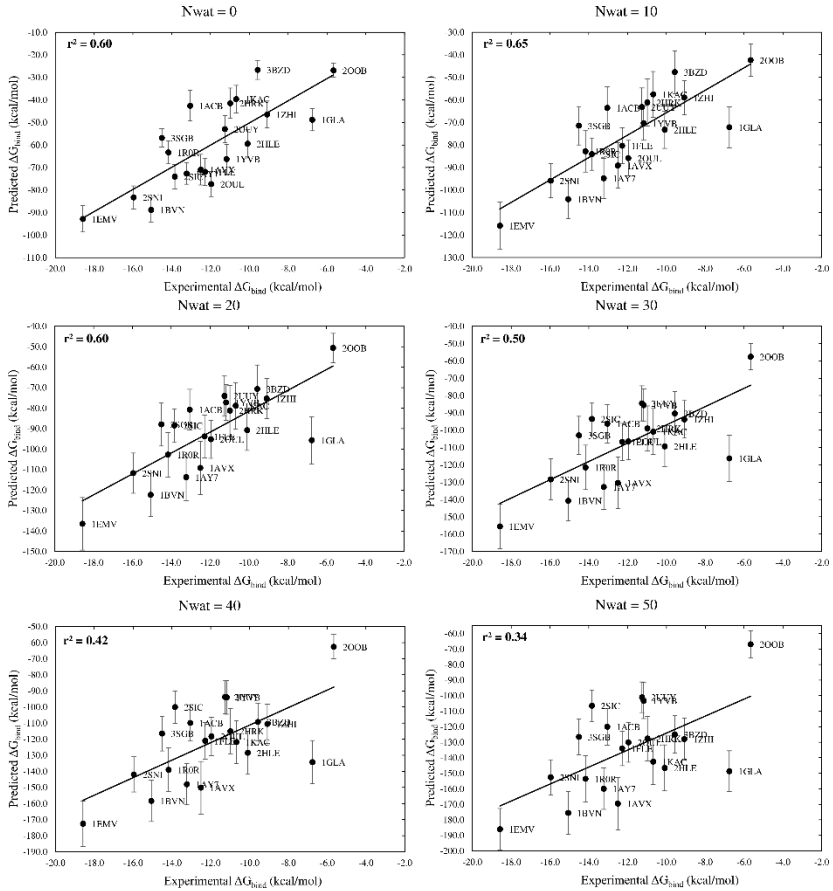

Figure 10.26. Correlation between experimental ΔG_{bind} and predicted binding energies obtained from the analysis MMGBSA analysis (cutoff = 0.75, ALL interfacial residues, GB-OBC(II)) of the 4th ns of the ff14SB, TIP3P MD simulations.

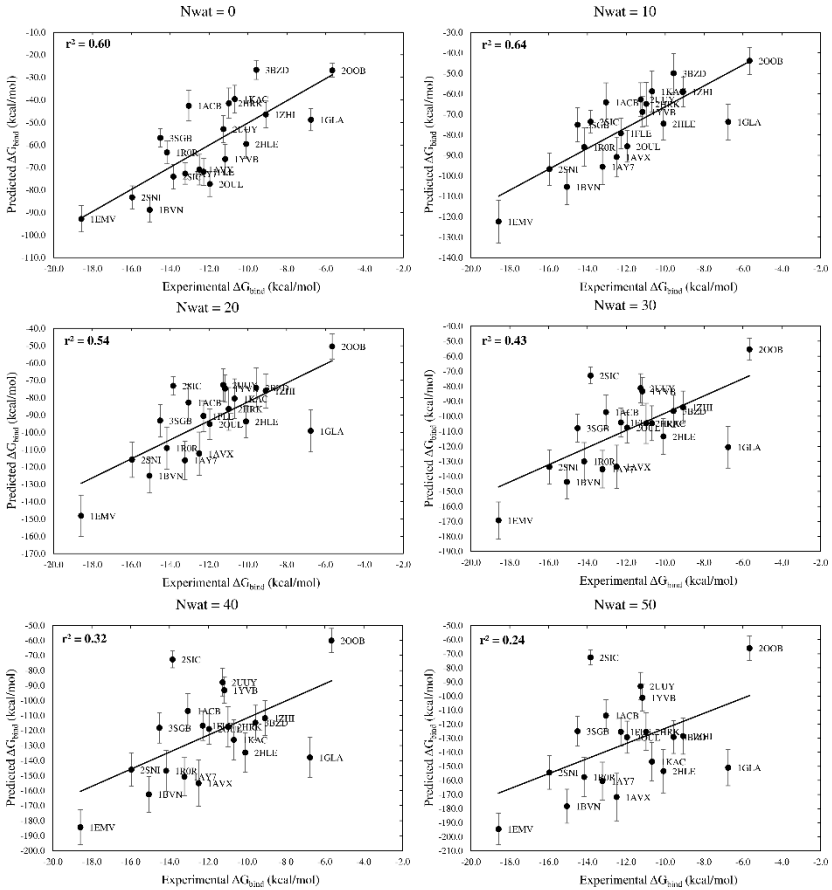

Figure 10.27. Correlation between experimental ΔG_{bind} and predicted binding energies obtained from the analysis MMGBSA analysis (cutoff = 0.75, POLAR interfacial residues, GB-OBC(II)) of the 4th ns of the ff14SB, TIP3P MD simulations.

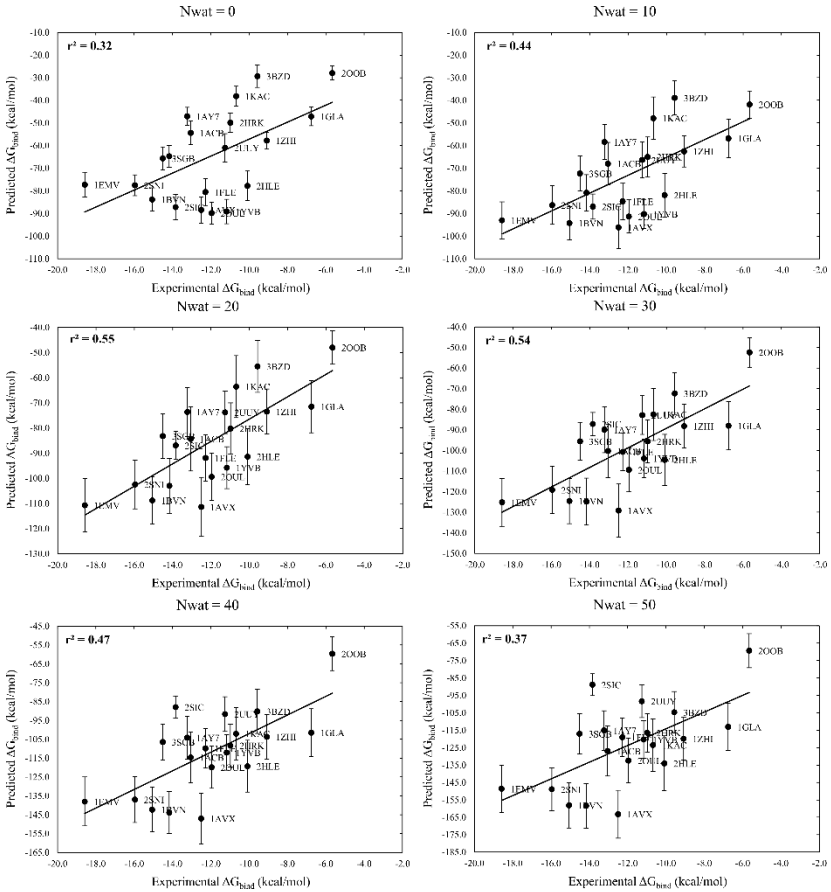

Figure 10.28. Correlation between experimental ΔG_{bind} and predicted binding energies obtained from the analysis MMGBSA analysis (cutoff = 0.50, POLAR interfacial residues, GB-Neck2) of the 4th ns of the ff99SBildn, TIP3P MD simulations.

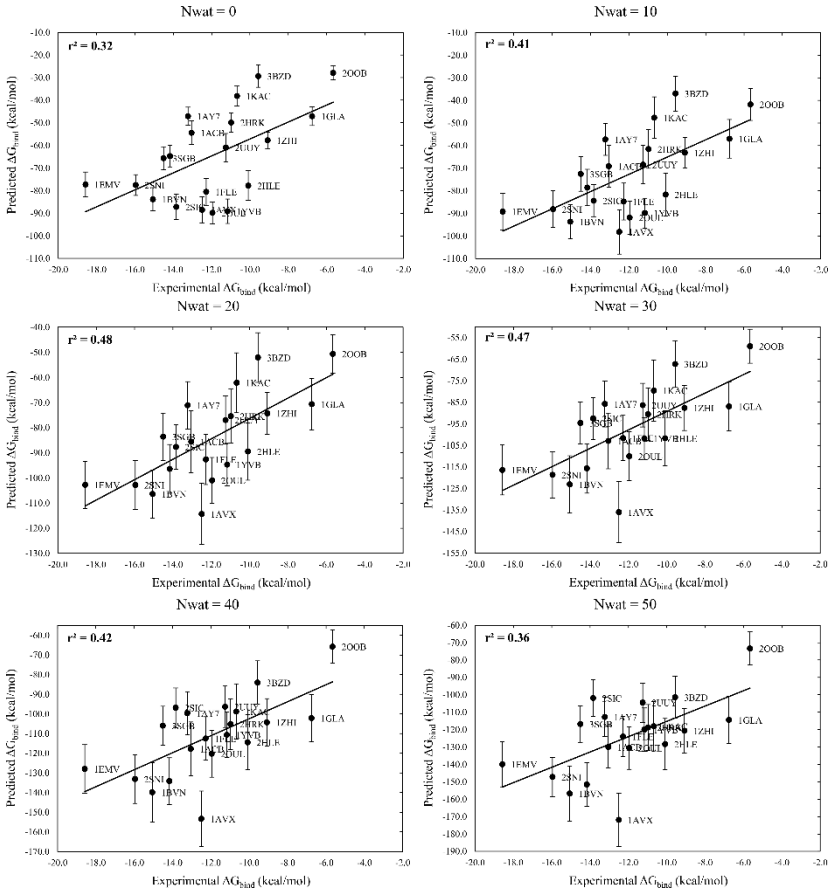

Figure 10.29. Correlation between experimental ΔG_{bind} and predicted binding energies obtained from the analysis MMGBSA analysis (cutoff = 0.50, ALL interfacial residues, GB-Neck2) of the 4th ns of the ff99SBildn, TIP3P MD simulations.

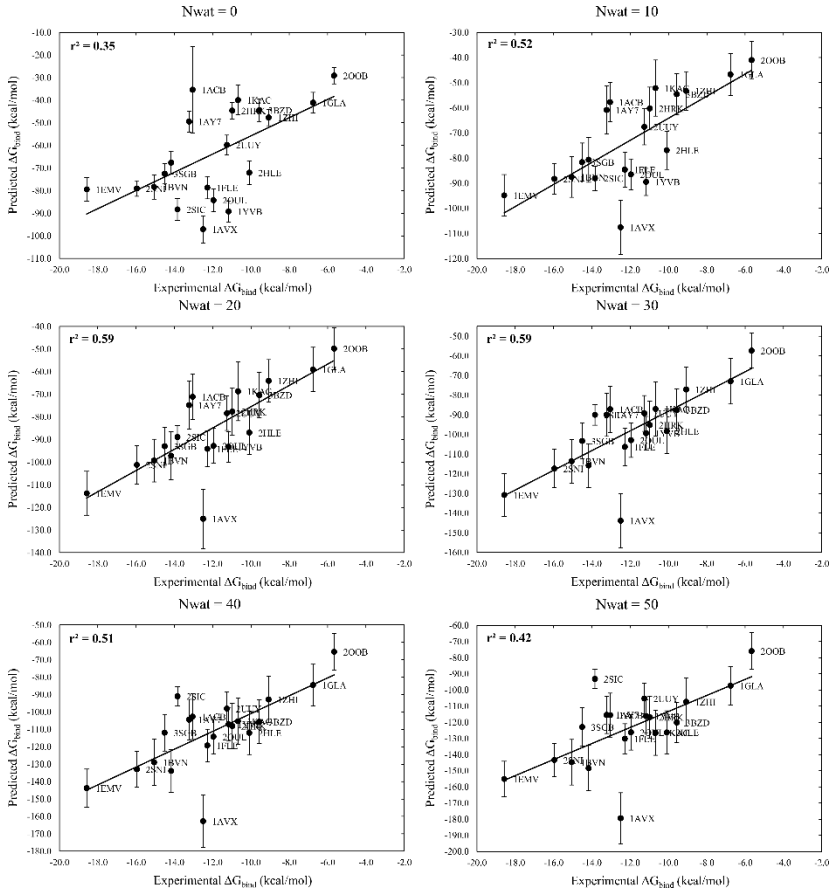

Figure 10.30. Correlation between experimental ΔG_{bind} and predicted binding energies obtained from the analysis MMGBSA analysis (cutoff = 0.50, POLAR interfacial residues, GB-Neck2) of the 12th ns of the ff99SBildn, TIP3P MD simulations.

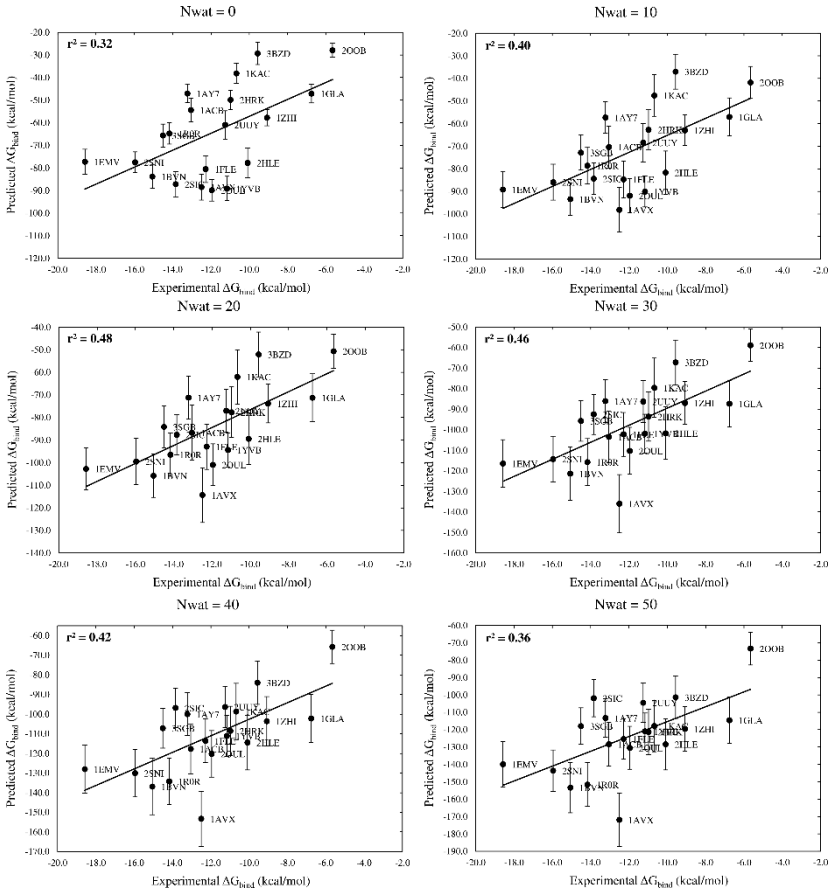

Figure 10.31. Correlation between experimental ΔG_{bind} and predicted binding energies obtained from the analysis MMGBSA analysis (cutoff = 0.75, ALL interfacial residues, GB-Neck2) of the 4th ns of the ff99SBildn, TIP3P MD simulations.

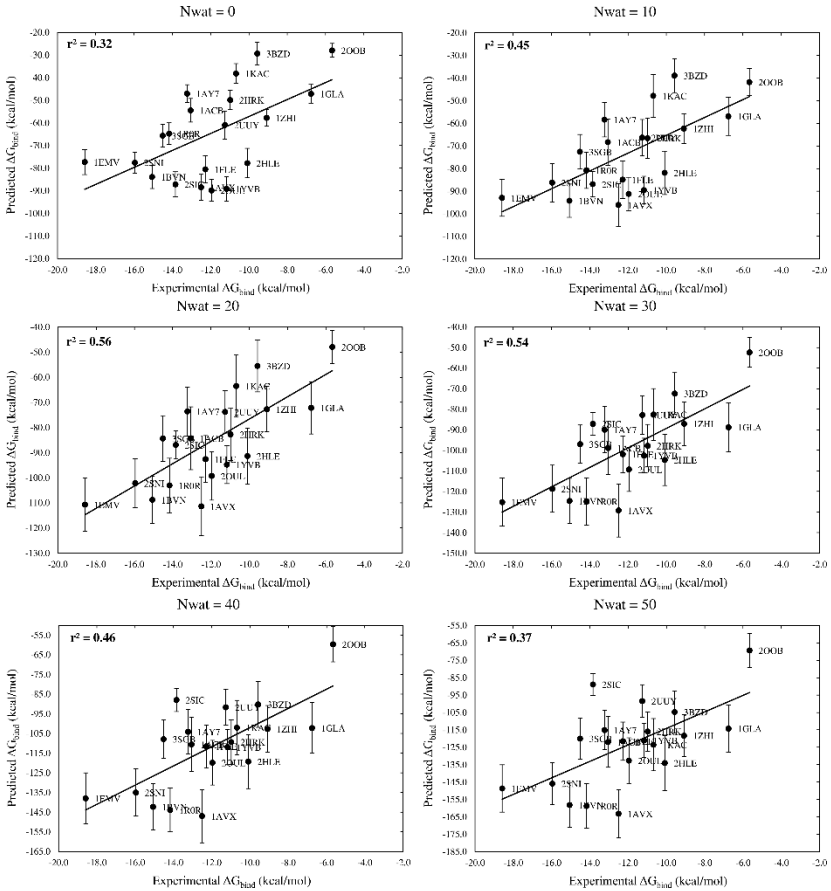

Figure 10.32. Correlation between experimental ΔG_{bind} and predicted binding energies obtained from the analysis MMGBSA analysis (cutoff = 0.75, POLAR interfacial residues, GB-Neck2) of the 4th ns of the ff99SBildn, TIP3P MD simulations.

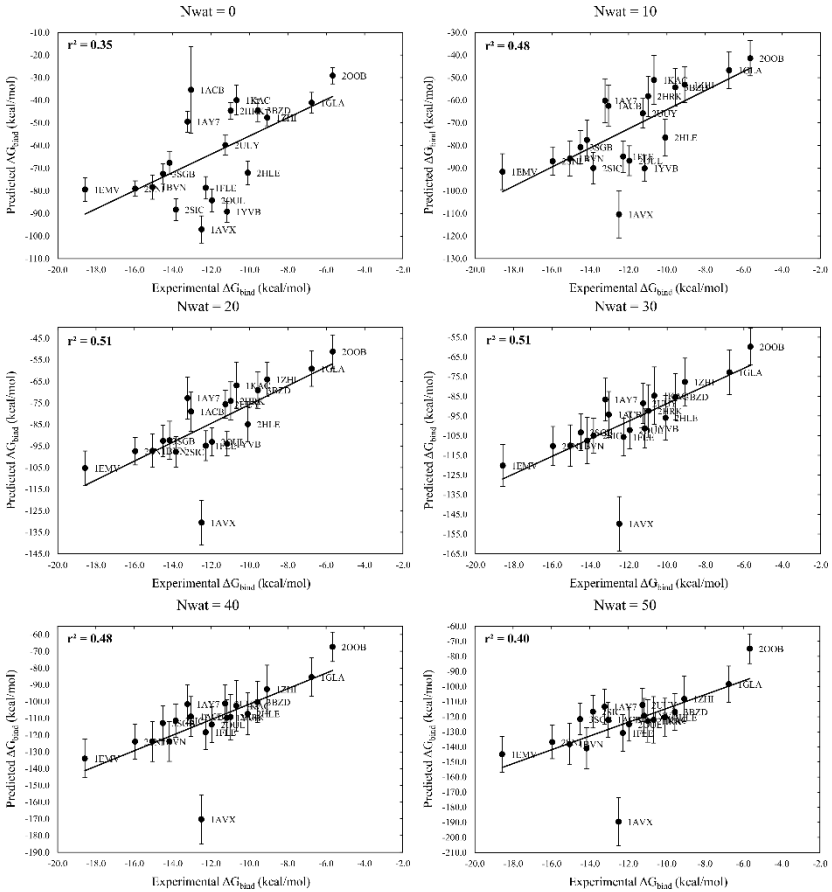

Figure 10.33. Correlation between experimental ΔG_{bind} and predicted binding energies obtained from the analysis MMGBSA analysis (cutoff = 0.75, ALL interfacial residues, GB-Neck2) of the 12h ns of the ff99SBildn, TIP3P MD simulations.

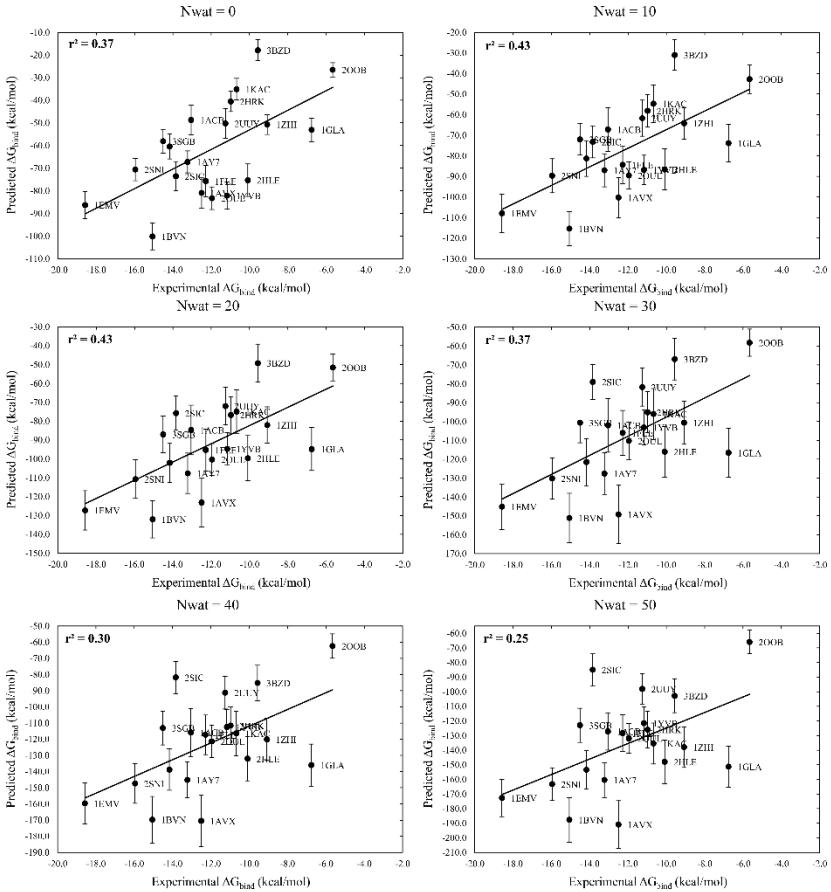

Figure 10.34. Correlation between experimental ΔG_{bind} and predicted binding energies obtained from the analysis MMGBSA analysis (cutoff = 0.50, ALL interfacial residues, GB-OBC(II)) of the 4th ns of the ff99SBildn, TIP3P MD simulations.

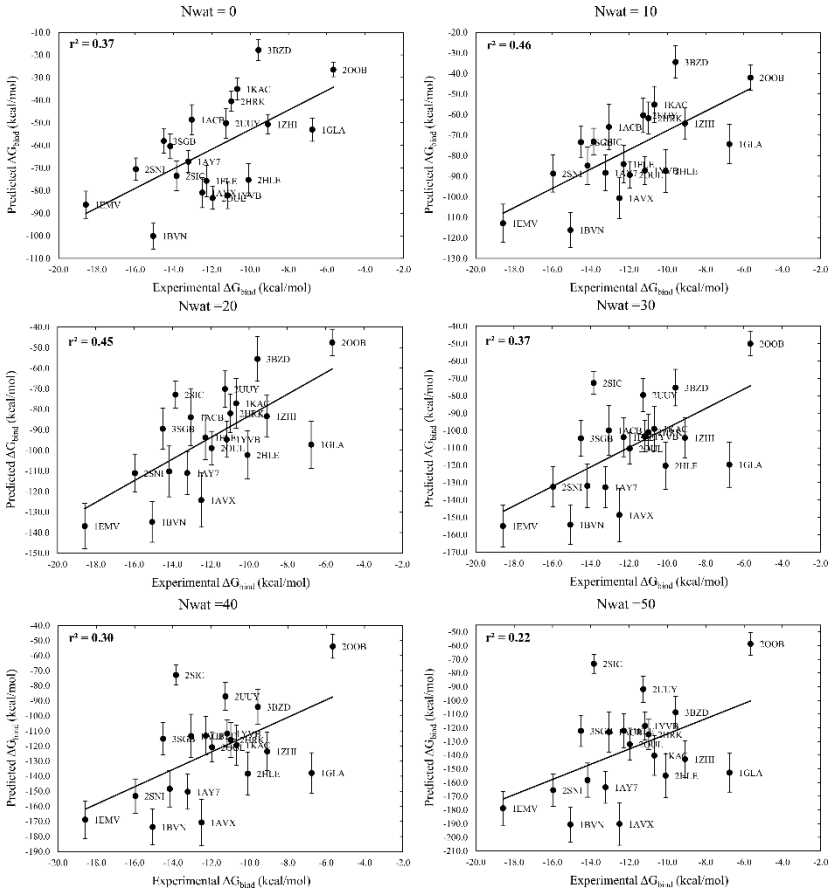

Figure 10.35. Correlation between experimental ΔG_{bind} and predicted binding energies obtained from the analysis MMGBSA analysis (cutoff = 0.50, POLAR interfacial residues, GB-OBC(II)) of the 4th ns of the ff99SBildn, TIP3P MD simulations.

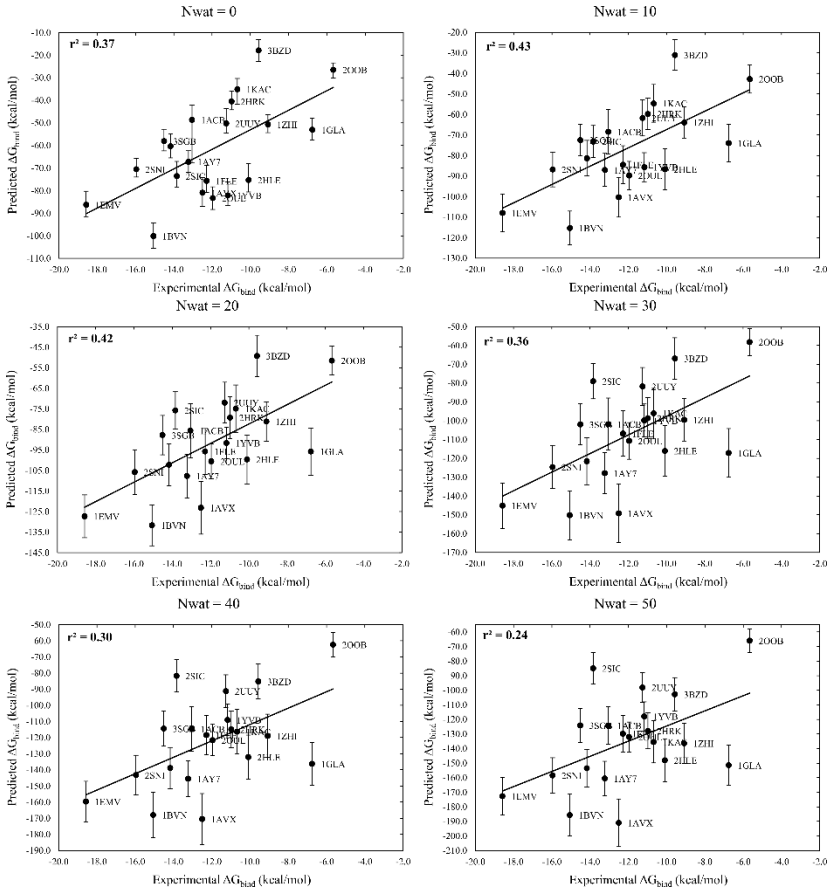

Figure 10.36. Correlation between experimental ΔG_{bind} and predicted binding energies obtained from the analysis MMGBSA analysis (cutoff = 0.75, ALL interfacial residues, GB-OBC(II)) of the 4th ns of the ff99SBildn, TIP3P MD simulations.

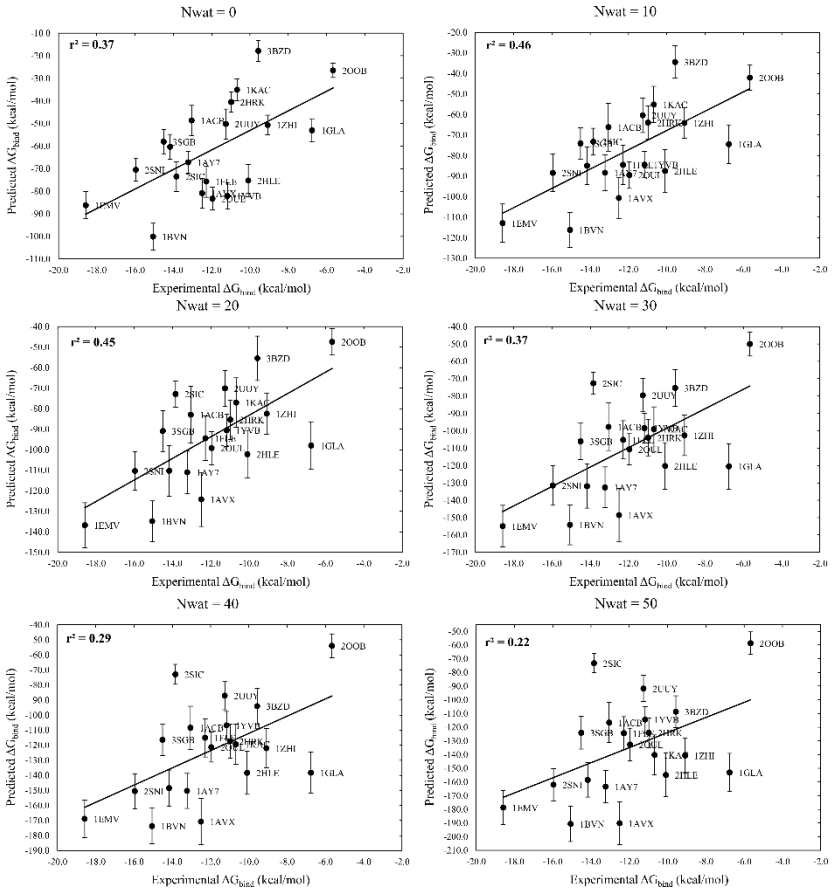

Figure 10.37. Correlation between experimental ΔG_{bind} and predicted binding energies obtained from the analysis MMGBSA analysis (cutoff = 0.75, POLAR interfacial residues, GB-OBC(II)) of the 4th ns of the ff99SBildn, TIP3P MD simulations.

11 APPLICATION OF THE NWAT-MMGBSA PROTOCOL TO PPI-INHIBITOR COMPLEXES

11.1 INTRODUCTION

In Chapter 10 the application of an automated Nwat-MMGBSA approach to the prediction of binding energies in PPI complexes has been described. In particular, the best protocol conditions in terms of correlation between MMGBSA predicted binding energies and experimental data for this particular kind of systems were found. Summarizing, the highest correlation in terms of r^2 has been obtained by submitting the last of 4 ns of MD simulations, performed by using the ff14SB[135] force field and the TIP3P[292] explicit solvent model, to Nwat-MMGBSA calculations, where the GB-Neck2[173] was used as implicit solvent model and 20 – 30 water molecules were explicitly included during the analysis.

Therefore, the optimized protocol had to be tested on systems where one of the two PPI protein partners is inhibited by a small molecule or a peptide-like ligand. Indeed, when the other protein partner is replaced by a decidedly smaller molecule, Nwat-MMGBSA results might be significantly affected. Indeed, in classical protein-ligand systems the ligand is generally buried in the receptor; in PPI complexes, on the other hand, there is a wide contact surface and waters are generally placed in between. Conversely, in complexes made by a ligand bound to a protein surface, the Nwat-MMGBSA procedure might lead to the selection of water molecules located on the solvent-exposed side. Since explicit water are considered as part of the receptor, this might be detrimental for the prediction of binding energy.

At the light of this, we initially applied the optimized MD/Nwat-MMGBSA protocol to the previously studied penicillopepsin system (see Chapter 9), which is inhibited by peptide-like molecules with known experimental ΔG_{bind}, in order to compare this updated protocol to the initial one. Successively, three additional systems consisting of one protein usually involved in PPIs complexed with inhibitors with known experimental activities have been tested, namely the MDM2 protein, involved in the MDM2-p53 PPI, complexed with 10 inhibitors with known IC_{50}

(Figure 11.15),[315] the BCL-X_L inhibited by 7 small molecules with known IC_{50} (Figure 11.14),[316] and XIAP-BIR2 in complex with 8 inhibitors with known IC_{50} (Figure 11.16).[317] In addition, HIV1-protease and 6 of its mutants complexed with amprenavir[318] and two HIV1-protease mutants complexed with ritonavir[319] (Figure 11.17) with known k_i were also considered (Table 11.9), in order to verify if the Nwat-MMGBSA approach can be also applied to predict the activity of a particular ligand on different mutants of the same protein target.

For these systems we verified if the explicit inclusion of water molecules during the MMGBSA analysis positively affected the correlation between predicted binding energy and available experimental activities in terms of r^2, and we evaluated the optimal number of solvent residues to consider during the calculations.

Furthermore, aiming to make this protocol fast enough to be applied for drug design/discovery purposes, we compared Nwat-MMGBSA calculations made on the first or on the fourth ns of production run. Calculations conducted on a classical HPC infrastructure, using 128 Xeon cores, were also compared with MD simulations run on a single GPU GTX card that, in terms of performance, equalled the 128 cores. To provide statistical significance, 3 independent simulations (using a random seed for the guess of initial forces) were conducted for each system on each hardware.

11.2 Results and Discussion

Before discussing the results obtained by the application of the Nwat-MMGBSA protocol to the selected systems, it is important to underline that this study has been particularly challenging, because only few dataset of more than 5 PPIs modulators with known activity data and crystallized in complex with their target are reported in literature. In addition, the choice of the dataset had to be done carefully, selecting complexes covering a wide range of binding energies and, possibly, evaluated within the same set of experiments or at least from very robust and validated experiments. Indeed, bad correlations were often obtained by us, during preliminary evaluations, when selecting complexes reported in different publications and with binding energies determined through different experimental setups. Furthermore, when a dataset of PPI modulators is made of congeneric compounds, but where only one or few

crystallographic structures of the complexes are available, other complexes must be reconstructed by manually modifying the ligand, as done for the MDM2, the BCL-X_L and the XIAP-BIR2 systems.

Penicillopepsin. The results obtained from the application of the updated Nwat-MMGBSA protocol on penicillopepsin system globally agreed with those previously discussed (see Chapter 9), and grid analysis showed in this case also the presence of many high water density areas (Figure 11.1B). Indeed, the inclusion of explicit water molecules during the MMGBSA calculations significantly increased the correlation between experimental and predicted binding energies, and the highest r^2 obtained was of about 0.70, except for the analysis performed on the 4th of MD simulations run on CPU hardware (Figure 11.1A).

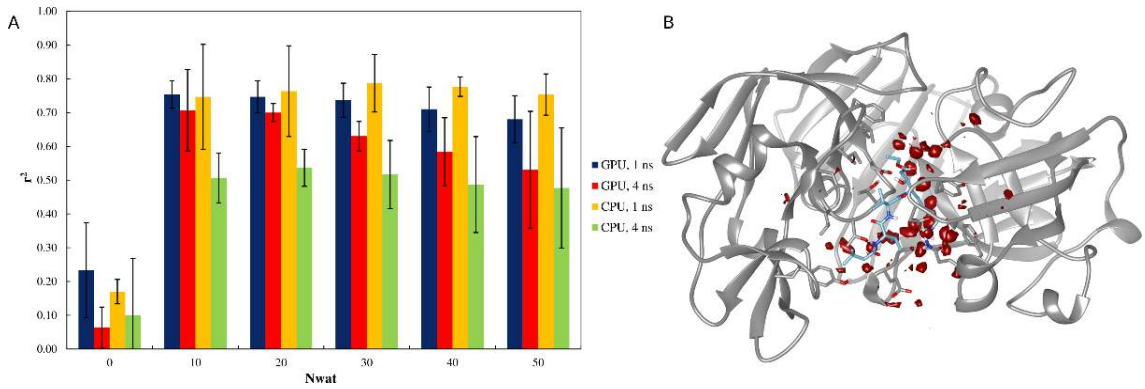

Figure 11.1. A) Trend of r^2 in dependency of Nwat for penicillopepsin. B) Water density plots obtained by grid analysis of penicillopepsin-APT complex (visualization with Chimera, step = 1 and level = 15).

However, some differences have to be highlighted and additional observations can be extrapolated from these results. In particular, the average correlations obtained when Nwat = 0 are lower than that obtained with the previous protocol (r^2 = 0.46, see Chapter 8.1), thus making the improvement given by the consideration of solute-solvent interactions more significant. This can be due to the different setup used for the MD simulations (ff14SB force field instead of ff99SB, Langevin MD with restraints instead of constraints in equilibration steps, longer equilibration, see Material and Methods) and to the different method used to derive the point charges of penicillopepsin ligands (Figure 9.3), because in this case a fast and less accurate semi-

empirical AM1-BCC method has been used instead of the accurate but time consuming *ab initio* RESP method.

Although, when Nwat ≠ 0 the r^2 values are not statistically different from those previously obtained, with this new protocol a plateau value is immediately reached with Nwat = 10 – 30. This might be due to a longer NPT equilibration (see Materials and Methods section) which can lead to a better positioning of water molecules around the ligands, allowing the formation of stable and relevant solute-solvent H-bonds also with lower Nwat values. Indeed, in this case the prediction of the binding energy of all the complexes (and not only APU, as showed in Chapter 9) is equally affected by the inclusion of water molecules during the MMGBSA analysis (Figure 11.2),.

Table 11.1. Values of r^2 as a function of Nwat obtained by the analysis of the first and fourth ns of MD simulations run on both GPU and CPU hardwares. Average values and standard deviations are also reported.

GPU, 1 ns					**CPU, 1 ns**			
Nwat	**r^2 run1**	**r^2 run2**	**r^2 run3**	**Avg r^2 ± SD**	**r^2 run1**	**r^2 run2**	**r^2 run3**	**Avg r^2 ± SD**
0	0.38	0.22	0.10	0.23 ± 0.14	0.18	0.13	0.20	0.17 ± 0.04
10	0.80	0.73	0.73	0.75 ± 0.04	0.57	0.86	0.81	0.75 ± 0.16
20	0.80	0.71	0.73	0.75 ± 0.05	0.61	0.86	0.82	0.76 ± 0.13
30	0.79	0.69	0.73	0.74 ± 0.05	0.69	0.85	0.82	0.79 ± 0.09
40	0.78	0.65	0.70	0.71 ± 0.07	0.76	0.81	0.76	0.78 ±0.03
50	0.76	0.63	0.65	0.68 ± 0.07	0.82	0.74	0.70	0.75 ± 0.06
GPU, 4 ns					**CPU, 4 ns**			
Nwat	**r^2 run1**	**r^2 run2**	**r^2 run3**	**Avg r^2 ± SD**	**r^2 run1**	**r^2 run2**	**r^2 run3**	**Avg r^2 ±SD**
0	0.13	0.05	0.01	0.06 ± 0.06	0.23	-0.09	0.16	0.10 ± 0.17
10	0.83	0.70	0.59	0.71 ± 0.12	0.59	0.48	0.45	0.51 ± 0.07
20	0.73	0.68	0.69	0.70 ± 0.03	0.59	0.48	0.54	0.54 ± 0.06
30	0.68	0.61	0.60	0.63 ± 0.04	0.61	0.41	0.53	0.52 ± 0.10
40	0.70	0.53	0.52	0.58 ± 0.10	0.64	0.36	0.46	0.49 ± 0.14
50	0.73	0.44	0.42	0.53 ± 0.17	0.68	0.35	0.40	0.48 ± 0.18

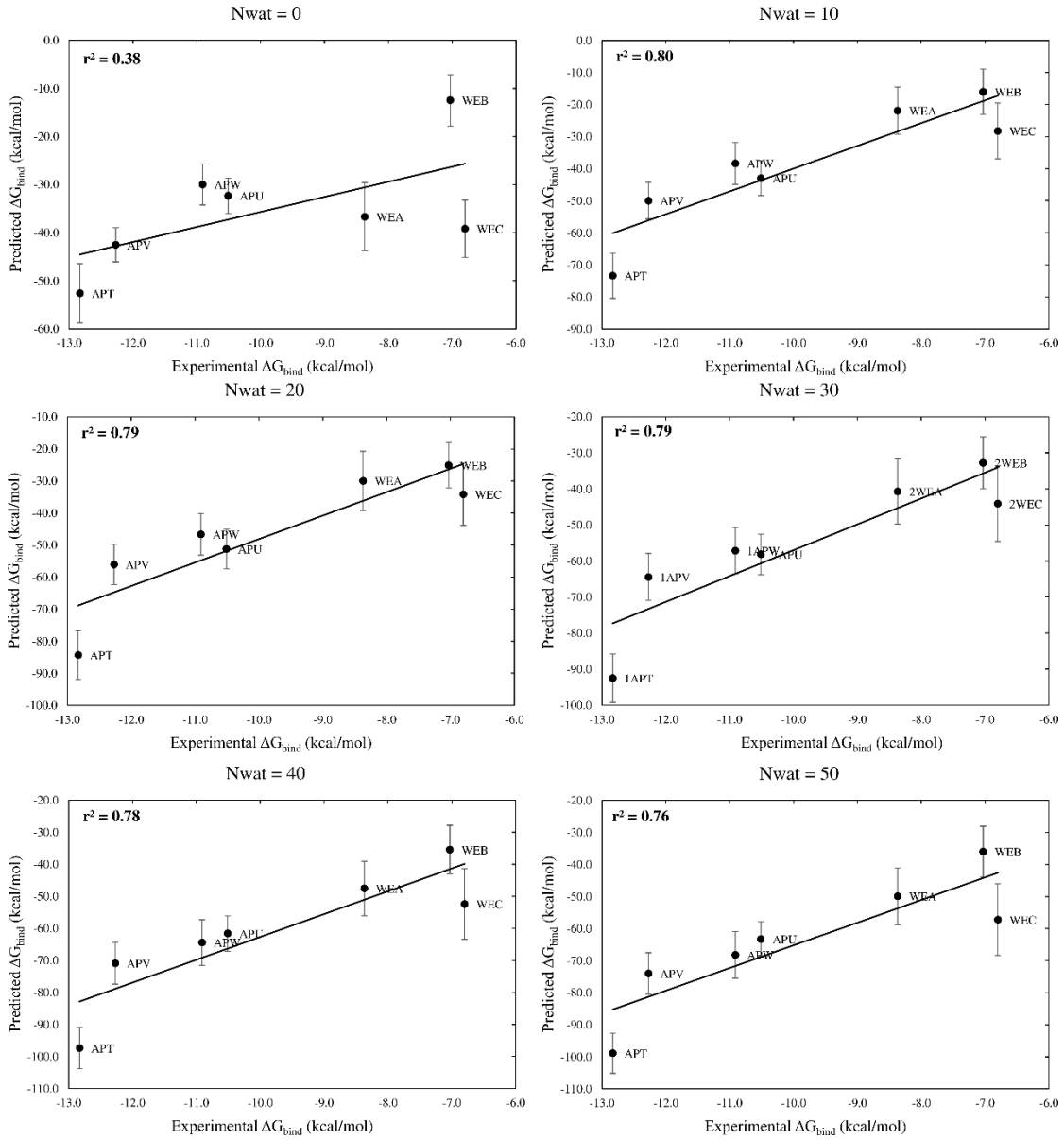

Figure 11.2. Correlation between experimental free energy of binding and predicted binding energies obtained for penicillopepsin by analyzing the first ns of one of the three MD simulations run on a GPU hardware.

Moreover, the performances of GPU and CPU hardware are generally statistically equivalent, and the same is true for the analyses performed on either the first or the 4th ns of MD. The only exception is represented by the MMGBSA results obtained from the analysis of the 4th ns of the MD simulations run on a CPU hardware, which are worse in terms of r^2 than the others at any Nwat (Figures 11.1 and 11.4). However, the analyses carried out on the 4th ns of GPU MD simulations also gave worse results than

those performed on the first ns of the MD simulations. This is mainly ascribable to the WEC complex, (Figure 11.4) whose binding energy is decidedly overestimated and has a high standard deviation (> 10%), not observed in the analysis on the first ns of GPU MD runs. The incorrect prediction of the binding energy of WEC when performing the MMGBSA calculation on the 4th ns of the CPU MD simulations can probably be attributed to problems in the MD simulations on this complex, which can be noticed, although at minor extent, also from Figure 11.2, where the correlations between experimental free energy of binding and predicted binding energies obtained for penicillopepsin by analyzing the first ns of one of the three MD simulations run on a GPU hardware are showed. The instability of the WEC complex is also proved by the RMSD of the backbone atoms from the crystallographic structure computed on the 4th ns of a CPU MD simulation. Indeed, this RMSD is higher than that computed on the first ns of the same simulation, whereas the RMSD computed on a CPU simulation of APU, whose predicted binding energy well correlated with experiments, are superimposable (Figure 11.3). In addition, it should be noted that the WEC RMSD are more fluctuating, explaining the high standard deviations of the predicted binding energy for this complex.

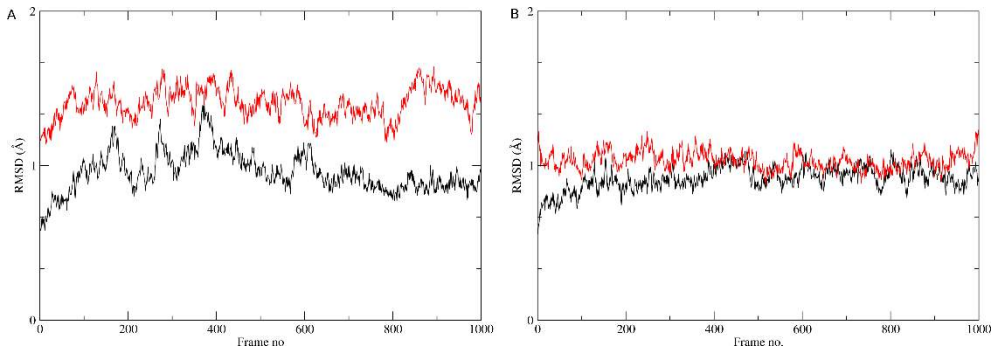

Figure 11.3. RMSD from the crystallographic structure of A) WEC and B) APU complexes computed on the 1st ns (black) and at the 4th ns (red) of one of the MD simulations run on CPUs.

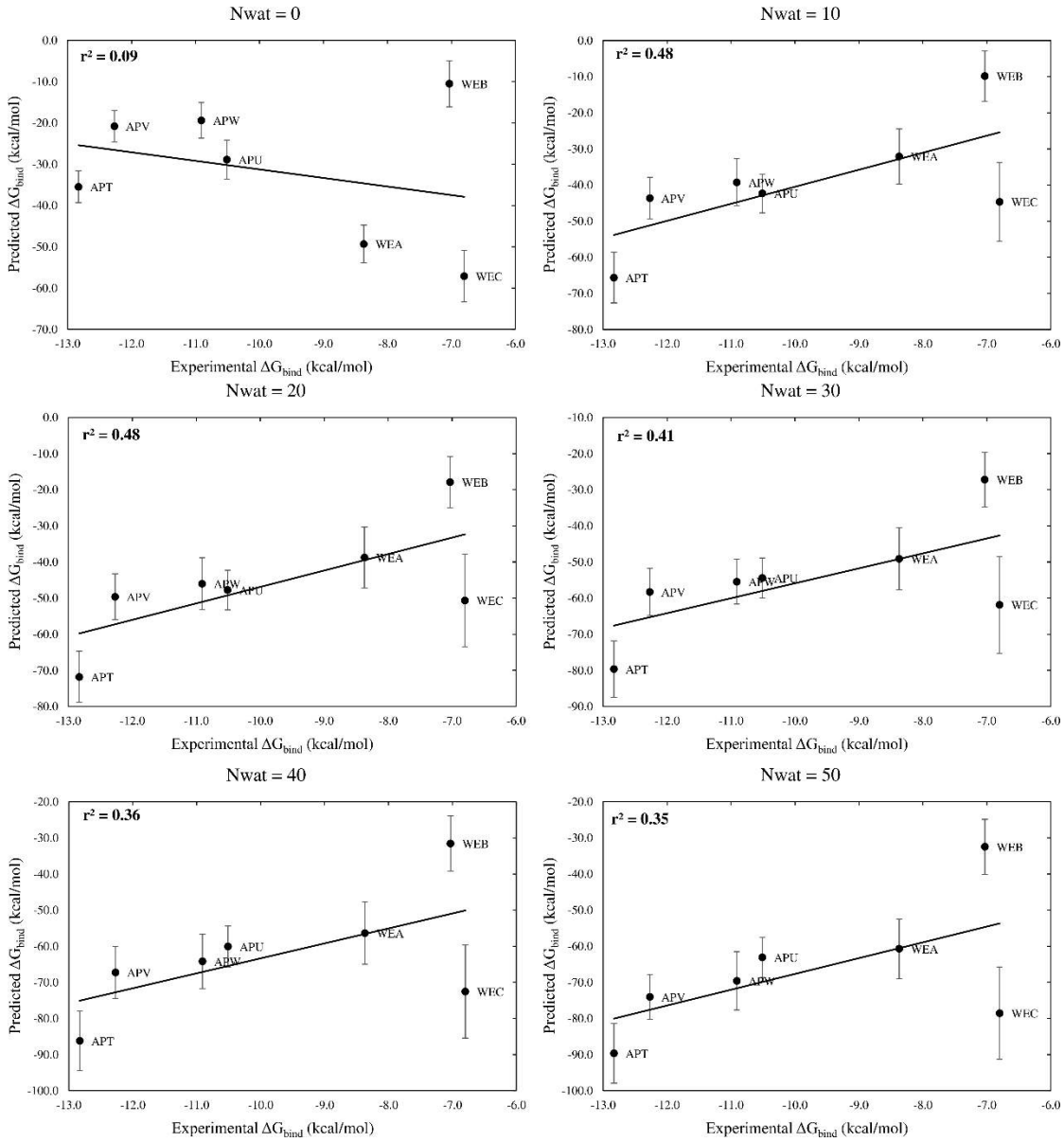

Figure 11.4. Correlation between experimental free energy of binding and predicted binding energies obtained for penicillopepsin by analyzing the 4th ns of one of the three MD simulations run on a CPU hardware.

Therefore, as observed in Chapter 10, multiple simulation runs, although shorter are recommended over a single and long simulation. Conversely, the nature of the hardware does not seem to significantly affect the results.

MDM2. For the MDM2 system an acceptable correlation between predicted binding energies and $-\log_{10}(IC_{50})$ could not be obtained by MMGBSA analyses with Nwat = 0, and the inclusion of up to 70 water molecules around the ligands

during the MMGBSA calculations slightly improved the r^2 value, which reached ~ 0.50 with Nwat = 70 (Figure 11.5A and Table 11.2). This increment in correlation of about 20 % can be explained by observing the water density plots obtained by grid analysis: for this system few and small areas of relevant water density are present around the inhibitors (Figure 11.5B), suggesting that the explicit consideration of solute-solvent interactions is advantageous, but not fundamental for the MDM2 system. Therefore, as observed for other systems (see Chapter 9) the small, but statistically significant, increase in r^2 might be due to the explicit inclusion of a few water molecules that, although not firmly bridging the ligand−receptor interactions, contribute in defining a water buffer between the ligands and the MDM2. This hypothesis explain why up to 70 water molecules are needed to have a significant increase of the correlation index.

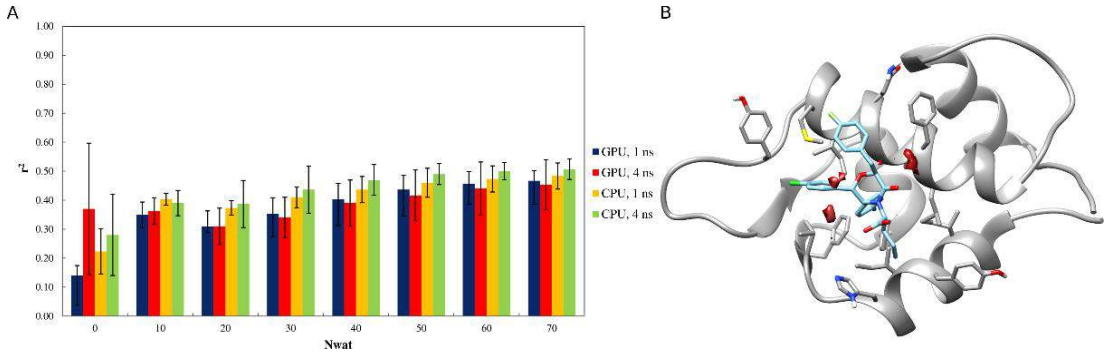

Figure 11.5. A) Trend of r^2 in dependency of Nwat for MDM2. B) Water density plots obtained by grid analysis of MDM2-4JVE complex (visualization with Chimera, step = 1 and level = 15).

Table 11.2. Values of r^2 as a function of Nwat obtained by the analysis of the first and fourth ns of MD simulations run on both GPU and CPU hardwares for MDM2 system. Average values and standard deviations are also reported.

GPU, 1 ns					**CPU, 1 ns**			
Nwat	**r^2 run1**	**r^2 run2**	**r^2 run3**	**Avg r^2 ± SD**	**r^2 run1**	**r^2 run2**	**r^2 run3**	**Avg r^2 ± SD**
0	0.10	0.16	0.16	0.14 ± 0.03	0.16	0.2	0.31	0.22 ± 0.08
10	0.33	0.40	0.32	0.35 ± 0.04	0.41	0.42	0.38	0.40 ± 0.02
20	0.33	0.35	0.25	0.31 ± 0.05	0.4	0.37	0.35	0.37 ± 0.03
30	0.38	0.39	0.29	0.35 ± 0.06	0.44	0.42	0.37	0.41 ± 0.04
40	0.43	0.44	0.34	0.40 ± 0.06	0.48	0.44	0.39	0.44 ± 0.05
50	0.46	0.47	0.38	0.44 ± 0.05	0.51	0.46	0.41	0.46 ± 0.05
60	0.47	0.49	0.41	0.46 ± 0.04	0.52	0.47	0.43	0.47 ± 0.05
70	0.47	0.50	0.43	0.47 ± 0.04	0.53	0.48	0.44	0.48 ± 0.05
GPU, 4 ns					**CPU, 4 ns**			

Nwat	r^2 run1	r^2 run2	r^2 run3	Avg r^2 ± SD	r^2 run1	r^2 run2	r^2 run3	Avg r^2 ±SD
0	0.16	0.61	0.34	0.37 ± 0.23	0.18	0.22	0.44	0.28 ± 0.14
10	0.32	0.41	0.36	0.36 ± 0.05	0.44	0.37	0.36	0.39 ± 0.04
20	0.29	0.38	0.26	0.31 ± 0.06	0.48	0.33	0.35	0.39 ± 0.08
30	0.37	0.39	0.26	0.34 ± 0.07	0.53	0.38	0.4	0.44 ± 0.08
40	0.45	0.42	0.30	0.39 ± 0.08	0.53	0.45	0.43	0.47 ± 0.05
50	0.49	0.44	0.32	0.42 ± 0.09	0.53	0.48	0.46	0.49 ± 0.04
60	0.52	0.46	0.34	0.44 ± 0.09	0.53	0.50	0.47	0.50 ± 0.03
70	0.53	0.47	0.36	0.45 ± 0.09	0.54	0.51	0.47	0.51 ± 0.04

The difficulty in having a correlation between predicted binding energies and experimental activities above 50% might also be attributed to the fact that some of the considered MDM2 inhibitors (Figure 11.6 and 8.48) were tested as racemates but only the complex of a single enantiomer was available, and thus considered.

Therefore, the poor correlation reached might also be due to the inhibitors data set, but, anyway, it is significantly improved when solute – solvent interactions are taken in account, although the role of water in mediating protein-ligand interactions is poor (Figure 11.5B). Moreover, it should be underlined that when Nwat ≠ 0 the standard deviation of r^2 decreases, suggesting that the Nwat-MMGBSA approach improve the reproducibility of the results, the contribute of the MDM2 protein to the binding energy is better estimated in the presence of explicit water.

Also in this case, simulations run on GPUs gave equivalent results to those run on CPUs, most of all when Nwat ≠ 0, making the GPU-based hardware a fast, cheap and reliable choice for MD simulations.

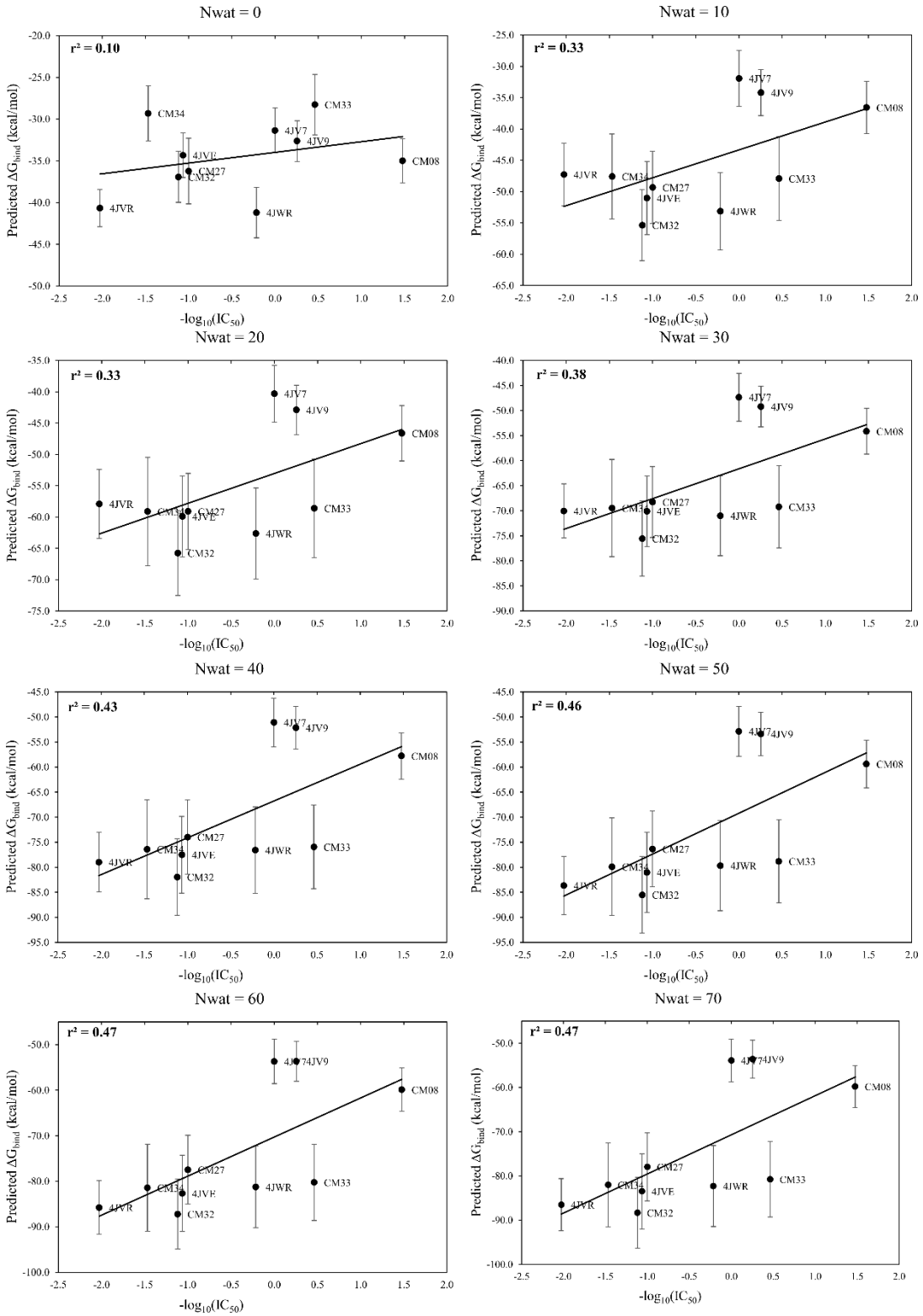

Figure 11.6. Correlation between experimental free energy of binding and predicted binding energies obtained for MDM2 with Nwat = 0 - 70 by analyzing the first ns of a MD simulation run on a GPU hardware.

BCL-X_L. For the BCL-X_L system a high correlation index ($r^2 \approx 0.70$) was obtained even with Nwat = 0, suggesting that water does not play a relevant role in mediating protein-ligand interactions or in stabilizing the complex. Indeed, including a hydration shell of 10 to 50 water molecules around the ligands when computing the binding energies did not minimally affect the correlation with $-\log_{10}(IC_{50})$ (Figure 11.7A and Table 11.3). As a further proof, grid analyses performed on the MD simulations showed the presence of decidedly small high water density areas, mainly located around protein loops and not at the protein -ligand boundary (Figure 11.7B).

It is important to emphasize that, although water has not a particular importance in this system, the inclusion of explicit hydration shells is neither detrimental nor time consuming. This aspect is fundamental, because it allows to automatically and safely apply the Nwat-MMGBSA approach in drug design/discovery protocols.

In addition, as previously observed for the other systems, it could not be found any significant difference between the MMGBSA results obtained from the analyses of the MD simulations performed on either GPUs or CPUs, indicating that the highly performing and innovative GPUs can be reliably used for MD simulations.

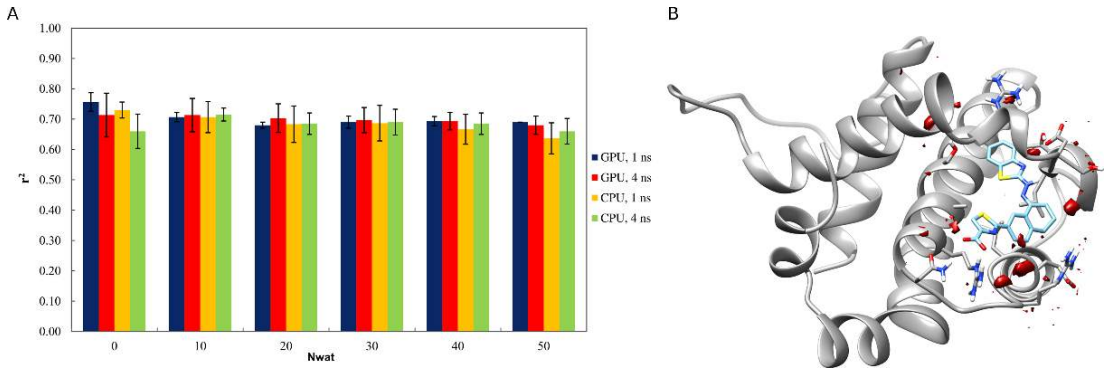

Figure 11.7. A) Trend of r^2 in dependency of Nwat for BCL-X_L. B) Water density plots obtained by grid analysis of BCL-X_L-3ZC4 (visualization with Chimera, step = 1 and level = 15).

Table 11.3. Values of r^2 as a function of Nwat obtained by the analysis of the first and fourth ns of BCL-X_L MD simulations run on both GPU and CPU hardwares. Average values and standard deviations are also reported.

GPU, 1 ns					**CPU, 1 ns**			
Nwat	**r^2 run1**	**r^2 run2**	**r^2 run3**	**Avg r^2 ± SD**	**r^2 run1**	**r^2 run2**	**r^2 run3**	**Avg r^2 ± SD**
0	0.75	0.73	0.79	0.76 ± 0.03	0.70	0.75	0.74	0.73 ± 0.03
10	0.71	0.69	0.72	0.71 ± 0.02	0.75	0.72	0.65	0.71 ± 0.05
20	0.67	0.68	0.69	0.68 ± 0.01	0.74	0.69	0.62	0.68 ± 0.06

30	0.67	0.71	0.69	0.69 ± 0.02	0.73	0.71	0.62	0.69 ± 0.06
40	0.68	0.71	0.69	0.69 ± 0.02	0.69	0.70	0.61	0.67 ± 0.05
50	0.69	0.69	0.69	0.69 ± 0.00	0.65	0.68	0.58	0.64 ± 0.05
GPU, 4 ns					**CPU, 4 ns**			
Nwat	**r^2 run1**	**r^2 run2**	**r^2 run3**	**Avg r^2 ± SD**	**r^2 run1**	**r^2 run2**	**r^2 run3**	**Avg r^2 ±SD**
0	0.63	0.76	0.75	0.71 ± 0.07	0.62	0.7	0.76	0.66 ± 0.06
10	0.65	0.75	0.74	0.71 ± 0.06	0.73	0.7	0.65	0.72 ± 0.02
20	0.65	0.74	0.72	0.70 ± 0.05	0.71	0.66	0.64	0.69 ± 0.04
30	0.65	0.73	0.71	0.70 ± 0.04	0.72	0.66	0.65	0.69 ± 0.04
40	0.66	0.71	0.71	0.69 ± 0.03	0.71	0.66	0.66	0.69 ± 0.04
50	0.65	0.68	0.71	0.68 ± 0.03	0.69	0.63	0.66	0.66 ± 0.04

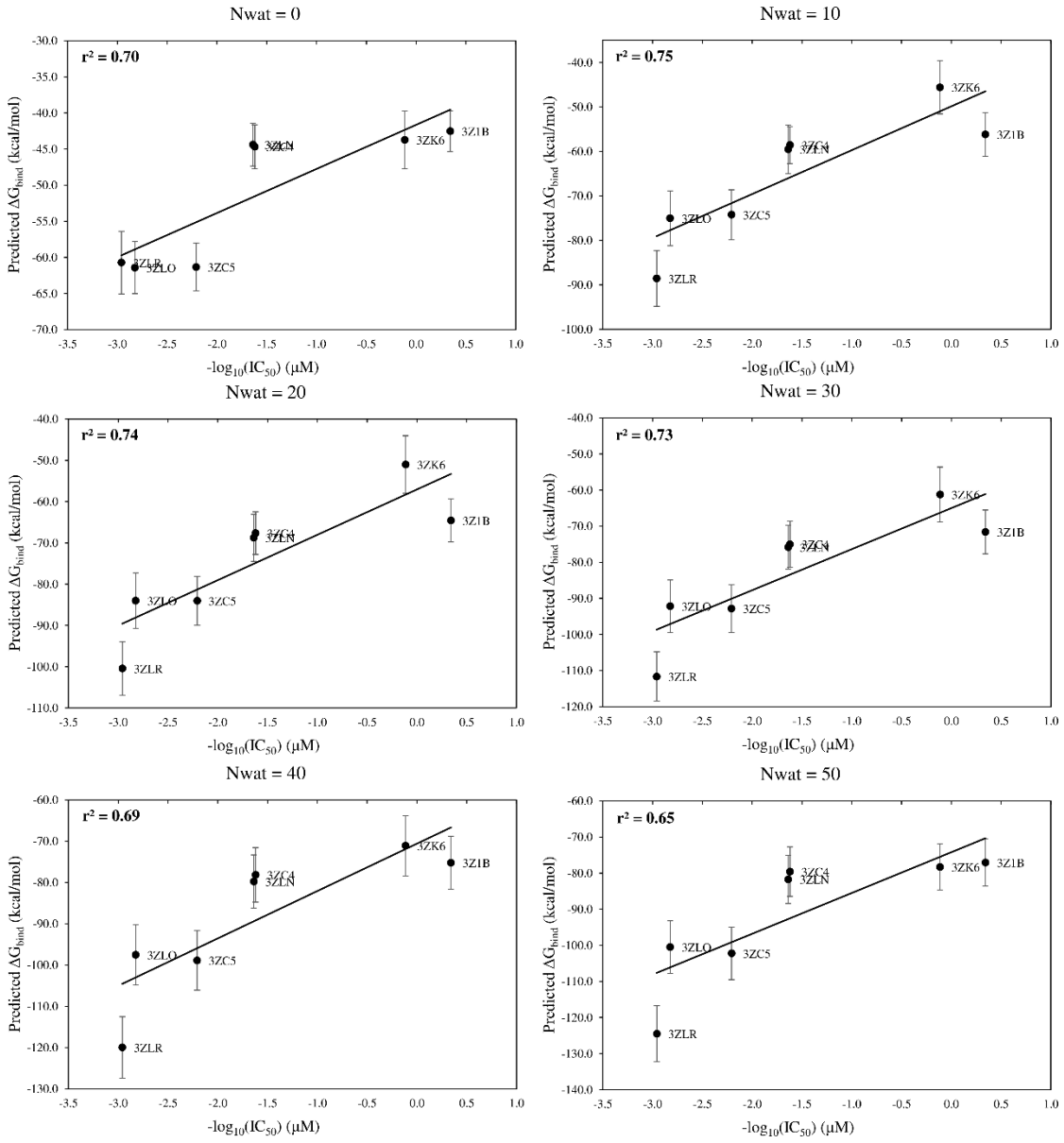

Figure 11.8. Correlation between experimental free energy of binding and predicted binding energies obtained for BCL-X_L with Nwat = 0 - 50 by analyzing the first ns of a MD simulation run on a HPC hardware.

XIAP-BIR2. The study of XIAP-BIR2 system required the extension of the hydration shell around the ligand up to Nwat = 90, in order to verify the convergence in terms of r^2. Indeed, this system behaved in a completely different way compared to the previously considered complexes. In detail, the correlation between predicted binding energies and $-\log_{10}(IC_{50})$ was already high ($0.64 < r^2 < 0.72$) without considering any explicit solvent model during the MMGBSA calculations (Nwat = 0).

Then, with Nwat = 10 – 30 a drastic decrease in the r^2 values was observed ($0.01 < r^2 < 0.13$), followed by an improvement in correlation up to values 10% higher than those obtained with Nwat = 0 ($0.74 < r^2 < 0.84$) with Nwat = 80 – 90 (Figures 8.42A and 8.43, and Table 11.4).

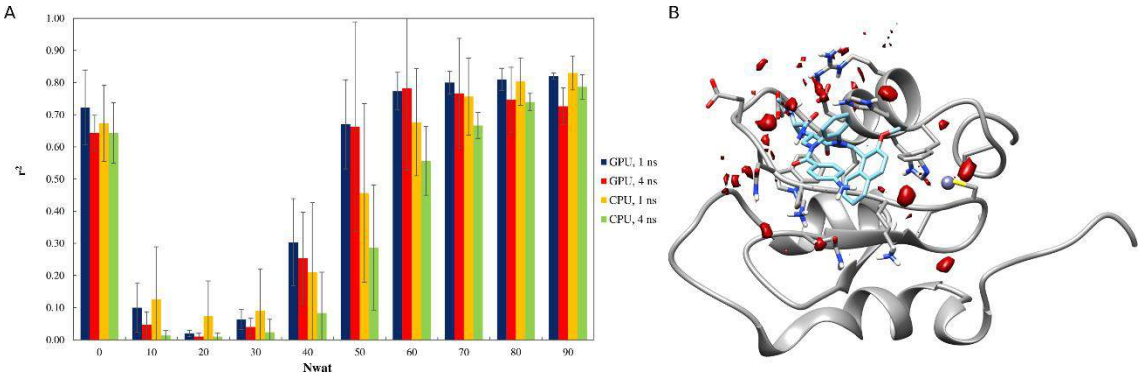

Figure 11.9. A) Trend of r^2 in dependency of Nwat for XIAP-BIR2. B) Water density plots obtained by grid analysis of XIAP-BIR2-21J (visualization with Chimera, step = 1 and level = 15).

Table 11.4. Values of r^2 as a function of Nwat obtained by the analysis of the first and fourth ns of MD simulations run on both GPU and CPU hardwares for MDM2 system. Average values and standard deviations are also reported.

GPU, 1 ns					**CPU, 1 ns**			
Nwat	**r^2 run1**	**r^2 run2**	**r^2 run3**	**Avg r^2 ± SD**	**r^2 run1**	**r^2 run2**	**r^2 run3**	**Avg r^2 ± SD**
0	0.83	0.74	0.60	0.72 ± 0.12	0.60	0.81	0.61	0.67 ± 0.12
10	0.18	0.03	0.09	0.10 ± 0.08	0.07	0.31	0.00	0.13 ± 0.16
20	0.03	0.01	0.02	0.02 ±0.01	0.01	0.20	0.01	0.07 ± 0.11
30	0.09	0.07	0.03	0.06 ± 0.03	0.03	0.24	0.00	0.09 ± 0.13
40	0.23	0.46	0.22	0.30 ± 0.14	0.18	0.44	0.01	0.21 ± 0.22
50	0.59	0.83	0.59	0.67 ± 0.14	0.50	0.71	0.16	0.46 ± 0.28
60	0.75	0.84	0.73	0.77 ± 0.06	0.73	0.81	0.49	0.68 ± 0.17
70	0.81	0.83	0.76	0.80 ± 0.04	0.81	0.84	0.62	0.76 ± 0.12
80	0.83	0.83	0.77	0.81 ± 0.03	0.83	0.86	0.72	0.80 ± 0.07
90	0.83	0.82	0.81	0.82 ± 0.01	0.87	0.85	0.77	0.83 ± 0.05
GPU, 4 ns					**CPU, 4 ns**			
Nwat	**r^2 run1**	**r^2 run2**	**r^2 run3**	**Avg r^2 ± SD**	**r^2 run1**	**r^2 run2**	**r^2 run3**	**Avg r^2 ±SD**
0	0.68	0.67	0.58	0.64 ± 0.06	0.61	0.75	0.57	0.64 ± 0.09
10	0.01	0.09	0.04	0.05 ± 0.04	0.00	0.03	0.01	0.01 ± 0.02
20	0.00	0.02	0.01	0.01 ± 0.01	0.01	0.02	0.00	0.01 ± 0.01
30	0.07	0.02	0.03	0.04 ± 0.03	0.00	0.07	0.00	0.02 ± 0.04
40	0.36	0.09	0.31	0.25 ± 0.14	0.01	0.23	0.01	0.08 ± 0.13
50	0.81	0.29	0.89	0.66 ± 0.33	0.16	0.51	0.19	0.29 ± 0.19
60	0.90	0.49	0.96	0.78 ± 0.26	0.49	0.68	0.50	0.56 ± 0.11
70	0.85	0.57	0.88	0.77 ± 0.17	0.62	0.69	0.69	0.67 ± 0.04

80	0.81	0.63	0.80	0.75 ± 0.10	0.72	0.73	0.77	0.74 ± 0.03
90	0.76	0.66	0.76	0.73 ± 0.06	0.77	0.76	0.83	0.79 ± 0.04

The decrease in r^2 values when Nwat = 10 -30 can be mainly attribute to the C09 complex. Indeed, for this complex the inclusion of small hydration shells around the ligands is detrimental, while it does not have any effect on the other complexes. This is probably due to the fact that, among the considered ligands, C09 is the only one with a secondary amine on the benzodiazepine ring (Figure 11.16), which can interact with water molecules (Figure 11.10). This additional interaction leads to an overestimation of the binding energy of the related complex when Nwat = 10 -30 is used, while with larger hydration shell it is not observed because additional water-mediated H-bonds within the protein reduce the impact of the complex contribute in the binding energy computation (Table 11.5).

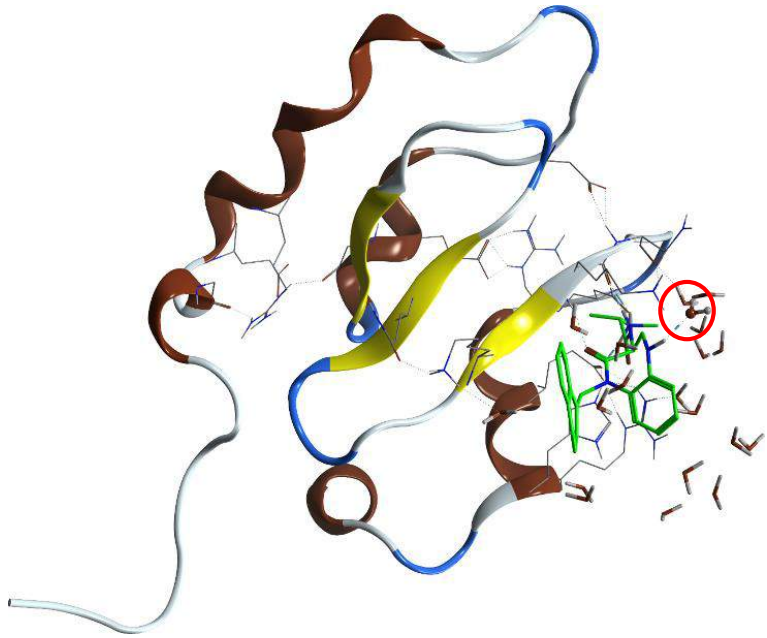

Figure 11.10. XIAP-BI2-C09 complex with Nwat = 20. C09 is represented in green, while the water molecule involved in the interaction with C09(N7) is represented in ball and stick and circled in red.

Therefore, if C09 was omitted from the dataset, results are similar to those obtained for the BCL-X_L system. It should also be considered that the overestimation of the binding energy in the C09 complex was reduced when considering larger hydration shells, and that the use of the Nwat-MMGBSA approach with Nwat $\neq 0$.

Table 11.5. Water-mediated H-bonds with occupancy > 20% detected from the analysis of a CPU MD simulation of the C09 complex.

Nwat = 20		**Nwat = 70**	
Residues involved	**Occ%**	**Residues involved**	**Occ%**
65:ASP 70:GLU	39.0	65:ASP 70:GLU	68.0
93:ARG 115:GLY	34.0	63:PRO 65:ASP	54.0
17:ARG 39:GLY	33.0	60:ASN 62:GLU	35.0
62:GLU 65:ASP	28.0	93:ARG 115:GLY	34.0
60:ASN 62:GLU	27.0	17:ARG 39:GLY	33.0
		62:GLU 65:ASP	33.0
		69:SER 70:GLU	20.0

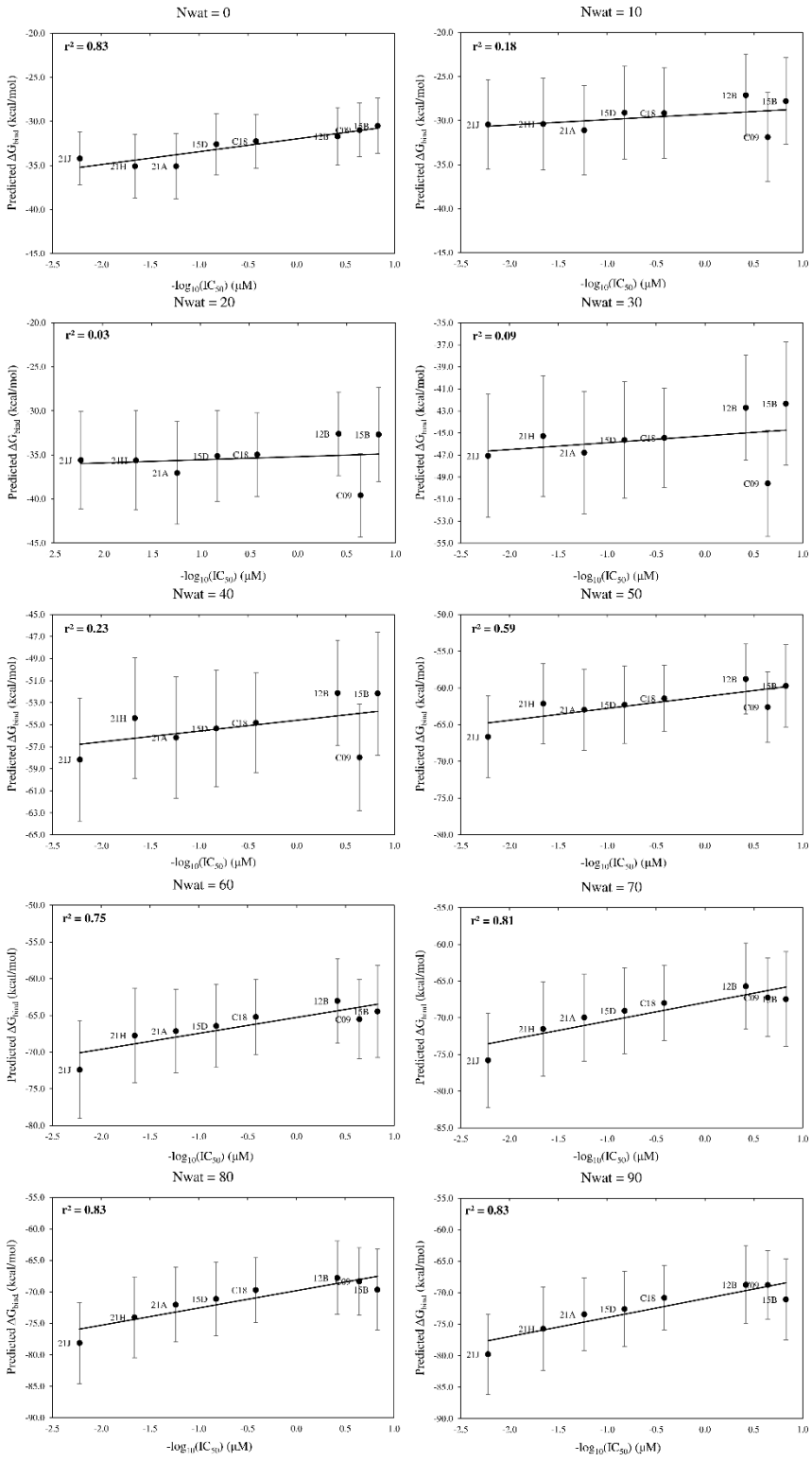

Figure 11.11. Correlation between experimental free energy of binding and predicted binding energies obtained for XIAP-BIR2 with Nwat = 0 - 90 by analyzing the first ns of a MD simulation run on a GPU hardware.

HIV1-protease. It is known that water is fundamental for the catalytic activity of this aspartic protease, where a water molecule, located between two aspartate residues, is activated through an acid-base mechanism and attacks the amidic carbonyl of the cleavage site.[320] Thus, it is not surprising that for this system many and relatively wide areas of high water density between the protein and the ligand have been detected by grid analysis (Figure 11.12B).

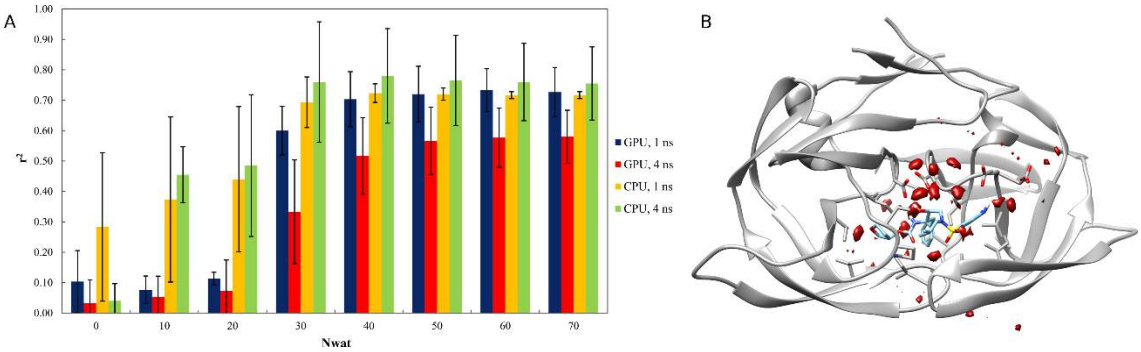

Figure 11.12. A) Trend of r^2 in dependency of Nwat for HIV1-protease. B) Water density plots obtained by grid analysis of HIV1-protease-3NUO (visualization with Chimera, step = 1 and level = 15).

In addition, among the considered systems, the HIV1-protease is the most affected by solute-solvent interactions. Indeed, the inclusion of a hydration shell of 30 – 70 molecules increased the correlation between predicted binding energies and k_i of about 50 – 60 % compared to the r^2 obtained with Nwat = 0 (Figure 11.11A and Table 11.5). In all the performed runs, the inclusion of 10 – 20 water molecules during the MMGBSA analysis did not significantly affect the r^2 (Table 11.6). This suggests that small hydration shells around the ligand are not enough to correctly treat the solute – solvent interactions, which, in this case, may differently involve the HIV1-protease mutants. Indeed, water-mediated H-bond analyses showed that only one or two stable (occupancy > 20%) water-mediated interactions involved the ligand, while in most of the cases water is needed to bridge interactions within the HIV1-protease. In addition, the water-mediated interactions between HIV1-protease and the ligand have the same occupancies with both Nwat = 10 and Nwat = 70, although the correlation with experiments is greater with Nwat = 70 than with Nwat =10. This is showed in Tables 8.26 and 8.27, where 3NUO, which is highly affected by the inclusion of solvent

molecules during the MMGBSA analysis, and 3NDW, which well correlated with experiments also with Nwat = 0, are taken as example. It can be observed that the number of water-mediated H-bonds within the protein decidedly increases when passing from Nwat = 10 to Nwat = 70 for 3NUO, evidencing the importance of water in this system. Conversely, with Nwat = 10 and Nwat = 70 the water-mediated interactions detected in 3NDW are equivalent and significantly lower than those obtained by analysing the 3NUO trajectory.

Table 11.6. Values of r^2 as a function of Nwat obtained by the analysis of the first and fourth ns of MD simulations run on both GPU and CPU hardwares for HIV1-protease system. Average values and standard deviations are also reported.

GPU, 1 ns					**CPU, 1 ns**			
Nwat	**r^2 run1**	**r^2 run2**	**r^2 run3**	**Avg r^2 ± SD**	**r^2 run1**	**r^2 run2**	**r^2 run3**	**Avg r^2 ± SD**
0	0.22	0.06	0.03	0.10 ± 0.10	0.48	0.36	0.01	0.28 ± 0.24
10	0.08	0.03	0.12	0.08 ± 0.05	0.34	0.66	0.12	0.37 ± 0.27
20	0.13	0.09	0.12	0.11 ± 0.02	0.39	0.70	0.23	0.44 ± 0.24
30	0.52	0.60	0.68	0.60 ± 0.08	0.72	0.76	0.6	0.69 ± 0.08
40	0.60	0.77	0.74	0.70 ± 0.09	0.73	0.75	0.69	0.72 ± 0.03
50	0.62	0.80	0.74	0.72 ± 0.09	0.72	0.74	0.70	0.72 ± 0.02
60	0.63	0.80	0.74	0.72 ± 0.09	0.71	0.73	0.71	0.72 ± 0.01
70	0.63	0.80	0.74	0.72 ± 0.09	0.71	0.73	0.71	0.72 ± 0.01
GPU, 4 ns					**CPU, 4 ns**			
Nwat	**r^2 run1**	**r^2 run2**	**r^2 run3**	**Avg r^2 ± SD**	**r^2 run1**	**r^2 run2**	**r^2 run3**	**Avg r^2 ±SD**
0	0.12	-0.02	0.00	0.03 ± 0.08	0.08	0.00	0.01	0.04 ± 0.06
10	0.13	0.00	0.03	0.05 ± 0.07	0.52	0.39	0.10	0.46 ± 0.09
20	0.19	0.01	0.02	0.07 ± 0.10	0.32	0.65	0.00	0.49 ± 0.23
30	0.53	0.24	0.23	0.33 ± 0.17	0.62	0.90	0.52	0.76 ± 0.20
40	0.65	0.50	0.40	0.52 ± 0.13	0.67	0.89	0.70	0.78 ± 0.16
50	0.67	0.58	0.45	0.57 ± 0.11	0.66	0.87	0.72	0.77 ± 0.15
60	0.66	0.60	0.47	0.58 ± 0.10	0.67	0.85	0.72	0.76 ± 0.13
70	0.64	0.62	0.48	0.58 ± 0.09	0.67	0.84	0.71	0.76 ± 0.12

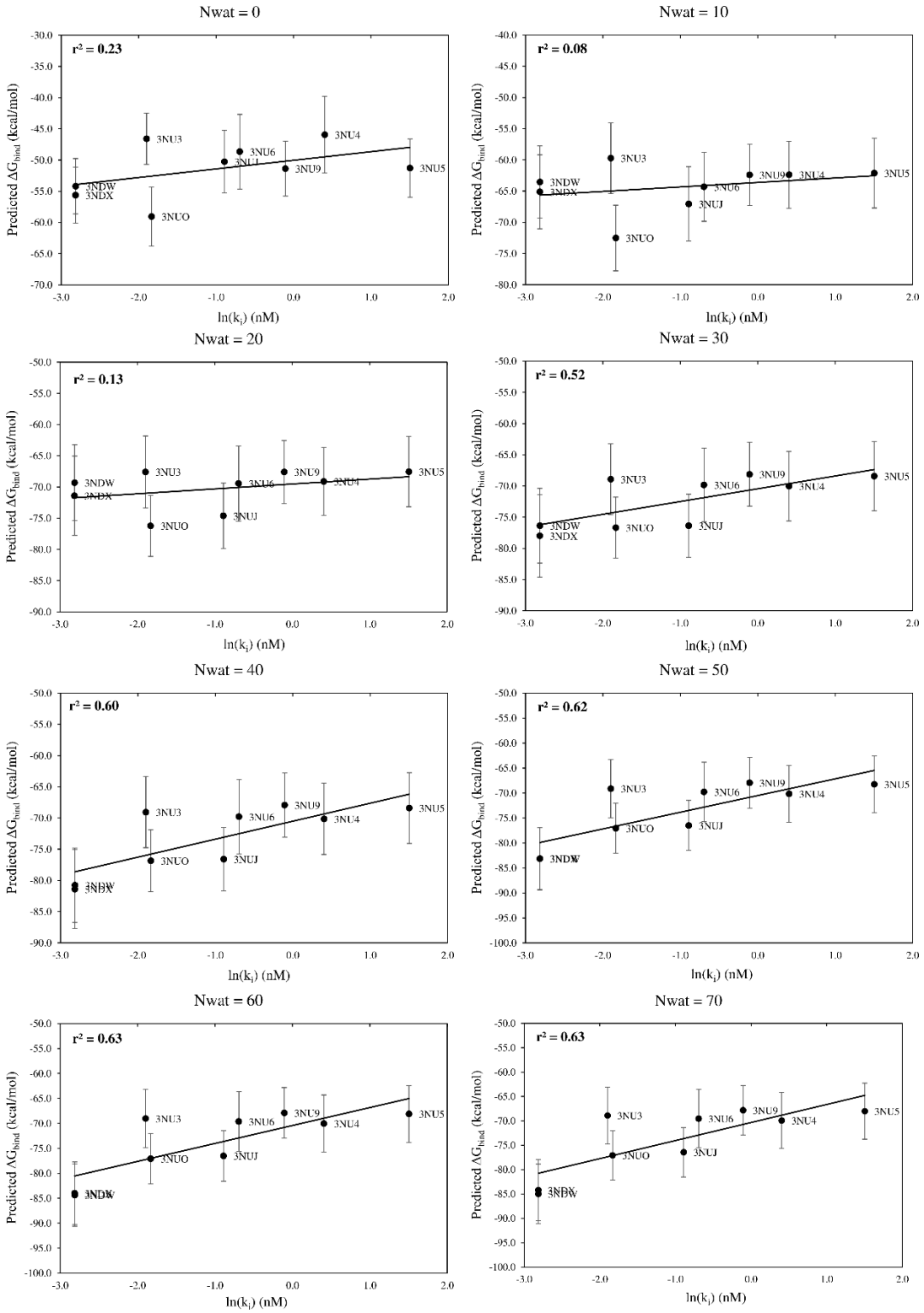

Figure 11.13. Correlation between experimental free energy of binding and predicted binding energies obtained for HIV1-protease with Nwat = 0 - 70 by analyzing the first ns of a MD simulation run on a GPU hardware.

Table 11.7. Water-mediated H-bonds with occupancy > 20% detected from the analysis of a CPU MD simulation of 3NUO. The water-mediated H-bonds involving amprenavir are reported in bold.

Nwat = 10		**Nwat = 70**	
Residues involved	**occ%**	**Residues involved**	**occ%**
31:ASP 203:AMP	**58.0**	**31:ASP 203:AMP**	**58.0**
90:LEU 91:MET	54.0	129:GLY 131:ASP	56.0
129:GLY 131:ASP	51.0	90:LEU 91:MET	54.0
132:ASP 203:AMP	**47.0**	80:PRO 152:ILE	54.0
191:LEU 192:MET	41.0	**132:ASP 203:AMP**	**47.0**
		191:LEU 192:MET	41.0
		27:THR 28:GLY	34.0
		52:GLY 181:PRO	30.0
		30:ASP 31:ASP	28.0
		31:ASP 46:LYS	21.0
		128:THR 129:GLY	20.0

Table 11.8. Water-mediated H-bonds with occupancy > 20% detected from the analysis of a CPU MD simulation of 3NDW. The water-mediated H-bonds involving ritonavir are reported in bold.

Nwat = 10		**Nwat = 70**	
Residues involved	**occ%**	**Residues involved**	**occ%**
191:LEU 192:LEU	73.0	26:ASP 127:ASP	86.0
26:ASP 127:ASP	70.0	191:LEU 192:LEU	73.0
132:ASP 203:RIT	**54.0**	**132:ASP 203:RIT**	**54.0**
90:LEU 91:LEU	53.0	90:LEU 91:LEU	53.0
176:THR 177:VAL	36.0	28:GLY 30:ASP	38.0
		176:THR 177:VAL	36.0

Moreover, when Nwat > 30 the standard deviations of r^2 generally decreased, and this is particularly evident for the MMGBSA analyses performed on the 1st ns of CPU MD simulations. This observation is consistent with what previously noticed for the MDM2 and the XIAP-BIR2 systems.

Therefore, this study confirmed the reliability and robustness of the Nwat-MMGBSA approach, which gave reproducible results within different independent MD simulations and independently from the hardware on which the simulations run. Indeed, the standard deviation of the correlation index within 3 independent MD simulations was generally lower when the optimal Nwat was considered than when Nwat = 0. Furthermore, the inclusion of variably wide hydration shells around the

ligands improved or, at least, did not worsened the correlation between predicted binding energies and experimental activities, such as ΔG_{bind}, k_i and IC_{50}.

Although, the definition of an optimal Nwat valid for all sytems is still an issue, generally Nwat = 50 – 60 gave good results, not significantly different from the best obtainable for each system. Therefore, in PPI systems larger hydration shells have to be considered during the MMGBSA calculations, compared to what observed for classical receptor-ligand or protein-protein complexes. Indeed, considering that explicit waters are considered as a part of the receptor, the selection of a limited number of water molecules around the ligand might lead to an overestimation of the binding energy when solvent-exposed hydrophilic groups are present on the ligand.

These observations indicate that the Nwat-MMGBSA approach represents a promising protocol for drug design/discovery studies, also because short MD simulations (even 1 ns) and fast and cheap GPU cards can be safely used at this scope. Furthermore, the whole protocol, including ligands parametrization, MD simulations, MMGBSA calculations and additional trajectory analysis, has been automatized (Annex 11.F) and a "single-click" is necessary to go from PDB complexes to MMGBSA results.

11.3 Materials and Methods

Preparation of complexes. For BCL-X_L (Figure 11.14), MDM2 (Figure 11.15) and XIAP-BIR2 (Figure 11.16) ligands not all the crystallographic structures of the complexes were available. In detail a X-ray structure was available for BCL-X_L 3ZK6, 3ZLN, 3ZLO and 3ZLR complexes,[316] for the MDM2 4JV7, 4JV9, 4JVE, 4JVR and 4JWR,[315] whereas for the XIAP-BIR2 system only the crystallographic structure of 21J was available.[317] Therefore, the starting geometries of the ligands without an X-ray structures were manually generated with MOE software[227] starting from those available.

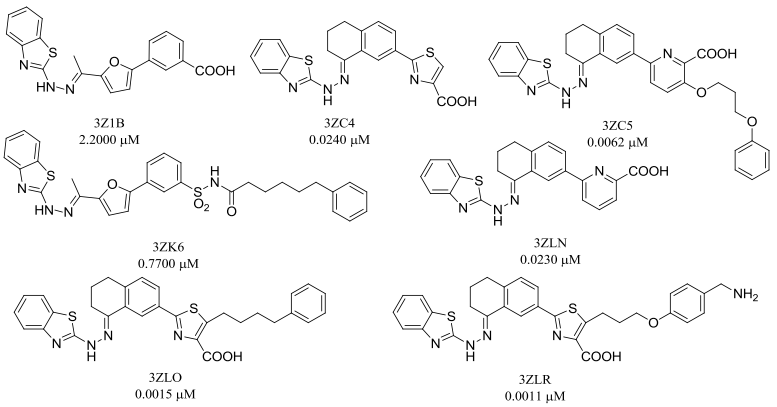

Figure 11.14. BCL-X_L ligands with IC_{50} values.

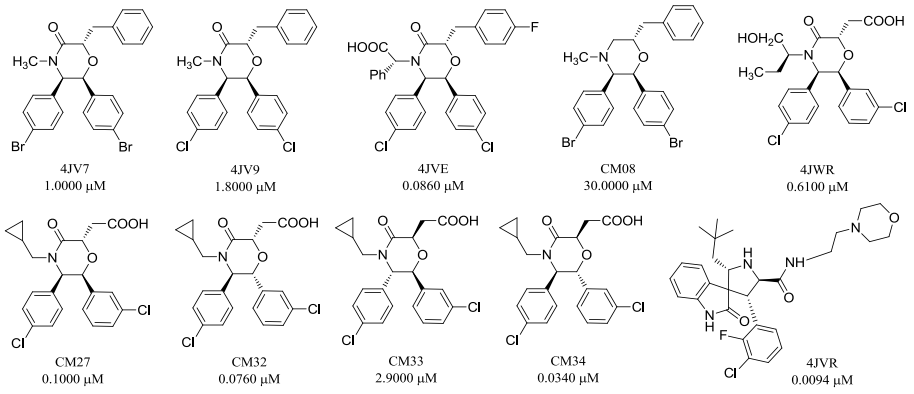

Figure 11.15. MDM2 ligands with IC_{50} values.

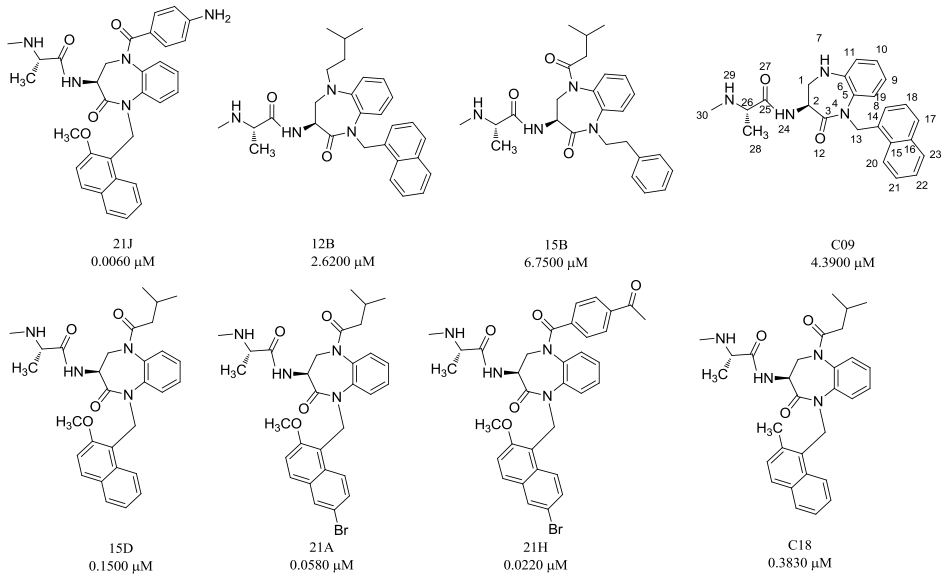

Figure 11.16. XIAP-BIR2 ligands with IC_{50} values.

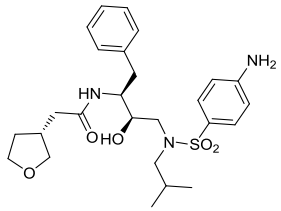

Amprenavir

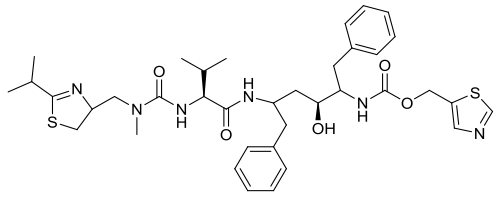

Ritonavir

Figure 11.17. HIV1-protease ligands.

Table 11.9. HIV1-protease complexes with related mutations and k_i values (APV= amprenavir, RTV = ritonavir).

Complex	Mutation	Ligand	k_i (nM)
3NU3	Wild type	APV	0.150
3NU4	V32I	APV	1.500
3NU5	I50V	APV	4.500
3NU6	I54M	APV	0.500
3NUJ	I54V	APV	0.410
3NU9	I84V	APV	0.900
3NUO	L90M	APV	0.160
3NDW	Q7K	RTV	0.055
3NDX	Q7K	RTV	0.055

Ligand partial charges were derived with the AM1-BCC method by the *antechamber*[321] software of AMBER14 package.

From the available crystallographic structures, crystallographic water molecules or crystal stabilizers have been manually removed, and the protonation states of the proteins were determined by MOE software through the *Protonate 3D* tool.

MD simulations. MD simulations were performed with the *pmemd* module of Amber14 package,[192] using the ff14SB[135] and *gaff*[322] force fields. In each complex, the total charge was neutralized by adding an adequate number of Na^+/Cl^- ions, and the systems were solvated with an octahedral box of TIP3P[292] water added up to a distance of 10 Å from the solute. The systems where then relaxed by minimizing hydrogens (1000 cycles of steepest descent and 5000 cycles of conjugated gradient), ions and waters (2000 cycles of steepest descent and 5000 cycles of conjugated gradient). The solvent box was equilibrated at 300 K by 100 ps of NVT and 100 ps of NPT simulation using a Langevin thermostat with a collision frequency of 2.0 ps^{-1}. Successively, a minimization of side chains, water and ions with restraints on

backbone and ligand of 25 kcal/mol and a total minimization (2500 cycles of steepest descent and 5000 cycles of conjugated gradient) were performed. The systems were then heated up to 300 K in 6 steps of 5 ps each (ΔT = 50 K), where backbone and ligand restraints were reduced from 10.0 kcal/mol to 5 kcal/mol. Full equilibration was performed in the NVT ensemble (100 ps, ligand and backbone restraints = 5.0 kcal/mol) and in the NPT ensemble (1 step of 200 ps, ligand and backbone restraints = 5 kcal/mol; 3 steps of 100 ps each, reducing the ligand and backbone restraints from 5.0 kcal/mol to 1.0 kcal/mol, and 1 step 1 ns with 1.0 kcal/mol of ligand and backbone restraints). Finally, unrestrained production runs were run at 300K for 4 ns. An electrostatic cutoff of 8.0 Å, and the SHAKE algorithm were applied to all the calculations. Six independent simulations for each complex were run on GPU and on CPUs.

When needed, RMSD analyses of backbone atoms were made to assess the system stability, and solute – solvent H-bonds (donor – acceptor distance = 4.0 Å, angle = 150°) and grid (cubic box 50 Å ×50 Å ×50 Å, mesh = 0.5 Å, centered on interfacial residues) analyses were performed with *cpptraj*.

Nwat-MMPB/GBSA. MMGBSA analyses were performed with the MMPBSA.py python script implemented in the Amber14 package. The analyses were conducted on either the 1st or the 4th ns of the production runs by selecting 100 evenly spaced out snapshots. The GB-Neck2 implicit solvent model was chosen for the GB calculations, and a salt molar concentration in solution was set at 0.15 M. During the analyses the entropic term was neglected.

When explicit water molecules were considered during the MMPB/GBSA calculations the same approach described in Chapter 8.1.3 was followed.

The water molecules (depending on the chosen Nwat) were considered as part of the protein considered as the receptor.

The square of Pearson's correlation coefficient (r^2) between experimental ΔG_{bind} and computed binding energies was used as an evaluation metric.

The whole process (from ligand parametrization to MMGBSA) has been automatized with a *tcsh* script reported as Annex 11.F.

12 CONCLUSIONS

In the wide field of PPIs, this PhD project has been focused on the optimization and application of computational methods for the design of PPIs modulators, with a particular interest toward peptide modulators targeting PPIs involving helical motifs.

In this contest, the first part of the project has been aimed to define the rationales behind the helical secondary structure stabilization and the helical screw sense selectivity exerted by chiral Cα-tetrasubstituted amino acids (cCTAAs) through REMD simulations and QTAIM analyses, and the mechanisms responsible of the helical screw sense inversion through PNEB simulations.

In detail, it has been found that the helical motif is stabilized by two complementary mechanisms: the first depends on the steric hindrance exerted by the cCTAA in an area parallel to the peptide helix axis and downstream of the cCTAA itself, whereas the second consists in the strengthening of the helical H-bond network thanks to peculiar C-H···O=C interactions. Analogously, *P*-helical screw sense selectivity is ascribable to the cCTAA steric hindrance parallel to the peptide helix axis, without particular preferences for the region downstream and upstream of the cCTAA, together with quite strong noncovalent interactions, consisting of classical N – H···O=C H-bonds and weak C – H···O=C interactions. Furthermore, PNEB simulations performed on achiral peptides of different lengths suggest that the helical screw sense inversion requires the formation of γ-turns, although a preferential screw sense inversion direction was not found.

Therefore, the knowledge gained from these studies could be helpful in designing stable helical peptides, having a preferential screw sense and that can be in principle activated *in situ* by inducing a conformational switch from *P* to *M* helix or *vice versa*.

Conversely, the second part of the project has been focused on the optimization of an MMGBSA based method, called Nwat-MMGBSA, aimed to improve the correlation between predicted binding energies of PPI complexes and experimental data. This approach, consisting in the inclusion, as part of the receptor, of hydration shells around the ligand during the MMGBSA calculations, was initially tested on

classical receptor-ligand complexes and, then, automatized, optimized and tested on PPI complexes.

This approach turned out to be good for the evaluation of PPI modulators activities, from different points of view. First of all, when water played a significant role in mediating protein-ligand interactions, the application of Nwat-MMGBSA improved the correlation between predicted and experimental data. On the other hand, if the solvent does not explicitly participate to the interaction, it did not give detrimental results compared to those obtained with the standard approach. In addition, the protocol proved to be robust and reproducible, giving equivalent results by using different setups. Furthermore, although an optimal number of water molecules to include in the hydration shell could not be found, in the case of PPI interactions inhibited by small molecules the inclusion of 50 – 60 water molecules appears to be a good choice. A non-negligible advantage of this approach is represented by the possibility to automatize it, making it applicable for drug design/discovery purposes.

Therefore, although further evaluations are needed, most of all on larger datasets, the knowledge coming from the combination of both parts of the project can be exploited for the design of stable non-natural peptides targeting PPIs.

13 BIBLIOGRAPHY

(1) Fischer, P. M. *Drug Des. Rev. - Online* **2005**, *2*, 179.

(2) Metz, A.; Ciglia, E.; Gohlke, H. *Curr. Pharm. Des.* **2012**, *18*, 4630.

(3) Zinzalla, G.; Thurston, D. E. *Future Med. Chem.* **2009**, *1*, 65.

(4) Cory, S.; Adams, J. M. *Nat. Rev. Cancer* **2002**, *2*, 647.

(5) Villunger, A.; Scott, C.; Bouillet, P.; Strasser, A. *Blood* **2003**, *101*, 2393.

(6) Xenarios, I.; Eisenberg, D. *Curr. Opin. Biotechnol.* **2001**, *12*, 334.

(7) Wells, J. a; McClendon, C. L. *Nature* **2007**, *450*, 1001.

(8) Blazer, L. L.; Neubig, R. R. *Neuropsychopharmacology* **2009**, *34*, 126.

(9) Ryan, D. P.; Matthews, J. M. *Curr. Opin. Struct. Biol.* **2005**, *15*, 441.

(10) Arkin, M. R.; Whitty, A. *Curr. Opin. Chem. Biol.* **2009**, *13*, 284.

(11) Chène, P. *ChemMedChem* **2006**, *1*, 400.

(12) Gerrard, J. A.; Hutton, C. A.; Perugini, M. A. *Mini-Reviews Med. Chem.* **2007**, *7*, 151.

(13) Mullard, A. *Nat. Rev. Drug Discov.* **2012**, *11*, 173.

(14) Fry, D. C. *Biopolymers* **2006**, *84*, 535.

(15) Cheng, A. C.; Coleman, R. G.; Smyth, K. T.; Cao, Q.; Soulard, P.; Caffrey, D. R.; Salzberg, A. C.; Huang, E. S. *Nat. Biotechnol.* **2007**, *25*, 71.

(16) Horton, N.; Lewis, M. *Protein Sci.* **2008**, *1*, 169.

(17) Janin, J.; Chothia, C. *J. Biol. Chem.* **1990**, *265*, 16027.

(18) Jones, S.; Thornton, J. M. *Proc. Natl. Acad. Sci. U. S. A.* **1996**, *93*, 13.

(19) Lo Conte, L.; Chothia, C.; Janin, J. *J. Mol. Biol.* **1999**, *285*, 2177.

(20) Hopkins, A. L.; Groom, C. R. *Nat. Rev. Drug Discov.* **2002**, *1*, 727.

(21) Deeds, E. J.; Ashenberg, O.; Gerardin, J.; Shakhnovich, E. I. *Proc. Natl. Acad. Sci.* **2007**, *104*, 14952.

(22) Keskin, O.; Ma, B.; Nussinov, R. *J. Mol. Biol.* **2005**, *345*, 1281.

(23) Berg, T. *Angew. Chemie Int. Ed.* **2003**, *42*, 2462.

(24) Checco, J. W.; Lee, E. F.; Evangelista, M.; Sleebs, N. J.; Rogers, K.; Pettikiriarachchi, A.; Kershaw, N. J.; Eddinger, G. A.; Belair, D. G.; Wilson, J. L.; Eller, C. H.; Raines, R. T.; Murphy, W. L.; Smith, B. J.; Gellman, S. H.; Fairlie, W. D. *J. Am. Chem. Soc.* **2015**, *137*, 11365.

(25) Pieraccini, S.; Saladino, G.; Cappelletti, G.; Cartelli, D.; Francescato, P.;

Speranza, G.; Manitto, P.; Sironi, M. *Nat. Chem.* **2009**, *1*, 642.

(26) Miller, M. *Curr. Protein Pept. Sci.* **2009**, *10*, 244.

(27) Ferri, N.; Corsini, A.; Bottino, P.; Clerici, F.; Contini, A. *J. Med. Chem.* **2009**, *52*, 4087.

(28) Moreira, I. S.; Fernandes, P. A.; Ramos, M. J. *Proteins* **2007**, *68*, 803.

(29) DeLano, W. L. *Curr. Opin. Struct. Biol.* **2002**, *12*, 14.

(30) Bogan, A. A.; Thorn, K. S. *J. Mol. Biol.* **1998**, *280*, 1.

(31) Thorn, K. S.; Bogan, A. A. *Bioinformatics* **2001**, *17*, 284.

(32) Keskin, O.; Gursoy, A.; Ma, B.; Nussinov, R. *Chem. Rev.* **2008**, *108*, 1225.

(33) Reichmann, D.; Rahat, O.; Albeck, S.; Meged, R.; Dym, O.; Schreiber, G. *Proc. Natl. Acad. Sci. U. S. A.* **2005**, *102*, 57.

(34) Nero, T. L.; Morton, C. J.; Holien, J. K.; Wielens, J.; Parker, M. W. *Nat. Rev. Cancer* **2014**, *14*, 248.

(35) Rodier, F.; Bahadur, R. P.; Chakrabarti, P.; Janin, J. *Proteins Struct. Funct. Bioinforma.* **2005**, *60*, 36.

(36) Lawrence, M. C.; Colman, P. M. *J. Mol. Biol.* **1993**, *234*, 946.

(37) Chakrabarti, P.; Janin, J. *Proteins Struct. Funct. Genet.* **2002**, *47*, 334.

(38) Lichtarge, O.; Bourne, H. R.; Cohen, F. E. *J. Mol. Biol.* **1996**, *257*, 342.

(39) Ma, B.; Elkayam, T.; Wolfson, H.; Nussinov, R. *Proc. Natl. Acad. Sci. U. S. A.* **2003**, *100*, 5772.

(40) Fernández, A. *FEBS Lett.* **2002**, *527*, 166.

(41) Sheinerman, F. *Curr. Opin. Struct. Biol.* **2000**, *10*, 153.

(42) Xu, D.; Lin, S. L.; Nussinov, R. *J. Mol. Biol.* **1997**, *265*, 68.

(43) Egner, U.; Hillig, R. C. *Expert Opin. Drug Discov.* **2008**.

(44) Bullock, B. N.; Jochim, A. L.; Arora, P. S. *J. Am. Chem. Soc.* **2011**, *133*, 14220.

(45) Jochim, A. L.; Arora, P. S. *Mol. Biosyst.* **2009**, *5*, 924.

(46) Kussie, P. H. *Science (80-.).* **1996**, *274*, 948.

(47) Janin, J. *Structure* **1999**, *7*, R277.

(48) Pelletier, H.; Kraut, J. *Science (80-.).* **1992**, *258*, 1748.

(49) Chong, S.-H.; Ham, S. *Proc. Natl. Acad. Sci.* **2012**, *109*, 7636.

(50) Ahmed, M. H.; Spyrakis, F.; Cozzini, P.; Tripathi, P. K.; Mozzarelli, A.;

Scarsdale, J. N.; Safo, M. A.; Kellogg, G. E. *PLoS One* **2011**, *6*, e24712.

(51) Sackett, D. L.; Sept, D. *Nat. Chem.* **2009**, *1*, 596.

(52) Thiel, P.; Kaiser, M.; Ottmann, C. *Angew. Chemie Int. Ed.* **2012**, *51*, 2012.

(53) Gao, Y.; Dickerson, J. B.; Guo, F.; Zheng, J.; Zheng, Y. *Proc. Natl. Acad. Sci. U. S. A.* **2004**, *101*, 7618.

(54) Zhang, G.; Liu, Y.; Ruoho, A. E.; Hurley, J. H. *Nature* **1997**, *386*, 247.

(55) Löwe, J.; Li, H.; Downing, K. H.; Nogales, E. *J. Mol. Biol.* **2001**, *313*, 1045.

(56) Vassiliev, V.; National, N. C. I. **2011**.

(57) Grasberger, B. L.; Lu, T.; Schubert, C.; Parks, D. J.; Carver, T. E.; Koblish, H. K.; Cummings, M. D.; LaFrance, L. V; Milkiewicz, K. L.; Calvo, R. R.; Maguire, D.; Lattanze, J.; Franks, C. F.; Zhao, S.; Ramachandren, K.; Bylebyl, G. R.; Zhang, M.; Manthey, C. L.; Petrella, E. C.; Pantoliano, M. W.; Deckman, I. C.; Spurlino, J. C.; Maroney, A. C.; Tomczuk, B. E.; Molloy, C. J.; Bone, R. F. *J. Med. Chem.* **2005**, *48*, 909.

(58) Azzarito, V.; Long, K.; Murphy, N. S.; Wilson, A. J. *Nat. Chem.* **2013**, *5*, 161.

(59) Orner, B. P.; Ernst, J. T.; Hamilton, A. D. *J. Am. Chem. Soc.* **2001**, *123*, 5382.

(60) Ernst, J. T.; Kutzki, O.; Debnath, A. K.; Jiang, S.; Lu, H.; Hamilton, A. D. *Angew. Chem. Int. Ed. Engl.* **2002**, *41*, 278.

(61) Kutzki, O.; Park, H. S.; Ernst, J. T.; Orner, B. P.; Yin, H.; Hamilton, A. D. *J. Am. Chem. Soc.* **2002**, *124*, 11838.

(62) Ahrens, V. M.; Bellmann-Sickert, K.; Beck-Sickinger, A. G. *Future Med. Chem.* **2012**, *4*, 1567.

(63) Rubinstein, M.; Niv, M. Y. *Biopolymers* **2009**, *91*, 505.

(64) Venkatraman, J.; Shankaramma, S. C.; Balaram, P. *Chem. Rev.* **2001**, *101*, 3131.

(65) Marshall, S. A.; Lazar, G. A.; Chirino, A. J.; Desjarlais, J. R. *Drug Discov. Today* **2003**, *8*, 212.

(66) Andrews, M. J. I.; Tabor, A. B. *Tetrahedron* **1999**, *55*, 11711.

(67) Garner, J.; Harding, M. M. *Org. Biomol. Chem.* **2007**, *5*, 3577.

(68) Patgiri, A.; Jochim, A. L.; Arora, P. S. *Acc. Chem. Res.* **2008**, *41*, 1289.

(69) Blackwell, H. E.; Grubbs, R. H. *Angew. Chemie Int. Ed.* **1998**, *37*, 3281.

(70) Schafmeister, C. E.; Po, J.; Verdine, G. L. *J. Am. Chem. Soc.* **2000**, *122*, 5891.

(71) Cheng, R. P.; Gellman, S. H.; DeGrado, W. F. *Chem. Rev.* **2001**, *101*, 3219.

(72) Maffucci, I.; Pellegrino, S.; Clayden, J.; Contini, A. *J. Phys. Chem. B* **2015**, *119*, 1350.

(73) Pellegrino, S.; Bonetti, A.; Clerici, F.; Contini, A.; Moretto, A.; Soave, R.; Gelmi, M. L. *J. Org. Chem.* **2015**, *80*, 5507.

(74) Zhou, P.; Wang, C.; Ren, Y.; Yang, C.; Tian, F. *Curr. Med. Chem.* **2013**, *20*, 1985.

(75) Pérot, S.; Sperandio, O.; Miteva, M. A.; Camproux, A.-C.; Villoutreix, B. O. *Drug Discov. Today* **2010**, *15*, 656.

(76) Brylinski, M.; Skolnick, J. *Proc. Natl. Acad. Sci. U. S. A.* **2008**, *105*, 129.

(77) Najmanovich, R.; Kurbatova, N.; Thornton, J. *Bioinformatics* **2008**, *24*, i105.

(78) Eyrisch, S.; Helms, V. *J. Med. Chem.* **2007**, *50*, 3457.

(79) Metz, A.; Pfleger, C.; Kopitz, H.; Pfeiffer-Marek, S.; Baringhaus, K.-H.; Gohlke, H. *J. Chem. Inf. Model.* **2012**, *52*, 120.

(80) Moreira, I.; Fernandes, P.; Ramos, M. In *Molecular Materials with Specific Interactions – Modeling and Design SE - 6*; Sokalski, W. A., Ed.; Challenges and Advances in Computational Chemistry and Physics; Springer Netherlands, 2007; Vol. 4, pp 305–339.

(81) Gohlke, H.; Case, D. A. *J. Comput. Chem.* **2004**, *25*, 238.

(82) Bienstock, R. J. *Curr. Pharm. Des.* **2012**, *18*, 1240.

(83) Aqvist, J.; Luzhkov, V. B.; Brandsdal, B. O. *Acc. Chem. Res.* **2002**, *35*, 358.

(84) Pearlman, D. A.; Charifson, P. S. *J. Med. Chem.* **2001**, *44*, 3417.

(85) Price, D. J.; Jorgensen, W. L. *J. Comput. Aided. Mol. Des. 15*, 681.

(86) Maffucci, I.; Clayden, J.; Contini, A. *J. Phys. Chem. B* **2015**, *119*, 14003.

(87) Clerici, F.; Ruffoni, A.; Contini, A.; Soave, R.; Lo Presti, L.; Esposto, I.; Nava, D.; Pellegrino, S.; Gelmi, M. L.; Maffucci, I. *RSC Adv.* **2015**, 32643.

(88) Maffucci, I.; Contini, A. *under Revis.*

(89) Maffucci, I.; Contini, A. *J. Chem. Theory Comput.* **2013**, *9*, 2706.

(90) Maffucci, I.; Contini, A. In *Frontiers in Computational Chemistry Volume 1*; Bentham Science, 2015; pp 82–120.

(91) Gentilucci, L.; De Marco, R.; Cerisoli, L. *Curr. Pharm. Des.* **2010**, *16*, 3185.

(92) Pellegrino, S.; Contini, A.; Gelmi, M. L.; Lo Presti, L.; Soave, R.; Erba, E. *J. Org. Chem.* **2014**, *79*, 3094.

(93) Pellegrino, S.; Contini, A.; Clerici, F.; Gori, A.; Nava, D.; Gelmi, M. L. *Chem. – A Eur. J.* **2012**, *18*, 8705.

(94) Clayden, J.; Castellanos, A.; Solà, J.; Morris, G. A. *Angew. Chemie Int. Ed.* **2009**, *48*, 5962.

(95) Zotti, M. De; Formaggio, F.; Crisma, M.; Peggion, C.; Moretto, A.; Toniolo, C. *J. Pept. Sci.* **2014**, *20*, 307.

(96) Byrne, L.; Solà, J.; Boddaert, T.; Marcelli, T.; Adams, R. W.; Morris, G. A.; Clayden, J. *Angew. Chemie Int. Ed.* **2014**, *53*, 151.

(97) Chilakamarri, K. B.; Criner, O. H. *Adv. Chem. Model.* **2011**, *1*, 377.

(98) Novotny, M.; Kleywegt, G. J. *J. Mol. Biol.* **2005**, *347*, 231.

(99) Brioche, J.; Pike, S. J.; Tshepelevitsh, S.; Leito, I.; Morris, G. A.; Webb, S. J.; Clayden, J. *J. Am. Chem. Soc.* **2015**, *137*, 6680.

(100) Nevola, L.; Giralt, E. *Chem. Commun.* **2015**, *51*, 3302.

(101) Rognan, D. *Med Chem Commun* **2015**, *6*, 51.

(102) Adcock, S. A.; McCammon, J. A. *Chem. Rev.* **2006**, *106*, 1589.

(103) Sugita, Y.; Okamoto, Y. *Chem. Phys. Lett.* **1999**, *314*, 141.

(104) Leach, A. R. Molecular Modelling: Principles and applications. *Molecular Modelling: Principles and applications*, 2001, 26–161.

(105) Bader. *Atoms in Molecules: A Quantum Theory*; Clarenson: Oxford, U.K., 1990.

(106) Boyd, R. J. *An Introduction to the Quantum Theory of Atoms in Molecules*; 2007.

(107) Mills, G.; Jónsson, H. *Phys. Rev. Lett.* **1994**, *72*, 1124.

(108) Mills, G.; Jónsson, H.; Schenter, G. K. *Surf. Sci.* **1995**, *324*, 305.

(109) Bergonzo, C.; Campbell, A. J.; Walker, R. C.; Simmerling, C. *Int. J. Quantum Chem.* **2009**, *109*, 3781.

(110) Pearlman, D. A.; Charifson, P. S. *J. Med. Chem.* **2001**, *44*, 3417.

(111) Srivastava, H. K.; Sastry, G. N. *J. Chem. Inf. Model.* **2012**, *52*, 3088.

(112) Massova, I.; Kollman, P. A. *Perspect. Drug Discov. Des. 18*, 113.

(113) Kollman, P. A.; Massova, I.; Reyes, C.; Kuhn, B.; Huo, S.; Chong, L.; Lee, M.; Lee, T.; Duan, Y.; Wang, W.; Donini, O.; Cieplak, P.; Srinivasan, J.; Case, D. A.; Cheatham, T. E. *Acc. Chem. Res.* **2000**, *33*, 889.

(114) Xu, L.; Sun, H.; Li, Y.; Wang, J.; Hou, T. *J. Phys. Chem. B* **2013**, *117*, 8408.

(115) Jackson, J. D. *Classical Electrodynamics*; Wiley: New York, 1999.

(116) Still, W. C.; Tempczyk, A.; Hawley, R. C.; Hendrickson, T. *J. Am. Chem. Soc.*

1990, *112*, 6127.

(117) Constanciel, R.; Contreras, R. *Theor. Chim. Acta* **1984**, *65*, 1.

(118) Homeyer, N.; Gohlke, H. *Mol. Inform.* **2012**, *31*, 114.

(119) Wallnoefer, H. G.; Liedl, K. R.; Fox, T. *J. Comput. Chem.* **2011**, *32*, 1743.

(120) Wong, S.; Amaro, R. E.; McCammon, J. A. *J. Chem. Theory Comput.* **2009**, *5*, 422.

(121) Ruffoni, A.; Ferri, N.; Bernini, S. K.; Ricci, C.; Corsini, A.; Maffucci, I.; Clerici, F.; Contini, A. *J. Med. Chem.* **2014**, *57*, 2953.

(122) Craik, D. J.; Fairlie, D. P.; Liras, S.; Price, D. *Chem. Biol. Drug Des.* **2013**, *81*, 136.

(123) Ruffoni, A.; Contini, A.; Soave, R.; Lo Presti, L.; Esposto, I.; Maffucci, I.; Nava, D.; Pellegrino, S.; Gelmi, M. L.; Clerici, F. *RSC Adv.* **2015**, 32643.

(124) Best, R. B. *Curr. Opin. Struct. Biol.* **2012**, *22*, 52.

(125) Nguyen, H.; Maier, J.; Huang, H.; Perrone, V.; Simmerling, C. *J. Am. Chem. Soc.* **2014**, 1.

(126) Chowdhury, S.; Lee, M. C.; Xiong, G.; Duan, Y. *J. Mol. Biol.* **2003**, *327*, 711.

(127) Jayachandran, G.; Vishal, V.; Pande, V. S. *J. Chem. Phys.* **2006**, *124*.

(128) Pitera, J. W.; Swope, W. *Proc. Natl. Acad. Sci. U. S. A.* **2003**, *100*, 7587.

(129) Lei, H.; Wu, C.; Liu, H.; Duan, Y. *Proc. Natl. Acad. Sci. U. S. A.* **2007**, *104*, 4925.

(130) Shaw, D. E.; Dror, R. O.; Salmon, J. K.; Grossman, J. P.; Mackenzie, K M, et al. In *Proceedings of the Conference on High Performance Computing, Networking, Storage and Analysis (SC09)*; New York: ACM, 2009.

(131) Shaw, D. E.; Maragakis, P.; Lindorff-Larsen, K.; Piana, S.; Shan, Y.; Wriggers, W. *Science (80-.).* **2010**, *330*, 341.

(132) Stone, J. E.; Hardy, D. J.; Ufimtsev, I. S.; Schulten, K. *J. Mol. Graph. Model.* **2010**, *29*, 116.

(133) Prinz, J. H.; Wu, H.; Sarich, M.; Keller, B.; Senne, M.; Held, M.; Chodera, J. D.; Schtte, C.; Noé, F. *J. Chem. Phys.* **2011**, *134*.

(134) Lei, H.; Duan, Y. *Curr. Opin. Struct. Biol.* **2007**, 187.

(135) Maier, J. A.; Martinez, C.; Kasavajhala, K.; Wickstrom, L.; Hauser, K. E.; Simmerling, C. *J. Chem. Theory Comput.* **2015**, *11*, 3696.

(136) Lindorff-Larsen, K.; Piana, S.; Palmo, K.; Maragakis, P.; Klepeis, J. L.; Dror, R. O.; Shaw, D. E. *Proteins Struct. Funct. Bioinforma.* **2010**, *78*, 1950.

(137) Shell, M. S.; Ritterson, R.; Dill, K. A. *J. Phys. Chem. B* **2008**, *112*, 6878.

(138) Lindorff-Larsen, K.; Maragakis, P.; Piana, S.; Eastwood, M. P.; Dror, R. O.; Shaw, D. E. *PLoS One* **2012**, *7*, 1.

(139) Lange, O. F.; Spoel, D. Van Der; Groot, B. L. De. *Biophys. J.* **2010**, *99*, 647.

(140) Best, R. B.; Buchete, N.-V.; Hummer, G. *Biophys. J.* **2008**, *95*, L07.

(141) Hornak, V.; Abel, R.; Okur, A.; Strockbine, B.; Roitberg, A.; Simmerling, C. *Proteins Struct. Funct. Bioinforma.* **2006**, *65*, 712.

(142) Kührová, P.; De Simone, A.; Otyepka, M.; Best, R. B. *Biophys. J.* **2012**, *102*, 1897.

(143) Lwin, T.; Luo, R. *Protein Sci.* **2006**, *15*, 2642.

(144) Martín-García, F.; Papaleo, E.; Gomez-Puertas, P.; Boomsma, W.; Lindorff-Larsen, K. *PLoS One* **2015**, *10*, e0121114.

(145) Piana, S.; Lindorff-Larsen, K.; Shaw, D. E. *Biophys. J.* **2011**, *100*, L47.

(146) Raucci, R.; Colonna, G.; Castello, G.; Costantini, S. *Int. J. Pept. Res. Ther.* **2013**, *19*, 117.

(147) Todorova, N.; Legge, F. S.; Treutlein, H.; Yarovsky, I. *J. Phys. Chem. B* **2008**, *112*, 11137.

(148) Yoda, T.; Sugita, Y.; Okamoto, Y. *Chem. Phys. Lett.* **2004**, *386*, 460.

(149) Yoda, T.; Sugita, Y.; Okamoto, Y. *Chem. Phys.* **2004**, *307*, 269.

(150) Zagrovic, B.; Sorin, E. J.; Pande, V. *J. Mol. Biol.* **2001**, *313*, 151.

(151) Zhou, R.; Berne, B. J. *Proc. Natl. Acad. Sci. U. S. A.* **2002**, *99*, 12777.

(152) Ono, S.; Nakajima, N.; Higo, J.; Nakamura, H. *J. Comput. Chem.* **2000**, *21*, 748.

(153) Henriques, J.; Cragnell, C.; Skepö, M. *J. Chem. Theory Comput.* **2015**, 150616124431001.

(154) Palazzesi, F.; Prakash, M. K.; Bonomi, M.; Barducci, A. *J. Chem. Theory Comput.* **2015**, *11*, 2.

(155) Best, R. B.; Mittal, J. *J. Phys. Chem. B* **2010**, *114*, 8790.

(156) Cino, E. a.; Choy, W. Y.; Karttunen, M. *J. Chem. Theory Comput.* **2012**, *8*, 2725.

(157) Simmerling, C.; Strockbine, B.; Roitberg, A. E.; Gaines, V. *J. Am. Chem. Soc.* **2002**, *124*, 11258.

(158) Yang, C.; Kim, E.; Pak, Y. *Bull. Korean Chem. Soc.* **2014**, *35*, 4.

(159) Zhou, R. *Proteins Struct.* **2003**, *161*, 148.

(160) Ozkan, S. B.; Wu, G. A.; Chodera, J. D.; Dill, K. a. *Proc. Natl. Acad. Sci. U. S. A.* **2007**, *104*, 11987.

(161) Jang, S.; Shin, S.; Pak, Y. *J. Am. Chem. Soc.* **2002**, *124*, 4976.

(162) Jang, S.; Kim, E.; Pak, Y. *Proteins* **2006**, *62*, 663.

(163) Dyson, H. J.; Wright, P. E. *Nat. Rev. Mol. Cell Biol.* **2005**, *6*, 197.

(164) Tompa, P. *Trends Biochem. Sci.* **2012**, *37*, 509.

(165) De Simone, A.; Kitchen, C.; Kwan, A. H.; Sunde, M.; Dobson, C. M.; Frenkel, D. *Proc. Natl. Acad. Sci. U. S. A.* **2012**, *109*, 6951.

(166) Barducci, A.; Bonomi, M.; Prakash, M. K.; Parrinello, M. *Proc. Natl. Acad. Sci. U. S. A.* **2013**, *110*, E4708.

(167) Kollman, P. A. *Acc. Chem. Res.* **1996**, *29*, 461.

(168) Nerenberg, P. S.; Head-gordon, T. *J. Chem. Theory Comput.* **2011**, *7*, 1220.

(169) Zgarbová, M.; Otyepka, M.; Šponer, J.; Mládek, A.; Banáš, P.; Cheatham, T. E.; Jurečka, P. *J. Chem. Theory Comput.* **2011**, *7*, 2886.

(170) Maier, J. A.; Martinez, C.; Kasavajhala, K.; Wickstrom, L.; Hauser, K. E.; Simmerling, C. *J. Chem. Theory Comput.* **2015**, *ASAP*.

(171) Hawkins, G. D.; Cramer, C. J.; Truhlar, D. G. *Chem. Phys. Lett.* **1995**, *246*, 122.

(172) Onufriev, A.; Bashford, D.; Case, D. A. *Proteins Struct. Funct. Bioinforma.* **2004**, *55*, 383.

(173) Nguyen, H.; Roe, D. R.; Simmerling, C. *J. Chem. Theory Comput.* **2013**, *9*, 2020.

(174) D'Andrea, L. D.; Iaccarino, G.; Fattorusso, R.; Sorriento, D.; Carannante, C.; Capasso, D.; Trimarco, B.; Pedone, C. *Proc. Natl. Acad. Sci. U. S. A.* **2005**, *102*, 14215.

(175) Francis, A. K.; Iqbal, M.; Balaram, P.; Vijayan, M. *Biopolymers* **1983**, *22*, 1499.

(176) Blanco, F. J.; Rivas, G.; Serrano, L. *Nature* **1994**, *12*, 994.

(177) Cochran, A. G.; Skelton, N. J.; Starovasnik, M. A. *Proc. Natl. Acad. Sci. U. S. A.* **2002**, *99*, 4145.

(178) Vijay-Kumar, S.; Bugg, C. E.; Cook, W. J. *J. Mol. Biol.* **1987**, *194*, 531.

(179) de Souza, B. M.; Da Silva, A. V. R.; Resende, V. M. F.; Arcuri, H. A.; dos Santos Cabrera, M. P.; Ruggiero Neto, J.; Palma, M. S. *Peptides* **2009**, *30*, 1387.

(180) Charpentier, T. H.; Thompson, L. E.; Liriano, M. A.; Varney, K. M.; Wilder, P. T.; Pozharski, E.; Toth, E. A.; Weber, D. J. *J. Mol. Biol.* **2010**, *396*, 1227.

(181) Chen, J. *J. Am. Chem. Soc.* **2009**, *131*, 2088.

(182) Rustandi, R. R.; Baldisseri, D. M.; Weber, D. J. *Nat. Struct. Biol.* **2000**, *7*, 570.

(183) Staneva, I.; Huang, Y.; Liu, Z.; Wallin, S. *PLoS Comput. Biol.* **2012**, *8*, 1.

(184) Toniolo, C.; Maria, G.; Vincenzo, B.; Bavoso, A.; Benedetti, E.; Blasio, B. Di; Grimaldi, P.; Lelj, F.; Pavone, V.; Pedoneb, C. *Macromolecules* **1985**, *18*, 895.

(185) Longo, E.; Moretto, A.; Formaggio, F.; Toniolo, C. *Chirality* **2011**, *23*, 756.

(186) Karle, I. L. *Pept. Sci.* **2001**, *60*, 351.

(187) Ruffoni, A.; Contini, A.; Soave, R.; Lo Presti, L.; Esposto, I.; Maffucci, I.; Nava, D.; Pellegrino, S.; Gelmi, M. L.; Clerici, F. *RSC Adv.* **2015**, *5*, 32643.

(188) García, A. E.; Sanbonmatsu, K. Y. *Proc. Natl. Acad. Sci. U. S. A.* **2002**, *99*, 2782.

(189) Freddolino, P. L.; Liu, F.; Gruebele, M.; Schulten, K. *Biophys. J.* **2008**, *94*, L75.

(190) Pak, Y.; Kim, E.; Jang, S. *J. Chem. Phys.* **2004**, *121*, 9184.

(191) Geney, R.; Layten, M.; Gomperts, R.; Hornak, V.; Simmerling, C. *J. Chem. Theory Comput.* **2006**, *2*, 115.

(192) Case, D. A.; Babin, V.; Berryman, J. T.; Betz, R. M.; Cai, Q.; Cerutti, D. S.; T.E. Cheatham, I.; Darden, T. A.; Duke, R. E.; Gohlke, H.; Goetz, A. W.; Gusarov, S.; Homeyer, N.; Janowski, P.; Kaus, J.; Kolossváry, I.; Kovalenko, A.; Lee, T. S.; LeGrand, S.; Luchko, T.; Luo, R.; Madej, B.; Merz, K. M.; Paesani, F.; Roe, D. R.; Roitberg, A.; Sagui, C.; Salomon-Ferrer, R.; Seabra, G.; Simmerling, C. L.; Smith, W.; Swails, J.; Walker, R. C.; Wang, J.; Wolf, R. M.; Wu, X.; Kollman, P. A. *AMBER 14*; University of California, San Francisco, 2014.

(193) Toniolo, C.; Formaggio, F.; Kaptein, B.; Broxterman, Q. B. *Synlett* **2006**, *2006*, 1295.

(194) Crisma, M.; Peggion, C.; Moretto, A.; Banerjee, R.; Supakar, S.; Formaggio, F.; Toniolo, C. *Pept. Sci.* **2014**, *102*, 145.

(195) Boddaert, T.; Sola, J.; Helliwell, M.; Clayden, J. *Chem. Commun. (Camb).* **2012**, *48*, 3397.

(196) Ballano, G.; Zanuy, D.; Jiménez, A. I.; Cativiela, C.; Nussinov, R.; Alemán, C. *J. Phys. Chem. B* **2008**, *112*, 13101.

(197) Alemán, C.; Zanuy, D.; Casanovas, J.; Cativiela, C.; Nussinov, R. *J. Phys. Chem. B* **2006**, *110*, 21264.

(198) Maity, P.; König, B. *Pept. Sci.* **2008**, *90*, 8.

(199) Tanaka, M. *Chem. Pharm. Bull.* **2007**, *55*, 349.

(200) Ma, D.; Ding, K.; Tian, H.; Wang, B.; Cheng, D. *Tetrahedron: Asymmetry* **2002**, *13*, 961.

(201) Yamazaki, H.; Horikawa, H.; Nishitani, T.; Iwasaki, T.; Nosaka, K.; Tamaki, H. *Chem. Pharm. Bull. (Tokyo).* **1992**, *40*, 102.

(202) Cativiela, C.; López, P.; Mayoral, J. *Tetrahedron: Asymmetry* **1990**, *1*, 379.

(203) Caputo, F.; Clerici, F.; Gelmi, M. L.; Pellegrino, S.; Pocar, D. *Tetrahedron: Asymmetry* **2006**, *17*, 1430.

(204) Maki, Y.; Masugi, T.; Hiramitsu, T.; Ogiso, T. *Chem. Pharm. Bull. (Tokyo).* **1973**, *21*, 2460.

(205) Casanovas, J.; Revilla-López, G.; Crisma, M.; Toniolo, C.; Alemán, C. *J. Phys. Chem. B* **2012**, *116*, 13297.

(206) De Poli, M.; De Zotti, M.; Raftery, J.; Aguilar, J. A.; Morris, G. A.; Clayden, J. *J. Org. Chem.* **2013**, *78*, 2248.

(207) Demizu, Y.; Doi, M.; Kurihara, M.; Maruyama, T.; Suemune, H.; Tanaka, M. *Chem. – A Eur. J.* **2012**, *18*, 2430.

(208) Solà, J.; Morris, G. A.; Clayden, J. *J. Am. Chem. Soc.* **2011**, *133*, 3712.

(209) Pengo, Barbara Formaggio, Fernando Crisma, M.; Toniolo, C.; Bonora, Gian Maria Broxterman, Quirinus B. Kamphuis, J.; Saviano, M.; Iacovino, R.; Rossi, F.; Benedetti, E. *J. Chem. Soc. Perkin Trans. 2 Phys. Org. Chem.* **1998**, 1651.

(210) Inai, Y.; Kurokawa, Y.; Ida, A.; Hirabayashi, T. *Bull. Chem. Soc. Jpn.* **1999**, *72*, 55.

(211) Inai, Y.; Kurokawa, Y.; Kojima, N. *J. Chem. Soc. Perkin Trans. 2* **2002**, 1850.

(212) Avbelj, F.; Moult, J. *Biochemistry* **1995**, *34*, 755.

(213) Wang, J.; Purisima, E. O. *J. Am. Chem. Soc.* **1996**, *118*, 995.

(214) LaPointe, S. M.; Farrag, S.; Bohórquez, H. J.; Boyd, R. J. *J. Phys. Chem. B* **2009**, *113*, 10957.

(215) Shi, Z.; Olson, C. A.; Bell, A. J.; Kallenbach, N. R. *Pept. Sci.* **2001**, *60*, 366.

(216) Chang, C.; Bader, R. F. W. *J. Phys. Chem.* **1992**, *96*, 1654.

(217) Scheiner, S. *J. Phys. Chem. B* **2006**, *110*, 18670.

(218) Scheiner, S.; Kar, T.; Pattanayak, J. *J. Am. Chem. Soc.* **2002**, *124*, 13257.

(219) Dixon, S. L.; Smondyrev, A. M.; Knoll, E.; Rao, S. N.; Shaw, D.; Friesner, R. *J. Comput. Aided. Mol. Des.* **2006**, *67*, 647.

(220) Leone, S.; Mutti, C.; Kazantsev, A.; Sturlese, M.; Moro, S.; Cattaneo, E.; Rigamonti, D.; Contini, A. *Bioorg. Med. Chem.* **2008**, *16*, 5695.

(221) Caputo, F.; Clerici, F.; Gelmi, M. L.; Pellegrino, S.; Pocar, D. *Tetrahedron: Asymmetry* **2006**, *17*, 1430.

(222) Vener, M. V; Egorova, A. N.; Fomin, D. P.; Tsirelson, V. G. *Chem. Phys. Lett.* **2007**, *440*, 279.

(223) Koch, U.; Popelier, P. L. A. *J. Phys. Chem.* **1995**, *99*, 9747.

(224) Tang, T.-H.; Hu, W.-J.; Yan, D.-Y.; Cui, Y.-P. *J. Mol. Struct. THEOCHEM* **1990**, *207*, 319.

(225) Ruffoni, A.; Ferri, N.; Bernini, S. K.; Ricci, C.; Corsini, A.; Maffucci, I.; Clerici, F.; Contini, A. *J. Med. Chem.* **2014**, *57*, 2953.

(226) Wang, Z.-X.; Wu, C.; Lei, H.; Duan, Y. *J. Chem. Theory Comput.* **2007**, *3*, 1527.

(227) *Molecular Operating Environment (MOE)*, 2013.08 ed.; Chemical Computing Group Inc.: Montreal, 2013.

(228) Dupradeau, F.-Y.; Pigache, A.; Zaffran, T.; Savineau, C.; Lelong, R.; Grivel, N.; Lelong, D.; Rosanski, W.; Cieplak, P. *Phys. Chem. Chem. Phys.* **2010**, *12*, 7821.

(229) Caliński, T.; Harabasz, J. *Commun. Stat.* **1974**, *3*, 1.

(230) Kabsch, W.; Sander, C. *Biopolymers* **1983**, *22*, 2577.

(231) Humphrey, W.; Dalke, A.; Schulten, K. *J. Mol. Graph.* **1996**, *14*, 33.

(232) Grossfield, A. *WHAM: the weighted histogram analysis method*, 2.0.9 ed.

(233) Frisch, M. J.; Trucks, G. W.; Schlegel, H. B.; Scuseria, G. E.; Robb, M. A.; Cheeseman, J. R.; Scalmani, G.; Barone, V.; Mennucci, B.; Petersson, G. A.; Nakatsuji, H.; Caricato, M.; Li, X.; Hratchian, H. P.; Izmaylov, A. F.; Bloino, J.; Zheng, G.; Sonnenberg, J. L.; Hada, M.; Ehara, M.; Toyota, K.; Fukuda, R.; Hasegawa, J.; Ishida, M.; Nakajima, T.; Honda, Y.; Kitao, O.; Nakai, H.; Vreven, T.; Montgomery, J. A., J.; Peralta, J. E.; Ogliaro, F.; Bearpark, M.; Heyd, J. J.; Brothers, E.; Kudin, K. N.; Staroverov, V. N.; Kobayashi, R.; Normand, J.; Raghavachari, K.; Rendell, A.; Burant, J. C.; Iyengar, S. S.; Tomasi, J.; Cossi, M.; Rega, N.; Millam, J. M.; Klene, M.; Knox, J. E.; Cross, J. B.; Bakken, V.; Adamo, C.; Jaramillo, J.; Gomperts, R.; Stratmann, R. E.; Yazyev, O.; Austin, A. J.; Cammi, R.; Pomelli, C.; Ochterski, J. W.; Martin, R. L.; Morokuma, K.; Zakrzewski, V. G.; Voth, G. A.; Salvador, P.; Dannenberg, J. J.; Dapprich, S.; Daniels, A. D.; Farkas, Ö.; Foresman, J. B.; Ortiz, J. V.; Cioslowski, J.; Fox, D. J. *Gaussian 09*; Gaussian Inc.: Wallingford CT, 2009.

(234) Zhao, Y.; Truhlar, D. G. *J. Phys. Chem. A* **2004**, *108*, 6908.

(235) Contini, A.; Erba, E. *RSC Adv.* **2012**, *2*, 10652.

(236) Cossi, M.; Rega, N.; Scalmani, G.; Barone, V. *J. Comput. Chem.* **2003**, *24*, 669.

(237) Konig, F.B., F. B.; Schonbohm, J., J.; Bayles, D., D. *J. Comput. Chem.* **2001**, *22*, 545.

(238) De Poli, M.; De Zotti, M.; Raftery, J.; Aguilar, J. A.; Morris, G. A.; Clayden, J. *J. Org. Chem.* **2013**, *78*, 2248.

(239) Andreetto, E.; Peggion, C.; Crisma, M.; Toniolo, C. *Biopolymers* **2006**, *84*, 490.

(240) Shepherd, N. E.; Hoang, H. N.; Abbenante, G.; Fairlie, D. P. *J. Am. Chem. Soc.* **2009**, *131*, 15877.

(241) Grauer, A. A.; Cabrele, C.; Zabel, M.; König, B. *J. Org. Chem.* **2009**, *74*, 3718.

(242) Inai, Y.; Ashitaka, S.; Hirabayashi, T. *Polym. J.* **1999**, *31*, 246.

(243) Brown, R. A.; Marcelli, T.; De Poli, M.; Solà, J.; Clayden, J. *Angew. Chemie* **2012**, *51*, 1395.

(244) Royo, S.; De Borggraeve, W. M.; Peggion, C.; Formaggio, F.; Crisma, M.; Jiménez, A. I.; Cativiela, C.; Toniolo, C. *J. Am. Chem. Soc.* **2005**, *127*, 2036.

(245) De Poli, M.; Byrne, L.; Brown, R. A.; Solà, J.; Castellanos, A.; Boddaert, T.; Wechsel, R.; Beadle, J. D.; Clayden, J. *J. Org. Chem.* **2014**, *79*, 4659.

(246) Yamazaki, H.; Horikawa, H.; Nishitani, T.; Iwasaki, T.; Nosaka, K.; Tamaki, H. *Chem. Pharm. Bull.* **1992**, *40*, 102.

(247) Némethy, G.; Printz, M. P. *Macromolecules* **1972**, *5*, 755.

(248) Crisma, M.; Toniolo, C. *Biopolymers* **2015**, *104*, 46.

(249) Contini, A.; Erba, E. *RSC Adv.* **2012**, *2*, 10652.

(250) Konig, F. B.; Schonbohm, J., J.; Bayles, D., D. *J. Comput. Chem.* **2001**, *22*, 545.

(251) Smith, C. A.; Ban, D.; Pratihar, S.; Giller, K.; Schwiegk, C.; de Groot, B. L.; Becker, S.; Griesinger, C.; Lee, D. *Angew. Chem. Int. Ed. Engl.* **2015**, *54*, 207.

(252) Nevola, L.; Giralt, E. *Chem. Commun. (Camb).* **2015**, *51*, 3302.

(253) Nevola, L.; Martín-Quirós, A.; Eckelt, K.; Camarero, N.; Tosi, S.; Llobet, A.; Giralt, E.; Gorostiza, P. *Angew. Chemie Int. Ed.* **2013**, *52*, 7704.

(254) Kumita, J. R.; Smart, O. S.; Woolley, G. A. *Proc. Natl. Acad. Sci.* **2000**, *97*, 3803.

(255) Schierling, B.; Noël, A.-J.; Wende, W.; Hien, L. T.; Volkov, E.; Kubareva, E.; Oretskaya, T.; Kokkinidis, M.; Römpp, A.; Spengler, B.; Pingoud, A. *Proc. Natl. Acad. Sci. U. S. A.* **2010**, *107*, 1361.

(256) Yoshida, K.; Yamaguchi, T.; Okamoto, Y. *Chem. Phys. Lett.* **2005**, *412*, 280.

(257) Hwang, S.; Shao, Q.; Williams, H.; Hilty, C.; Gao, Y. Q. *J. Phys. Chem. B* **2011**, *115*, 6653.

(258) Bergonzo, C.; Campbell, A. J.; Walker, R. C.; Simmerling, C. *Int. J. Quantum Chem.* **2009**, *109*, 3781.

(259) D.A. Case, V. Babin, J.T. Berryman, R.M. Betz, Q. Cai, D.S. Cerutti, T.E. Cheatham, III, T.A. Darden, R.E. Duke, H. Gohlke, A.W. Goetz, S. Gusarov, N. Homeyer, P. Janowski, J. Kaus, I. Kolossváry, A. Kovalenko, T.S. Lee, S. LeGrand, T. Luchko, R. Luo, B., X. W. and P. A. K. AMBER 14, 2014.

(260) Calinski, T.; Harabasz, J. *Commun. Stat.* **1974**, *22*, 2577.

(261) Crisma, M.; De Zotti, M.; Moretto, A.; Peggion, C.; Drouillat, B.; Wright, K.; Couty, F.; Toniolo, C.; Formaggio, F. *New J. Chem.* **2015**.

(262) Grossfield, A. WHAM: the weighted histogram analysis method.

(263) Bergonzo, C.; Campbell, A. J.; de los Santos, C.; Grollman, A. P.; Simmerling, C. *J. Am. Chem. Soc.* **2011**, *133*, 14504.

(264) Van Nostrand, K. P.; Kennedy, S. D.; Turner, D. H.; Mathews, D. H. *J. Chem. Theory Comput.* **2011**, *7*, 3779.

(265) Ferri, N.; Radice, T.; Antonino, M.; Beccalli, E. M.; Tinelli, S.; Zunino, F.; Corsini, A.; Pratesi, G.; Ragg, E. M.; Gelmi, M. L.; Contini, A. *Bioorg. Med. Chem.* **2011**, *19*, 5291.

(266) Contini, A.; Cappelletti, G.; Cartelli, D.; Fontana, G.; Gelmi, M. L. *Mol. Biosyst.* **2012**, *8*, 3254.

(267) Hou, T.; Wang, J.; Li, Y.; Wang, W. *J. Chem. Inf. Model.* **2011**, *51*, 69.

(268) Hou, T.; Wang, J.; Li, Y.; Wang, W. *J. Comput. Chem.* **2011**, *32*, 866.

(269) Yang, T.; Wu, J. C.; Yan, C.; Wang, Y.; Luo, R.; Gonzales, M. B.; Dalby, K. N.; Ren, P. *Proteins* **2011**, *79*, 1940.

(270) Genheden, S.; Ryde, U. *Proteins* **2012**, *80*, 1326.

(271) Abel, R.; Salam, N. K.; Shelley, J.; Farid, R.; Friesner, R. A.; Sherman, W. *ChemMedChem* **2011**, *6*, 1049.

(272) Greenidge, P. A.; Kramer, C.; Mozziconacci, J.-C.; Wolf, R. M. *J. Chem. Inf. Model.* **2013**, *53*, 201.

(273) Checa, A.; Ortiz, A. R.; de Pascual-Teresa, B.; Gago, F. *J. Med. Chem.* **1997**, *40*, 4136.

(274) Greenidge, P. A.; Kramer, C.; Mozziconacci, J.-C.; Sherman, W. *J. Chem. Inf. Model.* **2014**, *54*, 2697.

(275) Treesuwan, W.; Hannongbua, S. *J. Mol. Graph. Model.* **2009**, *27*, 921.

(276) Henchman, R. H.; McCammon, J. A. *Protein Sci.* **2002**, *11*, 2080.

(277) Mikulskis, P.; Genheden, S.; Ryde, U. *J. Mol. Model.* **2014**, *20*, 2273.

(278) Staker, B. L.; Hjerrild, K.; Feese, M. D.; Behnke, C. A.; Burgin, A. B.; Stewart, L. *Proc. Natl. Acad. Sci. U. S. A.* **2002**, *99*, 15387.

(279) Genheden, S.; Ryde, U. *J. Comput. Chem.* **2010**, *31*, 837.

(280) Samorì, C.; Guerrini, A.; Varchi, G.; Fontana, G.; Bombardelli, E.; Tinelli, S.; Beretta, G. L.; Basili, S.; Moro, S.; Zunino, F.; Battaglia, A. *J. Med. Chem.* **2009**, *52*, 1029.

(281) Schiffer, C.; Hermans, J. Promise of advances in simulation methods for protein crystallography: implicit solvent models, time-averaging refinement, and quantum mechanical modeling. *Biochemistry and Molecular Pharmacology Publications and Presentations*, 2003, 412–461.

(282) Kongsted, J.; Ryde, U. *J. Comput. Aided. Mol. Des.* **2009**, *23*, 63.

(283) Weis, A.; Katebzadeh, K.; Söderhjelm, P.; Nilsson, I.; Ryde, U. *J. Med. Chem.* **2006**, *49*, 6596.

(284) Chhatriwala, H.; Jafri, N.; Salgia, R. *Cancer Biol. Ther.* **2014**, *5*, 1600.

(285) Case, D. A.; Cheatham, T. E.; Darden, T.; Gohlke, H.; Luo, R.; Merz, K. M.; Onufriev, A.; Simmerling, C.; Wang, B.; Woods, R. J. *J. Comput. Chem.* **2005**, *26*, 1668.

(286) Anandakrishnan, R.; Aguilar, B.; Onufriev, A. V. *Nucleic Acids Res.* **2012**, *40*, W537.

(287) C. Cézard, E. Vanquelef, J. Pecher, P. Sonnet, P. Cieplak, E. D.; Dupradeau, F.-Y. In *236th ACS National Meeting, Philadelphia, PA, USA, August 17*; 2008.

(288) Pugliese, L.; Coda, A.; Malcovati, M.; Bolognesi, M. *J. Mol. Biol.* **1993**, *231*, 698.

(289) Green, N. M. *Biochem. J.* **1966**, *101*, 774.

(290) Kuhn, B.; Kollman, P. A. *J. Med. Chem.* **2000**, *43*, 3786.

(291) Vreven, T.; Hwang, H.; Pierce, B. G.; Weng, Z. *Protein Sci.* **2012**, *21*, 396.

(292) Jorgensen, W. L.; Chandrasekhar, J.; Madura, J. D.; Impey, R. W.; Klein, M. L. *J. Chem. Phys.* **1983**, *79*, 926.

(293) Horn, H. W.; Swope, W. C.; Pitera, J. W.; Madura, J. D.; Dick, T. J.; Hura, G. L.; Head-Gordon, T. *J. Chem. Phys.* **2004**, *120*, 9665.

(294) Frigerio, F.; Coda, A.; Pugliese, L.; Lionetti, C.; Menegatti, E.; Amiconi, G.; Schnebli, H. .; Ascenzi, P.; Bolognesi, M. *J.Mol.Biol.* **1992**, *225*, 107.

(295) Hou, Z.; Bernstein, D. .; Fox, C. .; Keck, J. L. *Proc.Natl.Acad.Sci.Usa* **2005**, *102*, 8489.

(296) Song, H. .; Suh, S. W. *J.Mol.Biol.* **1998**, *275*, 347.

(297) Chrencik, J. .; Brooun, A.; Kraus, M. .; Recht, M. .; Kolatkar, A. .; Han, G. .; Seifert, J. .; Widmer, H.; Auer, M.; Kuhn, P. *J.Biol.Chem.* **2006**, *281*, 28185.

(298) Sevcik, J.; Urbanikova, L.; Dauter, Z.; Wilson, K. S. *Acta Crystallogr.,Sect.D* **1998**, *54*, 954.

(299) Simader, H.; Hothorn, M.; Kohler, C.; Basquin, J.; Simos, G.; Suck, D. *Nucleic Acids Res.* **2006**, *34*, 3968.

(300) Wiegand, G.; Epp, O.; Huber, R. *J.Mol.Biol.* **1995**, *247*, 99.

(301) Peschard, P.; Kozlov, G.; Lin, T.; Mirza, I. .; Berghuis, A. .; Lipkowitz, S.; Park, M.; Gehring, K. *Mol.Cell* **2007**, *27*, 474.

(302) Kuhlmann, U. .; Pommer, A. .; Moore, G. .; James, R.; Kleanthous, C. *J.Mol.Biol.* **2000**, *301*, 1163.

(303) Wang, S. .; Pandey, K. .; Scharfstein, J.; Whisstock, J.; Huang, R. .; Jacobelli, J.; Fletterick, R. .; Rosenthal, P. .; Abrahamson, M.; Brinen, L. .; Rossi, A.; Sali, A.; McKerrow, J. H. *Structure* **2007**, *15*, 535.

(304) Tsunemi, M.; Matsuura, Y.; Sakakibara, S.; Katsube, Y. *Biochemistry* **1996**, *35*, 11570.

(305) Takeuchi, Y.; Satow, Y.; Nakamura, K. .; Mitsui, Y. *J.Mol.Biol.* **1991**, *221*, 309.

(306) Hurley, J. .; Faber, H. .; Worthylake, D.; Meadow, N. .; Roseman, S.; Pettigrew, D. .; Remington, S. J. *Science (80-.).* **1993**, *259*, 673.

(307) McPhalen, C. .; James, M. N. *Biochemistry* **1988**, *27*, 6582.

(308) Bewley, M. .; Springer, K.; Zhang, Y. .; Freimuth, P.; Flanagan, J. M. *Science (80-.).* **1999**, *286*, 1579.

(309) Paesen, G. .; Siebold, C.; Harlos, K.; Peacey, M. .; Nuttall, P. .; Stuart, D. I. *J.Mol.Biol.* **2007**, *368*, 1172.

(310) Horn, J. .; Ramaswamy, S.; Murphy, K. P. *J.Mol.Biol.* **2003**, *331*, 497.

(311) Cho, S.; Swaminathan, C. .; Kerzic, M. .; Guan, R.; Yang, J.; Kieke, M. .; Andersen, P. .; Krantz, D. .; Mariuzza, R. .; Eric, S. J. *To be Publ.*

(312) Wang, S. .; Pandey, K. .; Somoza, J. .; Sijwali, P. .; Kortemme, T.; Brinen, L. .; Fletterick, R. .; Rosenthal, P. .; McKerrow, J. H. *Proc.Natl.Acad.Sci.Usa* **2006**, *103*, 11503.

(313) Read, R. .; Fujinaga, M.; Sielecki, A. .; James, M. N. *Biochemistry* **1983**, *22*, 4420.

(314) Oehme, D. P.; Brownlee, R. T. C.; Wilson, D. J. D. *J. Comput. Chem.* **2012**, *33*, 2566.

(315) De Turiso, F. G. L.; Sun, D.; Rew, Y.; Bartberger, M. D.; Beck, H. P.; Canon, J.; Chen, A.; Chow, D.; Correll, T. L.; Huang, X.; Julian, L. D.; Kayser, F.; Lo, M. C.; Long, A. M.; McMinn, D.; Oliner, J. D.; Osgood, T.; Powers, J. P.; Saiki, A. Y.; Schneider, S.; Shaffer, P.; Xiao, S. H.; Yakowec, P.; Yan, X.; Ye, Q.; Yu, D.; Zhao, X.; Zhou, J.; Medina, J. C.; Olson, S. H. *J. Med. Chem.* **2013**, *56*, 4053.

(316) Lessene, G.L., Czabotar, P.E., Sleebs, B.E., Zobel, K., Lowes, K.L., Adams, J.M., Baell, J.B., Colman, P.M., Deshayes, K., Fairbrother, W.J., Flygare, J.A., Gibbons, P., Kersten, W.J.A., Kulasegaram, S., Moss, R.M., Parisot, J.P., Smith, B. J. *Nat. Chem. Biol.* **2013**, *9*, 390.

(317) Kester, R. F.; Donnell, A. F.; Lou, Y.; Remiszewski, S. W.; Lombardo, L. J.; Chen, S.; Le, N. T.; Lo, J.; Moliterni, J. a.; Han, X.; Heather Hogg, J.; Liang, W.; Michoud, C.; Rupert, K. C.; Mischke, S.; Le, K.; Weisel, M.; Janson, C. a.; Lukacs, C. M.; Fretland, A. J.; Hong, K.; Polonskaia, A.; Gao, L.; Li, S.; Solis, D. S.; Aguilar, D.; Tardell, C.; Dvorozniak, M.; Tannu, S.; Lee, E. C.; Schutt, A. D.; Goggin, B. *J. Med. Chem.* **2013**, *56*, 7788.

(318) Shen, C. H. *Febs J.* **2010**, *277*, 3699.

(319) Olajuyigbe, F. M. . D. N. . G. S. *Cryst.Growth Des.* **2011**, *11*, 4378.

(320) Brik, A.; Wong, C.-H. *Org. Biomol. Chem.* **2003**, *1*, 5.

(321) Wang, J.; Wang, W.; Kollman, P. A.; Case, D. A. *J. Mol. Graph. Model.* **2006**, *25*, 247.

(322) Wang, J.; Wolf, R. M.; Caldwell, J. W.; Kollman, P. A.; Case, D. A. *J. Comput. Chem.* **2004**, *25*, 1157.

ANNEXES

ANNEX 4.A. Additional information for peptide **H1**.

H-bond analysis of the 300.37 K trajectory extracted from REMD simulations of peptide **H1**. Data are related to H-bonds involving the backbone (donor backbone N-H, acceptor backbone C=O).

ff96/ GB-HCT				**ff96/ GB-OBC(II)**				**ff96/ GB-Neck2**		
donor	acceptor	occ%		donor	acceptor	occ%		donor	acceptor	occ%
GLU7	LEU3	30.68		TYR13	TYR9	72.91		LYS12	LEU8	69.15
LYS14	GLN10	35.35		LYS14	GLN10	62.96		GLN6	LYS14	8.80
GLN6	LYS2	19.22		TYR9	TRP5	74.06		TRP5	LYS14	6.82
GLY15	GLN10	10.03		LYS12	LEU8	79.69		ILE16	LEU3	7.87
LEU11	GLU7	35.42		GLN10	GLN6	81.16		LEU8	LYS12	7.06
LYS12	LEU8	42.26		LEU11	GLU7	78.83		LEU3	ILE16	6.62
GLN10	GLN6	36.85		GLN6	LYS2	38.66		LYS14	GLN10	47.49
TYR13	TYR9	40.04		LEU8	THR4	58.01		TYR13	TYR9	51.86
LEU8	THR4	30.61		GLU7	LEU3	46.24		LEU11	GLU7	61.36
TYR9	TRP5	52.09		GLY15	GLN10	11.79		LEU8	THR4	33.15
GLU7	TYR13	5.14		GLY15	LEU11	17.47		GLN10	GLN6	37.37
LYS14	TYR9	5.14		LYS14	TYR9	5.84		GLY15	GLN10	8.33
GLY15	LYS2	6.16						TYR9	TRP5	36.06
GLY15	LEU11	11.54						LEU11	LEU8	5.62
THR4	LYS12	7.10						LYS14	GLN6	6.38
LYS12	THR4	10.12						GLY15	LEU11	15.35
								GLU7	LEU3	14.22
								GLN6	LYS2	14.04
ff99SB/ GB-HCT				**ff99SB/ GB-OBC(II)**				**ff99SB/ GB-Neck2**		
donor	acceptor	occ%		donor	acceptor	occ%		donor	acceptor	occ%
GLU7	LEU3	22.98		LYS12	TYR9	12.36		LEU11	GLU7	22.56
TRP5	LYS2	16.62		LYS12	LEU8	26.07		TYR13	LEU8	6.93
GLY15	LEU11	11.42		TYR13	GLN10	11.99		GLN6	LEU3	24.60
TYR13	GLN10	21.61		GLU7	LEU3	25.44		LEU8	THR4	34.54
LYS14	GLN10	22.98		LEU8	TRP5	10.24		GLU7	THR4	17.66
ILE16	TYR13	8.64		LEU11	LEU8	11.39		TYR9	TRP5	41.27
LYS12	TYR9	15.29		TYR9	TRP5	30.46		TYR13	TYR9	16.54
TYR13	TYR9	15.47		GLU7	THR4	12.02		LYS12	LEU8	26.77
GLN6	LEU3	29.56		GLN10	GLU7	13.97		LEU11	LEU8	16.33
TYR9	GLN6	17.45		LEU8	THR4	26.93		TYR13	GLN10	12.92
GLN10	GLN6	20.31		GLN6	LEU3	27.49		LYS12	GLN6	7.29
LEU11	GLU7	18.10		LEU11	GLU7	28.66		LYS14	GLN10	16.24
GLY15	LYS12	5.30		TYR13	TYR9	22.38		GLN10	GLU7	17.59
LEU11	LEU8	11.85		GLN10	GLN6	29.96		TYR9	GLN6	6.87

TYR9	TRP5	21.34		ILE16	TYR13	9.36		ILE16	TYR13	9.78
GLN6	LYS2	10.67		GLN6	LYS2	16.80		GLN10	GLN6	25.78
LEU8	THR4	20.39		TYR9	GLN6	12.38		GLU7	LEU3	32.97
GLY15	GLN10	5.97		LYS14	LEU11	8.62		GLY15	LYS12	5.23
LEU8	TRP5	13.85		TRP5	LYS2	13.60		TRP5	LYS2	13.75
GLU7	THR4	14.49		LYS12	GLU7	5.30		LEU8	TRP5	10.41
LYS12	LEU8	16.66		LYS14	GLN10	19.89		GLN6	LYS2	17.18
LYS14	LEU11	12.50		GLY15	LEU11	8.62		TYR13	GLU7	8.13
GLN10	GLU7	12.60						LYS12	GLU7	7.02
LEU11	TRP5	5.94						LYS12	TYR9	7.43
LYS12	GLU7	7.60						LYS14	LEU11	9.70
								GLY15	LEU11	6.47
								LEU11	GLN6	8.02
								GLY15	GLN10	5.15
ff99SBildn/ GB-HCT				**ff99SBildn/ GB-OBC(II)**				**ff99SBildn/ GB-Neck2**		
donor	acceptor	occ%		donor	acceptor	occ%		donor	acceptor	occ%
TYR9	TRP5	15.27		LEU11	LEU8	21.48		GLY15	LYS12	6.99
LEU8	THR4	18.74		LYS12	TYR9	18.51		GLU7	THR4	25.32
GLY15	TYR9	5.40		GLY15	LEU11	8.77		LEU8	THR4	36.82
LEU11	GLU7	15.66		LEU8	THR4	21.04		LYS14	LEU11	8.86
LYS12	LEU8	14.49		TYR13	TYR9	17.69		GLN6	LEU3	34.00
LEU11	LEU8	21.86		LEU8	TRP5	17.71		TYR9	TRP5	29.49
GLN6	LEU3	37.18		GLN6	LEU3	30.13		GLY15	LEU11	5.10
GLU7	LEU3	20.73		GLU7	LEU3	20.83		TYR13	GLN10	9.60
TYR13	TYR9	11.62		LYS12	LEU8	14.66		GLU7	LEU3	22.24
LYS14	LEU11	17.22		GLU7	THR4	18.21		LEU11	GLU7	25.77
GLN10	GLU7	12.51		LEU11	GLU7	17.49		GLN10	GLN6	19.86
TYR9	GLN6	19.31		TYR13	GLN10	9.03		LYS12	LEU8	23.12
LYS12	GLU7	9.52		ILE16	TYR13	9.83		LYS12	TYR9	17.29
GLN10	GLN6	22.86		TYR9	GLN6	16.20		LYS14	GLN10	14.52
GLU7	THR4	16.02		LYS14	LEU11	14.98		TYR13	TYR9	22.19
LEU8	TRP5	13.02		GLN10	GLU7	16.43		LEU11	LEU8	22.94
GLY15	LYS12	12.17		GLY15	LYS12	6.53		GLN6	LYS2	9.66
ILE16	TYR13	15.62		GLN10	GLN6	18.56		TRP5	LYS2	8.90
TYR13	GLN10	15.41		TYR9	TRP5	19.09		LEU8	TRP5	14.54
LYS14	GLN10	14.26		LYS14	GLN10	12.88		ILE16	LEU11	6.79
LYS12	TYR9	17.25		TRP5	LYS2	9.47		TYR9	GLN6	11.98
TRP5	LYS2	7.18		GLN6	LYS2	5.93		GLN10	GLU7	17.57
ILE16	LEU11	9.80		GLN10	TRP5	8.00		TYR13	LEU8	9.26
								ILE16	TYR13	9.23
								LEU11	GLN6	6.52
ff99SBildn-φ/ GB-HCT				**ff99SBildn-φ/ GB-OBC(II)**				**ff99SBildn-φ/ GB-Neck2**		
donor	acceptor	occ%		donor	acceptor	occ%		donor	acceptor	occ%

TYR9	GLN6	12.90		GLU7	LEU3	24.54		LEU8	THR4	33.18
LEU8	TRP5	13.93		LEU8	THR4	31.10		TYR9	TRP5	26.89
GLN6	LEU3	29.06		TYR9	TRP5	35.99		LEU11	GLU7	32.41
LEU11	LEU8	14.49		GLN10	GLN6	32.75		TYR13	LEU8	24.58
GLN10	GLN6	14.38		TYR13	TYR9	27.26		GLN6	LEU3	38.89
GLY15	LYS12	15.25		LYS12	LEU8	23.34		LEU8	TRP5	10.79
TYR9	TRP5	25.57		GLY15	LEU11	7.99		GLU7	THR4	19.26
GLU7	LEU3	25.20		ILE16	LEU11	11.05		GLN10	GLU7	16.05
LEU8	THR4	27.07		GLN6	LEU3	28.29		LYS12	LEU8	29.35
TYR13	GLN10	17.11		GLU7	THR4	17.03		GLY15	LYS12	7.93
LEU11	TRP5	7.58		TRP5	LYS2	9.22		TYR13	TYR9	16.68
GLU7	THR4	17.69		LEU11	LEU8	18.55		LEU11	GLN6	5.20
LYS12	TYR9	15.37		LYS12	TYR9	19.48		TYR9	GLN6	15.10
LYS14	GLN10	25.95		TYR13	GLN10	8.91		LYS14	LEU11	9.28
GLY15	LEU11	11.03		LEU11	GLU7	25.45		GLN10	GLN6	23.66
LYS14	LEU11	13.92		LYS14	GLN10	21.37		LYS14	GLN10	12.66
TRP5	LYS2	9.74		GLY15	LYS12	9.98		GLY15	TYR9	8.20
ILE16	TYR13	7.76		TYR9	GLN6	11.07		ILE16	LEU11	5.26
LEU11	GLU7	8.57		GLN10	GLU7	10.13		GLU7	LEU3	24.76
GLN10	GLU7	15.17		TYR13	LEU8	9.75		LEU11	LEU8	12.56
LYS12	GLN6	9.94		LEU8	TRP5	13.77		TYR13	GLN10	7.87
ILE16	LEU11	17.59		LYS14	LEU11	6.83		LYS12	TYR9	11.10
GLN6	LYS2	10.04		GLN6	LYS2	11.70		ILE16	TYR13	15.13
LEU11	GLN6	8.18		ILE16	TYR13	13.50		TRP5	LYS2	9.63
TYR13	TYR9	14.03						LYS12	GLU7	5.74
LYS12	LEU8	12.77						GLN6	LYS2	6.76
ff12SB/ GB-HCT				**ff12SB/ GB-OBC(II)**				**ff12SB/ GB-Neck2**		
donor	acceptor	occ%		donor	acceptor	occ%		donor	acceptor	occ%
LEU8	THR4	47.55		LYS12	LEU8	53.91		LYS14	GLN10	48.09
LYS12	TYR9	11.65		TYR13	TYR9	56.36		GLN6	LYS2	31.64
GLU7	LEU3	38.02		LEU11	GLU7	52.22		GLU7	LEU3	40.12
LEU11	GLU7	30.38		LEU8	THR4	58.82		TYR13	TYR9	56.90
LYS14	LEU11	17.08		GLN6	LYS2	37.39		ILE16	LEU11	16.50
TYR9	TRP5	43.74		GLU7	LEU3	41.16		TYR9	TRP5	61.76
GLN10	GLN6	40.38		GLY15	LEU11	17.33		GLN10	GLN6	52.59
GLY15	LEU11	12.17		TYR9	TRP5	67.77		LEU8	THR4	50.20
LYS12	LEU8	32.97		GLN10	GLN6	60.84		GLY15	LEU11	14.93
ILE16	TYR13	14.52		TRP5	LYS2	8.24		TRP5	LYS2	12.14
LYS14	GLN10	29.22		ILE16	LEU11	11.98		LYS12	LEU8	55.68
ILE16	LEU11	9.62		GLY15	LYS12	10.33		LYS14	LEU11	8.79
TYR13	TYR9	34.10		LYS14	GLN10	49.29		LEU11	GLU7	49.81
GLN6	LYS2	14.85		TYR13	LEU8	8.92		GLN6	LEU3	17.97
GLY15	LYS12	12.96		LYS12	TYR9	6.92		GLY15	GLN10	8.00

TYR13	GLN10	13.11		GLN6	LEU3	10.00		GLY15	LYS12	11.02
GLN6	LEU3	18.23		ILE16	TYR13	15.19		GLU7	THR4	12.02
TRP5	LYS2	7.05		LYS14	LEU11	8.86		TYR13	LEU8	5.03
LEU8	TRP5	5.96		GLU7	THR4	7.34		ILE16	TYR13	6.86
TYR9	GLN6	6.37		ILE16	LYS12	6.11				
GLU7	THR4	11.64								
TYR13	LEU8	8.33								
LEU11	LEU8	7.89								
GLY15	GLN10	5.82								
ff14SB/ GB-HCT				**ff14SB/ GB-OBC(II)**				**ff14SB/ GB-Neck2**		
donor	acceptor	occ%		donor	acceptor	occ%		donor	acceptor	occ%
GLU7	LEU3	27.81		LEU11	LEU8	11.69		GLY15	LYS12	13.39
LEU8	TRP5	11.14		GLU7	LEU3	35.54		LYS14	GLN10	44.36
TYR9	GLN6	13.52		GLN6	LYS2	27.76		ILE16	LEU11	24.73
LYS12	TYR9	19.53		GLN10	GLN6	39.71		LYS12	LEU8	42.43
GLN6	LEU3	18.33		GLY15	LYS12	12.20		LEU11	GLU7	49.22
TRP5	LYS2	13.12		LEU8	THR4	42.76		TYR9	TRP5	45.40
LYS14	LEU11	9.83		LYS12	LEU8	38.19		LEU8	THR4	45.80
GLY15	LYS12	13.68		TYR9	TRP5	45.14		GLU7	THR4	18.44
GLN6	LYS2	16.65		LEU11	GLU7	34.83		LEU8	TRP5	6.73
ILE16	TYR13	8.75		TYR13	TYR9	39.13		GLN10	GLN6	36.49
GLN10	GLU7	10.37		TRP5	LYS2	14.21		GLY15	LEU11	9.70
LEU11	GLU7	16.67		GLY15	LEU11	12.44		TYR9	GLN6	8.67
LYS12	LEU8	19.04		LYS14	GLN10	43.21		TYR13	TYR9	39.67
GLU7	THR4	13.57		LEU8	TRP5	9.13		LYS12	TYR9	10.42
GLN10	GLN6	27.30		LYS12	TYR9	14.65		TRP5	LYS2	18.89
TYR9	TRP5	30.88		GLN10	GLU7	7.14		TYR13	GLN10	8.52
TYR13	TYR9	20.73		ILE16	TYR13	15.05		GLN10	GLU7	10.41
LYS14	GLN10	43.52		GLN6	LEU3	15.71		ILE16	TYR13	11.28
ILE16	LEU11	18.87		ILE16	LEU11	16.27		TYR13	LEU8	10.18
LEU8	THR4	35.01		TYR9	GLN6	9.25		LEU11	LEU8	8.74
GLY15	LEU11	15.57		LYS14	LEU11	6.04		GLN6	LEU3	19.60
TYR13	GLN10	18.57		TYR13	GLN10	9.88		GLN6	LYS2	19.12
LEU11	LEU8	16.29		GLU7	THR4	11.12		GLU7	LEU3	21.69

ANNEX 4.B. Additional information for peptide **H2**.

H-bond analysis of the 300.37 K trajectory extracted from REMD simulations of peptide **H2**. Data are related to H-bonds involving the backbone (donor backbone N-H, acceptor backbone C=O).

ff96/ GB-HCT				**ff96/ GB-OBC(II)**				**ff96/ GB-Neck2**		
donor	acceptor	occ%		donor	acceptor	occ%		donor	acceptor	occ%
AIB6	ALA2	8.19		AIB6	ALA2	10.63		/	/	/
ff99SB/ GB-HCT				**ff99SB/ GB-OBC(II)**				**ff99SB/ GB-Neck2**		

donor	acceptor	occ%		donor	acceptor	occ%		donor	acceptor	occ%
AIB6	ALA2	7.76		AIB5	ALA2	41.21		AIB5	ALA2	42.53
AIB5	ALA2	42.85		AIB6	ALA2	6.83		AIB6	AIB3	26.33
AIB6	AIB3	23.96		AIB6	AIB3	22.44				
ff99SBildn/ GB-HCT				**ff99SBildn/ GB-OBC(II)**				**ff99SBildn/ GB-Neck2**		
donor	acceptor	occ%		donor	acceptor	occ%		donor	acceptor	occ%
AIB5	ALA2	45.61		AIB6	AIB3	25.32		AIB6	AIB3	25.43
AIB6	AIB3	23.14		AIB5	ALA2	41.65		AIB5	ALA2	45.52
AIB6	ALA2	6.86		AIB6	ALA2	7.79				
ff99SBildn-φ/ GB-HCT				**ff99SBildn-φ/ GB-OBC(II)**				**ff99SBildn-φ/ GB-Neck2**		
donor	acceptor	occ%		donor	acceptor	occ%		donor	acceptor	occ%
AIB5	ALA2	46.40		AIB5	ALA2	44.66		AIB5	ALA2	43.30
AIB6	AIB3	22.33		AIB6	AIB3	21.97		AIB6	AIB3	26.37
AIB6	ALA2	7.22		AIB6	ALA2	8.02				
ff12SB/ GB-HCT				**ff12SB/ GB-OBC(II)**				**ff12SB/ GB-Neck2**		
donor	acceptor	occ%		donor	acceptor	occ%		donor	acceptor	occ%
AIB6	ALA2	25.73		AIB5	ALA2	27.51		AIB6	ALA2	11.92
AIB5	ALA2	29.29		AIB6	ALA2	21.62		AIB5	ALA2	36.17
AIB6	AIB3	12.43		AIB6	AIB3	11.60		AIB6	AIB3	15.59
ff14SB/ GB-HCT				**ff14SB/ GB-OBC(II)**				**ff14SB/ GB-Neck2**		
donor	acceptor	occ%		donor	acceptor	occ%		donor	acceptor	occ%
AIB6	AIB3	11.80		AIB6	AIB3	11.67		AIB5	ALA2	32.69
AIB5	ALA2	26.51		AIB5	ALA2	28.89		AIB6	AIB3	13.30
AIB6	ALA2	22.78		AIB6	ALA2	23.78		AIB6	ALA2	12.22

ANNEX 4.C. Additional information for peptide **B1.**

H-bonds of the native conformation of **B1**

donor	acceptor
GLU2	THR15
THR15	GLU2
THR13	THR4
ASP6	THR11
THR9	ASP6
LYS10	ASP7

H-bond analysis of the 300.37 K trajectory extracted from REMD simulations of peptide B1. Data are related to H-bonds involving the backbone (donor backbone N-H, acceptor backbone C=O).

ff96/ GB-HCT				**ff96/ GB-OBC(II)**				**ff96/ GB-Neck2**		
donor	acceptor	occ%		donor	acceptor	occ%		donor	acceptor	occ%
LYS10	ASP7	12.14		LYS10	ASP6	46.56		THR11	ASP7	36.04
ASP6	PHE12	4.61		ALA8	THR4	27.15		LYS10	ASP7	21.76
VAL14	LYS10	22.17		THR11	ASP7	61.57		THR15	GLY1	5.14

PHE12	ALA8	38.33		THR9	TYR5	34.81		TRP3	THR13	6.16
THR13	THR9	23.49		THR13	THR9	19.41		TRP3	VAL14	5.06
THR11	ASP7	56.38		PHE12	ALA8	36.34		ASP7	LYS10	6.12
THR4	THR13	9.14		VAL14	LYS10	12.55		VAL14	TRP3	6.14
ASP6	**THR11**	**5.87**		LYS10	ASP7	7.42		TYR5	PHE12	6.39
THR13	**THR4**	**7.70**		ASP7	TRP3	5.26		PHE12	TYR5	6.75
ASP6	GLU2	7.45								
LYS10	ASP6	20.13								
THR9	TYR5	16.82								
THR15	THR11	6.39								
ASP7	TRP3	11.04								
ALA8	THR4	9.37								
THR15	**GLU2**	**5.03**								
ff99SB/ GB-HCT				**ff99SB/ GB-OBC(II)**				**ff99SB/ GB-Neck2**		
donor	acceptor	occ%		donor	acceptor	occ%		donor	acceptor	occ%
THR15	PHE12	17.77		THR13	LYS10	13.53		ASP6	GLU2	27.34
VAL14	THR11	18.74		LYS10	ASP7	25.19		THR9	TYR5	10.51
VAL14	LYS10	8.46		ASP7	TRP3	14.60		ASP7	TRP3	27.42
PHE12	THR9	26.65		VAL14	LYS10	5.56		PHE12	ALA8	12.19
THR13	THR9	15.38		THR9	ASP6	27.50		ALA8	THR4	13.17
TYR5	GLU2	31.89		ASP6	TRP3	10.96		LYS10	ASP6	16.65
THR9	**ASP6**	**16.85**		THR13	THR9	10.06		THR11	ASP7	10.21
THR4	GLY1	15.42		TYR5	GLU2	18.93		THR15	PHE12	12.81
THR13	LYS10	25.41		ASP7	THR4	12.20		THR13	LYS10	19.02
THR11	ALA8	19.47		PHE12	THR9	21.17		LYS10	ASP7	34.17
LYS10	ASP7	29.18		THR15	PHE12	10.60		ALA8	TRP3	10.30
ASP7	TRP3	19.00		ASP6	GLU2	11.36		TYR5	GLU2	35.91
ASP6	TRP3	22.90		VAL14	THR11	11.60		VAL14	THR11	18.01
GLU16	THR13	5.14		LYS10	ASP6	21.45		THR15	THR11	5.62
ASP6	GLU2	15.50		ALA8	THR4	10.42		THR11	ALA8	17.65
PHE12	ALA8	8.06		THR9	TYR5	8.01		PHE12	THR9	31.54
THR11	ASP7	9.90		ALA8	TYR5	15.23		**THR9**	**ASP6**	**24.00**
LYS10	ASP6	11.22		THR11	ALA8	12.42		ASP6	TRP3	14.85
ALA8	TYR5	5.42		PHE12	ALA8	5.91		ASP7	THR4	6.50
ALA8	THR4	8.74		**ASP6**	**THR11**	**5.53**		THR13	THR9	15.09
THR9	TYR5	7.73		**THR13**	**THR4**	**7.86**		ALA8	TYR5	8.42
				THR4	THR13	5.67		GLU16	THR13	6.80
								VAL14	LYS10	8.71
ff99SBildn/ GB-HCT				**ff99SBildn/ GB-OBC(II)**				**ff99SBildn/ GB-Neck2**		
donor	acceptor	occ%		donor	acceptor	occ%		donor	acceptor	occ%
THR15	PHE12	13.97		**THR9**	**ASP6**	**29.14**		LYS10	ASP7	29.50
LYS10	ASP7	31.85		LYS10	ASP6	29.01		THR13	LYS10	26.68
THR4	GLY1	5.38		PHE12	THR9	38.48		**THR9**	**ASP6**	**30.76**

ASP6	GLU2	17.61		THR13	THR9	18.59		LYS10	ASP6	24.88
ASP6	TRP3	5.30		VAL14	LYS10	14.68		PHE12	THR9	25.27
VAL14	THR11	20.19		VAL14	THR11	13.12		VAL14	LYS10	11.14
PHE12	THR9	25.65		ALA8	THR4	5.76		THR11	ALA8	12.48
THR13	LYS10	27.93		THR13	LYS10	19.43		THR13	THR9	11.18
TYR5	GLU2	24.09		TYR5	GLU2	8.68		THR15	PHE12	14.08
THR11	ASP7	6.34		THR15	PHE12	10.00		TYR5	GLU2	22.73
VAL14	LYS10	14.21		LYS10	ASP7	22.73		ASP6	GLU2	11.12
THR11	ALA8	21.05		THR11	ASP7	5.57		ALA8	THR4	8.10
THR9	**ASP6**	**11.71**		THR11	ALA8	12.58		VAL14	THR11	24.87
PHE12	TRP3	7.06		ASP7	THR4	5.06		THR15	THR11	8.92
TYR5	LYS10	8.17		ALA8	TYR5	5.81		GLU16	THR13	6.00
ALA8	TYR5	10.55						PHE12	ALA8	6.38
THR13	THR9	12.68						THR11	ASP7	9.08
THR15	THR11	5.72						ALA8	TYR5	8.94
LYS10	ASP6	7.22						ASP7	THR4	7.00
ff99SBildn-φ/ GB-HCT				**ff99SBildn-φ/ GB-OBC(II)**				**ff99SBildn-φ/ GB-Neck2**		
donor	acceptor	occ%		donor	acceptor	occ%		donor	acceptor	occ%
ASP6	GLU2	16.77		ASP6	TRP3	7.94		THR15	PHE12	18.14
VAL14	THR11	20.58		TYR5	GLU2	17.10		VAL14	THR11	19.89
LYS10	ASP7	30.45		PHE12	THR9	29.89		LYS10	ASP6	23.60
THR11	ASP7	9.37		LYS10	ASP7	33.78		ASP7	THR4	7.72
GLU16	THR13	7.91		THR9	ASP6	27.27		THR9	TYR5	7.91
THR13	LYS10	25.90		ALA8	TYR5	12.91		GLU16	THR13	10.10
THR9	ASP6	18.28		THR13	THR9	13.99		THR9	ASP6	29.09
TYR5	GLU2	34.61		THR15	PHE12	18.42		ASP7	TRP3	12.03
ASP6	TRP3	12.89		THR13	LYS10	20.88		ASP6	GLU2	14.49
THR15	PHE12	24.69		THR11	ASP7	8.14		PHE12	THR9	34.11
THR4	GLY1	16.78		ASP6	GLU2	7.10		LYS10	ASP7	31.36
THR11	ALA8	19.71		LYS10	ASP6	17.28		THR13	LYS10	21.20
THR15	THR11	6.68		VAL14	THR11	18.07		VAL14	LYS10	10.77
PHE12	ALA8	7.05		ASP7	TRP3	10.31		TYR5	GLU2	29.14
PHE12	THR9	26.28		THR11	ALA8	16.79		THR11	ALA8	17.28
ASP7	TRP3	8.54		THR9	TYR5	6.87		THR11	ASP7	9.15
ALA8	TYR5	5.69		ASP7	THR4	5.79		ALA8	TYR5	10.07
VAL14	LYS10	9.90		VAL14	LYS10	9.55		THR13	THR9	16.22
LYS10	ASP6	11.90		PHE12	ALA8	6.40		PHE12	ALA8	10.26
THR13	THR9	16.21		GLU16	THR13	7.05		THR15	THR11	6.30
THR9	TYR5	5.18		ALA8	THR4	9.92		ASP6	TRP3	9.89
								ALA8	THR4	12.05
ff12SB/ GB-HCT				**ff12SB/ GB-OBC(II)**				**ff12SB/ GB-Neck2**		
donor	acceptor	occ%		donor	acceptor	occ%		donor	acceptor	occ%
THR9	ASP6	18.23		THR11	ASP7	8.46		ASP7	THR4	17.67

ASP6	GLU2	9.95		ALA8	TYR5	22.05		THR11	ASP7	15.60
VAL14	THR11	21.08		THR9	ASP6	18.60		TYR5	GLU2	26.64
VAL14	LYS10	5.83		ASP7	THR4	13.95		ASP6	GLU2	9.01
PHE12	ALA8	5.51		TYR5	GLU2	22.81		PHE12	ALA8	10.55
LYS10	ASP7	19.25		ASP6	TRP3	7.38		THR13	LYS10	20.41
THR13	THR9	7.04		VAL14	THR9	7.35		ASP6	TRP3	14.58
THR4	GLY1	19.18		PHE12	THR9	18.87		LYS10	ASP6	17.01
LYS10	ASP6	24.34		THR13	THR9	10.50		THR9	ASP6	21.31
TYR5	GLU2	27.13		GLU16	THR13	10.88		GLU16	THR13	14.00
THR13	LYS10	21.79		THR11	ALA8	14.49		ALA8	TYR5	27.97
THR11	ALA8	13.67		VAL14	THR11	20.93		LYS10	ASP7	31.42
PHE12	THR9	22.95		THR13	LYS10	22.37		VAL14	THR11	16.75
THR15	PHE12	19.85		LYS10	ASP6	12.18		THR15	THR11	5.46
THR11	ASP7	16.85		VAL14	LYS10	10.44		THR11	ALA8	13.96
GLU16	THR13	15.16		LYS10	ASP7	33.59		THR15	PHE12	19.75
ALA8	THR4	6.24		PHE12	ALA8	5.53		ALA8	THR4	6.94
PHE12	ASP7	6.46		ASP6	GLU2	8.98		VAL14	ALA8	6.06
ASP7	THR4	10.3		ALA8	THR4	5.15		THR13	THR9	10.38
THR9	TYR5	8.15		THR9	TYR5	10.62		VAL14	LYS10	9.63
ALA8	TYR5	9.78		THR15	PHE12	17.57		ASP7	TRP3	6.08
ASP6	TRP3	15.06		THR11	ASP6	9.79		THR9	TYR5	6.28
				THR4	GLY1	5.94		PHE12	THR9	27.46
ff14SB/ GB-HCT				**ff14SB/ GB-OBC(II)**				**ff14SB/ GB-Neck2**		
donor	acceptor	occ%		donor	acceptor	occ%		donor	acceptor	occ%
LYS10	ASP6	61.51		THR15	PHE12	16.42		THR11	ASP7	65.05
THR13	THR9	34.97		GLU16	THR13	6.11		VAL14	LYS10	49.96
THR15	THR11	17.63		**THR9**	**ASP6**	**7.74**		PHE12	ALA8	76.46
GLU16	PHE12	12.14		LYS10	ASP6	63.91		ALA8	THR4	48.73
ASP7	TRP3	20.95		ASP7	THR4	5.95		ASP6	TRP3	8.74
THR11	ASP7	43.84		THR11	ASP7	49.06		THR9	TYR5	60.72
VAL14	LYS10	37.01		VAL14	THR11	11.63		TYR5	GLU2	21.19
PHE12	ALA8	59.65		ALA8	THR4	33.81		LYS10	ASP6	74.91
ALA8	THR4	22.55		THR9	TYR5	35.37		THR15	THR11	25.80
ASP6	GLU2	20.91		VAL14	LYS10	37.05		GLU16	PHE12	19.19
THR4	GLY1	21.06		PHE12	ALA8	56.17		GLU16	THR13	6.66
ASP6	TRP3	13.90		THR15	THR11	16.99		THR13	THR9	36.07
THR9	TYR5	32.95		THR13	THR9	31.25		ASP6	GLU2	16.97
TYR5	GLU2	32.18		TYR5	GLU2	11.73		ASP7	TRP3	26.72
VAL14	THR11	11.21		ASP7	TRP3	11.29		THR15	PHE12	9.40
PHE12	THR9	6.73		THR4	GLY1	5.62		ASP7	THR4	5.19
THR15	PHE12	13.51		ASP6	GLU2	7.23		VAL14	THR11	6.22
THR13	LYS10	9.30		THR13	LYS10	10.21		THR13	LYS10	5.32
THR11	ALA8	6.30		LYS10	ASP7	7.73				

GLU16	THR13	5.46		PHE12	THR9	11.14				
				GLU16	PHE12	7.30				
				THR11	ALA8	7.54				

Salt bridge analysis of the 300.37 K trajectory extracted from REMD simulations of peptide **B1**.

ff96/ GB-HCT				**ff96/ GB-OBC(II)**				**ff96/ GB-Neck2**		
donor	acceptor	occ%		donor	acceptor	occ%		donor	acceptor	occ%
LYS10	ASP6	44.89		LYS10	ASP6	41.46		LYS10	ASP6	18.17
ff99SB/ GB-HCT				**ff99SB/ GB-OBC(II)**				**ff99SB/ GB-Neck2**		
donor	acceptor	occ%		donor	acceptor	occ%		donor	acceptor	occ%
LYS10	ASP6	16.08		LYS10	ASP6	12.67		LYS10	ASP7	17.90
LYS10	ASP7	15.68		LYS10	ASP7	22.35				
ff99SBildn/ GB-HCT				**ff99SBildn/ GB-OBC(II)**				**ff99SBildn/ GB-Neck2**		
LYS10	ASP6	23.49		LYS10	ASP6	15.11		LYS10	ASP7	5.44
LYS10	ASP7	25.70		LYS10	ASP7	22.02				
ff99SBildn-φ/ GB-HCT				**ff99SBildn-φ/ GB-OBC(II)**				**ff99SBildn-φ/ GB-Neck2**		
LYS10	ASP6	15.16		LYS10	ASP6	8.59		LYS10	ASP7	14.65
LYS10	ASP7	23.53		LYS10	ASP7	19.92				
ff12SB/ GB-HCT				**ff12SB/ GB-OBC(II)**				**ff12SB/ GB-Neck2**		
LYS10	ASP7	32.04		LYS10	ASP7	23.40		LYS10	ASP7	11.83
ff14SB/ GB-HCT				**ff14SB/ GB-OBC(II)**				**ff14SB/ GB-Neck2**		
LYS10	ASP6	13.80		LYS10	ASP6	14.32		/	/	/
LYS10	ASP7	37.66		LYS10	ASP7	18.34				

ANNEX 4.D. Additional information for peptide **B2.**

H-bonds of the native conformation of **B2**

donor	acceptor
SER1	LYS12
THR3	THR10
THR3 (OH Side chain)	TRP2
LYS12	SER1
THR10	THR3
LYS8	GLU5
GLU5	LYS8

H-bond analysis of the 300.37 K trajectory extracted from REMD simulations of peptide **B2**. Data are related to H-bonds involving the backbone (donor backbone N-H, acceptor backbone C=O).

ff96/ GB-HCT				**ff96/ GB-OBC(II)**				**ff96/ GB-Neck2**		
donor	acceptor	occ%		donor	acceptor	occ%		donor	acceptor	occ%
ASN6	TRP2	18.41		TRP9	GLU5	11.99		TRP11	TRP4	5.04
LYS8	**GLU5**	**5.60**		GLY7	THR3	5.00				

LYS12	**SER1**	**5.82**		GLY7	TRP9	6.50				
TRP4	THR10	7.80		LYS12	TRP2	6.31				
GLY7	THR10	6.60		TRP4	THR10	7.46				
LYS12	TRP2	8.92		THR10	TRP4	5.94				
SER1	**LYS12**	**5.96**		ASN6	LYS8	5.24				
GLY7	THR3	8.26								
TRP4	GLY7	6.90								
GLY7	TRP9	8.10								
THR10	GLU5	5.61								
TRP9	GLU5	15.03								
TRP9	TRP2	6.56								
ff99SB/ GB-HCT				**ff99SB/ GB-OBC(II)**				**ff99SB/ GB-Neck2**		
donor	acceptor	occ%		donor	acceptor	occ%		donor	acceptor	occ%
TRP4	SER1	17.08		ASN6	TRP2	5.86		GLU5	TRP2	28.17
GLU5	SER1	14.51		LYS12	TRP9	10.81		ASN6	THR3	20.73
TRP9	ASN6	9.13		GLY7	TRP4	15.35		TRP9	ASN6	7.33
TRP11	LYS8	13.73		TRP11	LYS8	20.85		THR10	GLY7	19.21
ASN6	TRP2	19.79		LYS12	LYS8	5.74		LYS12	LYS8	7.41
GLY7	TRP2	5.84		TRP9	ASN6	10.66		TRP11	GLY7	6.89
TRP11	GLY7	9.92		TRP11	GLY7	6.07		TRP11	LYS8	15.03
ASN6	THR3	12.81		GLU5	TRP2	18.32		LYS12	TRP9	5.66
THR10	GLY7	14.04		ASN6	THR3	17.11		**LYS8**	**GLU5**	**11.34**
GLY7	TRP4	11.36		THR10	GLY7	15.59		GLY7	TRP4	10.72
GLY7	THR3	6.39		GLY7	THR3	4.95		GLY7	THR3	6.23
LYS12	TRP9	17.59		**LYS8**	**GLU5**	**16.40**		ASN6	TRP2	14.07
GLU5	TRP2	26.14						TRP9	GLU5	5.22
LYS8	**GLU5**	**17.28**						TRP4	SER1	7.03
								GLU5	SER1	6.33
								GLY7	TRP2	6.02
ff99SBildn/ GB-HCT				**ff99SBildn/ GB-OBC(II)**				**ff99SBildn/ GB-Neck2**		
donor	acceptor	occ%		donor	acceptor	occ%		donor	acceptor	occ%
ASN6	TRP2	28.15		TRP9	LYS12	7.98		ASN6	THR3	25.72
GLU5	SER1	13.99		TRP9	ASN6	9.11		GLU5	TRP2	26.50
TRP4	SER1	16.70		GLU5	TRP2	14.29		TRP11	GLY7	7.82
THR10	GLY7	13.48		ASN6	THR3	24.07		THR10	GLY7	14.07
GLY7	TRP2	9.50		LYS12	TRP9	16.32		TRP9	ASN6	8.45
LYS12	TRP9	21.77		THR10	GLY7	18.13		LYS12	TRP9	6.85
GLU5	TRP2	26.90		GLY7	TRP4	19.64		GLY7	THR3	7.00
TRP11	LYS8	14.67		TRP11	GLY7	8.89		**LYS8**	**GLU5**	**12.81**
GLY7	THR3	6.40		GLY7	THR3	6.06		GLY7	TRP4	16.42
LYS8	THR3	7.31		TRP11	LYS8	11.38		ASN6	TRP2	10.50

GLY7	TRP4	15.15		GLU5	SER1	5.90		TRP9	GLU5	7.17
ASN6	THR3	15.98		TRP4	SER1	6.62		TRP11	LYS8	13.82
LYS8	**GLU5**	**9.10**		**LYS8**	**GLU5**	**9.91**				
TRP9	ASN6	11.27		ASN6	TRP2	7.58				
TRP11	GLY7	7.48								
ff99SBildn-φ/ GB-HCT				**ff99SBildn-φ/ GB-OBC(II)**				**ff99SBildn-φ/ GB-Neck2**		
donor	acceptor	occ%		donor	acceptor	occ%		donor	acceptor	occ%
GLU5	TRP2	26.25		GLU5	TRP2	18.05		THR10	GLY7	20.37
ASN6	THR3	15.85		ASN6	TRP2	7.52		ASN6	TRP2	15.79
TRP11	LYS8	25.99		THR10	GLY7	28.11		GLU5	SER1	5.68
GLY7	TRP4	17.47		GLY7	TRP4	24.76		TRP4	SER1	7.19
ASN6	TRP2	25.47		TRP11	GLY7	10.26		GLU5	TRP2	33.06
THR10	GLY7	18.30		ASN6	THR3	32.01		TRP11	LYS8	19.92
LYS8	THR3	7.92		TRP9	ASN6	7.58		GLY7	TRP4	21.76
TRP9	ASN6	7.07		LYS8	GLU5	9.99		ASN6	THR3	26.52
TRP4	SER1	18.04		TRP11	LYS8	25.03		TRP11	GLY7	7.09
LYS12	TRP9	23.34		GLY7	THR3	9.26		GLY7	THR3	6.88
GLY7	THR3	5.81		LYS12	LYS8	6.46		LYS8	THR3	6.45
TRP11	GLY7	5.85		LYS12	TRP9	12.28		LYS12	LYS8	6.66
LYS8	**GLU5**	**11.27**						LYS12	TRP9	10.18
GLU5	SER1	15.79						**LYS8**	**GLU5**	**8.90**
								TRP9	ASN6	8.49
ff12SB/ GB-HCT				**ff12SB/ GB-OBC(II)**				**ff12SB/ GB-Neck2**		
donor	acceptor	occ%		donor	acceptor	occ%		donor	acceptor	occ%
GLY7	TRP4	19.84		TRP9	ASN6	8.06		ASN6	THR3	41.12
ASN6	THR3	26.27		ASN6	THR3	45.80		GLY7	THR3	7.66
LYS8	**GLU5**	**17.47**		GLY7	TRP4	29.01		TRP11	LYS8	17.13
GLY7	THR3	14.29		THR10	GLY7	23.51		LYS12	LYS8	7.62
TRP9	ASN6	8.50		**LYS8**	**GLU5**	**18.12**		THR10	GLY7	21.46
ASN6	TRP2	19.96		GLY7	THR3	12.49		LYS12	TRP9	15.79
THR10	GLY7	24.79		LYS12	TRP9	10.98		ASN6	TRP2	8.73
TRP11	LYS8	24.73		LYS8	TRP4	7.16		GLY7	TRP4	30.96
LYS12	LYS8	9.42		TRP11	GLY7	5.25		TRP9	ASN6	9.06
LYS8	TRP4	7.46		TRP11	LYS8	18.66		GLU5	TRP2	13.03
LYS12	TRP9	20.12						**LYS8**	**GLU5**	**17.37**
GLU5	TRP2	11.59						TRP9	GLU5	6.12
GLU5	SER1	9.47								
TRP4	SER1	12.42								
TRP11	GLY7	6.24								
ff14SB/ GB-HCT				**ff14SB/ GB-OBC(II)**				**ff14SB/ GB-Neck2**		
donor	acceptor	occ%		donor	acceptor	occ%		donor	acceptor	occ%

GLY7	THR3	18.97		ASN6	THR3	44.07		THR10	GLY7	34.27
LYS8	**GLU5**	**21.05**		GLY7	THR3	10.66		LYS12	TRP9	8.04
TRP11	LYS8	26.53		LYS8	TRP4	10.33		GLY7	TRP4	26.08
LYS12	TRP9	19.47		THR10	GLY7	28.70		TRP11	LYS8	24.07
ASN6	TRP2	15.48		TRP11	LYS8	26.09		TRP9	GLU5	10.02
TRP4	SER1	9.78		TRP11	GLY7	10.19		LYS8	TRP4	20.19
TRP9	ASN6	16.81		GLY7	TRP4	28.61		ASN6	THR3	43.44
LYS8	TRP4	17.76		LYS12	TRP9	12.95		**LYS8**	**GLU5**	**15.34**
LYS12	LYS8	5.66		TRP9	ASN6	12.60		TRP9	ASN6	12.10
ASN6	THR3	30.68		**LYS8**	**GLU5**	**24.10**		TRP11	GLY7	16.15
THR10	GLY7	30.86		GLU5	TRP2	5.05		GLY7	THR3	16.12
GLY7	TRP4	18.77		THR10	ASN6	5.22		GLU5	TRP2	6.59
TRP11	GLY7	14.21		TRP9	GLU5	5.12		LYS12	LYS8	7.43
GLU5	TRP2	9.64						THR10	ASN6	6.71
GLU5	SER1	6.05								
THR10	ASN6	6.52								

Salt bridge analysis of the 300.37 K trajectory extracted from REMD simulations of peptide **B2**.

ff96/ GB-HCT				**ff96/ GB-OBC(II)**				**ff96/ GB-Neck2**		
donor	acceptor	occ%		donor	acceptor	occ%		donor	acceptor	occ%
LYS8	GLU5	12.12		/	/	/		/	/	/
ff99SB/ GB-HCT				**ff99SB/ GB-OBC(II)**				**ff99SB/ GB-Neck2**		
donor	acceptor	occ%		donor	acceptor	occ%		donor	acceptor	occ%
/	/	/		LYS8	GLU5	12.66		/	/	/
ff99SBildn/ GB-HCT				**ff99SBildn/ GB-OBC(II)**				**ff99SBildn/ GB-Neck2**		
donor	acceptor	occ%		donor	acceptor	occ%		donor	acceptor	occ%
/	/	/		/	/	/		/	/	/
ff99SBildn-φ/ GB-HCT				**ff99SBildn-φ/ GB-OBC(II)**				**ff99SBildn-φ/ GB-Neck2**		
donor	acceptor	occ%		donor	acceptor	occ%		donor	acceptor	occ%
/	/	/		/	/	/		/	/	/
ff12SB/ GB-HCT				**ff12SB/ GB-OBC(II)**				**ff12SB/ GB-Neck2**		
donor	acceptor	occ%		donor	acceptor	occ%		donor	acceptor	occ%
LYS8	GLU5	31.15		LYS8	GLU5	24.56		/	/	/
ff14SB/ GB-HCT				**ff14SB/ GB-OBC(II)**				**ff14SB/ GB-Neck2**		
donor	acceptor	occ%		donor	acceptor	occ%		donor	acceptor	occ%
LYS8	GLU5	43.31		LYS8	GLU5	34.18		LYS8	GLU5	18.29

ANNEX 4.E. Additional information for peptide **B3.**

H-bonds of the native conformation of **B3**

donor	acceptor

ILE2	LEU14
LEU14	ILE2
VAL4	ILE12
ILE12	VAL4
THR6	LYS10
GLY9	THR6
THR8	THR6 (OH Side chain)

H-bond analysis of the 300.37 K trajectory extracted from REMD simulations of peptide **B3**. Data are related to H-bonds involving the backbone (donor backbone N-H, acceptor backbone C=O).

ff96/ GB-HCT				**ff96/ GB-OBC(II)**				**ff96/ GB-Neck2**		
donor	acceptor	occ%		donor	acceptor	occ%		donor	acceptor	occ%
LYS10	LYS5	7.31		**ILE2**	**LEU14**	**11.18**		LEU14	PHE3	46.86
THR8	VAL4	6.09		**ILE12**	**VAL4**	**14.89**		PHE3	LEU14	29.04
GLY9	LYS5	5.22		**LEU14**	**ILE2**	**13.07**		ILE12	LYS5	48.36
LEU14	**ILE2**	**24.05**		**VAL4**	**ILE12**	**15.35**		LYS5	ILE12	51.80
VAL4	**ILE12**	**26.27**		LEU14	PHE3	9.33		LEU7	LYS10	21.74
LEU14	PHE3	19.01		LYS5	ILE12	18.21		LYS10	LEU7	9.79
LYS5	ILE12	23.20		ILE12	LYS5	14.44		LYS10	THR8	5.15
ILE12	LYS5	21.42		LEU7	LYS10	7.22				
LEU7	LYS10	13.83		ILE12	PHE3	8.31				
PHE3	LEU14	7.61		THR8	VAL4	14.04				
ILE2	**LEU14**	**23.81**		GLY9	VAL4	7.02				
THR11	VAL4	9.64		PHE3	LEU14	5.89				
ILE12	**VAL4**	**17.96**		ILE12	THR6	8.22				
THR6	GLY9	8.94		THR6	ILE12	9.35				
ILE12	LEU7	5.94		**THR6**	**LYS10**	**10.50**				
GLN1	GLU15	5.05								
THR11	LYS5	5.41								
THR6	**LYS10**	**9.58**								
LYS5	THR11	6.46								
GLU15	PHE3	6.34								
ILE12	PHE3	6.44								
PHE3	ILE12	5.14								
ff99SB/ GB-HCT				**ff99SB/ GB-OBC(II)**				**ff99SB/ GB-Neck2**		
donor	acceptor	occ%		donor	acceptor	occ%		donor	acceptor	occ%
LYS10	LYS5	20.55		LEU7	PHE3	10.18		LYS5	ILE12	31.02
THR6	ILE2	12.92		THR13	LYS10	12.03		LEU7	LYS10	31.78
LEU14	THR11	24.53		LEU14	THR11	12.17		ILE12	LYS5	32.13
LEU7	PHE3	18.89		THR8	VAL4	19.20		LYS10	LEU7	32.07
THR13	LYS10	24.85		ILE12	GLY9	6.66		LEU14	THR11	16.40
LYS5	ILE2	20.97		THR8	LYS5	8.10		THR8	VAL4	18.35
LEU7	VAL4	13.92		GLY9	LYS5	13.84		LEU7	PHE3	12.12

THR8	VAL4	28.53		LYS5	THR11	13.48		**GLY9**	**THR6**	**11.07**
THR6	PHE3	16.74		GLU15	ILE12	8.50		GLY9	LYS5	5.50
GLY9	**THR6**	**21.25**		**GLY9**	**THR6**	**19.01**		LEU14	PHE3	25.34
LEU14	LYS10	8.83		LEU14	LYS10	7.53		PHE3	LEU14	15.81
VAL4	GLN1	7.57		LEU7	VAL4	17.91		THR8	LYS5	6.79
THR8	LYS5	11.5		THR13	PHE3	8.78		THR6	PHE3	8.60
VAL4	**ILE12**	**7.94**		**THR6**	**LYS10**	**13.05**		LEU7	VAL4	16.50
LEU14	**ILE2**	**7.18**		**ILE12**	**VAL4**	**16.57**		ILE12	GLY9	7.78
ILE2	**LEU14**	**6.18**		**VAL4**	**ILE12**	**15.66**		THR13	LYS10	14.32
LYS5	LYS10	6.05		THR6	PHE3	7.71		GLU15	THR11	7.37
				ILE2	**LEU14**	**11.56**		LEU14	LYS10	5.57
				LEU14	**ILE2**	**12.18**				
ff99SBildn/ GB-HCT				**ff99SBildn/ GB-OBC(II)**				**ff99SBildn/ GB-Neck2**		
donor	acceptor	occ%		donor	acceptor	occ%		donor	acceptor	occ%
LEU14	THR11	26.22		THR13	LYS10	9.86		LYS10	LEU7	17.49
GLY9	THR6	18.85		LEU14	LYS10	12.18		LEU7	LYS10	11.50
THR8	LYS5	17.06		THR6	PHE3	7.73		ILE12	LYS5	13.05
THR6	ILE2	7.35		GLY9	LYS5	9.45		LEU14	PHE3	12.90
THR8	VAL4	25.99		LEU14	THR11	19.27		PHE3	LEU14	10.54
LEU7	VAL4	23.45		THR8	LYS5	7.43		LYS5	ILE12	13.64
LYS10	LYS5	26.10		LEU7	VAL4	33.49		**GLY9**	**THR6**	**19.54**
THR13	LYS10	25.77		LYS10	LEU7	5.46		**ILE12**	**VAL4**	**17.23**
LEU14	LYS10	11.42		LEU7	PHE3	6.75		**VAL4**	**ILE12**	**17.22**
LYS5	ILE2	23.88		THR8	VAL4	22.73		**LEU14**	**ILE2**	**15.64**
THR6	PHE3	27.09		ILE12	GLY9	19.28		LEU14	THR11	18.80
LEU7	PHE3	12.68		THR13	GLY9	14.31		**THR6**	**LYS10**	**12.48**
ILE2	GLU15	11.06		GLY9	THR6	15.19		ILE12	GLY9	9.85
				THR6	LYS10	5.34		THR8	VAL4	11.26
								LEU7	PHE3	6.21
								THR13	LYS10	10.83
								ILE12	PHE3	5.08
								LYS5	LYS10	6.99
								GLY9	LYS5	7.11
								ILE2	**LEU14**	**5.98**
								THR8	LYS5	8.40
								THR6	PHE3	7.72
								LEU7	VAL4	18.32
								GLU15	THR11	5.53
ff99SBildn-φ/ GB-HCT				**ff99SBildn-φ/ GB-OBC(II)**				**ff99SBildn-φ/ GB-Neck2**		
donor	acceptor	occ%		donor	acceptor	occ%		donor	acceptor	occ%
LEU14	THR11	39.79		LEU7	VAL4	31.18		THR8	VAL4	25.18
LYS10	LYS5	20.60		THR8	VAL4	27.13		THR6	PHE3	15.09
THR13	LYS10	24.98		GLY9	LYS5	12.18		LEU7	PHE3	16.30

ILE2	GLU15	5.01		THR13	LYS10	8.14		LEU14	LYS10	7.80
LYS5	ILE2	21.57		LEU14	LYS10	10.12		LYS5	ILE2	5.67
THR6	PHE3	23.91		ILE12	GLY9	13.62		LYS10	LEU7	14.81
THR8	VAL4	26.70		LEU7	PHE3	7.41		THR11	THR8	6.11
LEU14	LYS10	9.98		THR8	LYS5	7.94		**GLY9**	**THR6**	**18.20**
LEU7	VAL4	17.56		LEU14	THR11	25.91		ILE12	GLY9	17.53
LYS5	LYS10	8.82		LYS10	LEU7	7.63		THR8	LYS5	13.01
GLY9	**THR6**	**26.21**		ILE12	PHE3	6.02		GLY9	LYS5	8.52
LEU7	PHE3	20.77		LYS5	LYS10	9.31		LEU7	VAL4	24.33
THR6	ILE2	9.94		THR13	GLY9	6.76		**ILE12**	**VAL4**	**5.66**
ILE12	PHE3	6.39		THR6	PHE3	9.97		LEU14	THR11	20.55
THR8	LYS5	13.09		**GLY9**	**THR6**	**12.08**		GLU15	THR11	5.96
VAL4	GLN1	6.54						THR13	GLY9	6.51
								THR13	LYS10	18.88
								LYS5	ILE12	6.02
								ILE12	LYS5	5.96
								LEU7	LYS10	5.27
								LYS5	LYS10	4.97
								ILE12	PHE3	5.00
								LEU14	**ILE2**	**5.20**
								VAL4	**ILE12**	**6.18**
ff12SB/ GB-HCT				**ff12SB/ GB-OBC(II)**				**ff12SB/ GB-Neck2**		
donor	acceptor	occ%		donor	acceptor	occ%		donor	acceptor	occ%
LEU7	PHE3	26.81		LYS5	ILE2	13.74		LYS10	LEU7	13.81
LEU14	THR11	21.69		LEU14	THR11	27.00		LEU7	VAL4	31.45
GLU15	ILE12	8.17		THR6	PHE3	16.46		THR6	PHE3	22.24
THR8	VAL4	31.97		LYS10	LEU7	18.47		LYS5	ILE2	17.56
LYS10	LYS5	9.26		LEU7	VAL4	25.32		THR8	LYS5	15.25
THR6	ILE2	15.01		LEU14	GLY9	8.81		LEU7	PHE3	18.86
GLY9	**THR6**	**20.17**		LEU7	PHE3	18.63		LEU14	THR11	30.89
LYS10	LEU7	11.47		THR8	LYS5	9.61		GLU15	ILE12	12.50
VAL4	GLN1	7.25		ILE12	GLY9	13.90		GLY9	VAL4	6.50
LYS5	ILE2	34.94		GLY9	THR6	22.53		THR8	VAL4	20.09
THR6	PHE3	29.63		THR6	LYS10	6.24		ILE12	GLY9	19.11
LEU7	VAL4	19.67		THR13	LYS10	9.23		THR13	LYS10	17.72
THR8	LYS5	9.46		THR8	VAL4	20.64		GLY9	THR6	13.97
THR11	LYS5	24.54		GLY9	LYS5	7.72		GLU15	THR11	7.85
THR13	LYS10	7.06		THR13	GLY9	10.02		GLY9	LYS5	9.77
GLN1	GLU15	5.44		GLU15	ILE12	5.26		THR11	THR8	5.70
								LEU14	GLY9	8.91
								THR13	GLY9	9.64
ff14SB/ GB-HCT				**ff14SB/ GB-OBC(II)**				**ff14SB/ GB-Neck2**		
donor	acceptor	occ%		donor	acceptor	occ%		donor	acceptor	occ%

VAL4	GLN1	6.32		LYS10	LEU7	5.22		GLU15	ILE12	5.81
THR8	VAL4	40.00		THR6	PHE3	15.71		GLU15	THR11	6.10
LYS5	ILE2	17.38		LEU7	VAL4	13.64		LEU14	THR11	14.45
LEU7	PHE3	48.50		THR13	GLY9	26.23		**GLY9**	**THR6**	**8.81**
GLY9	LYS5	6.69		GLY9	LYS5	21.21		THR13	LYS10	19.27
LYS10	LYS5	23.79		LYS10	THR6	18.85		ILE12	GLY9	14.57
LEU14	THR11	44.05		ILE12	THR8	12.76		THR11	THR8	8.29
GLY9	**THR6**	**23.99**		LEU7	PHE3	50.64		LEU14	GLY9	10.28
THR6	ILE2	26.21		LEU14	THR11	29.07		THR8	VAL4	68.67
LYS5	GLN1	11.96		THR8	LYS5	7.86		LYS5	GLN1	26.58
LEU7	VAL4	10.39		THR8	VAL4	44.06		LEU7	PHE3	76.23
THR6	PHE3	17.32		THR11	LEU7	13.13		THR6	ILE2	28.77
THR8	LYS5	9.69		LEU14	LYS10	10.54		ILE12	THR8	43.28
THR13	LYS10	17.37		THR6	ILE2	6.30		LEU14	LYS10	13.33
THR11	LYS5	8.21		**GLY9**	**THR6**	**15.30**		THR11	LEU7	29.01
ILE12	GLY9	7.11		LYS10	LYS5	11.75		GLY9	LYS5	43.80
				THR13	LYS10	8.09		THR13	GLY9	18.88
				ILE12	GLY9	13.45		LYS10	THR6	42.83
				THR11	THR8	5.18		GLU15	GLY9	9.39
								THR6	PHE3	7.62

Salt bridge analysis of the 300.37 K trajectory extracted from REMD simulations of peptide **B3**.

ff96/ GB-HCT				**ff96/ GB-OBC(II)**				**ff96/ GB-Neck2**		
donor	acceptor	occ%		donor	acceptor	occ%		donor	acceptor	occ%
/	/	/		LYS5	GLU15	6.74		/	/	/
ff99SB/ GB-HCT				**ff99SB/ GB-OBC(II)**				**ff99SB/ GB-Neck2**		
donor	acceptor	occ%		donor	acceptor	occ%		donor	acceptor	occ%
LYS5	GLU15	25.94		LYS5	GLU15	7.68		/	/	/
LYS10	GLU15	19.52								
ff99SBildn/ GB-HCT				**ff99SBildn/ GB-OBC(II)**				**ff99SBildn/ GB-Neck2**		
donor	acceptor	occ%		donor	acceptor	occ%		donor	acceptor	occ%
LYS5	GLU15	33.12		LYS5	GLU15	6.18		/	/	/
LYS10	GLU15	15.62		LYS10	GLU15	9.19				
ff99SBildn-φ/ GB-HCT				**ff99SBildn-φ/ GB-OBC(II)**				**ff99SBildn-φ/ GB-Neck2**		
donor	acceptor	occ%		donor	acceptor	occ%		donor	acceptor	occ%
LYS5	GLU15	26.24		LYS10	GLU15	8.6		/	/	/
LYS10	GLU15	13.89								
ff12SB/ GB-HCT				**ff12SB/ GB-OBC(II)**				**ff12SB/ GB-Neck2**		
donor	acceptor	occ%		donor	acceptor	occ%		donor	acceptor	occ%
LYS5	GLU15	36.48		LYS10	GLU15	12.05		LYS10	GLU15	5.67
LYS10	GLU15	20.41								
ff14SB/ GB-HCT				**ff14SB/ GB-OBC(II)**				**ff14SB/ GB-Neck2**		
donor	acceptor	occ%		donor	acceptor	occ%		donor	acceptor	occ%

LYS5	GLU15	36.53		LYS5	GLU15	19.52		/	/	/
LYS10	GLU15	14.21		LYS10	GLU15	14.89				

ANNEX 4.F. Additional information for peptide **ID1**.

H-bond analysis of the 300.37 K trajectory extracted from REMD simulations of peptide **ID1**. Data are related to H-bonds involving the backbone (donor backbone N-H, acceptor backbone C=O).

ff96/ GB-HCT				**ff96/ GB-OBC(II)**				**ff96/ GB-Neck2**		
donor	acceptor	occ%		donor	acceptor	occ%		donor	acceptor	occ%
TRP3	ILE11	8.38		LEU14	ASN2	6.34		VAL10	GLY7	8.91
ILE11	TRP3	6.87		LEU4	ASP12	5.89		LEU4	ASP12	10.86
LYS5	MET9	23.11		LEU6	ASN2	5.00		LEU14	ASN2	11.02
MET9	LEU6	11.22		ILE11	LEU4	42.74		ASP12	LEU4	9.78
ILE1	ALA13	23.00		GLY7	MET9	14.41		GLY7	VAL10	10.57
LEU6	MET9	37.68		ALA13	ASN2	29.73		ILE11	LEU4	20.09
ALA13	ILE1	7.89		LEU4	ILE11	36.47		LEU4	ILE11	16.10
ALA13	ASN2	25.59		LEU6	MET9	29.77		LEU6	MET9	16.93
ILE11	LEU4	43.83		MET9	LEU6	9.90		MET9	LEU6	9.03
ASN2	ALA13	14.20		GLY7	VAL10	7.48		ALA13	ASN2	9.66
LEU4	ILE11	31.24		VAL10	GLY7	3.52		ASN2	LEU14	6.19
MET9	LYS5	17.87		ILE11	LYS5	5.73		MET9	LYS5	6.41
GLY7	MET9	14.90		ALA13	TRP3	6.77		LYS5	ASP12	7.42
ASN2	ILE11	15.11		LYS5	ILE11	7.68		ASP12	LYS5	6.56
LEU4	MET9	6.63		ASP12	LEU4	5.34		LYS5	MET9	5.36
ILE11	ASN2	18.62								
LYS8	LYS5	8.83								
ASP12	LEU4	8.90								
LEU4	ASP12	8.78								
ff99SB/ GB-HCT				**ff99SB/ GB-OBC(II)**				**ff99SB/ GB-Neck2**		
donor	acceptor	occ%		donor	acceptor	occ%		donor	acceptor	occ%
MET9	LEU6	7.81		ALA13	VAL10	17.10		GLY7	TRP3	14.44
ASP12	MET9	26.69		LEU14	VAL10	15.93		VAL10	LEU6	8.06
ALA13	VAL10	14.83		LYS8	LYS5	7.44		ILE11	LYS8	23.03
LEU14	ILE11	21.91		MET9	LYS5	6.37		ASP12	LYS8	14.79
GLY7	TRP3	16.60		LEU6	ASN2	27.31		LEU6	ASN2	18.81
LYS5	ASN2	21.14		GLY7	TRP3	23.64		MET9	LYS5	7.08
LYS8	LYS5	20.60		LEU6	TRP3	14.05		ALA13	MET9	23.65
LEU6	ASN2	33.35		ALA13	MET9	25.59		ASP12	MET9	30.61
ALA13	MET9	20.78		ASP12	MET9	33.36		LEU6	TRP3	11.74
LEU14	VAL10	12.02		GLY7	LEU4	12.47		MET9	LEU6	18.13
MET9	LYS5	12.86		LYS5	ASN2	16.18		LEU14	MET9	7.74
MET9	LEU4	7.45		MET9	LEU6	13.03		ILE11	LEU4	14.09
ILE11	LYS8	12.02		VAL10	LEU6	10.59		ASN2	LEU14	5.46

LEU6	TRP3	10.56		LYS8	TRP3	12.97		LEU14	ASN2	10.76
GLY7	LEU4	8.66		ILE11	LYS8	12.72		LEU4	ASP12	12.83
VAL10	LYS5	10.31		LEU14	ILE11	21.62		LEU6	MET9	14.55
ASP12	LYS8	7.26		VAL10	GLY7	12.02		ASP12	LEU4	9.79
LYS8	TRP3	8.62		ILE11	GLY7	9.91		LYS5	ASN2	17.52
				ASP12	LYS8	9.34		LEU14	ILE11	12.13
				LYS8	LEU4	5.70		LYS8	LYS5	11.61
								ALA13	VAL10	16.03
								GLY7	LEU4	7.15
								LEU14	VAL10	13.88
								VAL10	GLY7	8.95
								LYS8	TRP3	7.02
ff99SBildn/ GB-HCT				**ff99SBildn/ GB-OBC(II)**				**ff99SBildn/ GB-Neck2**		
donor	acceptor	occ%		donor	acceptor	occ%		donor	acceptor	occ%
ASN2	VAL10	16.95		MET9	LYS5	5.46		GLY7	LEU4	14.09
VAL10	ASN2	18.12		LYS8	LYS5	6.46		LEU14	ILE11	19.19
LEU14	ILE11	33.51		GLY7	TRP3	12.57		ILE11	GLY7	7.06
GLY7	LEU4	20.79		GLY7	LEU4	15.09		VAL10	GLY7	11.70
MET9	LYS5	9.19		LYS5	ASN2	17.94		ILE11	LYS8	17.24
LEU6	TRP3	11.93		ALA13	MET9	11.10		LYS5	ASN2	26.54
LYS8	LYS5	12.31		LEU14	ILE11	30.30		LEU6	TRP3	19.91
ASP12	MET9	13.61		ILE11	LYS8	7.65		LEU14	VAL10	9.42
LEU6	ASN2	16.02		ASP12	MET9	13.21		ALA13	VAL10	13.48
ALA13	VAL10	13.23		LEU6	TRP3	18.01		MET9	LYS5	6.22
LYS8	TRP3	10.27		VAL10	GLY7	9.14		GLY7	TRP3	14.49
LYS5	ASN2	16.93		MET9	LEU6	11.42		LYS8	TRP3	8.95
LEU4	MET9	7.00		LEU14	VAL10	11.86		LEU6	ASN2	11.50
ILE11	ASN2	8.03		ASP12	LYS8	7.62		ALA13	MET9	9.58
ASN2	ILE11	5.29		LEU6	ASN2	13.22		LYS8	LYS5	5.87
MET9	LEU4	5.53		LYS8	TRP3	10.92		ASP12	LYS8	10.25
LEU14	VAL10	7.81		ALA13	VAL10	20.43		MET9	LEU6	11.90
LEU4	LYS8	13.99		ILE11	GLY7	7.18		VAL10	LEU6	8.68
ALA13	MET9	8.82						ASP12	MET9	11.64
GLY7	TRP3	10.86						ILE11	LEU6	7.25
LYS8	LEU4	5.63						ILE11	LEU4	6.37
LYS5	MET9	6.22						LEU6	MET9	5.90
								LEU4	ILE11	5.05
ff99SBildn-φ/ GB-HCT				**ff99SBildn-φ/ GB-OBC(II)**				**ff99SBildn-φ/ GB-Neck2**		
donor	acceptor	occ%		donor	acceptor	occ%		donor	acceptor	occ%
ASP12	MET9	14.09		LEU14	ILE11	36.85		ALA13	ASN2	5.96
LEU14	ILE11	31.75		LEU14	VAL10	11.11		ILE11	LEU4	13.26
GLY7	TRP3	14.65		LEU6	TRP3	19.43		LEU6	MET9	11.57
LEU6	TRP3	18.76		ALA13	VAL10	18.30		ILE11	LYS8	11.08

LEU6	ASN2	22.26		LYS5	ASN2	21.35		ASP12	LYS8	7.01
LYS8	LYS5	12.23		GLY7	TRP3	17.63		LYS5	ASN2	22.32
MET9	LYS5	9.21		MET9	LEU6	11.92		LEU6	TRP3	18.22
LEU14	VAL10	14.08		VAL10	LEU6	5.76		ILE11	GLY7	7.07
LYS5	ASN2	22.60		ILE11	GLY7	10.12		LEU6	ASN2	10.26
VAL10	LYS5	5.02		ASP12	MET9	11.94		GLY7	LEU4	9.54
ALA13	VAL10	21.01		VAL10	GLY7	13.70		VAL10	GLY7	13.09
MET9	LEU6	11.52		LEU6	ASN2	16.47		LYS8	LYS5	12.27
ALA13	MET9	9.22		GLY7	LEU4	18.89		LEU14	VAL10	8.85
GLY7	LEU4	18.20		LYS8	TRP3	10.10		LEU14	ILE11	16.32
LYS8	TRP3	12.99		LYS8	LEU4	5.63		GLY7	TRP3	15.46
ILE11	LYS8	6.39		ASP12	LYS8	13.17		MET9	LYS5	7.44
MET9	LEU4	5.02		ILE11	LYS8	13.78		LYS5	MET9	5.26
				ALA13	MET9	12.65		ILE11	TRP3	5.26
				MET9	LYS5	6.52		ALA13	VAL10	12.49
				LYS8	LYS5	6.81		ASP12	MET9	9.17
								LEU4	ILE11	11.66
								MET9	LEU6	12.95
								ALA13	MET9	7.81
ff12SB/ GB-HCT				**ff12SB/ GB-OBC(II)**				**ff12SB/ GB-Neck2**		
donor	acceptor	occ%		donor	acceptor	occ%		donor	acceptor	occ%
LEU6	ASN2	42.56		LEU14	ILE11	40.72		LYS5	ASN2	28.08
ALA13	MET9	15.45		LEU6	ASN2	38.36		LEU6	TRP3	16.06
VAL10	LEU6	10.54		MET9	LYS5	21.85		GLY7	TRP3	36.74
GLY7	TRP3	24.31		ILE11	GLY7	34.77		ALA13	VAL10	20.35
LYS8	LYS5	8.88		ASP12	LYS8	58.20		ASP12	LYS8	39.36
MET9	LYS5	18.84		LYS8	LEU4	22.76		VAL10	GLY7	21.89
ILE11	LYS8	11.97		GLY7	TRP3	43.00		ILE11	GLY7	20.39
ASP12	LYS8	44.35		ALA13	MET9	19.69		MET9	LEU6	9.31
LEU14	ILE11	41.05		VAL10	LEU6	19.47		ILE11	LYS8	17.35
LYS5	ASN2	18.63		LEU14	VAL10	14.85		ALA13	MET9	14.87
MET9	LEU6	6.44		LEU6	TRP3	13.17		GLY7	LEU4	10.81
LYS8	LEU4	15.99		ALA13	VAL10	18.93		LEU6	ASN2	38.55
VAL10	GLY7	17.65		MET9	LEU6	9.49		VAL10	LEU6	19.84
LYS8	TRP3	9.39		LYS8	LYS5	6.57		LEU14	ILE11	31.01
ILE11	GLY7	16.82		ILE11	LYS8	9.14		LYS8	LYS5	9.14
ALA13	VAL10	15.19		LYS5	ASN2	20.43		ASP12	MET9	7.38
LEU14	VAL10	11.21		VAL10	GLY7	20.10		LEU14	VAL10	13.73
GLY7	LEU4	11.78		GLY7	LEU4	9.08		LYS8	LEU4	12.07
LEU6	TRP3	9.16		LYS8	TRP3	5.38		MET9	LYS5	20.02
MET9	TRP3	6.33						LYS8	TRP3	6.65
ASP12	MET9	5.36						LEU14	MET9	5.26
ff14SB/ GB-HCT				**ff14SB/ GB-OBC(II)**				**ff14SB/ GB-Neck2**		

donor	acceptor	occ%		donor	acceptor	occ%		donor	acceptor	occ%
ASP12	LYS8	28.86		ALA13	MET9	21.81		ILE11	GLY7	23.13
MET9	TRP3	9.95		LEU14	ILE11	39.69		LEU14	ILE11	27.04
VAL10	GLY7	10.80		VAL10	GLY7	19.66		MET9	LYS5	19.02
LEU6	TRP3	8.40		ASP12	LYS8	53.28		ASP12	LYS8	38.54
ASP12	MET9	5.68		ILE11	LYS8	11.59		LYS5	ASN2	30.79
GLY7	LEU4	15.00		LEU6	ASN2	30.65		VAL10	LEU6	19.13
LEU14	ILE11	35.31		LYS8	TRP3	7.74		LEU6	ASN2	35.63
ALA13	VAL10	14.98		ILE11	GLY7	33.78		GLY7	LEU4	10.66
LYS8	LEU4	8.77		GLY7	TRP3	30.73		VAL10	GLY7	19.71
ILE11	GLY7	12.95		LYS5	ASN2	18.21		LEU14	VAL10	20.04
TRP3	LYS8	7.38		LEU6	TRP3	13.61		ALA13	VAL10	18.33
LYS8	LYS5	18.22		GLY7	LEU4	14.26		LEU6	TRP3	17.07
VAL10	LEU4	5.20		LEU14	VAL10	17.40		ILE11	LYS8	15.90
LYS5	ASN2	18.80		VAL10	LEU6	17.09		ALA13	MET9	17.56
MET9	LYS5	10.39		MET9	LYS5	19.58		LYS8	LYS5	10.72
LEU6	ASN2	37.38		LYS8	LEU4	19.72		GLY7	TRP3	33.49
ALA13	MET9	13.13		ALA13	VAL10	13.12		ASP12	MET9	11.97
LYS8	TRP3	9.17		LYS8	LYS5	5.25		MET9	LEU6	8.59
LEU4	ILE1	5.50		MET9	LEU6	6.54		LYS8	LEU4	11.89
LEU14	VAL10	11.26						LYS8	TRP3	5.73
GLY7	TRP3	21.79								
MET9	LEU6	5.61								
VAL10	LEU6	6.34								
ILE11	LYS8	9.66								

Salt bridge analysis of the 300.37 K trajectory extracted from REMD simulations of peptide **ID1**.

ff96/ GB-HCT				**ff96/ GB-OBC(II)**				**ff96/ GB-Neck2**		
donor	acceptor	occ%		donor	acceptor	occ%		donor	acceptor	occ%
/	/	/		/	/	/		/	/	/
ff99SB/ GB-HCT				**ff99SB/ GB-OBC(II)**				**ff99SB/ GB-Neck2**		
donor	acceptor	occ%		donor	acceptor	occ%		donor	acceptor	occ%
LYS5	ASP12	17.98		LYS8	ASP12	11.16		/	/	/
LYS8	ASP12	5.18								
ff99SBildn/ GB-HCT				**ff99SBildn/ GB-OBC(II)**				**ff99SBildn/ GB-Neck2**		
donor	acceptor	occ%		donor	acceptor	occ%		donor	acceptor	occ%
LYS8	ASP12	11.31		/	/	/		/	/	/
ff99SBildn-φ/ GB-HCT				**ff99SBildn-φ/ GB-OBC(II)**				**ff99SBildn-φ/ GB-Neck2**		
donor	acceptor	occ%		donor	acceptor	occ%		donor	acceptor	occ%
LYS8	ASP12	15.08		/	/	/		/	/	/
ff12SB/ GB-HCT				**ff12SB/ GB-OBC(II)**				**ff12SB/ GB-Neck2**		
donor	acceptor	occ%		donor	acceptor	occ%		donor	acceptor	occ%
LYS8	ASP12	36.08		LYS8	ASP12	41.85		LYS8	ASP12	21.86

ff14SB/ GB-HCT				ff14SB/ GB-OBC(II)				ff14SB/ GB-Neck2		
donor	acceptor	occ%		donor	acceptor	occ%		donor	acceptor	occ%
LYS5	ASP12	14.22		LYS8	ASP12	30.55		LYS8	ASP12	14.88
LYS8	ASP12	31.14								

ANNEX 4.G. Additional information for peptide **ID2**.

H-bond analysis of the 300.37 K trajectory extracted from REMD simulations of peptide **ID2**. Data are related to H-bonds involving the backbone (donor backbone N-H, acceptor backbone C=O).

ff96/ GB-HCT				ff96/ GB-OBC(II)				ff96/ GB-Neck2		
donor	acceptor	occ%		donor	acceptor	occ%		donor	acceptor	occ%
ILE5	LYS9	10.18		ASN8	LYS4	69.51		/	/	/
LEU11	THR3	12.92		LYS9	ILE5	59.21				
THR3	LEU11	7.89		TRP7	THR3	82.16				
ASN8	LYS4	10.71		ILE10	ASP6	70.32				
TRP7	THR3	27.19								
ILE10	ASP6	10.74								
ARG2	LEU11	23.33								
ASP6	LYS9	14.45								
THR1	SER12	7.53								
ARG2	ILE10	25.62								
ILE10	ARG2	25.77								
LYS4	ASN8	19.50								
ILE5	ASN8	13.82								
LEU11	ARG2	12.29								
LYS9	ILE5	7.30								
ff99SB/ GB-HCT				**ff99SB/ GB-OBC(II)**				**ff99SB/ GB-Neck2**		
donor	acceptor	occ%		donor	acceptor	occ%		donor	acceptor	occ%
LEU11	TRP7	17.41		ILE10	ASP6	16.92		ASN8	LYS4	23.10
ILE5	ARG2	5.09		LEU11	TRP7	11.78		ASP6	THR3	35.17
LEU11	ASN8	27.16		TRP7	THR3	37.96		LEU11	TRP7	16.65
ASN8	ILE5	23.81		ASN8	LYS4	33.70		ILE10	TRP7	20.97
THR1	SER12	9.92		LYS9	ASP6	24.93		ILE5	ARG2	6.53
ILE10	TRP7	25.04		ASP6	THR3	25.33		ASN8	ILE5	10.98
TRP7	LYS4	12.99		LEU11	ASN8	17.42		TRP7	THR3	14.91
ASN8	LYS4	17.13		LYS9	ILE5	8.38		LYS9	ASP6	17.37
LYS9	ILE5	7.97		TRP7	LYS4	13.99		TRP7	LYS4	16.74
ASP6	THR3	11.10		ASN8	ILE5	13.13		LEU11	ASN8	14.79
LYS9	ASP6	22.11		ILE10	TRP7	17.38				
SER12	ASN8	13.38		SER12	TRP7	6.60				
TRP7	THR3	6.58								
ff99SBildn/ GB-HCT				**ff99SBildn/ GB-OBC(II)**				**ff99SBildn/ GB-Neck2**		
donor	acceptor	occ%		donor	acceptor	occ%		donor	acceptor	occ%

ARG2	LEU11	17.17		ASP6	ILE10	10.10		TRP7	LYS4	7.46
LEU11	ARG2	16.45		ILE10	ASP6	18.55		ASN8	ILE5	16.89
LYS4	LYS9	14.35		TRP7	THR3	7.29		ILE10	ASP6	17.00
ASN8	ILE5	10.95		ASN8	ILE5	19.54		LEU11	ASP6	9.33
LEU11	ASN8	5.62		LYS9	ASP6	23.58		LYS9	ASP6	31.93
TRP7	LYS4	22.77		ASP6	THR3	6.59		LYS9	ILE5	6.13
ILE10	TRP7	21.90		LEU11	TRP7	5.88		LEU11	TRP7	21.13
LYS9	ILE5	7.10		ILE10	TRP7	6.78		LEU11	ASN8	7.70
ASN8	LYS4	16.38		LYS9	ILE5	6.20				
LYS9	ASP6	12.42		LEU11	ASN8	10.00				
ILE10	ASP6	6.19		SER12	ASN8	5.13				
THR3	LYS9	6.58								
LEU11	THR1	7.16								
ASP6	THR3	6.76								
THR1	SER12	9.96								
TRP7	THR3	5.30								
LEU11	TRP7	21.77								
ff99SBildn-φ/ GB-HCT				**ff99SBildn-φ/ GB-OBC(II)**				**ff99SBildn-φ/ GB-Neck2**		
donor	acceptor	occ%		donor	acceptor	occ%		donor	acceptor	occ%
ILE10	ARG2	6.02		ASN8	ILE5	30.13		LEU11	TRP7	21.76
ARG2	ILE10	5.91		ILE10	ASP6	35.53		LYS9	ASP6	29.41
LYS4	ASN8	5.22		LYS9	ASP6	37.01		ASN8	ILE5	11.87
TRP7	LYS4	28.74		TRP7	LYS4	13.11		ILE10	ASP6	11.43
LEU11	TRP7	17.37		LEU11	TRP7	10.58		ILE10	TRP7	16.17
ILE10	ASP6	12.43		LYS9	ILE5	8.26		ASP6	ARG2	6.54
ASN8	ILE5	24.20		ILE10	TRP7	9.66		LEU11	ASN8	9.06
LYS9	ASP6	36.33		LEU11	ASN8	9.29		ILE5	ARG2	5.78
THR1	SER12	10.72		ASN8	LYS4	5.62		TRP7	THR3	6.08
LEU11	ASN8	16.05		TRP7	THR3	12.57				
SER12	TRP7	6.66								
LYS9	ILE5	9.46								
ILE10	TRP7	17.76								
ASN8	LYS4	8.72								
ARG2	LEU11	12.23								
LYS4	LYS9	9.94								
LEU11	ARG2	10.70								
ff12SB/ GB-HCT				**ff12SB/ GB-OBC(II)**				**ff12SB/ GB-Neck2**		
donor	acceptor	occ%		donor	acceptor	occ%		donor	acceptor	occ%
ILE10	ASP6	16.96		TRP7	THR3	36.51		ILE10	TRP7	23.85
ILE10	TRP7	22.52		LYS9	ILE5	27.80		LEU11	TRP7	43.71
THR1	SER12	8.91		ILE10	ASP6	53.88		LYS9	ASP6	30.94
LYS9	ILE5	17.93		LYS9	ASP6	22.29		ILE10	ASP6	14.09
ASN8	ILE5	17.16		ASN8	ILE5	19.64		TRP7	THR3	10.17

LEU11	ASN8	15.46		ASP6	THR3	7.31		SER12	ASN8	10.42
TRP7	THR3	8.23		TRP7	LYS4	5.66		LYS9	ILE5	14.26
ASN8	LYS4	24.45		ASN8	LYS4	33.84		ASN8	LYS4	21.29
LYS9	ASP6	17.24		LEU11	ASN8	6.74		ASP6	ARG2	5.03
SER12	LYS9	6.38		ILE10	TRP7	6.38		ILE5	ARG2	5.04
TRP7	LYS4	21.22		LEU11	TRP7	11.46		SER12	LYS9	6.53
SER12	ASN8	5.24						ASP6	THR3	11.26
LEU11	TRP7	20.83						TRP7	LYS4	19.12
ARG2	SER12	6.11						ASN8	ILE5	18.15
THR3	SER12	5.86						LEU11	ASN8	8.71
LYS4	THR1	6.73								
ASP6	ARG2	5.61								
ff14SB/ GB-HCT				**ff14SB/ GB-OBC(II)**				**ff14SB/ GB-Neck2**		
donor	acceptor	occ%		donor	acceptor	occ%		donor	acceptor	occ%
ASN8	ILE5	19.37		TRP7	THR3	38.71		ASP6	THR3	18.59
ILE10	TRP7	21.47		LEU11	TRP7	21.23		ASN8	LYS4	37.92
ASN8	LYS4	24.05		ILE10	ASP6	39.88		LYS9	ASP6	25.27
LEU11	ASN8	11.13		ASN8	LYS4	31.81		LEU11	TRP7	55.09
LYS9	ILE5	8.15		LYS9	ASP6	26.37		ILE10	ASP6	23.25
LEU11	TRP7	31.43		ASN8	ILE5	14.47		LYS9	ILE5	21.63
LYS9	ASP6	29.97		TRP7	LYS4	7.23		TRP7	THR3	38.33
TRP7	THR3	10.38		LYS9	ILE5	19.41		ILE10	TRP7	23.41
ASP6	THR3	7.06		ASP6	ARG2	6.30		SER12	ASN8	13.73
TRP7	LYS4	16.16		ASP6	THR3	7.65		ASN8	ILE5	13.31
SER12	LYS9	7.12		ILE10	TRP7	12.64		SER12	LYS9	7.98
ILE10	ASP6	18.42		ILE10	ILE5	7.14		TRP7	LYS4	14.48
ILE5	THR3	13.93								
ASP6	ARG2	22.09								
SER12	ASN8	7.23								
ILE10	ILE5	8.90								

Salt bridge analysis of the 300.37 K trajectory extracted from REMD simulations of peptide **ID2**.

ff96/ GB-HCT				**ff96/ GB-OBC(II)**				**ff96/ GB-Neck2**		
donor	acceptor	occ%		donor	acceptor	occ%		donor	acceptor	occ%
ARG2	ASP6	36.67		ARG2	ASP6	102.37		/	/	/
ff99SB/ GB-HCT				**ff99SB/ GB-OBC(II)**				**ff99SB/ GB-Neck2**		
donor	acceptor	occ%		donor	acceptor	occ%		donor	acceptor	occ%
LYS9	ASP6	26.59		ARG2	ASP6	87.69		ARG2	ASP6	22.56
ff99SBildn/ GB-HCT				**ff99SBildn/ GB-OBC(II)**				**ff99SBildn/ GB-Neck2**		
donor	acceptor	occ%		donor	acceptor	occ%		donor	acceptor	occ%
LYS4	ASP6	15.53		ARG2	ASP6	86.72		/	/	/
LYS9	ASP6	17.66		LYS9	ASP6	5.06				
ff99SBildn-φ/ GB-HCT				**ff99SBildn-φ/ GB-OBC(II)**				**ff99SBildn-φ/ GB-Neck2**		

donor	acceptor	occ%		donor	acceptor	occ%		donor	acceptor	occ%
ARG2	ASP6	50.02		ARG2	ASP6	117.45		/	/	/
LYS4	ASP6	23.57								
LYS9	ASP6	10.48								
ff12SB/ GB-HCT				**ff12SB/ GB-OBC(II)**				**ff12SB/ GB-Neck2**		
donor	acceptor	occ%		donor	acceptor	occ%		donor	acceptor	occ%
ARG2	ASP6	72.46		ARG2	ASP6	100.70		/	/	/
LYS4	ASP6	5.39								
LYS9	ASP6	23.02								
ff14SB/ GB-HCT				**ff14SB/ GB-OBC(II)**				**ff14SB/ GB-Neck2**		
donor	acceptor	occ%		donor	acceptor	occ%		donor	acceptor	occ%
ARG2	ASP6	89.71		ARG2	ASP6	82.41		/	/	/
LYS9	ASP6	20.18								

ANNEX 4.H. Additional information for peptide **ID2**.

H-bond analysis of the 300.37 K trajectory extracted from REMD simulations of peptide **ID3**. Data are related to H-bonds involving the backbone (donor backbone N-H, acceptor backbone C=O).

ff96/ GB-HCT				**ff96/ GB-OBC(II)**				**ff96/ GB-Neck2**		
donor	acceptor	occupancy		donor	acceptor	occupancy		donor	acceptor	occupancy
MET10	HIP6	12.20		HIP6	GLU14	10.56		LYS7	THR3	7.33
LEU9	SER2	6.62		PHE11	LYS7	23.58		HIP6	SER2	7.57
LYS8	PHE11	6.94		LYS7	GLU14	13.50				
GLU14	HIP6	10.50		GLU14	HIP6	10.39				
THR13	HIP6	6.21		MET10	HIP6	5.10				
PHE11	LYS8	5.29		LYS7	THR3	7.29				
HIP6	GLU14	9.45		LYS8	SER4	7.17				
SER4	LYS7	7.72		LEU9	ARG5	7.46				
LYS12	LYS8	13.96		HIP6	SER2	7.50				
LYS7	GLU14	7.44		ARG5	ACE1	5.12				
LYS7	THR3	18.42		HIP6	LEU9	5.26				
LYS8	SER4	16.33								
LEU9	ARG5	17.08								
HIP6	SER2	18.33								
LYS12	ARG5	5.59								
PHE11	LYS7	13.75								
ff99SB/ GB-HCT				**ff99SB/ GB-OBC(II)**				**ff99SB/ GB-Neck2**		
donor	acceptor	occupancy		donor	acceptor	occupancy		donor	acceptor	occupancy
MET10	ARG5	6.05		LYS12	LYS8	6.14		HIP6	THR3	18.85
ARG5	SER2	25.88		PHE11	LYS8	12.33		PHE11	LYS8	10.64

LEU9	ARG5	21.22		ARG5	SER2	20.82		ARG5	SER2	24.93
LYS8	SER4	16.28		LYS7	THR3	8.54		LYS7	SER4	10.03
HIP6	SER2	17.54		HIP6	THR3	20.41		LYS7	THR3	8.34
LEU9	HIP6	6.11		MET10	LYS7	8.01		HIP6	SER2	10.25
MET10	HIP6	7.14		LYS7	SER4	19.67		LYS8	ARG5	5.74
LYS7	THR3	12.02		LYS12	LEU9	7.49		LEU9	ARG5	8.17
LYS12	LEU9	10.85		LYS8	ARG5	9.95		LYS12	LEU9	8.21
LYS8	ARG5	15.56		LYS8	SER4	16.37		LYS8	SER4	7.38
LYS7	SER4	18.08		LEU9	ARG5	9.80		MET10	LYS7	6.06
HIP6	THR3	21.53		HIP6	SER2	9.56				
MET10	LYS7	11.10		MET10	HIP6	6.06				
PHE11	LYS7	6.20								
PHE11	LYS8	9.31								
LYS12	LYS8	5.57								
LEU9	SER4	5.62								
THR13	MET10	5.74								
ff99SBildn/ GB-HCT				**ff99SBildn/ GB-OBC(II)**				**ff99SBildn/ GB-Neck2**		
donor	acceptor	occupancy		donor	acceptor	occupancy		donor	acceptor	occupancy
HIP6	THR3	15.64		ARG5	SER2	18.48		MET10	LYS7	6.70
LYS7	SER4	16.65		PHE11	ARG5	11.41		ARG5	SER2	27.00
MET10	LYS7	7.11		HIP6	SER2	5.97		HIP6	THR3	21.94
ARG5	SER2	24.36		HIP6	THR3	13.96		HIP6	SER2	8.50
LEU9	ARG5	32.00		LYS8	SER4	16.64		LYS12	LEU9	9.94
LYS8	ARG5	19.69		LYS7	SER4	11.11		LYS7	SER4	9.94
LYS12	LEU9	12.16		LEU9	SER4	8.97		LYS7	THR3	6.11
HIP6	SER2	18.55		LYS7	THR3	7.74		LEU9	HIP6	5.72
LYS8	SER4	21.43		GLU14	PHE11	8.90		LYS8	ARG5	6.03
PHE11	ARG5	5.37		LEU9	ARG5	7.14		LEU9	ARG5	6.61
LEU9	HIP6	8.36		LEU9	HIP6	11.34		PHE11	LYS8	7.35
MET10	HIP6	11.63		MET10	LYS7	13.47				
MET10	ARG5	10.46		LYS12	LEU9	12.09				
LYS7	THR3	11.86								
PHE11	LYS8	7.49								
LEU9	SER4	6.27								
PHE11	LYS7	9.63								
LYS12	LYS8	6.92								
GLU14	LYS8	5.08								

ff99SBildn-φ/ GB-HCT			**ff99SBildn-φ/ GB-OBC(II)**			**ff99SBildn-φ/ GB-Neck2**		
donor	acceptor	occupancy	donor	acceptor	occupancy	donor	acceptor	occupancy
HIP6	THR3	12.69	LYS7	SER4	14.81	HIP6	THR3	21.43
ARG5	SER2	18.39	LYS8	ARG5	5.39	LYS12	LEU9	9.42
HIP6	GLU14	5.44	ARG5	SER2	19.48	LYS7	SER4	10.38
LYS8	ARG5	13.11	LYS12	LEU9	17.73	MET10	LYS7	5.24
ARG5	GLU14	7.61	LEU9	ARG5	18.44	LYS8	ARG5	5.82
LYS12	LEU9	9.30	THR13	LEU9	9.18	HIP6	SER2	9.46
LEU9	ARG5	26.65	LYS8	SER4	18.12	ARG5	SER2	24.55
LYS7	SER4	21.07	LYS7	THR3	8.79	LYS7	THR3	6.90
LYS8	SER4	23.39	HIP6	SER2	9.22	LEU9	HIP6	5.04
MET10	HIP6	13.69	MET10	LYS7	13.70	LYS8	SER4	6.13
PHE11	LYS8	6.01	HIP6	THR3	15.22	LEU9	ARG5	5.33
HIP6	SER2	14.28	PHE11	LYS8	5.62			
MET10	LYS7	7.13	LEU9	SER4	5.90			
LYS7	THR3	7.22	LEU9	HIP6	9.70			
LEU9	HIP6	10.05	PHE11	ARG5	5.72			
MET10	ARG5	9.48	PHE11	LYS7	8.55			
PHE11	ARG5	11.58	LYS7	GLU14	5.83			
LYS12	HIP6	9.55						
ff12SB/ GB-HCT			**ff12SB/ GB-OBC(II)**			**ff12SB/ GB-Neck2**		
donor	acceptor	occupancy	donor	acceptor	occupancy	donor	acceptor	occupancy
LYS8	SER4	38.20	HIP6	THR3	14.28	MET10	HIP6	27.35
MET10	HIP6	40.33	ARG5	SER2	22.87	LEU9	ARG5	50.29
GLU14	LYS8	13.53	PHE11	LYS8	7.44	LYS8	SER4	38.23
PHE11	LYS7	31.49	LYS12	LYS8	12.82	LYS7	THR3	32.22
LYS7	THR3	29.21	LYS8	SER4	25.78	HIP6	SER2	30.96
HIP6	SER2	29.39	LEU9	ARG5	49.56	ARG5	SER2	29.42
LYS7	SER4	16.40	LYS7	SER4	9.99	HIP6	THR3	19.45
LYS12	LYS8	26.66	MET10	HIP6	14.20	PHE11	LYS7	10.45
MET10	LYS7	5.56	PHE11	LYS7	11.89	LEU9	HIP6	7.38
HIP6	THR3	14.26	LYS7	THR3	17.67	PHE11	LYS8	7.84
LEU9	ARG5	49.13	HIP6	GLU14	15.49	LYS12	MET10	5.83
PHE11	LYS8	12.51	LYS12	LEU9	31.28	MET10	LYS7	10.40
THR13	LYS8	9.22	MET10	LYS7	9.54	THR13	MET10	14.66

ARG5	SER2	20.53		HIP6	SER2	10.93		GLU14	MET10	5.55
LYS8	ARG5	8.69		LYS8	ARG5	14.57		LYS7	SER4	16.11
LYS12	LEU9	6.05		SER4	LEU9	7.38		LYS8	ARG5	7.02
								LYS12	LEU9	8.69
								LYS12	LYS8	6.43
ff14SB/ GB-HCT				**ff14SB/ GB-OBC(II)**				**ff14SB/ GB-Neck2**		
donor	acceptor	occupancy		donor	acceptor	occupancy		donor	acceptor	occupancy
HIP6	THR3	19.44		LYS8	SER4	37.49		LYS7	SER4	15.62
LYS7	SER4	17.64		ARG5	SER2	27.67		ARG5	SER2	26.13
LYS7	THR3	22.91		HIP6	THR3	20.23		HIP6	SER2	21.54
LYS12	HIP6	7.93		THR13	MET10	11.03		LYS8	ARG5	10.52
LEU9	ARG5	29.21		LYS7	SER4	13.52		LEU9	HIP6	9.86
MET10	HIP6	15.89		MET10	LYS7	7.60		PHE11	LYS8	11.46
LYS8	SER4	29.77		LYS8	ARG5	5.23		LYS7	THR3	24.13
LYS12	LEU9	9.82		LEU9	ARG5	14.12		THR13	MET10	11.60
THR13	MET10	16.21		LYS7	THR3	18.48		HIP6	THR3	24.56
GLU14	PHE11	6.13		LEU9	HIP6	7.54		LYS12	LEU9	18.98
ARG5	SER2	25.74		LYS12	LEU9	14.41		MET10	LYS7	10.58
MET10	LYS7	12.90		PHE11	LYS8	6.22		GLU14	MET10	5.80
PHE11	LYS7	10.62		HIP6	SER2	9.16		GLU14	PHE11	5.52
PHE11	LYS8	6.78		GLU14	PHE11	7.42		LYS12	LYS8	9.79
LYS8	ARG5	11.38		MET10	ARG5	6.22		THR13	LEU9	7.52
LEU9	HIP6	10.88		LEU9	SER4	6.50		LYS8	SER4	28.69
SER4	MET10	5.58		PHE11	ARG5	12.00		THR13	LYS8	5.59
								MET10	HIP6	19.31
								LEU9	ARG5	29.52
								PHE11	LYS7	22.55

Salt bridge analysis of the 300.37 K trajectory extracted from REMD simulations of peptide **ID3**.

ff96/ GB-HCT				**ff96/ GB-OBC(II)**				**ff96/ GB-Neck2**		
donor	acceptor	occ%		donor	acceptor	occ%		donor	acceptor	occ%
ARG5	GLU14	65.51		ARG5	GLU14	35.78		/	/	/
HIP6	GLU14	29.43		HIP6	GLU14	35.93				
LYS7	GLU14	15.29		LYS7	GLU14	6.59				
LYS8	GLU14	5.55								
LYS12	GLU14	18.81								
ff99SB/ GB-HCT				**ff99SB/ GB-OBC(II)**				**ff99SB/ GB-Neck2**		
donor	acceptor	occ%		donor	acceptor	occ%		donor	acceptor	occ%
ARG5	GLU14	37.00		ARG5	GLU14	48.53		/	/	/

HIP6	GLU14	8.09		HIP6	GLU14	6.64				
LYS12	GLU14	21.66		LYS12	GLU14	11.77				
ff99SBildn/ GB-HCT				**ff99SBildn/ GB-OBC(II)**				**ff99SBildn/ GB-Neck2**		
donor	acceptor	occ%		donor	acceptor	occ%		donor	acceptor	occ%
ARG5	GLU14	42.41		ARG5	GLU14	60.05		/	/	/
HIP6	GLU14	5.33		HIP6	GLU14	14.59				
LYS7	GLU14	5.06		LYS12	GLU14	5.25				
LYS8	GLU14	13.73								
LYS12	GLU14	28.53								
ff99SBildn-φ/ GB-HCT				**ff99SBildn-φ/ GB-OBC(II)**				**ff99SBildn-φ/ GB-Neck2**		
donor	acceptor	occ%		donor	acceptor	occ%		donor	acceptor	occ%
ARG5	GLU14	35.82		ARG5	GLU14	56.98		/	/	/
HIP6	GLU14	20.02		HIP6	GLU14	9.06				
LYS12	GLU14	25.21		LYS12	GLU14	14.71				
ff12SB/ GB-HCT				**ff12SB/ GB-OBC(II)**				**ff12SB/ GB-Neck2**		
donor	acceptor	occ%		donor	acceptor	occ%		donor	acceptor	occ%
ARG5	GLU14	47.60		ARG5	GLU14	51.19		HIP6	GLU14	20.19
HIP6	GLU14	6.02		LYS12	GLU14	9.82				
LYS8	GLU14	27.77								
LYS12	GLU14	28.10								
ff14SB/ GB-HCT				**ff14SB/ GB-OBC(II)**				**ff14SB/ GB-Neck2**		
donor	acceptor	occ%		donor	acceptor	occ%		donor	acceptor	occ%
ARG5	GLU14	42.49		ARG5	GLU14	93.63		/	/	/
HIP6	GLU14	8.69								
LYS7	GLU14	5.26								
LYS8	GLU14	11.09								

ANNEX 5.A. Additional information about QM calculations

Cartesian coordinates (pdb format) and energies (a.u.) of all structures optimized at the MPW1B95/6-31+G(d,p) level with the CPCM solvent model for water. 310R = right-handed 3_{10} helix; 310L = left-handed 3_{10} helix; ext = extended. Vibrational analysis has been conducted at standard conditions (T = 298.15 K; P = 1 atm)

COMPND Ac-L-Ala-R-I-L-Ala-Aib-L-Ala-NHMe_310R
REMARK Energy(ZPE)= -1735.026859
REMARK #IF = 0
ATOM 1 C P01 1 5.632 -2.163 -1.911
ATOM 2 H P01 1 5.339 -1.678 -2.841
ATOM 3 H P01 1 6.582 -1.756 -1.572
ATOM 4 H P01 1 5.755 -3.227 -2.117
ATOM 5 C P01 1 4.531 -1.998 -0.910
ATOM 6 O P01 1 3.361 -2.299 -1.161
ATOM 7 N P01 1 4.865 -1.488 0.295
ATOM 8 H P01 1 5.834 -1.303 0.500
ATOM 9 C P01 1 3.908 -1.455 1.379
ATOM 10 H P01 1 3.482 -2.452 1.513
ATOM 11 C P01 1 4.579 -1.005 2.667
ATOM 12 H P01 1 5.012 -0.010 2.558
ATOM 13 H P01 1 3.848 -0.980 3.473
ATOM 14 H P01 1 5.367 -1.706 2.942
ATOM 15 C P01 1 2.709 -0.570 1.071
ATOM 16 O P01 1 1.625 -0.784 1.612
ATOM 17 N P01 1 2.898 0.439 0.203
ATOM 18 H P01 1 3.814 0.547 -0.205
ATOM 19 C P01 1 1.836 1.351 -0.189
ATOM 20 C P01 1 1.379 2.168 1.033
ATOM 21 H P01 1 2.256 2.343 1.662
ATOM 22 H P01 1 0.706 1.552 1.626
ATOM 23 C P01 1 0.685 3.486 0.745
ATOM 24 H P01 1 0.020 3.744 1.565
ATOM 25 H P01 1 0.102 3.464 -0.173
ATOM 26 N P01 1 1.657 4.622 0.640
ATOM 27 H P01 1 2.269 4.606 1.457
ATOM 28 H P01 1 1.140 5.499 0.714
ATOM 29 C P01 1 2.487 4.680 -0.601
ATOM 30 H P01 1 1.804 4.918 -1.415
ATOM 31 H P01 1 3.170 5.516 -0.467
ATOM 32 C P01 1 3.244 3.400 -0.893
ATOM 33 H P01 1 3.922 3.647 -1.711
ATOM 34 H P01 1 3.883 3.127 -0.049
ATOM 35 C P01 1 2.359 2.235 -1.333
ATOM 36 H P01 1 2.900 1.593 -2.030
ATOM 37 H P01 1 1.502 2.622 -1.889
ATOM 38 C P01 1 0.633 0.580 -0.748
ATOM 39 O P01 1 -0.485 1.100 -0.719
ATOM 40 N P01 1 0.853 -0.617 -1.302
ATOM 41 H P01 1 1.773 -1.048 -1.258
ATOM 42 C P01 1 -0.236 -1.353 -1.904
ATOM 43 H P01 1 -0.726 -0.712 -2.640
ATOM 44 C P01 1 0.284 -2.609 -2.584
ATOM 45 H P01 1 0.794 -3.257 -1.871
ATOM 46 H P01 1 -0.547 -3.154 -3.028
ATOM 47 H P01 1 0.987 -2.342 -3.374
ATOM 48 C P01 1 -1.344 -1.704 -0.913
ATOM 49 O P01 1 -2.473 -1.957 -1.342
ATOM 50 N P01 1 -1.033 -1.715 0.389
ATOM 51 H P01 1 -0.091 -1.463 0.672
ATOM 52 C P01 1 -2.004 -1.997 1.439
ATOM 53 C P01 1 -1.324 -1.732 2.782
ATOM 54 H P01 1 -0.492 -2.424 2.919
ATOM 55 H P01 1 -0.938 -0.713 2.835
ATOM 56 H P01 1 -2.039 -1.885 3.589
ATOM 57 C P01 1 -2.484 -3.441 1.369
ATOM 58 H P01 1 -3.196 -3.633 2.169
ATOM 59 H P01 1 -2.965 -3.644 0.414
ATOM 60 H P01 1 -1.628 -4.106 1.487
ATOM 61 C P01 1 -3.203 -1.038 1.350
ATOM 62 O P01 1 -4.293 -1.356 1.822
ATOM 63 N P01 1 -2.978 0.175 0.812
ATOM 64 H P01 1 -2.075 0.394 0.404
ATOM 65 C P01 1 -4.016 1.179 0.765
ATOM 66 H P01 1 -4.610 1.086 1.676
ATOM 67 C P01 1 -3.406 2.570 0.692
ATOM 68 H P01 1 -2.779 2.675 -0.194
ATOM 69 H P01 1 -4.199 3.314 0.649
ATOM 70 H P01 1 -2.795 2.757 1.575
ATOM 71 C P01 1 -5.010 0.983 -0.380
ATOM 72 O P01 1 -6.012 1.702 -0.444
ATOM 73 N P01 1 -4.733 0.038 -1.279
ATOM 74 H P01 1 -3.911 -0.541 -1.157
ATOM 75 C P01 1 -5.613 -0.222 -2.392
ATOM 76 H P01 1 -6.595 -0.552 -2.049
ATOM 77 H P01 1 -5.749 0.675 -2.997
ATOM 78 H P01 1 -5.173 -1.002 -3.008
END

COMPND Ac-L-Ala-R-II-L-Ala-Aib-L-Ala-NHMe_310R
REMARK Energy(ZPE)= -1792.373533
REMARK #IF = 0
ATOM 1 C P02 1 5.965 -1.967 -1.698
ATOM 2 H P02 1 5.647 -1.601 -2.675
ATOM 3 H P02 1 6.883 -1.462 -1.407
ATOM 4 H P02 1 6.157 -3.035 -1.792
ATOM 5 C P02 1 4.846 -1.766 -0.723
ATOM 6 O P02 1 3.728 -2.258 -0.894
ATOM 7 N P02 1 5.099 -0.998 0.358
ATOM 8 H P02 1 6.033 -0.654 0.513
ATOM 9 C P02 1 4.123 -0.868 1.419
ATOM 10 H P02 1 3.822 -1.864 1.753
ATOM 11 C P02 1 4.708 -0.089 2.586
ATOM 12 H P02 1 5.012 0.912 2.278
ATOM 13 H P02 1 3.966 0.001 3.377
ATOM 14 H P02 1 5.575 -0.612 2.989
ATOM 15 C P02 1 2.830 -0.223 0.940
ATOM 16 O P02 1 1.768 -0.466 1.514
ATOM 17 N P02 1 2.922 0.611 -0.106
ATOM 18 H P02 1 3.838 0.767 -0.500
ATOM 19 C P02 1 1.793 1.276 -0.723
ATOM 20 C P02 1 2.218 1.905 -2.072
ATOM 21 H P02 1 2.216 1.182 -2.888
ATOM 22 H P02 1 3.237 2.281 -1.954
ATOM 23 C P02 1 1.266 3.083 -2.277
ATOM 24 H P02 1 1.707 3.874 -2.884

```
ATOM     25  H   P02     1       0.348   2.755  -2.774
ATOM     26  C   P02     1       1.263   2.482   0.026
ATOM     27  C   P02     1       1.068   2.643   1.390
ATOM     28  H   P02     1       1.293   1.842   2.081
ATOM     29  C   P02     1       0.577   3.860   1.853
ATOM     30  H   P02     1       0.428   4.009   2.916
ATOM     31  C   P02     1       0.276   4.888   0.963
ATOM     32  H   P02     1      -0.103   5.830   1.338
ATOM     33  C   P02     1       0.466   4.716  -0.406
ATOM     34  H   P02     1       0.239   5.520  -1.096
ATOM     35  C   P02     1       0.967   3.507  -0.869
ATOM     36  C   P02     1       0.662   0.281  -1.022
ATOM     37  O   P02     1      -0.504   0.670  -1.096
ATOM     38  N   P02     1       0.997  -0.992  -1.282
ATOM     39  H   P02     1       1.956  -1.315  -1.182
ATOM     40  C   P02     1      -0.032  -1.939  -1.652
ATOM     41  H   P02     1      -0.552  -1.571  -2.539
ATOM     42  C   P02     1       0.577  -3.300  -1.947
ATOM     43  H   P02     1       1.080  -3.705  -1.069
ATOM     44  H   P02     1      -0.207  -3.992  -2.250
ATOM     45  H   P02     1       1.300  -3.221  -2.758
ATOM     46  C   P02     1      -1.124  -2.067  -0.595
ATOM     47  O   P02     1      -2.252  -2.439  -0.933
ATOM     48  N   P02     1      -0.795  -1.780   0.671
ATOM     49  H   P02     1       0.140  -1.433   0.868
ATOM     50  C   P02     1      -1.743  -1.856   1.776
ATOM     51  C   P02     1      -1.064  -1.266   3.012
ATOM     52  H   P02     1      -0.184  -1.857   3.269
ATOM     53  H   P02     1      -0.749  -0.237   2.838
ATOM     54  H   P02     1      -1.757  -1.290   3.852
ATOM     55  C   P02     1      -2.156  -3.297   2.044
ATOM     56  H   P02     1      -2.870  -3.328   2.865
ATOM     57  H   P02     1      -2.617  -3.739   1.163
ATOM     58  H   P02     1      -1.274  -3.877   2.316
ATOM     59  C   P02     1      -2.987  -0.995   1.500
ATOM     60  O   P02     1      -4.053  -1.244   2.060
ATOM     61  N   P02     1      -2.828   0.074   0.699
ATOM     62  H   P02     1      -1.950   0.225   0.211
ATOM     63  C   P02     1      -3.919   0.985   0.446
ATOM     64  H   P02     1      -4.470   1.119   1.379
ATOM     65  C   P02     1      -3.388   2.329  -0.030
ATOM     66  H   P02     1      -2.822   2.220  -0.955
ATOM     67  H   P02     1      -4.220   3.008  -0.206
ATOM     68  H   P02     1      -2.735   2.763   0.727
ATOM     69  C   P02     1      -4.949   0.451  -0.550
ATOM     70  O   P02     1      -6.010   1.062  -0.710
ATOM     71  N   P02     1      -4.639  -0.655  -1.229
ATOM     72  H   P02     1      -3.772  -1.143  -1.036
ATOM     73  C   P02     1      -5.560  -1.221  -2.186
ATOM     74  H   P02     1      -6.492  -1.523  -1.704
ATOM     75  H   P02     1      -5.801  -0.498  -2.966
ATOM     76  H   P02     1      -5.097  -2.093  -2.640
END

COMPND Ac-L-Ala-RRR-IIIa-L-Ala-Aib-L-Ala-
NHMe_310R
REMARK Energy(ZPE)= -1905.640014
REMARK #IF = 0
ATOM      1  C   P03     1      -4.607   3.731  -1.872
ATOM      2  H   P03     1      -4.216   3.552  -2.872
ATOM      3  H   P03     1      -5.624   3.351  -1.806
ATOM      4  H   P03     1      -4.621   4.809  -1.709
ATOM      5  C   P03     1      -3.681   3.113  -0.870
ATOM      6  O   P03     1      -2.462   3.309  -0.893
ATOM      7  N   P03     1      -4.231   2.316   0.070
ATOM      8  H   P03     1      -5.233   2.214   0.105
ATOM      9  C   P03     1      -3.448   1.828   1.185
ATOM     10  H   P03     1      -2.917   2.668   1.640
ATOM     11  C   P03     1      -4.350   1.172   2.218
ATOM     12  H   P03     1      -4.900   0.336   1.784
ATOM     13  H   P03     1      -3.749   0.799   3.045
ATOM     14  H   P03     1      -5.061   1.900   2.609
ATOM     15  C   P03     1      -2.343   0.874   0.758
ATOM     16  O   P03     1      -1.361   0.699   1.481
ATOM     17  N   P03     1      -2.489   0.243  -0.418
ATOM     18  H   P03     1      -3.337   0.392  -0.942
ATOM     19  C   P03     1      -1.489  -0.665  -0.931
ATOM     20  C   P03     1      -1.992  -1.390  -2.204
ATOM     21  H   P03     1      -2.949  -1.004  -2.553
ATOM     22  H   P03     1      -1.267  -1.304  -3.011
ATOM     23  C   P03     1      -2.052  -2.854  -1.725
ATOM     24  H   P03     1      -2.027  -3.599  -2.515
ATOM     25  O   P03     1      -0.864  -2.911  -0.928
ATOM     26  C   P03     1      -1.228  -1.906   0.011
ATOM     27  H   P03     1      -0.454  -1.756   0.755
ATOM     28  C   P03     1      -2.581  -2.386   0.460
ATOM     29  C   P03     1      -3.124  -2.988  -0.675
ATOM     30  C   P03     1      -4.404  -3.507  -0.667
ATOM     31  H   P03     1      -4.836  -3.967  -1.547
ATOM     32  C   P03     1      -5.125  -3.435   0.527
ATOM     33  H   P03     1      -6.122  -3.855   0.574
ATOM     34  C   P03     1      -4.580  -2.840   1.661
ATOM     35  H   P03     1      -5.160  -2.803   2.575
ATOM     36  C   P03     1      -3.296  -2.291   1.637
ATOM     37  H   P03     1      -2.881  -1.810   2.515
ATOM     38  C   P03     1      -0.166   0.061  -1.182
ATOM     39  O   P03     1       0.887  -0.571  -1.284
ATOM     40  N   P03     1      -0.188   1.399  -1.269
ATOM     41  H   P03     1      -1.050   1.926  -1.167
ATOM     42  C   P03     1       1.054   2.118  -1.442
ATOM     43  H   P03     1       1.558   1.751  -2.339
ATOM     44  C   P03     1       0.790   3.609  -1.573
ATOM     45  H   P03     1       0.286   3.997  -0.687
ATOM     46  H   P03     1       1.733   4.137  -1.705
ATOM     47  H   P03     1       0.157   3.802  -2.438
ATOM     48  C   P03     1       2.047   1.847  -0.314
ATOM     49  O   P03     1       3.255   1.997  -0.522
ATOM     50  N   P03     1       1.554   1.459   0.869
ATOM     51  H   P03     1       0.553   1.321   0.967
ATOM     52  C   P03     1       2.397   1.138   2.014
ATOM     53  C   P03     1       1.501   0.512   3.083
ATOM     54  H   P03     1       0.752   1.236   3.409
ATOM     55  H   P03     1       0.984  -0.367   2.698
ATOM     56  H   P03     1       2.105   0.224   3.942
ATOM     57  C   P03     1       3.078   2.386   2.559
ATOM     58  H   P03     1       3.706   2.122   3.408
ATOM     59  H   P03     1       3.699   2.853   1.796
ATOM     60  H   P03     1       2.317   3.096   2.885
ATOM     61  C   P03     1       3.453   0.083   1.647
ATOM     62  O   P03     1       4.506   0.011   2.279
ATOM     63  N   P03     1       3.132  -0.798   0.681
ATOM     64  H   P03     1       2.284  -0.679   0.135
```

ATOM 65 C P03 1 4.023 -1.881 0.335
ATOM 66 H P03 1 4.484 -2.239 1.257
ATOM 67 C P03 1 3.253 -3.016 -0.323
ATOM 68 H P03 1 2.770 -2.682 -1.241
ATOM 69 H P03 1 3.939 -3.826 -0.564
ATOM 70 H P03 1 2.487 -3.393 0.355
ATOM 71 C P03 1 5.193 -1.464 -0.557
ATOM 72 O P03 1 6.092 -2.276 -0.792
ATOM 73 N P03 1 5.180 -0.230 -1.065
ATOM 74 H P03 1 4.439 0.415 -0.817
ATOM 75 C P03 1 6.248 0.236 -1.917
ATOM 76 H P03 1 6.355 -0.407 -2.791
ATOM 77 H P03 1 6.016 1.246 -2.246
ATOM 78 H P03 1 7.201 0.247 -1.384
END

COMPND Ac-L-Ala-RSR-IIIb-L-Ala-Aib-L-Ala-NHMe_310R
REMARK Energy(ZPE)= -1905.640304
REMARK #IF = 0
ATOM 1 C P04 1 -5.843 -1.372 2.206
ATOM 2 H P04 1 -5.492 -0.677 2.967
ATOM 3 H P04 1 -6.755 -0.986 1.756
ATOM 4 H P04 1 -6.064 -2.320 2.698
ATOM 5 C P04 1 -4.747 -1.598 1.212
ATOM 6 O P04 1 -3.605 -1.921 1.552
ATOM 7 N P04 1 -5.049 -1.422 -0.092
ATOM 8 H P04 1 -6.000 -1.217 -0.355
ATOM 9 C P04 1 -4.101 -1.773 -1.127
ATOM 10 H P04 1 -3.775 -2.805 -0.980
ATOM 11 C P04 1 -4.733 -1.624 -2.501
ATOM 12 H P04 1 -5.066 -0.600 -2.674
ATOM 13 H P04 1 -4.009 -1.889 -3.269
ATOM 14 H P04 1 -5.589 -2.293 -2.594
ATOM 15 C P04 1 -2.821 -0.954 -1.039
ATOM 16 O P04 1 -1.765 -1.401 -1.489
ATOM 17 N P04 1 -2.906 0.257 -0.468
ATOM 18 H P04 1 -3.815 0.592 -0.184
ATOM 19 C P04 1 -1.764 1.138 -0.349
ATOM 20 C P04 1 -1.329 1.708 -1.720
ATOM 21 H P04 1 -1.871 1.200 -2.515
ATOM 22 H P04 1 -0.260 1.606 -1.885
ATOM 23 C P04 1 -1.773 3.181 -1.596
ATOM 24 H P04 1 -2.030 3.678 -2.526
ATOM 25 O P04 1 -2.930 3.066 -0.746
ATOM 26 C P04 1 -2.269 2.445 0.354
ATOM 27 H P04 1 -2.951 2.268 1.183
ATOM 28 C P04 1 -1.112 3.374 0.590
ATOM 29 C P04 1 -0.802 3.868 -0.675
ATOM 30 C P04 1 -0.393 3.744 1.708
ATOM 31 H P04 1 -0.629 3.354 2.691
ATOM 32 C P04 1 0.250 4.743 -0.862
ATOM 33 H P04 1 0.506 5.122 -1.843
ATOM 34 C P04 1 0.655 4.650 1.531
ATOM 35 H P04 1 1.228 4.979 2.389
ATOM 36 C P04 1 0.972 5.138 0.267
ATOM 37 H P04 1 1.787 5.843 0.159
ATOM 38 C P04 1 -0.627 0.466 0.415
ATOM 39 O P04 1 0.540 0.826 0.253
ATOM 40 N P04 1 -0.958 -0.494 1.292
ATOM 41 H P04 1 -1.915 -0.827 1.369
ATOM 42 C P04 1 0.070 -1.147 2.070
ATOM 43 H P04 1 0.626 -0.392 2.630
ATOM 44 C P04 1 -0.553 -2.144 3.035
ATOM 45 H P04 1 -1.130 -2.897 2.498
ATOM 46 H P04 1 0.230 -2.638 3.608
ATOM 47 H P04 1 -1.217 -1.628 3.728
ATOM 48 C P04 1 1.129 -1.833 1.212
ATOM 49 O P04 1 2.251 -2.033 1.690
ATOM 50 N P04 1 0.791 -2.198 -0.031
ATOM 51 H P04 1 -0.132 -1.961 -0.384
ATOM 52 C P04 1 1.722 -2.847 -0.947
ATOM 53 C P04 1 1.050 -2.923 -2.318
ATOM 54 H P04 1 0.155 -3.542 -2.258
ATOM 55 H P04 1 0.764 -1.934 -2.676
ATOM 56 H P04 1 1.738 -3.374 -3.032
ATOM 57 C P04 1 2.079 -4.247 -0.464
ATOM 58 H P04 1 2.764 -4.716 -1.167
ATOM 59 H P04 1 2.551 -4.212 0.516
ATOM 60 H P04 1 1.169 -4.845 -0.401
ATOM 61 C P04 1 2.998 -2.007 -1.123
ATOM 62 O P04 1 4.053 -2.539 -1.465
ATOM 63 N P04 1 2.875 -0.676 -0.971
ATOM 64 H P04 1 2.000 -0.280 -0.642
ATOM 65 C P04 1 3.987 0.216 -1.197
ATOM 66 H P04 1 4.584 -0.199 -2.011
ATOM 67 C P04 1 3.489 1.600 -1.587
ATOM 68 H P04 1 2.855 2.023 -0.807
ATOM 69 H P04 1 4.340 2.261 -1.742
ATOM 70 H P04 1 2.913 1.544 -2.510
ATOM 71 C P04 1 4.951 0.322 -0.015
ATOM 72 O P04 1 5.992 0.975 -0.140
ATOM 73 N P04 1 4.615 -0.294 1.120
ATOM 74 H P04 1 3.764 -0.842 1.171
ATOM 75 C P04 1 5.476 -0.240 2.277
ATOM 76 H P04 1 6.445 -0.699 2.068
ATOM 77 H P04 1 5.649 0.792 2.584
ATOM 78 H P04 1 4.998 -0.778 3.092
END

COMPND Ac-L-Ala-SRR-IV-L-Ala-Aib-L-Ala-NHMe_310R
REMARK Energy(ZPE)= -1717.366164
REMARK #IF = 0
ATOM 1 C P05 1 5.683 -2.068 -1.874
ATOM 2 H P05 1 5.385 -1.658 -2.838
ATOM 3 H P05 1 6.609 -1.596 -1.551
ATOM 4 H P05 1 5.856 -3.136 -2.007
ATOM 5 C P05 1 4.559 -1.885 -0.900
ATOM 6 O P05 1 3.408 -2.255 -1.147
ATOM 7 N P05 1 4.853 -1.279 0.271
ATOM 8 H P05 1 5.810 -1.036 0.471
ATOM 9 C P05 1 3.881 -1.204 1.339
ATOM 10 H P05 1 3.466 -2.200 1.514
ATOM 11 C P05 1 4.533 -0.690 2.614
ATOM 12 H P05 1 4.961 0.302 2.463
ATOM 13 H P05 1 3.791 -0.632 3.407
ATOM 14 H P05 1 5.324 -1.370 2.931
ATOM 15 C P05 1 2.675 -0.346 0.981
ATOM 16 O P05 1 1.608 -0.506 1.576
ATOM 17 N P05 1 2.836 0.570 0.016
ATOM 18 H P05 1 3.748 0.654 -0.407

```
ATOM     19  C   P05     1       1.771   1.456  -0.414
ATOM     20  C   P05     1       1.340   2.494   0.659
ATOM     21  H   P05     1       0.610   2.092   1.359
ATOM     22  C   P05     1       2.273   2.368  -1.575
ATOM     23  H   P05     1       3.272   2.077  -1.909
ATOM     24  H   P05     1       1.606   2.292  -2.435
ATOM     25  C   P05     1       3.251   3.873   0.155
ATOM     26  H   P05     1       3.417   4.914   0.439
ATOM     27  H   P05     1       4.217   3.462  -0.146
ATOM     28  C   P05     1       2.598   3.073   1.309
ATOM     29  H   P05     1       3.256   2.315   1.732
ATOM     30  H   P05     1       2.299   3.734   2.124
ATOM     31  C   P05     1       2.214   3.771  -0.972
ATOM     32  H   P05     1       2.286   4.559  -1.721
ATOM     33  C   P05     1       0.898   3.684  -0.200
ATOM     34  H   P05     1       0.039   3.464  -0.832
ATOM     35  H   P05     1       0.693   4.569   0.406
ATOM     36  C   P05     1       0.574   0.629  -0.883
ATOM     37  O   P05     1      -0.568   1.096  -0.871
ATOM     38  N   P05     1       0.817  -0.605  -1.353
ATOM     39  H   P05     1       1.749  -1.002  -1.308
ATOM     40  C   P05     1      -0.266  -1.406  -1.875
ATOM     41  H   P05     1      -0.779  -0.840  -2.656
ATOM     42  C   P05     1       0.266  -2.707  -2.453
ATOM     43  H   P05     1       0.788  -3.289  -1.693
ATOM     44  H   P05     1      -0.560  -3.298  -2.845
ATOM     45  H   P05     1       0.960  -2.499  -3.267
ATOM     46  C   P05     1      -1.354  -1.689  -0.843
ATOM     47  O   P05     1      -2.493  -1.967  -1.231
ATOM     48  N   P05     1      -1.015  -1.629   0.452
ATOM     49  H   P05     1      -0.073  -1.341   0.702
ATOM     50  C   P05     1      -1.962  -1.863   1.534
ATOM     51  C   P05     1      -1.257  -1.530   2.849
ATOM     52  H   P05     1      -0.413  -2.204   2.996
ATOM     53  H   P05     1      -0.886  -0.505   2.851
ATOM     54  H   P05     1      -1.954  -1.659   3.676
ATOM     55  C   P05     1      -2.436  -3.311   1.546
ATOM     56  H   P05     1      -3.135  -3.464   2.365
ATOM     57  H   P05     1      -2.929  -3.566   0.610
ATOM     58  H   P05     1      -1.575  -3.965   1.687
ATOM     59  C   P05     1      -3.167  -0.913   1.427
ATOM     60  O   P05     1      -4.245  -1.209   1.939
ATOM     61  N   P05     1      -2.954   0.273   0.828
ATOM     62  H   P05     1      -2.063   0.467   0.381
ATOM     63  C   P05     1      -3.990   1.278   0.764
ATOM     64  H   P05     1      -4.558   1.229   1.696
ATOM     65  C   P05     1      -3.379   2.662   0.610
ATOM     66  H   P05     1      -2.801   2.732  -0.313
ATOM     67  H   P05     1      -4.169   3.409   0.584
ATOM     68  H   P05     1      -2.718   2.876   1.449
ATOM     69  C   P05     1      -5.016   1.034  -0.343
ATOM     70  O   P05     1      -6.019   1.750  -0.413
ATOM     71  N   P05     1      -4.760   0.051  -1.208
ATOM     72  H   P05     1      -3.936  -0.522  -1.079
ATOM     73  C   P05     1      -5.667  -0.257  -2.287
ATOM     74  H   P05     1      -6.637  -0.580  -1.906
ATOM     75  H   P05     1      -5.825   0.616  -2.921
ATOM     76  H   P05     1      -5.238  -1.057  -2.884
END

COMPND Ac-L-Ala-SRR-IV-L-Ala-Aib-L-Ala-NHMe_ext
REMARK Energy(ZPE)= -1717.338937
REMARK #IF = 0
ATOM      1  C   P05     1       9.672  -2.049  -1.040
ATOM      2  H   P05     1      10.498  -2.246  -0.357
ATOM      3  H   P05     1       9.707  -2.802  -1.827
ATOM      4  H   P05     1       9.805  -1.064  -1.484
ATOM      5  C   P05     1       8.378  -2.192  -0.289
ATOM      6  O   P05     1       8.063  -3.249   0.265
ATOM      7  N   P05     1       7.585  -1.108  -0.255
ATOM      8  H   P05     1       7.836  -0.256  -0.735
ATOM      9  C   P05     1       6.311  -1.102   0.416
ATOM     10  H   P05     1       5.808  -2.049   0.203
ATOM     11  C   P05     1       6.467  -0.949   1.928
ATOM     12  H   P05     1       6.940   0.005   2.167
ATOM     13  H   P05     1       5.502  -0.998   2.433
ATOM     14  H   P05     1       7.093  -1.757   2.302
ATOM     15  C   P05     1       5.503   0.057  -0.171
ATOM     16  O   P05     1       6.071   0.966  -0.773
ATOM     17  N   P05     1       4.186  -0.015   0.078
ATOM     18  H   P05     1       3.893  -0.844   0.574
ATOM     19  C   P05     1       3.096   0.885  -0.299
ATOM     20  C   P05     1       2.806   1.984   0.746
ATOM     21  H   P05     1       2.349   1.606   1.662
ATOM     22  C   P05     1       3.318   1.722  -1.599
ATOM     23  H   P05     1       4.302   1.554  -2.025
ATOM     24  H   P05     1       2.573   1.436  -2.343
ATOM     25  C   P05     1       4.289   3.604  -0.274
ATOM     26  H   P05     1       4.237   4.676  -0.071
ATOM     27  H   P05     1       5.245   3.394  -0.751
ATOM     28  C   P05     1       4.085   2.784   1.021
ATOM     29  H   P05     1       4.934   2.147   1.265
ATOM     30  H   P05     1       3.916   3.435   1.880
ATOM     31  C   P05     1       3.103   3.166  -1.138
ATOM     32  H   P05     1       2.875   3.845  -1.960
ATOM     33  C   P05     1       2.005   2.993  -0.087
ATOM     34  H   P05     1       1.074   2.601  -0.500
ATOM     35  H   P05     1       1.790   3.908   0.469
ATOM     36  C   P05     1       1.921  -0.081  -0.567
ATOM     37  O   P05     1       2.028  -0.942  -1.440
ATOM     38  N   P05     1       0.817   0.052   0.175
ATOM     39  H   P05     1       0.721   0.773   0.875
ATOM     40  C   P05     1      -0.357  -0.760  -0.033
ATOM     41  H   P05     1      -0.510  -0.875  -1.108
ATOM     42  C   P05     1      -0.211  -2.140   0.604
ATOM     43  H   P05     1      -0.087  -2.050   1.684
ATOM     44  H   P05     1      -1.085  -2.758   0.401
ATOM     45  H   P05     1       0.667  -2.632   0.187
ATOM     46  C   P05     1      -1.528   0.004   0.580
ATOM     47  O   P05     1      -1.325   0.891   1.412
ATOM     48  N   P05     1      -2.737  -0.390   0.172
ATOM     49  H   P05     1      -2.829  -1.103  -0.543
ATOM     50  C   P05     1      -4.006   0.128   0.657
ATOM     51  C   P05     1      -4.135   1.620   0.342
ATOM     52  H   P05     1      -3.329   2.160   0.836
ATOM     53  H   P05     1      -4.071   1.794  -0.733
ATOM     54  H   P05     1      -5.085   2.014   0.702
ATOM     55  C   P05     1      -4.156  -0.137   2.157
ATOM     56  H   P05     1      -5.103   0.254   2.529
ATOM     57  H   P05     1      -4.114  -1.206   2.366
ATOM     58  H   P05     1      -3.348   0.362   2.689
ATOM     59  C   P05     1      -5.068  -0.661  -0.127
```

```
ATOM     60  O   P05     1      -4.751  -1.501  -0.972
ATOM     61  N   P05     1      -6.340  -0.376   0.161
ATOM     62  H   P05     1      -6.592   0.343   0.827
ATOM     63  C   P05     1      -7.449  -1.000  -0.518
ATOM     64  H   P05     1      -7.222  -1.042  -1.586
ATOM     65  C   P05     1      -7.708  -2.415  -0.005
ATOM     66  H   P05     1      -7.975  -2.394   1.052
ATOM     67  H   P05     1      -8.517  -2.889  -0.561
ATOM     68  H   P05     1      -6.805  -3.010  -0.131
ATOM     69  C   P05     1      -8.660  -0.102  -0.289
ATOM     70  O   P05     1      -8.656   0.757   0.594
ATOM     71  N   P05     1      -9.717  -0.330  -1.072
ATOM     72  H   P05     1      -9.652  -1.019  -1.802
ATOM     73  C   P05     1     -10.947   0.417  -0.922
ATOM     74  H   P05     1     -10.780   1.479  -1.104
ATOM     75  H   P05     1     -11.671   0.042  -1.640
ATOM     76  H   P05     1     -11.347   0.297   0.085
END

COMPND Ac-L-Ala-RRR-V-L-Ala-Aib-L-Ala-NHMe_310R
REMARK Energy(ZPE)= -1716.159420
REMARK #IF = 0
ATOM      1  C   P06     1       5.720  -1.957  -1.869
ATOM      2  H   P06     1       5.428  -1.512  -2.820
ATOM      3  H   P06     1       6.645  -1.500  -1.526
ATOM      4  H   P06     1       5.890  -3.020  -2.039
ATOM      5  C   P06     1       4.591  -1.804  -0.896
ATOM      6  O   P06     1       3.443  -2.176  -1.155
ATOM      7  N   P06     1       4.877  -1.222   0.289
ATOM      8  H   P06     1       5.832  -0.977   0.498
ATOM      9  C   P06     1       3.897  -1.165   1.351
ATOM     10  H   P06     1       3.494  -2.167   1.519
ATOM     11  C   P06     1       4.534  -0.648   2.632
ATOM     12  H   P06     1       4.946   0.352   2.489
ATOM     13  H   P06     1       3.787  -0.606   3.422
ATOM     14  H   P06     1       5.334  -1.316   2.950
ATOM     15  C   P06     1       2.685  -0.321   0.987
ATOM     16  O   P06     1       1.607  -0.511   1.553
ATOM     17  N   P06     1       2.853   0.616   0.043
ATOM     18  H   P06     1       3.779   0.750  -0.331
ATOM     19  C   P06     1       1.791   1.509  -0.382
ATOM     20  C   P06     1       1.373   2.542   0.723
ATOM     21  H   P06     1       0.686   2.127   1.455
ATOM     22  C   P06     1       2.301   2.440  -1.519
ATOM     23  H   P06     1       3.307   2.169  -1.840
ATOM     24  H   P06     1       1.649   2.380  -2.391
ATOM     25  C   P06     1       3.186   3.875   0.273
ATOM     26  H   P06     1       4.156   4.355   0.261
ATOM     27  C   P06     1       2.679   3.100   1.237
ATOM     28  H   P06     1       3.152   2.813   2.166
ATOM     29  C   P06     1       2.218   3.851  -0.884
ATOM     30  H   P06     1       2.308   4.657  -1.609
ATOM     31  C   P06     1       0.890   3.717  -0.136
ATOM     32  H   P06     1       0.050   3.464  -0.781
ATOM     33  H   P06     1       0.656   4.593   0.470
ATOM     34  C   P06     1       0.593   0.687  -0.860
ATOM     35  O   P06     1      -0.552   1.142  -0.824
ATOM     36  N   P06     1       0.845  -0.531  -1.364
ATOM     37  H   P06     1       1.781  -0.920  -1.331
ATOM     38  C   P06     1      -0.232  -1.327  -1.907
ATOM     39  H   P06     1      -0.749  -0.745  -2.674
ATOM     40  C   P06     1       0.312  -2.608  -2.517
ATOM     41  H   P06     1       0.842  -3.202  -1.771
ATOM     42  H   P06     1      -0.508  -3.198  -2.922
ATOM     43  H   P06     1       1.003  -2.373  -3.326
ATOM     44  C   P06     1      -1.319  -1.645  -0.884
ATOM     45  O   P06     1      -2.457  -1.916  -1.281
ATOM     46  N   P06     1      -0.980  -1.625   0.412
ATOM     47  H   P06     1      -0.043  -1.334   0.673
ATOM     48  C   P06     1      -1.930  -1.898   1.484
ATOM     49  C   P06     1      -1.229  -1.610   2.812
ATOM     50  H   P06     1      -0.384  -2.287   2.938
ATOM     51  H   P06     1      -0.861  -0.584   2.850
ATOM     52  H   P06     1      -1.928  -1.768   3.632
ATOM     53  C   P06     1      -2.398  -3.347   1.444
ATOM     54  H   P06     1      -3.098  -3.532   2.256
ATOM     55  H   P06     1      -2.889  -3.571   0.499
ATOM     56  H   P06     1      -1.535  -4.003   1.563
ATOM     57  C   P06     1      -3.137  -0.950   1.407
ATOM     58  O   P06     1      -4.212  -1.264   1.913
ATOM     59  N   P06     1      -2.931   0.254   0.840
ATOM     60  H   P06     1      -2.043   0.466   0.396
ATOM     61  C   P06     1      -3.974   1.253   0.803
ATOM     62  H   P06     1      -4.536   1.183   1.737
ATOM     63  C   P06     1      -3.372   2.643   0.672
ATOM     64  H   P06     1      -2.802   2.736  -0.254
ATOM     65  H   P06     1      -4.166   3.387   0.668
ATOM     66  H   P06     1      -2.704   2.844   1.510
ATOM     67  C   P06     1      -5.004   1.024  -0.302
ATOM     68  O   P06     1      -6.017   1.728  -0.347
ATOM     69  N   P06     1      -4.742   0.067  -1.194
ATOM     70  H   P06     1      -3.910  -0.501  -1.085
ATOM     71  C   P06     1      -5.653  -0.225  -2.274
ATOM     72  H   P06     1      -6.616  -0.570  -1.895
ATOM     73  H   P06     1      -5.826   0.663  -2.884
ATOM     74  H   P06     1      -5.218  -1.003  -2.896
END

COMPND Ac-L-Ala-RRR-V-L-Ala-Aib-L-Ala-NHMe_ext
REMARK Energy(ZPE)= -1716.131699
REMARK #IF = 0
ATOM      1  C   P06     1       9.535  -2.371  -1.234
ATOM      2  H   P06     1       9.465  -3.369  -1.667
ATOM      3  H   P06     1       9.526  -1.633  -2.033
ATOM      4  H   P06     1      10.484  -2.308  -0.702
ATOM      5  C   P06     1       8.414  -2.190  -0.249
ATOM      6  O   P06     1       8.265  -2.948   0.713
ATOM      7  N   P06     1       7.585  -1.158  -0.476
ATOM      8  H   P06     1       7.700  -0.555  -1.278
ATOM      9  C   P06     1       6.462  -0.862   0.375
ATOM     10  H   P06     1       5.974  -1.804   0.637
ATOM     11  C   P06     1       6.893  -0.148   1.656
ATOM     12  H   P06     1       7.353   0.812   1.420
ATOM     13  H   P06     1       6.042   0.024   2.317
ATOM     14  H   P06     1       7.618  -0.768   2.181
ATOM     15  C   P06     1       5.504   0.017  -0.431
ATOM     16  O   P06     1       5.914   0.626  -1.416
ATOM     17  N   P06     1       4.261   0.052   0.079
ATOM     18  H   P06     1       4.122  -0.550   0.877
ATOM     19  C   P06     1       3.093   0.863  -0.249
ATOM     20  C   P06     1       2.905   2.004   0.811
ATOM     21  H   P06     1       2.524   1.659   1.772
```

```
ATOM     22  C   P06     1       3.162   1.670  -1.579
ATOM     23  H   P06     1       4.044   1.430  -2.160
ATOM     24  H   P06     1       2.278   1.454  -2.182
ATOM     25  C   P06     1       4.371   3.380  -0.293
ATOM     26  H   P06     1       5.246   3.910  -0.644
ATOM     27  C   P06     1       4.240   2.711   0.856
ATOM     28  H   P06     1       4.983   2.575   1.630
ATOM     29  C   P06     1       3.121   3.142  -1.101
ATOM     30  H   P06     1       2.916   3.852  -1.899
ATOM     31  C   P06     1       2.081   3.028   0.019
ATOM     32  H   P06     1       1.116   2.661  -0.336
ATOM     33  H   P06     1       1.943   3.955   0.574
ATOM     34  C   P06     1       1.936  -0.145  -0.369
ATOM     35  O   P06     1       2.050  -1.121  -1.108
ATOM     36  N   P06     1       0.823   0.097   0.333
ATOM     37  H   P06     1       0.725   0.901   0.936
ATOM     38  C   P06     1      -0.352  -0.732   0.216
ATOM     39  H   P06     1      -0.481  -0.994  -0.836
ATOM     40  C   P06     1      -0.230  -2.014   1.038
ATOM     41  H   P06     1      -0.124  -1.780   2.098
ATOM     42  H   P06     1      -1.107  -2.646   0.905
ATOM     43  H   P06     1       0.649  -2.566   0.708
ATOM     44  C   P06     1      -1.533   0.112   0.688
ATOM     45  O   P06     1      -1.347   1.113   1.383
ATOM     46  N   P06     1      -2.733  -0.340   0.314
ATOM     47  H   P06     1      -2.808  -1.161  -0.276
ATOM     48  C   P06     1      -4.014   0.243   0.679
ATOM     49  C   P06     1      -4.125   1.672   0.142
ATOM     50  H   P06     1      -3.323   2.274   0.566
ATOM     51  H   P06     1      -4.042   1.684  -0.945
ATOM     52  H   P06     1      -5.077   2.123   0.424
ATOM     53  C   P06     1      -4.211   0.204   2.196
ATOM     54  H   P06     1      -5.173   0.636   2.474
ATOM     55  H   P06     1      -4.169  -0.821   2.564
ATOM     56  H   P06     1      -3.423   0.785   2.672
ATOM     57  C   P06     1      -5.054  -0.664  -0.003
ATOM     58  O   P06     1      -4.713  -1.653  -0.655
ATOM     59  N   P06     1      -6.333  -0.319   0.160
ATOM     60  H   P06     1      -6.609   0.520   0.653
ATOM     61  C   P06     1      -7.414  -1.069  -0.433
ATOM     62  H   P06     1      -7.128  -1.335  -1.454
ATOM     63  C   P06     1      -7.713  -2.346   0.350
ATOM     64  H   P06     1      -8.034  -2.106   1.365
ATOM     65  H   P06     1      -8.496  -2.928  -0.136
ATOM     66  H   P06     1      -6.811  -2.954   0.399
ATOM     67  C   P06     1      -8.624  -0.144  -0.466
ATOM     68  O   P06     1      -8.651   0.892   0.200
ATOM     69  N   P06     1      -9.648  -0.545  -1.224
ATOM     70  H   P06     1      -9.554  -1.382  -1.774
ATOM     71  C   P06     1     -10.877   0.212  -1.305
ATOM     72  H   P06     1     -10.702   1.194  -1.745
ATOM     73  H   P06     1     -11.582  -0.335  -1.925
ATOM     74  H   P06     1     -11.306   0.350  -0.312
END

COMPND Ac-L-Ala-R-VI-L-Ala-Aib-L-Ala-NHMe_310R
REMARK Energy(ZPE)= -1963.151409
REMARK #IF = 0
ATOM      1  C   P07     1       6.589  -0.356   1.572
ATOM      2  H   P07     1       6.165  -0.628   2.538
ATOM      3  H   P07     1       7.207  -1.172   1.206
ATOM      4  H   P07     1       7.212   0.526   1.721
ATOM      5  C   P07     1       5.473   0.004   0.639
ATOM      6  O   P07     1       4.641   0.873   0.915
ATOM      7  N   P07     1       5.397  -0.678  -0.524
ATOM      8  H   P07     1       6.120  -1.343  -0.752
ATOM      9  C   P07     1       4.455  -0.299  -1.555
ATOM     10  H   P07     1       4.552   0.773  -1.746
ATOM     11  C   P07     1       4.725  -1.076  -2.833
ATOM     12  H   P07     1       4.636  -2.151  -2.666
ATOM     13  H   P07     1       4.009  -0.783  -3.599
ATOM     14  H   P07     1       5.728  -0.859  -3.199
ATOM     15  C   P07     1       3.006  -0.475  -1.120
ATOM     16  O   P07     1       2.116   0.184  -1.660
ATOM     17  N   P07     1       2.765  -1.355  -0.140
ATOM     18  H   P07     1       3.547  -1.872   0.236
ATOM     19  C   P07     1       1.440  -1.602   0.406
ATOM     20  C   P07     1       0.557  -2.349  -0.607
ATOM     21  H   P07     1       0.165  -1.631  -1.330
ATOM     22  H   P07     1       1.210  -3.032  -1.161
ATOM     23  C   P07     1      -0.548  -3.095   0.058
ATOM     24  C   P07     1      -0.643  -3.268   1.409
ATOM     25  C   P07     1       0.329  -2.750   2.402
ATOM     26  H   P07     1      -0.067  -1.852   2.888
ATOM     27  H   P07     1       0.517  -3.478   3.193
ATOM     28  C   P07     1       1.637  -2.438   1.685
ATOM     29  H   P07     1       2.320  -1.911   2.354
ATOM     30  H   P07     1       2.118  -3.375   1.389
ATOM     31  N   P07     1      -1.788  -3.962   1.711
ATOM     32  H   P07     1      -2.075  -4.236   2.635
ATOM     33  C   P07     1      -2.453  -4.259   0.549
ATOM     34  C   P07     1      -3.646  -4.947   0.342
ATOM     35  H   P07     1      -4.213  -5.352   1.171
ATOM     36  C   P07     1      -4.083  -5.092  -0.965
ATOM     37  H   P07     1      -5.008  -5.621  -1.159
ATOM     38  C   P07     1      -3.350  -4.565  -2.041
ATOM     39  H   P07     1      -3.723  -4.696  -3.050
ATOM     40  C   P07     1      -2.163  -3.884  -1.831
ATOM     41  H   P07     1      -1.605  -3.482  -2.668
ATOM     42  C   P07     1      -1.696  -3.722  -0.521
ATOM     43  C   P07     1       0.798  -0.267   0.808
ATOM     44  O   P07     1      -0.423  -0.109   0.771
ATOM     45  N   P07     1       1.619   0.692   1.267
ATOM     46  H   P07     1       2.627   0.583   1.212
ATOM     47  C   P07     1       1.078   1.930   1.780
ATOM     48  H   P07     1       0.362   1.700   2.572
ATOM     49  C   P07     1       2.193   2.802   2.337
ATOM     50  H   P07     1       2.933   3.026   1.568
ATOM     51  H   P07     1       1.775   3.734   2.712
ATOM     52  H   P07     1       2.693   2.290   3.159
ATOM     53  C   P07     1       0.261   2.707   0.754
ATOM     54  O   P07     1      -0.577   3.524   1.151
ATOM     55  N   P07     1       0.492   2.473  -0.542
ATOM     56  H   P07     1       1.146   1.740  -0.803
ATOM     57  C   P07     1      -0.257   3.131  -1.607
ATOM     58  C   P07     1       0.110   2.450  -2.925
ATOM     59  H   P07     1       1.173   2.588  -3.130
ATOM     60  H   P07     1      -0.099   1.381  -2.890
ATOM     61  H   P07     1      -0.461   2.899  -3.737
ATOM     62  C   P07     1       0.081   4.614  -1.673
ATOM     63  H   P07     1      -0.481   5.087  -2.477
ATOM     64  H   P07     1      -0.163   5.111  -0.736
```

```
ATOM     65  H   P07     1       1.147   4.727  -1.871
ATOM     66  C   P07     1      -1.770   2.938  -1.413
ATOM     67  O   P07     1      -2.568   3.752  -1.873
ATOM     68  N   P07     1      -2.166   1.805  -0.803
ATOM     69  H   P07     1      -1.481   1.178  -0.390
ATOM     70  C   P07     1      -3.565   1.479  -0.659
ATOM     71  H   P07     1      -4.083   1.861  -1.542
ATOM     72  C   P07     1      -3.755  -0.027  -0.572
ATOM     73  H   P07     1      -3.199  -0.444   0.270
ATOM     74  H   P07     1      -4.811  -0.255  -0.441
ATOM     75  H   P07     1      -3.402  -0.502  -1.487
ATOM     76  C   P07     1      -4.247   2.167   0.523
ATOM     77  O   P07     1      -5.463   2.027   0.688
ATOM     78  N   P07     1      -3.486   2.897   1.342
ATOM     79  H   P07     1      -2.496   3.009   1.152
ATOM     80  C   P07     1      -4.060   3.591   2.469
ATOM     81  H   P07     1      -4.809   4.314   2.143
ATOM     82  H   P07     1      -4.541   2.890   3.153
ATOM     83  H   P07     1      -3.267   4.114   2.996
END

COMPND Ac-L-Ala-RSS-IV-L-Ala-Aib-L-Ala-NHMe_310L
REMARK Energy(ZPE)= -1717.360697
REMARK #IF = 0
ATOM      1  C   P12     1       5.660  -2.146   1.897
ATOM      2  H   P12     1       5.339  -1.725   2.849
ATOM      3  H   P12     1       5.743  -3.226   2.024
ATOM      4  H   P12     1       6.636  -1.743   1.635
ATOM      5  C   P12     1       4.607  -1.869   0.867
ATOM      6  O   P12     1       3.425  -2.182   1.042
ATOM      7  N   P12     1       5.002  -1.242  -0.259
ATOM      8  H   P12     1       5.983  -1.056  -0.388
ATOM      9  C   P12     1       4.122  -1.070  -1.403
ATOM     10  H   P12     1       4.659  -0.419  -2.098
ATOM     11  C   P12     1       3.802  -2.381  -2.100
ATOM     12  H   P12     1       3.278  -3.055  -1.425
ATOM     13  H   P12     1       3.172  -2.198  -2.968
ATOM     14  H   P12     1       4.728  -2.851  -2.429
ATOM     15  C   P12     1       2.853  -0.305  -1.030
ATOM     16  O   P12     1       1.788  -0.515  -1.610
ATOM     17  N   P12     1       2.982   0.633  -0.076
ATOM     18  H   P12     1       3.891   0.761   0.340
ATOM     19  C   P12     1       1.898   1.508   0.336
ATOM     20  C   P12     1       1.428   2.496  -0.769
ATOM     21  H   P12     1       0.691   2.056  -1.438
ATOM     22  C   P12     1       2.400   2.475   1.452
ATOM     23  H   P12     1       3.406   2.215   1.785
ATOM     24  H   P12     1       1.743   2.424   2.322
ATOM     25  C   P12     1       3.325   3.922  -0.356
ATOM     26  H   P12     1       4.302   3.535  -0.058
ATOM     27  H   P12     1       3.473   4.952  -0.683
ATOM     28  C   P12     1       2.663   3.069  -1.466
ATOM     29  H   P12     1       2.336   3.695  -2.298
ATOM     30  H   P12     1       3.325   2.307  -1.874
ATOM     31  C   P12     1       2.310   3.850   0.793
ATOM     32  H   P12     1       2.383   4.670   1.508
ATOM     33  C   P12     1       0.982   3.713   0.050
ATOM     34  H   P12     1       0.752   4.569  -0.588
ATOM     35  H   P12     1       0.139   3.506   0.707
ATOM     36  C   P12     1       0.719   0.678   0.851
ATOM     37  O   P12     1      -0.426   1.139   0.863
ATOM     38  N   P12     1       0.996  -0.551   1.307
ATOM     39  H   P12     1       1.938  -0.919   1.224
ATOM     40  C   P12     1      -0.030  -1.429   1.827
ATOM     41  H   P12     1       0.440  -2.411   1.921
ATOM     42  C   P12     1      -0.538  -0.998   3.193
ATOM     43  H   P12     1      -0.987  -0.007   3.138
ATOM     44  H   P12     1      -1.286  -1.701   3.552
ATOM     45  H   P12     1       0.294  -0.974   3.897
ATOM     46  C   P12     1      -1.180  -1.620   0.837
ATOM     47  O   P12     1      -2.313  -1.895   1.240
ATOM     48  N   P12     1      -0.886  -1.515  -0.467
ATOM     49  H   P12     1       0.052  -1.244  -0.745
ATOM     50  C   P12     1      -1.885  -1.688  -1.514
ATOM     51  C   P12     1      -2.327  -3.141  -1.614
ATOM     52  H   P12     1      -1.464  -3.761  -1.860
ATOM     53  H   P12     1      -2.755  -3.482  -0.673
ATOM     54  H   P12     1      -3.077  -3.247  -2.396
ATOM     55  C   P12     1      -1.256  -1.232  -2.830
ATOM     56  H   P12     1      -1.984  -1.324  -3.635
ATOM     57  H   P12     1      -0.923  -0.195  -2.770
ATOM     58  H   P12     1      -0.395  -1.859  -3.066
ATOM     59  C   P12     1      -3.105  -0.784  -1.260
ATOM     60  O   P12     1      -4.220  -1.105  -1.665
ATOM     61  N   P12     1      -2.861   0.388  -0.647
ATOM     62  H   P12     1      -1.938   0.567  -0.266
ATOM     63  C   P12     1      -3.897   1.368  -0.395
ATOM     64  H   P12     1      -3.418   2.152   0.197
ATOM     65  C   P12     1      -4.440   2.000  -1.667
ATOM     66  H   P12     1      -4.904   1.248  -2.303
ATOM     67  H   P12     1      -5.183   2.754  -1.416
ATOM     68  H   P12     1      -3.625   2.474  -2.214
ATOM     69  C   P12     1      -5.022   0.838   0.500
ATOM     70  O   P12     1      -6.125   1.391   0.507
ATOM     71  N   P12     1      -4.720  -0.173   1.319
ATOM     72  H   P12     1      -3.832  -0.654   1.231
ATOM     73  C   P12     1      -5.703  -0.709   2.230
ATOM     74  H   P12     1      -6.092   0.075   2.881
ATOM     75  H   P12     1      -6.544  -1.153   1.694
ATOM     76  H   P12     1      -5.230  -1.474   2.841
END

COMPND Ac-L-Ala-RSS-IV-L-Ala-Aib-L-Ala-
NHMe_310R
REMARK Energy(ZPE)= -1717.366358
REMARK #IF = 0
ATOM      1  C   P12     1       5.620  -1.975  -1.963
ATOM      2  H   P12     1       5.368  -1.391  -2.847
ATOM      3  H   P12     1       6.576  -1.639  -1.567
ATOM      4  H   P12     1       5.707  -3.018  -2.268
ATOM      5  C   P12     1       4.501  -1.863  -0.972
ATOM      6  O   P12     1       3.337  -2.154  -1.259
ATOM      7  N   P12     1       4.813  -1.408   0.259
ATOM      8  H   P12     1       5.778  -1.229   0.487
ATOM      9  C   P12     1       3.839  -1.421   1.330
ATOM     10  H   P12     1       3.400  -2.420   1.398
ATOM     11  C   P12     1       4.503  -1.062   2.651
ATOM     12  H   P12     1       4.951  -0.069   2.607
ATOM     13  H   P12     1       3.762  -1.074   3.448
ATOM     14  H   P12     1       5.278  -1.789   2.891
ATOM     15  C   P12     1       2.656  -0.500   1.069
ATOM     16  O   P12     1       1.582  -0.702   1.640
```

```
ATOM     17  N   P12     1       2.843   0.518   0.219
ATOM     18  H   P12     1       3.742   0.607  -0.227
ATOM     19  C   P12     1       1.790   1.459  -0.107
ATOM     20  C   P12     1       2.278   2.521  -1.133
ATOM     21  H   P12     1       2.304   2.142  -2.155
ATOM     22  C   P12     1       1.355   2.339   1.097
ATOM     23  H   P12     1       1.894   2.049   1.999
ATOM     24  H   P12     1       0.287   2.216   1.272
ATOM     25  C   P12     1       3.196   3.942   0.594
ATOM     26  H   P12     1       3.673   3.569   1.502
ATOM     27  H   P12     1       3.466   4.994   0.490
ATOM     28  C   P12     1       3.603   3.137  -0.662
ATOM     29  H   P12     1       3.968   3.796  -1.451
ATOM     30  H   P12     1       4.403   2.422  -0.469
ATOM     31  C   P12     1       1.674   3.764   0.638
ATOM     32  H   P12     1       1.153   4.529   1.214
ATOM     33  C   P12     1       1.319   3.680  -0.848
ATOM     34  H   P12     1       1.589   4.575  -1.412
ATOM     35  H   P12     1       0.273   3.435  -1.026
ATOM     36  C   P12     1       0.595   0.710  -0.710
ATOM     37  O   P12     1      -0.541   1.189  -0.677
ATOM     38  N   P12     1       0.831  -0.469  -1.310
ATOM     39  H   P12     1       1.754  -0.894  -1.297
ATOM     40  C   P12     1      -0.256  -1.188  -1.934
ATOM     41  H   P12     1      -0.746  -0.532  -2.657
ATOM     42  C   P12     1       0.263  -2.430  -2.640
ATOM     43  H   P12     1       0.768  -3.095  -1.940
ATOM     44  H   P12     1      -0.568  -2.962  -3.100
ATOM     45  H   P12     1       0.970  -2.148  -3.421
ATOM     46  C   P12     1      -1.363  -1.561  -0.954
ATOM     47  O   P12     1      -2.498  -1.790  -1.385
ATOM     48  N   P12     1      -1.048  -1.633   0.346
ATOM     49  H   P12     1      -0.110  -1.378   0.640
ATOM     50  C   P12     1      -2.023  -1.961   1.380
ATOM     51  C   P12     1      -1.349  -1.769   2.738
ATOM     52  H   P12     1      -0.520  -2.470   2.843
ATOM     53  H   P12     1      -0.960  -0.756   2.848
ATOM     54  H   P12     1      -2.070  -1.963   3.531
ATOM     55  C   P12     1      -2.508  -3.398   1.235
ATOM     56  H   P12     1      -3.225  -3.627   2.022
ATOM     57  H   P12     1      -2.984  -3.551   0.269
ATOM     58  H   P12     1      -1.655  -4.072   1.325
ATOM     59  C   P12     1      -3.219  -0.996   1.337
ATOM     60  O   P12     1      -4.309  -1.332   1.795
ATOM     61  N   P12     1      -2.992   0.241   0.855
ATOM     62  H   P12     1      -2.092   0.476   0.447
ATOM     63  C   P12     1      -4.033   1.242   0.851
ATOM     64  H   P12     1      -4.617   1.120   1.765
ATOM     65  C   P12     1      -3.428   2.637   0.813
ATOM     66  H   P12     1      -2.813   2.771  -0.077
ATOM     67  H   P12     1      -4.224   3.379   0.802
ATOM     68  H   P12     1      -2.806   2.800   1.693
ATOM     69  C   P12     1      -5.039   1.077  -0.288
ATOM     70  O   P12     1      -6.052   1.783  -0.311
ATOM     71  N   P12     1      -4.759   0.176  -1.231
ATOM     72  H   P12     1      -3.931  -0.402  -1.142
ATOM     73  C   P12     1      -5.652  -0.048  -2.342
ATOM     74  H   P12     1      -6.623  -0.411  -2.001
ATOM     75  H   P12     1      -5.811   0.874  -2.902
ATOM     76  H   P12     1      -5.208  -0.791  -3.000
END
```

```
COMPND Ac-L-Ala-SSS-V-L-Ala-Aib-L-Ala-NHMe_310L
REMARK Energy(ZPE)= -1716.153965
REMARK #IF = 0
ATOM      1  C   P13     1       5.718  -2.002   1.912
ATOM      2  H   P13     1       5.399  -1.556   2.853
ATOM      3  H   P13     1       5.822  -3.075   2.073
ATOM      4  H   P13     1       6.683  -1.591   1.625
ATOM      5  C   P13     1       4.649  -1.777   0.886
ATOM      6  O   P13     1       3.473  -2.095   1.088
ATOM      7  N   P13     1       5.025  -1.190  -0.269
ATOM      8  H   P13     1       6.003  -1.002  -0.417
ATOM      9  C   P13     1       4.127  -1.062  -1.405
ATOM     10  H   P13     1       4.649  -0.434  -2.130
ATOM     11  C   P13     1       3.802  -2.399  -2.049
ATOM     12  H   P13     1       3.296  -3.051  -1.338
ATOM     13  H   P13     1       3.154  -2.251  -2.910
ATOM     14  H   P13     1       4.724  -2.876  -2.378
ATOM     15  C   P13     1       2.860  -0.292  -1.037
ATOM     16  O   P13     1       1.787  -0.528  -1.590
ATOM     17  N   P13     1       3.000   0.673  -0.113
ATOM     18  H   P13     1       3.924   0.842   0.254
ATOM     19  C   P13     1       1.924   1.562   0.288
ATOM     20  C   P13     1       1.464   2.531  -0.860
ATOM     21  H   P13     1       0.769   2.070  -1.556
ATOM     22  C   P13     1       2.437   2.561   1.364
ATOM     23  H   P13     1       3.453   2.324   1.681
ATOM     24  H   P13     1       1.801   2.536   2.250
ATOM     25  C   P13     1       3.263   3.914  -0.518
ATOM     26  H   P13     1       4.225   4.409  -0.551
ATOM     27  C   P13     1       2.750   3.083  -1.430
ATOM     28  H   P13     1       3.211   2.755  -2.353
ATOM     29  C   P13     1       2.319   3.935   0.658
ATOM     30  H   P13     1       2.411   4.779   1.339
ATOM     31  C   P13     1       0.979   3.741  -0.054
ATOM     32  H   P13     1       0.719   4.580  -0.700
ATOM     33  H   P13     1       0.157   3.508   0.621
ATOM     34  C   P13     1       0.744   0.747   0.823
ATOM     35  O   P13     1      -0.404   1.202   0.814
ATOM     36  N   P13     1       1.024  -0.467   1.316
ATOM     37  H   P13     1       1.969  -0.830   1.249
ATOM     38  C   P13     1       0.002  -1.335   1.862
ATOM     39  H   P13     1       0.480  -2.310   1.989
ATOM     40  C   P13     1      -0.511  -0.863   3.212
ATOM     41  H   P13     1      -0.978   0.117   3.123
ATOM     42  H   P13     1      -1.244  -1.566   3.601
ATOM     43  H   P13     1       0.322  -0.798   3.912
ATOM     44  C   P13     1      -1.144  -1.570   0.877
ATOM     45  O   P13     1      -2.273  -1.849   1.289
ATOM     46  N   P13     1      -0.852  -1.496  -0.429
ATOM     47  H   P13     1       0.083  -1.220  -0.715
ATOM     48  C   P13     1      -1.850  -1.709  -1.470
ATOM     49  C   P13     1      -2.272  -3.171  -1.532
ATOM     50  H   P13     1      -1.400  -3.785  -1.756
ATOM     51  H   P13     1      -2.701  -3.491  -0.584
ATOM     52  H   P13     1      -3.016  -3.309  -2.315
ATOM     53  C   P13     1      -1.228  -1.281  -2.799
ATOM     54  H   P13     1      -1.961  -1.389  -3.598
ATOM     55  H   P13     1      -0.894  -0.243  -2.762
ATOM     56  H   P13     1      -0.369  -1.912  -3.028
ATOM     57  C   P13     1      -3.080  -0.814  -1.239
```

```
ATOM     58  O   P13     1      -4.191  -1.157  -1.638
ATOM     59  N   P13     1      -2.850   0.375  -0.655
ATOM     60  H   P13     1      -1.928   0.574  -0.280
ATOM     61  C   P13     1      -3.898   1.348  -0.426
ATOM     62  H   P13     1      -3.429   2.151   0.149
ATOM     63  C   P13     1      -4.446   1.945  -1.713
ATOM     64  H   P13     1      -4.898   1.173  -2.334
ATOM     65  H   P13     1      -5.201   2.693  -1.479
ATOM     66  H   P13     1      -3.637   2.419  -2.268
ATOM     67  C   P13     1      -5.019   0.825   0.478
ATOM     68  O   P13     1      -6.128   1.365   0.472
ATOM     69  N   P13     1      -4.707  -0.167   1.318
ATOM     70  H   P13     1      -3.813  -0.639   1.241
ATOM     71  C   P13     1      -5.686  -0.698   2.236
ATOM     72  H   P13     1      -6.522  -1.157   1.705
ATOM     73  H   P13     1      -5.207  -1.450   2.857
ATOM     74  H   P13     1      -6.082   0.091   2.876
END

COMPND Ac-L-Ala-SSS-V-L-Ala-Aib-L-Ala-NHMe_310R
REMARK Energy(ZPE)= -1716.161003
REMARK #IF = 0
ATOM      1  C   P13     1      -5.640  -1.901   1.945
ATOM      2  H   P13     1      -5.398  -1.284   2.810
ATOM      3  H   P13     1      -6.601  -1.591   1.540
ATOM      4  H   P13     1      -5.711  -2.934   2.284
ATOM      5  C   P13     1      -4.522  -1.800   0.952
ATOM      6  O   P13     1      -3.359  -2.094   1.240
ATOM      7  N   P13     1      -4.833  -1.352  -0.282
ATOM      8  H   P13     1      -5.798  -1.173  -0.512
ATOM      9  C   P13     1      -3.856  -1.363  -1.349
ATOM     10  H   P13     1      -3.424  -2.364  -1.426
ATOM     11  C   P13     1      -4.509  -0.983  -2.668
ATOM     12  H   P13     1      -4.949   0.014  -2.615
ATOM     13  H   P13     1      -3.765  -0.992  -3.462
ATOM     14  H   P13     1      -5.290  -1.700  -2.921
ATOM     15  C   P13     1      -2.668  -0.455  -1.065
ATOM     16  O   P13     1      -1.581  -0.673  -1.606
ATOM     17  N   P13     1      -2.861   0.568  -0.224
ATOM     18  H   P13     1      -3.789   0.721   0.142
ATOM     19  C   P13     1      -1.811   1.512   0.099
ATOM     20  C   P13     1      -2.330   2.571   1.145
ATOM     21  H   P13     1      -2.381   2.184   2.161
ATOM     22  C   P13     1      -1.400   2.406  -1.095
ATOM     23  H   P13     1      -1.927   2.109  -2.001
ATOM     24  H   P13     1      -0.328   2.330  -1.270
ATOM     25  C   P13     1      -3.273   3.878  -0.488
ATOM     26  H   P13     1      -3.943   4.356  -1.190
ATOM     27  C   P13     1      -3.611   3.131   0.568
ATOM     28  H   P13     1      -4.609   2.882   0.905
ATOM     29  C   P13     1      -1.771   3.833  -0.616
ATOM     30  H   P13     1      -1.315   4.627  -1.204
ATOM     31  C   P13     1      -1.370   3.730   0.860
ATOM     32  H   P13     1      -0.321   3.473   1.002
ATOM     33  H   P13     1      -1.629   4.618   1.437
ATOM     34  C   P13     1      -0.614   0.771   0.701
ATOM     35  O   P13     1       0.522   1.249   0.660
ATOM     36  N   P13     1      -0.854  -0.397   1.321
ATOM     37  H   P13     1      -1.777  -0.822   1.306
ATOM     38  C   P13     1       0.229  -1.110   1.956
ATOM     39  H   P13     1       0.726  -0.442   2.663
ATOM     40  C   P13     1      -0.297  -2.331   2.693
ATOM     41  H   P13     1      -0.811  -3.008   2.010
ATOM     42  H   P13     1       0.531  -2.860   3.161
ATOM     43  H   P13     1      -0.998  -2.026   3.470
ATOM     44  C   P13     1       1.332  -1.516   0.983
ATOM     45  O   P13     1       2.464  -1.747   1.419
ATOM     46  N   P13     1       1.014  -1.611  -0.315
ATOM     47  H   P13     1       0.076  -1.353  -0.612
ATOM     48  C   P13     1       1.983  -1.979  -1.341
ATOM     49  C   P13     1       1.311  -1.817  -2.704
ATOM     50  H   P13     1       0.472  -2.509  -2.788
ATOM     51  H   P13     1       0.938  -0.802  -2.845
ATOM     52  H   P13     1       2.030  -2.045  -3.490
ATOM     53  C   P13     1       2.452  -3.417  -1.158
ATOM     54  H   P13     1       3.169  -3.672  -1.936
ATOM     55  H   P13     1       2.924  -3.551  -0.187
ATOM     56  H   P13     1       1.593  -4.084  -1.234
ATOM     57  C   P13     1       3.189  -1.026  -1.323
ATOM     58  O   P13     1       4.275  -1.385  -1.776
ATOM     59  N   P13     1       2.975   0.223  -0.871
ATOM     60  H   P13     1       2.078   0.474  -0.469
ATOM     61  C   P13     1       4.024   1.215  -0.889
ATOM     62  H   P13     1       4.601   1.074  -1.806
ATOM     63  C   P13     1       3.430   2.615  -0.868
ATOM     64  H   P13     1       2.822   2.767   0.025
ATOM     65  H   P13     1       4.231   3.351  -0.875
ATOM     66  H   P13     1       2.803   2.770  -1.746
ATOM     67  C   P13     1       5.037   1.060   0.244
ATOM     68  O   P13     1       6.060   1.751   0.243
ATOM     69  N   P13     1       4.753   0.184   1.210
ATOM     70  H   P13     1       3.917  -0.386   1.142
ATOM     71  C   P13     1       5.653  -0.026   2.317
ATOM     72  H   P13     1       6.615  -0.411   1.975
ATOM     73  H   P13     1       5.832   0.907   2.852
ATOM     74  H   P13     1       5.206  -0.746   2.998
END

COMPND Ac-L-Ala-Aib-L-Ala-Aib-L-Ala-NHMe_310R
REMARK Energy(ZPE)= -1562.672596
REMARK #IF = 0
ATOM      1  C   P15     1      -6.045  -0.765   1.967
ATOM      2  H   P15     1      -5.728  -0.195   2.840
ATOM      3  H   P15     1      -6.951  -0.325   1.558
ATOM      4  H   P15     1      -6.259  -1.782   2.295
ATOM      5  C   P15     1      -4.915  -0.810   0.983
ATOM      6  O   P15     1      -3.791  -1.216   1.290
ATOM      7  N   P15     1      -5.171  -0.370  -0.268
ATOM      8  H   P15     1      -6.110  -0.096  -0.511
ATOM      9  C   P15     1      -4.197  -0.522  -1.326
ATOM     10  H   P15     1      -3.876  -1.566  -1.369
ATOM     11  C   P15     1      -4.800  -0.116  -2.662
ATOM     12  H   P15     1      -5.127   0.924  -2.646
ATOM     13  H   P15     1      -4.059  -0.234  -3.450
ATOM     14  H   P15     1      -5.654  -0.751  -2.897
ATOM     15  C   P15     1      -2.918   0.260  -1.062
ATOM     16  O   P15     1      -1.855  -0.107  -1.566
ATOM     17  N   P15     1      -3.014   1.340  -0.274
ATOM     18  H   P15     1      -3.923   1.576   0.095
ATOM     19  C   P15     1      -1.880   2.190   0.061
ATOM     20  C   P15     1      -2.328   3.148   1.165
ATOM     21  H   P15     1      -3.127   3.792   0.795
```

```
ATOM     22  H   P15     1      -2.687   2.603   2.039
ATOM     23  H   P15     1      -1.493   3.779   1.465
ATOM     24  C   P15     1      -1.397   2.968  -1.156
ATOM     25  H   P15     1      -0.555   3.601  -0.881
ATOM     26  H   P15     1      -1.082   2.291  -1.948
ATOM     27  H   P15     1      -2.209   3.595  -1.522
ATOM     28  C   P15     1      -0.738   1.339   0.633
ATOM     29  O   P15     1       0.435   1.704   0.531
ATOM     30  N   P15     1      -1.083   0.230   1.307
ATOM     31  H   P15     1      -2.048  -0.083   1.313
ATOM     32  C   P15     1      -0.080  -0.572   1.966
ATOM     33  H   P15     1       0.519   0.077   2.609
ATOM     34  C   P15     1      -0.734  -1.658   2.806
ATOM     35  H   P15     1      -1.346  -2.315   2.188
ATOM     36  H   P15     1       0.035  -2.252   3.298
ATOM     37  H   P15     1      -1.369  -1.210   3.569
ATOM     38  C   P15     1       0.933  -1.182   1.005
ATOM     39  O   P15     1       2.025  -1.559   1.446
ATOM     40  N   P15     1       0.595  -1.274  -0.286
ATOM     41  H   P15     1      -0.305  -0.911  -0.590
ATOM     42  C   P15     1       1.502  -1.798  -1.302
ATOM     43  C   P15     1       0.863  -1.561  -2.670
ATOM     44  H   P15     1      -0.064  -2.131  -2.748
ATOM     45  H   P15     1       0.633  -0.507  -2.823
ATOM     46  H   P15     1       1.544  -1.896  -3.450
ATOM     47  C   P15     1       1.757  -3.286  -1.095
ATOM     48  H   P15     1       2.433  -3.654  -1.864
ATOM     49  H   P15     1       2.200  -3.471  -0.118
ATOM     50  H   P15     1       0.810  -3.822  -1.166
ATOM     51  C   P15     1       2.832  -1.029  -1.290
ATOM     52  O   P15     1       3.862  -1.552  -1.711
ATOM     53  N   P15     1       2.790   0.254  -0.884
ATOM     54  H   P15     1       1.929   0.640  -0.509
ATOM     55  C   P15     1       3.965   1.092  -0.916
ATOM     56  H   P15     1       4.530   0.841  -1.816
ATOM     57  C   P15     1       3.567   2.559  -0.957
ATOM     58  H   P15     1       2.966   2.825  -0.086
ATOM     59  H   P15     1       4.460   3.180  -0.968
ATOM     60  H   P15     1       2.985   2.765  -1.855
ATOM     61  C   P15     1       4.934   0.845   0.240
ATOM     62  O   P15     1       6.037   1.400   0.234
ATOM     63  N   P15     1       4.530   0.046   1.229
ATOM     64  H   P15     1       3.631  -0.420   1.169
ATOM     65  C   P15     1       5.386  -0.242   2.354
ATOM     66  H   P15     1       6.280  -0.785   2.042
ATOM     67  H   P15     1       5.703   0.680   2.843
ATOM     68  H   P15     1       4.834  -0.850   3.066
END

COMPND Ac-L-Ala-RRR-IIIamb-L-Ala-Aib-L-Ala-
NHMe_310R
REMARK Energy(ZPE)= -1869.719615
REMARK #IF = 0
ATOM      1  C   P16     1       4.576  -3.704  -1.802
ATOM      2  H   P16     1       4.284  -3.410  -2.809
ATOM      3  H   P16     1       5.603  -3.396  -1.619
ATOM      4  H   P16     1       4.515  -4.790  -1.743
ATOM      5  C   P16     1       3.603  -3.120  -0.825
ATOM      6  O   P16     1       2.384  -3.274  -0.939
ATOM      7  N   P16     1       4.112  -2.398   0.196
ATOM      8  H   P16     1       5.112  -2.332   0.301
ATOM      9  C   P16     1       3.271  -1.936   1.278
ATOM     10  H   P16     1       2.694  -2.779   1.665
ATOM     11  C   P16     1       4.120  -1.342   2.391
ATOM     12  H   P16     1       4.710  -0.500   2.027
ATOM     13  H   P16     1       3.477  -0.990   3.195
ATOM     14  H   P16     1       4.792  -2.100   2.794
ATOM     15  C   P16     1       2.217  -0.936   0.819
ATOM     16  O   P16     1       1.183  -0.787   1.472
ATOM     17  N   P16     1       2.471  -0.252  -0.305
ATOM     18  H   P16     1       3.363  -0.395  -0.754
ATOM     19  C   P16     1       1.559   0.728  -0.858
ATOM     20  C   P16     1       2.173   1.349  -2.148
ATOM     21  H   P16     1       3.091   0.839  -2.442
ATOM     22  H   P16     1       1.472   1.276  -2.981
ATOM     23  C   P16     1       2.384   2.830  -1.771
ATOM     24  H   P16     1       2.588   3.470  -2.627
ATOM     25  C   P16     1       1.087   3.081  -0.993
ATOM     26  H   P16     1       0.188   2.890  -1.578
ATOM     27  H   P16     1       1.042   4.074  -0.543
ATOM     28  C   P16     1       1.362   1.989   0.055
ATOM     29  H   P16     1       0.629   1.836   0.843
ATOM     30  C   P16     1       2.747   2.381   0.486
ATOM     31  C   P16     1       3.390   2.884  -0.651
ATOM     32  C   P16     1       4.716   3.277  -0.598
ATOM     33  H   P16     1       5.224   3.662  -1.474
ATOM     34  C   P16     1       5.386   3.181   0.624
ATOM     35  H   P16     1       6.418   3.501   0.695
ATOM     36  C   P16     1       4.743   2.685   1.754
ATOM     37  H   P16     1       5.282   2.625   2.692
ATOM     38  C   P16     1       3.412   2.266   1.692
ATOM     39  H   P16     1       2.916   1.869   2.570
ATOM     40  C   P16     1       0.206   0.078  -1.154
ATOM     41  O   P16     1      -0.824   0.754  -1.203
ATOM     42  N   P16     1       0.183  -1.245  -1.377
ATOM     43  H   P16     1       1.023  -1.809  -1.287
ATOM     44  C   P16     1      -1.070  -1.898  -1.678
ATOM     45  H   P16     1      -1.528  -1.408  -2.541
ATOM     46  C   P16     1      -0.843  -3.369  -1.987
ATOM     47  H   P16     1      -0.379  -3.879  -1.142
ATOM     48  H   P16     1      -1.794  -3.848  -2.210
ATOM     49  H   P16     1      -0.190  -3.474  -2.853
ATOM     50  C   P16     1      -2.104  -1.746  -0.567
ATOM     51  O   P16     1      -3.303  -1.842  -0.845
ATOM     52  N   P16     1      -1.656  -1.529   0.677
ATOM     53  H   P16     1      -0.658  -1.407   0.831
ATOM     54  C   P16     1      -2.541  -1.383   1.828
ATOM     55  C   P16     1      -1.686  -0.977   3.029
ATOM     56  H   P16     1      -0.976  -1.770   3.263
ATOM     57  H   P16     1      -1.129  -0.062   2.828
ATOM     58  H   P16     1      -2.330  -0.820   3.893
ATOM     59  C   P16     1      -3.271  -2.686   2.126
ATOM     60  H   P16     1      -3.918  -2.557   2.992
ATOM     61  H   P16     1      -3.878  -2.997   1.278
ATOM     62  H   P16     1      -2.538  -3.463   2.345
ATOM     63  C   P16     1      -3.553  -0.249   1.604
ATOM     64  O   P16     1      -4.621  -0.234   2.211
ATOM     65  N   P16     1      -3.173   0.751   0.787
ATOM     66  H   P16     1      -2.302   0.682   0.272
ATOM     67  C   P16     1      -4.012   1.908   0.580
ATOM     68  H   P16     1      -4.469   2.166   1.538
ATOM     69  C   P16     1      -3.183   3.080   0.076
```

```
ATOM     70  H   P16     1      -2.712   2.842  -0.878
ATOM     71  H   P16     1      -3.824   3.949  -0.058
ATOM     72  H   P16     1      -2.402   3.325   0.796
ATOM     73  C   P16     1      -5.184   1.654  -0.366
ATOM     74  O   P16     1      -6.059   2.515  -0.495
ATOM     75  N   P16     1      -5.195   0.501  -1.038
ATOM     76  H   P16     1      -4.471  -0.187  -0.866
ATOM     77  C   P16     1      -6.265   0.179  -1.950
ATOM     78  H   P16     1      -7.224   0.135  -1.431
ATOM     79  H   P16     1      -6.342   0.929  -2.739
ATOM     80  H   P16     1      -6.061  -0.789  -2.400
END

COMPND Ac-L-Ala-RRR-IIIawr-L-Ala-Aib-L-Ala-
NHMe_310R
REMARK Energy(ZPE)= -1752.081494
REMARK #IF = 0
ATOM      1  C   P17     1       4.129  -3.551  -0.805
ATOM      2  H   P17     1       4.155  -3.228  -1.845
ATOM      3  H   P17     1       5.130  -3.489  -0.383
ATOM      4  H   P17     1       3.798  -4.589  -0.788
ATOM      5  C   P17     1       3.128  -2.721  -0.065
ATOM      6  O   P17     1       1.956  -2.613  -0.445
ATOM      7  N   P17     1       3.550  -2.072   1.036
ATOM      8  H   P17     1       4.491  -2.213   1.367
ATOM      9  C   P17     1       2.607  -1.365   1.877
ATOM     10  H   P17     1       1.806  -2.048   2.165
ATOM     11  C   P17     1       3.299  -0.827   3.119
ATOM     12  H   P17     1       4.098  -0.132   2.857
ATOM     13  H   P17     1       2.578  -0.305   3.745
ATOM     14  H   P17     1       3.722  -1.648   3.697
ATOM     15  C   P17     1       1.911  -0.240   1.125
ATOM     16  O   P17     1       0.756   0.082   1.397
ATOM     17  N   P17     1       2.625   0.403   0.184
ATOM     18  H   P17     1       3.584   0.135   0.026
ATOM     19  C   P17     1       2.054   1.512  -0.548
ATOM     20  C   P17     1       3.066   2.116  -1.551
ATOM     21  H   P17     1       4.013   1.578  -1.567
ATOM     22  H   P17     1       2.661   2.127  -2.562
ATOM     23  C   P17     1       3.187   3.562  -1.012
ATOM     24  H   P17     1       3.528   4.298  -1.733
ATOM     25  O   P17     1       1.834   3.805  -0.627
ATOM     26  C   P17     1       1.753   2.766   0.341
ATOM     27  H   P17     1       0.785   2.748   0.826
ATOM     28  C   P17     1       2.992   2.998   1.171
ATOM     29  H   P17     1       3.122   2.713   2.205
ATOM     30  C   P17     1       3.890   3.497   0.322
ATOM     31  H   P17     1       4.933   3.719   0.492
ATOM     32  C   P17     1       0.772   1.046  -1.254
ATOM     33  O   P17     1      -0.232   1.746  -1.324
ATOM     34  N   P17     1       0.850  -0.165  -1.838
ATOM     35  H   P17     1       1.640  -0.763  -1.637
ATOM     36  C   P17     1      -0.283  -0.722  -2.539
ATOM     37  H   P17     1      -0.738   0.070  -3.134
ATOM     38  C   P17     1       0.163  -1.869  -3.434
ATOM     39  H   P17     1       0.643  -2.652  -2.845
ATOM     40  H   P17     1      -0.695  -2.297  -3.951
ATOM     41  H   P17     1       0.870  -1.506  -4.179
ATOM     42  C   P17     1      -1.382  -1.185  -1.585
ATOM     43  O   P17     1      -2.572  -0.996  -1.856
ATOM     44  N   P17     1      -0.979  -1.813  -0.474
ATOM     45  H   P17     1       0.016  -1.942  -0.318
ATOM     46  C   P17     1      -1.915  -2.382   0.490
ATOM     47  C   P17     1      -1.116  -2.821   1.715
ATOM     48  H   P17     1      -0.396  -3.591   1.432
ATOM     49  H   P17     1      -0.582  -1.977   2.151
ATOM     50  H   P17     1      -1.789  -3.240   2.462
ATOM     51  C   P17     1      -2.664  -3.565  -0.105
ATOM     52  H   P17     1      -3.359  -3.971   0.627
ATOM     53  H   P17     1      -3.225  -3.266  -0.988
ATOM     54  H   P17     1      -1.946  -4.339  -0.381
ATOM     55  C   P17     1      -2.905  -1.301   0.954
ATOM     56  O   P17     1      -4.067  -1.573   1.243
ATOM     57  N   P17     1      -2.395  -0.063   1.090
ATOM     58  H   P17     1      -1.411   0.085   0.901
ATOM     59  C   P17     1      -3.167   1.022   1.649
ATOM     60  H   P17     1      -3.792   0.616   2.448
ATOM     61  C   P17     1      -2.238   2.085   2.213
ATOM     62  H   P17     1      -1.588   2.481   1.431
ATOM     63  H   P17     1      -2.826   2.904   2.622
ATOM     64  H   P17     1      -1.617   1.664   3.003
ATOM     65  C   P17     1      -4.147   1.659   0.665
ATOM     66  O   P17     1      -4.931   2.523   1.068
ATOM     67  N   P17     1      -4.102   1.258  -0.606
ATOM     68  H   P17     1      -3.479   0.506  -0.877
ATOM     69  C   P17     1      -5.005   1.802  -1.592
ATOM     70  H   P17     1      -6.044   1.601  -1.326
ATOM     71  H   P17     1      -4.879   2.882  -1.678
ATOM     72  H   P17     1      -4.789   1.342  -2.553
END

COMPND Ac-L-Ala-RRR-Vdm-L-Ala-Aib-L-Ala-
NHMe_310R
REMARK Energy(ZPE)= -1794.699892
REMARK #IF = 0
ATOM      1  C   P18     1      -5.205  -2.869   1.895
ATOM      2  H   P18     1      -5.023  -2.364   2.842
ATOM      3  H   P18     1      -6.184  -2.583   1.516
ATOM      4  H   P18     1      -5.197  -3.943   2.085
ATOM      5  C   P18     1      -4.088  -2.546   0.950
ATOM      6  O   P18     1      -2.907  -2.764   1.232
ATOM      7  N   P18     1      -4.423  -1.986  -0.232
ATOM      8  H   P18     1      -5.398  -1.863  -0.457
ATOM      9  C   P18     1      -3.443  -1.792  -1.278
ATOM     10  H   P18     1      -2.871  -2.716  -1.396
ATOM     11  C   P18     1      -4.130  -1.449  -2.589
ATOM     12  H   P18     1      -4.743  -0.552  -2.490
ATOM     13  H   P18     1      -3.383  -1.276  -3.362
ATOM     14  H   P18     1      -4.766  -2.275  -2.905
ATOM     15  C   P18     1      -2.385  -0.752  -0.925
ATOM     16  O   P18     1      -1.311  -0.743  -1.531
ATOM     17  N   P18     1      -2.667   0.106   0.062
ATOM     18  H   P18     1      -3.583   0.060   0.480
ATOM     19  C   P18     1      -1.713   1.072   0.578
ATOM     20  C   P18     1      -1.415   2.258  -0.401
ATOM     21  H   P18     1      -0.684   2.003  -1.167
ATOM     22  C   P18     1      -2.327   1.814   1.801
ATOM     23  H   P18     1      -3.300   1.401   2.074
ATOM     24  H   P18     1      -1.678   1.730   2.674
ATOM     25  C   P18     1      -3.369   3.333   0.152
ATOM     26  C   P18     1      -4.748   3.873   0.275
ATOM     27  H   P18     1      -4.734   4.926   0.569
```

```
ATOM     28  H   P18     1      -5.308   3.340   1.050
ATOM     29  H   P18     1      -5.306   3.789  -0.658
ATOM     30  C   P18     1      -2.768   2.735  -0.890
ATOM     31  C   P18     1      -3.272   2.472  -2.264
ATOM     32  H   P18     1      -3.204   1.412  -2.519
ATOM     33  H   P18     1      -2.667   3.004  -3.005
ATOM     34  H   P18     1      -4.308   2.786  -2.389
ATOM     35  C   P18     1      -2.399   3.279   1.315
ATOM     36  H   P18     1      -2.587   3.990   2.118
ATOM     37  C   P18     1      -1.061   3.376   0.584
ATOM     38  H   P18     1      -0.199   3.147   1.210
ATOM     39  H   P18     1      -0.923   4.332   0.078
ATOM     40  C   P18     1      -0.420   0.353   0.976
ATOM     41  O   P18     1       0.667   0.934   0.947
ATOM     42  N   P18     1      -0.514  -0.920   1.393
ATOM     43  H   P18     1      -1.400  -1.417   1.377
ATOM     44  C   P18     1       0.667  -1.617   1.849
ATOM     45  H   P18     1       1.129  -1.043   2.656
ATOM     46  C   P18     1       0.305  -3.004   2.353
ATOM     47  H   P18     1      -0.156  -3.600   1.565
ATOM     48  H   P18     1       1.203  -3.512   2.700
ATOM     49  H   P18     1      -0.396  -2.930   3.185
ATOM     50  C   P18     1       1.754  -1.713   0.784
ATOM     51  O   P18     1       2.928  -1.872   1.136
ATOM     52  N   P18     1       1.379  -1.638  -0.499
ATOM     53  H   P18     1       0.407  -1.435  -0.718
ATOM     54  C   P18     1       2.323  -1.716  -1.607
ATOM     55  C   P18     1       1.562  -1.403  -2.895
ATOM     56  H   P18     1       0.774  -2.142  -3.048
ATOM     57  H   P18     1       1.103  -0.415  -2.854
ATOM     58  H   P18     1       2.248  -1.443  -3.739
ATOM     59  C   P18     1       2.949  -3.102  -1.694
ATOM     60  H   P18     1       3.665  -3.130  -2.514
ATOM     61  H   P18     1       3.464  -3.354  -0.769
ATOM     62  H   P18     1       2.165  -3.836  -1.880
ATOM     63  C   P18     1       3.419  -0.647  -1.474
ATOM     64  O   P18     1       4.510  -0.799  -2.020
ATOM     65  N   P18     1       3.093   0.480  -0.814
ATOM     66  H   P18     1       2.198   0.553  -0.338
ATOM     67  C   P18     1       4.016   1.586  -0.718
ATOM     68  H   P18     1       4.567   1.641  -1.659
ATOM     69  C   P18     1       3.263   2.889  -0.490
ATOM     70  H   P18     1       2.687   2.849   0.435
ATOM     71  H   P18     1       3.971   3.712  -0.426
ATOM     72  H   P18     1       2.577   3.075  -1.317
ATOM     73  C   P18     1       5.084   1.404   0.359
ATOM     74  O   P18     1       6.002   2.224   0.450
ATOM     75  N   P18     1       4.962   0.357   1.176
ATOM     76  H   P18     1       4.207  -0.304   1.036
ATOM     77  C   P18     1       5.929   0.106   2.218
ATOM     78  H   P18     1       6.918  -0.089   1.799
ATOM     79  H   P18     1       6.008   0.965   2.885
ATOM     80  H   P18     1       5.609  -0.760   2.790
END

COMPND Ac-L-Ala-RSR-IIIbmb-L-Ala-Aib-L-Ala-
NHMe_310R
REMARK Energy(ZPE)= -1869.718581
REMARK #IF = 0
ATOM      1  C   P19     1       5.851   1.400   2.200
ATOM      2  H   P19     1       5.535   0.674   2.948
ATOM      3  H   P19     1       6.766   1.055   1.724
ATOM      4  H   P19     1       6.051   2.341   2.714
ATOM      5  C   P19     1       4.730   1.618   1.231
ATOM      6  O   P19     1       3.587   1.903   1.599
ATOM      7  N   P19     1       5.014   1.474  -0.081
ATOM      8  H   P19     1       5.966   1.297  -0.362
ATOM      9  C   P19     1       4.048   1.830  -1.098
ATOM     10  H   P19     1       3.686   2.844  -0.907
ATOM     11  C   P19     1       4.684   1.766  -2.478
ATOM     12  H   P19     1       5.054   0.762  -2.694
ATOM     13  H   P19     1       3.948   2.035  -3.233
ATOM     14  H   P19     1       5.514   2.469  -2.542
ATOM     15  C   P19     1       2.798   0.964  -1.052
ATOM     16  O   P19     1       1.740   1.379  -1.529
ATOM     17  N   P19     1       2.908  -0.246  -0.489
ATOM     18  H   P19     1       3.805  -0.516  -0.112
ATOM     19  C   P19     1       1.784  -1.159  -0.370
ATOM     20  C   P19     1       1.346  -1.723  -1.748
ATOM     21  H   P19     1       1.904  -1.219  -2.537
ATOM     22  H   P19     1       0.282  -1.575  -1.919
ATOM     23  C   P19     1       1.729  -3.220  -1.669
ATOM     24  H   P19     1       1.812  -3.706  -2.639
ATOM     25  C   P19     1       2.999  -3.147  -0.809
ATOM     26  H   P19     1       3.796  -2.559  -1.268
ATOM     27  H   P19     1       3.385  -4.127  -0.525
ATOM     28  C   P19     1       2.299  -2.440   0.367
ATOM     29  H   P19     1       2.886  -2.209   1.255
ATOM     30  C   P19     1       1.133  -3.368   0.574
ATOM     31  C   P19     1       0.784  -3.858  -0.688
ATOM     32  C   P19     1       0.432  -3.739   1.706
ATOM     33  H   P19     1       0.700  -3.356   2.684
ATOM     34  C   P19     1      -0.283  -4.723  -0.840
ATOM     35  H   P19     1      -0.565  -5.103  -1.816
ATOM     36  C   P19     1      -0.630  -4.632   1.559
ATOM     37  H   P19     1      -1.185  -4.955   2.432
ATOM     38  C   P19     1      -0.985  -5.115   0.303
ATOM     39  H   P19     1      -1.811  -5.809   0.212
ATOM     40  C   P19     1       0.636  -0.489   0.386
ATOM     41  O   P19     1      -0.532  -0.839   0.208
ATOM     42  N   P19     1       0.957   0.461   1.279
ATOM     43  H   P19     1       1.912   0.795   1.371
ATOM     44  C   P19     1      -0.077   1.096   2.063
ATOM     45  H   P19     1      -0.640   0.327   2.597
ATOM     46  C   P19     1       0.536   2.064   3.064
ATOM     47  H   P19     1       1.116   2.835   2.556
ATOM     48  H   P19     1      -0.253   2.537   3.645
ATOM     49  H   P19     1       1.196   1.528   3.746
ATOM     50  C   P19     1      -1.127   1.808   1.217
ATOM     51  O   P19     1      -2.248   2.009   1.698
ATOM     52  N   P19     1      -0.788   2.192  -0.020
ATOM     53  H   P19     1       0.128   1.948  -0.385
ATOM     54  C   P19     1      -1.723   2.855  -0.922
ATOM     55  C   P19     1      -1.060   2.949  -2.296
ATOM     56  H   P19     1      -0.163   3.567  -2.233
ATOM     57  H   P19     1      -0.776   1.964  -2.669
ATOM     58  H   P19     1      -1.751   3.411  -3.000
ATOM     59  C   P19     1      -2.075   4.249  -0.419
ATOM     60  H   P19     1      -2.764   4.727  -1.113
ATOM     61  H   P19     1      -2.541   4.203   0.562
ATOM     62  H   P19     1      -1.164   4.845  -0.355
ATOM     63  C   P19     1      -3.001   2.019  -1.102
```

```
ATOM     64  O   P19     1      -4.057   2.556  -1.430
ATOM     65  N   P19     1      -2.878   0.685  -0.970
ATOM     66  H   P19     1      -2.002   0.282  -0.652
ATOM     67  C   P19     1      -3.992  -0.203  -1.204
ATOM     68  H   P19     1      -4.590   0.223  -2.013
ATOM     69  C   P19     1      -3.495  -1.582  -1.611
ATOM     70  H   P19     1      -2.863  -2.014  -0.835
ATOM     71  H   P19     1      -4.345  -2.241  -1.776
ATOM     72  H   P19     1      -2.916  -1.515  -2.532
ATOM     73  C   P19     1      -4.952  -0.322  -0.021
ATOM     74  O   P19     1      -5.996  -0.970  -0.153
ATOM     75  N   P19     1      -4.611   0.276   1.121
ATOM     76  H   P19     1      -3.759   0.823   1.176
ATOM     77  C   P19     1      -5.467   0.208   2.281
ATOM     78  H   P19     1      -6.433   0.677   2.086
ATOM     79  H   P19     1      -5.646  -0.829   2.570
ATOM     80  H   P19     1      -4.982   0.727   3.103
END

COMPND Ac-L-Ala-RSR-IIIbwr-L-Ala-Aib-L-Ala-
NHMe_310R
REMARK Energy(ZPE)= -1752.084225
REMARK #IF = 0
ATOM      1  C   P20     1       5.716  -1.576  -2.025
ATOM      2  H   P20     1       5.444  -0.910  -2.843
ATOM      3  H   P20     1       6.667  -1.259  -1.604
ATOM      4  H   P20     1       5.823  -2.579  -2.436
ATOM      5  C   P20     1       4.602  -1.588  -1.023
ATOM      6  O   P20     1       3.445  -1.890  -1.329
ATOM      7  N   P20     1       4.906  -1.232   0.243
ATOM      8  H   P20     1       5.867  -1.047   0.486
ATOM      9  C   P20     1       3.932  -1.355   1.305
ATOM     10  H   P20     1       3.535  -2.373   1.312
ATOM     11  C   P20     1       4.570  -1.043   2.649
ATOM     12  H   P20     1       4.975  -0.030   2.667
ATOM     13  H   P20     1       3.827  -1.134   3.439
ATOM     14  H   P20     1       5.376  -1.748   2.854
ATOM     15  C   P20     1       2.714  -0.471   1.077
ATOM     16  O   P20     1       1.628  -0.766   1.578
ATOM     17  N   P20     1       2.886   0.624   0.324
ATOM     18  H   P20     1       3.816   0.845  -0.001
ATOM     19  C   P20     1       1.807   1.549   0.047
ATOM     20  C   P20     1       1.432   2.390   1.287
ATOM     21  H   P20     1       1.936   1.995   2.167
ATOM     22  H   P20     1       0.359   2.413   1.459
ATOM     23  C   P20     1       1.998   3.777   0.885
ATOM     24  H   P20     1       2.298   4.422   1.704
ATOM     25  O   P20     1       3.129   3.405   0.086
ATOM     26  C   P20     1       2.396   2.672  -0.883
ATOM     27  H   P20     1       3.038   2.297  -1.676
ATOM     28  C   P20     1       1.289   3.623  -1.257
ATOM     29  H   P20     1       0.761   3.630  -2.198
ATOM     30  C   P20     1       1.056   4.333  -0.155
ATOM     31  H   P20     1       0.282   5.063   0.028
ATOM     32  C   P20     1       0.627   0.828  -0.596
ATOM     33  O   P20     1      -0.520   1.266  -0.490
ATOM     34  N   P20     1       0.900  -0.268  -1.322
ATOM     35  H   P20     1       1.837  -0.662  -1.346
ATOM     36  C   P20     1      -0.165  -0.960  -2.011
ATOM     37  H   P20     1      -0.693  -0.246  -2.648
ATOM     38  C   P20     1       0.397  -2.087  -2.863
ATOM     39  H   P20     1       0.944  -2.804  -2.250
ATOM     40  H   P20     1      -0.416  -2.602  -3.370
ATOM     41  H   P20     1       1.077  -1.686  -3.614
ATOM     42  C   P20     1      -1.239  -1.491  -1.070
ATOM     43  O   P20     1      -2.369  -1.722  -1.513
ATOM     44  N   P20     1      -0.906  -1.687   0.211
ATOM     45  H   P20     1       0.024  -1.427   0.526
ATOM     46  C   P20     1      -1.859  -2.166   1.205
ATOM     47  C   P20     1      -1.194  -2.063   2.578
ATOM     48  H   P20     1      -0.314  -2.706   2.612
ATOM     49  H   P20     1      -0.880  -1.041   2.790
ATOM     50  H   P20     1      -1.895  -2.388   3.346
ATOM     51  C   P20     1      -2.264  -3.607   0.926
ATOM     52  H   P20     1      -2.984  -3.938   1.673
ATOM     53  H   P20     1      -2.716  -3.698  -0.060
ATOM     54  H   P20     1      -1.380  -4.243   0.976
ATOM     55  C   P20     1      -3.104  -1.265   1.243
ATOM     56  O   P20     1      -4.184  -1.707   1.630
ATOM     57  N   P20     1      -2.927   0.030   0.921
ATOM     58  H   P20     1      -2.033   0.349   0.560
ATOM     59  C   P20     1      -4.007   0.984   1.018
ATOM     60  H   P20     1      -4.614   0.709   1.884
ATOM     61  C   P20     1      -3.456   2.389   1.206
ATOM     62  H   P20     1      -2.817   2.673   0.369
ATOM     63  H   P20     1      -4.280   3.097   1.272
ATOM     64  H   P20     1      -2.870   2.443   2.123
ATOM     65  C   P20     1      -4.971   0.954  -0.167
ATOM     66  O   P20     1      -5.991   1.651  -0.137
ATOM     67  N   P20     1      -4.658   0.173  -1.202
ATOM     68  H   P20     1      -3.828  -0.408  -1.167
ATOM     69  C   P20     1      -5.521   0.083  -2.356
ATOM     70  H   P20     1      -6.501  -0.314  -2.083
ATOM     71  H   P20     1      -5.667   1.064  -2.808
ATOM     72  H   P20     1      -5.060  -0.579  -3.084
END

COMPND Ac-L-Ala-RSR-Vb-L-Ala-Aib-L-Ala-
NHMe_310R
REMARK Energy(ZPE)= -1716.159907
REMARK #IF = 0
ATOM      1  C   P21     1      -5.743  -1.569   2.047
ATOM      2  H   P21     1      -5.459  -0.940   2.891
ATOM      3  H   P21     1      -6.684  -1.214   1.633
ATOM      4  H   P21     1      -5.878  -2.583   2.421
ATOM      5  C   P21     1      -4.624  -1.575   1.051
ATOM      6  O   P21     1      -3.473  -1.896   1.358
ATOM      7  N   P21     1      -4.919  -1.195  -0.210
ATOM      8  H   P21     1      -5.877  -0.991  -0.451
ATOM      9  C   P21     1      -3.951  -1.326  -1.278
ATOM     10  H   P21     1      -3.553  -2.343  -1.275
ATOM     11  C   P21     1      -4.603  -1.034  -2.621
ATOM     12  H   P21     1      -5.013  -0.024  -2.646
ATOM     13  H   P21     1      -3.865  -1.131  -3.415
ATOM     14  H   P21     1      -5.407  -1.746  -2.810
ATOM     15  C   P21     1      -2.730  -0.437  -1.081
ATOM     16  O   P21     1      -1.663  -0.725  -1.628
ATOM     17  N   P21     1      -2.879   0.647  -0.309
ATOM     18  H   P21     1      -3.783   0.814   0.107
ATOM     19  C   P21     1      -1.790   1.567  -0.024
ATOM     20  C   P21     1      -1.355   2.375  -1.273
ATOM     21  H   P21     1      -0.284   2.292  -1.443
```

ATOM 22 H P21 1 -1.884 2.002 -2.150
ATOM 23 C P21 1 -1.789 3.826 -0.930
ATOM 24 H P21 1 -1.863 4.478 -1.798
ATOM 25 C P21 1 -3.074 3.557 -0.143
ATOM 26 H P21 1 -3.830 3.022 -0.721
ATOM 27 H P21 1 -3.507 4.457 0.292
ATOM 28 C P21 1 -2.363 2.696 0.911
ATOM 29 H P21 1 -2.952 2.296 1.736
ATOM 30 C P21 1 -1.219 3.607 1.281
ATOM 31 H P21 1 -0.710 3.597 2.235
ATOM 32 C P21 1 -0.882 4.287 0.183
ATOM 33 H P21 1 -0.039 4.953 0.061
ATOM 34 C P21 1 -0.627 0.821 0.627
ATOM 35 O P21 1 0.529 1.241 0.540
ATOM 36 N P21 1 -0.911 -0.295 1.322
ATOM 37 H P21 1 -1.852 -0.676 1.347
ATOM 38 C P21 1 0.151 -1.016 1.985
ATOM 39 H P21 1 0.693 -0.325 2.635
ATOM 40 C P21 1 -0.413 -2.159 2.813
ATOM 41 H P21 1 -0.967 -2.860 2.188
ATOM 42 H P21 1 0.401 -2.690 3.303
ATOM 43 H P21 1 -1.085 -1.772 3.578
ATOM 44 C P21 1 1.213 -1.534 1.022
ATOM 45 O P21 1 2.340 -1.802 1.454
ATOM 46 N P21 1 0.876 -1.675 -0.266
ATOM 47 H P21 1 -0.050 -1.388 -0.570
ATOM 48 C P21 1 1.824 -2.124 -1.279
ATOM 49 C P21 1 1.170 -1.940 -2.648
ATOM 50 H P21 1 0.276 -2.561 -2.716
ATOM 51 H P21 1 0.880 -0.902 -2.811
ATOM 52 H P21 1 1.868 -2.244 -3.427
ATOM 53 C P21 1 2.200 -3.584 -1.067
ATOM 54 H P21 1 2.920 -3.893 -1.823
ATOM 55 H P21 1 2.640 -3.732 -0.082
ATOM 56 H P21 1 1.304 -4.199 -1.155
ATOM 57 C P21 1 3.086 -1.246 -1.267
ATOM 58 O P21 1 4.164 -1.691 -1.656
ATOM 59 N P21 1 2.925 0.041 -0.905
ATOM 60 H P21 1 2.032 0.360 -0.540
ATOM 61 C P21 1 4.017 0.984 -0.966
ATOM 62 H P21 1 4.626 0.729 -1.836
ATOM 63 C P21 1 3.486 2.402 -1.113
ATOM 64 H P21 1 2.842 2.666 -0.273
ATOM 65 H P21 1 4.318 3.101 -1.150
ATOM 66 H P21 1 2.909 2.492 -2.034
ATOM 67 C P21 1 4.973 0.904 0.224
ATOM 68 O P21 1 6.003 1.584 0.223
ATOM 69 N P21 1 4.635 0.099 1.233
ATOM 70 H P21 1 3.797 -0.468 1.166
ATOM 71 C P21 1 5.484 -0.044 2.391
ATOM 72 H P21 1 6.450 -0.474 2.121
ATOM 73 H P21 1 5.662 0.923 2.861
ATOM 74 H P21 1 4.992 -0.701 3.104
END

COMPND Ac-L-Ala-RSR-Vbdm-L-Ala-Aib-L-Ala-NHMe_310R
REMARK Energy(ZPE)= -1794.702106
REMARK #IF = 0
ATOM 1 C P22 1 -5.809 -1.557 2.039
ATOM 2 H P22 1 -5.538 -0.870 2.839
ATOM 3 H P22 1 -6.726 -1.217 1.564
ATOM 4 H P22 1 -5.984 -2.535 2.488
ATOM 5 C P22 1 -4.659 -1.672 1.087
ATOM 6 O P22 1 -3.517 -1.947 1.466
ATOM 7 N P22 1 -4.914 -1.447 -0.220
ATOM 8 H P22 1 -5.863 -1.278 -0.512
ATOM 9 C P22 1 -3.914 -1.707 -1.233
ATOM 10 H P22 1 -3.511 -2.711 -1.083
ATOM 11 C P22 1 -4.526 -1.602 -2.621
ATOM 12 H P22 1 -4.939 -0.607 -2.794
ATOM 13 H P22 1 -3.763 -1.797 -3.373
ATOM 14 H P22 1 -5.319 -2.340 -2.739
ATOM 15 C P22 1 -2.703 -0.791 -1.117
ATOM 16 O P22 1 -1.624 -1.132 -1.606
ATOM 17 N P22 1 -2.870 0.371 -0.475
ATOM 18 H P22 1 -3.780 0.573 -0.086
ATOM 19 C P22 1 -1.784 1.314 -0.258
ATOM 20 C P22 1 -1.332 2.004 -1.567
ATOM 21 H P22 1 -0.258 1.904 -1.717
ATOM 22 H P22 1 -1.849 1.554 -2.415
ATOM 23 C P22 1 -1.760 3.478 -1.351
ATOM 24 H P22 1 -1.812 4.059 -2.271
ATOM 25 C P22 1 -3.057 3.290 -0.566
ATOM 26 H P22 1 -3.813 2.713 -1.103
ATOM 27 H P22 1 -3.486 4.229 -0.215
ATOM 28 C P22 1 -2.361 2.523 0.565
ATOM 29 H P22 1 -2.961 2.198 1.416
ATOM 30 C P22 1 -1.216 3.458 0.883
ATOM 31 C P22 1 -0.854 4.034 -0.274
ATOM 32 C P22 1 -0.631 0.625 0.472
ATOM 33 O P22 1 0.532 1.012 0.344
ATOM 34 C P22 1 -0.601 3.550 2.234
ATOM 35 H P22 1 0.221 4.265 2.256
ATOM 36 H P22 1 -0.210 2.581 2.557
ATOM 37 H P22 1 -1.339 3.858 2.981
ATOM 38 C P22 1 0.303 4.915 -0.574
ATOM 39 H P22 1 1.003 4.410 -1.248
ATOM 40 H P22 1 0.851 5.196 0.326
ATOM 41 H P22 1 -0.016 5.830 -1.081
ATOM 42 N P22 1 -0.936 -0.397 1.292
ATOM 43 H P22 1 -1.881 -0.768 1.346
ATOM 44 C P22 1 0.110 -1.047 2.046
ATOM 45 H P22 1 0.631 -0.300 2.650
ATOM 46 C P22 1 -0.477 -2.117 2.953
ATOM 47 H P22 1 -1.018 -2.866 2.373
ATOM 48 H P22 1 0.322 -2.606 3.507
ATOM 49 H P22 1 -1.168 -1.666 3.665
ATOM 50 C P22 1 1.202 -1.645 1.167
ATOM 51 O P22 1 2.328 -1.821 1.645
ATOM 52 N P22 1 0.890 -1.972 -0.094
ATOM 53 H P22 1 -0.032 -1.742 -0.453
ATOM 54 C P22 1 1.855 -2.556 -1.018
ATOM 55 C P22 1 1.205 -2.608 -2.401
ATOM 56 H P22 1 0.321 -3.246 -2.371
ATOM 57 H P22 1 0.903 -1.615 -2.736
ATOM 58 H P22 1 1.912 -3.025 -3.117
ATOM 59 C P22 1 2.253 -3.958 -0.577
ATOM 60 H P22 1 2.966 -4.380 -1.284
ATOM 61 H P22 1 2.708 -3.942 0.411
ATOM 62 H P22 1 1.364 -4.589 -0.551
ATOM 63 C P22 1 3.101 -1.665 -1.146

ATOM 64 O P22 1 4.180 -2.144 -1.489
ATOM 65 N P22 1 2.925 -0.345 -0.951
ATOM 66 H P22 1 2.032 0.004 -0.615
ATOM 67 C P22 1 4.005 0.594 -1.132
ATOM 68 H P22 1 4.624 0.230 -1.955
ATOM 69 C P22 1 3.460 1.972 -1.476
ATOM 70 H P22 1 2.807 2.342 -0.684
ATOM 71 H P22 1 4.286 2.670 -1.601
ATOM 72 H P22 1 2.889 1.930 -2.404
ATOM 73 C P22 1 4.953 0.692 0.063
ATOM 74 O P22 1 5.968 1.389 -0.025
ATOM 75 N P22 1 4.633 0.016 1.168
ATOM 76 H P22 1 3.802 -0.564 1.190
ATOM 77 C P22 1 5.482 0.057 2.335
ATOM 78 H P22 1 6.493 -0.273 2.091
ATOM 79 H P22 1 5.543 1.068 2.740
ATOM 80 H P22 1 5.065 -0.603 3.092
END

ANNEX 6.A. Additional information about QM calculations

Cartesian coordinates (pdb format) and energies (a.u.) of all structures optimized at MPW1B95/6-31+G(d,p) level with the CPCM solvent model. P310 = right-handed 3_{10}-helix; M310 = left-handed 3_{10}-helix. Vibrational analysis has been conducted at standard conditions (T = 298.15 K, P = 1 atm)

COMPND Ac-Aib$_2$-(R)-II-Aib$_2$-NHMe-P310
REMARK Energy(ZPE)= -1910.167821
REMARK #IF = 0
ATOM 1 C P01 1 6.2027 1.7476 -0.1735
ATOM 2 H P01 1 5.7937 2.5883 0.3843
ATOM 3 H P01 1 7.0755 1.3573 0.3456
ATOM 4 H P01 1 6.5098 2.1159 -1.1529
ATOM 5 C P01 1 5.1246 0.7239 -0.3682
ATOM 6 O P01 1 4.0034 1.0290 -0.7836
ATOM 7 N P01 1 5.4323 -0.5515 -0.0529
ATOM 8 H P01 1 6.3789 -0.7592 0.2244
ATOM 9 C P01 1 4.5592 -1.6802 -0.3582
ATOM 10 C P01 1 5.1534 -2.9218 0.3069
ATOM 11 H P01 1 6.1315 -3.1398 -0.1248
ATOM 12 H P01 1 5.2654 -2.7827 1.3828
ATOM 13 H P01 1 4.5062 -3.7798 0.1309
ATOM 14 C P01 1 4.4389 -1.8873 -1.8620
ATOM 15 H P01 1 3.7867 -2.7328 -2.0719
ATOM 16 H P01 1 4.0259 -1.0019 -2.3422
ATOM 17 H P01 1 5.4277 -2.0903 -2.2734
ATOM 18 C P01 1 3.1703 -1.4534 0.2526
ATOM 19 O P01 1 2.1569 -1.8923 -0.2908
ATOM 20 N P01 1 3.1324 -0.8113 1.4309
ATOM 21 H P01 1 4.0020 -0.4798 1.8208
ATOM 22 C P01 1 1.9128 -0.6315 2.2056
ATOM 23 C P01 1 2.2195 0.3477 3.3382
ATOM 24 H P01 1 2.9728 -0.0791 4.0024
ATOM 25 H P01 1 2.5859 1.2994 2.9511
ATOM 26 H P01 1 1.3169 0.5302 3.9196
ATOM 27 C P01 1 1.4251 -1.9608 2.7682
ATOM 28 H P01 1 0.5178 -1.8102 3.3501
ATOM 29 H P01 1 1.2118 -2.6647 1.9654
ATOM 30 H P01 1 2.1983 -2.3778 3.4136
ATOM 31 C P01 1 0.8147 0.0034 1.3434
ATOM 32 O P01 1 -0.3728 -0.1977 1.6027
ATOM 33 N P01 1 1.2049 0.8269 0.3588
ATOM 34 H P01 1 2.1939 0.9059 0.1381
ATOM 35 C P01 1 0.2596 1.5100 -0.5036
ATOM 36 C P01 1 0.9862 2.1042 -1.7335
ATOM 37 H P01 1 1.1432 1.3653 -2.5194
ATOM 38 H P01 1 1.9651 2.4540 -1.4016
ATOM 39 C P01 1 0.1309 3.2981 -2.1587
ATOM 40 H P01 1 0.7124 4.0661 -2.6693
ATOM 41 H P01 1 -0.6683 2.9841 -2.8364
ATOM 42 C P01 1 -0.3774 2.7461 0.0982
ATOM 43 C P01 1 -0.8434 2.9433 1.3900
ATOM 44 H P01 1 -0.7861 2.1507 2.1251
ATOM 45 C P01 1 -1.3867 4.1815 1.7215
ATOM 46 H P01 1 -1.7479 4.3575 2.7272
ATOM 47 C P01 1 -1.4671 5.1961 0.7706
ATOM 48 H P01 1 -1.8893 6.1555 1.0437
ATOM 49 C P01 1 -0.9983 4.9910 -0.5239
ATOM 50 H P01 1 -1.0514 5.7864 -1.2581
ATOM 51 C P01 1 -0.4481 3.7597 -0.8537
ATOM 52 C P01 1 -0.8131 0.5433 -1.0370
ATOM 53 O P01 1 -1.9459 0.9482 -1.3050
ATOM 54 N P01 1 -0.4166 -0.7142 -1.2807
ATOM 55 H P01 1 0.5120 -1.0106 -0.9916
ATOM 56 C P01 1 -1.2818 -1.6967 -1.9225
ATOM 57 C P01 1 -0.5897 -3.0567 -1.8381
ATOM 58 H P01 1 0.3512 -3.0312 -2.3891
ATOM 59 H P01 1 -0.3798 -3.3298 -0.8034
ATOM 60 H P01 1 -1.2296 -3.8184 -2.2819
ATOM 61 C P01 1 -1.5317 -1.3234 -3.3783
ATOM 62 H P01 1 -2.1766 -2.0632 -3.8483
ATOM 63 H P01 1 -2.0091 -0.3474 -3.4502
ATOM 64 H P01 1 -0.5781 -1.2957 -3.9062
ATOM 65 C P01 1 -2.6213 -1.8323 -1.1774
ATOM 66 O P01 1 -3.6339 -2.1877 -1.7772
ATOM 67 N P01 1 -2.5913 -1.6205 0.1508
ATOM 68 H P01 1 -1.7433 -1.2510 0.5688
ATOM 69 C P01 1 -3.7525 -1.7940 1.0136
ATOM 70 C P01 1 -3.3485 -1.3597 2.4228
ATOM 71 H P01 1 -2.5298 -1.9848 2.7831
ATOM 72 H P01 1 -3.0200 -0.3202 2.4370
ATOM 73 H P01 1 -4.1977 -1.4740 3.0952
ATOM 74 C P01 1 -4.2082 -3.2479 1.0331
ATOM 75 H P01 1 -5.0774 -3.3527 1.6797
ATOM 76 H P01 1 -4.4699 -3.5871 0.0329
ATOM 77 H P01 1 -3.4001 -3.8691 1.4211
ATOM 78 C P01 1 -4.9123 -0.8775 0.5881
ATOM 79 O P01 1 -6.0725 -1.1475 0.9090
ATOM 80 N P01 1 -4.5870 0.2551 -0.0437
ATOM 81 H P01 1 -3.6374 0.3970 -0.3672
ATOM 82 C P01 1 -5.6018 1.2026 -0.4351
ATOM 83 H P01 1 -6.1838 1.5217 0.4301
ATOM 84 H P01 1 -5.1181 2.0703 -0.8765
ATOM 85 H P01 1 -6.2899 0.7710 -1.1653
COMPND Ac-Aib$_2$-(R)-II-Aib$_2$-NHMe-M310
REMARK Energy(ZPE)= -1910.169435
REMARK #IF = 0
ATOM 1 C P01 1 6.1966 0.4517 -1.3243
ATOM 2 H P01 1 5.8516 0.6934 -2.3288
ATOM 3 H P01 1 6.5790 1.3686 -0.8756

ATOM 4 H P01 1 7.0028 -0.2763 -1.3846
ATOM 5 C P01 1 5.0284 -0.0231 -0.5128
ATOM 6 O P01 1 3.9957 0.6420 -0.4067
ATOM 7 N P01 1 5.1485 -1.2296 0.0811
ATOM 8 H P01 1 6.0325 -1.7093 0.0132
ATOM 9 C P01 1 4.1796 -1.7438 1.0437
ATOM 10 C P01 1 4.1876 -0.9119 2.3196
ATOM 11 H P01 1 5.1750 -0.9703 2.7777
ATOM 12 H P01 1 3.9572 0.1296 2.1005
ATOM 13 H P01 1 3.4463 -1.2939 3.0188
ATOM 14 C P01 1 4.5501 -3.1951 1.3482
ATOM 15 H P01 1 3.8263 -3.6226 2.0405
ATOM 16 H P01 1 4.5676 -3.8000 0.4408
ATOM 17 H P01 1 5.5340 -3.2347 1.8186
ATOM 18 C P01 1 2.7709 -1.7497 0.4338
ATOM 19 O P01 1 1.7757 -1.6152 1.1465
ATOM 20 N P01 1 2.6974 -1.9689 -0.8879
ATOM 21 H P01 1 3.5652 -2.0601 -1.3942
ATOM 22 C P01 1 1.4561 -2.1192 -1.6328
ATOM 23 C P01 1 0.7502 -3.4151 -1.2461
ATOM 24 H P01 1 1.4066 -4.2556 -1.4720
ATOM 25 H P01 1 0.5134 -3.4251 -0.1830
ATOM 26 H P01 1 -0.1726 -3.5212 -1.8127
ATOM 27 C P01 1 1.8067 -2.1290 -3.1201
ATOM 28 H P01 1 0.8957 -2.2207 -3.7092
ATOM 29 H P01 1 2.3234 -1.2138 -3.4124
ATOM 30 H P01 1 2.4471 -2.9839 -3.3428
ATOM 31 C P01 1 0.5153 -0.9314 -1.3974
ATOM 32 O P01 1 -0.6938 -1.0553 -1.6073
ATOM 33 N P01 1 1.0480 0.2342 -1.0014
ATOM 34 H P01 1 2.0474 0.3162 -0.8317
ATOM 35 C P01 1 0.1956 1.3847 -0.7736
ATOM 36 C P01 1 -0.3527 2.0108 -2.0717
ATOM 37 H P01 1 -1.3128 1.5817 -2.3485
ATOM 38 H P01 1 0.3664 1.7822 -2.8599
ATOM 39 C P01 1 -0.4063 3.5235 -1.8325
ATOM 40 H P01 1 -0.1807 4.0982 -2.7321
ATOM 41 H P01 1 -1.3989 3.8256 -1.4897
ATOM 42 C P01 1 0.9478 2.5354 -0.1369
ATOM 43 C P01 1 1.8101 2.4886 0.9488
ATOM 44 H P01 1 2.0659 1.5425 1.4131
ATOM 45 C P01 1 2.3550 3.6793 1.4163
ATOM 46 H P01 1 3.0406 3.6666 2.2543
ATOM 47 C P01 1 2.0237 4.8892 0.8092
ATOM 48 H P01 1 2.4577 5.8097 1.1799
ATOM 49 C P01 1 1.1404 4.9281 -0.2658
ATOM 50 H P01 1 0.8825 5.8740 -0.7272
ATOM 51 C P01 1 0.5960 3.7401 -0.7370
ATOM 52 C P01 1 -0.9462 1.0343 0.1938
ATOM 53 O P01 1 -2.0093 1.6574 0.1434
ATOM 54 N P01 1 -0.6985 0.0929 1.1141
ATOM 55 H P01 1 0.1808 -0.4183 1.0799
ATOM 56 C P01 1 -1.6562 -0.2477 2.1594
ATOM 57 C P01 1 -1.7923 0.8958 3.1567
ATOM 58 H P01 1 -0.8234 1.0804 3.6215
ATOM 59 H P01 1 -2.1287 1.8041 2.6591
ATOM 60 H P01 1 -2.5144 0.6333 3.9274
ATOM 61 C P01 1 -1.1534 -1.5070 2.8634
ATOM 62 H P01 1 -1.8677 -1.8063 3.6293
ATOM 63 H P01 1 -1.0262 -2.3291 2.1581
ATOM 64 H P01 1 -0.1941 -1.3079 3.3425
ATOM 65 C P01 1 -3.0332 -0.5857 1.5609
ATOM 66 O P01 1 -4.0559 -0.4068 2.2191
ATOM 67 N P01 1 -3.0380 -1.1488 0.3387
ATOM 68 H P01 1 -2.1688 -1.1926 -0.1838
ATOM 69 C P01 1 -4.2557 -1.5831 -0.3335
ATOM 70 C P01 1 -4.9230 -2.7264 0.4210
ATOM 71 H P01 1 -4.2330 -3.5694 0.4739
ATOM 72 H P01 1 -5.1925 -2.4219 1.4303
ATOM 73 H P01 1 -5.8237 -3.0368 -0.1052
ATOM 74 C P01 1 -3.8633 -2.0465 -1.7367
ATOM 75 H P01 1 -4.7554 -2.3541 -2.2806
ATOM 76 H P01 1 -3.3647 -1.2493 -2.2890
ATOM 77 H P01 1 -3.1836 -2.8974 -1.6702
ATOM 78 C P01 1 -5.2465 -0.4200 -0.5185
ATOM 79 O P01 1 -6.4490 -0.6453 -0.6785
ATOM 80 N P01 1 -4.7298 0.8099 -0.6000
ATOM 81 H P01 1 -3.7541 0.9686 -0.3729
ATOM 82 C P01 1 -5.5783 1.9541 -0.8273
ATOM 83 H P01 1 -6.1489 1.8344 -1.7488
ATOM 84 H P01 1 -6.2858 2.0951 -0.0071
ATOM 85 H P01 1 -4.9538 2.8400 -0.9104
COMPND Ac-Aib$_2$-(1R,2R,4R)-IIIa-Aib$_2$-NHMe-P310
REMARK Energy(ZPE)= -2023.432969
REMARK #IF = 0
ATOM 1 C P02 1 5.9583 0.4259 -0.8974
ATOM 2 H P02 1 5.7072 1.3895 -0.4562
ATOM 3 H P02 1 6.8349 0.0177 -0.3991
ATOM 4 H P02 1 6.192   0.5934 -1.9488
ATOM 5 C P02 1 4.7599 -0.4701 -0.8140
ATOM 6 O P02 1 3.6584 -0.1267 -1.2548
ATOM 7 N P02 1 4.9303 -1.665 -0.2143
ATOM 8 H P02 1 5.8604 -1.9257 0.0748
ATOM 9 C P02 1 3.9098 -2.7097 -0.2146
ATOM 10 C P02 1 4.3892 -3.827   0.7107
ATOM 11 H P02 1 5.3092 -4.2624 0.3175
ATOM 12 H P02 1 4.577 -3.4554 1.7187
ATOM 13 H P02 1 3.637 -4.6129 0.7618
ATOM 14 C P02 1 3.6799 -3.242 -1.6226
ATOM 15 H P02 1 2.9217 -4.0225 -1.6093
ATOM 16 H P02 1 3.3483 -2.4457 -2.2872
ATOM 17 H P02 1 4.6131 -3.6599 -2.0007
ATOM 18 C P02 1 2.5951 -2.1615 0.3602
ATOM 19 O P02 1 1.5083 -2.5602 -0.0566
ATOM 20 N P02 1 2.7139 -1.2805 1.3675
ATOM 21 H P02 1 3.6465 -1.0051 1.6369
ATOM 22 C P02 1 1.5999 -0.735   2.1316
ATOM 23 C P02 1 2.1765 0.2863 3.1102
ATOM 24 H P02 1 2.8423 -0.2156 3.8140
ATOM 25 H P02 1 2.7305 1.0677 2.5886
ATOM 26 H P02 1 1.3676 0.7508 3.6722
ATOM 27 C P02 1 0.8659 -1.8344 2.8938
ATOM 28 H P02 1 0.0596 -1.3988 3.4801
ATOM 29 H P02 1 0.4446 -2.5696 2.2103
ATOM 30 H P02 1 1.5683 -2.3299 3.5641
ATOM 31 C P02 1 0.6039 0.0041 1.2282
ATOM 32 O P02 1 -0.5401 0.2331 1.6281
ATOM 33 N P02 1 1.0268 0.4135 0.0226
ATOM 34 H P02 1 1.9711 0.2019 -0.2879
ATOM 35 C P02 1 0.1293 1.0878 -0.8903
ATOM 36 C P02 1 0.8982 1.5953 -2.1363
ATOM 37 H P02 1 1.9271 1.2412 -2.1552

ATOM 38 H P02 1 0.3984 1.2846 -3.0526
ATOM 39 C P02 1 0.7628 3.1223 -1.9835
ATOM 40 H P02 1 0.9051 3.6929 -2.8965
ATOM 41 O P02 1 -0.5915 3.2143 -1.5275
ATOM 42 C P02 1 -0.4305 2.4532 -0.334
ATOM 43 H P02 1 -1.363   2.3753 0.2126
ATOM 44 C P02 1 0.7318 3.1538 0.3127
ATOM 45 C P02 1 1.5188 3.5736 -0.7598
ATOM 46 C P02 1 2.7177 4.2263 -0.5515
ATOM 47 H P02 1 3.3405 4.5486 -1.3770
ATOM 48 C P02 1 3.0994 4.4791 0.7690
ATOM 49 H P02 1 4.0217 5.012   0.9647
ATOM 50 C P02 1 2.3082 4.0664 1.8371
ATOM 51 H P02 1 2.6255 4.2821 2.8499
ATOM 52 C P02 1 1.1114 3.3800 1.6197
ATOM 53 H P02 1 0.5039 3.0412 2.4508
ATOM 54 C P02 1 -1.0491 0.1897 -1.2785
ATOM 55 O P02 1 -2.0883 0.6821 -1.7236
ATOM 56 N P02 1 -0.9026 -1.1292 -1.0999
ATOM 57 H P02 1 -0.0285 -1.4972 -0.7346
ATOM 58 C P02 1 -1.9724 -2.0743 -1.3956
ATOM 59 C P02 1 -1.5747 -3.4244 -0.7993
ATOM 60 H P02 1 -0.6666 -3.7902 -1.2795
ATOM 61 H P02 1 -1.3883 -3.3411 0.2725
ATOM 62 H P02 1 -2.3731 -4.1467 -0.9649
ATOM 63 C P02 1 -2.1889 -2.2028 -2.8971
ATOM 64 H P02 1 -2.9928 -2.9088 -3.0967
ATOM 65 H P02 1 -2.4525 -1.2412 -3.3339
ATOM 66 H P02 1 -1.2710 -2.5667 -3.3596
ATOM 67 C P02 1 -3.2823 -1.6468 -0.709
ATOM 68 O P02 1 -4.3686 -1.9358 -1.2054
ATOM 69 N P02 1 -3.1636 -1.0279 0.4808
ATOM 70 H P02 1 -2.2406 -0.7641 0.8076
ATOM 71 C P02 1 -4.3061 -0.6341 1.2956
ATOM 72 C P02 1 -3.7678 0.1598 2.4858
ATOM 73 H P02 1 -3.1128 -0.4717 3.088
ATOM 74 H P02 1 -3.1993 1.0293 2.154
ATOM 75 H P02 1 -4.5983 0.4924 3.1073
ATOM 76 C P02 1 -5.0729 -1.8537 1.7919
ATOM 77 H P02 1 -5.9237 -1.5333 2.3904
ATOM 78 H P02 1 -5.4359 -2.4512 0.958
ATOM 79 H P02 1 -4.4128 -2.4647 2.4088
ATOM 80 C P02 1 -5.2501 0.3094 0.5291
ATOM 81 O P02 1 -6.4336 0.4113 0.8621
ATOM 82 N P02 1 -4.7031 1.0733 -0.4215
ATOM 83 H P02 1 -3.7603 0.8842 -0.7437
ATOM 84 C P02 1 -5.5018 2.0225 -1.1578
ATOM 85 H P02 1 -6.2750 1.5233 -1.7465
ATOM 86 H P02 1 -5.9920 2.7201 -0.4782
ATOM 87 H P02 1 -4.8519 2.5789 -1.8285

COMPND Ac-Aib$_2$-(1R,2R,4R)-IIIa-Aib$_2$-NHMe-M310
REMARK Energy(ZPE)= -2023.430125
REMARK #IF = 0
ATOM 1 C P02 1 -5.8049 -0.4134 -1.0589
ATOM 2 H P02 1 -5.8860 0.0053 -2.0606
ATOM 3 H P02 1 -6.6502 -1.0726 -0.8723
ATOM 4 H P02 1 -5.8430 0.4126 -0.3470
ATOM 5 C P02 1 -4.4792 -1.1034 -0.9253
ATOM 6 O P02 1 -3.4217 -0.5729 -1.2750
ATOM 7 N P02 1 -4.4886 -2.3263 -0.3565
ATOM 8 H P02 1 -5.3754 -2.7567 -0.1467
ATOM 9 C P02 1 -3.2928 -3.1552 -0.2741
ATOM 10 C P02 1 -2.8508 -3.6166 -1.6563
ATOM 11 H P02 1 -3.6516 -4.2022 -2.1081
ATOM 12 H P02 1 -2.6264 -2.7626 -2.2933
ATOM 13 H P02 1 -1.9592 -4.2357 -1.5773
ATOM 14 C P02 1 -3.6133 -4.3567 0.6142
ATOM 15 H P02 1 -2.7261 -4.9776 0.7304
ATOM 16 H P02 1 -3.9533 -4.0433 1.6019
ATOM 17 H P02 1 -4.3924 -4.9619 0.1483
ATOM 18 C P02 1 -2.1648 -2.3674 0.4027
ATOM 19 O P02 1 -0.9914 -2.5154 0.0639
ATOM 20 N P02 1 -2.5144 -1.5697 1.4253
ATOM 21 H P02 1 -3.4911 -1.4950 1.6675
ATOM 22 C P02 1 -1.5320 -0.9343 2.2926
ATOM 23 C P02 1 -0.8265 -1.9668 3.1603
ATOM 24 H P02 1 -1.5644 -2.4736 3.7823
ATOM 25 H P02 1 -0.3127 -2.7014 2.5422
ATOM 26 H P02 1 -0.0942 -1.4799 3.8012
ATOM 27 C P02 1 -2.2658 0.0889 3.1589
ATOM 28 H P02 1 -1.5545 0.6134 3.7956
ATOM 29 H P02 1 -2.7926 0.8211 2.5454
ATOM 30 H P02 1 -2.9858 -0.4205 3.8013
ATOM 31 C P02 1 -0.5054 -0.1650 1.4519
ATOM 32 O P02 1 0.6742 -0.0952 1.7946
ATOM 33 N P02 1 -0.9774 0.5161 0.3899
ATOM 34 H P02 1 -1.9190 0.3363 0.0543
ATOM 35 C P02 1 -0.1197 1.4341 -0.3265
ATOM 36 C P02 1 0.4283 2.5914 0.5481
ATOM 37 H P02 1 0.0801 2.5172 1.5757
ATOM 38 H P02 1 1.5150 2.5956 0.5323
ATOM 39 C P02 1 -0.1224 3.8297 -0.1827
ATOM 40 H P02 1 0.4490 4.7449 -0.0607
ATOM 41 O P02 1 -0.0920 3.3924 -1.5520
ATOM 42 C P02 1 -0.9314 2.2579 -1.3949
ATOM 43 H P02 1 -1.0948 1.7494 -2.3411
ATOM 44 C P02 1 -2.1327 2.8651 -0.7087
ATOM 45 C P02 1 -1.6031 3.8931 0.0704
ATOM 46 C P02 1 -2.4108 4.6753 0.8712
ATOM 47 H P02 1 -2.0029 5.4685 1.4856
ATOM 48 C P02 1 -3.7853 4.4252 0.8492
ATOM 49 H P02 1 -4.4489 5.0371 1.4474
ATOM 50 C P02 1 -4.3155 3.4118 0.0570
ATOM 51 H P02 1 -5.3866 3.2503 0.0457
ATOM 52 C P02 1 -3.4889 2.6076 -0.7313
ATOM 53 H P02 1 -3.8959 1.8118 -1.3393
ATOM 54 C P02 1 1.0453 0.7076 -1.0145
ATOM 55 O P02 1 2.0657 1.3192 -1.3384
ATOM 56 N P02 1 0.9074 -0.6065 -1.2449
ATOM 57 H P02 1 0.1020 -1.1072 -0.8826
ATOM 58 C P02 1 1.9739 -1.3797 -1.8709
ATOM 59 C P02 1 2.1524 -0.9802 -3.3300
ATOM 60 H P02 1 1.2258 -1.1804 -3.8689
ATOM 61 H P02 1 2.3965 0.0766 -3.4168
ATOM 62 H P02 1 2.9564 -1.5633 -3.7747
ATOM 63 C P02 1 1.6114 -2.8612 -1.7803
ATOM 64 H P02 1 2.4030 -3.4518 -2.2398
ATOM 65 H P02 1 1.4848 -3.1791 -0.7458
ATOM 66 H P02 1 0.6801 -3.0500 -2.3156
ATOM 67 C P02 1 3.2990 -1.2016 -1.1087
ATOM 68 O P02 1 4.3729 -1.3394 -1.6906

ATOM 69 N P02 1 3.2110 -0.9744 0.2160
ATOM 70 H P02 1 2.3005 -0.8119 0.6328
ATOM 71 C P02 1 4.3774 -0.8710 1.0835
ATOM 72 C P02 1 5.1265 -2.1957 1.1569
ATOM 73 H P02 1 4.4634 -2.9585 1.5667
ATOM 74 H P02 1 5.4618 -2.5066 0.1695
ATOM 75 H P02 1 5.9937 -2.0917 1.8065
ATOM 76 C P02 1 3.8825 -0.4774 2.4755
ATOM 77 H P02 1 4.7333 -0.3739 3.1476
ATOM 78 H P02 1 3.3326 0.4638 2.4474
ATOM 79 H P02 1 3.2201 -1.2511 2.8667
ATOM 80 C P02 1 5.3252 0.2496 0.6221
ATOM 81 O P02 1 6.5176 0.2272 0.9364
ATOM 82 N P02 1 4.7725 1.2784 -0.0297
ATOM 83 H P02 1 3.8186 1.2078 -0.3631
ATOM 84 C P02 1 5.5713 2.4004 -0.4588
ATOM 85 H P02 1 6.2893 2.1110 -1.2298
ATOM 86 H P02 1 4.9118 3.1650 -0.8617
ATOM 87 H P02 1 6.1262 2.8161 0.3821

COMPND Ac-Aib$_2$-(1S,2R,4R)-IV-Aib$_2$-NHMe-P310
REMARK Energy(ZPE)= -1835.160047
REMARK #IF = 0
ATOM 1 C P03 1 6.1757 1.3622 0.0064
ATOM 2 H P03 1 5.8363 2.1385 0.6905
ATOM 3 H P03 1 7.0240 0.8393 0.4430
ATOM 4 H P03 1 6.4958 1.8484 -0.9154
ATOM 5 C P03 1 5.0230 0.4574 -0.3096
ATOM 6 O P03 1 3.9356 0.8975 -0.6932
ATOM 7 N P03 1 5.2223 -0.8653 -0.1371
ATOM 8 H P03 1 6.1447 -1.1778 0.1229
ATOM 9 C P03 1 4.2671 -1.8803 -0.5720
ATOM 10 C P03 1 4.7539 -3.2312 -0.0491
ATOM 11 H P03 1 5.7163 -3.4774 -0.5004
ATOM 12 H P03 1 4.8643 -3.2210 1.0359
ATOM 13 H P03 1 4.0430 -4.0100 -0.3213
ATOM 14 C P03 1 4.1538 -1.9046 -2.0905
ATOM 15 H P03 1 3.4382 -2.6640 -2.3994
ATOM 16 H P03 1 3.8216 -0.9391 -2.4687
ATOM 17 H P03 1 5.1292 -2.1409 -2.5162
ATOM 18 C P03 1 2.8892 -1.6148 0.0519
ATOM 19 O P03 1 1.8564 -1.9140 -0.5461
ATOM 20 N P03 1 2.8906 -1.1008 1.2925
ATOM 21 H P03 1 3.7842 -0.8767 1.7038
ATOM 22 C P03 1 1.6948 -0.8903 2.0976
ATOM 23 C P03 1 2.1154 -0.1332 3.3568
ATOM 24 H P03 1 2.8036 -0.7437 3.9437
ATOM 25 H P03 1 2.6050 0.8100 3.1087
ATOM 26 H P03 1 1.2388 0.0776 3.9672
ATOM 27 C P03 1 1.0520 -2.2218 2.4708
ATOM 28 H P03 1 0.1680 -2.0497 3.0817
ATOM 29 H P03 1 0.7600 -2.7742 1.5789
ATOM 30 H P03 1 1.7686 -2.8151 3.0390
ATOM 31 C P03 1 0.6729 -0.0125 1.3621
ATOM 32 O P03 1 -0.5157 -0.0446 1.6915
ATOM 33 N P03 1 1.1225 0.8042 0.4008
ATOM 34 H P03 1 2.1033 0.7845 0.1380
ATOM 35 C P03 1 0.2240 1.6881 -0.3210
ATOM 36 C P03 1 -0.3309 2.8576 0.5390
ATOM 37 H P03 1 -1.2255 2.5812 1.0924
ATOM 38 C P03 1 1.0090 2.4383 -1.4410
ATOM 39 H P03 1 2.0165 2.0385 -1.5551
ATOM 40 H P03 1 0.4928 2.3343 -2.3975
ATOM 41 C P03 1 1.7740 4.0019 0.3358
ATOM 42 H P03 1 2.0253 5.0398 0.5599
ATOM 43 H P03 1 2.7111 3.4427 0.2736
ATOM 44 C P03 1 0.8100 3.4117 1.3927
ATOM 45 H P03 1 1.2778 2.6624 2.0302
ATOM 46 H P03 1 0.4155 4.1940 2.0438
ATOM 47 C P03 1 0.9732 3.8902 -0.9718
ATOM 48 H P03 1 1.2754 4.5975 -1.7438
ATOM 49 C P03 1 -0.4729 3.9864 -0.4884
ATOM 50 H P03 1 -1.2021 3.7756 -1.2696
ATOM 51 H P03 1 -0.7120 4.9403 -0.0126
ATOM 52 C P03 1 -0.9179 0.8821 -0.9434
ATOM 53 O P03 1 -2.0164 1.4033 -1.1556
ATOM 54 N P03 1 -0.6549 -0.3867 -1.2933
ATOM 55 H P03 1 0.2455 -0.7969 -1.0634
ATOM 56 C P03 1 -1.6345 -1.2265 -1.9694
ATOM 57 C P03 1 -1.0984 -2.6578 -1.9735
ATOM 58 H P03 1 -0.1668 -2.7043 -2.5389
ATOM 59 H P03 1 -0.9078 -3.0100 -0.9590
ATOM 60 H P03 1 -1.8242 -3.3182 -2.4465
ATOM 61 C P03 1 -1.8633 -0.7462 -3.3968
ATOM 62 H P03 1 -2.5924 -1.3826 -3.8943
ATOM 63 H P03 1 -2.2309 0.2785 -3.4043
ATOM 64 H P03 1 -0.9199 -0.7923 -3.9417
ATOM 65 C P03 1 -2.9682 -1.2534 -1.2038
ATOM 66 O P03 1 -4.0247 -1.4456 -1.8029
ATOM 67 N P03 1 -2.9000 -1.1474 0.1363
ATOM 68 H P03 1 -2.0149 -0.9043 0.5696
ATOM 69 C P03 1 -4.0706 -1.2521 0.9977
ATOM 70 C P03 1 -3.6204 -0.9517 2.4276
ATOM 71 H P03 1 -2.8806 -1.6874 2.7470
ATOM 72 H P03 1 -3.1752 0.0408 2.5004
ATOM 73 H P03 1 -4.4774 -1.0067 3.0977
ATOM 74 C P03 1 -4.6760 -2.6484 0.9290
ATOM 75 H P03 1 -5.5443 -2.7083 1.5824
ATOM 76 H P03 1 -4.9829 -2.8874 -0.0871
ATOM 77 H P03 1 -3.9325 -3.3752 1.2586
ATOM 78 C P03 1 -5.1278 -0.1931 0.6396
ATOM 79 O P03 1 -6.3150 -0.3692 0.9249
ATOM 80 N P03 1 -4.6770 0.9494 0.1117
ATOM 81 H P03 1 -3.7161 1.0113 -0.2045
ATOM 82 C P03 1 -5.5813 2.0256 -0.2116
ATOM 83 H P03 1 -6.1392 2.3383 0.6717
ATOM 84 H P03 1 -5.0023 2.8685 -0.5805
ATOM 85 H P03 1 -6.2999 1.7269 -0.9781

COMPND Ac-Aib$_2$-(1S,2R,4R)-IV-Aib$_2$-NHMe-M310
REMARK Energy(ZPE)= -1835.158057
REMARK #IF = 0
ATOM 1 C P03 1 -5.9940 1.3721 -0.6045
ATOM 2 H P03 1 -5.6832 2.2258 -0.0038
ATOM 3 H P03 1 -6.2018 1.7336 -1.6119
ATOM 4 H P03 1 -6.9041 0.9471 -0.1867
ATOM 5 C P03 1 -4.8606 0.3928 -0.6750
ATOM 6 O P03 1 -3.7227 0.7337 -1.0072
ATOM 7 N P03 1 -5.1338 -0.8854 -0.3401
ATOM 8 H P03 1 -6.0877 -1.1392 -0.1357
ATOM 9 C P03 1 -4.1704 -1.9637 -0.5294
ATOM 10 C P03 1 -3.9187 -2.2209 -2.0086

ATOM 11 H P03 1 -4.8533 -2.5214 -2.4824
ATOM 12 H P03 1 -3.5410 -1.3242 -2.4969
ATOM 13 H P03 1 -3.1858 -3.0164 -2.1298
ATOM 14 C P03 1 -4.7311 -3.2159 0.1439
ATOM 15 H P03 1 -4.0187 -4.0350 0.0548
ATOM 16 H P03 1 -4.9352 -3.0434 1.2013
ATOM 17 H P03 1 -5.6569 -3.5161 -0.3493
ATOM 18 C P03 1 -2.8532 -1.6083 0.1731
ATOM 19 O P03 1 -1.7667 -1.9326 -0.3045
ATOM 20 N P03 1 -2.9587 -0.9921 1.3614
ATOM 21 H P03 1 -3.8816 -0.7598 1.6971
ATOM 22 C P03 1 -1.8246 -0.7578 2.2458
ATOM 23 C P03 1 -1.2889 -2.0725 2.7976
ATOM 24 H P03 1 -2.0806 -2.5735 3.3550
ATOM 25 H P03 1 -0.9543 -2.7222 1.9903
ATOM 26 H P03 1 -0.4491 -1.8847 3.4635
ATOM 27 C P03 1 -2.3054 0.1442 3.3820
ATOM 28 H P03 1 -1.4771 0.3657 4.0536
ATOM 29 H P03 1 -2.7055 1.0832 2.9971
ATOM 30 H P03 1 -3.0826 -0.3645 3.9549
ATOM 31 C P03 1 -0.7089 -0.0001 1.5128
ATOM 32 O P03 1 0.4695 -0.1513 1.8401
ATOM 33 N P03 1 -1.0839 0.8900 0.5801
ATOM 34 H P03 1 -2.0408 0.8867 0.2429
ATOM 35 C P03 1 -0.1166 1.7611 -0.0623
ATOM 36 C P03 1 -0.8199 2.7694 -1.0127
ATOM 37 H P03 1 -1.1266 2.3204 -1.9576
ATOM 38 C P03 1 0.6076 2.7134 0.9322
ATOM 39 H P03 1 0.2659 2.5322 1.9516
ATOM 40 H P03 1 1.6820 2.5402 0.8917
ATOM 41 C P03 1 -1.2188 4.3883 0.7461
ATOM 42 H P03 1 -1.4674 5.4394 0.5880
ATOM 43 H P03 1 -1.4617 4.1447 1.7825
ATOM 44 C P03 1 -1.9583 3.4804 -0.2645
ATOM 45 H P03 1 -2.6723 2.8082 0.2057
ATOM 46 H P03 1 -2.5203 4.0736 -0.9879
ATOM 47 C P03 1 0.2543 4.1154 0.4292
ATOM 48 H P03 1 0.9376 4.8859 0.7859
ATOM 49 C P03 1 0.2126 3.8979 -1.0843
ATOM 50 H P03 1 1.1689 3.5916 -1.5035
ATOM 51 H P03 1 -0.1713 4.7611 -1.6322
ATOM 52 C P03 1 0.9085 0.9332 -0.8523
ATOM 53 O P03 1 2.0166 1.3990 -1.1382
ATOM 54 N P03 1 0.5557 -0.3050 -1.2289
ATOM 55 H P03 1 -0.3319 -0.6982 -0.9316
ATOM 56 C P03 1 1.4633 -1.1629 -1.9809
ATOM 57 C P03 1 1.6472 -0.6477 -3.4021
ATOM 58 H P03 1 0.6820 -0.6537 -3.9093
ATOM 59 H P03 1 2.0425 0.3662 -3.3979
ATOM 60 H P03 1 2.3375 -1.2908 -3.9446
ATOM 61 C P03 1 0.8709 -2.5716 -2.0073
ATOM 62 H P03 1 1.5446 -3.2376 -2.5452
ATOM 63 H P03 1 0.7188 -2.9560 -0.9986
ATOM 64 H P03 1 -0.0923 -2.5608 -2.5184
ATOM 65 C P03 1 2.8267 -1.2703 -1.2748
ATOM 66 O P03 1 3.8503 -1.4821 -1.9217
ATOM 67 N P03 1 2.8124 -1.2089 0.0702
ATOM 68 H P03 1 1.9490 -0.9608 0.5413
ATOM 69 C P03 1 4.0023 -1.3906 0.8913
ATOM 70 C P03 1 4.5508 -2.8054 0.7538
ATOM 71 H P03 1 3.7905 -3.5157 1.0808
ATOM 72 H P03 1 4.8175 -3.0187 -0.2794
ATOM 73 H P03 1 5.4355 -2.9200 1.3772
ATOM 74 C P03 1 3.6019 -1.1271 2.3431
ATOM 75 H P03 1 4.4754 -1.2285 2.9858
ATOM 76 H P03 1 3.1849 -0.1264 2.4613
ATOM 77 H P03 1 2.8505 -1.8524 2.6587
ATOM 78 C P03 1 5.0923 -0.3613 0.5444
ATOM 79 O P03 1 6.2748 -0.5897 0.8121
ATOM 80 N P03 1 4.6794 0.8094 0.0485
ATOM 81 H P03 1 3.7189 0.9141 -0.2584
ATOM 82 C P03 1 5.6189 1.8599 -0.2586
ATOM 83 H P03 1 6.2233 2.1006 0.6163
ATOM 84 H P03 1 6.2935 1.5716 -1.0682
ATOM 85 H P03 1 5.0652 2.7453 -0.5607

COMPND Ac-Aib$_2$-(1R,2R,4R)-IV-Aib$_2$-NHMe-P310
REMARK Energy(ZPE)= -1833.953184
REMARK #IF = 0
ATOM 1 C P04 1 6.1912 1.3959 0.1214
ATOM 2 H P04 1 5.8528 2.1117 0.8694
ATOM 3 H P04 1 7.0494 0.8496 0.5065
ATOM 4 H P04 1 6.4947 1.9577 -0.7621
ATOM 5 C P04 1 5.0429 0.5072 -0.2519
ATOM 6 O P04 1 3.9609 0.9659 -0.6293
ATOM 7 N P04 1 5.2389 -0.8220 -0.1353
ATOM 8 H P04 1 6.1578 -1.1470 0.1222
ATOM 9 C P04 1 4.2864 -1.8165 -0.6200
ATOM 10 C P04 1 4.7679 -3.1891 -0.1514
ATOM 11 H P04 1 5.7335 -3.4174 -0.6054
ATOM 12 H P04 1 4.8698 -3.2257 0.9338
ATOM 13 H P04 1 4.0582 -3.9545 -0.4621
ATOM 14 C P04 1 4.1845 -1.7776 -2.139
ATOM 15 H P04 1 3.4678 -2.5203 -2.4839
ATOM 16 H P04 1 3.8587 -0.7960 -2.4793
ATOM 17 H P04 1 5.1620 -2.0000 -2.5672
ATOM 18 C P04 1 2.9040 -1.5770 0.0042
ATOM 19 O P04 1 1.8755 -1.8465 -0.6148
ATOM 20 N P04 1 2.8962 -1.1199 1.2671
ATOM 21 H P04 1 3.7868 -0.9206 1.6974
ATOM 22 C P04 1 1.6945 -0.9462 2.0723
ATOM 23 C P04 1 2.1027 -0.2369 3.3627
ATOM 24 H P04 1 2.7930 -0.8648 3.9285
ATOM 25 H P04 1 2.5844 0.7195 3.1537
ATOM 26 H P04 1 1.2210 -0.0586 3.9761
ATOM 27 C P04 1 1.0539 -2.2936 2.3875
ATOM 28 H P04 1 0.1691 -2.1492 3.0041
ATOM 29 H P04 1 0.7632 -2.8077 1.4727
ATOM 30 H P04 1 1.7710 -2.9095 2.9303
ATOM 31 C P04 1 0.6756 -0.0443 1.3637
ATOM 32 O P04 1 -0.5166 -0.0967 1.6780
ATOM 33 N P04 1 1.1336 0.8124 0.4427
ATOM 34 H P04 1 2.1198 0.8150 0.2026
ATOM 35 C P04 1 0.2453 1.7236 -0.2549
ATOM 36 C P04 1 -0.2807 2.8841 0.6579
ATOM 37 H P04 1 -1.1156 2.5887 1.2870
ATOM 38 C P04 1 1.0254 2.5040 -1.3528
ATOM 39 H P04 1 2.0480 2.1423 -1.4473
ATOM 40 H P04 1 0.5362 2.3957 -2.3224
ATOM 41 C P04 1 1.6786 4.0597 0.4355
ATOM 42 H P04 1 2.6693 4.4767 0.5612
ATOM 43 C P04 1 0.9512 3.4143 1.3525

ATOM 44 H P04 1 1.2305 3.1945 2.3742
ATOM 45 C P04 1 0.9340 3.9748 -0.8733
ATOM 46 H P04 1 1.2128 4.6979 -1.6373
ATOM 47 C P04 1 -0.5127 3.9949 -0.3741
ATOM 48 H P04 1 -1.2419 3.7265 -1.1374
ATOM 49 H P04 1 -0.7845 4.9393 0.0993
ATOM 50 C P04 1 -0.9096 0.9437 -0.8894
ATOM 51 O P04 1 -2.0136 1.4682 -1.0578
ATOM 52 N P04 1 -0.6468 -0.3080 -1.2978
ATOM 53 H P04 1 0.2576 -0.7244 -1.0939
ATOM 54 C P04 1 -1.6284 -1.1202 -2.0044
ATOM 55 C P04 1 -1.0885 -2.5486 -2.0746
ATOM 56 H P04 1 -0.1577 -2.5674 -2.6427
ATOM 57 H P04 1 -0.8969 -2.9475 -1.0779
ATOM 58 H P04 1 -1.8136 -3.1877 -2.5771
ATOM 59 C P04 1 -1.8632 -0.5799 -3.4095
ATOM 60 H P04 1 -2.5912 -1.1979 -3.9312
ATOM 61 H P04 1 -2.2356 0.4425 -3.3749
ATOM 62 H P04 1 -0.9214 -0.5982 -3.9585
ATOM 63 C P04 1 -2.9600 -1.1870 -1.2378
ATOM 64 O P04 1 -4.0156 -1.3617 -1.8438
ATOM 65 N P04 1 -2.8903 -1.1360 0.1052
ATOM 66 H P04 1 -2.0074 -0.8977 0.5460
ATOM 67 C P04 1 -4.0596 -1.2824 0.9629
ATOM 68 C P04 1 -3.6086 -1.0436 2.4041
ATOM 69 H P04 1 -2.8662 -1.7903 2.6900
ATOM 70 H P04 1 -3.1665 -0.0539 2.5203
ATOM 71 H P04 1 -4.4650 -1.1311 3.0715
ATOM 72 C P04 1 -4.6601 -2.6766 0.8346
ATOM 73 H P04 1 -5.5293 -2.7650 1.4836
ATOM 74 H P04 1 -4.9650 -2.8746 -0.1910
ATOM 75 H P04 1 -3.9152 -3.4143 1.1353
ATOM 76 C P04 1 -5.1224 -0.2135 0.6540
ATOM 77 O P04 1 -6.3063 -0.4045 0.9436
ATOM 78 N P04 1 -4.6792 0.9492 0.1654
ATOM 79 H P04 1 -3.7205 1.0254 -0.1545
ATOM 80 C P04 1 -5.5868 2.0365 -0.1075
ATOM 81 H P04 1 -6.2932 1.7800 -0.9003
ATOM 82 H P04 1 -6.1579 2.2928 0.7853
ATOM 83 H P04 1 -5.0089 2.9033 -0.4184
COMPND Ac-Aib$_2$-(1R,2R,4R)-IV-Aib$_2$-NHMe-M310
REMARK Energy(ZPE)= -1833.952914
REMARK #IF = 0
ATOM 1 C P04 1 -6.0125 1.4475 -0.4733
ATOM 2 H P04 1 -5.7202 2.2374 0.2178
ATOM 3 H P04 1 -6.1888 1.9067 -1.4460
ATOM 4 H P04 1 -6.9351 0.9886 -0.1246
ATOM 5 C P04 1 -4.8788 0.4746 -0.6042
ATOM 6 O P04 1 -3.7445 0.8339 -0.9306
ATOM 7 N P04 1 -5.1467 -0.8179 -0.3258
ATOM 8 H P04 1 -6.0987 -1.0812 -0.1251
ATOM 9 C P04 1 -4.1871 -1.8878 -0.5750
ATOM 10 C P04 1 -3.9495 -2.0711 -2.0677
ATOM 11 H P04 1 -4.8922 -2.3340 -2.5480
ATOM 12 H P04 1 -3.5640 -1.1550 -2.5114
ATOM 13 H P04 1 -3.2299 -2.8696 -2.2383
ATOM 14 C P04 1 -4.7469 -3.1702 0.0396
ATOM 15 H P04 1 -4.0382 -3.9859 -0.0970
ATOM 16 H P04 1 -4.9406 -3.0503 1.1062
ATOM 17 H P04 1 -5.6780 -3.4422 -0.4601
ATOM 18 C P04 1 -2.8629 -1.5727 0.1335
ATOM 19 O P04 1 -1.7829 -1.8896 -0.3636
ATOM 20 N P04 1 -2.9563 -1.0002 1.3446
ATOM 21 H P04 1 -3.8755 -0.7703 1.6918
ATOM 22 C P04 1 -1.8144 -0.7958 2.2266
ATOM 23 C P04 1 -1.2715 -2.1293 2.7240
ATOM 24 H P04 1 -2.0563 -2.6499 3.2733
ATOM 25 H P04 1 -0.9478 -2.7498 1.8896
ATOM 26 H P04 1 -0.4232 -1.9649 3.3853
ATOM 27 C P04 1 -2.2852 0.0619 3.4003
ATOM 28 H P04 1 -1.4502 0.2596 4.0708
ATOM 29 H P04 1 -2.6909 1.0141 3.0557
ATOM 30 H P04 1 -3.0555 -0.4693 3.9620
ATOM 31 C P04 1 -0.7069 -0.0113 1.5099
ATOM 32 O P04 1 0.4744 -0.1638 1.8289
ATOM 33 N P04 1 -1.0888 0.8921 0.5949
ATOM 34 H P04 1 -2.0575 0.9276 0.2940
ATOM 35 C P04 1 -0.1303 1.7748 -0.0430
ATOM 36 C P04 1 -0.8792 2.7720 -1.0036
ATOM 37 H P04 1 -1.2014 2.3100 -1.9355
ATOM 38 C P04 1 0.5643 2.7467 0.9474
ATOM 39 H P04 1 0.2481 2.5484 1.9700
ATOM 40 H P04 1 1.6457 2.6359 0.8856
ATOM 41 C P04 1 -1.3571 4.2434 0.6939
ATOM 42 H P04 1 -1.8187 4.7963 1.5016
ATOM 43 C P04 1 -1.9615 3.4208 -0.1678
ATOM 44 H P04 1 -3.0080 3.1570 -0.2142
ATOM 45 C P04 1 0.1263 4.1475 0.4455
ATOM 46 H P04 1 0.7350 4.9630 0.8310
ATOM 47 C P04 1 0.1383 3.9149 -1.0687
ATOM 48 H P04 1 1.1128 3.6134 -1.4496
ATOM 49 H P04 1 -0.2471 4.7651 -1.6318
ATOM 50 C P04 1 0.9053 0.9666 -0.8359
ATOM 51 O P04 1 2.0098 1.4454 -1.1147
ATOM 52 N P04 1 0.5609 -0.2687 -1.2283
ATOM 53 H P04 1 -0.3284 -0.6686 -0.9438
ATOM 54 C P04 1 1.4746 -1.1142 -1.9864
ATOM 55 C P04 1 1.6584 -0.5858 -3.4028
ATOM 56 H P04 1 0.6936 -0.5890 -3.9108
ATOM 57 H P04 1 2.0517 0.4288 -3.3897
ATOM 58 H P04 1 2.3504 -1.2227 -3.9504
ATOM 59 C P04 1 0.8880 -2.5252 -2.0257
ATOM 60 H P04 1 1.5675 -3.1858 -2.5629
ATOM 61 H P04 1 0.7300 -2.9157 -1.0201
ATOM 62 H P04 1 -0.0719 -2.5145 -2.5428
ATOM 63 C P04 1 2.8373 -1.2212 -1.2792
ATOM 64 O P04 1 3.8627 -1.4211 -1.9269
ATOM 65 N P04 1 2.8209 -1.1726 0.0662
ATOM 66 H P04 1 1.9557 -0.9324 0.5388
ATOM 67 C P04 1 4.0113 -1.3576 0.8859
ATOM 68 C P04 1 4.5679 -2.7675 0.7317
ATOM 69 H P04 1 3.8118 -3.4860 1.0505
ATOM 70 H P04 1 4.8359 -2.9674 -0.3039
ATOM 71 H P04 1 5.4532 -2.8840 1.3540
ATOM 72 C P04 1 3.6093 -1.1142 2.3408
ATOM 73 H P04 1 4.4837 -1.2179 2.9819
ATOM 74 H P04 1 3.1864 -0.1176 2.4711
ATOM 75 H P04 1 2.8627 -1.8480 2.6477
ATOM 76 C P04 1 5.0958 -0.3182 0.5521
ATOM 77 O P04 1 6.2791 -0.5423 0.8200
ATOM 78 N P04 1 4.6771 0.8551 0.0672
ATOM 79 H P04 1 3.7163 0.9581 -0.2388

ATOM 80 C P04 1 5.6111 1.9146 -0.2257
ATOM 81 H P04 1 6.2909 1.6382 -1.0350
ATOM 82 H P04 1 5.0529 2.7992 -0.5218
ATOM 83 H P04 1 6.2102 2.1508 0.6540
COMPND Ac-Aib$_2$-(1S,2R,3S,4R)-VIIa-Aib$_2$-NHMe-P310
REMARK Energy(ZPE)= -2233.38737
REMARK #IF = 0
ATOM 1 C P05 1 -6.0818 1.2710 -0.369
ATOM 2 H P05 1 -5.7213 1.8855 -1.1929
ATOM 3 H P05 1 -6.9553 0.7087 -0.6915
ATOM 4 H P05 1 -6.3693 1.9401 0.4422
ATOM 5 C P05 1 -4.9608 0.3991 0.1097
ATOM 6 O P05 1 -3.8604 0.8665 0.4196
ATOM 7 N P05 1 -5.1991 -0.9262 0.1689
ATOM 8 H P05 1 -6.1296 -1.2526 -0.0404
ATOM 9 C P05 1 -4.2735 -1.8789 0.7758
ATOM 10 C P05 1 -4.8000 -3.2847 0.4894
ATOM 11 H P05 1 -5.7696 -3.422 0.9709
ATOM 12 H P05 1 -4.9103 -3.4585 -0.5818
ATOM 13 H P05 1 -4.1124 -4.0258 0.8945
ATOM 14 C P05 1 -4.1604 -1.6458 2.2764
ATOM 15 H P05 1 -3.4714 -2.3651 2.7146
ATOM 16 H P05 1 -3.794 -0.642   2.486
ATOM 17 H P05 1 -5.1432 -1.771 2.7314
ATOM 18 C P05 1 -2.889 -1.7608 0.1224
ATOM 19 O P05 1 -1.8642 -1.9694 0.7707
ATOM 20 N P05 1 -2.8796 -1.4794 -1.1914
ATOM 21 H P05 1 -3.7696 -1.3209 -1.6395
ATOM 22 C P05 1 -1.6831 -1.432 -2.0196
ATOM 23 C P05 1 -2.0991 -0.9256 -3.4005
ATOM 24 H P05 1 -2.7843 -1.6375 -3.8635
ATOM 25 H P05 1 -2.5908 0.0465 -3.337
ATOM 26 H P05 1 -1.2199 -0.8333 -4.0362
ATOM 27 C P05 1 -1.0421 -2.8107 -2.1365
ATOM 28 H P05 1 -0.1545 -2.7522 -2.7634
ATOM 29 H P05 1 -0.7547 -3.1897 -1.1571
ATOM 30 H P05 1 -1.7569 -3.4976 -2.5899
ATOM 31 C P05 1 -0.656 -0.4356 -1.4655
ATOM 32 O P05 1 0.5302 -0.5357 -1.7844
ATOM 33 N P05 1 -1.0993 0.5554 -0.6763
ATOM 34 H P05 1 -2.0787 0.5894 -0.4058
ATOM 35 C P05 1 -0.1874 1.5637 -0.1625
ATOM 36 C P05 1 0.4556 2.4546 -1.2662
ATOM 37 H P05 1 1.3512 2.0029 -1.6848
ATOM 38 C P05 1 -1.0098 2.6139 0.6748
ATOM 39 H P05 1 -2.0562 2.3098 0.7142
ATOM 40 S P05 1 -0.5863 2.7735 2.4397
ATOM 41 H P05 1 0.7213   3.034 2.2886
ATOM 42 C P05 1 -1.5708 3.7199 -1.4686
ATOM 43 H P05 1 -1.7405 4.6831 -1.9515
ATOM 44 H P05 1 -2.547 3.2515 -1.3207
ATOM 45 C P05 1 -0.6125 2.8286 -2.2904
ATOM 46 H P05 1 -1.1056 1.9685 -2.741
ATOM 47 H P05 1 -0.1436 3.3945 -3.0971
ATOM 48 C P05 1   -0.83 3.9021 -0.1316
ATOM 49 H P05 1 -1.1249 4.7885   0.427
ATOM 50 C P05 1 0.6343 3.7934 -0.5455
ATOM 51 H P05 1 1.3283 3.7462 0.2929
ATOM 52 H P05 1 0.9489 4.5853 -1.228
ATOM 53 C P05 1 0.9194 0.8932 0.6625
ATOM 54 O P05 1 2.0068 1.4556 0.8241
ATOM 55 N P05 1 0.6459 -0.3029 1.1936
ATOM 56 H P05 1 -0.2568 -0.7282 1.0082
ATOM 57 C P05 1 1.5919 -1.0139 2.0428
ATOM 58 C P05 1 1.0405 -2.4187 2.2838
ATOM 59 H P05 1 0.0737 -2.3576 2.7845
ATOM 60 H P05 1 0.9079 -2.9579   1.345
ATOM 61 H P05 1   1.729 -2.9761 2.9175
ATOM 62 C P05 1 1.7808 -0.2867 3.3677
ATOM 63 H P05 1 2.5122 -0.8129   3.978
ATOM 64 H P05 1 2.1257 0.7329 3.2014
ATOM 65 H P05 1 0.8271 -0.2552   3.895
ATOM 66 C P05 1 2.9458 -1.1798 1.3317
ATOM 67 O P05 1 3.9843 -1.2755 1.9824
ATOM 68 N P05 1   2.908 -1.2938 -0.0092
ATOM 69 H P05 1 2.0303 -1.1265 -0.4912
ATOM 70 C P05 1 4.0933 -1.5349 -0.8218
ATOM 71 C P05 1 3.6644 -1.4822 -2.2882
ATOM 72 H P05 1 2.9352 -2.2684 -2.4898
ATOM 73 H P05 1   3.211 -0.5212 -2.5328
ATOM 74 H P05 1 4.5329 -1.6398 -2.9264
ATOM 75 C P05 1 4.7046 -2.8962 -0.5119
ATOM 76 H P05 1 5.5891 -3.0488 -1.1275
ATOM 77 H P05 1 4.9894 -2.9648   0.536
ATOM 78 H P05 1   3.975 -3.675 -0.7365
ATOM 79 C P05 1   5.144 -0.4276 -0.6308
ATOM 80 O P05 1 6.3297 -0.6408 -0.8969
ATOM 81 N P05 1 4.6947 0.7783 -0.2692
ATOM 82 H P05 1 3.7342 0.8894 0.0341
ATOM 83 C P05 1 5.6004 1.8899 -0.1111
ATOM 84 H P05 1 6.1622 2.0618 -1.0296
ATOM 85 H P05 1 5.0222 2.7803 0.1224
ATOM 86 H P05 1 6.3157 1.7105 0.6948

COMPND Ac-Aib$_2$-(1S,2R,3S,4R)-VIIa-Aib$_2$-NHMe-M310
REMARK Energy(ZPE)= -2233.380876
REMARK #IF = 0
ATOM 1 C P05 1 -6.0427 1.3168 -1.0163
ATOM 2 H P05 1 -5.7297 2.2473 -0.5448
ATOM 3 H P05 1 -6.2001 1.5185 -2.0762
ATOM 4 H P05 1 -6.9810 0.9853 -0.5766
ATOM 5 C P05 1 -4.9395 0.3102 -0.8822
ATOM 6 O P05 1 -3.7780 0.5656 -1.2095
ATOM 7 N P05 1 -5.2708 -0.8927 -0.3682
ATOM 8 H P05 1 -6.2411 -1.0823 -0.1713
ATOM 9 C P05 1 -4.3393 -2.0149 -0.3430
ATOM 10 C P05 1 -4.0274 -2.5009 -1.7517
ATOM 11 H P05 1 -4.9511 -2.8302 -2.2277
ATOM 12 H P05 1 -3.5817 -1.7038 -2.3441
ATOM 13 H P05 1 -3.3296 -3.3352 -1.7131
ATOM 14 C P05 1 -4.9730 -3.1350 0.4816
ATOM 15 H P05 1 -4.2831 -3.9745 0.5560
ATOM 16 H P05 1 -5.2220 -2.7977 1.4883
ATOM 17 H P05 1 -5.8826 -3.4861 -0.0085
ATOM 18 C P05 1 -3.0454 -1.5957 0.3654
ATOM 19 O P05 1 -1.9511 -2.0288 0.0073
ATOM 20 N P05 1 -3.1769 -0.7932 1.4333
ATOM 21 H P05 1 -4.0997 -0.4692 1.6817
ATOM 22 C P05 1 -2.0635 -0.4781 2.3177
ATOM 23 C P05 1 -1.6184 -1.7113 3.0921
ATOM 24 H P05 1 -2.4530 -2.0760 3.6910
ATOM 25 H P05 1 -1.2944 -2.4985 2.4131

ATOM 26 H P05 1 -0.7912 -1.4586 3.7525
ATOM 27 C P05 1 -2.5274 0.6185 3.2760
ATOM 28 H P05 1 -1.7095 0.9006 3.9376
ATOM 29 H P05 1 -2.8590 1.5034 2.7311
ATOM 30 H P05 1 -3.3509 0.2504 3.8902
ATOM 31 C P05 1 -0.8866 0.0978 1.5174
ATOM 32 O P05 1 0.2724 -0.0580 1.8979
ATOM 33 N P05 1 -1.1951 0.8655 0.4539
ATOM 34 H P05 1 -2.1390 0.8386 0.0815
ATOM 35 C P05 1 -0.1800 1.6241 -0.2535
ATOM 36 C P05 1 -0.8151 2.5559 -1.3285
ATOM 37 H P05 1 -1.0663 2.0186 -2.2432
ATOM 38 C P05 1 0.4911 2.6767 0.7100
ATOM 39 H P05 1 -0.0245 2.6068 1.6679
ATOM 40 S P05 1 2.2281 2.4744 1.1948
ATOM 41 H P05 1 2.7738 2.8544 0.0305
ATOM 42 C P05 1 -1.2939 4.3369 0.2317
ATOM 43 H P05 1 -1.5046 5.3732 -0.0372
ATOM 44 H P05 1 -1.6061 4.1977 1.2687
ATOM 45 C P05 1 -1.9859 3.3519 -0.7352
ATOM 46 H P05 1 -2.7462 2.7412 -0.2545
ATOM 47 H P05 1 -2.4818 3.8819 -1.5501
ATOM 48 C P05 1 0.1932 4.0248 0.0345
ATOM 49 H P05 1 0.8624 4.8163 0.3670
ATOM 50 C P05 1 0.2446 3.6558 -1.4469
ATOM 51 H P05 1 1.2170 3.2921 -1.7748
ATOM 52 H P05 1 -0.0845 4.4675 -2.0984
ATOM 53 C P05 1 0.8025 0.6916 -0.9769
ATOM 54 O P05 1 1.8608 1.1152 -1.4477
ATOM 55 N P05 1 0.4268 -0.5898 -1.1233
ATOM 56 H P05 1 -0.4386 -0.9152 -0.7063
ATOM 57 C P05 1 1.2518 -1.5650 -1.8225
ATOM 58 C P05 1 1.3839 -1.2251 -3.3020
ATOM 59 H P05 1 0.3922 -1.2278 -3.7558
ATOM 60 H P05 1 1.8383 -0.2464 -3.4391
ATOM 61 H P05 1 2.0015 -1.9723 -3.7966
ATOM 62 C P05 1 0.5988 -2.9387 -1.6681
ATOM 63 H P05 1 1.2221 -3.6884 -2.1538
ATOM 64 H P05 1 0.4740 -3.2045 -0.6183
ATOM 65 H P05 1 -0.3831 -2.9385 -2.1416
ATOM 66 C P05 1 2.6407 -1.6718 -1.1744
ATOM 67 O P05 1 3.6017 -2.0716 -1.8283
ATOM 68 N P05 1 2.7186 -1.3896 0.1408
ATOM 69 H P05 1 1.9084 -1.0008 0.6121
ATOM 70 C P05 1 3.9451 -1.5556 0.9120
ATOM 71 C P05 1 4.3772 -3.0167 0.9512
ATOM 72 H P05 1 3.5823 -3.6099 1.4048
ATOM 73 H P05 1 4.5770 -3.3931 -0.0496
ATOM 74 H P05 1 5.2792 -3.1171 1.5520
ATOM 75 C P05 1 3.6663 -1.0626 2.3311
ATOM 76 H P05 1 4.5758 -1.1341 2.9263
ATOM 77 H P05 1 3.3204 -0.0289 2.3237
ATOM 78 H P05 1 2.8987 -1.6854 2.7938
ATOM 79 C P05 1 5.0774 -0.6826 0.3432
ATOM 80 O P05 1 6.2583 -0.9615 0.5659
ATOM 81 N P05 1 4.7096 0.4202 -0.3152
ATOM 82 H P05 1 3.7293 0.5702 -0.5165
ATOM 83 C P05 1 5.6856 1.3349 -0.8528
ATOM 84 H P05 1 6.2632 0.8744 -1.6575
ATOM 85 H P05 1 5.1690 2.2068 -1.2471
ATOM 86 H P05 1 6.3807 1.6543 -0.0760

COMPND Ac-Aib$_2$-(1S,2R,3R,4R)-VIIb-Aib$_2$-NHMe-P310
REMARK Energy(ZPE)= -2233.383227
REMARK #IF = 0
ATOM 1 C P06 1 -6.5936 0.1771 -1.2960
ATOM 2 H P06 1 -6.3441 0.7751 -2.1707
ATOM 3 H P06 1 -7.1406 -0.7106 -1.6072
ATOM 4 H P06 1 -7.2392 0.7780 -0.6540
ATOM 5 C P06 1 -5.3316 -0.1346 -0.5420
ATOM 6 O P06 1 -4.4817 0.7218 -0.3107
ATOM 7 N P06 1 -5.1755 -1.4244 -0.1494
ATOM 8 H P06 1 -5.9344 -2.0607 -0.3368
ATOM 9 C P06 1 -4.1532 -1.8911 0.7830
ATOM 10 C P06 1 -4.3144 -3.4061 0.9132
ATOM 11 H P06 1 -5.2944 -3.6390 1.3331
ATOM 12 H P06 1 -4.2181 -3.8999 -0.0548
ATOM 13 H P06 1 -3.5525 -3.7980 1.5849
ATOM 14 C P06 1 -4.3090 -1.2242 2.1450
ATOM 15 H P06 1 -3.5241 -1.5680 2.8163
ATOM 16 H P06 1 -4.2434 -0.1415 2.0516
ATOM 17 H P06 1 -5.2794 -1.4917 2.5636
ATOM 18 C P06 1 -2.7338 -1.6538 0.2442
ATOM 19 O P06 1 -1.7671 -1.6841 1.0080
ATOM 20 N P06 1 -2.6231 -1.4805 -1.0809
ATOM 21 H P06 1 -3.4811 -1.4810 -1.6099
ATOM 22 C P06 1 -1.3798 -1.3992 -1.8288
ATOM 23 C P06 1 -1.7387 -1.0863 -3.2811
ATOM 24 H P06 1 -2.3374 -1.8986 -3.6959
ATOM 25 H P06 1 -2.3039 -0.1560 -3.3580
ATOM 26 H P06 1 -0.8282 -0.9935 -3.8702
ATOM 27 C P06 1 -0.6140 -2.7185 -1.7474
ATOM 28 H P06 1 0.3039 -2.6503 -2.3275
ATOM 29 H P06 1 -0.3616 -2.9568 -0.7148
ATOM 30 H P06 1 -1.2372 -3.5152 -2.1539
ATOM 31 C P06 1 -0.4704 -0.2703 -1.3366
ATOM 32 O P06 1 0.7120 -0.2633 -1.6911
ATOM 33 N P06 1 -0.9725 0.6891 -0.5453
ATOM 34 H P06 1 -1.9485 0.6772 -0.2604
ATOM 35 C P06 1 -0.0948 1.7203 -0.0297
ATOM 36 C P06 1 0.2795 2.7928 -1.0873
ATOM 37 H P06 1 1.1419 2.5066 -1.6848
ATOM 38 C P06 1 -0.7649 2.6000 1.0932
ATOM 39 H P06 1 -0.0233 2.7497 1.8783
ATOM 40 S P06 1 -2.2453 1.9358 1.8968
ATOM 41 H P06 1 -1.6244 0.9376 2.5447
ATOM 42 C P06 1 -1.9055 3.7535 -0.8195
ATOM 43 H P06 1 -2.3099 4.7101 -1.1510
ATOM 44 H P06 1 -2.7556 3.1085 -0.5790
ATOM 45 C P06 1 -0.9817 3.1209 -1.8875
ATOM 46 H P06 1 -1.4252 2.2571 -2.3801
ATOM 47 H P06 1 -0.7268 3.8460 -2.6620
ATOM 48 C P06 1 -0.9732 3.9397 0.3896
ATOM 49 H P06 1 -1.2669 4.7317 1.0767
ATOM 50 C P06 1 0.4056 4.0739 -0.2592
ATOM 51 H P06 1 1.2237 4.0566 0.4611
ATOM 52 H P06 1 0.4961 4.9581 -0.8926
ATOM 53 C P06 1 1.1263 1.0731 0.6242
ATOM 54 O P06 1 2.2183 1.6428 0.6408
ATOM 55 N P06 1 0.8933 -0.0882 1.2615
ATOM 56 H P06 1 -0.0167 -0.5287 1.1551
ATOM 57 C P06 1 1.8842 -0.7657 2.0877

ATOM 58 C P06 1 1.3096 -2.1296 2.4693
ATOM 59 H P06 1 0.4014 -1.9969 3.0588
ATOM 60 H P06 1 1.0646 -2.7159 1.5826
ATOM 61 H P06 1 2.0362 -2.6776 3.0672
ATOM 62 C P06 1 2.1837 0.0471 3.3413
ATOM 63 H P06 1 2.9193 -0.4709 3.9533
ATOM 64 H P06 1 2.5751 1.0294 3.0824
ATOM 65 H P06 1 1.2638 0.1691 3.9139
ATOM 66 C P06 1 3.1859 -1.0295 1.3131
ATOM 67 O P06 1 4.2475 -1.1614 1.9189
ATOM 68 N P06 1 3.0817 -1.1752 -0.0201
ATOM 69 H P06 1 2.1953 -0.9717 -0.4704
ATOM 70 C P06 1 4.2238 -1.4757 -0.8737
ATOM 71 C P06 1 3.7411 -1.4278 -2.3234
ATOM 72 H P06 1 2.9678 -2.1811 -2.4818
ATOM 73 H P06 1 3.3246 -0.4507 -2.5689
ATOM 74 H P06 1 4.5754 -1.6380 -2.9913
ATOM 75 C P06 1 4.7941 -2.8541 -0.5636
ATOM 76 H P06 1 5.6393 -3.0586 -1.2181
ATOM 77 H P06 1 5.1272 -2.9127 0.4705
ATOM 78 H P06 1 4.0222 -3.6053 -0.7347
ATOM 79 C P06 1 5.3174 -0.4019 -0.7376
ATOM 80 O P06 1 6.4907 -0.6632 -1.0135
ATOM 81 N P06 1 4.9116 0.8299 -0.4117
ATOM 82 H P06 1 3.9563 0.9817 -0.1096
ATOM 83 C P06 1 5.8510 1.9201 -0.3131
ATOM 84 H P06 1 6.3968 2.0437 -1.2490
ATOM 85 H P06 1 5.3030 2.8343 -0.0996
ATOM 86 H P06 1 6.5784 1.7492 0.4835

COMPND Ac-Aib$_2$-(1S,2R,3R,4R)-VIIb-Aib$_2$-NHMe-M310
REMARK Energy(ZPE)= -2233.382783
REMARK #IF = 0
ATOM 1 C P06 1 -6.1867 0.8444 -0.4855
ATOM 2 H P06 1 -5.9353 1.7218 0.1093
ATOM 3 H P06 1 -6.4592 1.1877 -1.4835
ATOM 4 H P06 1 -7.0402 0.3389 -0.0386
ATOM 5 C P06 1 -4.9721 -0.0288 -0.5971
ATOM 6 O P06 1 -3.8962 0.3976 -1.0212
ATOM 7 N P06 1 -5.1014 -1.3095 -0.1886
ATOM 8 H P06 1 -6.0117 -1.6399 0.0908
ATOM 9 C P06 1 -4.0542 -2.3018 -0.3969
ATOM 10 C P06 1 -3.8600 -2.5926 -1.8788
ATOM 11 H P06 1 -4.7881 -2.9923 -2.2878
ATOM 12 H P06 1 -3.5917 -1.6853 -2.4173
ATOM 13 H P06 1 -3.0665 -3.3251 -2.0150
ATOM 14 C P06 1 -4.4583 -3.5728 0.3498
ATOM 15 H P06 1 -3.6799 -4.3273 0.2447
ATOM 16 H P06 1 -4.6162 -3.3793 1.4116
ATOM 17 H P06 1 -5.3797 -3.9736 -0.0760
ATOM 18 C P06 1 -2.7400 -1.8051 0.2189
ATOM 19 O P06 1 -1.6532 -2.0733 -0.2915
ATOM 20 N P06 1 -2.8402 -1.1334 1.3775
ATOM 21 H P06 1 -3.7626 -0.9570 1.7467
ATOM 22 C P06 1 -1.6897 -0.7982 2.2058
ATOM 23 C P06 1 -1.0622 -2.0527 2.7991
ATOM 24 H P06 1 -1.8001 -2.5604 3.4203
ATOM 25 H P06 1 -0.7314 -2.7280 2.0115
ATOM 26 H P06 1 -0.2020 -1.7872 3.4108
ATOM 27 C P06 1 -2.1756 0.1350 3.3139
ATOM 28 H P06 1 -1.3357 0.4376 3.9375
ATOM 29 H P06 1 -2.6388 1.0309 2.8986
ATOM 30 H P06 1 -2.9009 -0.3853 3.9417
ATOM 31 C P06 1 -0.6426 -0.0306 1.3885
ATOM 32 O P06 1 0.5564 -0.1468 1.6312
ATOM 33 N P06 1 -1.1064 0.8302 0.4614
ATOM 34 H P06 1 -2.0879 0.7867 0.2107
ATOM 35 C P06 1 -0.2242 1.6662 -0.3240
ATOM 36 C P06 1 -0.9802 2.3377 -1.5001
ATOM 37 H P06 1 -1.2410 1.6264 -2.2834
ATOM 38 C P06 1 0.3692 2.9202 0.4067
ATOM 39 H P06 1 1.4523 2.8239 0.3981
ATOM 40 S P06 1 -0.1623 3.0226 2.1489
ATOM 41 H P06 1 0.5478 4.1267 2.4221
ATOM 42 C P06 1 -1.5305 4.4040 -0.3480
ATOM 43 H P06 1 -1.7819 5.3000 -0.9181
ATOM 44 H P06 1 -1.8329 4.5677 0.6853
ATOM 45 C P06 1 -2.1770 3.1453 -0.9647
ATOM 46 H P06 1 -2.7880 2.5978 -0.2493
ATOM 47 H P06 1 -2.8337 3.3951 -1.7989
ATOM 48 C P06 1 -0.0412 4.1074 -0.4859
ATOM 49 H P06 1 0.6061 4.9722 -0.3414
ATOM 50 C P06 1 -0.0066 3.4588 -1.8719
ATOM 51 H P06 1 0.9792 3.1103 -2.1735
ATOM 52 H P06 1 -0.4132 4.1130 -2.6450
ATOM 53 C P06 1 0.9221 0.8182 -0.9166
ATOM 54 O P06 1 2.0478 1.2916 -1.0919
ATOM 55 N P06 1 0.6100 -0.4251 -1.3069
ATOM 56 H P06 1 -0.2892 -0.8215 -1.0540
ATOM 57 C P06 1 1.5487 -1.2767 -2.0277
ATOM 58 C P06 1 1.7775 -0.7436 -3.4365
ATOM 59 H P06 1 0.8280 -0.7378 -3.9722
ATOM 60 H P06 1 2.1769 0.2688 -3.4090
ATOM 61 H P06 1 2.4818 -1.3818 -3.9665
ATOM 62 C P06 1 0.9529 -2.6830 -2.0899
ATOM 63 H P06 1 1.6322 -3.3403 -2.6310
ATOM 64 H P06 1 0.7855 -3.0861 -1.0912
ATOM 65 H P06 1 -0.0029 -2.6587 -2.6149
ATOM 66 C P06 1 2.8907 -1.3985 -1.2864
ATOM 67 O P06 1 3.9248 -1.6275 -1.9112
ATOM 68 N P06 1 2.8491 -1.3293 0.0563
ATOM 69 H P06 1 1.9847 -1.0493 0.5077
ATOM 70 C P06 1 4.0249 -1.5117 0.8978
ATOM 71 C P06 1 4.5629 -2.9324 0.7846
ATOM 72 H P06 1 3.7939 -3.6323 1.1136
ATOM 73 H P06 1 4.8379 -3.1614 -0.2430
ATOM 74 H P06 1 5.4408 -3.0458 1.4179
ATOM 75 C P06 1 3.6060 -1.2289 2.3409
ATOM 76 H P06 1 4.4664 -1.3452 2.9987
ATOM 77 H P06 1 3.2110 -0.2182 2.4462
ATOM 78 H P06 1 2.8332 -1.9351 2.6488
ATOM 79 C P06 1 5.1275 -0.4951 0.5529
ATOM 80 O P06 1 6.3065 -0.7317 0.8283
ATOM 81 N P06 1 4.7272 0.6757 0.0468
ATOM 82 H P06 1 3.7676 0.7869 -0.2596
ATOM 83 C P06 1 5.6780 1.7138 -0.2679
ATOM 84 H P06 1 6.2635 1.9790 0.6129
ATOM 85 H P06 1 6.3695 1.3984 -1.0525
ATOM 86 H P06 1 5.1353 2.5918 -0.6091

COMPND Ac-Aib$_2$-(1R,2S,4R)-IIIb-Aib$_2$-NHMe-P310

REMARK Energy(ZPE)= -2023.434992
REMARK #IF = 0
ATOM 1 C P07 1 -6.0390 1.7071 -0.4465
ATOM 2 H P07 1 -5.6581 2.1659 -1.3576
ATOM 3 H P07 1 -6.9859 1.2144 -0.6564
ATOM 4 H P07 1 -6.2076 2.5023 0.2802
ATOM 5 C P07 1 -4.9974 0.7788 0.1010
ATOM 6 O P07 1 -3.8273 1.1378 0.2653
ATOM 7 N P07 1 -5.3900 -0.4770 0.3955
ATOM 8 H P07 1 -6.3672 -0.7070 0.3035
ATOM 9 C P07 1 -4.5385 -1.4262 1.1069
ATOM 10 C P07 1 -5.2411 -2.7833 1.0955
ATOM 11 H P07 1 -6.1841 -2.7165 1.6404
ATOM 12 H P07 1 -5.4447 -3.1185 0.0779
ATOM 13 H P07 1 -4.6166 -3.5264 1.5893
ATOM 14 C P07 1 -4.2881 -0.9657 2.5366
ATOM 15 H P07 1 -3.6429 -1.6758 3.0501
ATOM 16 H P07 1 -3.8083 0.0117 2.5482
ATOM 17 H P07 1 -5.2406 -0.9042 3.0630
ATOM 18 C P07 1 -3.2036 -1.5906 0.3677
ATOM 19 O P07 1 -2.1564 -1.7954 0.9801
ATOM 20 N P07 1 -3.2590 -1.5609 -0.9742
ATOM 21 H P07 1 -4.1520 -1.3847 -1.4095
ATOM 22 C P07 1 -2.1119 -1.8235 -1.8321
ATOM 23 C P07 1 -2.5153 -1.4755 -3.2646
ATOM 24 H P07 1 -3.3336 -2.1225 -3.5849
ATOM 25 H P07 1 -2.8344 -0.4355 -3.3452
ATOM 26 H P07 1 -1.6710 -1.6360 -3.9333
ATOM 27 C P07 1 -1.6812 -3.2820 -1.7402
ATOM 28 H P07 1 -0.8173 -3.4531 -2.3796
ATOM 29 H P07 1 -1.4152 -3.5417 -0.7169
ATOM 30 H P07 1 -2.5025 -3.9183 -2.0699
ATOM 31 C P07 1 -0.9381 -0.9099 -1.4611
ATOM 32 O P07 1 0.2216 -1.2464 -1.7104
ATOM 33 N P07 1 -1.2293 0.2852 -0.9288
ATOM 34 H P07 1 -2.1882 0.5200 -0.6865
ATOM 35 C P07 1 -0.1818 1.2465 -0.6512
ATOM 36 C P07 1 0.4216 1.8423 -1.9455
ATOM 37 H P07 1 0.0124 1.3249 -2.8112
ATOM 38 H P07 1 1.5064 1.7760 -1.9578
ATOM 39 C P07 1 -0.0880 3.2970 -1.8837
ATOM 40 H P07 1 -0.2063 3.7979 -2.8397
ATOM 41 O P07 1 -1.3624 3.1247 -1.2402
ATOM 42 C P07 1 -0.8703 2.5184 -0.0466
ATOM 43 H P07 1 -1.6778 2.2985 0.6456
ATOM 44 C P07 1 0.1868 3.4977 0.3831
ATOM 45 C P07 1 0.6884 4.0126 -0.8101
ATOM 46 C P07 1 0.6919 3.8857 1.6075
ATOM 47 H P07 1 0.3108 3.4755 2.5349
ATOM 48 C P07 1 1.7218 4.9279 -0.8140
ATOM 49 H P07 1 2.1269 5.3245 -1.7370
ATOM 50 C P07 1 1.7184 4.8327 1.6128
ATOM 51 H P07 1 2.1246 5.1764 2.5559
ATOM 52 C P07 1 2.2257 5.3431 0.4213
ATOM 53 H P07 1 3.0199 6.0787 0.4535
ATOM 54 C P07 1 0.8800 0.6645 0.2822
ATOM 55 O P07 1 2.0423 1.0717 0.2455
ATOM 56 N P07 1 0.4670 -0.2660 1.1552
ATOM 57 H P07 1 -0.4839 -0.6171 1.0961
ATOM 58 C P07 1 1.3530 -0.8539 2.1521
ATOM 59 C P07 1 0.6119 -2.0217 2.8020
ATOM 60 H P07 1 -0.2778 -1.6560 3.3163
ATOM 61 H P07 1 0.3052 -2.7577 2.0586
ATOM 62 H P07 1 1.2614 -2.5028 3.5320
ATOM 63 C P07 1 1.7351 0.1773 3.2069
ATOM 64 H P07 1 2.3688 -0.2806 3.9638
ATOM 65 H P07 1 2.2728 1.0112 2.7592
ATOM 66 H P07 1 0.8272 0.5514 3.6813
ATOM 67 C P07 1 2.6207 -1.4332 1.5017
ATOM 68 O P07 1 3.6639 -1.5186 2.1463
ATOM 69 N P07 1 2.4972 -1.9011 0.2459
ATOM 70 H P07 1 1.6351 -1.7303 -0.2612
ATOM 71 C P07 1 3.5897 -2.5471 -0.4712
ATOM 72 C P07 1 3.1081 -2.8276 -1.8946
ATOM 73 H P07 1 2.2485 -3.4994 -1.8701
ATOM 74 H P07 1 2.8124 -1.9087 -2.4011
ATOM 75 H P07 1 3.9077 -3.3044 -2.4602
ATOM 76 C P07 1 3.9908 -3.8531 0.2034
ATOM 77 H P07 1 4.8004 -4.3222 -0.3525
ATOM 78 H P07 1 4.3201 -3.6779 1.2255
ATOM 79 H P07 1 3.1324 -4.5259 0.2148
ATOM 80 C P07 1 4.8072 -1.6138 -0.5940
ATOM 81 O P07 1 5.9352 -2.0776 -0.7798
ATOM 82 N P07 1 4.5608 -0.2999 -0.5933
ATOM 83 H P07 1 3.6393 0.0392 -0.3431
ATOM 84 C P07 1 5.6281 0.6570 -0.7546
ATOM 85 H P07 1 6.3399 0.6049 0.0724
ATOM 86 H P07 1 6.1724 0.4735 -1.6814
ATOM 87 H P07 1 5.1991 1.6552 -0.7877

COMPND Ac-Aib$_2$-(1R,2S,4R)-IIIb-Aib$_2$-NHMe-M310
REMARK Energy(ZPE)= -2023.430559
REMARK #IF = 0
ATOM 1 C P07 1 6.0159 2.2780 0.0049
ATOM 2 H P07 1 5.5705 2.8781 -0.7875
ATOM 3 H P07 1 6.1228 2.9151 0.8828
ATOM 4 H P07 1 7.0003 1.9380 -0.3096
ATOM 5 C P07 1 5.0811 1.1562 0.3436
ATOM 6 O P07 1 3.9043 1.3627 0.6558
ATOM 7 N P07 1 5.5761 -0.0956 0.2708
ATOM 8 H P07 1 6.5567 -0.2101 0.0673
ATOM 9 C P07 1 4.8455 -1.2728 0.7309
ATOM 10 C P07 1 4.6639 -1.2451 2.2422
ATOM 11 H P07 1 5.6445 -1.2267 2.7179
ATOM 12 H P07 1 4.1009 -0.3652 2.5487
ATOM 13 H P07 1 4.1270 -2.1328 2.5707
ATOM 14 C P07 1 5.6441 -2.5062 0.3097
ATOM 15 H P07 1 5.1142 -3.4095 0.6084
ATOM 16 H P07 1 5.7982 -2.5310 -0.7698
ATOM 17 H P07 1 6.6163 -2.5028 0.8051
ATOM 18 C P07 1 3.4772 -1.3505 0.0390
ATOM 19 O P07 1 2.4984 -1.8212 0.6168
ATOM 20 N P07 1 3.4340 -0.9355 -1.2376
ATOM 21 H P07 1 4.2782 -0.5569 -1.6401
ATOM 22 C P07 1 2.2560 -1.0443 -2.0867
ATOM 23 C P07 1 1.9416 -2.5022 -2.3994
ATOM 24 H P07 1 2.7852 -2.9418 -2.9316
ATOM 25 H P07 1 1.7647 -3.0644 -1.4837
ATOM 26 H P07 1 1.0531 -2.5644 -3.0246
ATOM 27 C P07 1 2.5379 -0.2711 -3.3747
ATOM 28 H P07 1 1.6655 -0.3117 -4.0250
ATOM 29 H P07 1 2.7720 0.7739 -3.1670

ATOM 30 H P07 1 3.3788 -0.7250 -3.9014
ATOM 31 C P07 1 1.0423 -0.3823 -1.4243
ATOM 32 O P07 1 -0.1010 -0.7275 -1.7310
ATOM 33 N P07 1 1.2729 0.6157 -0.5563
ATOM 34 H P07 1 2.2251 0.8591 -0.2990
ATOM 35 C P07 1 0.1722 1.3623 0.0236
ATOM 36 C P07 1 0.7233 2.4674 0.9609
ATOM 37 H P07 1 1.7840 2.3149 1.1518
ATOM 38 H P07 1 0.1962 2.5006 1.9128
ATOM 39 C P07 1 0.4786 3.7389 0.1161
ATOM 40 H P07 1 1.1844 4.5481 0.2772
ATOM 41 O P07 1 0.5886 3.2226 -1.2178
ATOM 42 C P07 1 -0.4537 2.2453 -1.1091
ATOM 43 H P07 1 -0.5935 1.7105 -2.0427
ATOM 44 C P07 1 -1.5927 3.0909 -0.6081
ATOM 45 C P07 1 -0.9883 4.0687 0.1777
ATOM 46 C P07 1 -2.9586 3.0756 -0.8083
ATOM 47 H P07 1 -3.4335 2.3142 -1.4146
ATOM 48 C P07 1 -1.7340 5.0389 0.8191
ATOM 49 H P07 1 -1.2692 5.7928 1.4427
ATOM 50 C P07 1 -3.7168 4.0701 -0.1906
ATOM 51 H P07 1 -4.7894 4.0952 -0.3398
ATOM 52 C P07 1 -3.1156 5.0331 0.6166
ATOM 53 H P07 1 -3.7276 5.7950 1.0834
ATOM 54 C P07 1 -0.7847 0.4330 0.7682
ATOM 55 O P07 1 -1.9597 0.7482 0.9609
ATOM 56 N P07 1 -0.2542 -0.7051 1.2401
ATOM 57 H P07 1 0.7127 -0.9267 1.0240
ATOM 58 C P07 1 -1.0099 -1.6626 2.0368
ATOM 59 C P07 1 -1.3415 -1.0855 3.4069
ATOM 60 H P07 1 -0.4126 -0.8512 3.9276
ATOM 61 H P07 1 -1.9359 -0.1787 3.3116
ATOM 62 H P07 1 -1.9030 -1.8119 3.9909
ATOM 63 C P07 1 -0.1510 -2.9182 2.1881
ATOM 64 H P07 1 -0.6939 -3.6616 2.7702
ATOM 65 H P07 1 0.1020 -3.3430 1.2161
ATOM 66 H P07 1 0.7762 -2.6741 2.7078
ATOM 67 C P07 1 -2.3009 -2.0918 1.3191
ATOM 68 O P07 1 -3.2710 -2.4807 1.9661
ATOM 69 N P07 1 -2.2716 -2.0844 -0.0260
ATOM 70 H P07 1 -1.4575 -1.7042 -0.4969
ATOM 71 C P07 1 -3.3906 -2.5184 -0.8522
ATOM 72 C P07 1 -3.6593 -4.0081 -0.6743
ATOM 73 H P07 1 -2.7660 -4.5663 -0.9572
ATOM 74 H P07 1 -3.9108 -4.2379 0.3592
ATOM 75 H P07 1 -4.4849 -4.3144 -1.3139
ATOM 76 C P07 1 -3.0258 -2.2281 -2.3080
ATOM 77 H P07 1 -3.8584 -2.5033 -2.9541
ATOM 78 H P07 1 -2.7947 -1.1724 -2.4542
ATOM 79 H P07 1 -2.1523 -2.8150 -2.5958
ATOM 80 C P07 1 -4.6614 -1.7084 -0.5432
ATOM 81 O P07 1 -5.7755 -2.1702 -0.8028
ATOM 82 N P07 1 -4.4899 -0.4660 -0.0805
ATOM 83 H P07 1 -3.5671 -0.1547 0.1997
ATOM 84 C P07 1 -5.6234 0.3774 0.2102
ATOM 85 H P07 1 -6.3055 -0.1110 0.9087
ATOM 86 H P07 1 -5.2649 1.3025 0.6543
ATOM 87 H P07 1 -6.1811 0.6132 -0.6977

COMPND Ac-Aib$_2$-(1S,2S,3S,4R)-VIIIa-Aib$_2$-NHMe-P310
REMARK Energy(ZPE)= -1910.359438
REMARK #IF = 0
ATOM 1 C P08 1 5.9944 1.6913 -0.2977
ATOM 2 H P08 1 5.6094 2.4803 0.3463
ATOM 3 H P08 1 6.9077 1.2853 0.1319
ATOM 4 H P08 1 6.2258 2.1358 -1.2662
ATOM 5 C P08 1 4.9242 0.6601 -0.4921
ATOM 6 O P08 1 3.7753 0.9676 -0.8237
ATOM 7 N P08 1 5.2660 -0.6255 -0.2717
ATOM 8 H P08 1 6.2299 -0.8357 -0.0638
ATOM 9 C P08 1 4.3851 -1.7455 -0.5895
ATOM 10 C P08 1 5.0252 -3.0160 -0.0313
ATOM 11 H P08 1 5.9778 -3.2007 -0.5304
ATOM 12 H P08 1 5.1989 -2.9358 1.0424
ATOM 13 H P08 1 4.3743 -3.8691 -0.2173
ATOM 14 C P08 1 4.1800 -1.8657 -2.0937
ATOM 15 H P08 1 3.5237 -2.7047 -2.3159
ATOM 16 H P08 1 3.7325 -0.9578 -2.4950
ATOM 17 H P08 1 5.1453 -2.0326 -2.5719
ATOM 18 C P08 1 3.0305 -1.5651 0.1100
ATOM 19 O P08 1 1.9924 -1.9765 -0.4078
ATOM 20 N P08 1 3.0592 -0.9981 1.3268
ATOM 21 H P08 1 3.9516 -0.6865 1.6795
ATOM 22 C P08 1 1.8958 -0.8620 2.1924
ATOM 23 C P08 1 2.3131 -0.0113 3.3918
ATOM 24 H P08 1 3.0786 -0.5347 3.9670
ATOM 25 H P08 1 2.7106 0.9544 3.0754
ATOM 26 H P08 1 1.4542 0.1572 4.0396
ATOM 27 C P08 1 1.4044 -2.2275 2.6593
ATOM 28 H P08 1 0.5435 -2.1087 3.3138
ATOM 29 H P08 1 1.1171 -2.8472 1.8112
ATOM 30 H P08 1 2.2049 -2.7234 3.2084
ATOM 31 C P08 1 0.7565 -0.1170 1.4811
ATOM 32 O P08 1 -0.4085 -0.2803 1.8472
ATOM 33 N P08 1 1.0891 0.7448 0.5055
ATOM 34 H P08 1 2.0554 0.8023 0.1954
ATOM 35 C P08 1 0.0909 1.5431 -0.1806
ATOM 36 C P08 1 -0.7133 2.4973 0.7588
ATOM 37 H P08 1 -1.5789 2.0125 1.2055
ATOM 38 C P08 1 0.8020 2.5544 -1.1580
ATOM 39 H P08 1 1.8720 2.3522 -1.1926
ATOM 40 O P08 1 0.3586 2.4461 -2.4925
ATOM 41 H P08 1 -0.6052 2.5026 -2.5080
ATOM 42 C P08 1 1.1795 3.9645 0.8476
ATOM 43 H P08 1 1.2590 4.9941 1.1970
ATOM 44 H P08 1 2.1942 3.5600 0.7992
ATOM 45 C P08 1 0.2584 3.1211 1.7587
ATOM 46 H P08 1 0.7973 2.3927 2.3617
ATOM 47 H P08 1 -0.3050 3.7572 2.4434
ATOM 48 C P08 1 0.4829 3.9030 -0.5225
ATOM 49 H P08 1 0.7197 4.7323 -1.1880
ATOM 50 C P08 1 -0.9828 3.7087 -0.1404
ATOM 51 H P08 1 -1.6408 3.4960 -0.9822
ATOM 52 H P08 1 -1.3956 4.5473 0.4233
ATOM 53 C P08 1 -0.8828 0.6577 -0.9582
ATOM 54 O P08 1 -1.9460 1.1363 -1.3767
ATOM 55 N P08 1 -0.5597 -0.6231 -1.1516
ATOM 56 H P08 1 0.3320 -0.9756 -0.8140
ATOM 57 C P08 1 -1.4772 -1.5613 -1.7873
ATOM 58 C P08 1 -0.9234 -2.9702 -1.5774
ATOM 59 H P08 1 0.0404 -3.0696 -2.0771
ATOM 60 H P08 1 -0.7868 -3.1869 -0.5170

ATOM 61 H P08 1 -1.6128 -3.6996 -2.0008
ATOM 62 C P08 1 -1.6207 -1.2663 -3.2739
ATOM 63 H P08 1 -2.2999 -1.9827 -3.7319
ATOM 64 H P08 1 -2.0102 -0.2626 -3.4324
ATOM 65 H P08 1 -0.6428 -1.3505 -3.7490
ATOM 66 C P08 1 -2.8548 -1.5103 -1.1000
ATOM 67 O P08 1 -3.8775 -1.7662 -1.7311
ATOM 68 N P08 1 -2.8565 -1.2516 0.2218
ATOM 69 H P08 1 -1.9834 -1.0133 0.6814
ATOM 70 C P08 1 -4.0658 -1.2564 1.0346
ATOM 71 C P08 1 -3.6758 -0.7948 2.4392
ATOM 72 H P08 1 -2.9568 -1.4917 2.8726
ATOM 73 H P08 1 -3.2252 0.1984 2.4186
ATOM 74 H P08 1 -4.5611 -0.7685 3.0732
ATOM 75 C P08 1 -4.6796 -2.6493 1.1007
ATOM 76 H P08 1 -5.5814 -2.6250 1.7097
ATOM 77 H P08 1 -4.9371 -3.0072 0.1057
ATOM 78 H P08 1 -3.9619 -3.3347 1.5530
ATOM 79 C P08 1 -5.1005 -0.2454 0.5107
ATOM 80 O P08 1 -6.2983 -0.3887 0.7681
ATOM 81 N P08 1 -4.6272 0.8291 -0.1290
ATOM 82 H P08 1 -3.6568 0.8580 -0.4200
ATOM 83 C P08 1 -5.5187 1.8567 -0.6090
ATOM 84 H P08 1 -6.1241 2.2511 0.2075
ATOM 85 H P08 1 -4.9254 2.6637 -1.0314
ATOM 86 H P08 1 -6.1941 1.4740 -1.3776

COMPND Ac-Aib$_2$-(1S,2S,3S,4R)-VIIIa-Aib$_2$-NHMe-M310
REMARK Energy(ZPE)= -1910.350961
REMARK #IF = 0
ATOM 1 C P08 1 -5.8824 1.6065 -1.0531
ATOM 2 H P08 1 -5.5242 2.5117 -0.5651
ATOM 3 H P08 1 -6.0147 1.8301 -2.1121
ATOM 4 H P08 1 -6.8434 1.3223 -0.6297
ATOM 5 C P08 1 -4.8390 0.5378 -0.9199
ATOM 6 O P08 1 -3.6573 0.7381 -1.2124
ATOM 7 N P08 1 -5.2479 -0.6583 -0.4481
ATOM 8 H P08 1 -6.2321 -0.7985 -0.2812
ATOM 9 C P08 1 -4.3864 -1.8356 -0.4353
ATOM 10 C P08 1 -4.0670 -2.2955 -1.8511
ATOM 11 H P08 1 -4.9944 -2.5631 -2.3575
ATOM 12 H P08 1 -3.5678 -1.5048 -2.4087
ATOM 13 H P08 1 -3.4128 -3.1648 -1.8214
ATOM 14 C P08 1 -5.1108 -2.9377 0.3365
ATOM 15 H P08 1 -4.4810 -3.8245 0.3921
ATOM 16 H P08 1 -5.3565 -2.6196 1.3502
ATOM 17 H P08 1 -6.0322 -3.2075 -0.1821
ATOM 18 C P08 1 -3.0873 -1.5196 0.3171
ATOM 19 O P08 1 -2.0159 -2.0233 -0.0184
ATOM 20 N P08 1 -3.1969 -0.7221 1.3910
ATOM 21 H P08 1 -4.1032 -0.3372 1.6115
ATOM 22 C P08 1 -2.0860 -0.4547 2.2936
ATOM 23 C P08 1 -1.7124 -1.7040 3.0797
ATOM 24 H P08 1 -2.5748 -2.0296 3.6616
ATOM 25 H P08 1 -1.4099 -2.5065 2.4086
ATOM 26 H P08 1 -0.8883 -1.4872 3.7564
ATOM 27 C P08 1 -2.5159 0.6665 3.2389
ATOM 28 H P08 1 -1.6983 0.9138 3.9147
ATOM 29 H P08 1 -2.7949 1.5639 2.6844
ATOM 30 H P08 1 -3.3674 0.3406 3.8387
ATOM 31 C P08 1 -0.8692 0.0612 1.5109
ATOM 32 O P08 1 0.2736 -0.1644 1.9058
ATOM 33 N P08 1 -1.1229 0.8499 0.4482
ATOM 34 H P08 1 -2.0614 0.8787 0.0613
ATOM 35 C P08 1 -0.0670 1.5639 -0.2476
ATOM 36 C P08 1 -0.6429 2.6339 -1.2211
ATOM 37 H P08 1 -0.9464 2.2079 -2.1773
ATOM 38 C P08 1 0.7436 2.4532 0.7649
ATOM 39 H P08 1 0.3172 2.3114 1.7604
ATOM 40 O P08 1 2.1093 2.0970 0.7861
ATOM 41 H P08 1 2.5130 2.5423 1.5364
ATOM 42 C P08 1 -0.9590 4.2372 0.5505
ATOM 43 H P08 1 -1.1197 5.3118 0.4567
ATOM 44 H P08 1 -1.2502 3.9505 1.5641
ATOM 45 C P08 1 -1.7380 3.4510 -0.5265
ATOM 46 H P08 1 -2.5543 2.8564 -0.1222
ATOM 47 H P08 1 -2.1765 4.1254 -1.2643
ATOM 48 C P08 1 0.5009 3.8746 0.2552
ATOM 49 H P08 1 1.2291 4.5827 0.6518
ATOM 50 C P08 1 0.4933 3.6619 -1.2565
ATOM 51 H P08 1 1.4298 3.2580 -1.6339
ATOM 52 H P08 1 0.2148 4.5552 -1.8194
ATOM 53 C P08 1 0.8297 0.6037 -1.0467
ATOM 54 O P08 1 1.8261 1.0009 -1.6499
ATOM 55 N P08 1 0.4726 -0.6924 -1.0683
ATOM 56 H P08 1 -0.3747 -1.0009 -0.6067
ATOM 57 C P08 1 1.3293 -1.7018 -1.6721
ATOM 58 C P08 1 1.3894 -1.5640 -3.1876
ATOM 59 H P08 1 0.3817 -1.6663 -3.5920
ATOM 60 H P08 1 1.7945 -0.5966 -3.4748
ATOM 61 H P08 1 2.0178 -2.3478 -3.6071
ATOM 62 C P08 1 0.7717 -3.0761 -1.3001
ATOM 63 H P08 1 1.4292 -3.8529 -1.6890
ATOM 64 H P08 1 0.6909 -3.1897 -0.2182
ATOM 65 H P08 1 -0.2193 -3.2054 -1.7353
ATOM 66 C P08 1 2.7396 -1.6203 -1.0631
ATOM 67 O P08 1 3.7281 -1.9601 -1.7097
ATOM 68 N P08 1 2.8044 -1.2606 0.2339
ATOM 69 H P08 1 1.9699 -0.9090 0.6925
ATOM 70 C P08 1 4.0475 -1.2820 0.9943
ATOM 71 C P08 1 4.5858 -2.7001 1.1298
ATOM 72 H P08 1 3.8531 -3.3117 1.6576
ATOM 73 H P08 1 4.7797 -3.1373 0.1525
ATOM 74 H P08 1 5.5146 -2.6882 1.6974
ATOM 75 C P08 1 3.7475 -0.7056 2.3770
ATOM 76 H P08 1 4.6676 -0.6362 2.9566
ATOM 77 H P08 1 3.3002 0.2847 2.2932
ATOM 78 H P08 1 3.0531 -1.3584 2.9083
ATOM 79 C P08 1 5.1015 -0.3738 0.3366
ATOM 80 O P08 1 6.3071 -0.6197 0.4333
ATOM 81 N P08 1 4.6330 0.7261 -0.2563
ATOM 82 H P08 1 3.6325 0.8695 -0.3229
ATOM 83 C P08 1 5.5178 1.6918 -0.8575
ATOM 84 H P08 1 6.2424 2.0622 -0.1306
ATOM 85 H P08 1 6.0697 1.2580 -1.6942
ATOM 86 H P08 1 4.9252 2.5266 -1.2230

COMPND Ac-Aib$_2$-(1S,2S,3R,4R)-VIIIb-Aib$_2$-NHMe-P310
REMARK Energy(ZPE)= -1910.35777
REMARK #IF = 0
ATOM 1 C P09 1 6.8066 0.5709 0.5416
ATOM 2 H P09 1 6.6200 1.4106 1.2087

ATOM 3 H P09 1 7.3680 -0.1958 1.0721
ATOM 4 H P09 1 7.4106 0.9345 -0.2907
ATOM 5 C P09 1 5.4948 0.0796 -0.0022
ATOM 6 O P09 1 4.6486 0.8438 -0.4583
ATOM 7 N P09 1 5.2897 -1.2600 0.0555
ATOM 8 H P09 1 6.0462 -1.8344 0.3921
ATOM 9 C P09 1 4.1844 -1.9488 -0.6000
ATOM 10 C P09 1 4.3381 -3.4407 -0.2979
ATOM 11 H P09 1 5.2718 -3.8083 -0.7265
ATOM 12 H P09 1 4.3438 -3.6303 0.7767
ATOM 13 H P09 1 3.5142 -3.9925 -0.7470
ATOM 14 C P09 1 4.1946 -1.7177 -2.1071
ATOM 15 H P09 1 3.3690 -2.2576 -2.5667
ATOM 16 H P09 1 4.0966 -0.6591 -2.3397
ATOM 17 H P09 1 5.1340 -2.0890 -2.5174
ATOM 18 C P09 1 2.8269 -1.5335 -0.0161
ATOM 19 O P09 1 1.7923 -1.7521 -0.6486
ATOM 20 N P09 1 2.8309 -1.0023 1.2159
ATOM 21 H P09 1 3.7291 -0.8985 1.6636
ATOM 22 C P09 1 1.6454 -0.8203 2.0437
ATOM 23 C P09 1 2.0773 -0.0699 3.3036
ATOM 24 H P09 1 2.7835 -0.6770 3.8725
ATOM 25 H P09 1 2.5515 0.8807 3.0554
ATOM 26 H P09 1 1.2094 0.1227 3.9323
ATOM 27 C P09 1 1.0393 -2.1710 2.4113
ATOM 28 H P09 1 0.1700 -2.0302 3.0499
ATOM 29 H P09 1 0.7331 -2.7131 1.5174
ATOM 30 H P09 1 1.7846 -2.7596 2.9467
ATOM 31 C P09 1 0.5868 0.0424 1.3487
ATOM 32 O P09 1 -0.5944 -0.0445 1.6930
ATOM 33 N P09 1 0.9853 0.9151 0.4139
ATOM 34 H P09 1 1.9494 0.9449 0.1007
ATOM 35 C P09 1 0.0225 1.7610 -0.2588
ATOM 36 C P09 1 -0.5843 2.8743 0.6373
ATOM 37 H P09 1 -1.4709 2.5434 1.1721
ATOM 38 C P09 1 0.7407 2.5978 -1.3772
ATOM 39 H P09 1 0.1389 2.5486 -2.2912
ATOM 40 O P09 1 2.0152 2.0591 -1.6128
ATOM 41 H P09 1 2.4887 2.6158 -2.2371
ATOM 42 C P09 1 1.4792 4.0929 0.4832
ATOM 43 H P09 1 1.7138 5.1259 0.7415
ATOM 44 H P09 1 2.4255 3.5546 0.3976
ATOM 45 C P09 1 0.5275 3.4452 1.5162
ATOM 46 H P09 1 1.0163 2.6989 2.1407
ATOM 47 H P09 1 0.0985 4.1978 2.1802
ATOM 48 C P09 1 0.6824 4.0207 -0.8262
ATOM 49 H P09 1 0.9575 4.7684 -1.5704
ATOM 50 C P09 1 -0.7689 4.0320 -0.3512
ATOM 51 H P09 1 -1.4871 3.8218 -1.1434
ATOM 52 H P09 1 -1.0479 4.9584 0.1538
ATOM 53 C P09 1 -1.0802 0.9134 -0.8992
ATOM 54 O P09 1 -2.2039 1.3863 -1.0907
ATOM 55 N P09 1 -0.7517 -0.3275 -1.2844
ATOM 56 H P09 1 0.1711 -0.6953 -1.0692
ATOM 57 C P09 1 -1.6890 -1.2059 -1.9718
ATOM 58 C P09 1 -1.0694 -2.6030 -2.0076
ATOM 59 H P09 1 -0.1246 -2.5752 -2.5518
ATOM 60 H P09 1 -0.8736 -2.9724 -1.0003
ATOM 61 H P09 1 -1.7459 -3.2911 -2.5129
ATOM 62 C P09 1 -1.9527 -0.7098 -3.3875
ATOM 63 H P09 1 -2.6556 -1.3706 -3.8908
ATOM 64 H P09 1 -2.3686 0.2963 -3.3726
ATOM 65 H P09 1 -1.0136 -0.7001 -3.9414
ATOM 66 C P09 1 -3.0140 -1.3232 -1.1990
ATOM 67 O P09 1 -4.0636 -1.5555 -1.7955
ATOM 68 N P09 1 -2.9403 -1.2445 0.1429
ATOM 69 H P09 1 -2.0639 -0.9702 0.5746
ATOM 70 C P09 1 -4.0955 -1.4250 1.0129
ATOM 71 C P09 1 -3.6428 -1.1387 2.4449
ATOM 72 H P09 1 -2.8652 -1.8463 2.7368
ATOM 73 H P09 1 -3.2437 -0.1284 2.5384
ATOM 74 H P09 1 -4.4881 -1.2515 3.1225
ATOM 75 C P09 1 -4.6356 -2.8463 0.9173
ATOM 76 H P09 1 -5.4986 -2.9571 1.5712
ATOM 77 H P09 1 -4.9342 -3.0791 -0.1026
ATOM 78 H P09 1 -3.8591 -3.5449 1.2312
ATOM 79 C P09 1 -5.2065 -0.4097 0.6940
ATOM 80 O P09 1 -6.3773 -0.6461 1.0029
ATOM 81 N P09 1 -4.8224 0.7607 0.1746
ATOM 82 H P09 1 -3.8725 0.8764 -0.1597
ATOM 83 C P09 1 -5.7843 1.7980 -0.1070
ATOM 84 H P09 1 -6.3286 2.0744 0.7967
ATOM 85 H P09 1 -5.2559 2.6708 -0.4821
ATOM 86 H P09 1 -6.5117 1.4753 -0.8551

COMPND Ac-Aib$_2$-(1S,2S,3R,4R)-VIIIb-Aib$_2$-NHMe-M310
REMARK Energy(ZPE)= -1910.358165
REMARK #IF = 0
ATOM 1 C P09 1 -5.9499 1.2567 -0.8589
ATOM 2 H P09 1 -6.8626 0.8893 -0.3944
ATOM 3 H P09 1 -5.6378 2.1777 -0.3690
ATOM 4 H P09 1 -6.1550 1.4895 -1.9043
ATOM 5 C P09 1 -4.8212 0.2711 -0.8048
ATOM 6 O P09 1 -3.6729 0.5732 -1.1397
ATOM 7 N P09 1 -5.1140 -0.9681 -0.3580
ATOM 8 H P09 1 -6.0754 -1.1924 -0.1539
ATOM 9 C P09 1 -4.1598 -2.0692 -0.4242
ATOM 10 C P09 1 -3.8794 -2.4659 -1.8669
ATOM 11 H P09 1 -4.8092 -2.7901 -2.3344
ATOM 12 H P09 1 -3.4704 -1.6257 -2.4253
ATOM 13 H P09 1 -3.1618 -3.2837 -1.8961
ATOM 14 C P09 1 -4.7484 -3.2483 0.3502
ATOM 15 H P09 1 -4.0411 -4.0765 0.3579
ATOM 16 H P09 1 -4.9774 -2.9747 1.3808
ATOM 17 H P09 1 -5.6641 -3.5889 -0.1357
ATOM 18 C P09 1 -2.8540 -1.6634 0.2704
ATOM 19 O P09 1 -1.7611 -2.0363 -0.1533
ATOM 20 N P09 1 -2.9735 -0.9423 1.3971
ATOM 21 H P09 1 -3.8981 -0.6742 1.6993
ATOM 22 C P09 1 -1.8460 -0.6467 2.2709
ATOM 23 C P09 1 -1.3157 -1.9134 2.9293
ATOM 24 H P09 1 -2.1105 -2.3636 3.5241
ATOM 25 H P09 1 -0.9813 -2.6286 2.1798
ATOM 26 H P09 1 -0.4779 -1.6728 3.5806
ATOM 27 C P09 1 -2.3308 0.3441 3.3301
ATOM 28 H P09 1 -1.5073 0.6140 3.9899
ATOM 29 H P09 1 -2.7230 1.2520 2.8705
ATOM 30 H P09 1 -3.1140 -0.1177 3.9335
ATOM 31 C P09 1 -0.7291 0.0540 1.4888
ATOM 32 O P09 1 0.4531 -0.0597 1.8367
ATOM 33 N P09 1 -1.1008 0.8647 0.4908
ATOM 34 H P09 1 -2.0636 0.8401 0.1710

ATOM 35 C P09 1 -0.1473 1.6774 -0.2294
ATOM 36 C P09 1 -0.8501 2.5902 -1.2664
ATOM 37 H P09 1 -1.1633 2.0515 -2.1611
ATOM 38 C P09 1 0.6053 2.7429 0.6724
ATOM 39 H P09 1 1.6763 2.5715 0.5505
ATOM 40 O P09 1 0.2557 2.7162 2.0315
ATOM 41 H P09 1 0.5987 1.8908 2.3970
ATOM 42 C P09 1 -1.2454 4.3755 0.3237
ATOM 43 H P09 1 -1.4823 5.4068 0.0579
ATOM 44 H P09 1 -1.4862 4.2382 1.3771
ATOM 45 C P09 1 -1.9853 3.3739 -0.5902
ATOM 46 H P09 1 -2.6953 2.7506 -0.0515
ATOM 47 H P09 1 -2.5523 3.8886 -1.3678
ATOM 48 C P09 1 0.2272 4.0774 0.0341
ATOM 49 H P09 1 0.9117 4.8784 0.3128
ATOM 50 C P09 1 0.1899 3.7015 -1.4470
ATOM 51 H P09 1 1.1454 3.3515 -1.8344
ATOM 52 H P09 1 -0.1879 4.5102 -2.0750
ATOM 53 C P09 1 0.8829 0.7941 -0.9458
ATOM 54 O P09 1 1.9862 1.2437 -1.2733
ATOM 55 N P09 1 0.5360 -0.4717 -1.2181
ATOM 56 H P09 1 -0.3510 -0.8383 -0.8877
ATOM 57 C P09 1 1.4333 -1.3761 -1.9275
ATOM 58 C P09 1 1.6015 -0.9435 -3.3783
ATOM 59 H P09 1 0.6299 -0.9737 -3.8724
ATOM 60 H P09 1 2.0020 0.0672 -3.4349
ATOM 61 H P09 1 2.2818 -1.6198 -3.8920
ATOM 62 C P09 1 0.8388 -2.7821 -1.8631
ATOM 63 H P09 1 1.5039 -3.4793 -2.3711
ATOM 64 H P09 1 0.7018 -3.1074 -0.8318
ATOM 65 H P09 1 -0.1317 -2.7991 -2.3599
ATOM 66 C P09 1 2.8058 -1.4418 -1.2341
ATOM 67 O P09 1 3.8189 -1.7053 -1.8779
ATOM 68 N P09 1 2.8107 -1.2797 0.1023
ATOM 69 H P09 1 1.9496 -1.0115 0.5644
ATOM 70 C P09 1 4.0098 -1.3973 0.9221
ATOM 71 C P09 1 4.5547 -2.8197 0.8913
ATOM 72 H P09 1 3.7947 -3.5005 1.2764
ATOM 73 H P09 1 4.8139 -3.1124 -0.1244
ATOM 74 H P09 1 5.4430 -2.8903 1.5163
ATOM 75 C P09 1 3.6230 -1.0150 2.3509
ATOM 76 H P09 1 4.5018 -1.0610 2.9927
ATOM 77 H P09 1 3.2056 -0.0080 2.3886
ATOM 78 H P09 1 2.8755 -1.7122 2.7326
ATOM 79 C P09 1 5.0959 -0.4014 0.4783
ATOM 80 O P09 1 6.2823 -0.6107 0.7436
ATOM 81 N P09 1 4.6771 0.7266 -0.1035
ATOM 82 H P09 1 3.7108 0.8103 -0.3966
ATOM 83 C P09 1 5.6143 1.7432 -0.5144
ATOM 84 H P09 1 6.2094 2.0833 0.3337
ATOM 85 H P09 1 6.2978 1.3697 -1.2801
ATOM 86 H P09 1 5.0593 2.5862 -0.9179

COMPND Ac-Aib$_2$-(S)-VI-Aib$_2$-NHMe-P310
REMARK Energy(ZPE)= -2080.946006
REMARK #IF = 0
ATOM 1 C P10 5.3822 1.2774 0.1719
ATOM 2 H P10 5.7746 0.8985 1.1159
ATOM 3 H P10 5.3528 0.4447 -0.5305
ATOM 4 H P10 6.0513 2.0468 -0.2075
ATOM 5 C P10 3.9834 1.7682 0.4009
ATOM 6 O P10 3.0736 1.0102 0.7446
ATOM 7 N P10 3.7518 3.0817 0.1949
ATOM 8 H P10 4.5317 3.6822 -0.0222
ATOM 9 C P10 2.4837 3.7161 0.5406
ATOM 10 C P10 2.5034 5.1373 -0.0213
ATOM 11 H P10 2.6683 5.1383 -1.0994
ATOM 12 H P10 1.5552 5.6313 0.1867
ATOM 13 H P10 3.2975 5.7127 0.4572
ATOM 14 C P10 2.2793 3.7416 2.0489
ATOM 15 H P10 1.3274 4.2112 2.2900
ATOM 16 H P10 2.2811 2.7320 2.4560
ATOM 17 H P10 3.0851 4.3152 2.5072
ATOM 18 C P10 1.3271 2.9649 -0.1345
ATOM 19 O P10 0.2344 2.8410 0.4175
ATOM 20 N P10 1.5603 2.5157 -1.3782
ATOM 21 H P10 2.4804 2.6537 -1.7686
ATOM 22 C P10 0.5326 1.9276 -2.2256
ATOM 23 C P10 1.2288 1.3421 -3.4536
ATOM 24 H P10 1.9913 0.6167 -3.1659
ATOM 25 H P10 0.4986 0.8496 -4.0944
ATOM 26 H P10 1.7017 2.1414 -4.0265
ATOM 27 C P10 -0.4897 2.9775 -2.6414
ATOM 28 H P10 -1.2480 2.5310 -3.2813
ATOM 29 H P10 -0.9785 3.4062 -1.7678
ATOM 30 H P10 0.0189 3.7695 -3.1915
ATOM 31 C P10 -0.1694 0.7682 -1.5032
ATOM 32 O P10 -1.3433 0.4949 -1.7615
ATOM 33 N P10 0.5729 0.0451 -0.6490
ATOM 34 H P10 1.5069 0.3641 -0.4070
ATOM 35 C P10 0.0673 -1.1529 0.0056
ATOM 36 C P10 1.1507 -1.6756 0.9648
ATOM 37 H P10 1.5202 -0.8502 1.5792
ATOM 38 H P10 0.6790 -2.3951 1.6406
ATOM 39 C P10 2.2617 -2.3010 0.1905
ATOM 40 C P10 2.1441 -2.6711 -1.1204
ATOM 41 C P10 0.9167 -2.5309 -1.9427
ATOM 42 H P10 1.0391 -1.7241 -2.6736
ATOM 43 H P10 0.7242 -3.4406 -2.5169
ATOM 44 C P10 -0.2672 -2.2440 -1.0271
ATOM 45 H P10 -1.1335 -1.9395 -1.6122
ATOM 46 H P10 -0.5405 -3.1422 -0.4727
ATOM 47 N P10 3.3374 -3.1836 -1.5640
ATOM 48 H P10 3.5093 -3.5321 -2.4911
ATOM 49 C P10 4.2492 -3.1580 -0.5398
ATOM 50 C P10 5.5819 -3.5628 -0.5063
ATOM 51 H P10 6.0647 -3.9802 -1.3812
ATOM 52 C P10 6.2677 -3.4091 0.6880
ATOM 53 H P10 7.3056 -3.7129 0.7464
ATOM 54 C P10 5.6419 -2.8688 1.8236
ATOM 55 H P10 6.2083 -2.7644 2.7409
ATOM 56 C P10 4.3167 -2.4695 1.7861
ATOM 57 H P10 3.8429 -2.0505 2.6661
ATOM 58 C P10 3.5998 -2.6077 0.5923
ATOM 59 C P10 -1.1809 -0.8534 0.8389
ATOM 60 O P10 -1.9587 -1.7672 1.1309
ATOM 61 N P10 -1.3634 0.4067 1.2538
ATOM 62 H P10 -0.7170 1.1304 0.9530
ATOM 63 C P10 -2.5070 0.8030 2.0660
ATOM 64 C P10 -2.5312 2.3300 2.1241
ATOM 65 H P10 -1.6149 2.6983 2.5868
ATOM 66 H P10 -2.6116 2.7628 1.1264

ATOM 67 H P10 -3.3813 2.6583 2.7208
ATOM 68 C P10 -2.4047 0.2249 3.4709
ATOM 69 H P10 -3.2676 0.5284 4.0607
ATOM 70 H P10 -2.3677 -0.8624 3.4401
ATOM 71 H P10 -1.4982 0.6013 3.9456
ATOM 72 C P10 -3.8239 0.3580 1.4058
ATOM 73 O P10 -4.8146 0.1104 2.0897
ATOM 74 N P10 -3.8391 0.3375 0.0600
ATOM 75 H P10 -2.9714 0.4950 -0.4423
ATOM 76 C P10 -5.0295 0.0253 -0.7200
ATOM 77 C P10 -4.6177 -0.0151 -2.1917
ATOM 78 H P10 -3.8229 -0.7431 -2.3588
ATOM 79 H P10 -5.4791 -0.2808 -2.8032
ATOM 80 H P10 -4.2578 0.9662 -2.5043
ATOM 81 C P10 -6.1121 1.0777 -0.5137
ATOM 82 H P10 -6.3999 1.1380 0.5341
ATOM 83 H P10 -5.7326 2.0478 -0.8366
ATOM 84 H P10 -6.9893 0.8239 -1.1060
ATOM 85 C P10 -5.5774 -1.3716 -0.3787
ATOM 86 O P10 -6.7591 -1.6497 -0.5984
ATOM 87 N P10 -4.6950 -2.2752 0.0587
ATOM 88 H P10 -3.7638 -1.9785 0.3262
ATOM 89 C P10 -5.1016 -3.6259 0.3599
ATOM 90 H P10 -5.5745 -4.0870 -0.5075
ATOM 91 H P10 -4.2209 -4.2025 0.6311
ATOM 92 H P10 -5.8124 -3.6545 1.1889

COMPND Ac-Aib$_2$-(S)-VI-Aib$_2$-NHMe-M310
REMARK Energy(ZPE)= -2080.945027
REMARK #IF = 0
ATOM 1 C P10 5.6352 -1.6465 1.3331
ATOM 2 H P10 6.4610 -2.1185 0.8052
ATOM 3 H P10 5.6761 -0.5691 1.1768
ATOM 4 H P10 5.7441 -1.8307 2.4019
ATOM 5 C P10 4.2909 -2.1478 0.8979
ATOM 6 O P10 3.2416 -1.6764 1.3446
ATOM 7 N P10 4.2744 -3.1295 -0.0263
ATOM 8 H P10 5.1509 -3.5312 -0.3202
ATOM 9 C P10 3.0493 -3.8196 -0.4159
ATOM 10 C P10 2.5101 -4.6642 0.7299
ATOM 11 H P10 1.5950 -5.1690 0.4262
ATOM 12 H P10 3.2551 -5.4123 1.0013
ATOM 13 H P10 2.2932 -4.0433 1.5971
ATOM 14 C P10 3.3717 -4.6990 -1.6236
ATOM 15 H P10 4.1050 -5.4566 -1.3429
ATOM 16 H P10 2.4704 -5.2085 -1.9616
ATOM 17 H P10 3.7716 -4.1111 -2.4506
ATOM 18 C P10 1.9965 -2.7944 -0.8575
ATOM 19 O P10 0.7999 -2.9621 -0.6239
ATOM 20 N P10 2.4450 -1.7482 -1.5693
ATOM 21 H P10 3.4379 -1.6663 -1.7293
ATOM 22 C P10 1.5537 -0.7893 -2.2076
ATOM 23 C P10 0.8232 -1.4280 -3.3806
ATOM 24 H P10 0.2324 -2.2800 -3.0476
ATOM 25 H P10 0.1564 -0.7043 -3.8453
ATOM 26 H P10 1.5543 -1.7641 -4.1159
ATOM 27 C P10 2.3996 0.3929 -2.6794
ATOM 28 H P10 2.9342 0.8521 -1.8468
ATOM 29 H P10 3.1219 0.0583 -3.4260
ATOM 30 H P10 1.7597 1.1445 -3.1400
ATOM 31 C P10 0.5411 -0.2445 -1.1902
ATOM 32 O P10 0.6017 0.0501 -1.5423
ATOM 33 N P10 0.9985 -0.0297 0.0561
ATOM 34 H P10 1.8930 -0.4308 0.3201
ATOM 35 C P10 0.2147 0.6463 1.0790
ATOM 36 C P10 0.1168 2.0888 0.6588
ATOM 37 H P10 0.5668 2.0799 -0.3349
ATOM 38 H P10 0.8796 2.4611 1.3457
ATOM 39 C P10 1.1117 2.9284 0.6891
ATOM 40 C P10 2.2192 2.6086 1.4210
ATOM 41 C P10 2.3728 1.3925 2.2551
ATOM 42 H P10 3.1249 0.7261 1.8232
ATOM 43 H P10 2.7333 1.6436 3.2563
ATOM 44 C P10 1.0314 0.6683 2.3836
ATOM 45 H P10 1.2035 -0.3545 2.7250
ATOM 46 H P10 0.4101 1.1656 3.1303
ATOM 47 N P10 3.1939 3.5569 1.2271
ATOM 48 H P10 4.1047 3.5496 1.6525
ATOM 49 C P10 2.7285 4.5110 0.3591
ATOM 50 C P10 3.3421 5.6564 -0.1426
ATOM 51 H P10 4.3512 5.9250 0.1449
ATOM 52 C P10 2.6155 6.4378 -1.0276
ATOM 53 H P10 3.0664 7.3333 -1.4370
ATOM 54 C P10 1.3076 6.0898 -1.4036
ATOM 55 H P10 0.7699 6.7233 -2.0984
ATOM 56 C P10 0.6993 4.9530 -0.8989
ATOM 57 H P10 0.3109 4.6927 -1.1930
ATOM 58 C P10 1.4091 4.1438 -0.0043
ATOM 59 C P10 1.0902 -0.1043 1.3767
ATOM 60 O P10 2.0313 0.4787 1.9241
ATOM 61 N P10 1.1444 -1.4025 1.0523
ATOM 62 H P10 0.3691 -1.8290 0.5535
ATOM 63 C P10 2.3364 -2.2095 1.2829
ATOM 64 C P10 2.5691 -2.4230 2.7727
ATOM 65 H P10 2.6967 -1.4701 3.2830
ATOM 66 H P10 3.4611 -3.0270 2.9272
ATOM 67 H P10 1.7094 -2.9442 3.1949
ATOM 68 C P10 2.1353 -3.5521 0.5820
ATOM 69 H P10 1.2780 -4.0701 1.0134
ATOM 70 H P10 3.0224 -4.1695 0.7171
ATOM 71 H P10 1.9521 -3.4177 -0.4844
ATOM 72 C P10 3.5698 -1.5485 0.6433
ATOM 73 O P10 4.6922 -1.7416 1.1053
ATOM 74 N P10 3.3537 -0.8257 -0.4726
ATOM 75 H P10 2.3998 -0.6637 -0.7815
ATOM 76 C P10 4.4320 -0.2221 -1.2456
ATOM 77 C P10 5.3391 -1.2880 -1.8477
ATOM 78 H P10 5.7876 -1.9009 -1.0682
ATOM 79 H P10 6.1323 -0.8160 -2.4245
ATOM 80 H P10 4.7501 -1.9247 -2.5090
ATOM 81 C P10 3.7949 0.6080 -2.3598
ATOM 82 H P10 4.5749 1.1131 -2.9282
ATOM 83 H P10 3.1104 1.3538 -1.9543
ATOM 84 H P10 3.2377 -0.0418 -3.0361
ATOM 85 C P10 5.2543 0.7524 -0.3850
ATOM 86 O P10 6.4159 1.0327 -0.6905
ATOM 87 N P10 4.6109 1.3441 0.6265
ATOM 88 H P10 3.6982 1.0007 0.9007
ATOM 89 C P10 5.2744 2.3052 1.4725
ATOM 90 H P10 5.6830 3.1223 0.8776
ATOM 91 H P10 6.0950 1.8480 2.0302
ATOM 92 H P10 4.5509 2.7079 2.1769

COMPND Ac-Aib$_5$ -NHMe-P310
REMARK Energy(ZPE)= -1680.465008
REMARK #IF = 0
ATOM 1 C P11 1 -6.1625 -1.9280 0.3925
ATOM 2 H P11 1 -5.8385 -2.4901 1.2670
ATOM 3 H P11 1 -7.0446 -1.3428 0.6439
ATOM 4 H P11 1 -6.4241 -2.6459 -0.3854
ATOM 5 C P11 1 -5.0179 -1.0927 -0.0985
ATOM 6 O P11 1 -3.8992 -1.5737 -0.2979
ATOM 7 N P11 1 -5.2639 0.2190 -0.2982
ATOM 8 H P11 1 -6.2083 0.5510 -0.1800
ATOM 9 C P11 1 -4.3147 1.1192 -0.9456
ATOM 10 C P11 1 -4.8742 2.5370 -0.8367
ATOM 11 H P11 1 -5.8163 2.6040 -1.3834
ATOM 12 H P11 1 -5.0488 2.8167 0.2030
ATOM 13 H P11 1 -4.1747 3.2459 -1.2772
ATOM 14 C P11 1 -4.1088 0.7351 -2.4048
ATOM 15 H P11 1 -3.4073 1.4197 -2.8773
ATOM 16 H P11 1 -3.7151 -0.2769 -2.4834
ATOM 17 H P11 1 -5.0650 0.7910 -2.9251
ATOM 18 C P11 1 -2.9706 1.0943 -0.2057
ATOM 19 O P11 1 -1.9116 1.2654 -0.8090
ATOM 20 N P11 1 -3.0225 0.9392 1.1267
ATOM 21 H P11 1 -3.9257 0.8037 1.5549
ATOM 22 C P11 1 -1.8501 0.9994 1.9884
ATOM 23 C P11 1 -2.2715 0.5236 3.3785
ATOM 24 H P11 1 -3.0224 1.2003 3.7896
ATOM 25 H P11 1 -2.6847 -0.4854 3.3434
ATOM 26 H P11 1 -1.4103 0.5252 4.0451
ATOM 27 C P11 1 -1.2983 2.4177 2.0558
ATOM 28 H P11 1 -0.4311 2.4513 2.7123
ATOM 29 H P11 1 -1.0011 2.7636 1.0670
ATOM 30 H P11 1 -2.0692 3.0801 2.4499
ATOM 31 C P11 1 -0.7630 0.0365 1.4901
ATOM 32 O P11 1 0.4264 0.2713 1.7142
ATOM 33 N P11 1 -1.1711 -1.0822 0.8742
ATOM 34 H P11 1 -2.1533 -1.1973 0.6409
ATOM 35 C P11 1 -0.2397 -2.1196 0.4504
ATOM 36 C P11 1 -1.0097 -3.1158 -0.4158
ATOM 37 H P11 1 -1.8007 -3.5820 0.1729
ATOM 38 H P11 1 -1.4665 -2.6231 -1.2744
ATOM 39 H P11 1 -0.3330 -3.8928 -0.7688
ATOM 40 C P11 1 0.3674 -2.8274 1.6549
ATOM 41 H P11 1 1.0585 -3.6006 1.3253
ATOM 42 H P11 1 0.9064 -2.1232 2.2866
ATOM 43 H P11 1 -0.4324 -3.2886 2.2344
ATOM 44 C P11 1 0.8730 -1.5274 -0.4275
ATOM 45 O P11 1 1.9839 -2.0625 -0.4770
ATOM 46 N P11 1 0.5491 -0.4612 -1.1726
ATOM 47 H P11 1 -0.3605 -0.0298 -1.0425
ATOM 48 C P11 1 1.4639 0.1523 -2.1259
ATOM 49 C P11 1 0.8348 1.4644 -2.5936
ATOM 50 H P11 1 -0.1161 1.2640 -3.0891
ATOM 51 H P11 1 0.6502 2.1348 -1.7537
ATOM 52 H P11 1 1.5008 1.9561 -3.3014
ATOM 53 C P11 1 1.7027 -0.7692 -3.3151
ATOM 54 H P11 1 2.3893 -0.3010 -4.0177
ATOM 55 H P11 1 2.1275 -1.7182 -2.9919
ATOM 56 H P11 1 0.7526 -0.9561 -3.8163
ATOM 57 C P11 1 2.8029 0.5121 -1.4607
ATOM 58 O P11 1 3.8349 0.5655 -2.1271
ATOM 59 N P11 1 2.7585 0.8348 -0.1553
ATOM 60 H P11 1 1.8911 0.7037 0.3560
ATOM 61 C P11 1 3.9298 1.2753 0.5904
ATOM 62 C P11 1 3.5195 1.4204 2.0560
ATOM 63 H P11 1 2.7363 2.1741 2.1498
ATOM 64 H P11 1 3.1423 0.4789 2.4559
ATOM 65 H P11 1 4.3802 1.7369 2.6439
ATOM 66 C P11 1 4.4435 2.6104 0.0660
ATOM 67 H P11 1 5.3248 2.9128 0.6285
ATOM 68 H P11 1 4.7050 2.5399 -0.9878
ATOM 69 H P11 1 3.6660 3.3650 0.1911
ATOM 70 C P11 1 5.0473 0.2186 0.5513
ATOM 71 O P11 1 6.2224 0.5429 0.7402
ATOM 72 N P11 1 4.6674 -1.0558 0.4114
ATOM 73 H P11 1 3.7091 -1.2719 0.1610
ATOM 74 C P11 1 5.6397 -2.1215 0.4124
ATOM 75 H P11 1 6.2176 -2.1150 1.3372
ATOM 76 H P11 1 5.1169 -3.0708 0.3284
ATOM 77 H P11 1 6.3370 -2.0254 -0.4228

COMPND Ac-Aib$_5$ -NHMe-M310
REMARK Energy(ZPE)= -1680.464965
REMARK #IF = 0
ATOM 1 C P11 1 6.1621 -1.9282 0.3937
ATOM 2 H P11 1 5.8375 -2.4910 1.2676
ATOM 3 H P11 1 6.4247 -2.6456 -0.3844
ATOM 4 H P11 1 7.0437 -1.3428 0.6463
ATOM 5 C P11 1 5.0176 -1.0931 -0.0979
ATOM 6 O P11 1 3.8989 -1.5740 -0.2971
ATOM 7 N P11 1 5.2638 0.2185 -0.2985
ATOM 8 H P11 1 6.2083 0.5504 -0.1804
ATOM 9 C P11 1 4.3148 1.1182 -0.9466
ATOM 10 C P11 1 4.1088 0.7329 -2.4055
ATOM 11 H P11 1 5.0650 0.7882 -2.9259
ATOM 12 H P11 1 3.7149 -0.2791 -2.4832
ATOM 13 H P11 1 3.4074 1.4172 -2.8786
ATOM 14 C P11 1 4.8746 2.5361 -0.8390
ATOM 15 H P11 1 4.1751 3.2447 -1.2800
ATOM 16 H P11 1 5.0493 2.8166 0.2004
ATOM 17 H P11 1 5.8166 2.6024 -1.3858
ATOM 18 C P11 1 2.9707 1.0942 -0.2067
ATOM 19 O P11 1 1.9117 1.2650 -0.8102
ATOM 20 N P11 1 3.0226 0.9402 1.1259
ATOM 21 H P11 1 3.9259 0.8048 1.5541
ATOM 22 C P11 1 1.8504 1.0015 1.9876
ATOM 23 C P11 1 1.2987 2.4198 2.0534
ATOM 24 H P11 1 2.0697 3.0827 2.4466
ATOM 25 H P11 1 1.0013 2.7646 1.0643
ATOM 26 H P11 1 0.4317 2.4543 2.7102
ATOM 27 C P11 1 2.2718 0.5272 3.3782
ATOM 28 H P11 1 1.4107 0.5296 4.0448
ATOM 29 H P11 1 2.6851 -0.4818 3.3442
ATOM 30 H P11 1 3.0229 1.2044 3.7884
ATOM 31 C P11 1 0.7632 0.0380 1.4905
ATOM 32 O P11 1 -0.4262 0.2730 1.7146
ATOM 33 N P11 1 1.1712 -1.0811 0.8754
ATOM 34 H P11 1 2.1534 -1.1965 0.6422
ATOM 35 C P11 1 0.2398 -2.1190 0.4527
ATOM 36 C P11 1 -0.3673 -2.8257 1.6579
ATOM 37 H P11 1 0.4326 -3.2863 2.2378

ATOM 38 H P11 1 -0.9063 -2.1210 2.2889
ATOM 39 H P11 1 -1.0583 -3.5993 1.3290
ATOM 40 C P11 1 1.0098 -3.1160 -0.4126
ATOM 41 H P11 1 0.3331 -3.8933 -0.7649
ATOM 42 H P11 1 1.4667 -2.6241 -1.2716
ATOM 43 H P11 1 1.8008 -3.5817 0.1765
ATOM 44 C P11 1 -0.8729 -1.5277 -0.4259
ATOM 45 O P11 1 -1.9838 -2.0629 -0.4750
ATOM 46 N P11 1 -0.5490 -0.4621 -1.1718
ATOM 47 H P11 1 0.3607 -0.0307 -1.0423
ATOM 48 C P11 1 -1.4638 0.1504 -2.1259
ATOM 49 C P11 1 -1.7023 -0.7723 -3.3143
ATOM 50 H P11 1 -0.7521 -0.9592 -3.8153
ATOM 51 H P11 1 -2.1267 -1.7211 -2.9901
ATOM 52 H P11 1 -2.3891 -0.3050 -4.0173
ATOM 53 C P11 1 -0.8349 1.4622 -2.5946
ATOM 54 H P11 1 -1.5009 1.9531 -3.3031
ATOM 55 H P11 1 -0.6508 2.1334 -1.7553
ATOM 56 H P11 1 0.1162 1.2616 -3.0897
ATOM 57 C P11 1 -2.8029 0.5106 -1.4612
ATOM 58 O P11 1 -3.8349 0.5630 -2.1277
ATOM 59 N P11 1 -2.7587 0.8345 -0.1560
ATOM 60 H P11 1 -1.8913 0.7040 0.3554
ATOM 61 C P11 1 -3.9301 1.2757 0.5890
ATOM 62 C P11 1 -4.4435 2.6104 0.0633
ATOM 63 H P11 1 -3.6660 3.3651 0.1880
ATOM 64 H P11 1 -4.7048 2.5390 -0.9905
ATOM 65 H P11 1 -5.3250 2.9133 0.6253
ATOM 66 C P11 1 -3.5201 1.4222 2.0546
ATOM 67 H P11 1 -4.3807 1.7396 2.6419
ATOM 68 H P11 1 -3.1433 0.4810 2.4556
ATOM 69 H P11 1 -2.7367 2.1757 2.1479
ATOM 70 C P11 1 -5.0477 0.2191 0.5507
ATOM 71 O P11 1 -6.2227 0.5437 0.7392
ATOM 72 N P11 1 -4.6678 -1.0555 0.4121
ATOM 73 H P11 1 -3.7094 -1.2718 0.1621
ATOM 74 C P11 1 -5.6400 -2.1212 0.4140
ATOM 75 H P11 1 -6.2179 -2.1139 1.3387
ATOM 76 H P11 1 -6.3373 -2.0259 -0.4213
ATOM 77 H P11 1 -5.1172 -3.0705 0.3308

COMPND Ac-Aib$_2$-(1R,2R,4R)-IIIawr-Aib$_2$-NHMe-P310
REMARK Energy(ZPE)= -1869.877938
REMARK #IF = 0
ATOM 1 C P12 6.1406 1.4622 -0.0553
ATOM 2 H P12 5.7925 2.2323 0.6316
ATOM 3 H P12 7.0083 0.9627 0.3701
ATOM 4 H P12 6.4333 1.9529 -0.9837
ATOM 5 C P12 5.0064 0.5275 -0.3493
ATOM 6 O P12 3.9071 0.9379 -0.7346
ATOM 7 N P12 5.2337 -0.7869 -0.1551
ATOM 8 H P12 6.1637 -1.0765 0.1048
ATOM 9 C P12 4.2947 -1.8281 -0.5624
ATOM 10 C P12 4.8080 -3.1584 -0.0125
ATOM 11 H P12 5.7724 -3.3973 -0.4636
ATOM 12 H P12 4.9238 -3.1224 1.0713
ATOM 13 H P12 4.1099 -3.9557 -0.2634
ATOM 14 C P12 4.1733 -1.8868 -2.079
ATOM 15 H P12 3.4707 -2.6661 -2.3675
ATOM 16 H P12 3.8201 -0.9359 -2.475
ATOM 17 H P12 5.1506 -2.1133 -2.5055
ATOM 18 C P12 2.9165 -1.5697 0.0635
ATOM 19 O P12 1.8837 -1.8777 -0.5297
ATOM 20 N P12 2.9177 -1.0499 1.3023
ATOM 21 H P12 3.8102 -0.8175 1.7117
ATOM 22 C P12 1.7209 -0.8435 2.1068
ATOM 23 C P12 2.1355 -0.0830 3.366
ATOM 24 H P12 2.8280 -0.6889 3.9523
ATOM 25 H P12 2.6173 0.8641 3.1183
ATOM 26 H P12 1.2569 0.1201 3.976
ATOM 27 C P12 1.0799 -2.1759 2.48
ATOM 28 H P12 0.1939 -2.0045 3.0881
ATOM 29 H P12 0.7922 -2.7305 1.5881
ATOM 30 H P12 1.7960 -2.7663 3.0517
ATOM 31 C P12 0.7002 0.0305 1.369
ATOM 32 O P12 -0.4889 0.0083 1.6965
ATOM 33 N P12 1.1509 0.8452 0.4043
ATOM 34 H P12 2.1308 0.8297 0.1368
ATOM 35 C P12 0.2426 1.7113 -0.3139
ATOM 36 C P12 0.9908 2.5442 -1.3843
ATOM 37 H P12 2.0405 2.2674 -1.4601
ATOM 38 H P12 0.5246 2.4341 -2.3626
ATOM 39 C P12 0.7592 3.9809 -0.8577
ATOM 40 H P12 0.8600 4.7674 -1.5996
ATOM 41 O P12 -0.5880 3.8731 -0.4010
ATOM 42 C P12 -0.3472 2.8675 0.5734
ATOM 43 H P12 -1.2523 2.6065 1.1098
ATOM 44 C P12 0.8263 3.4348 1.3372
ATOM 45 H P12 1.0773 3.2166 2.3645
ATOM 46 C P12 1.5212 4.1290 0.4369
ATOM 47 H P12 2.4786 4.6167 0.5491
ATOM 48 C P12 -0.8963 0.9063 -0.9461
ATOM 49 O P12 -1.9999 1.4191 -1.1404
ATOM 50 N P12 -0.6216 -0.3587 -1.2976
ATOM 51 H P12 0.2857 -0.7578 -1.0757
ATOM 52 C P12 -1.5939 -1.2074 -1.9743
ATOM 53 C P12 -1.0421 -2.6325 -1.9825
ATOM 54 H P12 -0.1137 -2.6686 -2.5537
ATOM 55 H P12 -0.8413 -2.9834 -0.9696
ATOM 56 H P12 -1.7636 -3.3002 -2.4520
ATOM 57 C P12 -1.8282 -0.7242 -3.3998
ATOM 58 H P12 -2.5504 -1.3668 -3.8992
ATOM 59 H P12 -2.2077 0.2964 -3.4040
ATOM 60 H P12 -0.8847 -0.7575 -3.9452
ATOM 61 C P12 -2.9273 -1.2499 -1.2088
ATOM 62 O P12 -3.9807 -1.4516 -1.8097
ATOM 63 N P12 -2.8623 -1.1455 0.1315
ATOM 64 H P12 -1.9802 -0.8978 0.5671
ATOM 65 C P12 -4.0335 -1.2651 0.9906
ATOM 66 C P12 -3.5893 -0.9604 2.4214
ATOM 67 H P12 -2.8425 -1.6883 2.7421
ATOM 68 H P12 -3.1550 0.0369 2.4954
ATOM 69 H P12 -4.4469 -1.0248 3.0899
ATOM 70 C P12 -4.6213 -2.6687 0.9190
ATOM 71 H P12 -5.4904 -2.7399 1.5702
ATOM 72 H P12 -4.9230 -2.9101 -0.0982
ATOM 73 H P12 -3.8698 -3.3868 1.2494
ATOM 74 C P12 -5.1031 -0.2191 0.6308
ATOM 75 O P12 -6.2887 -0.4108 0.9123
ATOM 76 N P12 -4.6652 0.9297 0.1056
ATOM 77 H P12 -3.7043 1.0032 -0.2073
ATOM 78 C P12 -5.5817 1.9944 -0.2215
ATOM 79 H P12 -6.1467 2.3005 0.6596
ATOM 80 H P12 -5.0119 2.8442 -0.5887
ATOM 81 H P12 -6.2936 1.6864 -0.9905
COMPND Ac-Aib$_2$-(1R,2R,4R)-IIIawr-Aib$_2$-NHMe-M310
REMARK Energy(ZPE)= -1869.8758
REMARK #IF = 0
ATOM 1 C P12 -6.0450 1.4168 -0.3682
ATOM 2 H P12 -5.7486 2.2051 0.3225
ATOM 3 H P12 -6.2599 1.8820 -1.3304
ATOM 4 H P12 -6.9472 0.9345 0.0018
ATOM 5 C P12 -4.8966 0.4690 -0.5430
ATOM 6 O P12 -3.7694 0.8603 -0.8599
ATOM 7 N P12 -5.1431 -0.8372 -0.3174
ATOM 8 H P12 -6.0903 -1.1211 -0.1218
ATOM 9 C P12 -4.1703 -1.8843 -0.6099
ATOM 10 C P12 -3.9316 -2.0030 -2.1090
ATOM 11 H P12 -4.8720 -2.2551 -2.5993
ATOM 12 H P12 -3.5553 -1.0654 -2.5148
ATOM 13 H P12 -3.2047 -2.7869 -2.3128
ATOM 14 C P12 -4.7130 -3.1972 -0.0466
ATOM 15 H P12 -3.9939 -3.9975 -0.2157
ATOM 16 H P12 -4.9069 -3.1217 1.0239
ATOM 17 H P12 -5.6411 -3.4615 -0.5560
ATOM 18 C P12 -2.8499 -1.5818 0.1102
ATOM 19 O P12 -1.7669 -1.8770 -0.3940
ATOM 20 N P12 -2.9472 -1.0409 1.3355
ATOM 21 H P12 -3.8674 -0.8247 1.6888
ATOM 22 C P12 -1.8044 -0.8413 2.2167
ATOM 23 C P12 -1.2410 -2.1773 2.6839
ATOM 24 H P12 -2.0155 -2.7185 3.2277
ATOM 25 H P12 -0.9148 -2.7770 1.8355
ATOM 26 H P12 -0.3908 -2.0146 3.3432
ATOM 27 C P12 -2.2788 -0.0137 3.4107
ATOM 28 H P12 -1.4419 0.1806 4.0798
ATOM 29 H P12 -2.6991 0.9399 3.0888
ATOM 30 H P12 -3.0383 -0.5667 3.9659
ATOM 31 C P12 -0.7117 -0.0284 1.5114
ATOM 32 O P12 0.4714 -0.1586 1.8293
ATOM 33 N P12 -1.1084 0.8802 0.6042
ATOM 34 H P12 -2.0758 0.8943 0.2937
ATOM 35 C P12 -0.1492 1.7644 -0.0203
ATOM 36 C P12 0.5186 2.7599 0.9554
ATOM 37 H P12 0.1756 2.6111 1.9767
ATOM 38 H P12 1.6004 2.6644 0.9148

ATOM 39 C P12 0.0734 4.1158 0.3574
ATOM 40 H P12 0.7146 4.9633 0.5795
ATOM 41 O P12 0.0900 3.8168 -1.0422
ATOM 42 C P12 -0.8697 2.7788 -0.9951
ATOM 43 H P12 -1.0873 2.3858 -1.9845
ATOM 44 C P12 -1.9998 3.4113 -0.2138
ATOM 45 H P12 -3.0376 3.1264 -0.2873
ATOM 46 C P12 -1.4044 4.2558 0.6267
ATOM 47 H P12 -1.8443 4.8428 1.4197
ATOM 48 C P12 0.9077 0.9800 -0.8087
ATOM 49 O P12 2.0090 1.4737 -1.0622
ATOM 50 N P12 0.5726 -0.2502 -1.2256
ATOM 51 H P12 -0.3169 -0.6594 -0.9544
ATOM 52 C P12 1.4944 -1.0786 -1.9927
ATOM 53 C P12 1.6817 -0.5255 -3.3993
ATOM 54 H P12 0.7187 -0.5226 -3.9107
ATOM 55 H P12 2.0724 0.4898 -3.3689
ATOM 56 H P12 2.3775 -1.1514 -3.9548
ATOM 57 C P12 0.9137 -2.4910 -2.0582
ATOM 58 H P12 1.5988 -3.1402 -2.6021
ATOM 59 H P12 0.7511 -2.8983 -1.0600
ATOM 60 H P12 -0.0434 -2.4754 -2.5806
ATOM 61 C P12 2.8549 -1.1912 -1.2827
ATOM 62 O P12 3.8818 -1.3817 -1.9306
ATOM 63 N P12 2.8362 -1.1572 0.0631
ATOM 64 H P12 1.9697 -0.9252 0.5365
ATOM 65 C P12 4.0265 -1.3446 0.8826
ATOM 66 C P12 4.5878 -2.7515 0.7174
ATOM 67 H P12 3.8339 -3.4750 1.0296
ATOM 68 H P12 4.8573 -2.9418 -0.3197
ATOM 69 H P12 5.4732 -2.8700 1.3392
ATOM 70 C P12 3.6215 -1.1136 2.3385
ATOM 71 H P12 4.4958 -1.2146 2.9801
ATOM 72 H P12 3.1908 -0.1210 2.4746
ATOM 73 H P12 2.8804 -1.8552 2.6401
ATOM 74 C P12 5.1084 -0.2997 0.5569
ATOM 75 O P12 6.2925 -0.5239 0.8203
ATOM 76 N P12 4.6864 0.8769 0.0830
ATOM 77 H P12 3.7243 0.9807 -0.2184
ATOM 78 C P12 5.6176 1.9399 -0.2059
ATOM 79 H P12 6.2215 2.1691 0.6724
ATOM 80 H P12 6.2930 1.6714 -1.0215
ATOM 81 H P12 5.0568 2.8265 -0.4910

COMPND Ac-Aib$_2$-(1R,2R,4R)-Var-Aib$_2$-NHMe-P310
REMARK Energy(ZPE)= -1987.511795
REMARK #IF = 0
ATOM 1 C P13 6.0431 0.2238 -0.5211
ATOM 2 H P13 5.8216 1.1795 -0.0486
ATOM 3 H P13 6.8390 -0.2767 0.0263
ATOM 4 H P13 6.3862 0.4269 -1.5360
ATOM 5 C P13 4.7814 -0.5817 -0.6004
ATOM 6 O P13 3.7360 -0.1088 -1.0559
ATOM 7 N P13 4.8339 -1.8471 -0.1362
ATOM 8 H P13 5.7243 -2.2058 0.1719
ATOM 9 C P13 3.7523 -2.8097 -0.3203
ATOM 10 C P13 4.0985 -4.0575 0.4919
ATOM 11 H P13 5.0131 -4.5087 0.104
ATOM 12 H P13 4.2423 -3.8188 1.5464
ATOM 13 H P13 3.2961 -4.7888 0.4055
ATOM 14 C P13 3.5821 -3.1607 -1.7923
ATOM 15 H P13 2.7751 -3.8802 -1.9147
ATOM 16 H P13 3.3474 -2.2723 -2.3763
ATOM 17 H P13 4.5089 -3.5990 -2.1629
ATOM 18 C P13 2.4382 -2.2469 0.2402
ATOM 19 O P13 1.3576 -2.5391 -0.2706
ATOM 20 N P13 2.5443 -1.4847 1.3406
ATOM 21 H P13 3.4724 -1.2927 1.6867
ATOM 22 C P13 1.4140 -0.9682 2.1016
ATOM 23 C P13 1.9744 -0.0763 3.2078
ATOM 24 H P13 2.5803 -0.6733 3.8914
ATOM 25 H P13 2.5861 0.7281 2.7973
ATOM 26 H P13 1.1538 0.3651 3.7714
ATOM 27 C P13 0.5990 -2.1092 2.704
ATOM 28 H P13 -0.2278 -1.7051 3.2844
ATOM 29 H P13 0.1993 -2.7539 1.9221
ATOM 30 H P13 1.2422 -2.6976 3.3586
ATOM 31 C P13 0.4954 -0.1019 1.2286
ATOM 32 O P13 -0.6613 0.1247 1.5937
ATOM 33 N P13 0.9923 0.3984 0.0901
ATOM 34 H P13 1.9509 0.1955 -0.1754
ATOM 35 C P13 0.1774 1.2035 -0.7997
ATOM 36 C P13 0.9974 1.6022 -2.0623
ATOM 37 H P13 1.9607 1.0957 -2.0888
ATOM 38 H P13 0.4509 1.3403 -2.9697
ATOM 39 C P13 1.1064 3.1378 -1.9515
ATOM 40 H P13 1.4463 3.6171 -2.8675
ATOM 41 C P13 -0.3114 3.4631 -1.4667
ATOM 42 H P13 -1.0887 3.1246 -2.1493
ATOM 43 H P13 -0.4509 4.5187 -1.2295
ATOM 44 C P13 -0.2067 2.5992 -0.1985
ATOM 45 H P13 -1.0651 2.5578 0.4656
ATOM 46 C P13 1.0726 3.1404 0.3783
ATOM 47 C P13 1.8956 3.4562 -0.7097
ATOM 48 C P13 3.1809 3.9276 -0.5114
ATOM 49 H P13 3.8262 4.1689 -1.3482
ATOM 50 C P13 3.6274 4.1031 0.8008
ATOM 51 H P13 4.6227 4.4911 0.9806
ATOM 52 C P13 2.8071 3.7918 1.881
ATOM 53 H P13 3.1728 3.9392 2.8899
ATOM 54 C P13 1.5186 3.2925 1.6776
ATOM 55 H P13 0.8865 3.0355 2.5202
ATOM 56 C P13 -1.0808 0.4283 -1.2054
ATOM 57 O P13 -2.1099 1.0217 -1.5390
ATOM 58 N P13 -0.9925 -0.9093 -1.2103
ATOM 59 H P13 -0.1307 -1.3553 -0.9089
ATOM 60 C P13 -2.0942 -1.7698 -1.6209
ATOM 61 C P13 -1.7294 -3.2011 -1.2268
ATOM 62 H P13 -0.8231 -3.5095 -1.7493
ATOM 63 H P13 -1.5502 -3.2788 -0.1532
ATOM 64 H P13 -2.5394 -3.8756 -1.5013
ATOM 65 C P13 -2.3222 -1.6756 -3.1238
ATOM 66 H P13 -3.1462 -2.3221 -3.4194
ATOM 67 H P13 -2.5588 -0.6534 -3.4147
ATOM 68 H P13 -1.4168 -1.9938 -3.6414
ATOM 69 C P13 -3.3880 -1.4151 -0.8681
ATOM 70 O P13 -4.4843 -1.6197 -1.3852
ATOM 71 N P13 -3.2477 -0.9636 0.3922
ATOM 72 H P13 -2.3186 -0.7414 0.7360
ATOM 73 C P13 -4.3796 -0.6780 1.2648
ATOM 74 C P13 -3.8255 -0.0754 2.5560
ATOM 75 H P13 -3.1809 -0.7993 3.0570
ATOM 76 H P13 -3.2429 0.8238 2.3538
ATOM 77 H P13 -4.6494 0.1768 3.2225
ATOM 78 C P13 -5.1612 -1.9469 1.5821
ATOM 79 H P13 -5.9953 -1.7125 2.2408

ATOM 80 H P13 -5.5482 -2.4029 0.6732
ATOM 81 H P13 -4.5012 -2.6552 2.0842
ATOM 82 C P13 -5.3098 0.3816 0.6492
ATOM 83 O P13 -6.4912 0.4570 0.9964
ATOM 84 N P13 -4.7457 1.2613 -0.1839
ATOM 85 H P13 -3.8037 1.0974 -0.5205
ATOM 86 C P13 -5.5179 2.3235 -0.7802
ATOM 87 H P13 -6.0183 2.9110 -0.0102
ATOM 88 H P13 -4.8474 2.9707 -1.3401
ATOM 89 H P13 -6.2807 1.9333 -1.4583

COMPND Ac-Aib$_2$-(1R,2R,4R)-Var-Aib$_2$-NHMe-M310
REMARK Energy(ZPE)= -1987.5085
REMARK #IF = 0
ATOM 1 C P13 -5.8240 -0.3830 -1.0786
ATOM 2 H P13 -5.9014 0.0311 -2.0824
ATOM 3 H P13 -6.6776 -1.0295 -0.8855
ATOM 4 H P13 -5.8485 0.4477 -0.3716
ATOM 5 C P13 -4.5067 -1.0886 -0.9433
ATOM 6 O P13 -3.4466 -0.5812 -1.3151
ATOM 7 N P13 -4.5247 -2.2986 -0.3454
ATOM 8 H P13 -5.4133 -2.7164 -0.1185
ATOM 9 C P13 -3.3341 -3.1338 -0.2562
ATOM 10 C P13 -2.9028 -3.6217 -1.6328
ATOM 11 H P13 -3.7090 -4.2118 -2.0689
ATOM 12 H P13 -2.6792 -2.7800 -2.2862
ATOM 13 H P13 -2.0132 -4.2432 -1.5485
ATOM 14 C P13 -3.6568 -4.3184 0.6535
ATOM 15 H P13 -2.7728 -4.9429 0.7748
ATOM 16 H P13 -3.9890 -3.9868 1.6379
ATOM 17 H P13 -4.4425 -4.9264 0.2022
ATOM 18 C P13 -2.1967 -2.3426 0.4020
ATOM 19 O P13 -1.0259 -2.5086 0.0626
ATOM 20 N P13 -2.5360 -1.5253 1.4126
ATOM 21 H P13 -3.5118 -1.4388 1.6545
ATOM 22 C P13 -1.5471 -0.8961 2.2777
ATOM 23 C P13 -0.8586 -1.9333 3.1537
ATOM 24 H P13 -1.6051 -2.4254 3.7774
ATOM 25 H P13 -0.3542 -2.6793 2.5415
ATOM 26 H P13 -0.1203 -1.4532 3.7929
ATOM 27 C P13 -2.2703 0.1397 3.1376
ATOM 28 H P13 -1.5539 0.6587 3.7732
ATOM 29 H P13 -2.7877 0.8756 2.5206
ATOM 30 H P13 -2.9978 -0.3578 3.7811
ATOM 31 C P13 -0.5057 -0.1456 1.4364
ATOM 32 O P13 0.6749 -0.0988 1.7835
ATOM 33 N P13 -0.9606 0.5369 0.3709
ATOM 34 H P13 -1.9130 0.3982 0.0507
ATOM 35 C P13 -0.0959 1.4492 -0.3531
ATOM 36 C P13 0.4671 2.5903 0.5421
ATOM 37 H P13 0.1435 2.4648 1.5737
ATOM 38 H P13 1.5551 2.5848 0.5136
ATOM 39 C P13 -0.0783 3.8798 -0.1082
ATOM 40 H P13 0.4492 4.7832 0.1917
ATOM 41 C P13 -0.0225 3.4924 -1.5942
ATOM 42 H P13 0.9837 3.2606 -1.9369
ATOM 43 H P13 -0.4844 4.2343 -2.2463
ATOM 44 C P13 -0.9133 2.2513 -1.4265
ATOM 45 H P13 -1.1537 1.6701 -2.3155
ATOM 46 C P13 -2.0870 2.8767 -0.7088
ATOM 47 C P13 -1.5647 3.8855 0.1086
ATOM 48 C P13 -2.3915 4.6384 0.9218
ATOM 49 H P13 -1.9919 5.4174 1.5605
ATOM 50 C P13 -3.7655 4.3879 0.8837
ATOM 51 H P13 -4.4352 4.9797 1.4960
ATOM 52 C P13 -4.2854 3.3976 0.0570
ATOM 53 H P13 -5.3558 3.2319 0.0312
ATOM 54 C P13 -3.4455 2.6216 -0.7459
ATOM 55 H P13 -3.8466 1.8425 -1.3802
ATOM 56 C P13 1.0566 0.6909 -1.0285
ATOM 57 O P13 2.0877 1.2814 -1.3661
ATOM 58 N P13 0.9053 -0.6246 -1.2376
ATOM 59 H P13 0.0917 -1.1104 -0.8738
ATOM 60 C P13 1.9627 -1.4208 -1.8500
ATOM 61 C P13 2.1386 -1.0570 -3.3184
ATOM 62 H P13 1.2093 -1.2649 -3.8499
ATOM 63 H P13 2.3877 -0.0037 -3.4308
ATOM 64 H P13 2.9382 -1.6543 -3.7521
ATOM 65 C P13 1.5870 -2.8964 -1.7217
ATOM 66 H P13 2.3606 -3.5054 -2.1878
ATOM 67 H P13 1.4821 -3.1915 -0.6780
ATOM 68 H P13 0.6393 -3.0849 -2.2275
ATOM 69 C P13 3.2914 -1.2372 -1.0955
ATOM 70 O P13 4.3635 -1.3871 -1.6779
ATOM 71 N P13 3.2064 -0.9946 0.2268
ATOM 72 H P13 2.2968 -0.8201 0.6416
ATOM 73 C P13 4.3737 -0.8891 1.0928
ATOM 74 C P13 5.1166 -2.2165 1.1777
ATOM 75 H P13 4.4496 -2.9728 1.5932
ATOM 76 H P13 5.4514 -2.5373 0.1934
ATOM 77 H P13 5.9837 -2.1112 1.8273
ATOM 78 C P13 3.8809 -0.4821 2.4818
ATOM 79 H P13 4.7324 -0.3762 3.1526
ATOM 80 H P13 3.3343 0.4608 2.4462
ATOM 81 H P13 3.2158 -1.2502 2.8794
ATOM 82 C P13 5.3267 0.2233 0.6226
ATOM 83 O P13 6.5183 0.1995 0.9404
ATOM 84 N P13 4.7796 1.2475 -0.0408
ATOM 85 H P13 3.8268 1.1766 -0.3776
ATOM 86 C P13 5.5835 2.3628 -0.4777
ATOM 87 H P13 6.1397 2.7821 0.3607
ATOM 88 H P13 6.3009 2.0651 -1.2460
ATOM 89 H P13 4.9277 3.1274 -0.8864

COMPND Ac-Aib$_2$-(1R,2R,4R)-Vdm-Aib$_2$-NHMe-P310
REMARK Energy(ZPE)= -1912.493059
REMARK #IF = 0
ATOM 1 C P14 6.1314 0.6747 0.0912
ATOM 2 H P14 5.8143 1.5146 0.7076
ATOM 3 H P14 6.9009 0.1099 0.6131
ATOM 4 H P14 6.5526 1.0796 -0.8295
ATOM 5 C P14 4.9283 -0.1479 -0.2596
ATOM 6 O P14 3.9026 0.3628 -0.7183
ATOM 7 N P14 5.0062 -1.4760 -0.0363
ATOM 8 H P14 5.8830 -1.8590 0.2816
ATOM 9 C P14 3.9869 -2.4151 -0.4947
ATOM 10 C P14 4.3186 -3.7857 0.0942
ATOM 11 H P14 5.2775 -4.1332 -0.2937
ATOM 12 H P14 4.3708 -3.7485 1.1830
ATOM 13 H P14 3.5547 -4.5061 -0.1948
ATOM 14 C P14 3.9532 -2.4818 -2.0157
ATOM 15 H P14 3.2003 -3.1959 -2.3431
ATOM 16 H P14 3.7168 -1.5077 -2.4405
ATOM 17 H P14 4.9292 -2.8043 -2.3785
ATOM 18 C P14 2.6095 -2.0008 0.0446
ATOM 19 O P14 1.5878 -2.2058 -0.6095

ATOM 20 N P14 2.5985 -1.4716 1.2792
ATOM 21 H P14 3.4916 -1.3315 1.7273
ATOM 22 C P14 1.4012 -1.1316 2.0355
ATOM 23 C P14 1.8568 -0.5031 3.3505
ATOM 24 H P14 2.3942 -1.2434 3.9452
ATOM 25 H P14 2.5132 0.3507 3.1775
ATOM 26 H P14 0.9891 -0.1704 3.9180
ATOM 27 C P14 0.5620 -2.3763 2.3165
ATOM 28 H P14 -0.3144 -2.1018 2.9005
ATOM 29 H P14 0.2339 -2.8406 1.3876
ATOM 30 H P14 1.1622 -3.0903 2.8807
ATOM 31 C P14 0.5251 -0.1093 1.2951
ATOM 32 O P14 -0.6535 0.0334 1.6342
ATOM 33 N P14 1.0691 0.6036 0.3020
ATOM 34 H P14 2.0420 0.4602 0.0491
ATOM 35 C P14 0.2648 1.4985 -0.5155
ATOM 36 C P14 -0.1487 2.8243 0.2049
ATOM 37 H P14 -1.0061 2.7007 0.8624
ATOM 38 C P14 1.1099 2.0328 -1.7092
ATOM 39 H P14 2.0985 1.5764 -1.7322
ATOM 40 H P14 0.6166 1.8167 -2.6588
ATOM 41 C P14 1.9075 3.7837 -0.1616
ATOM 42 C P14 3.3075 4.2833 -0.1236
ATOM 43 H P14 3.3872 5.2705 -0.5872
ATOM 44 H P14 3.9720 3.6180 -0.6833
ATOM 45 H P14 3.6879 4.3554 0.8956
ATOM 46 C P14 1.1191 3.3590 0.8391
ATOM 47 C P14 1.3764 3.3001 2.3020
ATOM 48 H P14 1.2314 2.2878 2.6861
ATOM 49 H P14 0.6737 3.9391 2.8454
ATOM 50 H P14 2.3875 3.6194 2.5556
ATOM 51 C P14 1.1463 3.5560 -1.4516
ATOM 52 H P14 1.4919 4.1325 -2.3094
ATOM 53 C P14 -0.2912 3.7792 -0.9837
ATOM 54 H P14 -1.0442 3.4641 -1.7063
ATOM 55 H P14 -0.4787 4.8040 -0.6604
ATOM 56 C P14 -0.9658 0.7475 -1.0398
ATOM 57 O P14 -2.0352 1.3307 -1.2344
ATOM 58 N P14 -0.8051 -0.5556 -1.3211
ATOM 59 H P14 0.0789 -1.0109 -1.1095
ATOM 60 C P14 -1.8531 -1.3561 -1.9415
ATOM 61 C P14 -1.4133 -2.8192 -1.8946
ATOM 62 H P14 -0.4895 -2.9486 -2.4595
ATOM 63 H P14 -1.2402 -3.1458 -0.8686
ATOM 64 H P14 -2.1847 -3.4463 -2.3399
ATOM 65 C P14 -2.0810 -0.9222 -3.3838
ATOM 66 H P14 -2.8678 -1.5243 -3.8339
ATOM 67 H P14 -2.3746 0.1253 -3.4298
ATOM 68 H P14 -1.1577 -1.0607 -3.9471
ATOM 69 C P14 -3.1702 -1.2635 -1.1535
ATOM 70 O P14 -4.2481 -1.4117 -1.7263
ATOM 71 N P14 -3.0684 -1.1039 0.1789
ATOM 72 H P14 -2.1627 -0.8852 0.5815
ATOM 73 C P14 -4.2246 -1.0924 1.0647
ATOM 74 C P14 -3.7251 -0.7833 2.4761
ATOM 75 H P14 -3.0217 -1.5533 2.7975
ATOM 76 H P14 -3.2195 0.1817 2.5148
ATOM 77 H P14 -4.5692 -0.7715 3.1644
ATOM 78 C P14 -4.9362 -2.4401 1.0549
ATOM 79 H P14 -5.7986 -2.4048 1.7181
ATOM 80 H P14 -5.2731 -2.6947 0.0519
ATOM 81 H P14 -4.2476 -3.2092 1.4069
ATOM 82 C P14 -5.2081 0.0308 0.6927
ATOM 83 O P14 -6.3911 -0.0349 1.0369
ATOM 84 N P14 -4.6956 1.1040 0.0819
ATOM 85 H P14 -3.7453 1.0787 -0.2705
ATOM 86 C P14 -5.5302 2.2289 -0.2621
ATOM 87 H P14 -6.0265 2.6255 0.6241
ATOM 88 H P14 -4.9064 3.0062 -0.6963
ATOM 89 H P14 -6.3003 1.9484 -0.9842

COMPND Ac-Aib$_2$-(1R,2R,4R)-Vdm-Aib$_2$-NHMe-M310
REMARK Energy(ZPE)= -1912.4899
REMARK #IF = 0
ATOM 1 C P14 -5.7319 0.5957 -1.5142
ATOM 2 H P14 -5.6748 1.5177 -0.9357
ATOM 3 H P14 -5.6413 0.8600 -2.5667
ATOM 4 H P14 -6.7001 0.1311 -1.3403
ATOM 5 C P14 -4.5783 -0.2879 -1.1411
ATOM 6 O P14 -3.4098 0.0135 -1.3971
ATOM 7 N P14 -4.8777 -1.4248 -0.4766
ATOM 8 H P14 -5.8483 -1.6670 -0.3531
ATOM 9 C P14 -3.8894 -2.4650 -0.2208
ATOM 10 C P14 -3.4452 -3.1282 -1.5175
ATOM 11 H P14 -4.3109 -3.5799 -2.0023
ATOM 12 H P14 -2.9970 -2.3978 -2.1891
ATOM 13 H P14 -2.7090 -3.9022 -1.3081
ATOM 14 C P14 -4.5213 -3.4916 0.7188
ATOM 15 H P14 -3.7946 -4.2640 0.9671
ATOM 16 H P14 -4.8668 -3.0266 1.6428
ATOM 17 H P14 -5.3694 -3.9706 0.2268
ATOM 18 C P14 -2.6757 -1.8645 0.4955
ATOM 19 O P14 -1.5335 -2.2433 0.2399
ATOM 20 N P14 -2.9191 -0.9651 1.4623
ATOM 21 H P14 -3.8734 -0.6911 1.6435
ATOM 22 C P14 -1.8651 -0.4887 2.3511
ATOM 23 C P14 -1.3882 -1.6013 3.2734
ATOM 24 H P14 -2.2251 -1.9449 3.8817
ATOM 25 H P14 -0.9958 -2.4377 2.6972
ATOM 26 H P14 -0.6009 -1.2325 3.9283
ATOM 27 C P14 -2.4298 0.6759 3.1623
ATOM 28 H P14 -1.6571 1.0836 3.8131
ATOM 29 H P14 -2.7924 1.4727 2.5115
ATOM 30 H P14 -3.2524 0.3275 3.7891
ATOM 31 C P14 -0.6894 0.0545 1.5223
ATOM 32 O P14 0.4756 -0.0808 1.8961
ATOM 33 N P14 -1.0199 0.7690 0.4326
ATOM 34 H P14 -1.9608 0.6805 0.0638
ATOM 35 C P14 -0.0371 1.5140 -0.3318
ATOM 36 C P14 -0.7627 2.4810 -1.3395
ATOM 37 H P14 -1.1912 1.9623 -2.1974
ATOM 38 C P14 0.7751 2.5240 0.5297
ATOM 39 H P14 0.4635 2.4778 1.5721
ATOM 40 H P14 1.8391 2.2984 0.478
ATOM 41 C P14 -0.9958 4.1746 0.2051
ATOM 42 C P14 -1.4113 5.1418 1.2540
ATOM 43 H P14 -1.0242 6.1418 1.0403
ATOM 44 H P14 -1.0043 4.8516 2.2279
ATOM 45 H P14 -2.4946 5.2073 1.3527
ATOM 46 C P14 -1.7355 3.3235 -0.5230
ATOM 47 C P14 -3.2136 3.1507 -0.5214
ATOM 48 H P14 -3.5259 2.2538 0.0209
ATOM 49 H P14 -3.5984 3.0433 -1.5380
ATOM 50 H P14 -3.7071 4.0044 -0.0563
ATOM 51 C P14 0.4515 3.8909 -0.1183
ATOM 52 H P14 1.1556 4.6799 0.1451

ATOM 53 C P14 0.3427 3.5095 -1.595
ATOM 54 H P14 1.2566 3.0844 -2.006
ATOM 55 H P14 -0.0129 4.3319 -2.2164
ATOM 56 C P14 0.9336 0.5691 -1.0546
ATOM 57 O P14 1.9981 0.9924 -1.5201
ATOM 58 N P14 0.6142 -0.7308 -1.1369
ATOM 59 H P14 -0.2270 -1.0821 -0.6906
ATOM 60 C P14 1.5435 -1.6997 -1.7066
ATOM 61 C P14 1.6881 -1.5054 -3.2101
ATOM 62 H P14 0.7177 -1.6583 -3.6833
ATOM 63 H P14 2.0451 -0.5032 -3.4378
ATOM 64 H P14 2.3964 -2.2297 -3.6081
ATOM 65 C P14 1.0180 -3.1041 -1.4122
ATOM 66 H P14 1.7058 -3.8385 -1.83
ATOM 67 H P14 0.9223 -3.2766 -0.3404
ATOM 68 H P14 0.0378 -3.2402 -1.8702
ATOM 69 C P14 2.9181 -1.5899 -1.0226
ATOM 70 O P14 3.9432 -1.9009 -1.6252
ATOM 71 N P14 2.9189 -1.2206 0.2734
ATOM 72 H P14 2.0490 -0.9292 0.7083
ATOM 73 C P14 4.1302 -1.1575 1.08
ATOM 74 C P14 4.7428 -2.5411 1.2618
ATOM 75 H P14 4.0262 -3.1843 1.7738
ATOM 76 H P14 4.9954 -2.9832 0.2999
ATOM 77 H P14 5.6469 -2.4663 1.8631
ATOM 78 C P14 3.7457 -0.5777 2.4411
ATOM 79 H P14 4.6345 -0.4940 3.065
ATOM 80 H P14 3.2907 0.4080 2.3354
ATOM 81 H P14 3.0308 -1.2360 2.9369
ATOM 82 C P14 5.1662 -0.1964 0.4714
ATOM 83 O P14 6.3607 -0.3055 0.7601
ATOM 84 N P14 4.6978 0.8038 -0.2821
ATOM 85 H P14 3.7319 0.7940 -0.5888
ATOM 86 C P14 5.5927 1.7767 -0.8596
ATOM 87 H P14 6.1818 2.2655 -0.0832
ATOM 88 H P14 6.2835 1.3132 -1.5677
ATOM 89 H P14 5.0031 2.5263 -1.3811

COMPND Ac-Aib$_2$-(1R,2S,4R)-V-Aib$_2$-NHMe-P310
REMARK Energy(ZPE)= -1833.953988
REMARK #IF = 0
ATOM 1 C P15 -6.0930 1.5259 -0.2947
ATOM 2 H P15 -5.7344 2.1383 -1.1210
ATOM 3 H P15 -6.9816 0.9817 -0.6071
ATOM 4 H P15 -6.3560 2.1956 0.5242
ATOM 5 C P15 -4.9805 0.6307 0.1624
ATOM 6 O P15 -3.8713 1.0767 0.4690
ATOM 7 N P15 -5.2406 -0.6923 0.2046
ATOM 8 H P15 -6.1789 -1.0005 0.0028
ATOM 9 C P15 -4.3261 -1.6652 0.7948
ATOM 10 C P15 -4.8691 -3.0604 0.4877
ATOM 11 H P15 -5.8403 -3.1936 0.9670
ATOM 12 H P15 -4.9813 -3.2171 -0.5859
ATOM 13 H P15 -4.1905 -3.8156 0.8818
ATOM 14 C P15 -4.2077 -1.4573 2.2985
ATOM 15 H P15 -3.5218 -2.1875 2.7235
ATOM 16 H P15 -3.8346 -0.4593 2.5224
ATOM 17 H P15 -5.1901 -1.5834 2.7542
ATOM 18 C P15 -2.9420 -1.5524 0.1398
ATOM 19 O P15 -1.9168 -1.7661 0.7854
ATOM 20 N P15 -2.9335 -1.2732 -1.1746
ATOM 21 H P15 -3.8227 -1.1079 -1.6219
ATOM 22 C P15 -1.7372 -1.2459 -2.0045
ATOM 23 C P15 -2.1435 -0.7262 -3.3833
ATOM 24 H P15 -2.8550 -1.4141 -3.8430
ATOM 25 H P15 -2.5987 0.2632 -3.3168
ATOM 26 H P15 -1.2648 -0.6645 -4.0235
ATOM 27 C P15 -1.1226 -2.6359 -2.1244
ATOM 28 H P15 -0.2373 -2.5939 -2.7557
ATOM 29 H P15 -0.8366 -3.0198 -1.1463
ATOM 30 H P15 -1.8518 -3.3101 -2.5741
ATOM 31 C P15 -0.6954 -0.2673 -1.4486
ATOM 32 O P15 0.4941 -0.3942 -1.7512
ATOM 33 N P15 -1.1274 0.7432 -0.6830
ATOM 34 H P15 -2.1030 0.7932 -0.3999
ATOM 35 C P15 -0.2018 1.7462 -0.1787
ATOM 36 C P15 0.3546 2.6519 -1.3055
ATOM 37 H P15 1.4416 2.6807 -1.2914
ATOM 38 H P15 0.0234 2.2744 -2.2731
ATOM 39 C P15 -0.2768 4.0370 -0.9963
ATOM 40 H P15 -0.2691 4.7223 -1.8414
ATOM 41 C P15 -1.6403 3.6076 -0.4505
ATOM 42 H P15 -2.2323 3.0257 -1.1602
ATOM 43 H P15 -2.2311 4.4400 -0.0676
ATOM 44 C P15 -1.0337 2.7671 0.6809
ATOM 45 H P15 -1.7160 2.2734 1.3702
ATOM 46 C P15 -0.0656 3.7616 1.2712
ATOM 47 H P15 0.2762 3.7545 2.2970
ATOM 48 C P15 0.3792 4.5258 0.2705
ATOM 49 H P15 1.1599 5.2736 0.3175
ATOM 50 C P15 0.9041 1.0821 0.6432
ATOM 51 O P15 2.0133 1.6069 0.7674
ATOM 52 N P15 0.5890 -0.0763 1.2430
ATOM 53 H P15 -0.3175 -0.4923 1.0550
ATOM 54 C P15 1.5214 -0.7988 2.0972
ATOM 55 C P15 0.9227 -2.1753 2.3855
ATOM 56 H P15 -0.0400 -2.0659 2.8861
ATOM 57 H P15 0.7693 -2.7393 1.4648
ATOM 58 H P15 1.5943 -2.7353 3.0350
ATOM 59 C P15 1.7569 -0.0426 3.3983
ATOM 60 H P15 2.4552 -0.5903 4.0280
ATOM 61 H P15 2.1663 0.9467 3.2002
ATOM 62 H P15 0.8081 0.0616 3.9258
ATOM 63 C P15 2.8598 -1.0402 1.3780
ATOM 64 O P15 3.8998 -1.1595 2.0229
ATOM 65 N P15 2.8059 -1.1963 0.0420
ATOM 66 H P15 1.9345 -0.9999 -0.4419
ATOM 67 C P15 3.9749 -1.5181 -0.7658
ATOM 68 C P15 3.5457 -1.4955 -2.2329
ATOM 69 H P15 2.7780 -2.2512 -2.4065
ATOM 70 H P15 3.1392 -0.5229 -2.5111
ATOM 71 H P15 4.4043 -1.7178 -2.8651
ATOM 72 C P15 4.5235 -2.8954 -0.4118
ATOM 73 H P15 5.3902 -3.1177 -1.0315
ATOM 74 H P15 4.8184 -2.9399 0.6347
ATOM 75 H P15 3.7524 -3.6439 -0.5984
ATOM 76 C P15 5.0735 -0.4522 -0.6138
ATOM 77 O P15 6.2497 -0.7261 -0.8662
ATOM 78 N P15 4.6740 0.7851 -0.3032
ATOM 79 H P15 3.7177 0.9458 -0.0077
ATOM 80 C P15 5.6239 1.8643 -0.1878
ATOM 81 H P15 6.1962 1.9727 -1.1096
ATOM 82 H P15 5.0820 2.7872 0.0030
ATOM 83 H P15 6.3279 1.6917 0.6295

COMPND Ac-Aib$_2$-(1R,2S,4R)-V-Aib$_2$-NHMe-M310

REMARK Energy(ZPE)= -1833.9511
REMARK #IF = 0
ATOM 1 C P15 -6.1969 1.5168 0.2526
ATOM 2 H P15 -5.8388 2.1862 1.0336
ATOM 3 H P15 -6.4931 2.1294 -0.5991
ATOM 4 H P15 -7.0648 0.9700 0.6147
ATOM 5 C P15 -5.0708 0.6238 -0.1736
ATOM 6 O P15 -3.9752 1.0771 -0.5174
ATOM 7 N P15 -5.3011 -0.7046 -0.1452
ATOM 8 H P15 -6.2289 -1.0235 0.0866
ATOM 9 C P15 -4.3705 -1.6866 -0.6934
ATOM 10 C P15 -4.2719 -1.5576 -2.2075
ATOM 11 H P15 -5.2534 -1.7390 -2.6456
ATOM 12 H P15 -3.9316 -0.5623 -2.4885
ATOM 13 H P15 -3.5662 -2.2885 -2.5978
ATOM 14 C P15 -4.8764 -3.0755 -0.3056
ATOM 15 H P15 -4.1849 -3.8343 -0.6691
ATOM 16 H P15 -4.9705 -3.1773 0.7763
ATOM 17 H P15 -5.8502 -3.2562 -0.7636
ATOM 18 C P15 -2.9834 -1.5086 -0.0615
ATOM 19 O P15 -1.9599 -1.7478 -0.7010
ATOM 20 N P15 -2.9638 -1.1412 1.2300
ATOM 21 H P15 -3.8487 -0.9583 1.6790
ATOM 22 C P15 -1.7556 -1.0514 2.0372
ATOM 23 C P15 -1.1496 -2.4330 2.2593
ATOM 24 H P15 -1.8794 -3.0635 2.7674
ATOM 25 H P15 -0.8786 -2.8941 1.3104
ATOM 26 H P15 -0.2568 -2.3515 2.8756
ATOM 27 C P15 -2.1371 -0.4162 3.3735
ATOM 28 H P15 -1.2479 -0.3067 3.9924
ATOM 29 H P15 -2.5886 0.5666 3.2301
ATOM 30 H P15 -2.8447 -1.0581 3.9007
ATOM 31 C P15 -0.7146 -0.1333 1.3839
ATOM 32 O P15 0.4775 -0.2530 1.6781
ATOM 33 N P15 -1.1530 0.8102 0.5385
ATOM 34 H P15 -2.1369 0.8410 0.2884
ATOM 35 C P15 -0.2385 1.7508 -0.0924
ATOM 36 C P15 -1.0257 2.6347 -1.1037
ATOM 37 H P15 -0.5470 2.6559 -2.0819
ATOM 38 H P15 -2.0382 2.2518 -1.2307
ATOM 39 C P15 -1.0165 4.0349 -0.4298
ATOM 40 H P15 -1.8028 4.6957 -0.7893
ATOM 41 C P15 -1.0426 3.6450 1.0505
ATOM 42 H P15 -1.9234 3.0680 1.3396
ATOM 43 H P15 -0.9267 4.5016 1.7145
ATOM 44 C P15 0.2419 2.8080 0.9555
ATOM 45 H P15 0.6175 2.3445 1.8644
ATOM 46 C P15 1.1522 3.7998 0.2705
ATOM 47 H P15 2.2265 3.8206 0.3732
ATOM 48 C P15 0.3989 4.5452 -0.5426
ATOM 49 H P15 0.7370 5.2881 -1.2530
ATOM 50 C P15 0.8933 0.9886 -0.7826
ATOM 51 O P15 2.0183 1.4778 -0.9036
ATOM 52 N P15 0.5860 -0.2140 -1.2960
ATOM 53 H P15 -0.3302 -0.6182 -1.1217
ATOM 54 C P15 1.5416 -0.9889 -2.0770
ATOM 55 C P15 1.8011 -0.3227 -3.4227
ATOM 56 H P15 0.8637 -0.2613 -3.9763
ATOM 57 H P15 2.2016 0.6810 -3.2862
ATOM 58 H P15 2.5169 -0.9084 -3.9963
ATOM 59 C P15 0.9553 -2.3851 -2.2842
ATOM 60 H P15 1.6594 -2.9952 -2.8486
ATOM 61 H P15 0.7509 -2.8733 -1.3305
ATOM 62 H P15 0.0245 -2.3194 -2.8487
ATOM 63 C P15 2.8689 -1.1729 -1.3216
ATOM 64 O P15 3.9187 -1.3285 -1.9427
ATOM 65 N P15 2.7973 -1.2430 0.0204
ATOM 66 H P15 1.9234 -1.0022 0.4783
ATOM 67 C P15 3.9588 -1.4979 0.8631
ATOM 68 C P15 4.5262 -2.8892 0.6094
ATOM 69 H P15 3.7664 -3.6340 0.8488
ATOM 70 H P15 4.8236 -3.0033 -0.4310
ATOM 71 H P15 5.3956 -3.0504 1.2441
ATOM 72 C P15 3.5087 -1.3827 2.3196
ATOM 73 H P15 4.3588 -1.5624 2.9766
ATOM 74 H P15 3.0981 -0.3949 2.5300
ATOM 75 H P15 2.7402 -2.1278 2.5306
ATOM 76 C P15 5.0515 -0.4345 0.6575
ATOM 77 O P15 6.2253 -0.6803 0.9480
ATOM 78 N P15 4.6472 0.7749 0.2571
ATOM 79 H P15 3.6955 0.9056 -0.0669
ATOM 80 C P15 5.5881 1.8544 0.0853
ATOM 81 H P15 6.1455 2.0289 1.0061
ATOM 82 H P15 6.3056 1.6378 -0.7095
ATOM 83 H P15 5.0392 2.7568 -0.1723

COMPND Ac-Aib$_2$-(1R,2S,4R)-Vdm-Aib$_2$-NHMe-P310
REMARK Energy(ZPE)= -1912.494595
REMARK #IF = 0
ATOM 1 C P16 -6.1199 1.4515 -0.4865
ATOM 2 H P16 -5.7521 1.9815 -1.3638
ATOM 3 H P16 -7.0165 0.8939 -0.7494
ATOM 4 H P16 -6.3746 2.1958 0.2684
ATOM 5 C P16 -5.0208 0.5857 0.0525
ATOM 6 O P16 -3.8942 1.0323 0.2842
ATOM 7 N P16 -5.3130 -0.7156 0.2575
ATOM 8 H P16 -6.2625 -1.0220 0.1135
ATOM 9 C P16 -4.4099 -1.6314 0.9471
ATOM 10 C P16 -4.9971 -3.0376 0.8301
ATOM 11 H P16 -5.9604 -3.0783 1.3413
ATOM 12 H P16 -5.1384 -3.3248 -0.2125
ATOM 13 H P16 -4.3310 -3.7572 1.3039
ATOM 14 C P16 -4.2501 -1.2400 2.4101
ATOM 15 H P16 -3.5767 -1.9323 2.9115
ATOM 16 H P16 -3.8434 -0.2340 2.4975
ATOM 17 H P16 -5.2249 -1.2773 2.8968
ATOM 18 C P16 -3.0387 -1.6437 0.2559
ATOM 19 O P16 -2.0070 -1.8250 0.9015
ATOM 20 N P16 -3.0460 -1.5133 -1.0807
ATOM 21 H P16 -3.9347 -1.3570 -1.5320
ATOM 22 C P16 -1.8613 -1.6280 -1.9209
ATOM 23 C P16 -2.2663 -1.2427 -3.3433
ATOM 24 H P16 -3.0132 -1.9442 -3.7185
ATOM 25 H P16 -2.6795 -0.2335 -3.3777
ATOM 26 H P16 -1.3967 -1.2869 -3.9970
ATOM 27 C P16 -1.3127 -3.0503 -1.8931
ATOM 28 H P16 -0.4390 -3.1249 -2.5375
ATOM 29 H P16 -1.0275 -3.3363 -0.8818
ATOM 30 H P16 -2.0812 -3.7340 -2.2543
ATOM 31 C P16 -0.7716 -0.6410 -1.4811
ATOM 32 O P16 0.4097 -0.8556 -1.7659
ATOM 33 N P16 -1.1560 0.4695 -0.8403
ATOM 34 H P16 -2.1286 0.5906 -0.5708
ATOM 35 C P16 -0.1928 1.4869 -0.4442
ATOM 36 C P16 0.3978 2.2427 -1.6594
ATOM 37 H P16 1.4859 2.2334 -1.6421

ATOM 38 H P16 0.0566 1.7725 -2.5821
ATOM 39 C P16 -0.1809 3.6710 -1.5004
ATOM 40 H P16 -0.1397 4.2661 -2.4123
ATOM 41 C P16 -1.5622 3.3602 -0.9250
ATOM 42 H P16 -2.1775 2.7318 -1.5729
ATOM 43 H P16 -2.1182 4.2525 -0.6364
ATOM 44 C P16 -0.9867 2.6273 0.2899
ATOM 45 H P16 -1.6875 2.2372 1.0273
ATOM 46 C P16 0.0139 3.6466 0.7896
ATOM 47 C P16 0.4986 4.2778 -0.2907
ATOM 48 C P16 0.8882 0.8756 0.4513
ATOM 49 O P16 2.0228 1.3566 0.5069
ATOM 50 C P16 0.4063 3.7531 2.2194
ATOM 51 H P16 1.1728 4.5124 2.3749
ATOM 52 H P16 0.7983 2.8008 2.5869
ATOM 53 H P16 -0.4537 4.0042 2.8468
ATOM 54 C P16 1.6097 5.2582 -0.3980
ATOM 55 H P16 2.4436 4.8315 -0.9649
ATOM 56 H P16 1.9888 5.5586 0.5788
ATOM 57 H P16 1.2949 6.1576 -0.9342
ATOM 58 N P16 0.5246 -0.1839 1.1919
ATOM 59 H P16 -0.4026 -0.5784 1.0657
ATOM 60 C P16 1.4287 -0.8586 2.1140
ATOM 61 C P16 0.7531 -2.1556 2.5584
ATOM 62 H P16 -0.1790 -1.9297 3.0782
ATOM 63 H P16 0.5212 -2.7913 1.7033
ATOM 64 H P16 1.4114 -2.6961 3.2373
ATOM 65 C P16 1.7277 0.0182 3.3231
ATOM 66 H P16 2.3682 -0.5158 4.0222
ATOM 67 H P16 2.2328 0.9337 3.0203
ATOM 68 H P16 0.7906 0.2722 3.8195
ATOM 69 C P16 2.7458 -1.2553 1.4253
ATOM 70 O P16 3.7808 -1.3556 2.0818
ATOM 71 N P16 2.6822 -1.5558 0.1151
ATOM 72 H P16 1.8221 -1.3756 -0.3943
ATOM 73 C P16 3.8388 -2.0189 -0.6412
ATOM 74 C P16 3.4223 -2.1404 -2.1072
ATOM 75 H P16 2.6215 -2.8745 -2.2068
ATOM 76 H P16 3.0689 -1.1869 -2.4998
ATOM 77 H P16 4.2750 -2.4736 -2.6975
ATOM 78 C P16 4.3205 -3.3726 -0.1336
ATOM 79 H P16 5.1911 -3.6898 -0.7046
ATOM 80 H P16 4.5890 -3.3217 0.9194
ATOM 81 H P16 3.5237 -4.1060 -0.2641
ATOM 82 C P16 4.9850 -0.9930 -0.5985
ATOM 83 O P16 6.1482 -1.3465 -0.8084
ATOM 84 N P16 4.6429 0.2889 -0.4332
ATOM 85 H P16 3.6947 0.5285 -0.1657
ATOM 86 C P16 5.6440 1.3274 -0.4304
ATOM 87 H P16 6.2162 1.3131 -1.3585
ATOM 88 H P16 5.1477 2.2901 -0.3357
ATOM 89 H P16 6.3431 1.2062 0.4001

COMPND Ac-Aib$_2$-(1R,2S,4R)-Vdm-Aib$_2$-NHMe-M310
REMARK Energy(ZPE)= -1912.4903
REMARK #IF = 0
ATOM 1 C P16 6.2209 1.5587 -0.1608
ATOM 2 H P16 5.8727 2.1997 -0.9695
ATOM 3 H P16 6.4530 2.1972 0.6918
ATOM 4 H P16 7.1257 1.0418 -0.4730
ATOM 5 C P16 5.1130 0.6279 0.2311
ATOM 6 O P16 3.9855 1.0414 0.5164
ATOM 7 N P16 5.3977 -0.6905 0.2394
ATOM 8 H P16 6.3474 -0.9748 0.0570
ATOM 9 C P16 4.4846 -1.6984 0.7690
ATOM 10 C P16 4.3112 -1.5403 2.2737
ATOM 11 H P16 5.2785 -1.6674 2.7601
ATOM 12 H P16 3.9154 -0.5552 2.5152
ATOM 13 H P16 3.6207 -2.2932 2.6489
ATOM 14 C P16 5.0640 -3.0732 0.4377
ATOM 15 H P16 4.3900 -3.8519 0.7920
ATOM 16 H P16 5.2077 -3.1966 -0.6364
ATOM 17 H P16 6.0245 -3.2013 0.9396
ATOM 18 C P16 3.1207 -1.5947 0.0741
ATOM 19 O P16 2.0835 -1.8785 0.6726
ATOM 20 N P16 3.1326 -1.2422 -1.2210
ATOM 21 H P16 4.0219 -1.0213 -1.6431
ATOM 22 C P16 1.9442 -1.2138 -2.0620
ATOM 23 C P16 1.4220 -2.6245 -2.3087
ATOM 24 H P16 2.1909 -3.2054 -2.8184
ATOM 25 H P16 1.1706 -3.1128 -1.3682
ATOM 26 H P16 0.5301 -2.5865 -2.9309
ATOM 27 C P16 2.3267 -0.5467 -3.3825
ATOM 28 H P16 1.4514 -0.4823 -4.0271
ATOM 29 H P16 2.7170 0.4590 -3.2191
ATOM 30 H P16 3.0849 -1.1424 -3.8935
ATOM 31 C P16 0.8399 -0.3558 -1.4298
ATOM 32 O P16 -0.3409 -0.5549 -1.7273
ATOM 33 N P16 1.2143 0.6322 -0.6054
ATOM 34 H P16 2.1910 0.7240 -0.3420
ATOM 35 C P16 0.2398 1.5516 -0.0329
ATOM 36 C P16 0.9486 2.5020 0.9750
ATOM 37 H P16 0.4251 2.5387 1.9306
ATOM 38 H P16 1.9681 2.1635 1.1621
ATOM 39 C P16 0.9097 3.8672 0.2482
ATOM 40 H P16 1.6459 4.5790 0.6209
ATOM 41 C P16 1.0295 3.4271 -1.2117
ATOM 42 H P16 1.9447 2.8743 -1.4370
ATOM 43 H P16 0.9159 4.2538 -1.9131
ATOM 44 C P16 -0.2323 2.5535 -1.1418
ATOM 45 H P16 -0.5455 2.0410 -2.0498
ATOM 46 C P16 -1.2151 3.5590 -0.5731
ATOM 47 C P16 -0.5273 4.3463 0.2681
ATOM 48 C P16 -0.8531 0.7563 0.6828
ATOM 49 O P16 -2.0039 1.1819 0.7949
ATOM 50 C P16 -2.6469 3.6152 -0.9690
ATOM 51 H P16 -3.2035 4.3458 -0.3810
ATOM 52 H P16 -3.1226 2.6424 -0.8489
ATOM 53 H P16 -2.7418 3.8939 -2.0234
ATOM 54 C P16 -1.0035 5.4272 1.1707
ATOM 55 H P16 -0.8173 5.1695 2.2184
ATOM 56 H P16 -2.0713 5.6148 1.0580
ATOM 57 H P16 -0.4717 6.3640 0.9816
ATOM 58 N P16 -0.4644 -0.3984 1.2525
ATOM 59 H P16 0.4701 -0.7563 1.0773
ATOM 60 C P16 -1.3463 -1.1990 2.0914
ATOM 61 C P16 -1.6704 -0.4651 3.3876
ATOM 62 H P16 -0.7426 -0.2745 3.9279
ATOM 63 H P16 -2.1652 0.4829 3.1821
ATOM 64 H P16 -2.3246 -1.0744 4.0081
ATOM 65 C P16 -0.6288 -2.5131 2.3983
ATOM 66 H P16 -1.2805 -3.1546 2.9901
ATOM 67 H P16 -0.3497 -3.0335 1.4816
ATOM 68 H P16 0.2781 -2.3144 2.9708
ATOM 69 C P16 -2.6479 -1.5630 1.3599
ATOM 70 O P16 -3.6661 -1.8215 2.0001

ATOM 71 N P16 -2.5880 -1.6531 0.0192
ATOM 72 H P16 -1.7432 -1.3540 -0.4578
ATOM 73 C P16 -3.7345 -2.0309 -0.7960
ATOM 74 C P16 -4.1429 -3.4750 -0.5316
ATOM 75 H P16 -3.3051 -4.1306 -0.7716
ATOM 76 H P16 -4.4177 -3.6151 0.5119
ATOM 77 H P16 -4.9920 -3.7410 -1.1583
ATOM 78 C P16 -3.3366 -1.8656 -2.2626
ATOM 79 H P16 -4.1845 -2.1147 -2.8994
ATOM 80 H P16 -3.0206 -0.8438 -2.4737
ATOM 81 H P16 -2.5116 -2.5384 -2.5017
ATOM 82 C P16 -4.9262 -1.0890 -0.5507
ATOM 83 O P16 -6.0788 -1.4654 -0.7775
ATOM 84 N P16 -4.6414 0.1659 -0.1850
ATOM 85 H P16 -3.6960 0.4099 0.0890
ATOM 86 C P16 -5.6979 1.1217 0.0428
ATOM 87 H P16 -6.3606 0.7967 0.8479
ATOM 88 H P16 -5.2542 2.0758 0.3150
ATOM 89 H P16 -6.2996 1.2542 -0.8571

COMPND Ac-Aib$_2$-(1R,2S,4R)-IIIbwr-Aib$_2$-NHMe-P310
REMARK Energy(ZPE)= -1869.877922
REMARK #IF = 0
ATOM 1 C P17 -6.1033 1.4892 -0.3267
ATOM 2 H P17 -5.7550 2.0823 -1.1713
ATOM 3 H P17 -6.9905 0.9313 -0.6179
ATOM 4 H P17 -6.3640 2.1782 0.4768
ATOM 5 C P17 -4.9815 0.6133 0.1443
ATOM 6 O P17 -3.8746 1.0746 0.4368
ATOM 7 N P17 -5.2290 -0.7105 0.2153
ATOM 8 H P17 -6.1649 -1.0318 0.0232
ATOM 9 C P17 -4.3018 -1.6630 0.8191
ATOM 10 C P17 -4.8371 -3.0685 0.5477
ATOM 11 H P17 -5.8023 -3.1980 1.0400
ATOM 12 H P17 -4.9593 -3.2494 -0.5209
ATOM 13 H P17 -4.1489 -3.8100 0.9512
ATOM 14 C P17 -4.1726 -1.4211 2.3169
ATOM 15 H P17 -3.4796 -2.1383 2.7523
ATOM 16 H P17 -3.8031 -0.4165 2.5160
ATOM 17 H P17 -5.1506 -1.5421 2.7831
ATOM 18 C P17 -2.9234 -1.5547 0.1510
ATOM 19 O P17 -1.8926 -1.7534 0.7926
ATOM 20 N P17 -2.9247 -1.2970 -1.1677
ATOM 21 H P17 -3.8172 -1.1455 -1.6133
ATOM 22 C P17 -1.7317 -1.2720 -2.0025
ATOM 23 C P17 -2.1443 -0.7683 -3.3853
ATOM 24 H P17 -2.8528 -1.4654 -3.8358
ATOM 25 H P17 -2.6055 0.2188 -3.3283
ATOM 26 H P17 -1.2680 -0.7081 -4.0287
ATOM 27 C P17 -1.1091 -2.6595 -2.1097
ATOM 28 H P17 -0.2269 -2.6197 -2.7456
ATOM 29 H P17 -0.8163 -3.0304 -1.1287
ATOM 30 H P17 -1.8365 -3.3426 -2.5486
ATOM 31 C P17 -0.6952 -0.2835 -1.4552
ATOM 32 O P17 0.4978 -0.4122 -1.7415
ATOM 33 N P17 -1.1357 0.7367 -0.7070
ATOM 34 H P17 -2.1206 0.8132 -0.4650
ATOM 35 C P17 -0.2145 1.7403 -0.2097
ATOM 36 C P17 0.3083 2.6639 -1.3314
ATOM 37 H P17 -0.0162 2.2879 -2.2998
ATOM 38 H P17 1.3914 2.7533 -1.3174
ATOM 39 C P17 -0.4051 3.9946 -0.9805
ATOM 40 H P17 -0.5843 4.6682 -1.8128
ATOM 41 O P17 -1.6393 3.5164 -0.4358
ATOM 42 C P17 -1.0600 2.7714 0.6266
ATOM 43 H P17 -1.8200 2.3135 1.2534
ATOM 44 C P17 -0.1157 3.7684 1.2501
ATOM 45 H P17 0.2204 3.7559 2.2758
ATOM 46 C P17 0.2817 4.5453 0.2451
ATOM 47 H P17 1.0282 5.3259 0.2481
ATOM 48 C P17 0.9011 1.0999 0.6164
ATOM 49 O P17 2.0021 1.6430 0.7273
ATOM 50 N P17 0.5932 -0.0492 1.2346
ATOM 51 H P17 -0.3116 -0.4731 1.0523
ATOM 52 C P17 1.5269 -0.7536 2.1037
ATOM 53 C P17 0.9274 -2.1232 2.4210
ATOM 54 H P17 -0.0339 -2.0022 2.9215
ATOM 55 H P17 0.7713 -2.7054 1.5122
ATOM 56 H P17 1.6000 -2.6701 3.0803
ATOM 57 C P17 1.7610 0.0308 3.3883
ATOM 58 H P17 2.4567 -0.5043 4.0313
ATOM 59 H P17 2.1726 1.0149 3.1703
ATOM 60 H P17 0.8113 0.1480 3.9112
ATOM 61 C P17 2.8654 -1.0100 1.3897
ATOM 62 O P17 3.9042 -1.1203 2.0377
ATOM 63 N P17 2.8121 -1.1844 0.0561
ATOM 64 H P17 1.9396 -1.0019 -0.4309
ATOM 65 C P17 3.9804 -1.5216 -0.7465
ATOM 66 C P17 3.5501 -1.5237 -2.2135
ATOM 67 H P17 2.7839 -2.2838 -2.3739
ATOM 68 H P17 3.1412 -0.5567 -2.5073
ATOM 69 H P17 4.4086 -1.7547 -2.8427
ATOM 70 C P17 4.5279 -2.8932 -0.3693
ATOM 71 H P17 5.3916 -3.1289 -0.9882
ATOM 72 H P17 4.8269 -2.9196 0.6766
ATOM 73 H P17 3.7546 -3.6434 -0.5392
ATOM 74 C P17 5.0794 -0.4538 -0.6126
ATOM 75 O P17 6.2555 -0.7327 -0.8588
ATOM 76 N P17 4.6807 0.7894 -0.3242
ATOM 77 H P17 3.7238 0.9570 -0.0363
ATOM 78 C P17 5.6316 1.8700 -0.2300
ATOM 79 H P17 6.1994 1.9642 -1.1561
ATOM 80 H P17 5.0910 2.7958 -0.0504
ATOM 81 H P17 6.3393 1.7091 0.5864

COMPND Ac-Aib$_2$-(1R,2S,4R)-IIIbwr-Aib$_2$-NHMe-M310
REMARK Energy(ZPE)= -1869.8755
REMARK #IF = 0
ATOM 1 C P17 -6.1828 1.5766 0.1175
ATOM 2 H P17 -5.8301 2.2788 0.8715
ATOM 3 H P17 -6.4652 2.1510 -0.7650
ATOM 4 H P17 -7.0582 1.0514 0.4932
ATOM 5 C P17 -5.0572 0.6587 -0.2534
ATOM 6 O P17 -3.9522 1.0888 -0.5972
ATOM 7 N P17 -5.2993 -0.6656 -0.1754
ATOM 8 H P17 -6.2335 -0.9670 0.0539
ATOM 9 C P17 -4.3685 -1.6763 -0.6680
ATOM 10 C P17 -4.2393 -1.6063 -2.1837
ATOM 11 H P17 -5.2147 -1.7917 -2.6336
ATOM 12 H P17 -3.8804 -0.6268 -2.4953
ATOM 13 H P17 -3.5366 -2.3604 -2.5326
ATOM 14 C P17 -4.8956 -3.0446 -0.2375
ATOM 15 H P17 -4.2035 -3.8230 -0.5555
ATOM 16 H P17 -5.0142 -3.1025 0.8451
ATOM 17 H P17 -5.8608 -3.2349 -0.7095
ATOM 18 C P17 -2.9919 -1.4873 -0.0166

ATOM 19 O P17 -1.9592 -1.7605 -0.6276
ATOM 20 N P17 -2.9912 -1.0718 1.2603
ATOM 21 H P17 -3.8815 -0.8638 1.6873
ATOM 22 C P17 -1.7938 -0.9605 2.0818
ATOM 23 C P17 -1.2047 -2.3362 2.3730
ATOM 24 H P17 -1.9470 -2.9365 2.8992
ATOM 25 H P17 -0.9268 -2.8410 1.4490
ATOM 26 H P17 -0.3184 -2.2362 2.9962
ATOM 27 C P17 -2.1871 -0.2619 3.3827
ATOM 28 H P17 -1.3056 -0.1305 4.0081
ATOM 29 H P17 -2.6293 0.7163 3.1885
ATOM 30 H P17 -2.9064 -0.8742 3.9290
ATOM 31 C P17 -0.7379 -0.0836 1.3991
ATOM 32 O P17 0.4544 -0.2107 1.6884
ATOM 33 N P17 -1.1635 0.8429 0.5280
ATOM 34 H P17 -2.1488 0.9005 0.2898
ATOM 35 C P17 -0.2293 1.7368 -0.1279
ATOM 36 C P17 -0.9983 2.6562 -1.1100
ATOM 37 H P17 -2.0251 2.3153 -1.2293
ATOM 38 H P17 -0.5299 2.7054 -2.0911
ATOM 39 C P17 -0.9284 4.0126 -0.3588
ATOM 40 H P17 -1.7539 4.6919 -0.5487
ATOM 41 O P17 -0.9230 3.5809 1.0040
ATOM 42 C P17 0.2665 2.7991 0.9129
ATOM 43 H P17 0.5372 2.3715 1.8731
ATOM 44 C P17 1.2286 3.7587 0.2566
ATOM 45 H P17 2.3007 3.7372 0.3634
ATOM 46 C P17 0.4774 4.5354 -0.5216
ATOM 47 H P17 0.7876 5.2952 -1.2239
ATOM 48 C P17 0.8810 0.9510 -0.8219
ATOM 49 O P17 1.9996 1.4429 -0.9868
ATOM 50 N P17 0.5608 -0.2692 -1.2761
ATOM 51 H P17 -0.3560 -0.6589 -1.0738
ATOM 52 C P17 1.4957 -1.0962 -2.0281
ATOM 53 C P17 1.7306 -0.5168 -3.4172
ATOM 54 H P17 0.7830 -0.4875 -3.9558
ATOM 55 H P17 2.1350 0.4922 -3.3542
ATOM 56 H P17 2.4339 -1.1399 -3.9661
ATOM 57 C P17 0.8880 -2.4951 -2.1354
ATOM 58 H P17 1.5548 -3.1405 -2.7058
ATOM 59 H P17 0.7296 -2.9325 -1.1488
ATOM 60 H P17 -0.0739 -2.4435 -2.6471
ATOM 61 C P17 2.8349 -1.2483 -1.2869
ATOM 62 O P17 3.8727 -1.4476 -1.9152
ATOM 63 N P17 2.7849 -1.2373 0.0576
ATOM 64 H P17 1.9150 -0.9843 0.5154
ATOM 65 C P17 3.9541 -1.4577 0.8991
ATOM 66 C P17 4.4998 -2.8689 0.7195
ATOM 67 H P17 3.7329 -3.5879 1.0101
ATOM 68 H P17 4.7819 -3.0467 -0.3164
ATOM 69 H P17 5.3749 -3.0068 1.3519
ATOM 70 C P17 3.5213 -1.2501 2.3507
ATOM 71 H P17 4.3766 -1.3949 3.0093
ATOM 72 H P17 3.1189 -0.2483 2.5033
ATOM 73 H P17 2.7497 -1.9750 2.6149
ATOM 74 C P17 5.0572 -0.4227 0.6162
ATOM 75 O P17 6.2320 -0.6682 0.9020
ATOM 76 N P17 4.6628 0.7675 0.1524
ATOM 77 H P17 3.7077 0.8928 -0.1632
ATOM 78 C P17 5.6161 1.8210 -0.0961
ATOM 79 H P17 6.2019 2.0269 0.8001
ATOM 80 H P17 6.3071 1.5553 -0.8994
ATOM 81 H P17 5.0758 2.7204 -0.3803

COMPND Ac-Aib$_2$-(1R,2S,4R)-IIIbmb-Aib$_2$-NHMe-P310
REMARK Energy(ZPE)= -1987.512821
REMARK #IF = 0
ATOM 1 C P18 -6.0696 1.7257 -0.5413
ATOM 2 H P18 -5.6755 2.1817 -1.4480
ATOM 3 H P18 -7.0063 1.2203 -0.7660
ATOM 4 H P18 -6.2629 2.5243 0.1757
ATOM 5 C P18 -5.0289 0.8138 0.0359
ATOM 6 O P18 -3.8621 1.1810 0.2011
ATOM 7 N P18 -5.4225 -0.4363 0.3561
ATOM 8 H P18 -6.3992 -0.6678 0.2614
ATOM 9 C P18 -4.5821 -1.3668 1.1043
ATOM 10 C P18 -5.2845 -2.7241 1.1155
ATOM 11 H P18 -6.2352 -2.6446 1.6451
ATOM 12 H P18 -5.4735 -3.0833 0.1032
ATOM 13 H P18 -4.6670 -3.4549 1.6358
ATOM 14 C P18 -4.3543 -0.8712 2.5261
ATOM 15 H P18 -3.7144 -1.5667 3.0655
ATOM 16 H P18 -3.8777 0.1079 2.5215
ATOM 17 H P18 -5.3145 -0.7998 3.0370
ATOM 18 C P18 -3.2349 -1.5505 0.3919
ATOM 19 O P18 -2.2024 -1.7522 1.0299
ATOM 20 N P18 -3.2683 -1.5395 -0.9507
ATOM 21 H P18 -4.1550 -1.3598 -1.3972
ATOM 22 C P18 -2.1165 -1.8160 -1.7983
ATOM 23 C P18 -2.5201 -1.5056 -3.2394
ATOM 24 H P18 -3.3351 -2.1639 -3.5448
ATOM 25 H P18 -2.8436 -0.4691 -3.3458
ATOM 26 H P18 -1.6738 -1.6782 -3.9023
ATOM 27 C P18 -1.6794 -3.2704 -1.6711
ATOM 28 H P18 -0.8183 -3.4532 -2.3110
ATOM 29 H P18 -1.4063 -3.5036 -0.6432
ATOM 30 H P18 -2.4998 -3.9183 -1.9799
ATOM 31 C P18 -0.9430 -0.8912 -1.4529
ATOM 32 O P18 0.2125 -1.2250 -1.7262
ATOM 33 N P18 -1.2269 0.3017 -0.9127
ATOM 34 H P18 -2.1785 0.5224 -0.6304
ATOM 35 C P18 -0.1700 1.2584 -0.6301
ATOM 36 C P18 0.4622 1.8301 -1.9272
ATOM 37 H P18 0.0358 1.3187 -2.7901
ATOM 38 H P18 1.5414 1.6978 -1.9354
ATOM 39 C P18 0.0455 3.3192 -1.9124
ATOM 40 H P18 0.1153 3.8068 -2.8828
ATOM 41 C P18 -1.3474 3.2148 -1.2757
ATOM 42 H P18 -2.0411 2.5994 -1.8515
ATOM 43 H P18 -1.8015 4.1839 -1.0664
ATOM 44 C P18 -0.8377 2.5268 0.0030
ATOM 45 H P18 -1.5661 2.2793 0.7725
ATOM 46 C P18 0.2546 3.4822 0.3984
ATOM 47 C P18 0.8006 3.9775 -0.7897
ATOM 48 C P18 0.7499 3.8668 1.6299
ATOM 49 H P18 0.3326 3.4754 2.5505
ATOM 50 C P18 1.8611 4.8643 -0.7641
ATOM 51 H P18 2.2948 5.2488 -1.6799
ATOM 52 C P18 1.8059 4.7804 1.6596
ATOM 53 H P18 2.2013 5.1133 2.6115
ATOM 54 C P18 2.3547 5.2702 0.4784
ATOM 55 H P18 3.1715 5.9805 0.5239
ATOM 56 C P18 0.8775 0.6454 0.3016
ATOM 57 O P18 2.0477 1.0327 0.2826
ATOM 58 N P18 0.4511 -0.2980 1.1555
ATOM 59 H P18 -0.5052 -0.6329 1.0929
ATOM 60 C P18 1.3273 -0.9134 2.1430
ATOM 61 C P18 0.5820 -2.1036 2.7464
ATOM 62 H P18 -0.3350 -1.7619 3.2284
ATOM 63 H P18 0.3169 -2.8320 1.9796
ATOM 64 H P18 1.2107 -2.5874 3.4928
ATOM 65 C P18 1.6953 0.0861 3.2323
ATOM 66 H P18 2.3340 -0.3872 3.9755
ATOM 67 H P18 2.2225 0.9405 2.8112
ATOM 68 H P18 0.7823 0.4339 3.7169

ATOM 69 C P18 2.6020 -1.4711 1.4875
ATOM 70 O P18 3.6426 -1.5665 2.1351
ATOM 71 N P18 2.4846 -1.9174 0.2229
ATOM 72 H P18 1.6280 -1.7255 -0.2867
ATOM 73 C P18 3.5808 -2.5486 -0.5015
ATOM 74 C P18 3.1033 -2.8085 -1.9303
ATOM 75 H P18 2.2462 -3.4837 -1.9182
ATOM 76 H P18 2.8054 -1.8829 -2.4230
ATOM 77 H P18 3.9060 -3.2733 -2.5014
ATOM 78 C P18 3.9834 -3.8645 0.1530
ATOM 79 H P18 4.7920 -4.3251 -0.4115
ATOM 80 H P18 4.3145 -3.7047 1.1770
ATOM 81 H P18 3.1252 -4.5376 0.1557
ATOM 82 C P18 4.7977 -1.6126 -0.6084
ATOM 83 O P18 5.9253 -2.0727 -0.8069
ATOM 84 N P18 4.5514 -0.2992 -0.5797
ATOM 85 H P18 3.6307 0.0350 -0.3182
ATOM 86 C P18 5.6183 0.6604 -0.7257
ATOM 87 H P18 6.1646 0.4893 -1.6536
ATOM 88 H P18 5.1888 1.6590 -0.7466
ATOM 89 H P18 6.3286 0.5984 0.1020

COMPND Ac-Aib$_2$-(1R,2S,4R)-IIIbmb-Aib$_2$-NHMe-M310
REMARK Energy(ZPE)= -1987.5071
REMARK #IF = 0
ATOM 1 C P18 6.0363 2.2716 -0.1163
ATOM 2 H P18 5.5934 2.8350 -0.9366
ATOM 3 H P18 6.1418 2.9484 0.7316
ATOM 4 H P18 7.0210 1.9167 -0.4124
ATOM 5 C P18 5.0993 1.1679 0.2720
ATOM 6 O P18 3.9245 1.3909 0.5795
ATOM 7 N P18 5.5887 -0.0883 0.2489
ATOM 8 H P18 6.5677 -0.2172 0.0458
ATOM 9 C P18 4.8534 -1.2388 0.7657
ATOM 10 C P18 4.6760 -1.1363 2.2747
ATOM 11 H P18 5.6579 -1.1067 2.7472
ATOM 12 H P18 4.1244 -0.2351 2.5378
ATOM 13 H P18 4.1291 -2.0004 2.6466
ATOM 14 C P18 5.6433 -2.4955 0.4016
ATOM 15 H P18 5.1073 -3.3804 0.7417
ATOM 16 H P18 5.7961 -2.5709 -0.6757
ATOM 17 H P18 6.6159 -2.4763 0.8959
ATOM 18 C P18 3.4821 -1.3423 0.0834
ATOM 19 O P18 2.5077 -1.7932 0.6843
ATOM 20 N P18 3.4319 -0.9735 -1.2069
ATOM 21 H P18 4.2742 -0.6065 -1.6241
ATOM 22 C P18 2.2536 -1.1172 -2.0514
ATOM 23 C P18 1.9410 -2.5882 -2.2995
ATOM 24 H P18 2.7947 -3.0540 -2.7919
ATOM 25 H P18 1.7438 -3.1053 -1.3613
ATOM 26 H P18 1.0664 -2.6805 -2.9403
ATOM 27 C P18 2.5409 -0.4026 -3.3714
ATOM 28 H P18 1.6692 -0.4665 -4.0206
ATOM 29 H P18 2.7805 0.6493 -3.2088
ATOM 30 H P18 3.3804 -0.8826 -3.8769
ATOM 31 C P18 1.0359 -0.4268 -1.4231
ATOM 32 O P18 -0.1035 -0.7855 -1.7278
ATOM 33 N P18 1.2636 0.5991 -0.5878
ATOM 34 H P18 2.2166 0.8258 -0.3177
ATOM 35 C P18 0.1657 1.3694 -0.0201
ATOM 36 C P18 0.7284 2.4615 0.9359
ATOM 37 H P18 1.7924 2.3006 1.1074
ATOM 38 H P18 0.2239 2.4479 1.9015
ATOM 39 C P18 0.4744 3.7837 0.1730
ATOM 40 H P18 1.1133 4.6030 0.4964
ATOM 41 C P18 0.6097 3.3097 -1.2822
ATOM 42 H P18 1.5951 2.9068 -1.5215
ATOM 43 H P18 0.3434 4.0803 -2.0058
ATOM 44 C P18 -0.4843 2.2306 -1.1521
ATOM 45 H P18 -0.7241 1.6395 -2.0321
ATOM 46 C P18 -1.5987 3.0820 -0.6047
ATOM 47 C P18 -1.0064 4.0473 0.2142
ATOM 48 C P18 -2.9647 3.0722 -0.8165
ATOM 49 H P18 -3.4255 2.3282 -1.4557
ATOM 50 C P18 -1.7748 4.9905 0.8734
ATOM 51 H P18 -1.3208 5.7342 1.5180
ATOM 52 C P18 -3.7411 4.0392 -0.1782
ATOM 53 H P18 -4.8125 4.0602 -0.3388
ATOM 54 C P18 -3.1555 4.9814 0.6640
ATOM 55 H P18 -3.7769 5.7238 1.1502
ATOM 56 C P18 -0.7869 0.4415 0.7360
ATOM 57 O P18 -1.9669 0.7431 0.9209
ATOM 58 N P18 -0.2528 -0.6835 1.2385
ATOM 59 H P18 0.7153 -0.9115 1.0361
ATOM 60 C P18 -1.0168 -1.6231 2.0475
ATOM 61 C P18 -1.3401 -1.0269 3.4113
ATOM 62 H P18 -0.4077 -0.7951 3.9270
ATOM 63 H P18 -1.9257 -0.1154 3.3056
ATOM 64 H P18 -1.9075 -1.7398 4.0063
ATOM 65 C P18 -0.1717 -2.8867 2.2115
ATOM 66 H P18 -0.7230 -3.6201 2.7986
ATOM 67 H P18 0.0785 -3.3218 1.2431
ATOM 68 H P18 0.7570 -2.6482 2.7311
ATOM 69 C P18 -2.3133 -2.0464 1.3362
ATOM 70 O P18 -3.2958 -2.3947 1.9881
ATOM 71 N P18 -2.2741 -2.0887 -0.0082
ATOM 72 H P18 -1.4539 -1.7312 -0.4866
ATOM 73 C P18 -3.3923 -2.5401 -0.8260
ATOM 74 C P18 -3.6793 -4.0187 -0.5935
ATOM 75 H P18 -2.7906 -4.5976 -0.8478
ATOM 76 H P18 -3.9407 -4.2055 0.4463
ATOM 77 H P18 -4.5042 -4.3401 -1.2267
ATOM 78 C P18 -3.0135 -2.3096 -2.2891
ATOM 79 H P18 -3.8429 -2.6038 -2.9309
ATOM 80 H P18 -2.7732 -1.2622 -2.4744
ATOM 81 H P18 -2.1421 -2.9136 -2.5464
ATOM 82 C P18 -4.6566 -1.7055 -0.5583
ATOM 83 O P18 -5.7740 -2.1674 -0.8038
ATOM 84 N P18 -4.4737 -0.4457 -0.1507
ATOM 85 H P18 -3.5508 -0.1377 0.1346
ATOM 86 C P18 -5.5990 0.4210 0.1014
ATOM 87 H P18 -6.2054 0.5382 -0.7976
ATOM 88 H P18 -6.2391 0.0216 0.8913
ATOM 89 H P18 -5.2252 1.3952 0.4059

ANNEX 7.A. Convergence test for explicit MeOH REMD simulation

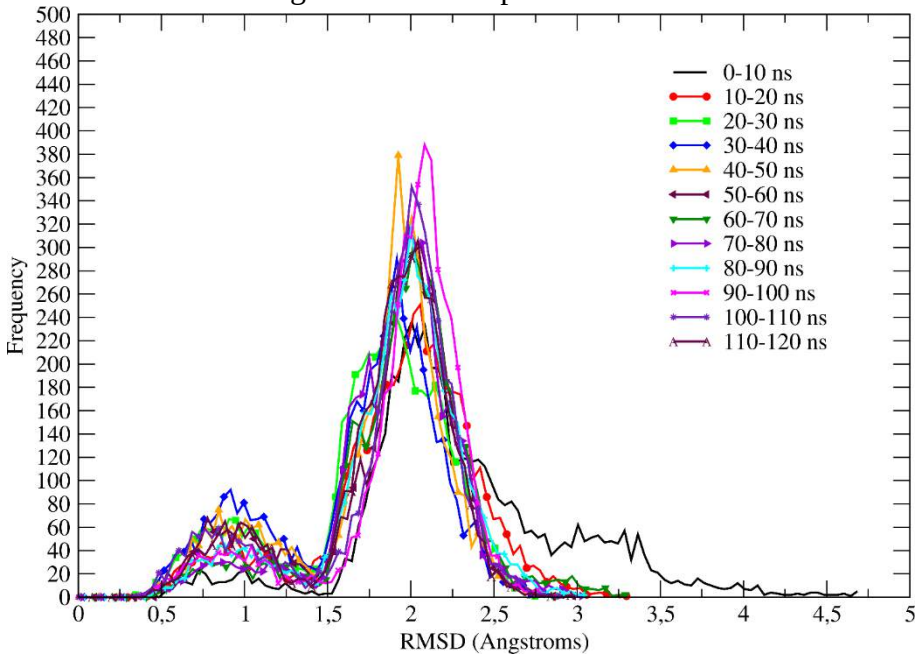

ANNEX 9.A. Correlation between MMPBSA results and available experimental data.

Correlations between MM-PBSA predicted and experimental binding energies for α-trombin.

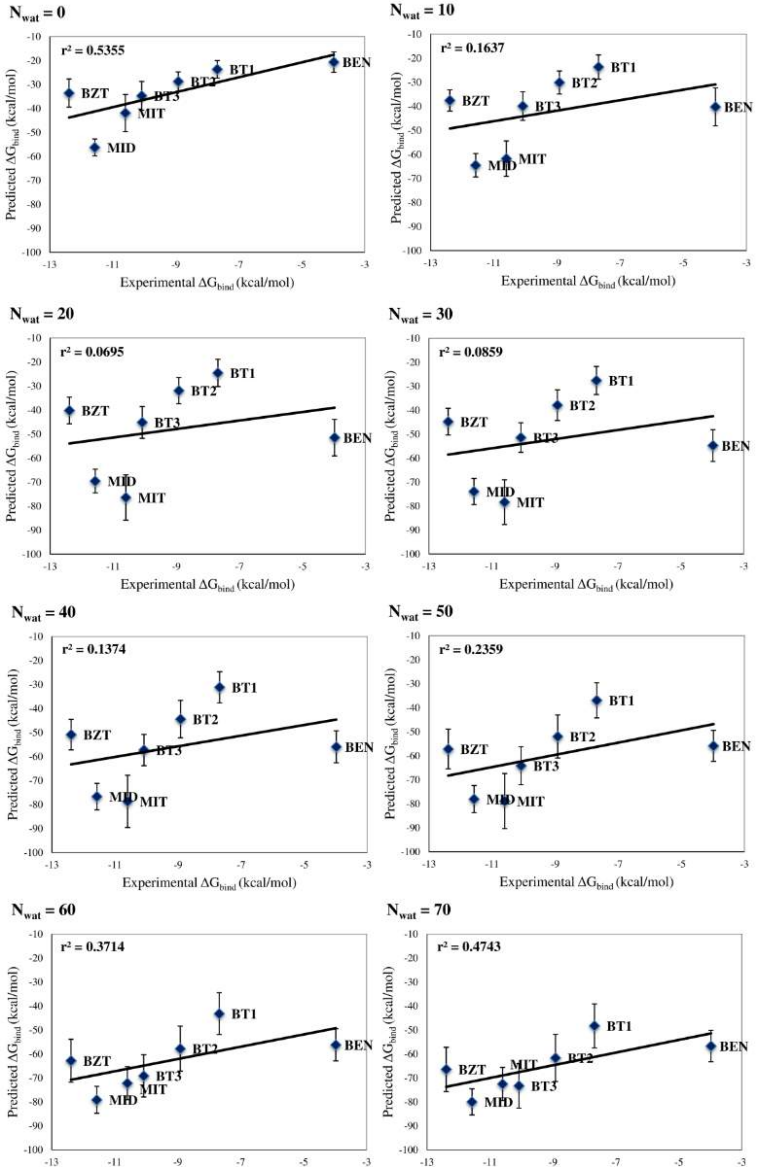

Correlations between MM-PBSA predicted and experimental binding energies for penicillopepsin.

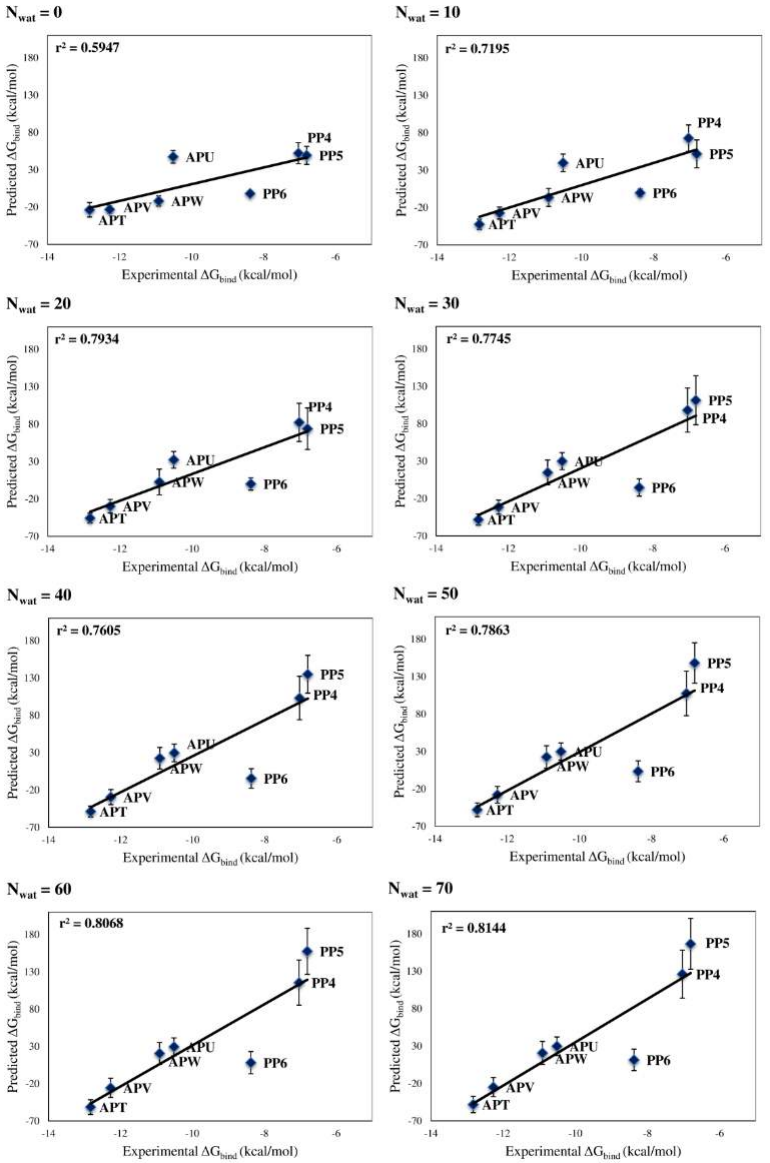

Correlations between MM-PBSA predicted and experimental binding energies for avidin.

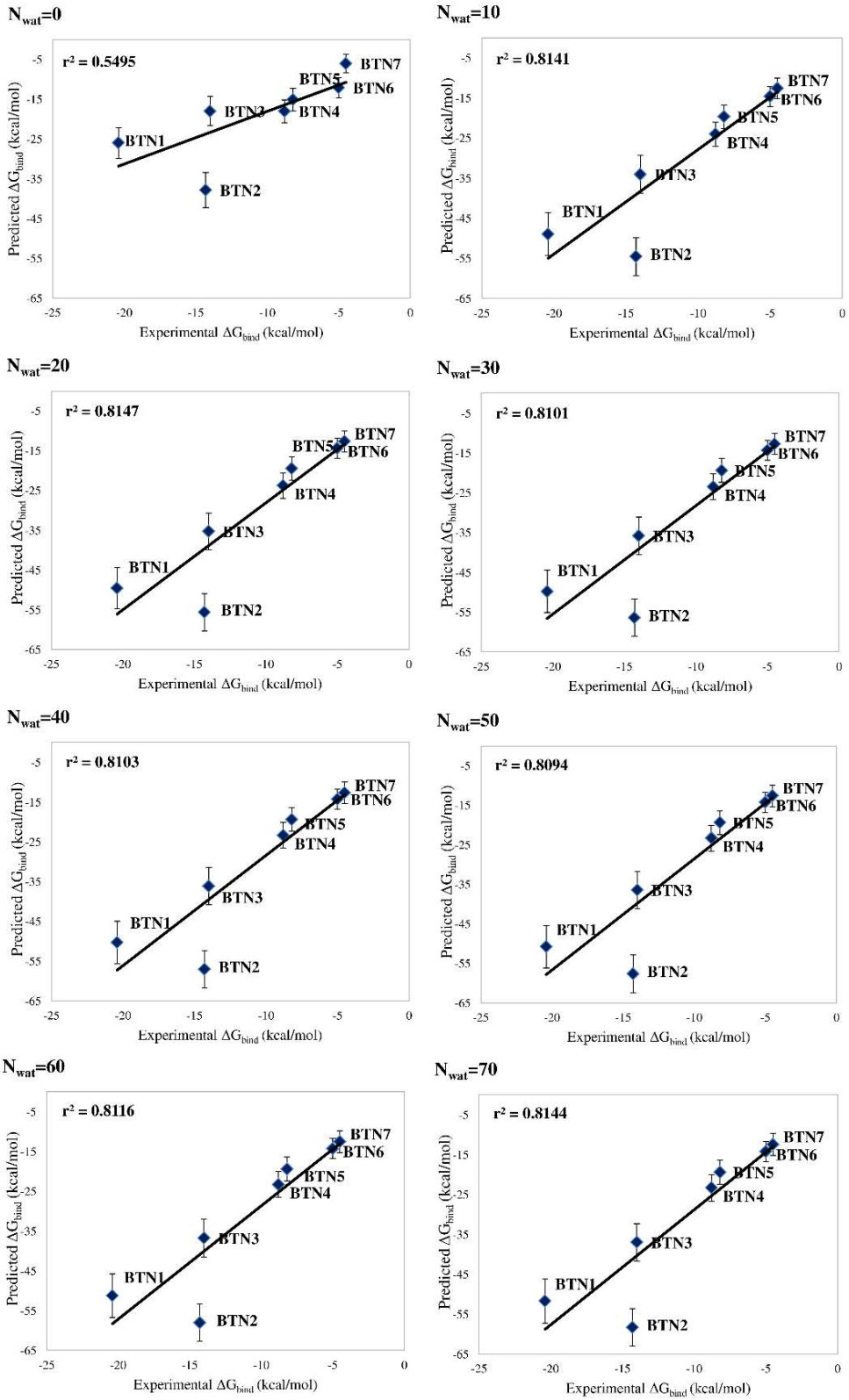

ANNEX 10.A. Scripts used for the automatization of MD/Nwat-MMGBSA protocol on PPIs.

Script for the selection of interfacial residues.

```
from pymol import stored

def interfaceResidues(cmpx, cA='c. A', cB='c. B', cutoff=1.0,
selName="interface"):
      """
      interfaceResidues -- finds 'interface' residues between two chains in
a complex.

      PARAMS
            cmpx
                  The complex containing cA and cB

            cA
                  The first chain in which we search for residues at an
interface
                  with cB

            cB
                  The second chain in which we search for residues at an
interface
                  with cA

            cutoff
                  The difference in area OVER which residues are considered
                  interface residues.  Residues whose dASA from the complex
to
                  a single chain is greater than this cutoff are kept.  Zero
                  keeps all residues.

            selName
                  The name of the selection to return.

      RETURNS
            * A selection of interface residues is created and named
                  depending on what you passed into selName
            * An array of values is returned where each value is:
                  ( modelName, residueNumber, dASA )

      NOTES
            If you have two chains that are not from the same PDB that you
want
            to complex together, use the create command like:
                  create myComplex, pdb1WithChainA or pdb2withChainX
            then pass myComplex to this script like:
                  interfaceResidues myComlpex, c. A, c. X

            This script calculates the area of the complex as a whole.
Then,
            it separates the two chains that you pass in through the
arguments
            cA and cB, alone.  Once it has this, it calculates the
difference
            and any residues ABOVE the cutoff are called interface residues.

      AUTHOR:
            Jason Vertrees, 2009.
      """
```

```
     # Save user's settings, before setting dot_solvent
     oldDS = cmd.get("dot_solvent")
     cmd.set("dot_solvent", 1)

     # set some string names for temporary objects/selections
     tempC, selName1 = "tempComplex", selName+"1"
     chA, chB = "chA", "chB"

     # operate on a new object & turn off the original
     cmd.create(tempC, cmpx)
     cmd.disable(cmpx)

     # remove cruft and inrrelevant chains
     cmd.remove(tempC + " and not (polymer and (%s or %s))" % (cA, cB))

     # get the area of the complete complex
     cmd.get_area(tempC, load_b=1)
     # copy the areas from the loaded b to the q, field.
     cmd.alter(tempC, 'q=b')

     # extract the two chains and calc. the new area
     # note: the q fields are copied to the new objects
     # chA and chB
     cmd.extract(chA, tempC + " and (" + cA + ")")
     cmd.extract(chB, tempC + " and (" + cB + ")")
     cmd.get_area(chA, load_b=1)
     cmd.get_area(chB, load_b=1)

     # update the chain-only objects w/the difference
     cmd.alter( "%s or %s" % (chA,chB), "b=b-q" )

     # The calculations are done.  Now, all we need to
     # do is to determine which residues are over the cutoff
     # and save them.
     stored.r, rVal, seen = [], [], []
     cmd.iterate('%s or %s' % (chA, chB),
'stored.r.append((model,resi,b))')

     cmd.enable(cmpx)
     cmd.select(selName1, None)
     for (model,resi,diff) in stored.r:
          key=resi+"-"+model
          if abs(diff)>=float(cutoff):
               if key in seen: continue
               else: seen.append(key)
               rVal.append( (model,resi,diff) )
               # expand the selection here; I chose to iterate over
stored.r instead of
               # creating one large selection b/c if there are too many
residues PyMOL
               # might crash on a very large selection.  This is pretty
much guaranteed
               # not to kill PyMOL; but, it might take a little longer to
run.
               cmd.select( selName1, selName1 + " or (%s and i. %s)" %
(model,resi))

     # this is how you transfer a selection to another object.
     cmd.select(selName, cmpx + " in " + selName1)
     # clean up after ourselves
```

```
      cmd.delete(selName1)
      cmd.delete(chA)
      cmd.delete(chB)
      cmd.delete(tempC)
      # show the selection
      cmd.enable(selName)

      # reset users settings
      cmd.set("dot_solvent", oldDS)

      return rVal

cmd.extend("interfaceResidues", interfaceResidues)
```

Script for the automatization of Nwat-MMGBSA calculations.

```
#!/bin/tcsh
#
# Written by I. Maffucci and A. Contini, 2014; based on the work reported
in J. Chem. Theory Comput., 2013, 9 (6), pp 2706-2717
#
# Given a "list" of PDB complexes, this script setup MMPBSA calculations
including $n explicit water closest to PPI interface.
# An input file called "complex_features.txt" and containing the
definitions of "receptor mask", "ligand mask" and "last residue" is also
required.
#
# The script assumes that solvated MD trajectories were previously obtained
and are stored in $TRAJ/$n.
#
# The following standard name are also used:
# solvated topology file: $z_complex_wat.top
# solvated trajectory file: $z_complex.prod4.mdcrd
# with $z = system name
#
# AmberTools14 needs to be installed and environment variables correctly
specified
# pymol needs to be installed to generate interfaces
#
# This scripts assumes that the solvated MD trajectory is made by 1000
frames.
#
#  run as: qsub NWAT_MMPBSA_PyPPIs_2.2_HPC.pbs
#
#########################################################
# HERE ARE VARIABLES THAT NEED TO BE MODIFIED BY USER#
#########################################################
#
#

#PBS -N MMPBSA_PPI
#PBS -l nodes=1:ppn=6
#PBS -o MMPBSA_PPI.log
#PBS -q batch
#PBS -l walltime=120:0:0

set AMBERV = 14 # amber version
#
setenv TRAJ "/home/studenti/giacomo/MMPBSA_ff14SB_TIP3P_4ns" # path to
trajectories
#
```

```
setenv INTPATH "/home/studenti/giacomo/Complexes" # path to complexes
#
setenv EXTPARAMS "/home/studenti/giacomo/MMPBSA_ff14SB_TIP3P_4ns/2SIC" #
path to parameters not included in standard ff, if any
#
set r = 10           # interval between trajectory frames selected for
MMGBSA calculation (suggested values for production = 10 or 20)
#
set g = 8       # kind of GB model for MMGBSA calculations (i.e. g = 1 for
igb=1; suggested values = 1, 5, 8)
#                 mind that the correct GB radius (mbondi, mbondi2 or
mbondi3) need to be set in the solvated prmtop
set cut = 0.50       # set interface cutoff for pymol interface definition
#
set argv = POLAR     # flag to set the kind of interface to be selected.
ALL = all residues; POLAR = polar residues
#
source /data/software/amber/amber$AMBERV/amber$AMBERV.csh # modify
accordingly to your amber installation
#
# flag to activate the strip of structural ions; 0 = no stripping; !=0 =
stripping accordingly to ionmask
# Note that if you want to strip structural ions such as CA or MG, you need
to create a modified "complex_features.txt" (complex_features_strip.txt)
# with updated recmask, ligmask and lastres to be used only in the
generation of MMGBSA input
#
set stripstructions = 0
if ($stripstructions != 0) then
     set ionmask = ":CA*"
else
     set ionmask = ""
endif
#
#########################################################
# END OF USER MODIFIABLE VARIABLES                      #
#########################################################
#
set NPROCS = `wc -l < $PBS_NODEFILE`
#
cd $PBS_O_WORKDIR
#
# option "ALL" or "POLAR"
#
if ($argv == ALL | $argv == POLAR) then
     echo "the interface will consider "$argv" residues"
     else
        echo "please specify POLAR or ALL"
        exit
endif

if (! -e interface.pymol) then
     echo "the interface.pymol script needs to be in the current
directory"
     exit
endif
#
@ f = (1000 / $r)    # total number of frames used in MMPBSA
#
echo "calculation begun on "`date`
```

```
#
echo "                    Average Delta         Std. Dev.   Std. Err. of
Mean" > RESULTS_"$argv".txt
#
foreach z (`awk 'f;/name/{f=1}' complex_features.txt | awk '{print $1}'`)
     echo 'run interface.pymol' > tmp.pml # Generate the input and run
Pymol
     echo 'load '$INTPATH'/complex_'$z'_leap.pdb' >> tmp.pml
     echo 'myInterfaceResidues = interfaceResidues("complex_'$z'_leap",
cA="c. A", cB="c. B", cutoff='$cut', selName="interface")' >> tmp.pml
     echo 'save '$z'_interface.pdb, interface' >> tmp.pml
     echo 'quit' >> tmp.pml
     pymol -c tmp.pml

     mkdir $z
        echo "$z" >> RESULTS_$argv.txt
        if ($argv == ALL) then
     # the following command create a mask for ALL residues
           awk '{print $6}' "$z"_interface.pdb | awk '\!x[$0]++' | awk
'/./' | awk '{print ":"$0","}' | awk '/ key (start|stop) / {next}
{printf("%s", $0)} END {print ""}' > "$z"_intmask_"$argv".txt

     else if ($argv == POLAR) then
           awk '/ARG/ || /ASH/ || /ASP/ || /GLH/ || /GLN/ || /GLU/ || /HID/
|| /HIE/ || /HIP/ || /LYN/ || /LYS/ || /SER/ || /THR/ || /TRP/ ||
/TYR/{print}' "$z"_interface.pdb | awk '{print $6}' | awk '\!x[$0]++' | awk
'/./' | awk '{print ":"$0","}' | awk '/ key (start|stop) / {next}
{printf("%s", $0)} END {print ""}' > "$z"_intmask_"$argv".txt
     endif
#
# set MMPBSA variables
#
     set intmask = `cat "$z"_intmask_"$argv".txt`                    # set
PP interface mask
     if ($stripstructions == 0) then
           set recmask = `awk "/"$z"/" complex_features.txt | awk '{print
$2}'`# set receptor mask
           set ligmask = `awk "/"$z"/" complex_features.txt | awk '{print
$3}'`# set ligand mask
           set lastres = `awk "/"$z"/" complex_features.txt | awk '{print
$4}'`# set last residue number
     else
           set recmask = `awk "/"$z"/" complex_features_strip.txt | awk
'{print $2}'`     # set receptor mask
           set ligmask = `awk "/"$z"/" complex_features_strip.txt | awk
'{print $3}'`     # set ligand mask
           set lastres = `awk "/"$z"/" complex_features_strip.txt | awk
'{print $4}'`     # set last residue number
     endif
#
#    cleanup
       rm "$z"_interface.pdb
       rm "$z"_intmask_"$argv".txt
       rm tmp.pml
#
# create a file named nwat.dat containing the nr. of closest water
molecules to include in top/mdcrd; modify to your needs
#
     cd $z
        printf %"s\n" 0 10 20 30 40 50 60 70 > nwat.dat # for production
```

```
       #printf %"s\n" 10 20 > nwat.dat # for debug

      foreach n (`cat nwat.dat`)

         # set variables for MMPBSA input
         @ a = $lastres + $n
      @ w = $lastres + 1
         @ b = $a + 1

         # create directories named nwatn, where n is nr. of closest water
molecules
                mkdir nwat$n
            cd nwat$n

         # generate ligand topologies
      cat > lig_gen.cpptraj << EOF
parmstrip $recmask,:Cl-,:Na+,:WAT,$ionmask
parmbox nobox
parmwrite out ligand.top amber
EOF

      $AMBERHOME/bin/cpptraj -i lig_gen.cpptraj -p
$TRAJ/$z/"$z"_complex_wat.top > lig_cpptraj.log

         # generate trajectory for nwat > 0
            if ($n != 0) then
                echo "trajin $TRAJ/$z/"$z"_complex_wat.prod4.mdcrd 1 1000
$r" > cmplx_trj_gen.cpptraj
                echo "center @CA,C,N mass origin\nimage origin
center\nstrip :Cl-,:Na+,"$ionmask"\nclosest $n $intmask noimage\ntrajout
nwat$n.$z.mdcrd nobox" >> cmplx_trj_gen.cpptraj
                        $AMBERHOME/bin/cpptraj -i cmplx_trj_gen.cpptraj -p
$TRAJ/$z/"$z"_complex_wat.top > cmplx_trj_cpptraj.log

      # generate complex pdb for nwat > 0
                echo "trajin $TRAJ/$z/"$z"_complex_wat.prod4.mdcrd 1 1" >
cmplx_pdb_gen.cpptraj
                echo "center @CA,C,N mass origin\nimage origin
center\nstrip :Cl-,:Na+,"$ionmask"" >> cmplx_pdb_gen.cpptraj
                        echo "closest $n $intmask noimage\ntrajout
nwat$n.$z.pdb pdb" >> cmplx_pdb_gen.cpptraj
                $AMBERHOME/bin/cpptraj -i cmplx_pdb_gen.cpptraj -p
$TRAJ/$z/"$z"_complex_wat.top > cmplx_pdb_gen_cpptraj.log

      # generate receptor pdb for nwat > 0
                echo "trajin $TRAJ/$z/"$z"_complex_wat.prod4.mdcrd 1 1" >
rec_pdb_gen.cpptraj
                echo "center @CA,C,N mass origin\nimage origin
center\nstrip :Cl-,:Na+,"$ionmask"" >> rec_pdb_gen.cpptraj
                        echo "closest $n $intmask noimage\nstrip
"$ligmask"\ntrajout nwat$n.$z.rec.pdb pdb" >> rec_pdb_gen.cpptraj
                $AMBERHOME/bin/cpptraj -i rec_pdb_gen.cpptraj -p
$TRAJ/$z/"$z"_complex_wat.top > rec_pdb_gen_cpptraj.log

         # use leap to generate the top
                echo "source leaprc.ff14SB\nsource
leaprc.gaff\nloadamberparams frcmod.ionsjc_tip3p\nloadamberparams
frcmod.ionslm_1264_tip3p" > leap.in
                        foreach l (`ls $EXTPARAMS/*off`)
                           echo "loadoff "$l"" >> leap.in
```

```
                end
                foreach m (`ls $EXTPARAMS/*prep`)
                     echo "loadamberprep "$m"" >> leap.in
                end
                foreach o (`ls $EXTPARAMS/*frcmod*`)
                     echo "loadamberparams "$o"" >> leap.in
                end
                echo "set default PBRadii mbondi3" >> leap.in
                echo "cmp=loadpdb nwat"$n"."$z".pdb" >> leap.in
                echo "rec=loadpdb nwat"$n"."$z".rec.pdb" >> leap.in
                echo "saveamberparm cmp nwat$n.$z.top nwat$n.$z.crd" >>
leap.in
                        echo "saveamberparm rec nwat$n.$z.rec.top
nwat$n.$z.crd" >> leap.in

                $AMBERHOME/bin/tleap -f leap.in

        # generate MMPBSA input for nwat > 0; change to modify MM-PBSA/GBSA
protocol. See Amber14 manual for details
                echo "&general\nreceptor_mask="$recmask":"$w"-"$a",
ligand_mask="$ligmask", startframe=1, endframe="$f", \
interval=1, verbose=1,\n/\n&pb\nistrng=0.15, radiopt=0" >
mmpbsa_closest_nwat$n.in

                else
     # generate trajectory for nwat = 0
                cat > gen0.cpptraj << EOF
trajin $TRAJ/$z/$z.complex_wat.prod4.mdcrd 1 1000 $r
autoimage
strip :Cl-,:Na+,:WAT,$ionmask
trajout nwat$n.$z.mdcrd nobox
EOF
                        # workaround for heredocs
                        sed -i 's/'$z'.complex/'$z'_complex/g' gen0.cpptraj

                        $AMBERHOME/bin/cpptraj -i gen0.cpptraj -p
$TRAJ/$z/"$z"_complex_wat.top > traj_nwat0_cpptraj.log


     # generate receptor and complex topologies for nwat=0
                cat > topgen0.cpptraj << EOF
parmstrip :Cl-,:Na+,:WAT,$ionmask
parmbox nobox
parmwrite out nwat$n.$z.top amber
parmstrip $ligmask
parmwrite out nwat$n.$z.rec.top amber
EOF

                        $AMBERHOME/bin/cpptraj -i topgen0.cpptraj -p
$TRAJ/$z/"$z"_complex_wat.top > top_nwat0_cpptraj.log

        # generate MMPBSA input for nwat = 0; change to modify MM-PBSA/GBSA
protocol. See Amber14 manual for details

                echo "&general\nreceptor_mask="$recmask",
ligand_mask="$ligmask", startframe=1, endframe="$f", \
interval=1, verbose=1,\n/\n&pb\nistrng=0.15, radiopt=0" >
mmpbsa_closest_nwat$n.in
```

```
          endif
#
# execute MMPBSA and print results
#
          if ($stripstructions == 0) then
                        $MPI_HOME/bin/mpirun -machinefile $PBS_NODEFILE -np
$NPROCS $AMBERHOME/bin/MMPBSA.py.MPI -O -i mmpbsa_closest_nwat$n.in -o
FINAL_RESULTS_CLOSEST$n -cp nwat$n.$z.top -rp nwat$n.$z.rec.top -lp
ligand.top -y nwat$n.$z.mdcrd > MMPBSA.out
                        grep "DELTA TOTAL" FINAL_RESULTS_CLOSEST"$n" | sed
"s/DELTA TOTAL/NWAT="$n"/g" >> $PBS_O_WORKDIR/RESULTS_"$argv".txt
                else

                        $MPI_HOME/bin/mpirun -machinefile $PBS_NODEFILE -np
$NPROCS $AMBERHOME/bin/MMPBSA.py.MPI -O -i mmpbsa_closest_nwat$n.in -o
FINAL_RESULTS_CLOSEST$n -cp nwat$n.$z.top -rp nwat$n.$z.rec.top -lp
ligand.top -y nwat$n.$z.mdcrd > MMPBSA.out
                        grep "DELTA TOTAL" FINAL_RESULTS_CLOSEST"$n" | sed
"s/DELTA TOTAL/NWAT="$n"/g" >>
$PBS_O_WORKDIR/RESULTS_strip_"$ionmask"_"$argv".txt
                endif
                cd ..
     end
     cd ..
        endif
end
#
# the script terminates
#
echo "calculations ended on "`date`
#
```

ANNEX 11.A. Additional information about penicillopesin system

Correlation between experimental free energy of binding and predicted binding energies obtained for penicillopepsin by analyzing the first ns of one of the three MD simulations run on a CPU hardware.

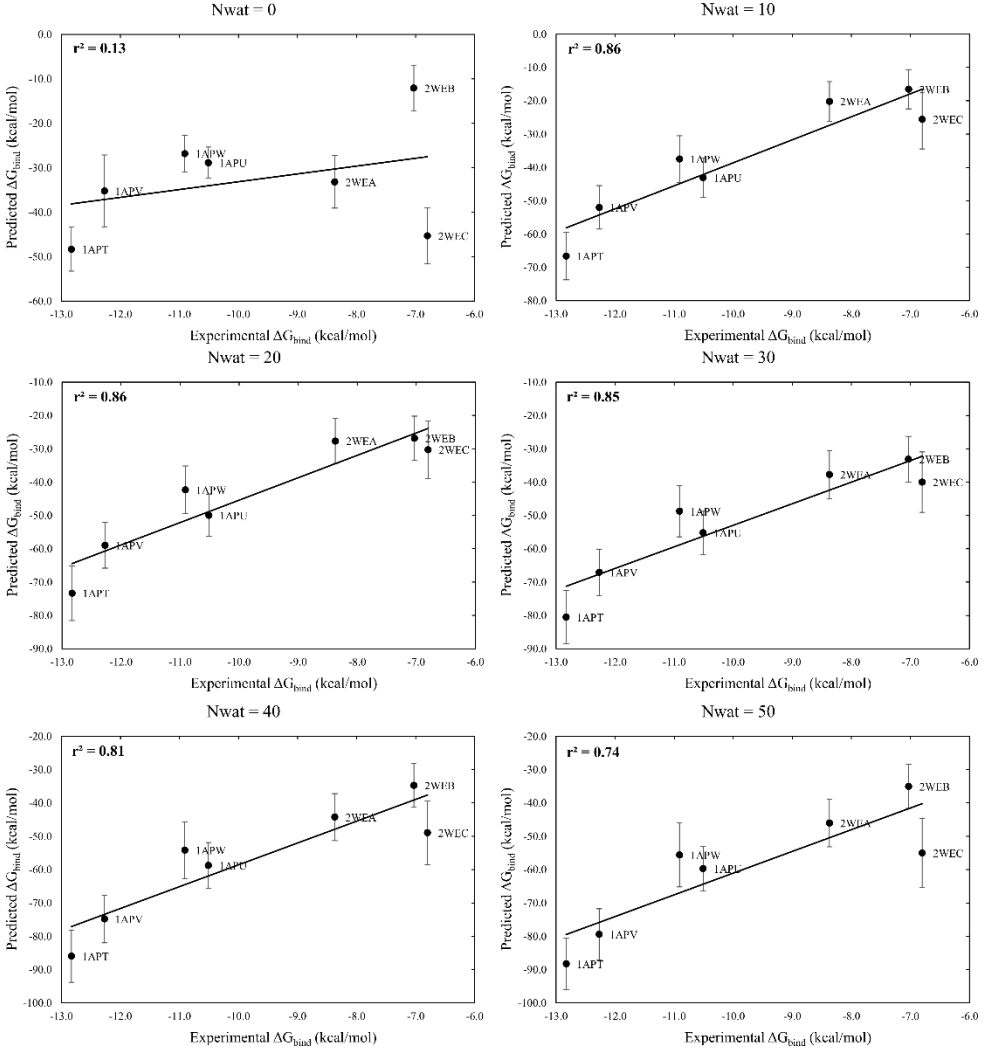

Correlation between experimental free energy of binding and predicted binding energies obtained for penicillopepsin by analyzing the 4th ns of one of the three MD simulations run on a GPU hardware.

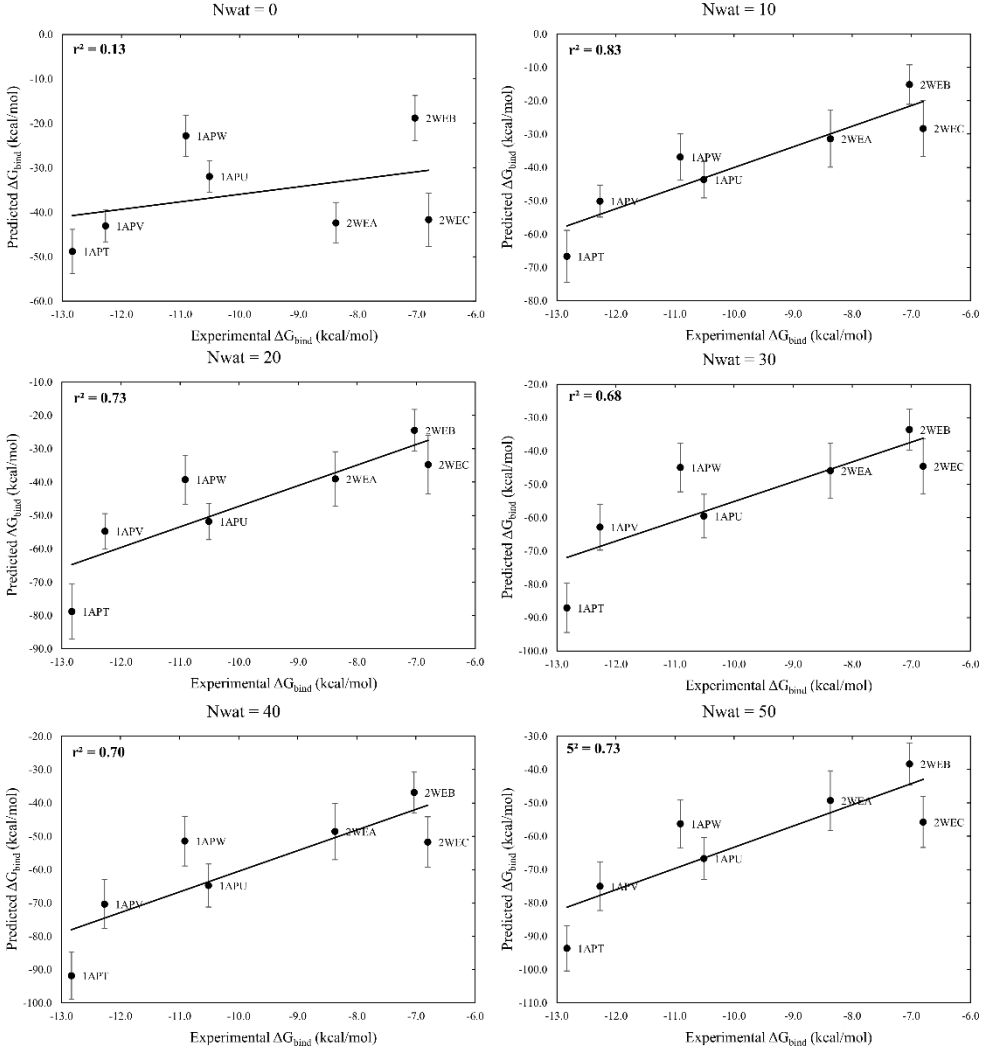

ANNEX 11.B. Additional information about MDM2 system.

Correlation between experimental free energy of binding and predicted binding energies obtained for MDM2 with Nwat = 0 - 70 by analyzing the first ns of a MD simulation run on a CPU hardware.

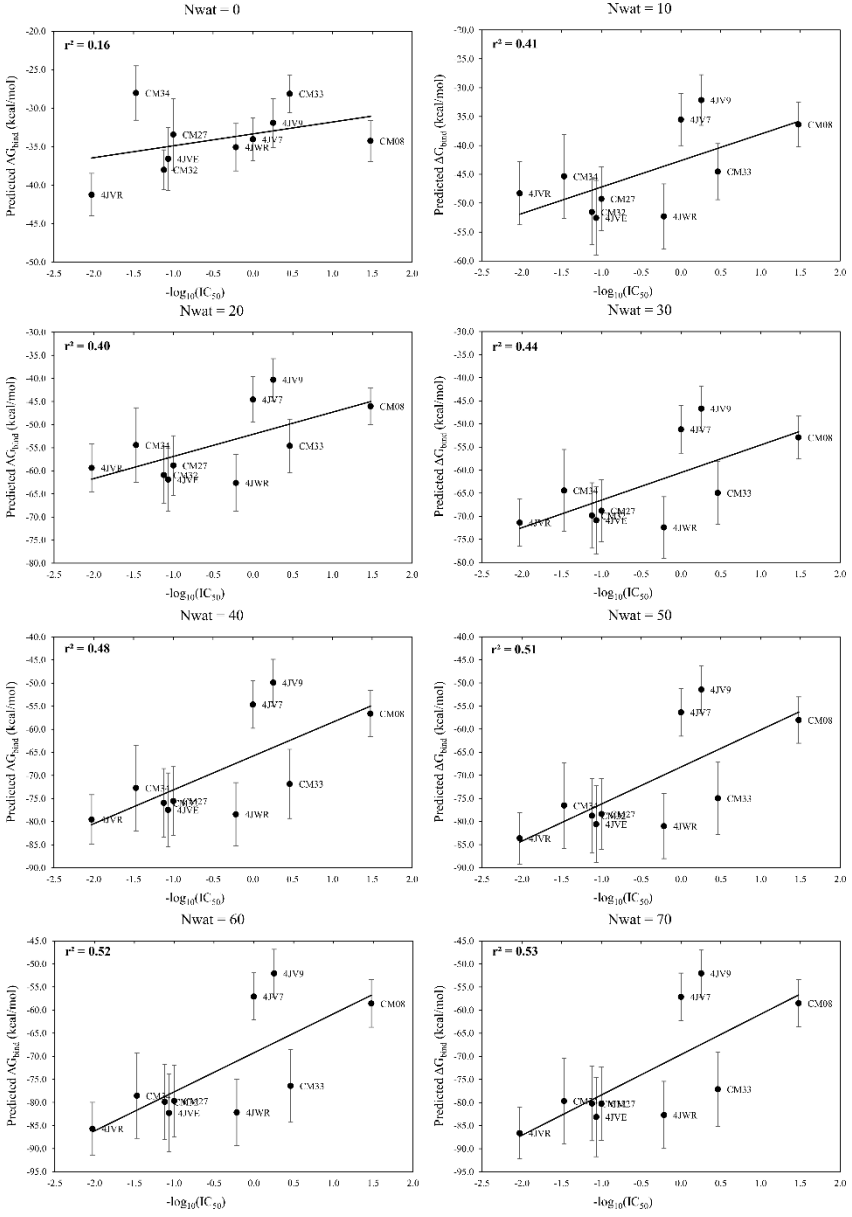

Correlation between experimental free energy of binding and predicted binding energies obtained for MDM2 with Nwat = 0 - 70 by analyzing the 4th ns of a MD simulation run on a GPU hardware.

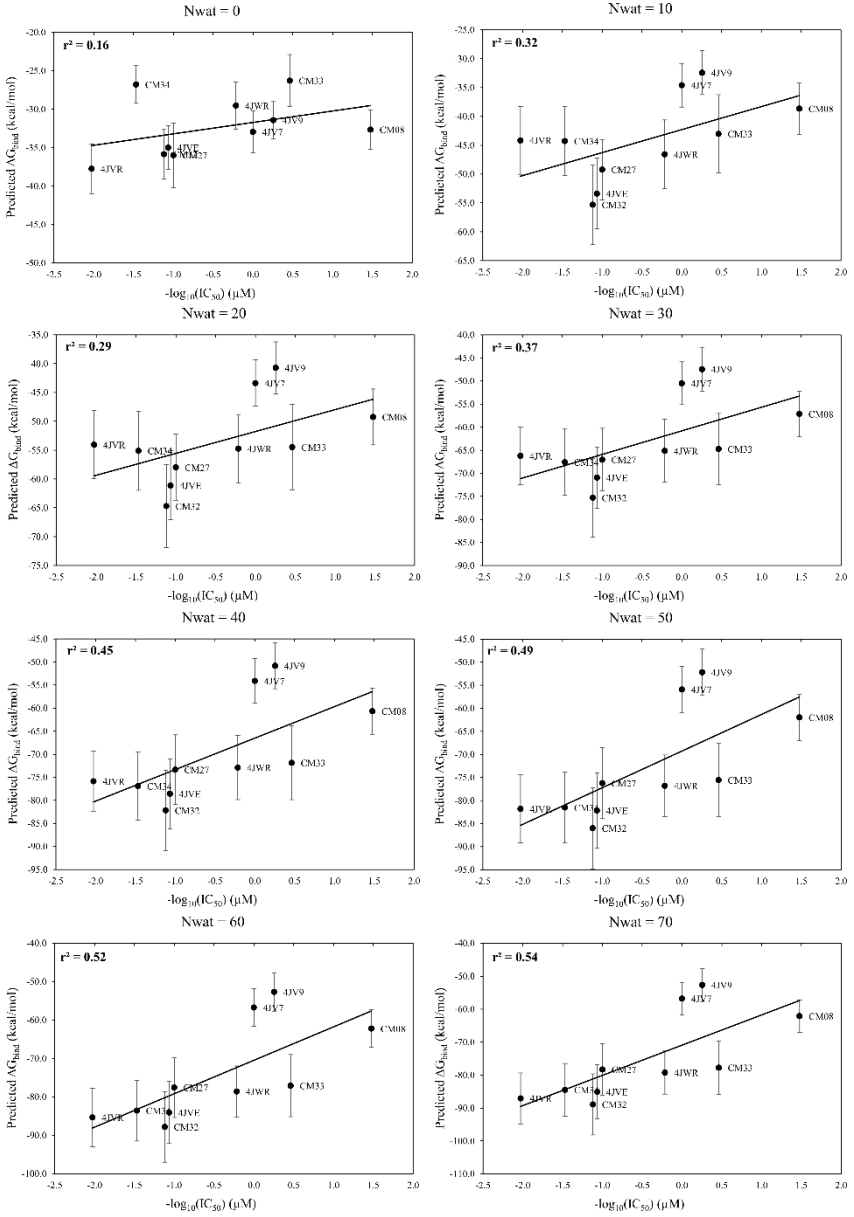

Correlation between experimental free energy of binding and predicted binding energies obtained for MDM2 with Nwat = 0 - 70 by analyzing the 4th ns of a MD simulation run on a CPU hardware.

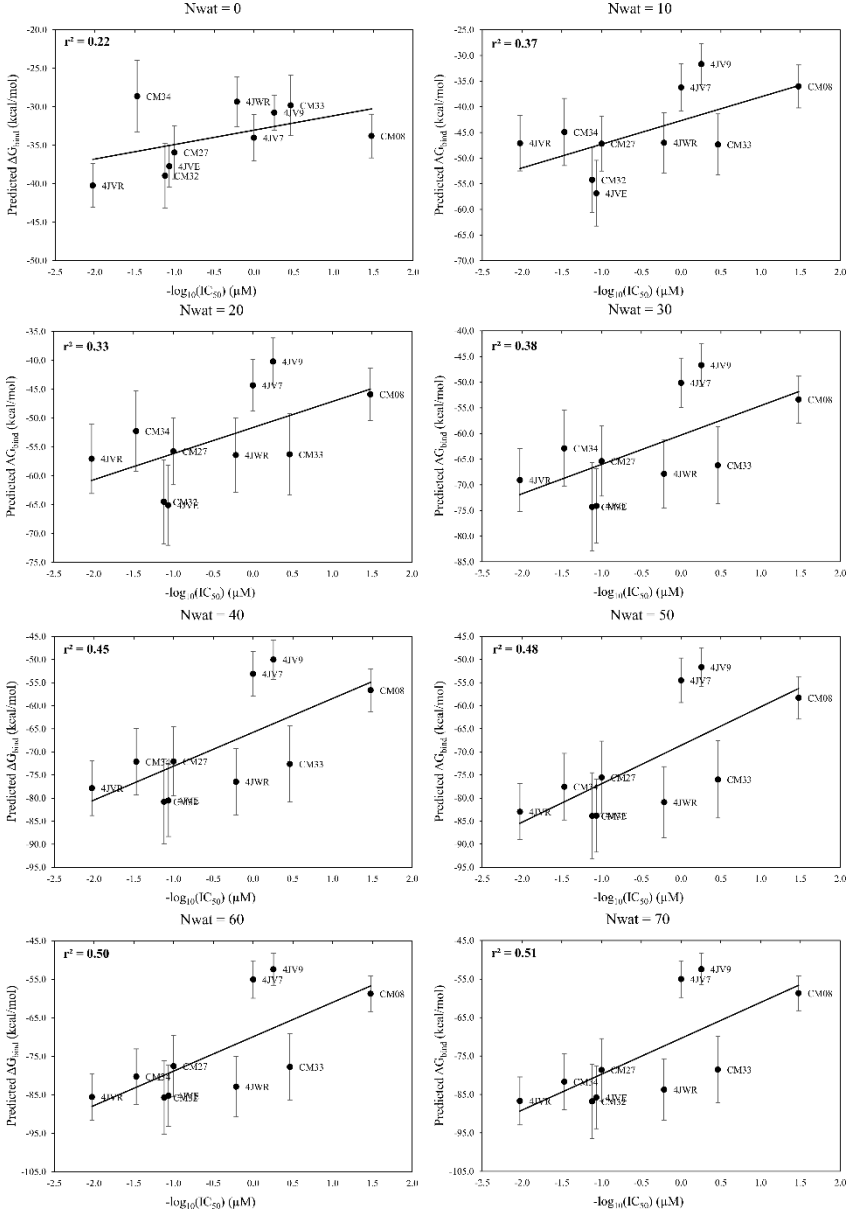

Correlation between experimental free energy of binding and predicted binding energies obtained for BCL-X_L with Nwat = 0 - 50 by analyzing the first ns of a MD simulation run on a GPU hardware.

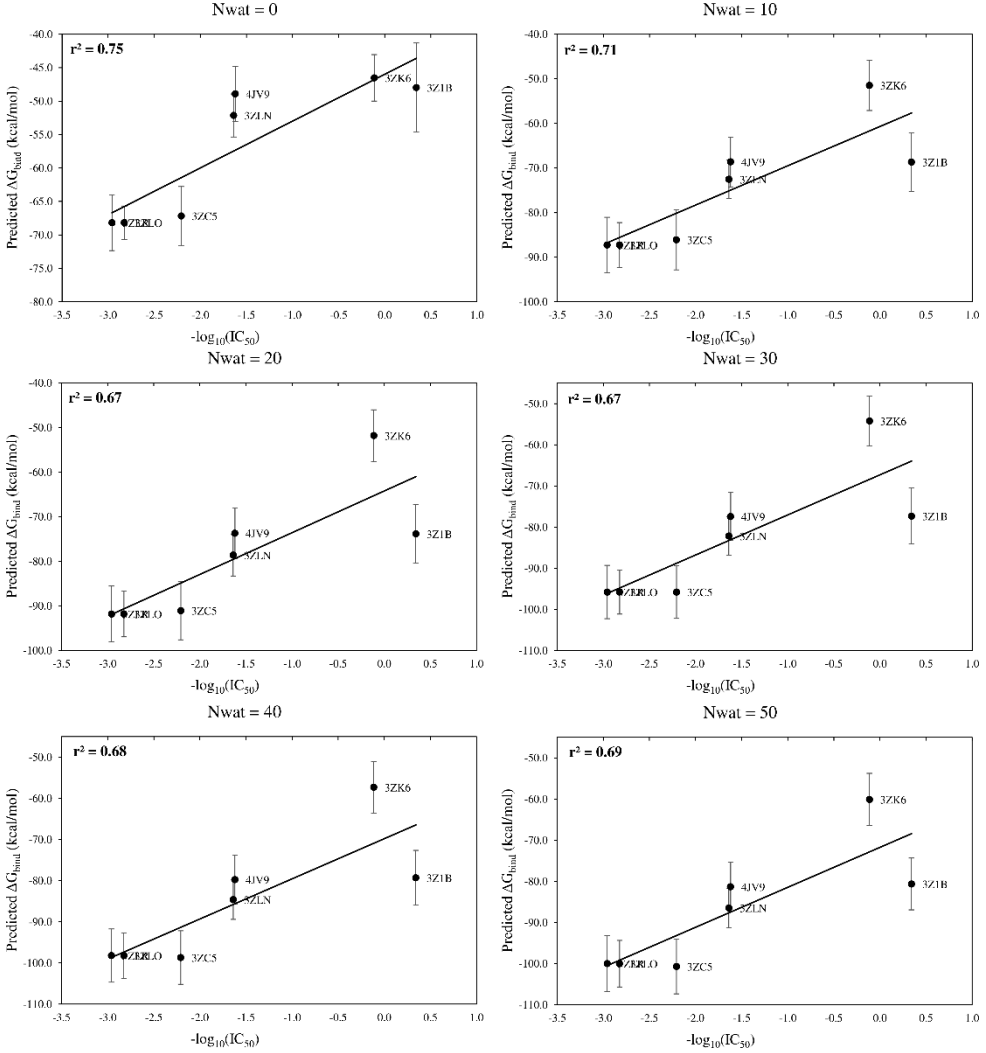

Correlation between experimental free energy of binding and predicted binding energies obtained for BCL-X_L with Nwat = 0 - 50 by analyzing the 4th ns of a MD simulation run on a GPU hardware.

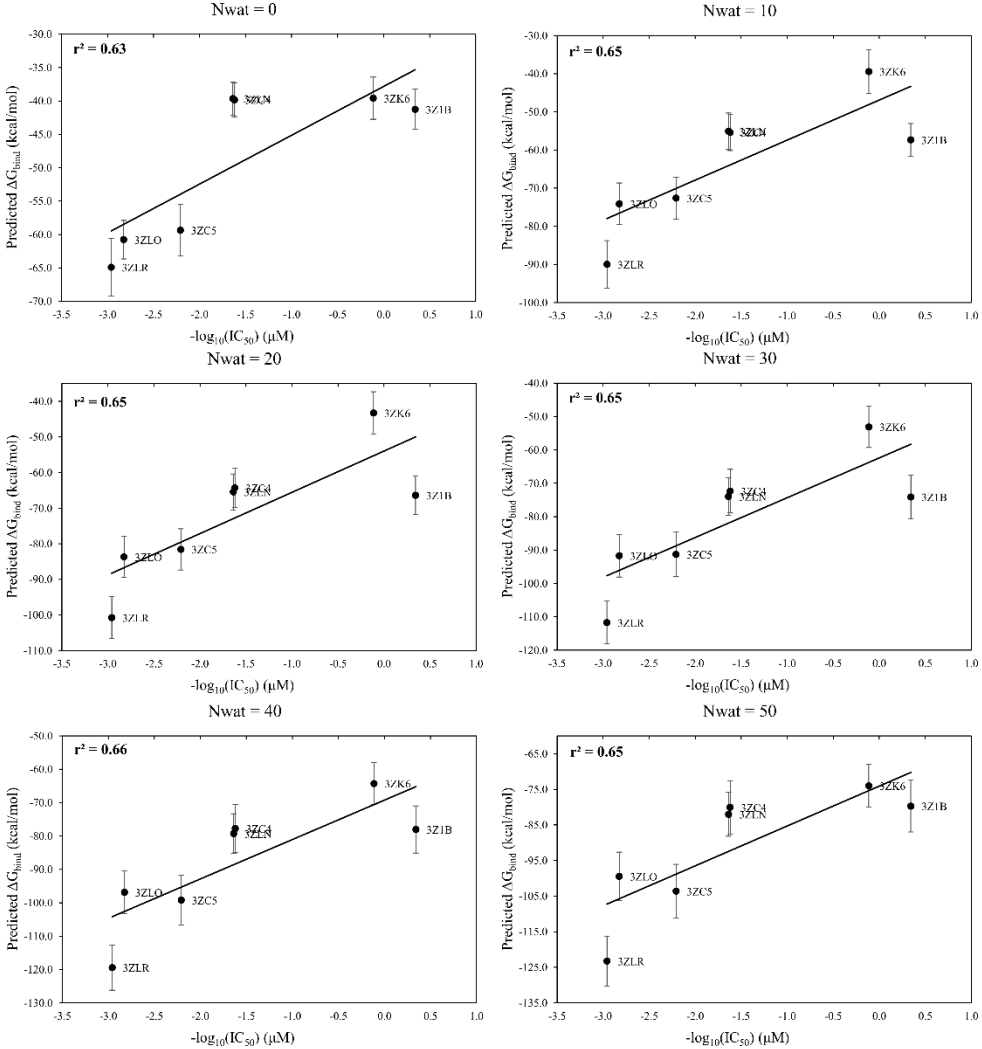

Correlation between experimental free energy of binding and predicted binding energies obtained for BCL-X_L with Nwat = 0 - 50 by analyzing the 4th ns of a MD simulation run on a CPU hardware.

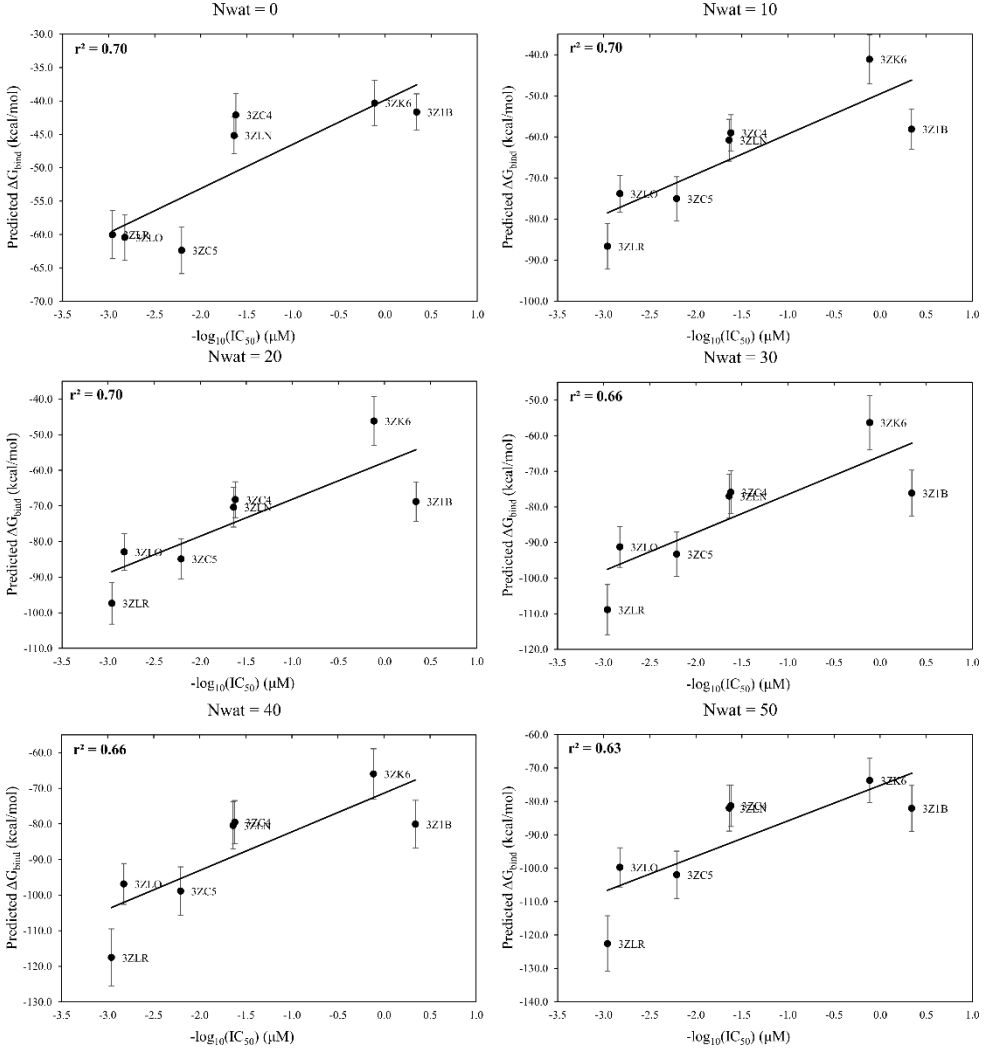

ANNEX 11.D. Additional information about XIAP-BIR2

Correlation between experimental free energy of binding and predicted binding energies obtained for XIAP-BIR2 with Nwat = 0 - 90 by analyzing the first ns of a MD simulation run on a CPU hardware.

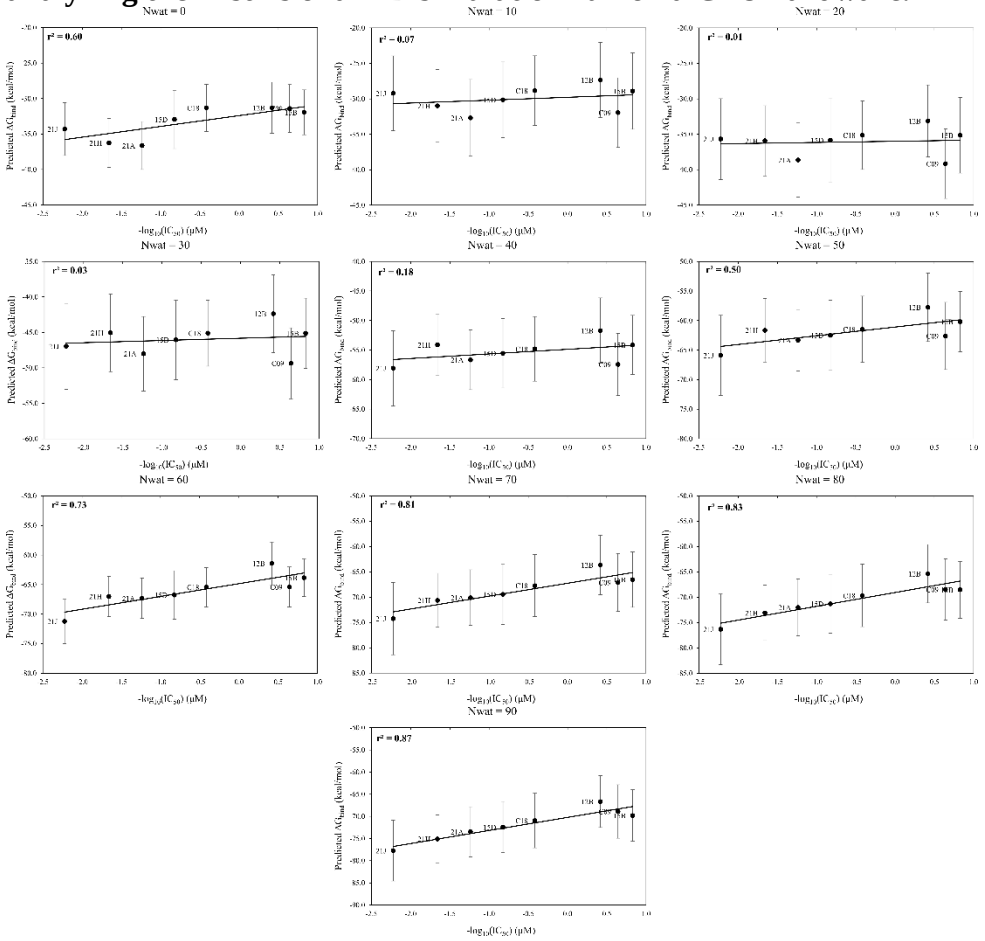

Correlation between experimental free energy of binding and predicted binding energies obtained for XIAP-BIR2 with Nwat = 0 - 90 by analyzing the 4th ns of a MD simulation run on a GPU hardware.

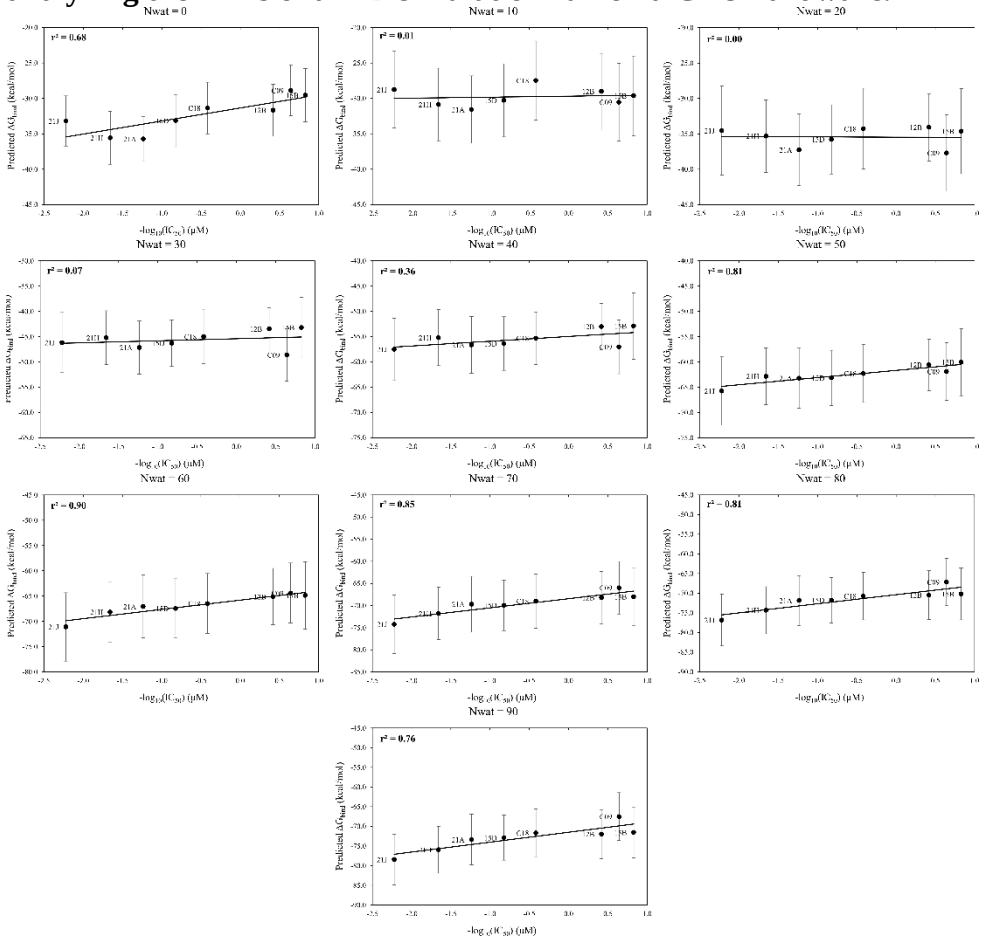

Correlation between experimental free energy of binding and predicted binding energies obtained for XIAP-BIR2 with Nwat = 0 - 90 by analyzing the 4th ns of a MD simulation run on a CPU hardware.

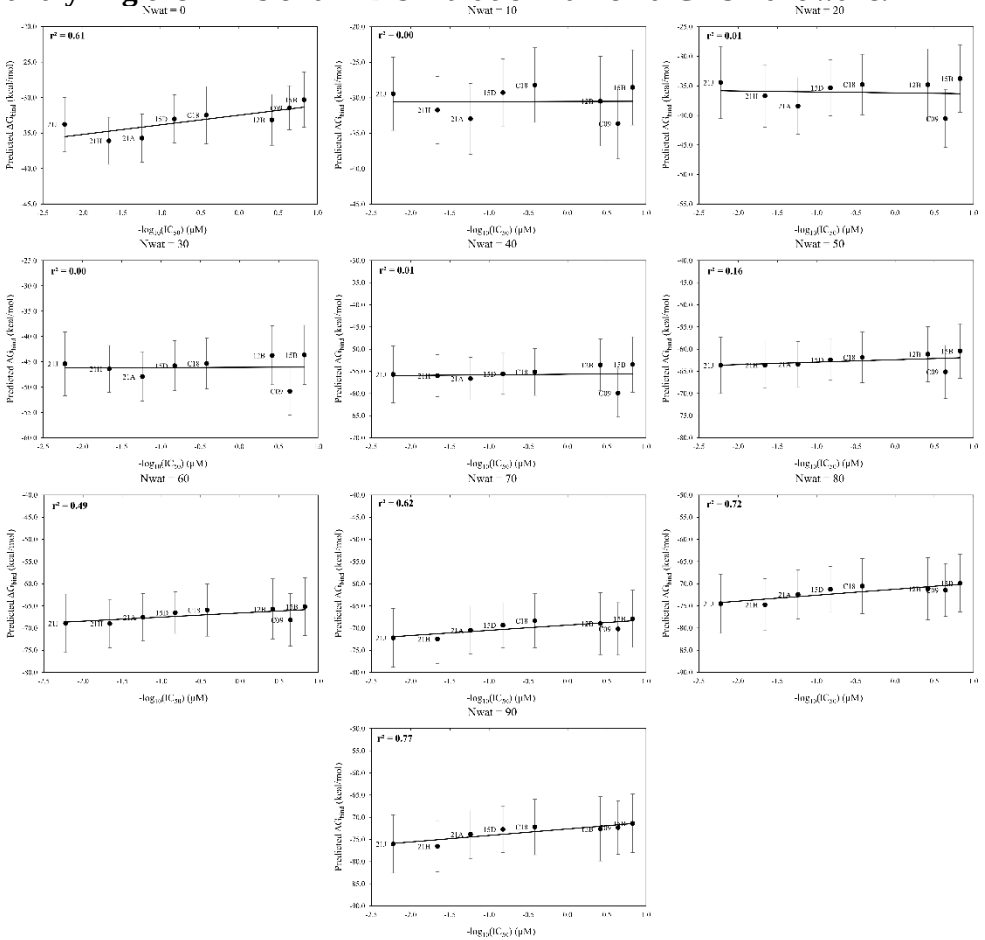

Correlation between experimental free energy of binding and predicted binding energies obtained for HIV1-protease with Nwat = 0 - 70 by analyzing the first ns of a MD simulation run on a CPU hardware.

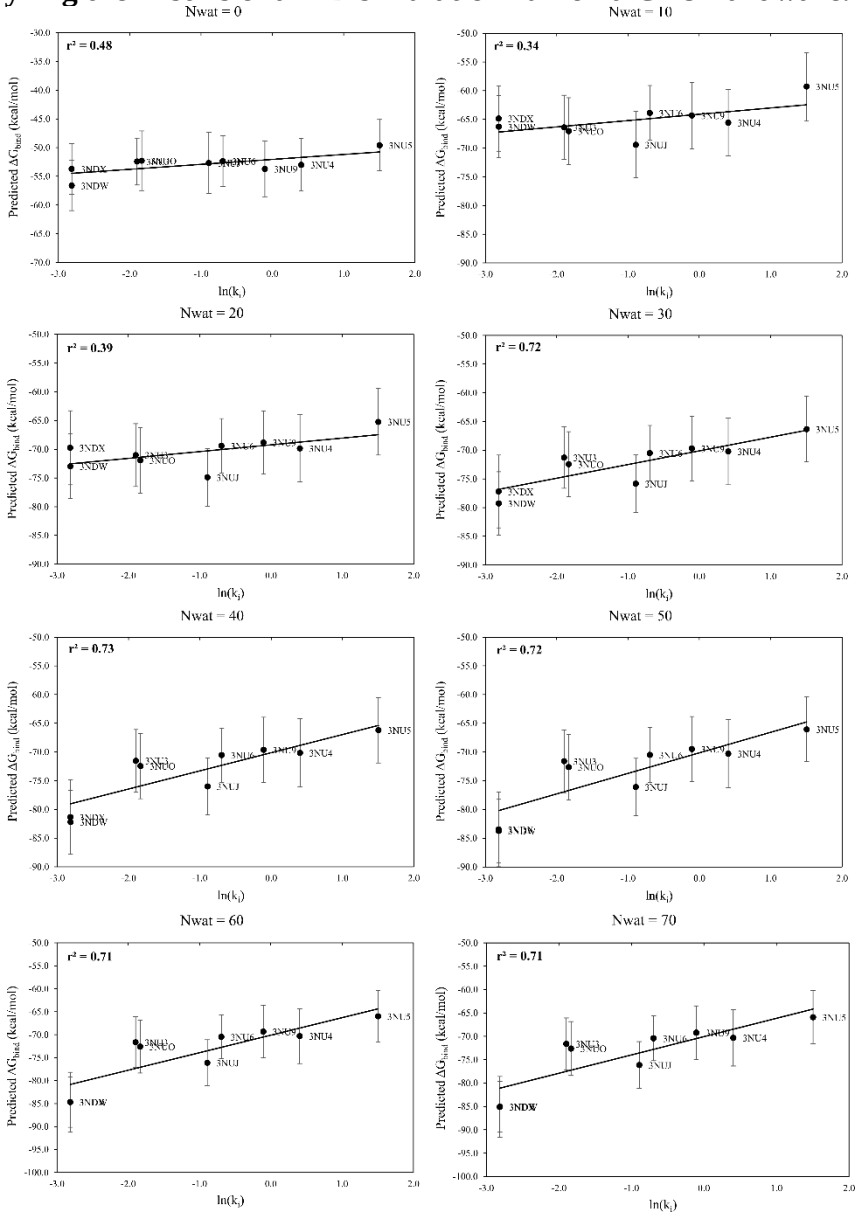

Correlation between experimental free energy of binding and predicted binding energies obtained for HIV1-protease with Nwat = 0 - 70 by analyzing the 4th ns of a MD simulation run on a GPU hardware.

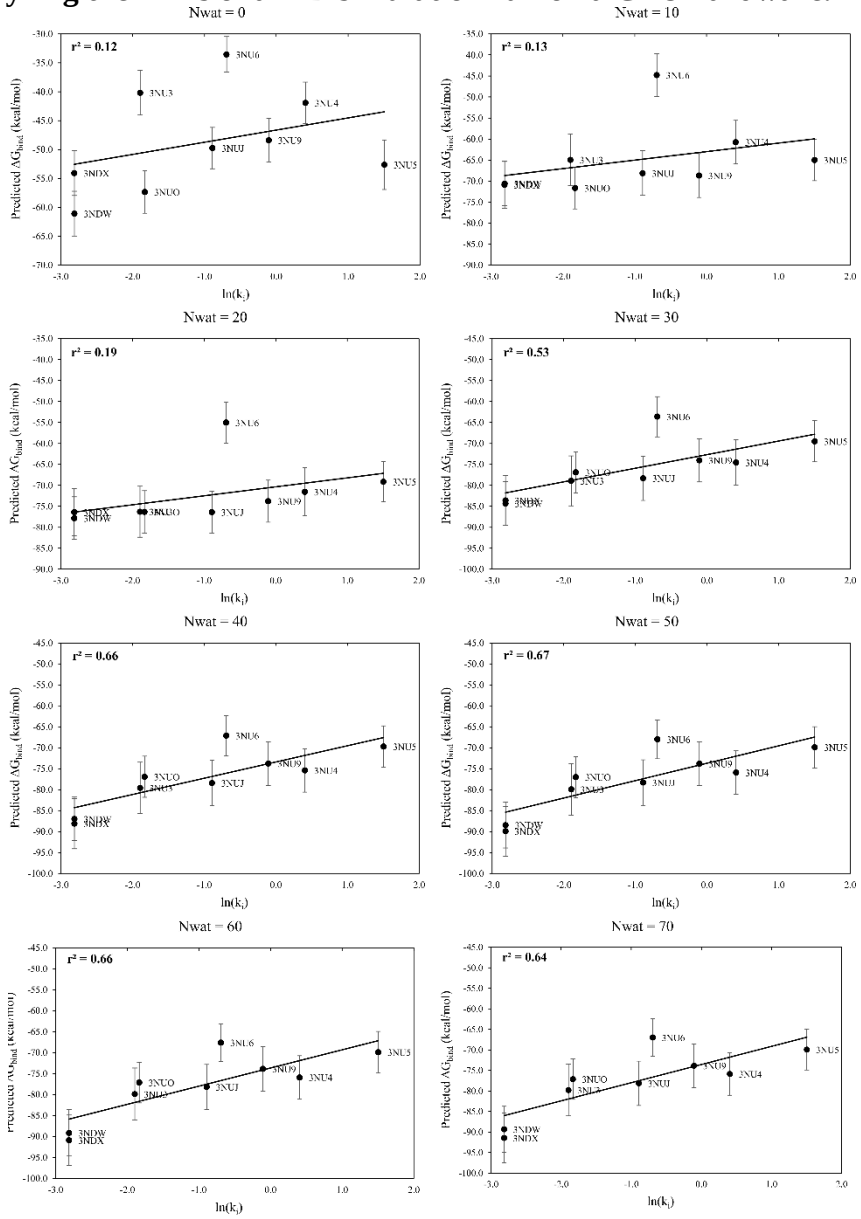

Correlation between experimental free energy of binding and predicted binding energies obtained for HIV1-protease with Nwat = 0 - 70 by analyzing the 4th ns of a MD simulation run on a CPU hardware.

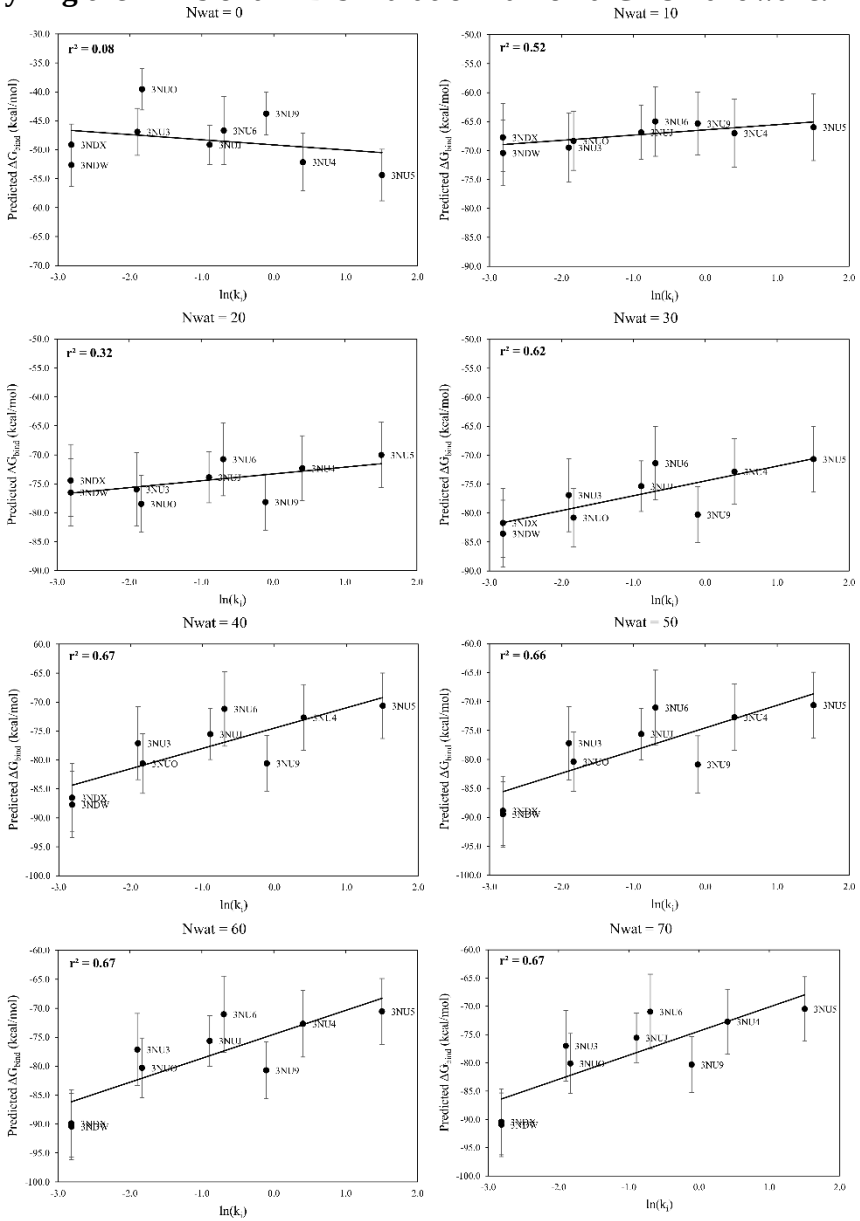

ANNEX 11.F. Scripts used for the automatization of the MD/Nwat-MMGBSA protocol

Ligand parametrization.

```
#!/bin/tcsh
# Alessandro Contini 2014
# Given a multimol2 named multimol2_c1.mol2, the scripts uses antechamber
and
# parmchk2 to generate .prep and .frcmods for each ligand
#
# usage: tcsh PARAMETERIZE_AC.csh
#
# do preliminary setup
source /usr/local/amber14/amber14.csh
setenv WORKDIR `pwd`
if (-e charges.txt) then
     rm charges.txt
endif
if (-e names.txt) then
     rm names.txt
endif
if (! -d BCC) then
     mkdir BCC
endif
if (! -e multimol2_c1.mol2) then
     echo "multimol2_c1.mol2 must be in the current directory"
else
     #edit multimol2s to delete the "Q" before the residue name (I guess
it is a bug in MOE)
        sed -i 's/1 Q/1 /g' multimol2*
        #create list
        awk '/@<TRIPOS>MOLECULE/{getline; print}' multimol2_c1.mol2 | awk
'{print substr($0,0,4)}' > list
     set max = `grep -o "@<TRIPOS>MOLECULE" multimol2_c1.mol2 | wc -l`
     set  a = 1
     #split the multimol2, calculate molecule net charge and grab residue
name
     foreach n (`cat list`)
          if ($a <= $max) then
               awk
"/^@<TRIPOS>MOLECULE/,/^MOE/{if(++m==1)n++;if(n=="$a")print;if(/^#/)m=0}"
multimol2_c1.mol2 > ligand_"$n".mol2
               babel -imol2 ligand_"$n".mol2 --partialcharge mmff94 -omol2
tmp
               set c = `awk '{print $9}' tmp | awk '{sum+=$1} END {print
sum}' | awk '{printf "%.0f\n", $1}'`
               rm tmp
               echo $c >> charges.txt # print charges for debug
               set name = `awk '/@<TRIPOS>ATOM/{getline; print}'
ligand_"$n".mol2 | awk '{print $(NF-1)}' | awk '{print substr( $0,
length($0) -2,length($0))}'`
               echo $name >> names.txt
     #run ac and parmchk
               antechamber -i ligand_$n.mol2 -fi mol2 -o $name.prep -fo
prepi -nc $c -c bcc -rn $name -pf y
               parmchk2 -i $name.prep -f prepi -o $name.frcmod
                       mv $name.prep BCC
                       mv $name.frcmod BCC
                          @ a ++
          endif
     end
endif
```

Nwat-MMGBSA.

```
#!/bin/tcsh
#
# Written by I. Maffucci and A. Contini, 2014; based on the work reported
in J. Chem. Theory Comput., 2013, 9 (6), pp 2706-2717
#
# Given a set of PDB complexes, this script setup MMGBSA calculations
including $n explicit water closest to ligand mask.
# The sript assumes that solvated .top and MD trajectories are stored in
$WORKDIR/$n.
#
# The following standard name are also used:
# solvated topology file: $z_complex_wat.top
# solvated trajectory file: $z_complex.prod$nprod.mdcrd
# with $z = system name and $nprod = production run number
#
# AmberTools14 needs to be installed and environment variables correctly
specified
#
# ATTENTION!
# Automatic ligand recognition only works if the ligand is a single chain
(no "TER" inbetween) and is the last residue or set of residues of the
complex.
# If ions or cofactors need to be considered as part of the receptor, they
must be placed "before" the ligand in the original PDB file.
#
# run as: tcsh NWAT_MMPBGBSA_5.1_MPI.csh >& NWAT_MMPBGBSA_5.1_MPI.log &
#
#########################################################
# HERE ARE VARIABLES THAT NEED TO BE MODIFIED BY USER#
#########################################################
#
set AMBERV = 14 # modify accordingly to your Amber installation
#
set solv = "GB"       # PB = MMPBSA; GB = MMGBSA
#
set nproc = 6         # set n° of processors for MMGBSA calculations (max 6
on born)
#
set nprod = 4         # which is the number of production run to be
analyzed?
#
set frames = 1000     # total number of frames in trajectory
#
set r = 10            # interval between trajectory frames selected for
MMGBSA calculation (suggested values for production = 10 or 20)
#
set nwat = "0 10 20 30 40 50" # set Nwat walues; typical values for
screening water effect are 0 10 20 30 40 50; for fixed Nwat run 0 30
#
# define residues/ions that are NOT receptor or ligand
set nonlig = ":Na+,:Cl-,:MG,:ZN,:ATP,:GTP"
#
#########################################################
# END OF USER MODIFIABLE VARIABLES                      #
#########################################################
#
source /usr/local/amber$AMBERV/amber$AMBERV.csh # modify accordingly to
your amber installation
```

```
#
setenv WORKDIR `pwd`
#
mkdir MM"$solv"SA
#
echo "MM"$solv"SA calculation begun on "`date`
#
echo "                      Average Delta          Std. Dev.   Std. Err. of
Mean" > $WORKDIR/MM"$solv"SA/RESULTS_$solv.txt
#
#foreach z (`cat $WORKDIR/list_debug`) # for debug
foreach z (`ls */*top | awk -F/ '{print $1F}'`)
        # check if trajectory exists and is compressed
     if (-e $WORKDIR/$z/"$z"_complex_wat.prod"$nprod".mdcrd.bz2) then
           set bz = ".bz2"
     else if (-e $WORKDIR/$z/"$z"_complex_wat.prod"$nprod".mdcrd.gz) then
           set bz = ".gz"
        else if (-e $WORKDIR/$z/"$z"_complex_wat.prod"$nprod".mdcrd) then
           set bz = ""
        else
           echo "I cannot find "$z"_complex_wat.prod"$nprod" trajectory"
           exit
        endif

        #see if ligand is a single residue or not
        # do a pdb file from coordinates
        cat << EOF | cpptraj -p $WORKDIR/$z/$z\_complex_wat.top
trajin $WORKDIR/$z/$z\_complex_wat.prod$nprod.mdcrd$bz 1 1
strip :WAT,$nonlig
trajout tmp.rst restart
EOF
        cat << EOF | cpptraj -p $WORKDIR/$z/$z\_complex_wat.top
parmstrip :WAT,$nonlig nobox
parmwrite out tmp1.top amber
EOF
ambpdb -p tmp1.top < tmp.rst > tmp
     #define last receptor residue
        set y = `tac tmp | awk '/TER/ && ++n ==1 {getline; print$5}'`
        #define first ligand residue
        @ f = $y + 1
        #define last ligand residue
        set l = `tac tmp | awk 'NR==2 {print$5}'`
        #rm tmp
        if ($f == $l) then
           set x = "$f"
        else
           set x = "$f-$l"
        endif
        echo ""$z" ligand residue numbers are: "$x""

        #start MM-PBSA/GBSA calculation
        mkdir MM"$solv"SA/$z
     echo "$z" >> MM"$solv"SA/RESULTS_$solv.txt
     cd $WORKDIR/MM"$solv"SA/$z

     if ($solv == GB) then
        # check the PBRadii set and define the GB model (only if GB method
is used)
           set radii = `awk '/FLAG RADIUS_SET/{getline;getline;print $NF}'
$WORKDIR/$z/"$z"_complex_wat.top | sed 's/(//g' | sed 's/)//g'`
```

```
                if ($radii == mbondi3) then
                set g = 8
                else if ($radii == mbondi2) then
                set g = 5
                else if ($radii == mbondi) then
                set g = 1
           else
                echo "cannot determine the RADIUS SET from topology"
                exit
           endif
           echo "the radius set is "$radii", setting igb="$g""
      endif

      # create a file named nwat.dat containing the nr. of closest water
molecules to include in top/mdcrd.
         printf %"s\n" "$nwat" > nwat.dat # for Nwat screen

      foreach n (`cat nwat.dat`)
                # set variables for MMPB/GBSA input
                set a = `echo $l+$n | bc`  # last water residue
           @ w = $l + 1               # first water residue
                @ b = $a + 1               # first ecluded water
                mkdir nwat$n # create directories named nwatn, where n is
nr. of closest water molecules
           cd nwat$n

      # generate ligand topologies
           echo "parmstrip :1-"$y","$nonlig",:WAT\nparmbox nobox\nparmwrite
out ligand.top amber" > lig_gen.cpptraj
           $AMBERHOME/bin/cpptraj -i lig_gen.cpptraj -p
"$WORKDIR"/"$z"/"$z"_complex_wat.top > lig_cpptraj.log

      # generate trajectory  for nwat > 0
           if ($n != 0) then
                echo "trajin
"$WORKDIR"/"$z"/"$z"_complex_wat.prod"$nprod".mdcrd"$bz" 1 $frames "$r"" >
cmplx_trj_gen.cpptraj
                echo "center @CA,C,N mass origin\nimage origin
center\nstrip "$nonlig"\nclosest "$n" :"$x" noimage" >>
cmplx_trj_gen.cpptraj
                echo "trajout nwat"$n"."$z".mdcrd nobox" >>
cmplx_trj_gen.cpptraj
                $AMBERHOME/bin/cpptraj -i cmplx_trj_gen.cpptraj -p
"$WORKDIR"/"$z"/"$z"_complex_wat.top > cmplx_trj_gen_cpptraj.log
      # generate complex topologies for nwat > 0
                echo "parmstrip "$nonlig"\nparmbox nobox\nparmwrite out
tmp.top amber" > cmplx_top1_gen.cpptraj
                $AMBERHOME/bin/cpptraj -i cmplx_top1_gen.cpptraj -p
"$WORKDIR"/"$z"/"$z"_complex_wat.top > cmplx_top1_nwat_cpptraj.log

                        #assuming max water number = 60000
                        echo "parmstrip :"$b"-60000\nparmbox
nobox\nparmwrite out nwat"$n"."$z".top amber" > cmplx_top2_gen.cpptraj
                $AMBERHOME/bin/cpptraj -i cmplx_top2_gen.cpptraj -p tmp.top
> cmplx_top2_nwat_cpptraj.log
      # generate receptor topologies for nwat > 0
                echo "parmstrip :"$x"\nparmbox nobox\nparmwrite out
nwat"$n"."$z"_rec.top amber" > rec_top_gen.cpptraj
                $AMBERHOME/bin/cpptraj -i rec_top_gen.cpptraj -p
nwat"$n"."$z".top > rec_top_nwat_cpptraj.log
```

```
        # generate MMPB/GBSA input for nwat > 0; change to modify MM-
PBSA/GBSA protocol. See Amber14 manual for details
                if ($solv == GB) then
                           echo "&general\nreceptor_mask=:1-"$y":"$w"-"$a",
ligand_mask=:"$x", \
interval=1, verbose=1,\n/\n&gb\nigb="$g", saltcon=0.15," >
mmpbsa_closest_nwat$n.in
                        else if ($solv == PB) then
                           echo "&general\nreceptor_mask=:1-"$y":"$w"-"$a",
ligand_mask=:"$x", \
interval=1, verbose=1,\n/\n&pb\nistrng=0.150, radiopt=0" >
mmpbsa_closest_nwat$n.in
                endif
            else
      # generate trajectory for nwat = 0
                echo "trajin
"$WORKDIR"/"$z"/"$z"_complex_wat.prod"$nprod".mdcrd"$bz" 1 $frames "$r"" >
gen0.cpptraj
                echo "autoimage\nstrip "$nonlig",:WAT\ntrajout
nwat"$n"."$z".mdcrd nobox" >> gen0.cpptraj
                $AMBERHOME/bin/cpptraj -i gen0.cpptraj -p
"$WORKDIR"/"$z"/"$z"_complex_wat.top > traj_nwat0_cpptraj.log

      # generate receptor and complex topologies for nwat=0
                echo "parmstrip "$nonlig",:WAT\nparmbox nobox\nparmwrite
out nwat"$n"."$z".top amber" > topgen0.cpptraj
                echo "parmstrip :"$x"\nparmwrite out nwat"$n"."$z"_rec.top
amber" >> topgen0.cpptraj
                $AMBERHOME/bin/cpptraj -i topgen0.cpptraj -p
"$WORKDIR"/"$z"/"$z"_complex_wat.top > top_nwat0_cpptraj.log

       # generate MMPB/GBSA input for nwat = 0; change to modify MM-
PBSA/GBSA protocol. See Amber14 manual for details
                        if ($solv == GB) then
                           echo "&general\nreceptor_mask=:1-"$y",
ligand_mask=:"$x", interval=1, verbose=1,\n/\n&gb\nigb="$g", saltcon=0.15,"
> mmpbsa_closest_nwat$n.in
                else if ($solv == PB) then
                           echo "&general\nreceptor_mask=:1-"$y",
ligand_mask=:"$x", interval=1, verbose=1,\n/\n&pb\nistrng=0.150, radiopt=0"
> mmpbsa_closest_nwat$n.in
                endif
                endif
# execute MMPB/GBSA and print results
           $MPI_HOME/bin/mpirun -np $nproc $AMBERHOME/bin/MMPBSA.py.MPI -O
-i mmpbsa_closest_nwat$n.in -o FINAL_RESULTS_CLOSEST$n \
                -cp nwat"$n"."$z".top -rp nwat"$n"."$z"_rec.top -lp
ligand.top -y nwat$n.$z.mdcrd >& MMPBSA.out
                grep "DELTA TOTAL" FINAL_RESULTS_CLOSEST"$n" | sed "s/DELTA
TOTAL/NWAT="$n"/g" >> $WORKDIR/MM"$solv"SA/RESULTS_$solv.txt
                cd ..
      end
      cd $WORKDIR
         rm tmp*
end
#
# the script terminates
#
echo "MM"$solv"SA calculations ended on "`date`
```